Journal of Immunology Research

# Cell Death Signaling and Mechanisms of Systemic Inflammation

Lead Guest Editor: Yi-Song Qian
Guest Editors: Meng-Hao Huang, Lifei Wang, Tingtao Chen, and Xuan Huang

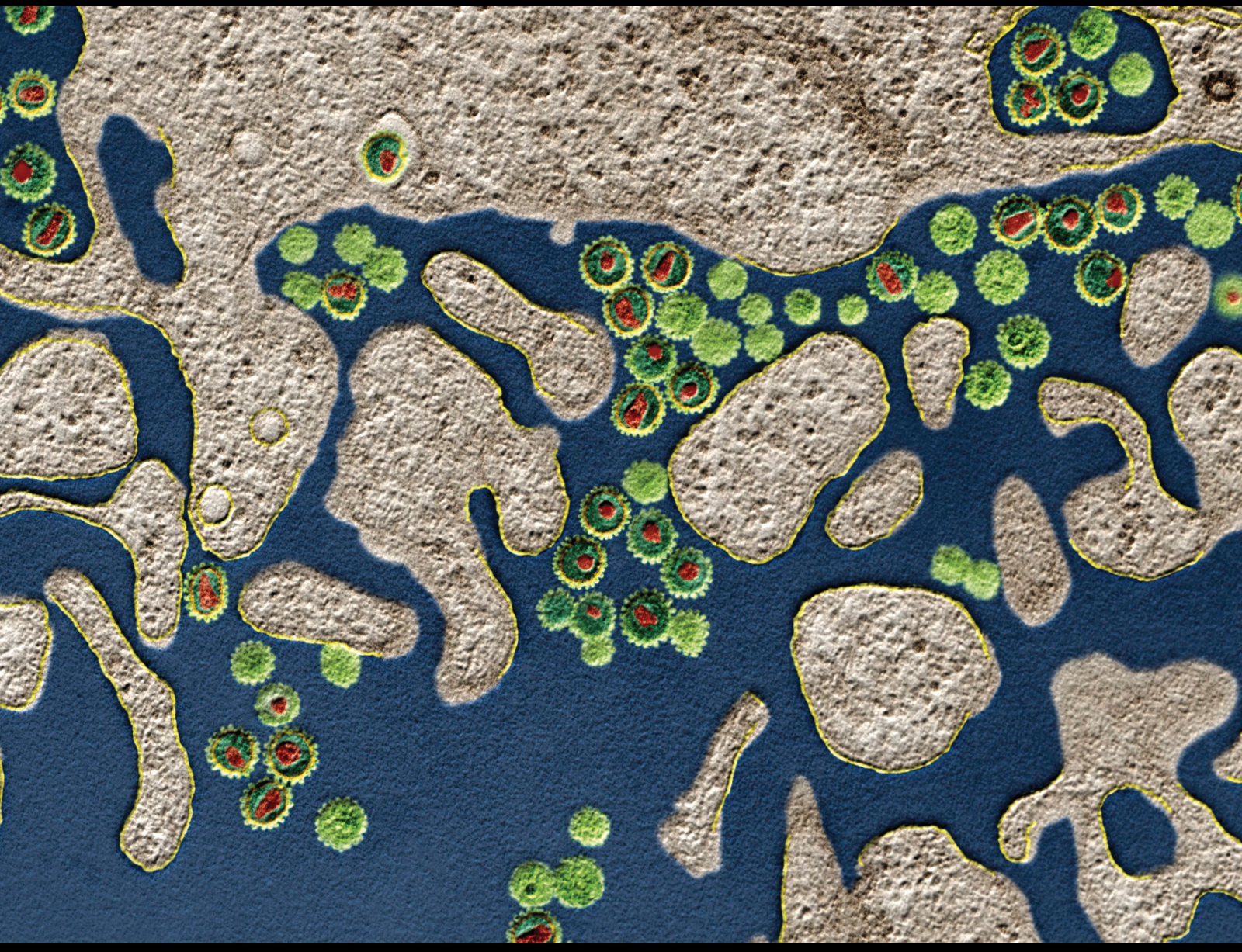

# Cell Death Signaling and Mechanisms of Systemic Inflammation

Journal of Immunology Research

# Cell Death Signaling and Mechanisms of Systemic Inflammation

Lead Guest Editor: Yi-Song Qian
Guest Editors: Meng-Hao Huang, Lifei Wang, Tingtao Chen, and Xuan Huang

# Contents

Hindawi
Journal of Immunology Research
Volume 2022, Article ID 9166370, 10 pages
https://doi.org/10.1155/2022/9166370

*Research Article*

# Ebosin Attenuates the Inflammatory Responses Induced by TNF-α through Inhibiting NF-κB and MAPK Pathways in Rat Fibroblast-Like Synoviocytes

**Yang Zhang**,[1,2] **Lifei Wang**,[1] **Liping Bai**,[1] **Rong Jiang**,[1] **Jianbo Wu**,[1] **and Yuan Li**[1]

[1]*NHC Key Laboratory of Biotechnology of Antibiotics, CAMS Key Laboratory of Synthetic Biology for Drug Innovation, Institute of Medicinal Biotechnology, Chinese Academy of Medical Sciences & Peking Union Medical College, No. 1 Tiantan Xili, 100050 Beijing, China*
[2]*Beijing Institute of Hepatology, Beijing Youan Hospital, Capital Medical University, Beijing 100069, China*

Correspondence should be addressed to Yuan Li; yuanwli@hotmail.com

Received 6 July 2021; Revised 4 December 2021; Accepted 22 January 2022; Published 17 March 2022

Academic Editor: Ran Wang



Tumor necrosis factor-α (TNF-α) lies at the apex of signal transduction cascades that results in induced destruction of joints in rheumatoid arthritis. It is therefore of great medicinal interest to modulate the cellular responses to TNF-α. Ebosin, a novel exopolysaccharide derived from *Streptomyces* sp, has been demonstrated to have remarkable therapeutic actions on collagen-induced arthritis in rats, while it also suppressed the production of IL-1β, TNF-α, and IL-6 at both mRNA and protein levels in cultured fibroblast-like synoviocytes. In order to further understand the potential mechanisms involved in the anti-inflammatory effects of ebosin at molecular level, we investigated the impact of it on the activation of MAPK and NF-κB pathways following TNF-α induced in fibroblast-like synoviocytes (FLS). The results showed that the phosphorylation levels of TNF-α-induced p38, JNK1, JNK2, IKKα, IKKβ, and IκB, as well as NF-κB nuclear translocation, were reduced significantly in FLS cells in response to ebosin. Furthermore, we proved that ebosin decreased the level of NF-κB in the nucleus and blocked the DNA-binding ability of NF-κB using electrophoresis mobility gel shift assay. Besides, low levels of matrix metalloproteinases (MMP-1 and MMP-3) and chemokines (interleukin-8 and RANTES) were found in TNF-α-stimulated fibroblast-like synoviocytes treated with ebosin. These results indicate that ebosin can suppress a range of activities in both MAPK and NF-κB pathways induced by TNF-α in rat fibroblast-like synoviocytes, which provides a rationale for examining the use of ebosin as a potential therapeutic candidate for rheumatic arthritis.

## 1. Introduction

Rheumatoid arthritis (RA) is a chronic destructive disease of the joints and cartilage. Proinflammatory cytokines such as tumor necrosis factor (TNF) produced by fibroblast-like synoviocytes (FLS) and inflammatory cells, which are expressed at high levels in rheumatoid joint tissue, where they contribute significantly to inflammation and articular destruction. Dysfunction of TNF-α is involved in the pathological process of different types of diseases including RA [1, 2], which was the first proinflammatory cytokine fully identified as a therapeutic target for RA [3]. TNF-targeted therapy has convincingly demonstrated significant benefit for the majority of RA patients treated. Using recombinant proteins including infliximab, adalimumab, and golimumab [4] to block TNF has emerged in recent years.

TNF-α elicits its biological activities through binding to two types of cell surface receptors TNF-R1 and TNF-R2. In most of the cells, TNF-R1 was considered to be a key mediator of TNF-α signal [5]. NF-κB is an important downstream target of TNF-α signaling, and it has been identified to be involved in inflammatory responses [6]. TNF-α triggers NF-κB activation by a variety of signaling molecules, including TRAF2 (TNF receptor-associated factor 2), RIP (receptor-interacting protein), and the IKK (IκB kinase) complex. Another signal pathway activated by TNF-α is mitogen-activated protein kinase

pathways (including p38, JNK, and ERK1/2), which has been strongly associated with many of the processes that mediate the pathological features of RA [7]. The p38 MAPK and JNK (Jun N-terminal kinase) pathway inhibitors attract more attention since they can reduce both the synthesis of proinflammatory cytokine and their intracellular signaling [8]. In addition, TNF-$\alpha$ also induces extracellular matrix (ECM) remodeling by regulating the expression of MMPs involved in joint damage in RA, as well as expression of multiple chemokines including IL-8, MCP-1, CCL3, CCL4, and RANTES, which contribute to chronic inflammatory [9–16]. Currently, anti-inflammatory therapy by inhibiting MAPK and NF-$\kappa$B pathways has been well recognized [17].

Ebosin, a novel exopolysaccharide (EPS) extracted from *Streptomyces* sp.139 of soil samples in China, remarkably inhibits the development of CIA (collagen-induced arthritis) in rats [18], which consisted of rhamnose, fucose, arabinose, mannose, xylose, glucose, galactose, and galacturonic acid [19]. This anti-inflammatory effect of ebosin on CIA has been identified to be related to attenuating the production of IL-1$\beta$ (interleukin-1$\beta$), IL-6 (interleukin-6), and TNF-$\alpha$ at the transcriptional and posttranscriptional levels [18].

Although anti-TNF agents have been shown to improve the outcome of the management of RA, a proportion of patients does not respond well to anti-TNF therapy and has increased the risk of adverse events such as infections [20–24]. Unlike antibody-based agents, ebosin is the first EPS produced by the *Streptomyces* genus with a novel structure [19]. In a previous study, we found that the inhibitory effect of ebosin on TNF-$\alpha$ secretion was stronger than other cytokines as IL-1$\beta$ and IL-6 in the CIA rat model and FLS cells, implicating that ebosin may improve rheumatoid arthritis symptoms through the TNF-$\alpha$ signaling pathway [18]. However, ebosin may have a wide application prospect due to its efficacy and high safety which have been proven by a long-term toxicity study (unpublished data). Based on the above, the purpose of this study was to investigate the impact of ebosin on TNF-$\alpha$-mediated MAPK and NF-$\kappa$B pathways, as well as on levels of MMPs and chemokines in rat fibroblast-like synoviocytes (FLS), which will help us to better understand the mechanism of action of ebosin.

## 2. Materials and Methods

*2.1. Isolation of FLSs.* Male Wistar rats (Certificate No.: SCXK 2005-0013) were obtained from the Institute of Experimental Animals, Chinese Academy of Medical Sciences, Beijing [18]. All rats were handled humanely and procedures under standard laboratory conditions with the approval of the Institute of Experimental Animals and Use Committee of the Chinese Academy of Medical Sciences. Chicken type II collagen (CII, Sigma)-induced arthritis (CIA) model and isolation of FLS were performed following the protocol described by Zhang et al. [18, 25]. In brief, Synovial tissues were isolated from the knee joint of CIA rats, which were sacrificed on day 30 after immunization, and then digested by 0.4% type II collagenase (Gibco). Isolated FLS were grown in DMEM high-glucose medium supplemented with 10% fetal bovine serum, 100 units/ml penicillin, and 100 $\mu$g/ml streptomycin and cultured at 37°C, 5% $CO_2$.

*2.2. Purification of Ebosin.* Ebosin-producing *Streptomyces*.139 was found from a soil sample in China and deposited in the China General Microbiology Culture Collection Center (No. 0405). Ebosin was purified from the supernatant of fermentation culture of *Streptomyces* sp.139 according to the protocol as described before [19].

*2.3. Cytoplasmic and Nuclear Protein Extraction.* FLS were cultivated in 6-well plates (at $1 \times 10^6$/ml) at 37°C for 24 h. Ebosin (80, 16, or 3.2 $\mu$g/ml) was diluted in DMEM and added into FLS for 3 h with TNF-$\alpha$ (10 ng/ml). Cells were collected in 0.25% trypsin-EDTA (HyClone) and harvested by centrifugation at 500 g for 5 min. Cytoplasmic and nuclear were extracted using NE-PER Nuclear and Cytoplasmic Extraction Reagents following the manufacturer's protocol [25]. The cytoplasmic and nuclear extracts were stored at -80°C. Determination of protein concentration was performed by the Bradford method [26].

*2.4. Western Blot Analysis.* The effect of Ebosin on MAPK and NF-$\kappa$B signaling pathways was determined by western blot assay as described previously [25]. The expression level of protein was detected with antibodies (Cell Signaling Technology) against phosphorylated or nonphosphorylated p38, JNK1, JNK2, ERK, IKK$\alpha$, IKK$\beta$, I$\kappa$B, and NF-$\kappa$B p65, respectively. The relative densities for the protein bands were quantitated using ImageQuant 300 (GE Healthcare) with Image J software.

*2.5. Enzyme-Linked Immunosorbent Assays (ELISAs).* ELISA was used to evaluate the levels of IL-8, RANTES, MMP-1, and MMP-3 in cell culture medium. FLS cells were plated in 24-well plates at $1 \times 10^6$/ml and cultivated at 37°C for 24 h and then received proper ebosin treatments (80, 16, and 3.2 $\mu$g/ml) for 12 h. Cells were further induced by adding 10 ng/ml TNF-$\alpha$ for 24 h before supernatants were collected. The level of MMP-1, MMP-3, RANTES, and IL-8 in the medium was detected using colorimetric ELISA kits (USCN Life Science Inc. and Boster, Elab).

*2.6. Electrophoretic Mobility Shift Analysis (EMSAs).* EMSA was performed to detect the effect of ebosin on the ability of NF-$\kappa$B binding to DNA in nuclei using the LightShift Chemiluminescent EMSA Kit (Thermo) following the instructions of the manufacturer [25]. Extraction of nuclear protein was performed as previously described. Oligonucleotides labeling with biotin (5′-AGTTGAGGGGACTTTCCCAGGC-3′; 3′-TCAA CTCCCCTGAAAGGGTCCG-5′), which contains the $\kappa$-chain binding site ($\kappa$B, 5′-GGGACTTTCC-3′), was synthesized from Beyotime Biotechnology Company. Unlabeled oligonucleotide and a 50-fold excess of cold $\kappa$B oligonucleotide were used as a control to confirm specific binding.

*2.7. Immunofluorescence Analysis.* FLS cells were cultivated in 96-well plates (at $1 \times 10^4$/ml) at 37°C for 12 h. Ebosin (80 $\mu$g/ml) was added in each well followed by cultivation

at 37°C for 12 h and then treated cell with TNF-$\alpha$ (10 ng/ml) for an additional 3 h. The cells were fixed in 5% paraformaldehyde (PFA)/PBS for 10 min at room temperature, permeabilized with PBS/0.1% Triton-X100 for 15 min, and blocked in PBS with 5% bovine serum albumin for 1 h. The cells were incubated with rabbit anti-NF-$\kappa$B p65 (Cell Signaling Technology) and Alexa Fluor 488 donkey anti-rabbit IgG (Molecular Probes). The fluorescent signals were detected by fluorescence microscopy (Olympus IX71, Japan).

*2.8. Statistical Analysis.* Data are presented as mean ± SD values. Evaluation of significance of differences between sample groups was performed by GraphPad Prism software (Version 6.0) using Student's $t$-test. All $P$ value < 0.05 was considered significant (∗).

## 3. Results

*3.1. Ebosin Downregulates TNF-α-Induced p38 MAPK Activation.* Phosphorylation of p38 MAPK is involved in the activation of proinflammatory cytokines including TNF-$\alpha$ [27]. In order to investigate the effect of ebosin on TNF-$\alpha$-induced p38 MAPK activation, FLS cells were treated with ebosin at a concentration of 0.128, 0.64, 3.2, 16, 80, and 400 $\mu$g/ml for 12 h. Phosphorylated active forms of p38 MAPK were detected by western blot in FLS cells following TNF-$\alpha$ stimulation. As shown in Figure 1(a), ebosin markedly reduced the level of phosphorylation of p38 MAPK by 63.67% ($P < 0.01$), 38.94% ($P < 0.001$), 25.21% ($P < 0.05$), 16.51% ($P < 0.01$), 10.16% ($P < 0.05$), and 3.62%, respectively, in a dose-dependent manner, while the levels of nonphosphorylated p38 in FLS did not change (Figure 1(a)), indicating that ebosin can downregulate p38 MAPK activation induced by TNF-$\alpha$.

*3.2. Ebosin Reduces the Production of Phosphorylated JNK1 and JNK2 MAPK.* JNK is one major group of MAPK cascades, which are activated by TNFR superfamily members [27]. To understand the effect of ebosin on TNF-$\alpha$-induced expression of JNKs in FLS, the supernatant of lysed cells was assessed by western blot after treating cells with TNF-$\alpha$ in the presence of ebosin. The results showed that ebosin in the range of 0.128~400 $\mu$g/ml significantly reduced the expression levels of phosphorylated JNK1 by 50.32% ($P < 0.01$), 34.84% ($P < 0.001$), 27.60% ($P < 0.01$), 13.51% ($P < 0.01$), 8.95%, and 1.19%, respectively (Figure 1(b)), while the phosphorylated JNK2 levels decreased by 59.09% ($P < 0.01$), 50.07% ($P < 0.01$), 43.00% ($P < 0.01$), 21.96% ($P < 0.05$), 13.29%, and 8.30%, respectively (Figure 1(b)), but does not affect nonphosphorylated forms of JNK1 and JNK2 (Figure 1(b)) at the same dosages.

*3.3. The Expression Levels of p42/44 MAPK (ERK1/2) Are Not Influenced by Ebosin.* The activation of p42/44 MAPK is associated with inflammatory response, synovial proliferation, and angiogenesis in RA [27]. To valuate effect of ebosin on TNF-$\alpha$-induced expression of p42/44 MAPK in FLS, we treated FLS cells with TNF-$\alpha$ in the presence of ebosin, and then, the phosphorylated (or nonphosphorylated) p42/44 protein level in the supernatant of lysed cells was determined using western blot. The results found that ebosin did not exert any action on both phosphorylated and nonphosphorylated forms of p42/44 MAPK (Figure 1(c)).

*3.4. Effect of Ebosin on Expression of IKKα and IKKβ.* The IKK complex has consisted of two catalytic subunits, IKK$\alpha$ and IKK$\beta$, and a noncatalytic subunit IKK$\gamma$. Activation of IKK complex by TNF-$\alpha$ stimulation requires the phosphorylation of IKK$\alpha/\beta$ in its activation loop and polyubiquitination of IKK$\gamma$ [28]. To expand these studies, we have analyzed the impact of ebosin on the phosphorylation level of IKK$\alpha$ and IKK$\beta$ in response to TNF-$\alpha$. Western blot results showed that 80, 16, and 3.2 $\mu$g/ml ebosin decreased the protein levels of phosphorylated IKK$\alpha$ by 53.85% ($P < 0.01$), 19.90% ($P < 0.05$), and 0.85% separately and IKK$\beta$ by 71.56% ($P < 0.01$), 58.11% ($P < 0.05$), and 40.28% ($P < 0.05$ ), respectively (Figure 2(a)), but not nonphosphorylated IKK$\alpha$ and IKK$\beta$ (Figure 2(a)).

*3.5. Ebosin Suppresses the Production of IκBα.* I$\kappa$Bs is an inhibitory factor of NF-$\kappa$B, and ubiquitination of I$\kappa$Bs leads to release NF-$\kappa$B entering the nucleus and activating transcription of appropriate gene targets [28]. Using western blot, we measured the expression level of TNF-$\alpha$-induced I$\kappa$B$\alpha$ with ebosin in FLS cells. As shown in Figure 2(b), ebosin reduced the expression levels of phosphorylated I$\kappa$B$\alpha$ by 35.27% ($P < 0.05$), 14.99% ($P < 0.05$), and 6.93%, respectively, at dosages 80, 16, and 3.2 $\mu$g/ml, but the levels of nonphosphorylated I$\kappa$B$\alpha$ were enhanced by 55.12% ($P < 0.05$), 45.08% ($P < 0.05$), and 32.78% ($P < 0.05$), respectively, at the same dosages (Figure 2(b)).

*3.6. Ebosin Attenuates NF-κB DNA-Binding Activity.* Once released from its inactive form complexed with I$\kappa$Bs, NF-$\kappa$B is presumably translocated to the nucleus and interacted with specific DNA-binding sequences to regulate gene transcription [29]. To confirm if ebosin can affect the NF-$\kappa$B's activity through interfering with its specific DNA, an electrophoretic mobility shift analysis (EMSA) was performed in FLS cells stimulated by TNF-$\alpha$ and then incubation with varying concentrations of ebosin. Results in Figure 3 showed that ebosin significantly blocked NF-$\kappa$B-DNA binding in a dose-dependent manner.

*3.7. Ebosin Inhibit NF-κB Nuclear Translocation.* For understanding the effect of ebosin on the activity of NF-$\kappa$B, we detected the NF-$\kappa$B protein level in the cytoplasm and nucleus using the NF-$\kappa$B p65 antibody. Western blot analysis showed (Figure 2(c)) that ebosin markedly enhanced the protein level of p65 in the cytoplasm induced with TNF-$\alpha$ by 51.72% ($P < 0.01$), 46.84% ($P < 0.05$), 40.33% ($P < 0.05$), 30.34% ($P < 0.05$), 23.12% ($P < 0.05$), and 14.34%, respectively, at dosages 400, 80, 16, 3.2, 0.64, and 0.128 $\mu$g/ml. However, it decreased the expression of NF-$\kappa$B in the nucleus of cells by 80.11% ($P < 0.001$), 77.02% ($P < 0.001$), 53.77% ($P < 0.001$), 19.25% ($P < 0.05$), 10.07% ($P < 0.05$), and 5.25%, respectively, at same dosages (Figure 2(c)). For further understanding the nuclear events that govern NF-$\kappa$B function by ebosin, immunofluorescence was performed to analyze the translocation of activated NF-$\kappa$B in the

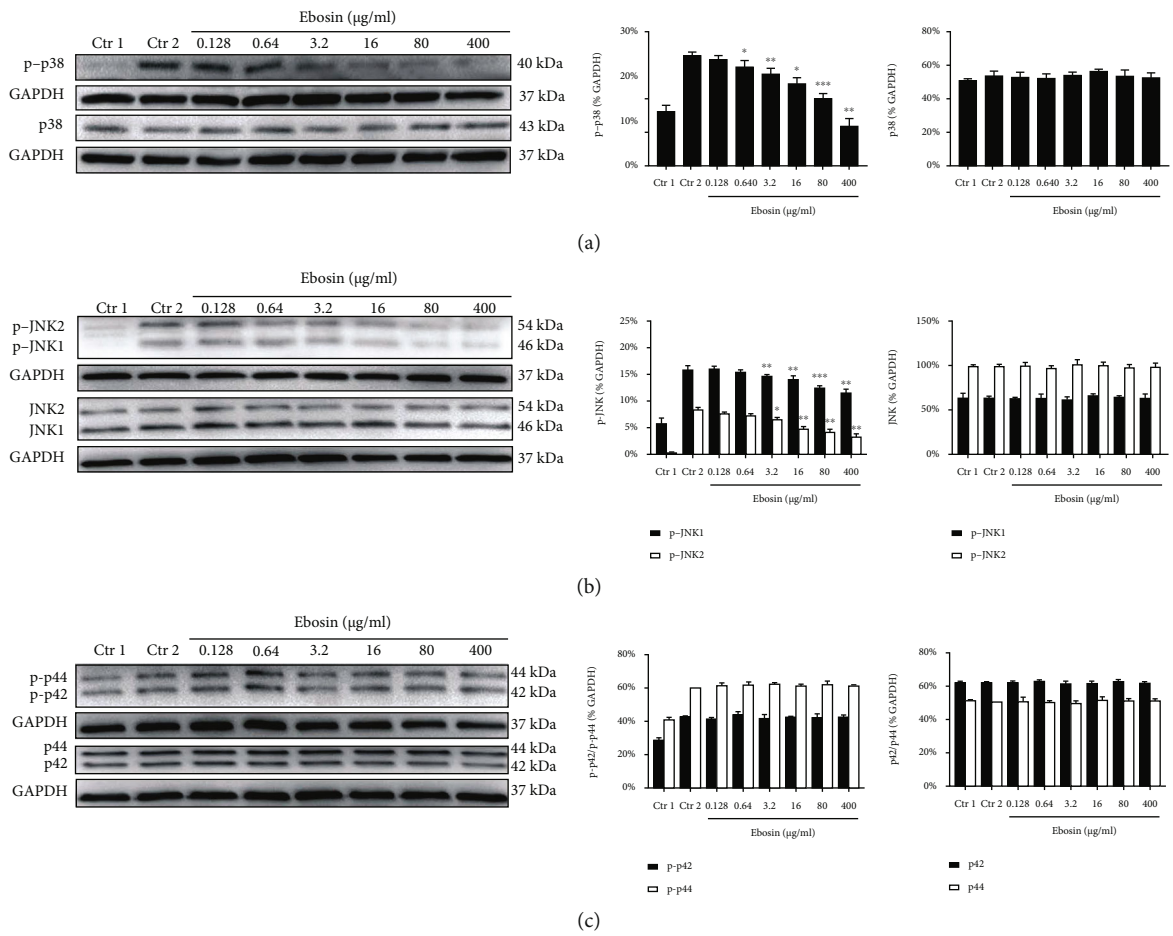


Figure 1: Ebosin inhibits the MAPK signaling pathway mediated by TNF-$\alpha$ in FLS. (a) Effect of ebosin on the phosphorylated and nonphosphorylated p38 MAPK separately. FLS cells ($1 \times 10^5$/ml) were incubated in the presence or absence of ebosin for 12 h then with TNF-$\alpha$ (10 ng/ml) 15 min. The phosphorylated and nonphosphorylated p38 MAPK were analyzed by western blot. (b) Effect of ebosin on the phosphorylated and nonphosphorylated JNK1 and JNK2 MAPK, respectively. The experimental protocol is the same as p38. (c) Effect of ebosin on phosphorylated and nonphosphorylated p42/44 MAPK (ERK1/2). The protocol is also the same as before. All of the data are expressed as the means ± SD from at least 3 independent experiments. $P < 0.001$, $P < 0.01$, and $P < 0.05$ compared to the control 2 (FLS incubated with TNF-$\alpha$).

nucleus (Figure 4) The cells were treated with ebosin at 80 $\mu$g/ml after TNF-$\alpha$ inducing and then incubated with rabbit NF-$\kappa$B p65 antibody. From these results, we observed that the process of NF-$\kappa$B from the cytoplasm into the nucleus was significantly suppressed in FLS by ebosin (Figure 4).

*3.8. Ebosin Reduced the Secretion of MMP1 and MMP3.* The increased level of MMP expression has been associated with destroy collagenous components of cartage in RA [30]. In order to study the therapeutic effects of ebosin, we measured the influence of ebosin on MMP-1 and MMP-3 secretion in TNF-$\alpha$-induced FLS cells by ELISA. As shown in Figure 5 (a), the concentration of MMP-1 in cell-cultured supernatant decreased by 44.16% ($P < 0.01$), 33.63% ($P < 0.05$), and 26.94% ($P < 0.05$), respectively, at dosages of 80, 16, and 3.2 $\mu$g/ml of ebosin, and meanwhile, the productions of MMP-3 in FLS were suppressed by 83.01% ($P < 0.01$), 70.81% ($P < 0.01$), and 32.63% ($P < 0.05$), respectively (Figure 5(b)).

*3.9. Effect of Ebosin on Secretion of Chemokines.* Clinical studies have demonstrated chemokines, produced by FLS cells, promoting inflammation and cartilage destruction in response to TNF-$\alpha$ [31]. In this study, we detect the concentration of TNF-$\alpha$-induced release of chemokines comprising RANTES and IL-8 in FLS treated with ebosin by ELISA. The results showed that ebosin at dosages 80, 16, and 3.2 $\mu$g/ml decreased the production of IL-8 by 68.08% ($P < 0.001$), 57.52% ($P < 0.001$), and 57.28% ($P < 0.001$), respectively (Figure 5(c)), and at the meantime, diminished the expression levels of RANTES by 53.08% ($P < 0.001$), 29.94% ($P < 0.01$), and 19.93% ($P < 0.01$) separately (Figure 5(d)).

## 4. Discussion

In the current study, we demonstrated that ebosin affects the TNF-$\alpha$-induced inflammatory responses in FLS largely due to its intervention in TNF-$\alpha$-induced MAPKs and NF-$\kappa$B pathways (Figure 6).

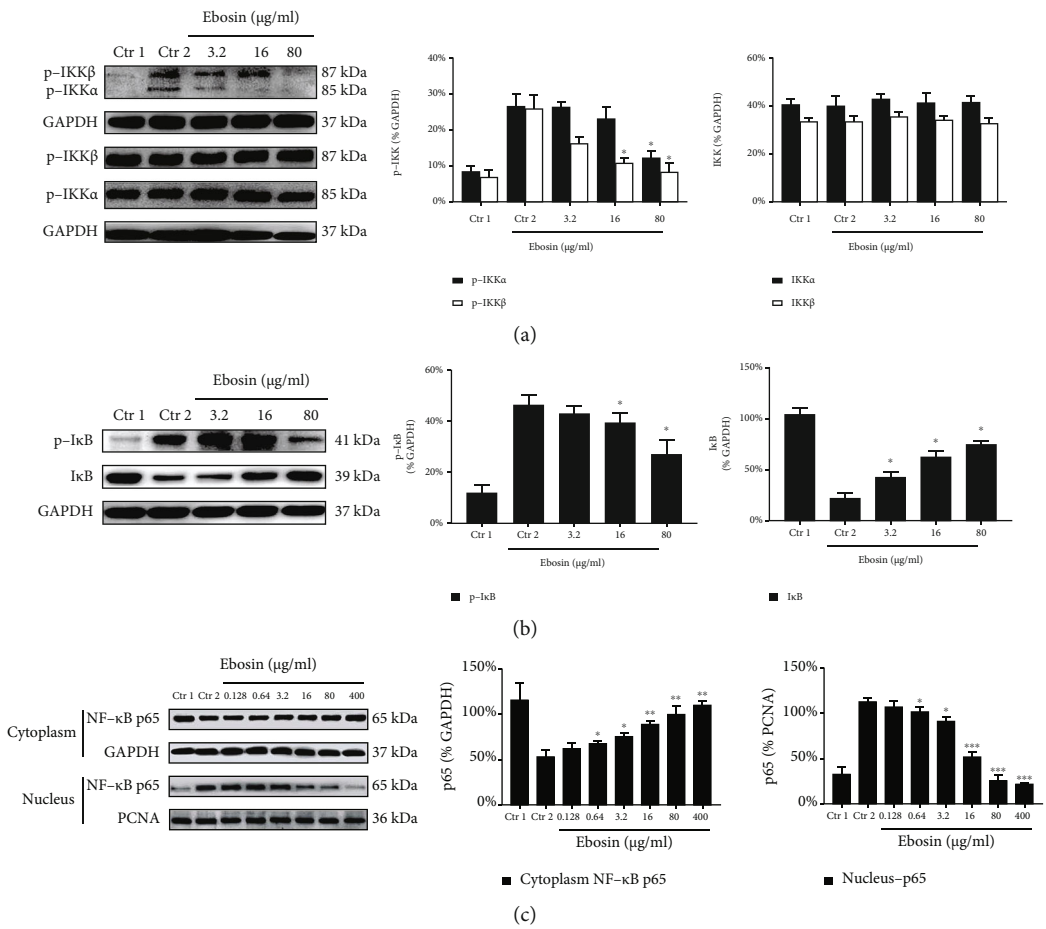


Figure 2: The influences of ebosin on the NF-$\kappa$B signaling pathway mediated by TNF-$\alpha$ in FLS. (a) Effects of ebosin on the expression of phosphorylated and nonphosphorylated IKK$\alpha$ and IKK$\beta$. FLS cells ($1 \times 10^5$/ml) were incubated in the presence or absence of ebosin for 12 h then with TNF-$\alpha$ (10 ng/ml) 3 h. The production of phosphorylated and nonphosphorylated IKK$\alpha$ and IKK$\beta$ was analyzed with western blot. (b) Effects of ebosin on production of phosphorylated I$\kappa$Ba and nonphosphorylated I$\kappa$Ba. The expression levels of phosphorylated and nonphosphorylated I$\kappa$Ba were identified with the same protocols as before. (c) Effect of ebosin on nuclear and cytoplasm NF-$\kappa$B of FLS. The production of nuclear and cytoplasm NF-$\kappa$B was determined by western blot also. All of the data are expressed as the means ± SD from at least 3 independent experiments. $P < 0.001$, $P < 0.01$, and $P < 0.05$ compared to the control 2 (FLS incubated with TNF-$\alpha$) individually for NF-$\kappa$B, IKK$\alpha$, IKK$\beta$, and I$\kappa$Ba.

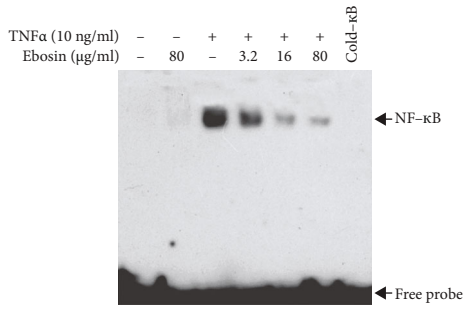


Figure 3: Ebosin inhibits NF-$\kappa$B DNA binding activity in FLS mediated by TNF-$\alpha$. The DNA binding activity in the nuclear extracts of FLS mediated by TNF-$\alpha$ was assessed in an electrophoretic mobility shift assay (EMSA) by a specific probe, an oligonucleotide labeled with biotin. A LightShift Chemiluminescent EMSA Kit was used following the instructions of the manufacturer. Specific binding was controlled by competition with a 50-fold excess of cold $\kappa$B oligonucleotide.

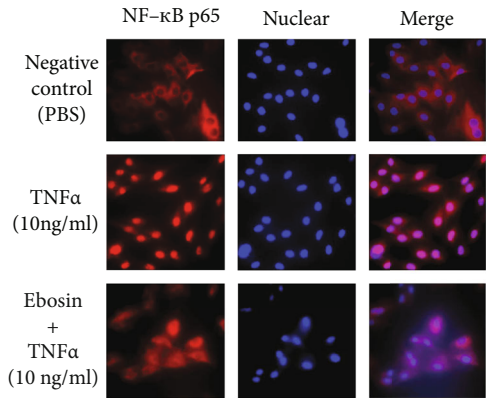


Figure 4: The effect of ebosin on nuclear translocation of NF-$\kappa$B mediated by TNF-$\alpha$ in FLS. Indirect immunofluorescence with the specific anti-NF-$\kappa$B p65 antibody was performed. Using a fluorescence microscope, the cells were counterstained by Hoechst 33528 for nuclear staining.

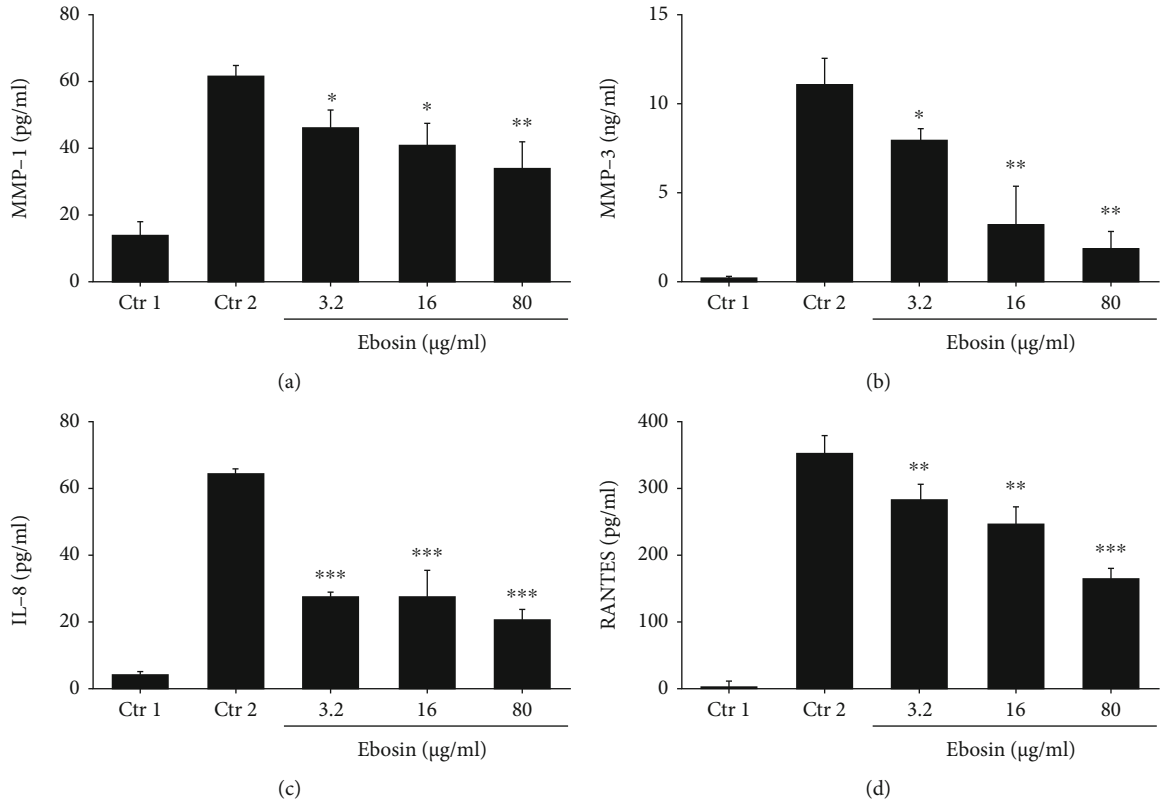


Figure 5: Ebosin suppresses production of MMPs and chemokines mediated by TNF-$\alpha$ in FLS. (a, b) Inhibition of ebosin on production of MMP1 and MMP3. FLS cells ($1 \times 10^6$/ml) were incubated in the presence or absence of ebosin for 12 h then with TNF-$\alpha$ (10 ng/ml) for 24 h. The expression levels of MMP1 and MMP3 were analyzed by ELISA kits individually. (c, d) Influences of ebosin on production of chemokines including RANTES and IL-8. The levels of RANTES and IL-8 were determined also by ELISA kits separately. $P < 0.001$, $P < 0.01$, and $P < 0.05$ compared to the control 2 (FLS incubated with TNF-$\alpha$).

Inflammation, a representative innate immune response and the cause of numerous diseases including cancer and arthritis [32], is characterized by the involvement of a common set of genes and endogenous mediators including growth factors, inflammatory cytokines, chemokines, MMPs, and toxic molecules (nitric oxide or free radicals) [33]. Efforts have been made to elucidate the mechanisms underlying the inflammatory responses to identify novel anti-inflammatory drug targets including the inflammation mediators such as TNF and IL-1 [34]. Several anti-TNF antibodies, including infliximab and adalimumab, have been approved by the FDA for the treatment of RA [20, 23]. However, long-term use of anti-TNF-$\alpha$ agents has also been reported to be closely associated with increasing risk of adverse events like serious infections, malignancies, skin, tuberculosis, and cancer [24]. Different from antibody-based agents, ebosin is a natural product that originates as secondary metabolites from *Streptomyces* sp.139 with efficacy and high safety properties, which may provide a more effective treatment option for RA.

Exopolysaccharides play a crucial role in several biological activities and have also remarkable industrial applications such as biothickeners in foods [35]. Numerous reports suggested that they can confer health benefits including anti-inflammation [36], cholesterol-lowering properties [37], antitumor activity [38], and antidiabetic activity [39]. EPSs isolated from *Trichoderma erinaceum* DG-312 exhibited a strong anti-inflammatory activity in inflamed mice [40]. Nowak et al. reported that EPS derived from *Lactobacillus rhamnosus* can significantly inhibit the production of arthritogenic antibodies, hence suppressing active CIA [41]. Recently, there has been growing interests in microbial EPS due to its broad medical applications in the field of immune regulation and antiviral activity, even against the coronavirus disease 2019 (COVID-19) [36, 42–45].

ERK1/2, JNK, and p38 MAPKs are the three major members of the MAPK family that respond to distinct signaling cascades [46]. The employment of p38 and JNK inhibitors has emerged as an attractive strategy to reduce both proinflammatory cytokine synthesis and its intracellular signaling [47]. Our results in this study showed that ebosin has a remarkably dose-dependent effect on reducing the phosphorylated p38, JNK1, and JNK2 MAPK protein levels in FLS induced by TNF-$\alpha$. More than 50% phosphorylated protein was inhibited by ebosin at high dosage (400 mg/ml) that has no significant influence on the cell viability by cytotoxicity assay as described in our previous study [18]. Meanwhile, our research indicated that ebosin did not affect the expression of p42/44 MAPK (ERK1/2) which plays a key role in cell proliferation, differentiation, and migration [48].

The transcription factor NF-$\kappa$B, which initially exists in the cytoplasm in an inactive complex with I$\kappa$B, is a

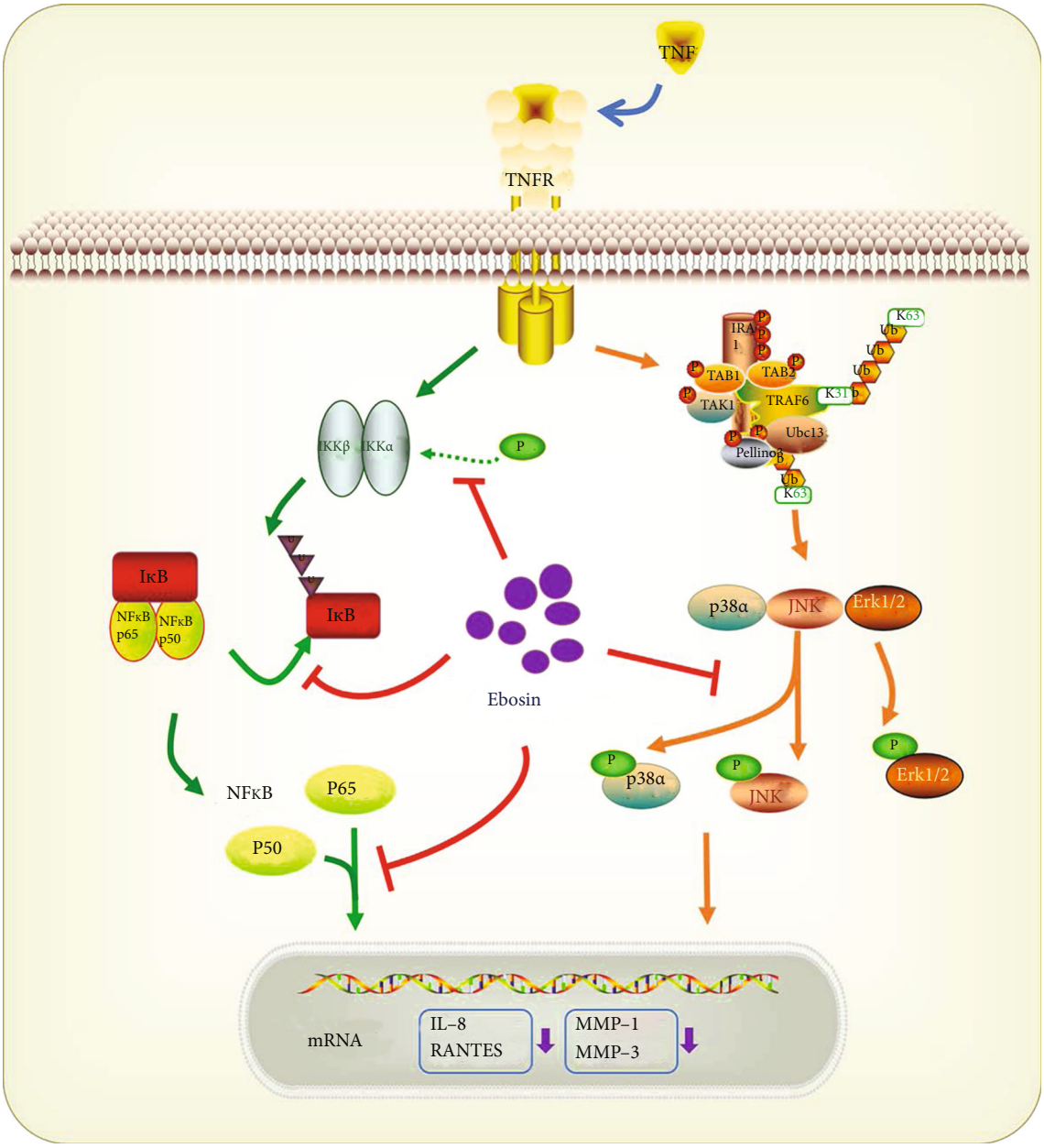


Figure 6: Schematic representation of TNF-$\alpha$-induced activation of MAPK and NF-$\kappa$B signaling pathways modulated by ebosin. The biological effects of TNF-$\alpha$ were attenuated by ebosin on two different pathways. First, phosphorylation of p38 and JNK MAPK was significantly inhibited by ebosin with a dose-dependent manner, which may contribute to reduce the nuclear translocation of p38 and JNK. Secondly, it has been shown ebosin can significantly decrease the phosphorylation level of IKK$\alpha$ and IKK$\beta$. And then, the increased level of I$\kappa$B with a concomitant decrease in the level of p-I$\kappa$B resulted in cytoplasmic retention of NF-$\kappa$B p65 and depression of the DNA binding ability of NF-$\kappa$B in the nucleus. Finally, the expression of MMP-1, MMP-3, interleukin-8, and RANTES which induced by TNF-$\alpha$ was significantly reduced responding to ebosin treatment in FLS cells.

pivotal regulator in the regulation of inflammation and immune responses by eliciting the transcriptional responses following different stimuli such as TNF-$\alpha$ or IL-1$\beta$ [28]. It has been reported that the activation of NF-$\kappa$B appears to precede disease onset, which suggested that inhibition of NF-$\kappa$B by different means may contribute to reduce the severity of disease [49]. In this study, we focused on the capacity of ebosin to counteract the level of NF-$\kappa$B in FLS induced by TNF-$\alpha$. Our results showed decreased levels of phosphorylated IKK$\alpha$ and IKK$\beta$ after treating with ebosin. Besides, ebosin was capable of downregulating the levels of phosphorylated I$\kappa$B$\alpha$. EMSA indicated that ebosin decreased the DNA-binding activity of NF-$\kappa$B in the nucleus, probably through affecting the phosphorylation of NF-$\kappa$B itself. Furthermore, we also demonstrated that ebosin can significantly inhibit the NF-$\kappa$B nuclear translocation process using western blot analysis and fluorescence microscopy. All of the results

mentioned above suggest that ebosin is an inhibitor of the NF-$\kappa$B-driven signaling pathway, which may be responsible for its anti-inflammatory effects *in vivo* [18].

MMP-1 and MMP-3, as targets of NF-$\kappa$B and major collagenolytic enzymes involved in tissue destruction, have been reported to be significantly elevated in the synovial fluid of RA patients [50]. In addition to MMPs, FLS produces chemokines into synovial tissue upon stimulation by proinflammatory cytokines that further enhance inflammation, hyperplasia, and cartilage destruction [51]. As a member of the CC subfamily of chemokines, RANTES is involved in the pathogenesis of RA by promoting leukocyte infiltration [52]. Another important chemokine, IL-8 has been reported to be strongly associated with leukocyte accumulation and inflammation in RA. In the current study, ELISA analysis demonstrated that MMP-1, MMP-3, RANTES, and IL-8 levels were suppressed by ebosin in FLS induced with TNF-$\alpha$. These results suggested that inhibition of ebosin on NF-$\kappa$B activation contributes to reduce the secretion of MMPs and chemokines, thereby protecting RA patients from joint destruction.

In conclusion, this study has demonstrated that ebosin is capable of inhibiting the inflammatory responses induced by TNF-$\alpha$ in isolated FLS, acting as an effective *in vitro* inhibitor of the MAPKs and NF-$\kappa$B signaling pathways (Figure 6). It is assumed that the anti-inflammatory activity of ebosin is at least partially due to inhibition of these pathways. Therefore, ebosin may be developed as a potential candidate for the treatment of RA. Additional investigations to identify its clinical usefulness should be explored.

## Abbreviations

| | |
|---|---|
| CIA: | Collagen-induced arthritis |
| FLS: | Fibroblast-like synoviocytes |
| MTT: | 3-(4,5-Dimethylthiazol-2-yl)-2,5-diphenyltetrazolium bromide |
| IL-1$\beta$: | Interleukin-1$\beta$ |
| TNF-$\alpha$: | Tumor necrosis factor-$\alpha$ |
| MAPK: | Mitogen-activated protein kinase |
| IKK: | I$\kappa$B kinase |
| NF-$\kappa$B: | Nuclear factor-kappa B |
| p38: | p38 mitogen-activated protein kinase |
| JNK: | Jun N-terminal kinase |
| ELISA: | Enzyme-linked immunosorbent assay |
| EMSA: | Electrophoretic mobility shift assay |
| MMP: | Matrix metalloproteinase |
| RANTES: | Reduced upon activation normal T expression and secreted |
| IL-8: | Interleukin-8 |
| TRAF2: | TNF receptor-associated factor2 |
| RIP: | Receptor interacting protein |
| DMEM: | Dulbecco's modified Eagle's medium |
| DMSO: | Dimethyl sulfoxide |
| RIPA: | Radio immunoprecipitation assay |
| HRP: | Horseradish peroxidase |
| PVDF: | Polyvinylidene fluoride |
| EDTA: | Ethylene diamino tetraacetic acid |
| PBS: | Phosphate-buffered saline |
| BCA: | Bicinchoninic acid. |

## Data Availability

The original data used to support the findings of this study are included within the article.

## Conflicts of Interest

All authors declare no conflict of interest.

## Authors' Contributions

Yang Zhang and Lifei Wang contributed equally to this work.

## Acknowledgments

This research was supported by grants from the National Natural Science Foundation of China (NSFC 30530830 and 82070627), the National Key Project of New Drug Study of China (2012ZX09301002-001-023-02), the Beijing Municipal Institute of Public Medical Research Development and Reform Pilot Project (2021-10), the Research Fund of Beijing Institute of Hepatology (Y-2021-6), and the Open Project of NHC Key Laboratory of Biotechnology of Antibiotics (NHC-KLBA201903).

## References

[1] D. I. Jang, A. H. Lee, H. Y. Shin et al., "The role of tumor necrosis factor alpha (TNF-$\alpha$) in autoimmune disease and current TNF-$\alpha$ inhibitors in therapeutics," *International Journal of Molecular Sciences*, vol. 22, no. 5, p. 2719, 2021.

[2] J. Holbrook, S. Lara-Reyna, H. Jarosz-Griffiths, and M. McDermott, "Tumour necrosis factor signalling in health and disease," *F1000Res*, vol. 8, 2019.

[3] P. C. Taylor and M. Feldmann, "Anti-TNF biologic agents: still the therapy of choice for rheumatoid arthritis," *Nature Reviews Rheumatology*, vol. 5, no. 10, pp. 578–582, 2009.

[4] J. Alam, I. Jantan, and S. N. A. Bukhari, "Rheumatoid arthritis: recent advances on its etiology, role of cytokines and pharmacotherapy," *Biomedicine & Pharmacotherapy*, vol. 92, pp. 615–633, 2017.

[5] M. Noack and P. Miossec, "Selected cytokine pathways in rheumatoid arthritis," *Seminars in Immunopathology*, vol. 39, no. 4, pp. 365–383, 2017.

[6] E. Jimi, N. Takakura, F. Hiura, I. Nakamura, and S. Hirata-Tsuchiya, "The role of NF-$\kappa$B in physiological bone development and inflammatory bone diseases: is NF-$\kappa$B inhibition "killing two birds with one stone"?," *Cell*, vol. 8, no. 12, p. 1636, 2019.

[7] Y. Shen, L. Teng, Y. Qu et al., "Anti-proliferation and anti-inflammation effects of corilagin in rheumatoid arthritis by downregulating NF-kappaB and MAPK signaling pathways," *Journal of Ethnopharmacology*, vol. 284, article 114791, 2022.

[8] Q. Fang, C. Zhou, and K. S. Nandakumar, "Molecular and cellular pathways contributing to joint damage in rheumatoid arthritis," *Mediators of Inflammation*, vol. 2020, Article ID 3830212, 20 pages, 2020.

[9] G. Zhang, B. Liu, Z. Zeng, Q. Chen, Y. Feng, and X. Ning, "Oxymatrine hydrazone (OMTH) synthesis and its protective effect for rheumatoid arthritis through downregulation of

MEK/NF-κB pathway," *Environmental Toxicology*, vol. 36, no. 12, pp. 2448–2453, 2021.

[10] N. Akhter, A. Wilson, R. Thomas et al., "ROS/TNF-α crosstalk triggers the expression of IL-8 and MCP-1 in human monocytic THP-1 cells via the NF-κB and ERK1/2 mediated signaling," *International Journal of Molecular Sciences*, vol. 22, no. 19, p. 10519, 2021.

[11] Z. Yu, Y. Wang, Y. Li et al., "Effect of moxibustion on the serum levels of MMP-1, MMP-3, and VEGF in patients with rheumatoid arthritis," *Evidence-based Complementary and Alternative Medicine*, vol. 2020, Article ID 7150605, 2020.

[12] X. Tong, H. Zeng, P. Gu, K. Wang, H. Zhang, and X. Lin, "Monocyte chemoattractant protein-1 promotes the proliferation, migration and differentiation potential of fibroblast-like synoviocytes via the PI3K/P38 cellular signaling pathway," *Molecular Medicine Reports*, vol. 21, no. 3, pp. 1623–1632, 2020.

[13] S. Sindhu, S. Kochumon, S. Shenouda, A. Wilson, F. Al-Mulla, and R. Ahmad, "The cooperative induction of CCL4 in human monocytic cells by TNF-α and palmitate requires MyD88 and involves MAPK/NF-κB signaling pathways," *International Journal of Molecular Sciences*, vol. 20, no. 18, p. 4658, 2019.

[14] P. Cai, T. Jiang, B. Li et al., "Comparison of rheumatoid arthritis (RA) and osteoarthritis (OA) based on microarray profiles of human joint fibroblast-like synoviocytes," *Cell Biochemistry and Function*, vol. 37, no. 1, pp. 31–41, 2019.

[15] W. Sun, N. Meednu, A. Rosenberg et al., "B cells inhibit bone formation in rheumatoid arthritis by suppressing osteoblast differentiation," *Nature Communications*, vol. 9, no. 1, p. 5127, 2018.

[16] P. S. Burrage, K. S. Mix, and C. E. Brinckerhoff, "Matrix metalloproteinases: role in arthritis," *Frontiers in Bioscience*, vol. 11, no. 1, pp. 529–543, 2006.

[17] H. Okamoto, T. P. Cujec, H. Yamanaka, and N. Kamatani, "Molecular aspects of rheumatoid arthritis: role of transcription factors," *The FEBS Journal*, vol. 275, no. 18, pp. 4463–4470, 2008.

[18] Y. Zhang, L. F. Wang, J. Y. Bai et al., "Anti-inflammatory effect of ebosin on rat collagen-induced arthritis through suppressing production of interleukin-1β, interleukin-6 and tumor necrosis factor-α," *Journal of Inflammation*, vol. 11, no. 3, pp. 697–708, 2013.

[19] C. Jing, W. Jianbo, L. Yuan, J. Rong, and L. Baoyi, "A new IL-1 receptor inhibitor 139A: fermentation, isolation, physicochemical properties and structure," *Journal of Antibiotics (Tokyo)*, vol. 56, no. 2, pp. 87–90, 2003.

[20] M. Pap, I. Sapina, N. Laktasic Zerjavic et al., "Anti-TNF therapy and the risk of malignancies and infections in inflammatory rheumatic diseases- our experience," *Psychiatria Danubina*, vol. 33, Suppl 4, pp. 625–631, 2021.

[21] S. Zhao, E. Mysler, and R. J. Moots, "Etanercept for the treatment of rheumatoid arthritis," *Immunotherapy*, vol. 10, no. 6, pp. 433–445, 2018.

[22] S. Bek, A. B. Bojesen, J. V. Nielsen et al., "Systematic review and meta-analysis: pharmacogenetics of anti-TNF treatment response in rheumatoid arthritis," *The Pharmacogenomics Journal*, vol. 17, no. 5, pp. 403–411, 2017.

[23] P. A. van Schouwenburg, T. Rispens, and G. J. Wolbink, "Immunogenicity of anti-TNF biologic therapies for rheumatoid arthritis," *Nature Reviews Rheumatology*, vol. 9, no. 3, pp. 164–172, 2013.

[24] J. Li, Z. Zhang, X. Wu, J. Zhou, D. Meng, and P. Zhu, "Risk of adverse events after anti-TNF treatment for inflammatory rheumatological disease. A meta-analysis," *Frontiers in Pharmacology*, vol. 12, article 746396, 2021.

[25] Y. Zhang, L. Wang, L. Bai et al., "Effect of ebosin on modulating interleukin-1β-induced inflammatory responses in rat fibroblast-like synoviocytes," *Cellular & Molecular Immunology*, vol. 13, no. 5, pp. 584–592, 2016.

[26] M. M. Bradford, "A rapid and sensitive method for the quantitation of microgram quantities of protein utilizing the principle of protein-dye binding," *Analytical Biochemistry*, vol. 72, no. 1-2, pp. 248–254, 1976.

[27] G. Sabio and R. J. Davis, "TNF and MAP kinase signalling pathways," *Seminars in Immunology*, vol. 26, no. 3, pp. 237–245, 2014.

[28] S. Mitchell, J. Vargas, and A. Hoffmann, "Signaling via theNFκBsystem," *Wiley Interdisciplinary Reviews. Systems Biology and Medicine*, vol. 8, no. 3, pp. 227–241, 2016.

[29] M. S. Hayden and S. Ghosh, "Regulation of NF-κB by TNF family cytokines," *Seminars in Immunology*, vol. 26, no. 3, pp. 253–266, 2014.

[30] F. Javed, H. B. Ahmed, T. Mikami, K. Almas, G. E. Romanos, and K. Al-Hezaimi, "Cytokine profile in the gingival crevicular fluid of rheumatoid arthritis patients with chronic periodontitis," *Journal of Investigative and Clinical Dentistry*, vol. 5, no. 1, pp. 1–8, 2014.

[31] S. E. Sweeney and G. S. Firestein, "Rheumatoid arthritis: regulation of synovial inflammation," *The International Journal of Biochemistry & Cell Biology*, vol. 36, no. 3, pp. 372–378, 2004.

[32] I. M. Rea, D. S. Gibson, V. McGilligan, S. E. McNerlan, H. D. Alexander, and O. A. Ross, "Age and age-related diseases: role of inflammation triggers and cytokines," *Frontiers in Immunology*, vol. 9, p. 586, 2018.

[33] K. D. Deane, M. K. Demoruelle, L. B. Kelmenson, K. A. Kuhn, J. M. Norris, and V. M. Holers, "Genetic and environmental risk factors for rheumatoid arthritis," *Best Practice & Research. Clinical Rheumatology*, vol. 31, no. 1, pp. 3–18, 2017.

[34] Z. Chen, A. Bozec, A. Ramming, and G. Schett, "Anti-inflammatory and immune-regulatory cytokines in rheumatoid arthritis," *Nature Reviews Rheumatology*, vol. 15, no. 1, pp. 9–17, 2019.

[35] I. C. Boels, M. Kleerebezem, and W. M. de Vos, "Engineering of carbon distribution between glycolysis and sugar nucleotide biosynthesis in Lactococcus lactis," *Applied and Environmental Microbiology*, vol. 69, no. 2, pp. 1129–1135, 2003.

[36] L. Q. Li, A. X. Song, J. Y. Yin, K. C. Siu, W. T. Wong, and J. Y. Wu, "Anti-inflammation activity of exopolysaccharides produced by a medicinal fungus Cordyceps sinensis Cs-HK1 in cell and animal models," *International Journal of Biological Macromolecules*, vol. 149, pp. 1042–1050, 2020.

[37] E. Korcz, Z. Kerenyi, and L. Varga, "Dietary fibers, prebiotics, and exopolysaccharides produced by lactic acid bacteria: potential health benefits with special regard to cholesterol-lowering effects," *Food & Function*, vol. 9, no. 6, pp. 3057–3068, 2018.

[38] J. Angelin and M. Kavitha, "Exopolysaccharides from probiotic bacteria and their health potential," *International Journal of Biological Macromolecules*, vol. 162, pp. 853–865, 2020.

[39] M. Jin, Z. Lu, M. Huang, Y. Wang, and Y. Wang, "Effects of Se-enriched polysaccharides produced by _Enterobacter cloacae_ Z0206 on alloxan-induced diabetic mice," *International*

*Journal of Biological Macromolecules*, vol. 50, no. 2, pp. 348–352, 2012.

[40] J. H. Joo and J. W. Yun, "Structure and molecular characterization of extracellular polysaccharides produced by Trichoderma erinaceum DG-312," *Journal of Microbiology and Biotechnology*, vol. 15, pp. 1250–1257, 2005.

[41] B. Nowak, M. Ciszek-Lenda, M. Srottek et al., "Lactobacillus rhamnosus exopolysaccharide ameliorates arthritis induced by the systemic injection of collagen and lipopolysaccharide in DBA/1 mice," *Archivum Immunologiae et Therapiae Experimentalis (Warsz)*, vol. 60, no. 3, pp. 211–220, 2012.

[42] M. Andrew and G. Jayaraman, "Marine sulfated polysaccharides as potential antiviral drug candidates to treat corona virus disease (COVID-19)," *Carbohydrate Research*, vol. 505, article 108326, 2021.

[43] L. Xiao, X. Ge, L. Yang et al., "Anticancer potential of an exopolysaccharide fromLactobacillus helveticusMB2-1 on human colon cancer HT-29 cellsviaapoptosis induction," *Food & Function*, vol. 11, no. 11, pp. 10170–10181, 2020.

[44] O. Y. A. Costa, J. M. Raaijmakers, and E. E. Kuramae, "Microbial extracellular polymeric substances: ecological function and impact on soil aggregation," *Frontiers in Microbiology*, vol. 9, p. 1636, 2018.

[45] M. Moscovici, "Present and future medical applications of microbial exopolysaccharides," *Frontiers in Microbiology*, vol. 6, p. 1012, 2015.

[46] K. Flores, S. S. Yadav, A. A. Katz, and R. Seger, "The nuclear translocation of mitogen-activated protein kinases: molecular mechanisms and use as novel therapeutic target," *Neuroendocrinology*, vol. 108, no. 2, pp. 121–1231, 2019.

[47] E. K. Kim and E. J. Choi, "Pathological roles of MAPK signaling pathways in human diseases," *Biochimica et Biophysica Acta*, vol. 1802, no. 4, pp. 396–405, 2010.

[48] M. Beloueche-Babari, L. E. Jackson, N. M. Al-Saffar, P. Workman, M. O. Leach, and S. M. Ronen, "Magnetic resonance spectroscopy monitoring of mitogen-activated protein kinase signaling inhibition," *Cancer Research*, vol. 65, no. 8, pp. 3356–3363, 2005.

[49] J. C. Keith Jr., L. M. Albert, Y. Leathurby et al., "The utility of pathway selective estrogen receptor ligands that inhibit nuclear factor-kappa B transcriptional activity in models of rheumatoid arthritis," *Arthritis Research & Therapy*, vol. 7, no. 3, pp. R427–R438, 2005.

[50] C. J. Malemud, "Matrix metalloproteinases and synovial joint pathology," *Progress in Molecular Biology and Translational Science*, vol. 148, pp. 305–325, 2017.

[51] B. Bartok and G. S. Firestein, "Fibroblast-like synoviocytes: key effector cells in rheumatoid arthritis," *Immunological Reviews*, vol. 233, no. 1, pp. 233–255, 2010.

[52] D. Wen, X. Du, Y. Qiao, J. Z. Dong, and C. S. Ma, "RANTES gene polymorphisms are not associated with rheumatoid arthritis and atopic dermatitis: a meta-analysis," *International Reviews of Immunology*, vol. 34, no. 6, pp. 500–508, 2015.

Hindawi
Journal of Immunology Research
Volume 2021, Article ID 4084566, 17 pages
https://doi.org/10.1155/2021/4084566

*Research Article*

# Mangiferin Ameliorates HFD-Induced NAFLD through Regulation of the AMPK and NLRP3 Inflammasome Signal Pathways

**Zhang Yong,[1] Wang Ruiqi,[2] Yao Hongji,[1] Ma Ning,[3] Jiang Chenzuo,[1] Zhou Yu,[1] Xia Zhixuan,[1] Liu Qiang,[1] Liu Qibing,[1] Lu Weiying,[3] and Zhang Xiaopo[2]**

[1]*Department of Pharmacology, Hainan Medical University, Haikou, Hainan 571199, China*
[2]*Key Laboratory of Tropical Translational Medicine of the Ministry of Education, Hainan Key Laboratory for Research and Development of Tropical Herbs, School of Pharmacy, Hainan Medical University, Haikou 571199, China*
[3]*Reproductive Medical Center, Hainan Women and Children's Medical Center, Haikou 570206, China*

Correspondence should be addressed to Lu Weiying; 2490206511@qq.com and Zhang Xiaopo; z_xp1412@163.com

Received 7 July 2021; Revised 28 August 2021; Accepted 11 October 2021; Published 25 October 2021

Academic Editor: Meng-Hao Huang



Nonalcoholic fatty liver disease (NAFLD) is closely related to glycolipid metabolism and liver inflammation. And there is no effective drug approved for its clinical therapy. In this study, we focused on mangiferin (Man) and explored its effects and mechanisms on NAFLD treatment based on the regulation of glycolipid metabolism and anti-inflammatory *in vivo* and *in vitro*. The results exhibited that Man can significantly attenuate liver injury, insulin resistance, and glucose tolerance in high-fat diet- (HFD-) induced NAFLD mice and significantly reduce fat accumulation and inflammation in hepatic tissue of NAFLD mice. The transcriptome level RNA-seq analysis showed that the significantly different expression genes between the Man treatment group and the HFD-induced NAFLD model group were mainly related to regulation of energy, metabolism, and inflammation in liver tissue. Furthermore, western blots, real-time PCR, and immunohistochemistry experiments confirmed that Man significantly activated the AMPK signal pathway and inhibited NLRP3 inflammasome activation and pyroptosis in NAFLD mice. In *in vitro* cell experiments, we further confirmed that Man can promote glucose consumption and reduce intracellular triglyceride (TG) accumulation induced by free fatty acids in HepG2 cells and further that it can be blocked by AMPK-specific inhibitors. Western blot results showed that Man upregulated p-AMPK$\alpha$ levels and exhibited a significant AMPK activation effect, which was blocked by compound C. At the same time, Man downregulated the expression of NLRP3 inflammasome-related proteins and inhibited the activation of NLRP3 inflammasome, alleviating cell pyroptosis and inflammation effects. These results indicate that Man anti-NAFLD activity is mediated through its regulation of glucolipid metabolism by AMPK activation and its anti-inflammatory effects by NLRP3 inflammasome inhibition. Our study indicates that Man is a promising prodrug for the therapy of NAFLD patients.

## 1. Introduction

As we know, excessive lipid accumulation and steatosis in hepatocytes are the two main characters for nonalcoholic fatty liver disease (NAFLD) patient [1]. NAFLD, as the most commonly liver-related disease, includes simple fatty liver, steatohepatitis, fibrosis, cirrhosis, and even hepatocellular carcinoma [2], which also causes a huge human health challenge and global medical burden [3]. In recent years, with continuous exploration and scientific improvement, the proposed pathogenesis of NAFLD has developed from the "two hit" theory to the "multiple parallel hits" hypothesis, which includes factors such as fat accumulation, lipotoxicity, oxidative stress, inflammation, insulin resistance, endoplasmic reticulum stress, and mitochondrial dysfunction [4–6]. Liver glucose and lipid metabolic disorder and inflammation are the most common initial predisposing factors for NAFLD development [7]. However, the exact pathogenesis is still

not fully elucidated, and no effective drug has been given a licence by the FDA to NAFLD treatment in clinical settings. Discovering and investigating effective therapeutic drugs for NAFLD is an urgent problem worldwide.

Glucose and lipid metabolic disorder in hepatocytes is considered to be one of the major NAFLD development risk factors and continually influences the progression of NAFLD. Regulating hepatocyte glucose and lipid metabolism can promote the prevention and treatment of NAFLD [8]. Many enzymes involved in glycolipid metabolism regulation [9]. AMP-activated protein kinase (AMPK), as a cell energy sensor, is one of the key regulatory enzymes for cellular glycolipid metabolism [10]. The metabolic effects of AMPK activation, such as the promotion of glucose consumption, glucose uptake and fatty acid oxidation, inhibition of lipid synthesis and glucose output, and especially its aptitude to arouse a change from fat synthesis to fat oxidation, would be expected to benefit patient with NAFLD, obesity, and type 2 diabetes [10–13]. Targeting AMPK activation is an effective strategy in the exploration of NAFLD treatment based on its regulatory effects on glucose and lipid metabolism.

Inflammation is another key risk factor for NAFLD, especially inflammation caused by lipotoxicity [14, 15]. NLRP3 is the most extensively studied Nod-like receptor associated with inflammation, which forms an inflammasome with its adaptor proteins, and can be activated by many danger factors from surroundings in hepatocyte, including lipotoxicity [14], mitochondrial reactive oxygen species (ROS) [16], and potassium efflux [17]. With activation of NLRP3 inflammasome by danger signals, the caspase-1 is activated and further processes the proinflammatory cytokines interleukin-1$\beta$ (pro-IL-1$\beta$) and pro-IL-18 and causes the release of mature inflammatory cytokines [16]. Activated caspase-1 also cleaves gasdermin D (GSDMD) to remove autoinhibition of its N-terminal domain (GSDMD-N) [18]. The GSDMD-N further triggers pyroptosis and promotes secretion of IL-1$\beta$ and IL-18 and then causes an inflammatory cascade [18]. The NLRP3 inflammasome and its associated pyroptosis have been proved to play a vital role in NAFLD development in animal models, especially steatohepatitis [19–21]. Suppression of inflammation by inhibiting the NLRP3 inflammasome and pyroptosis is one potential effective therapeutic strategy for NAFLD.

Mangiferin (C2-$\beta$-D-glycopyranosyl-1,3,6,7-tetrahydroxyxanthone; Man) is a naturally occurring carbon glycoside molecule and is particularly abundant in the leaves of mango, a tropical medicinal plant. Man has a rich biological activity in animal models, such as antioxidative [22], anti-inflammatory [23], anticancer [24], and antidiabetic [25] activity. In addition, a double-blind randomized controlled clinical trial showed that Man significantly reduced triglyceride (TG) and free fatty acid (FFA) levels in serum and improved lipid levels in overweight hyperlipidemia patients [26]. These results suggest that Man is a potential treatment for NAFLD. One recent research has suggested that GSDMD can promote inflammation and pyroptosis in hepatocytes and accelerate the development of NAFLD [27]. Thus, studies on Man could provide new insights for the prevention and treatment of NAFLD. In this study, we study on the effects of Man in the prevention and treatment of NAFLD and explore its mechanisms of glycolipid metabolism regulation and its anti-inflammatory activity based on the AMPK and NLRP3 inflammasome signal pathways.

## 2. Materials and Methods

*2.1. Animal Experiments.* The male C57BL/6J mice, 5 weeks old, were purchased from Vital River Laboratory Animal Technology Co., Ltd. (Beijing, China). Animal experiments were performed at the Animal Research Center of Hainan Medical University under the National Institutes of Health regulations. Our protocols were ratified by the medical ethics committee of Hainan Medical University. The mice were housed at the Animal Research Center of Hainan Medical College under typical environmental surroundings at 25 ± 0.5°C and 12 h light-dark cycle with ad libitum access to standard laboratory water and food.

All mice were randomly divided into 5 groups ($n = 8$ per group): in the normal group, mice were kept with basal diet; in the NAFLD model group, mice were kept with high-fat diet (HFD); in the Man-L group, mice were kept with HFD and administered 25 mg/kg/d Man, i.g.; in the Man-M group, mice were kept with HFD and administered 50 mg/kg/d Man, i.g.; and in the Man-H group, mice were kept with HFD and administered 100 mg/kg/d Man, i.g. The normal group and NAFLD model group mice were administered equal volumes of saline solution. The body weight and blood-glucose concentration after overnight fasting were tested once a week in all animals. After a 12-week treatment, all mice had an absolute diet for 8 h and had taken the whole blood samples from the orbits. Then, the serum samples were got from whole blood for further assay. After blood samples were taken, animals were euthanized with $CO_2$ and tissue samples were taken for further analysis.

*2.2. Oral Glucose Tolerance Test (OGTT) and Insulin Tolerance Test (ITT).* At the last treatment week, the OGTT and ITT were performed, respectively, as follows: (1) OGTT: after fasting overnight, the blood glucose levels were detected and defined as the 0 min time point blood glucose. 2 g/kg of glucose was given orally to all mice, and the concentration of blood glucose was detected at 30, 60, 120, and 180 min time points. (2) ITT: the blood glucose detected after 6 h of fasting, which was defined as the 0 min time point blood glucose. 0.5 U/kg of insulin was then administered by intraperitoneal injection to all mice, and the concentration of blood glucose was detected at 15, 30, 60, and 120 min time points after administration. The blood glucose levels were detected by glucose meter (Roche, ACCU-CHEK) for all glucose tests in this study.

*2.3. Biochemical Analysis.* The levels of serum TG, total cholesterol (TC), low-density lipoprotein cholesterol (LDL-c), high-density lipoprotein cholesterol (HDL-c), alanine aminotransferase (ALT), and aspartate aminotransferase (AST) were tested by appropriate kits from Beijing Strong

Biotechnologies, Inc. The serum IL-1$\beta$ level was assayed by IL-1$\beta$ ELISA kit (Beyotime Biotechnology, Nanjing, China).

*2.4. Liver Histopathological Examination.* A section of liver tissue from each mouse was excised from the same part of liver and fixed in 10% formalin for 48 h. The samples were then gone through paraffin embedding, histological section (4 $\mu$m), and hematoxylin and eosin (H&E) staining, taken pictures under a light microscope. Pathological liver changes were evaluated and scored by steatosis with 5 grades as follows: zero score is less than 5% of parenchyma involved, one score is between 5% and 25%, two score is between 25% and 50%, three score is between 50% and 75%, and 4 score is over 75%.

*2.5. RNA-Seq Assay.* Four mouse livers were isolated from the model group and the Man-H treatment group, respectively, after the experiment has finished. Total RNA from each mouse liver was extracted and its integrity was assessed. The RNA was then subjected to cDNA library construction, further evaluated the quality of cDNA library by the Agilent Bioanalyzer 2100 system. The clustering of the index-coded samples was performed on a cBot Cluster Generation System using TruSeq PE Cluster Kit v3-cBot-HS (Illumina) according to the manufacturer's instructions. After cluster generation, the library preparations were sequenced on an Illumina Novaseq platform and 150 bp paired-end reads were generated. Pearson correlations were performed between samples. The difference gene, Gene Ontology (GO), and Kyoto Encyclopedia of Genes and Genomes (KEGG) assays were performed for the RNA-seq results.

*2.6. Immunohistochemical Assay.* In brief, immunohistochemical assays were conducted on 4 $\mu$m liver sections after rehydration and antigen retrieval. The sections were first incubated with blocking buffer, then exposed to the primary antibody at 4°C for 12 h, followed by TBS washing 3 times and incubation with a properly diluted secondary antibody for 1–2 h at 25°C. Sections were washed with TBS 3 times and stained with diaminobenzidine substrate solution peroxidase substrate kit (Beyotime Biotechnology, Nanjing, China). All immunohistochemical analyses were repeated at least 3 times, and representative images were captured and presented.

*2.7. Cell Culture and Treatment.* HepG2 cells were cultured with Dulbecco's modified Eagle medium containing 10% fetal bovine serum (FBS) and appropriate antibiotics at 37°C in a cellular incubator with 5% $CO_2$. Man (Biopurify Phytochemicals Ltd., lot number B20837, purity ≥ 99%) and metformin (Met) (Shanghai Yuanye Bio-Technology Co., Ltd., lot number 20191008, purity ≥ 98%) were all dissolved in dimethylsulfoxide (DMSO). Met was used as the positive control for cellular experiments. The cells were seeded into cell culture plates (96/24/6-well) and cultured for approximately 24 h. Study drugs were added after overnight starvation in 0.5% FBS-containing medium.

*2.8. Cytotoxicity Assay.* The cell viability was evaluated by the MTT method. First, the HepG2 cells were seeded into 96-well plates at $2.0 \times 10^4$ cells per well. After 24 h of incubation and 8 h of serum starvation, Man was added at the specified concentration treatment for 24 h and each treatment with 5 replicates. Control treatment wells were added DMSO as equal concentration of 400 $\mu$M of Man treatment wells. Then, the media supernatants were discarded and cells were added with 50 $\mu$l MTT solution, incubated it at 37°C for 4 h. The OD values at 490 nm were read at a microplate reader for formazan level detection. Results were exhibited as percentages of controls wells, normalized to 100.

*2.9. Glucose Consumption Assay.* The HepG2 Cells cultured and seeded as above description. The cells were treated with DMSO, Man, or Met at the indicated concentrations for 24 h with 5 replicates. The glucose level of cellular culture supernatant was tested by the Randox glucose assay kit (Beijing Strong Biotechnologies, Inc.). The base glucose consumption of each compound treatment was calculated as glucose level of the fresh medium minus the cultured medium glucose level.

*2.10. Intracellular Triglyceride Assay.* The palmitic acid (PA) coupled with bovine serum albumin (BSA) method was described previously [28]. First, the fatty acid-free BSA was added to DMEM medium to achieve a 10% BSA solution. The PA powder then was added to 10% BSA solution to get a 7.5 mM solution of PA coupled with BSA (PA-BSA). The HepG2 cells were cultured and seeded as above description. After starving overnight, PA-BSA was added to wells at 300 $\mu$M concentration. The 10% BSA solution treatment was used as a control and performed at the same time. After 24 h incubation, PA-BSA, DMSO, Man, and Met at the indicated concentration were then added to wells for another 24 h incubation. The levels of intracellular TG were detected by tissue TG assay kit (Applygen Technologies Inc.) and normalized to sample protein concentrations.

*2.11. Oil Red O (ORO) Staining.* We further evaluate the intracellular lipid accumulation induced by PA-BSA in hepatocyte by ORO staining. Briefly, HepG2 cells were fixed with 10% formalin for 1 hour and stained then with ORO solution for 45 min. The cells were washed with deionized water and observed under a light microscope.

*2.12. Real-Time PCR Assay.* Total RNA was extracted from HepG2 cells and mouse liver tissues after treatment. The cDNA were made by the commercial kit per its protocols, which were used as the templates of real-time PCR. Real-time PCR was performed in an ABI PRISM 7900 High-Throughput Real-Time RCR System. The forward (F) and reverse (R) primer sequences were as follows: NLRP3 (F, 5′-tcacaactcgcccaaggaggaa-3′; R, 5′-aagagaccacggcagaagctag-3′); caspase-1 (F, 5′-acaaggcacgggacctatg-3′; R, 5′-tcccagtcagtcctggaaatg-3′); IL-1$\beta$ (F, 5′-cgacaaaatacctgtggcct-3′; R, 5′-ttctttgggtattgcttggg-3′); and $\beta$-actin (F, 5′-ggatgcagaaggagattactgc-3′; R, 5′-ccaccgatccacacagagta-3′).

*2.13. Western Blot.* Total proteins were extracted from cells or liver tissues. Western blots for each sample were

produced as follows: samples with 50 $\mu$g total protein were added to 10% or 12% sodium dodecyl sulfate-polyacrylamide gel electrophoresis (SDS-PAGE) and protein bands were electrically transferred to a PVDF membrane (Merck, Germany). After 5% skimmed milk blocking overnight at 4°C, detections of phospho-AMPK$\alpha$ (Thr172) (p-AMPK$\alpha$), AMPK$\alpha$, phospho-ACC (Ser79) (p-ACC), ACC, NLRP3, caspase-1, caspase-1 (p10), IL-1$\beta$, GSDMD-N, and $\beta$-actin proteins were achieved with specific monoclonal primary and secondary antibodies. The protein bands were developed by ECL kit (Beyotime Biotechnology, Nanjing, China). The blots were scanned and quantified, levels of p-AMPK$\alpha$ and p-ACC were normalized to that of AMPK$\alpha$ and ACC, respectively, and NLRP3, caspase-1, caspase-1 (p10), IL-1$\beta$, and GSDMD-N were normalized to that of $\beta$-catenin. The level of target protein was presented as fold of control treatment.

*2.14. Blocking Experiments.* HepG2 cells were cultured and seeded as above. Before drug treatment, the cells were pretreated with compound C (dissolved in DMSO) at 10 $\mu$M for 1 h, and DMSO was added to the untreated wells. Following pretreatment, the drugs were added to corresponding wells and cocultured with the cells for 24 h. Total cellular protein was extracted after treatment and detected by western blot. In parallel experiments, cell culture supernatants were centrifuged at 500 $g$ for 10 min, and glucose consumption of every treatment was tested by glucose assay kits as described above. In other parallel experiments, intracellular TG was detected by TG assay kit as described above and normalized to protein concentration from each treatment.

*2.15. Statistical Analysis.* All values from *in vitro* experiments are presented as the mean ± SD, and each experiment was replicated at least 3 times; all values from *in vivo* experimental results are shown as the mean ± SD; 8 mice were included in each group. Data processing and statistical analysis were used by GraphPad Prism 5.0 software. One-way ANOVA was used to detect the differences among studied groups. $p < 0.05$ is considered to be statistically significant.

## 3. Results

*3.1. Man Reduces Weight and Lowers Blood Glucose and Blood Lipids in HFD-Induced NAFLD Mice.* After 12 weeks of HFD, the weight of the model group NAFLD mice (31.32 ± 1.43 g) was obviously higher than that of the normal group (25.47 ± 0.87 g) (Figures 1(a) and 1(b), $p < 0.001$), and the levels of fasting blood glucose (FBG) (6.61 ± 0.42 mM), TG (1.02 ± 0.17 mM), LDL-c (2.04 ± 0.42 mM), and CHO (5.18 ± 1.12 mM) were more higher than those of the normal control group (FBG: 4.65 ± 0.66 mM; TG: 0.71 ± 0.04 mM; LDL-c: 0.65 ± 0.15 mM; CHO: 2.72 ± 0.45 mM) significantly, while the level of HLD-c (0.59 ± 0.18 mM) was lower than that of the normal group (0.78 ± 0.23 mM) significantly (Figures 1(d)–1(g), $p < 0.001$). After the 12-week experimental period, mice from the Man intervention treatment groups weighed significantly less than the NAFLD model group (31.32 ± 1.43 g), especially in the high-dose (Man-H) group (28.63 ± 1.64 g) (Figure 1(b), $p < 0.05$). Man treatment also significantly reduced FBG, improved serum lipid TG, LDL-c, and CHO-c levels (Figures 1(d)–1(g), $p < 0.05$), and exhibited dose dependency. At the same time, Man also increased HLD-c levels, which is conducive to regulating fat metabolism (Figure 1(g), $p < 0.01$).

*3.2. Man Improves Hepatic Fatty Deposition and Reduces Liver Damage.* In the HFD-induced NAFLD model mice, liver weight and liver index were obviously increased compared to that in the normal group mice (Figure 2(a), $p < 0.001$ or $p < 0.05$). At the same time, the liver TG was also significantly increased in NAFLD mice compared to the normal control group (Figure 2(b), $p < 0.001$), suggesting that hepatomegaly may be caused by liver TG accumulation in NAFLD model. However, for mice in the Man-M and Man-H groups, liver weight and liver index were significantly decreased compared to the model group (Figure 2(a), $p < 0.05$), and all doses of Man treatment inhibited liver TG increases (Figure 2(b), $p < 0.05$). Moreover, the levels of liver functions index of ALT and AST in the NAFLD model group mouse serum markedly increased compared to those in the normal group mice (Figures 2(c) and 2(d), $p < 0.05$), suggesting that excessive TG accumulation may cause liver injury. However, the levels of AST and ALT in the Man treatment group mouse serum were significantly decreased compared to those in the no-treatment model group (Figures 2(c) and 2(d), $p < 0.05$), suggesting that Man could reduce liver damage from adipopexis.

*3.3. Man Improved Insulin Resistance and Glucose Tolerance in NAFLD Mice.* The ITT and OGTT *in vivo* were executed to characterize whether Man could improve hepatic insulin resistance. As compared to the normal group, the HFD-induced NAFLD mouse group showed obvious impaired insulin resistance and glucose tolerance as marked by the important increase in the area under curve (AUC) of OGTT and ITT (Figures 3(a)–3(d), $p < 0.001$ vs. the normal group). After 12 weeks of Man treatment, the AUCs of OGTT and ITT were dose-dependently reduced, suggesting that insulin resistance of NAFLD mice was distinctly improved compared to the NAFLD model group mice (Figures 3(a)–3(d), $p < 0.01$ vs. the NAFLD model group).

*3.4. Man Improves Hepatic Steatosis of HFD-Induced NAFLD Mice.* In the liver histopathology examination, serious fatty accumulation and degeneration were also detected in NAFLD model mice, and more diffuse hepatocellular bullae steatosis were observed in liver pathology slice (Figure 4(a)), which may also damage the liver function. And the pathological steatosis scores were more higher than the normal group (Figure 4(b), $p < 0.05$), which indicated that more severe steatosis occurs in the liver of model mice and was effectively improved by Man treatment dose-dependently (Figure 4, $p < 0.05$ vs. the NAFLD model group), and the numbers of hepatocyte involved in liver diffuse bullae steatosis were also decreased seriously

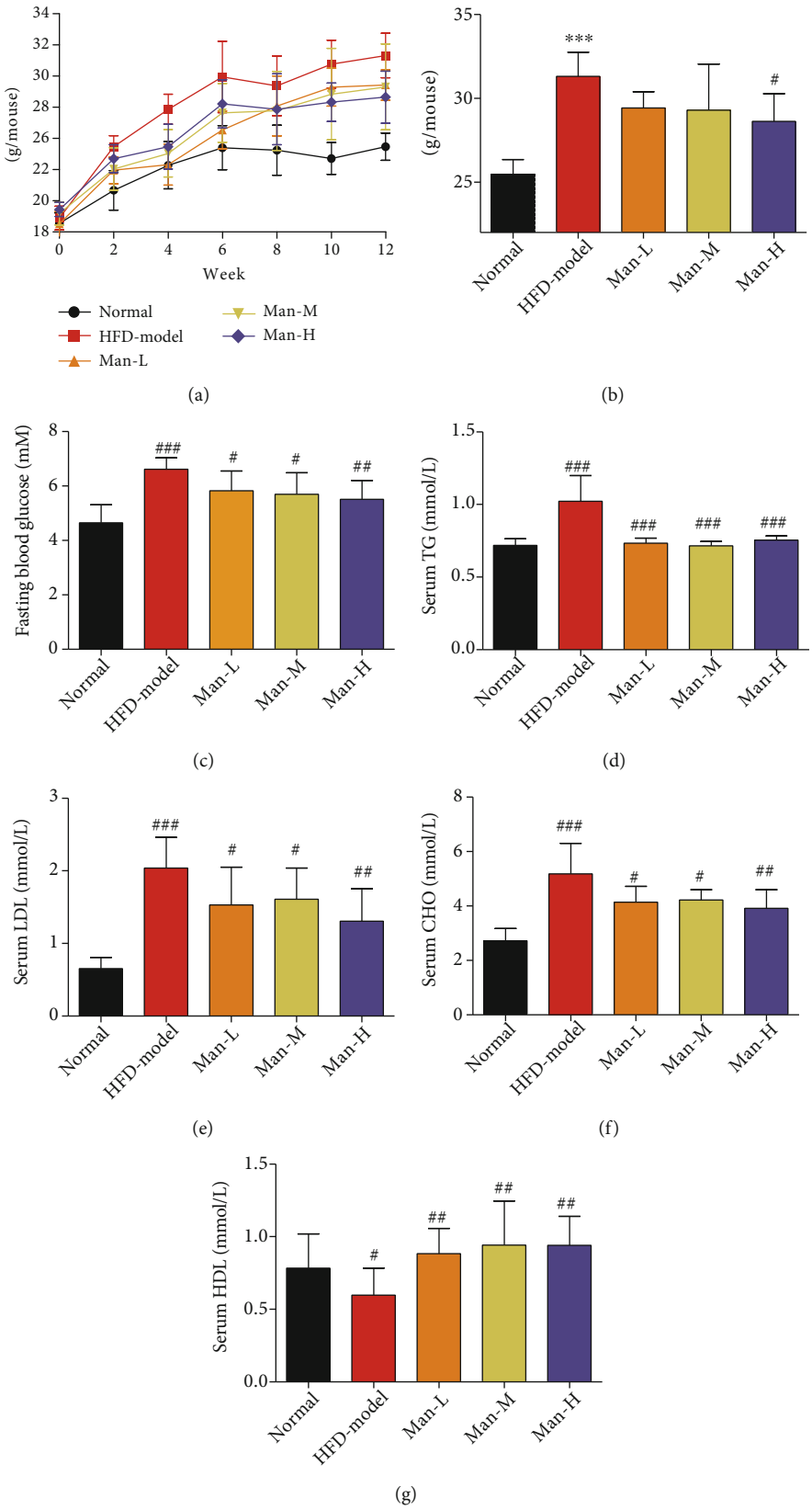


Figure 1: Man reduces weight and lowers blood glucose and blood lipids in HFD-induced NAFLD mice. (a) The body weight change of mice during experimental period. (b) The body weight of mice after a 12-week treatment. (c) The last FBG before the finished experiment. (d–g) Serum levels of TG (d), LDL-c (e), CHO (f), and HDL-c (g). The results represent as the mean ± SD, $n = 8$. $^{*}p < 0.05$, $^{**}p < 0.01$, and $^{***}p < 0.001$ vs. the normal group. $^{\#}p < 0.05$, $^{\#\#}p < 0.01$, and $^{\#\#\#}p < 0.001$ vs. the model group.

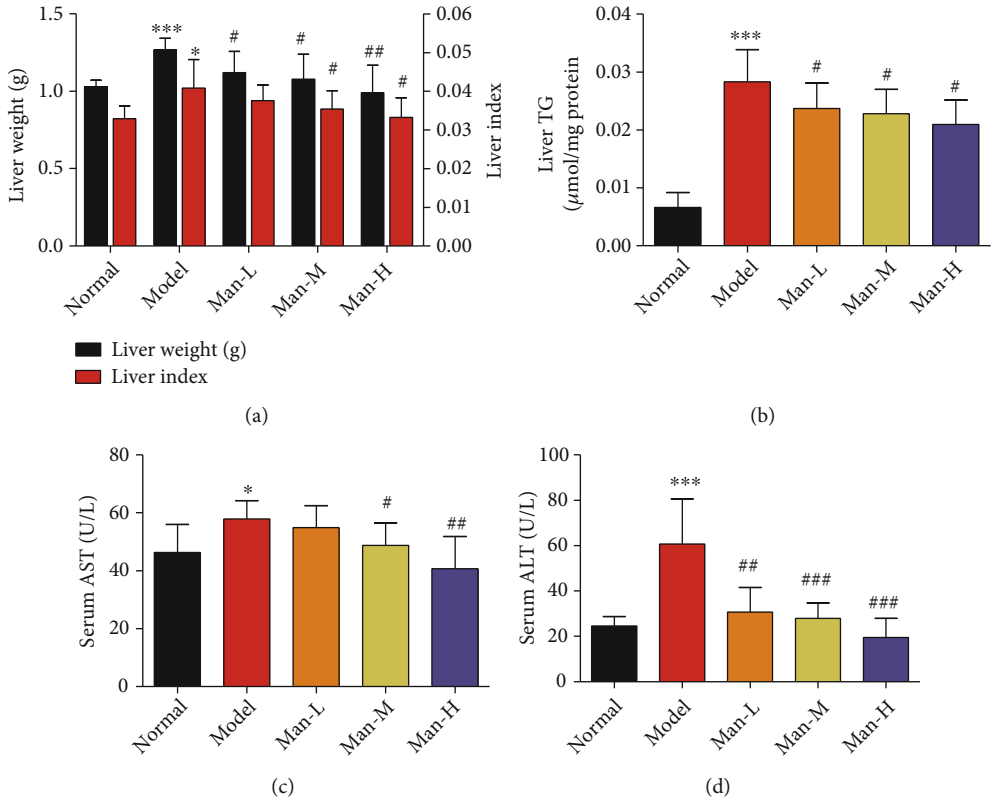


Figure 2: Man improves hepatic fatty deposition and reduces liver damage. (a) Liver weight and liver index of animals. (b) TG levels of liver. (c, d) The levels of AST and ALT in serums. All results represent as the mean ± SD, $n = 8$. $^{*}p < 0.05$, $^{**}p < 0.01$, and $^{***}p < 0.001$ vs. the normal group. $^{\#}p < 0.05$, $^{\#\#}p < 0.01$, and $^{\#\#\#}p < 0.001$ vs. the model group.

(Figure 4(a)). Our results suggest that Man can improve liver steatosis and function in histopathology level *in vivo*.

*3.5. RNA-Seq Assay of Man's Effects on NAFLD Treatment.* To explore the potential molecular mechanisms of Man's effects on NAFLD mouse livers, RNA-seq was performed on liver tissue from 4 mice with or without Man (100 mg/kg/d) treatment. The Pearson $R^2$ values of all Man-treated samples and NAFLD model mouse samples were over 0.92, suggesting that the samples exhibited good repeatability (Figure 5(a)). The 1601 differentially expressed genes ($|\log_2(\text{fold change})|>1$ and corrected $p$ value ($p$adj) $\leq 0.05$) were found using the DESeq2 R package (1.20.0) and visualized with volcano plot as shown in Figure 5(b), in which 448 genes were upregulated and 1153 genes were downregulated (Figure 5(b)). The heat map as shown in Figure 5(c) was also used to visualize the differentially expressed genes. The Gene Ontology (GO) enrichment analysis was done by the clusterProfiler R package, and GO terms with corrected $p$ value less than 0.05 were considered significantly enriched. The GO biological processes of significantly upregulated genes are shown in Figure 5(d), which were mainly related to energy derivation, cellular respiration, fatty acid metabolic processing, and generation of precursor metabolites and energy, and associated with liver metabolism of energy substances, such as glucose, free fatty acids, and lipids. We used the clusterProfiler R package to test the statistical enrichment of differentially expressed genes in KEGG pathways and found that Man could significantly promote fatty acid degradation signaling pathways by increasing the E6.2.1.3 gene expression (Figure 5(f)), which is one of the key enzymes for fatty acid oxidation (Figure 5(g), $p$ value = 0.00003). For the downregulated genes, the GO biological processes were mostly associated with inflammation, such as immune response, the Toll-like receptor signaling pathway, cytokine biosynthetic processing, the NF-KB signaling pathway, and programmed cell death, among others, and the representative 10 biological processes as shown in Figure 5(e). Those results suggested that Man might exhibit anti-inflammatory activity. The KEGG pathway assay of these downregulated genes found that Man could significantly inhibit the nod-like receptor signal pathway (Figures 5(h) and 5(i), $p$ value = 0.0019), which mainly downregulated NLRP3 gene expression and regulated the NLRP3/caspase-1/GSDMD signal pathway (Figure 5(j)). All these results showed that Man might possess beneficial effects on energy metabolism and inflammation for treatment of HFD-induced NAFLD mice.

*3.6. Man Activates AMPK and Inhibits the NLRP3/Caspase-1/GSDMD Signaling Pathway in Hepatocyte In Vivo.* AMPK is a key regulatory enzyme of energy balance in liver tissue cells, which is associated with hepatocyte glucolipid metabolism and is a potential target for NAFLD therapy. As our RNA-seq assay showed that genes significantly upregulated by Man treatment were mostly associated with energy

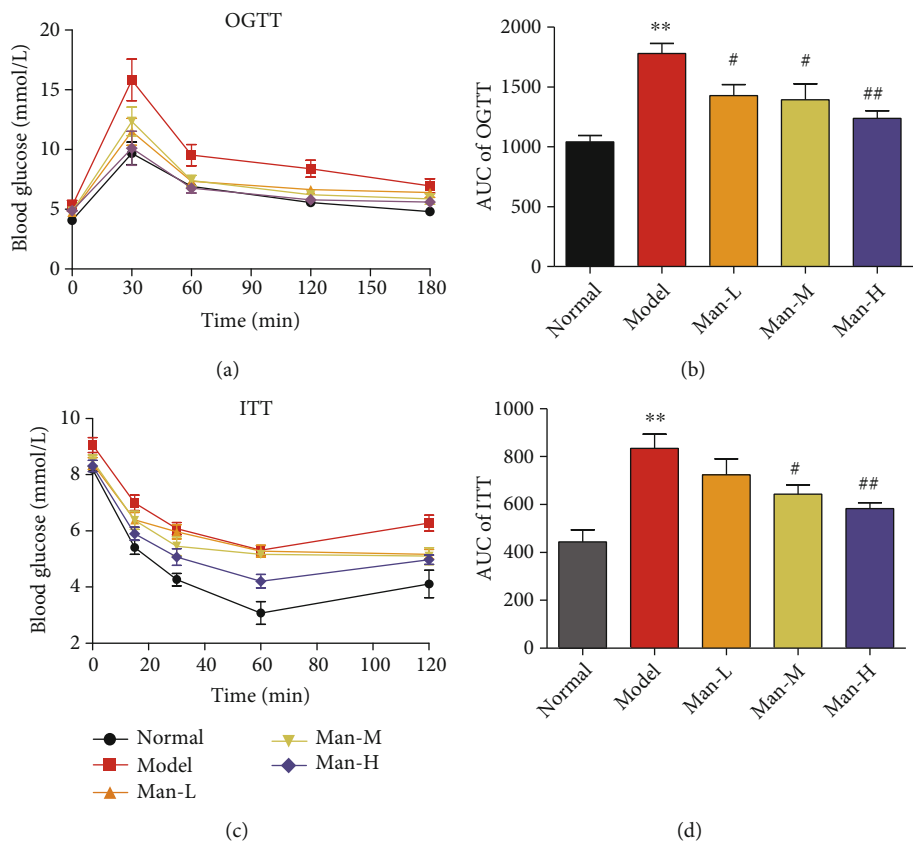


Figure 3: Man ameliorates insulin resistance and glucose tolerance in NAFLD mice. (a) The curve of OGTT. (b) The area under the curve of OGTT. (c) The curve of ITT. (d) The area under the curve of ITT. Data represent as the mean ± SD ($n = 8$). $^{**}p < 0.01$ vs. that of the normal group. $^{\#}p < 0.05$ and $^{\#\#}p < 0.01$ vs. that of the NAFLD model group.

metabolism (Figure 5(d)), the AMPK activation in mouse hepatocytes was detected by western blot. The results showed that AMPK activity in the NAFLD mouse liver tissues was significantly inhibited, while the level of p-AMPK$\alpha$ was potently upregulated in Man treatment mice dose-dependently (Figures 6(a) and 6(b)). Meanwhile, we further investigated the effects of Man on NLRP3-mediated hepatocyte inflammation and pyroptosis. Our results exhibited that liver NLRP3, caspase-1, caspase-1 (p10), and IL-1$\beta$ were significantly upregulated in the NAFLD model group mice (Figures 6(a), 6(c), and 6(d)) and which were significantly decreased in Man-treated mice (Figures 6(a), 6(c), and 6(d)). These suggested that Man can inhibit the activation of NLRP3 inflammasome. We further examined the GSDMD splicing and pyroptosis induced by NLRP3 inflammasome activation and found that Man could inhibit GSDMD splicing and pyroptosis mediated by NLRP3 inflammasome activation (Figures 6(a) and 6(c)), thus playing an anti-inflammatory effect. Through the quantification of serum IL-1$\beta$, we also found that serum IL-1$\beta$ levels significantly decreased with Man treatment (Figure 6(e), $p < 0.05$). The RT-PCR results demonstrated that Man significantly downregulated the transcription levels of NLRP3, caspase-1, and IL-1$\beta$ genes (Figures 6(f)–6(h), $p < 0.05$). Immunofluorescence assays showed that the positive staining degrees of NLRP3, caspase-1, GSDMD-N, and IL-1$\beta$ in NAFLD mouse liver tissues were visibly high compared to those of the normal control group, indicating upregulation of NLRP3, caspase-1, and GSDMD expression (Figure 6(i)), and Man could reduce the positive staining levels (Figure 6(i)), indicating downregulation of those proteins, which was consistent with the western blot and RT-PCR results.

*3.7. Man Cytotoxicity in HepG2 Cells.* As shown in Figure 7, 400 $\mu$M Man displayed no cytotoxicity with 24 h treatment in HepG2 cells. Importantly, it reduced the viability of HepG2 cells at higher concentrations (800 $\mu$M; Figure 7, $p < 0.05$ vs. DMSO).

*3.8. Man Activates AMPK to Regulate Hepatocyte Glucose and Lipid Metabolism In Vitro.* The effect of Man on glucose metabolism was investigated via glucose consumption assay. As shown in Figure 8(a), Man increases the basal glucose consumption level of HepG2 cells in a dose-dependent manner (Figure 8(a), $p < 0.01$ or $p < 0.001$ vs. DMSO). 25 $\mu$M Man significantly increased glucose consumption (Figure 8(a), $p < 0.01$ vs. DMSO), and 100 $\mu$M Man was comparable to that of 2 mM metformin (Figure 8(a)). Moreover, its activity was abolished by pretreatment with compound C (cc), an AMPK inhibitor. These results suggest that the effects of Man may be dependent on AMPK activation (Figure 8(b), $p < 0.01$ vs. Man). In fact, our results

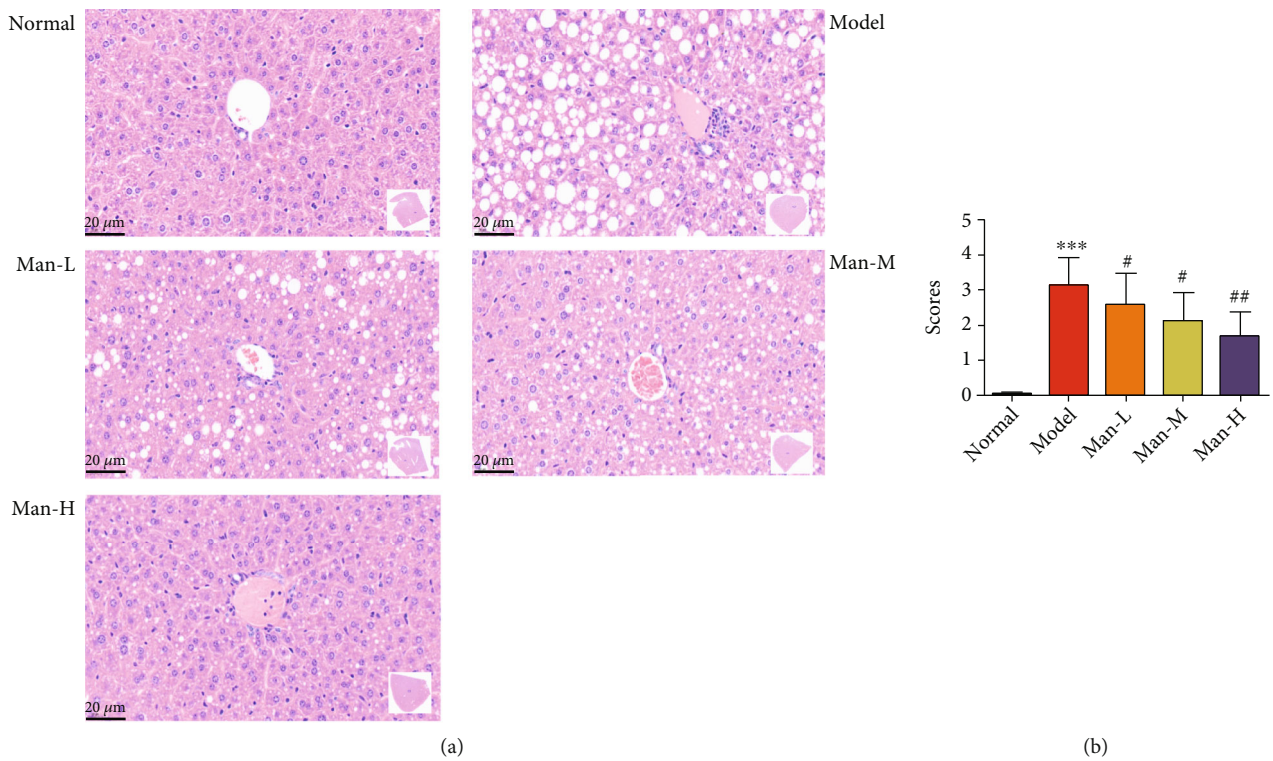


Figure 4: Man improves hepatic steatosis in HFD-induced NAFLD mice. (a) The H&E staining, one representativeness of pathological images of each group. (b) The steatosis scores of liver pathological changes. Data represent as the mean ± SD ($n = 8$). $^{***}p < 0.001$ vs. that of the normal group. $^{\#\#}p < 0.01$ vs. that of the NAFLD model group.

showed that Man could activate AMPK and dose-dependently increased the level of p-AMPK$\alpha$ (Thr172) and p-ACC (Ser79) in HepG2 cells after 24 h of administration (Figures 8(c) and 8(d), $p < 0.05$ or $p < 0.01$ or $p < 0.001$ vs. DMSO). The observed AMPK-stimulating activation of Man was completely blocked by cc (Figures 8(e) and 8(f), $p < 0.05$). To investigate Man effects on lipid metabolism, the hepatocyte of HepG2 cells was induced by PA-BSA to accumulate TG, and Man was administered to prevent PA-BSA-induced intracellular TG accumulation. As shown in Figure 8(g), 0.3 mM of PA-BSA treatment for 24 h increased intracellular TG levels dramatically (Figure 8(g), $p < 0.01$ vs. DMSO+10% BSA), which were dose-dependently reduced by Man (Figure 8(g), $p < 0.01$ or $p < 0.001$ vs. PA-BSA +DMSO). Furthermore, this effect of Man on reducing intracellular TG accumulation was blocked by cc pretreatment for 60 min in HepG2 cells (Figure 8(h), $^{\&}p < 0.05$ vs. PA-BSA+Man). ORO staining was performed to further determine Man effects on lipid metabolism. As shown in Figure 8(i), cells treated with PA-BSA and DMSO exhibited more red positive staining, which was significantly reduced by 100 $\mu$M Man treatment (Figure 8(i)), but not after cc pretreatment for 60 min before Man treatment compared to Man treatment alone (Figure 8(i)).

*3.9. Man Inhibits the NLRP3/Caspase-1/GSDMD Signal Pathway in Hepatocytes.* The inflammation from NLRP3 inflammasome activation plays a crucial role in many metabolic diseases including NAFLD, and our animal experiments showed that Man inhibits NLRP3-mediated inflammation and pyroptosis in hepatocytes by western blot and RNA-seq analysis. Similar results were obtained in HepG2 cells with free fatty acid (0.3 mM PA-BSA) induction of NLRP3 inflammasome activation, as shown in Figure 9. Compared to the DMSO+10% BSA treatment group, p-AMPK$\alpha$ levels were significantly decreased in PA-BSA-treated HepG2 cells (Figures 9(a) and 9(b), $p < 0.001$ vs. DMSO+10% BSA), which were significantly increased by Man (Figures 9(a) and 9(b), $p < 0.01$ or $p < 0.001$ vs. DMSO+PA-BSA). At the same time, the protein levels of NLRP3, caspase-1 (p10), IL-1$\beta$, and GSDMD-N were obviously increased in PA-BSA-induced HepG2 cells (Figure 9(a)), indicating that FFA (0.3 mM PA-BSA) can activate the NLRP3 inflammasome and cell pyroptosis to induce inflammation. However, mangiferin significantly reversed this phenomenon, reduced the expression of these proteins, inhibited the activation of NLRP3 inflammasomes and pyroptosis, and played an anti-inflammatory effect *in vitro* (Figures 9(c) and 9(d)).

## 4. Discussion

NAFLD is considered to be ultralimit lipid accumulation and steatosis in hepatocytes without ethanol consumption and encompasses a broad disease spectrum including simple fatty liver, steatohepatitis, fibrosis, cirrhosis, and liver cancer [1]. The "two-hit" and "multiple parallel hits" hypotheses had been used to explain NAFLD development, and the

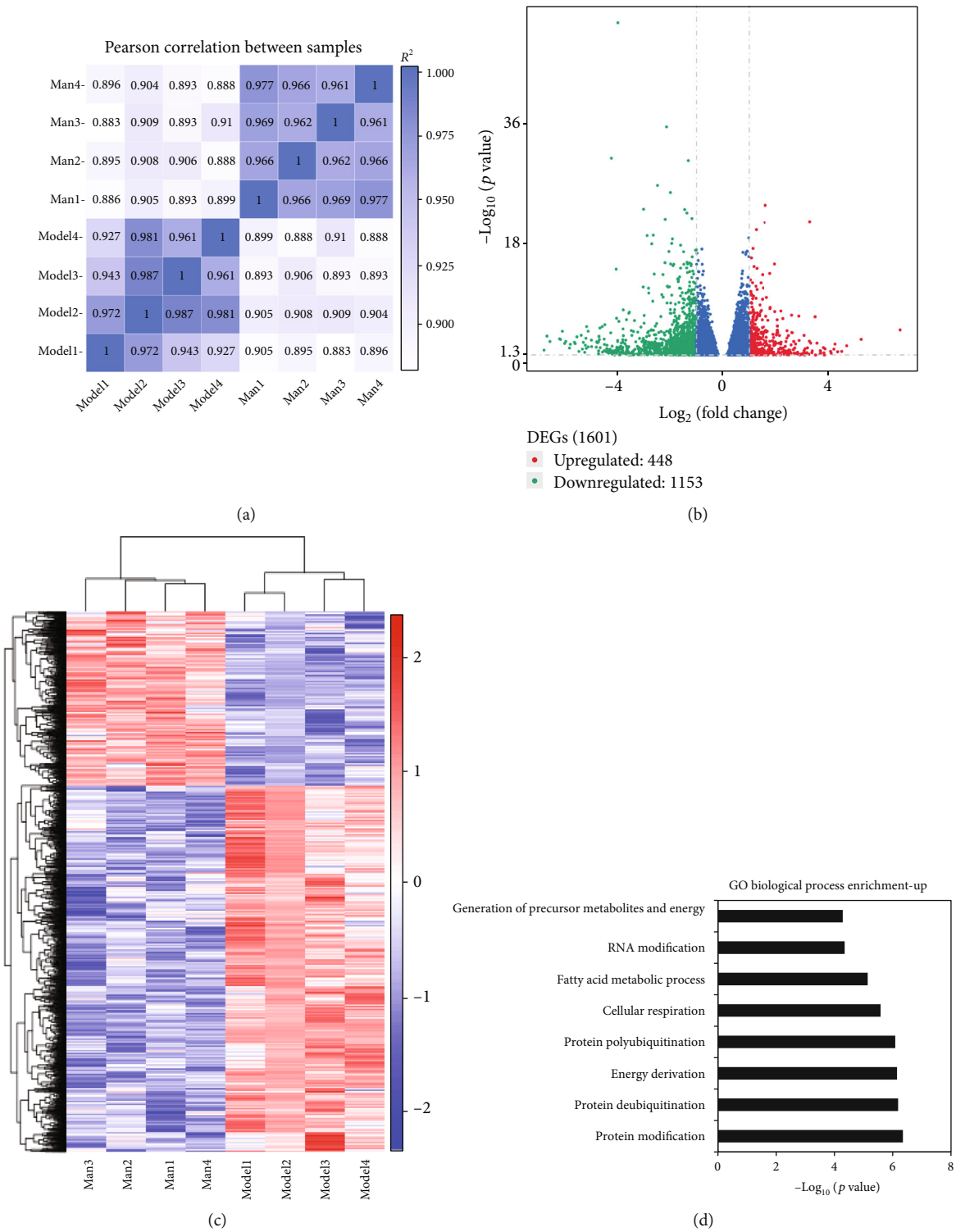


Figure 5: Continued.

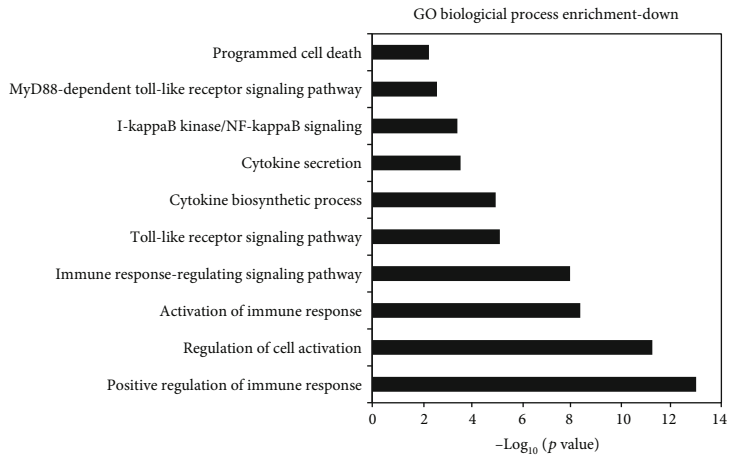


(e)

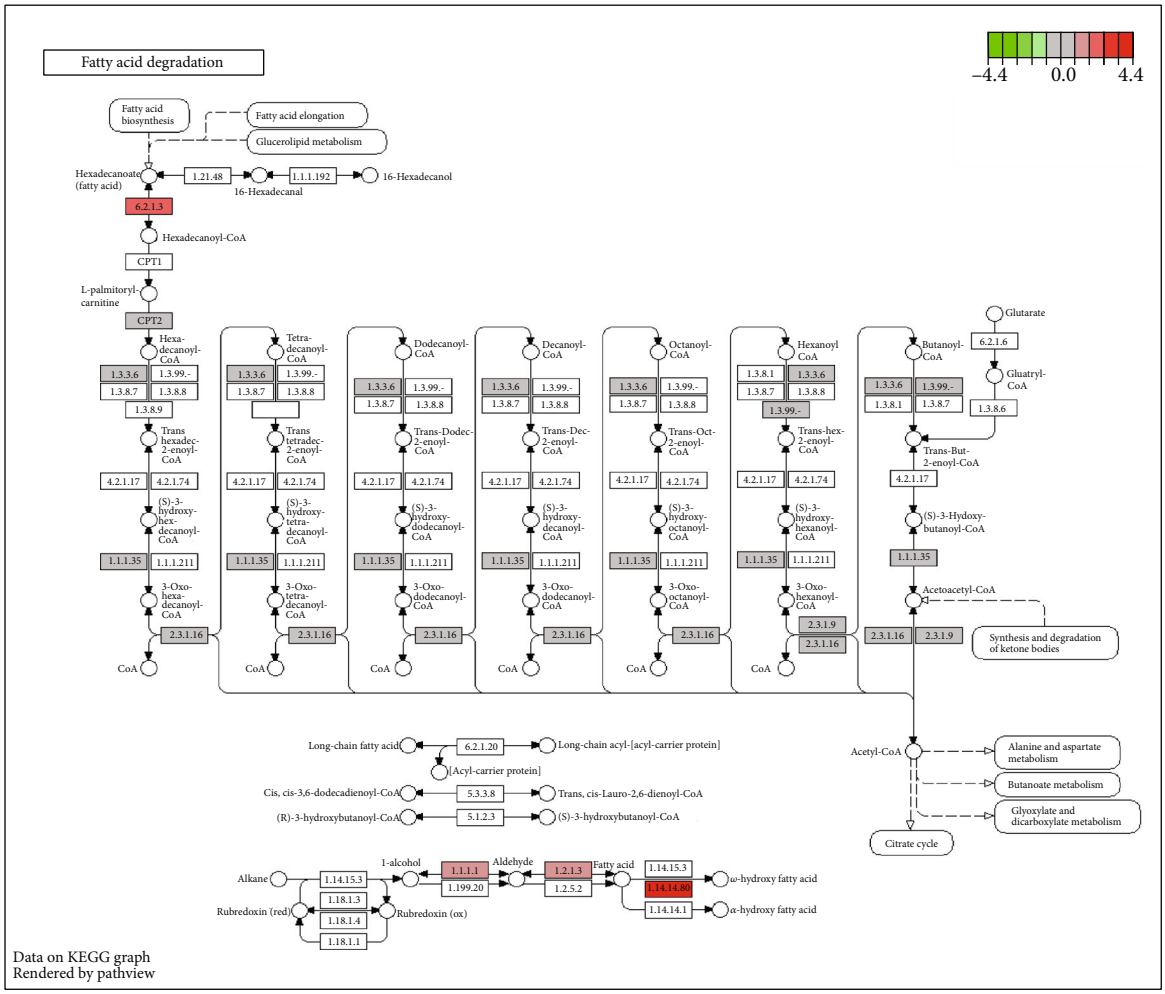


(f)

| KEGGID | Description | *p* value | *p* adj |
|---|---|---|---|
| mmu00071 | Fatty acid degradation | 0.0000295 | 0.0017906 |

(g)

Figure 5: Continued.

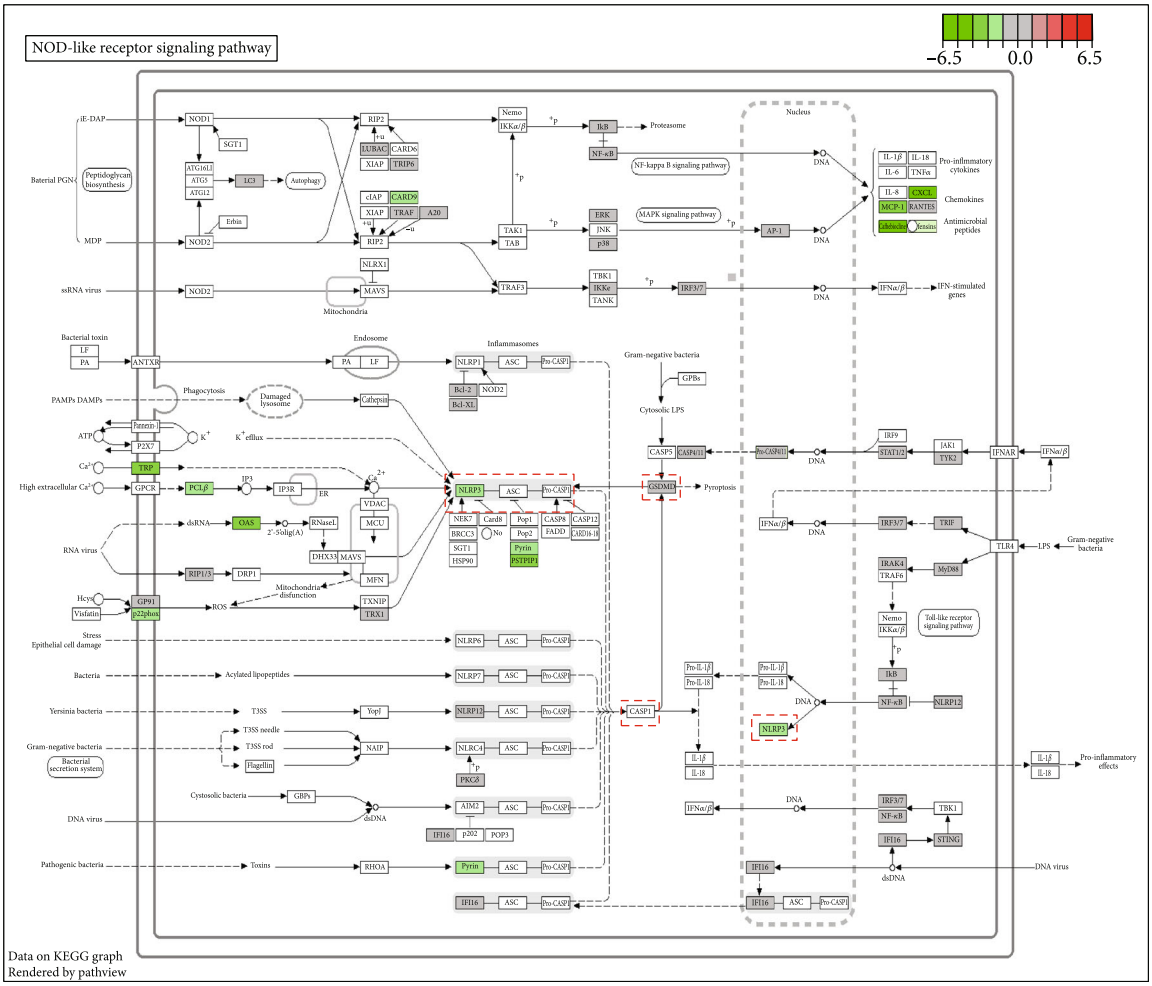


(h)

| KEGGID | Description | $p$ value | $p$ adj |
|---|---|---|---|
| mmu04621 | NOD–like receptor signaling | 0.0019831 | 0.0193833 |

(i)

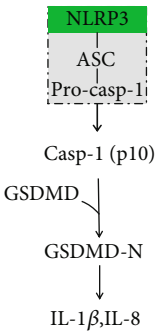


(j)

Figure 5: RNA-seq assay of mouse hepatocytes between Man treatment and NAFLD model groups. (a) The Pearson correlation between samples. (b) Differentially expressed gene volcano map ($|\log_2(\text{fold change})|>1$ and $p\text{adj} \leq 0.05$). (c) Differentially expressed genes clustering heat map of 1601 ($|\log_2(\text{fold change})|>1$ and $p\text{adj} \leq 0.05$). (d, e) The Gene Ontology (GO) biological process enrichment of upregulation (d) or downregulation (e) of differentially expressed genes, and the threshold value for significant enrichment of GO function was $p\text{adj} \leq 0.05$. (f, g) One of the representations of KEGG pathway (f) about upregulation of differentially expressed genes and its ID, description, $p$ value, and $p$adj value (g). (h, i) One of the representations of KEGG pathway (h) about downregulation of differentially expressed genes and its ID, description, $p$ value, and $p$adj value (i). (j) The NLRP3/Casp-1/GSDMD-mediated inflammatory signal pathway in (h), which is closely related to the effects of Man treatment.

latter hypothesis is more widely favored. Even so, the pathogenesis of NAFLD remains unclear and very complex. Risk factors leading to NAFLD development include lipotoxicity, oxidative stress, inflammation, endoplasmic reticulum stress, insulin resistance, and mitochondrial dysfunction, which are also potential therapeutic targets for the

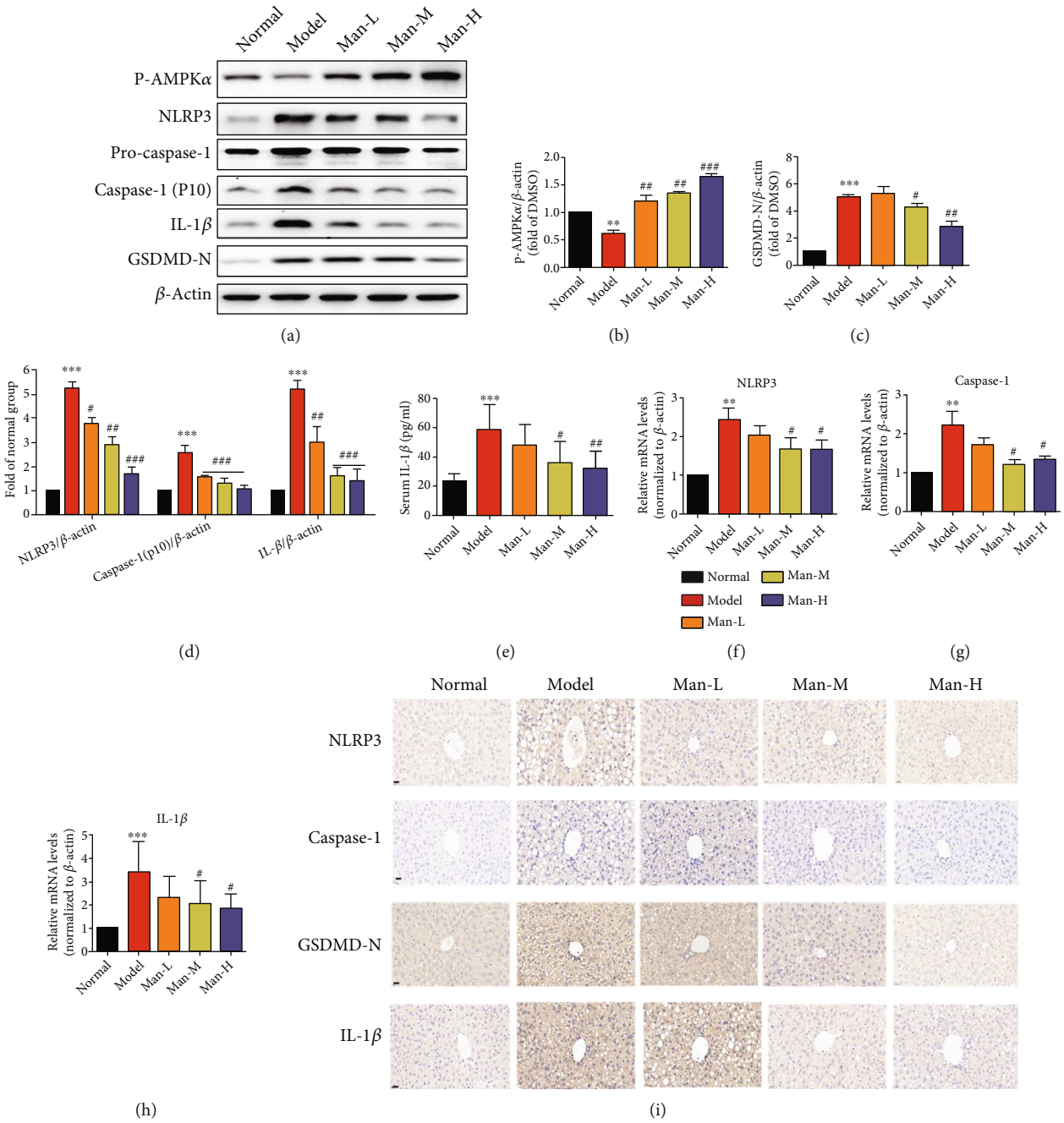


Figure 6: Man activates AMPK and regulates the NLRP3 inflammasome signaling pathway to exert anti-inflammatory effects *in vivo*. The total protein was extracted from animal liver of experiment. The p-AMPK, NLRP3, pro-caspase-1, caspase-1 (p10), IL-1$\beta$, and GSDMD-N protein levels were detected by Western blots and quantified by using ImageJ software. (a) Western blots. (b) The protein levels of p-AMPK were normalized to those of $\beta$-actin, respectively, and plotted as fold of the normal group. (c) The protein levels of GSDMD-N were normalized to those of $\beta$-actin, respectively, and plotted as fold of the normal group. (d) The protein levels of NLRP3, caspase-1 (p10), and IL-1$\beta$ were normalized to those of $\beta$-actin, respectively, and plotted as fold of the normal group. (f–h) The NLRP3 and ASC caspase-1 mRNA levels were detected by quantitative real-time PCR in animals' liver. The data are expressed as the mean ± SD ($n = 8$). $^{*}p < 0.05$, $^{**}p < 0.01$, and $^{***}p < 0.001$ vs. the normal group. $^{\#}p < 0.05$ and $^{\#\#}p < 0.01$ vs. the NAFLD model group.

development of NAFLD treatments [29]. At the present time, there is no long-term efficacious and approved standard therapy for NAFLD treatment. Clinically, the drugs such as hypoglycemic, lipid-lowering, and insulin sensitizers are usually chosen during the NAFLD treatment; at the same time, diet control and exercise are necessary [10, 29]. In this work, we are interested in the potential anti-NAFLD activity and mechanisms of Man and focusing on its regulation of glycolipid metabolism and anti-inflammatory *in vitro* and *in vivo*. In our experiments, HFD-fed-induced NAFLD mice indicated that Man treatment significantly reversed body and liver weight increases

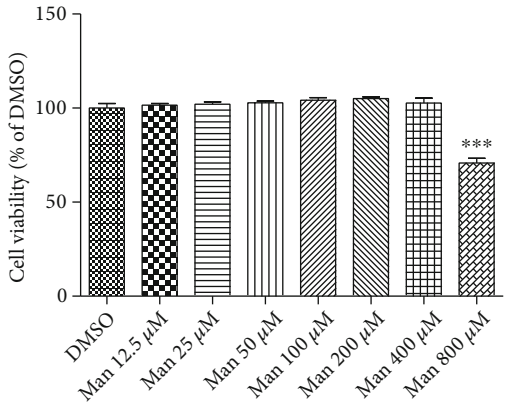


Figure 7: Man effects on cell viability. HepG2 cells were incubated with Man at indicated concentrations for 24 h; cell viabilities were tested by MTT assay. All result values are represented as the mean ± SD ($n = 5$). $^{***}p < 0.001$ vs. DMSO.

and improved liver index, dyslipidemia, liver damage, insulin resistance, and inflammation. In *in vitro* HepG2 cell experiments, Man significantly increased glucose consumption and decreased intracellular TG levels, lipid accumulation, and inflammation induced by PA-BSA. We further demonstrated that this protective effect of Man might contribute to its regulation effects on the AMPK and NLRP3 inflammasome signaling pathways.

The liver is a vital organ for controlling circulating glucolipid metabolism and plays a key role in the progress of NAFLD, T2D, and atherosclerosis [13]. AMPK is a highly conserved kinase that regulates energy balance, and is thought as an important and interesting target for the treatment of many glucose and lipid metabolic disorder diseases, such as NAFLD, diabetes, dyslipidemia, and obesity [13, 30, 31]. Activating liver AMPK can promote glucose metabolism and lipid oxidative decomposition to provide energy for the body [12]. AMPK agonists, such as metformin, berberine, and gastrodin, were considered potential drugs used for the treatment of a variety of diseases related to glucose and lipid metabolism disorders, including NAFLD, diabetes, and cardiovascular and cerebrovascular diseases [13, 31]. Our results show that Man significantly activates AMPK of hepatocytes with *in vitro* and *in vivo* experiments. Man accelerates HepG2 cell basal glucose consumption and reduces TG accumulation induced by PA-BSA, and its effects are abolished by an AMPK-specific inhibitor, compound C. Our ORO staining test also confirmed the lipid-lowering effect of Man and its dependence on AMPK activation. In the HFD-induced NAFLD animal experiments, we also observed the hypoglycemic and lipid-lowering effects of Man in serum. Liver histopathological and transcriptomic analyses also showed that Man significantly reduced fat storage and degeneration in liver tissue. Previous studies showed that Man reduces weight and lowers glucose and lipid in a diabetic rat model [32], which is consistent with our results. Obesity is also a common cause of NAFLD development, and several studies showed that AMPK activation is a potential therapeutic target for weight loss drugs [33, 34]. Our study showed that Man also has a weight loss effect in HFD-induced NAFLD model mice. Thus, AMPK activation by Man may be one of the key mechanisms of its anti-NAFLD effects. The AMPK signal pathway is mainly activated by two different ways, one is $Ca^{2+}$-dependent pathway regulation by CaMKK$\beta$ and another is AMP-dependent pathway mediated by LKB1, and the exact molecular mechanism of how Man activates AMPK is our focus for future work.

Inflammasomes are multiprotein complexes that mediate the production of inflammatory cytokines and produce potent inflammatory cascades [35]. The NLRP3 inflammasome is the most widely studied and characterized member of this family. As extensively reported, the NLRP3 inflammasome mediates inflammation induced by many noninfectious factors, such as lipid accumulation, oxidative stress from hyperglycemia, and hyperlipidemia [35, 36], and participates in the causing of many diseases, including NAFLD, obesity, diabetes, and cardiovascular diseases [16, 35, 37]. Many inflammasome inhibitors, such as isoliquiritigenin and GS9450, may be potential anti-NAFLD drugs. In our study, we confirmed that Man inhibits NLRP3 inflammasome activity at both the cellular and organism levels through a series of experiments. First, Man significantly downregulated the levels of NLRP3, caspase-1, and IL-1$\beta$ in the liver tissues of HFD-induced NAFLD mice as measured by western blot and RT-PCR. At the cellular level, Man significantly decreased the levels of NLRP3, caspase-1, and IL-1$\beta$ induced by PA-BSA treatment of HepG2 cells. Liver tissue immunohistochemical analysis also exhibited that Man distinctly inhibits NLRP3 inflammasome function, decreased inflammatory factor production and release, and then suppressed the occurrence of inflammation. At the same time, we also analyzed transcriptional sequencing and observed that the Man-treated groups exhibited significantly downregulated transcription of genes related to the biochemical process of inflammation. The KEGG pathway assay also showed that Man had a significant impact on the NLRP3 inflammasome signaling pathway. All these results indicated that Man exerts anti-inflammatory effects by inhibiting the activation of NLRP3 inflammasomes, which may be an important effect on NAFLD treatment.

Our study also found that Man can improve insulin resistance in HFD-induced NAFLD mice. Insulin resistance is also a common risk factor for the occurrence and development of NAFLD, especially in type 2 diabetic patients. It is recognized that improving insulin resistance can significantly improve the progression of NAFLD [38], and it is currently a common method for the clinical treatment of NAFLD. Others studies have reported that Man improves insulin resistance in diabetic mice, and we also observed a significant improvement in insulin resistance in NAFLD models [39]. This may be related to its ability to activate AMPK in hepatocytes because studies have shown that AMPK activation can improve insulin resistance, but the specific mechanism needs to be further studied. In addition, we also observed protective effects of Man on liver function, which may be associated with improved insulin resistance and glucose tolerance, and have a positive effect on the prevention and treatment of NAFLD.

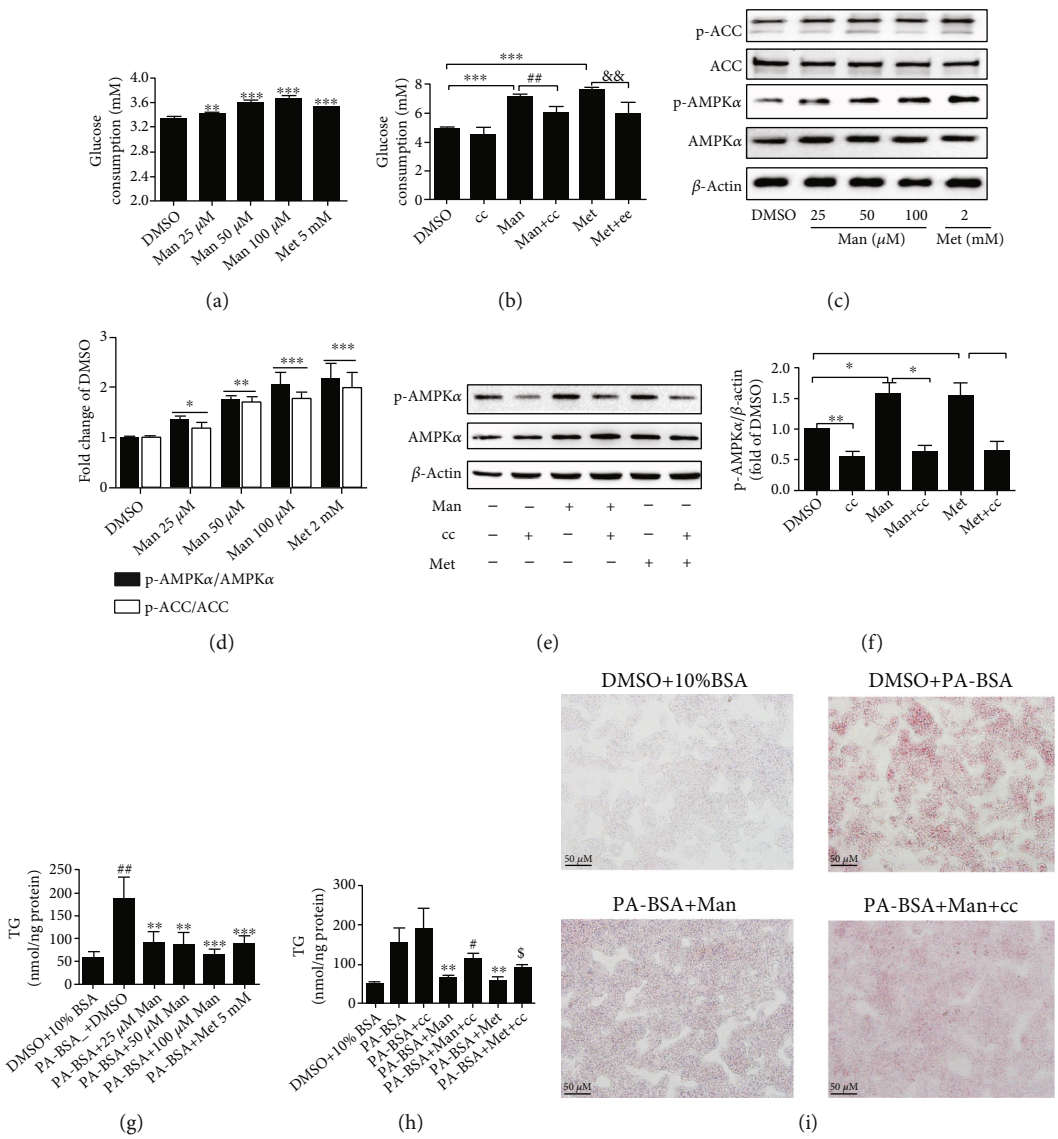


Figure 8: Man modulates cell glycolipid metabolism by activating the AMPK signal pathway. (a) Glucose consumptions. All result values are represented as the mean ± SD ($n = 5$). $^{**}p < 0.01$ or $^{***}p < 0.001$ vs. DMSO. (b) Glucose consumptions with compound C pretreatment. Values are represented as the mean ± SD ($n = 5$). $^{***}p < 0.001$ vs. DMSO, $^{\#\#}p < 0.01$ vs. Man, and $^{\&\&}p < 0.01$ vs. Met. (c) After Man treatment, the total cell proteins of every well were extracted; p-AMPK$\alpha$ (Thr172) (p-AMPK$\alpha$), AMPK$\alpha$, p-ACC (Ser79) (p-ACC), ACC, and $\beta$-actin were determined by western blot. Representative blot pictures as presented. (d) Normalizing the level of p-AMPK$\alpha$ and p-ACC to those of AMPK$\alpha$ and ACC, respectively, and plotted as fold of DMSO-treated cells. The values are represented as the mean ± SD ($n = 3$). $^{*}p < 0.05$, $^{**}p < 0.01$, and $^{***}p < 0.001$ vs. DMSO. (e) HepG2 cells were pretreated with cc for 60 min; then, Man was added and incubated for 24 h; total cell proteins were extracted; p-AMPK$\alpha$ (Thr172) (p-AMPK$\alpha$) and AMPK$\alpha$ were detected by western blot. Representative blot pictures as presented. (f) The protein level of p-AMPK$\alpha$ was normalized to AMPK$\alpha$, respectively, and plotted as fold of DMSO-treated cells. Values are represented as the mean ± SD ($n = 3$). $^{*}p < 0.05$, $^{**}p < 0.01$, and $^{***}p < 0.001$ vs. DMSO. (g) The intracellular TG levels of HepG2 cells were detected after PA-BSA or PA-BSA plus Man or Met treatment for 24 h and normalized to protein content of the sample. All result values are represented as the mean ± SD ($n = 4$). $^{**}p < 0.01$ vs. DMSO+10% BSA and $^{\#\#}p < 0.01$ or $^{\#\#\#}p < 0.001$ vs. PA-BSA+DMSO. (h) The intracellular TG levels of HepG2 cells were detected and normalized to protein content of the sample, each treatment with 4 replications. Values are represented as the mean ± SD ($n = 4$). $^{***}p < 0.001$ vs. 10% BSA+DMSO, $^{\#\#}p < 0.01$ vs. PA-BSA, $^{\&}p < 0.05$ vs. PA-BSA+Man, and $^{\$}p < 0.05$ vs. PA-BSA+Met. (i) ORO staining.

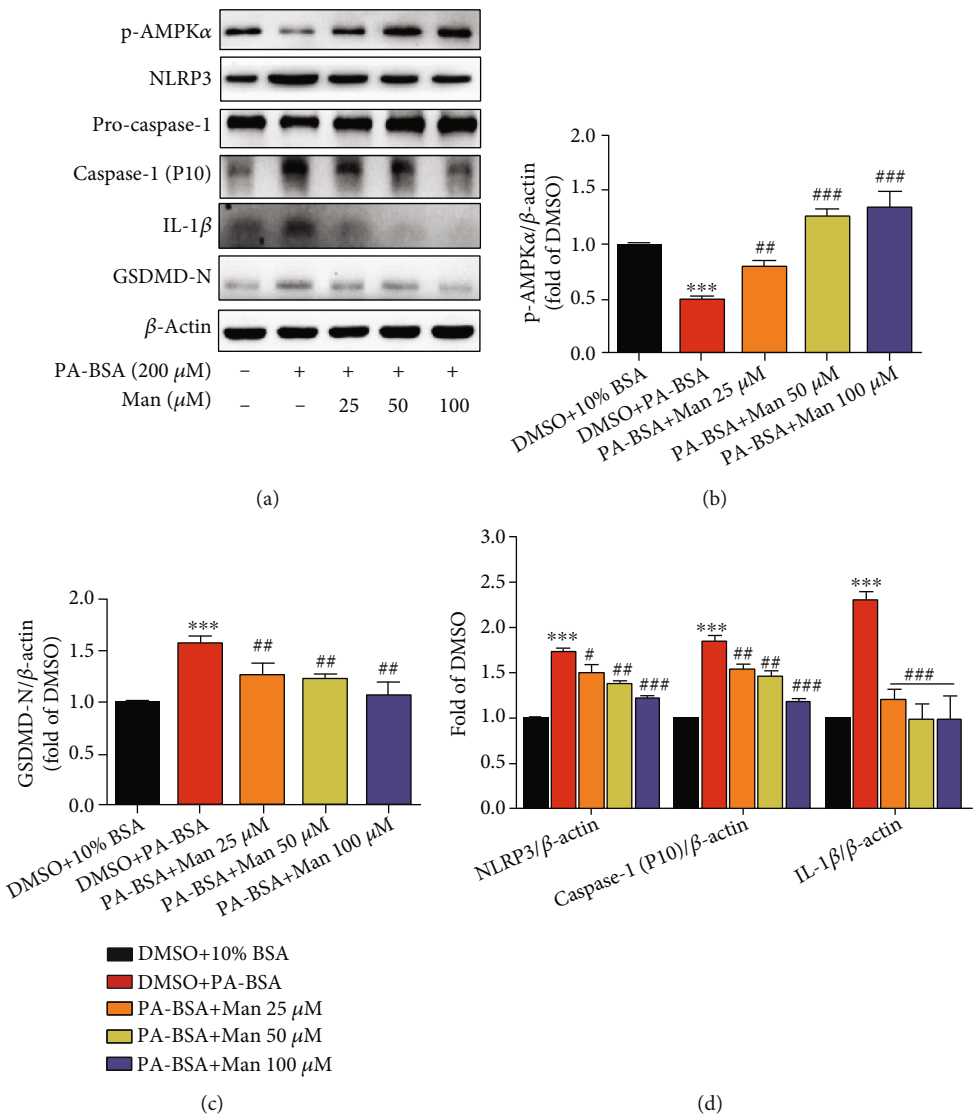


Figure 9: The effects of Man on NLRP3 inflammasome signal axis and its inhibition of NLRP3-mediated pyroptosis *in vitro*. (a) After serum starvation treatment, cells were untreated or treated with PA-BSA or PA-BSA+Man or PA-BSA+Met as indicated for 24 h. Then, total cell proteins were made; p-AMPKα (Thr172) (p-AMPKα), NLRP3, caspase-1, caspase-1 (P10), GSDMD-N, IL-1β, and β-actin were detected by western blot. Representative blot pictures as shown. The protein levels of p-AMPKα (b), GSDMD-N (c), and NLRP3/caspase-1 (p10)/IL-β (d) were normalized to β-actin, respectively, and plotted as fold of the DMSO+10% BSA-treated group. Values are represented as the mean ± SD ($n = 3$). $^{***}p < 0.001$ vs. DMSO+10% BSA and $^{\#\#}p < 0.01$ and $^{\#\#\#}p < 0.001$ vs. DMSO+PA-BSA.

## 5. Conclusion

Our study demonstrated that Man had a protective effect against NAFLD through AMPK activation and NLRP3 inflammasome inhibition. Its treatment obviously improved body weight, liver weight/index, serum glucolipid metabolism, and insulin resistance and alleviated hepatic lipid accumulation and steatosis and liver function in HFD-induced NAFLD mice *in vivo*. In *in vitro* experiments, Man promoted hepatocyte glucose consumption and decreased FFA-induced intracellular TG and lipid accumulation. In addition, its protective mechanisms might be associated with the activity to regulate the AMPK and NLRP3 signaling pathways. Our findings will provide a scientific basis for the clinical application of Man to treat or precaution NAFLD in the future.

## Data Availability

The data used to support the findings of this study are included within the article.

## Conflicts of Interest

The authors report no conflict of interest.

## Authors' Contributions

Zhang Yong and Lu Weiying designed this study and completed the data analysis, drafted all figures, and wrote of the manuscript. Wang Ruiqi, Yao Hongji, Jiang Chenzuo, and Zhou Yu performed the experiment and data collection. Zhang Xiaopo and Ma Ning revised the manuscript. All authors read and agreed with the final manuscript. Zhang Yong and Wang Ruiqi contributed equally to this paper.

## Acknowledgments

This work was financially supported by the Hainan Provincial Natural Science Foundation of China (819QN226), the Key Scientific Research Projects of Higher Education in Hainan Province (Hnky2019ZD-32), the Key Research and Development Program of Hainan Province (No. ZDYF2019157), and the National Natural Science Foundation of China (82060778 and 81760628).

## References

[1] M. Malaguarnera, M. di Rosa, F. Nicoletti, and L. Malaguarnera, "Molecular mechanisms involved in NAFLD progression," *Journal of Molecular Medicine*, vol. 87, no. 7, pp. 679–695, 2009.

[2] L. C. Katzelnick, L. Gresh, M. E. Halloran et al., "Antibody-dependent enhancement of severe dengue disease in humans," *Science*, vol. 358, no. 6365, pp. 929–932, 2017.

[3] Z. Younossi, Q. M. Anstee, M. Marietti et al., "Global burden of NAFLD and NASH: trends, predictions, risk factors and prevention," *Nature Reviews Gastroenterology & Hepatology*, vol. 15, no. 1, pp. 11–20, 2018.

[4] E. Buzzetti, M. Pinzani, and E. A. Tsochatzis, "The multiple-hit pathogenesis of non-alcoholic fatty liver disease (NAFLD)," *Metabolism*, vol. 65, no. 8, pp. 1038–1048, 2016.

[5] M. Huang, H. G. Kim, X. Zhong et al., "Sestrin 3 protects against diet-induced nonalcoholic steatohepatitis in mice through suppression of transforming growth factor $\beta$ signal transduction," *Hepatology*, vol. 71, no. 1, pp. 76–92, 2020.

[6] X. Zhong, M. Huang, H. G. Kim et al., "SIRT6 protects against liver fibrosis by deacetylation and suppression of SMAD3 in hepatic stellate cells," *Cellular and Molecular Gastroenterology and Hepatology*, vol. 10, no. 2, pp. 341–364, 2020.

[7] S. Chen, X. Zhao, J. Wan et al., "Dihydromyricetin improves glucose and lipid metabolism and exerts anti- inflammatory effects in nonalcoholic fatty liver disease: a randomized controlled trial," *Pharmacological Research*, vol. 99, pp. 74–81, 2015.

[8] S. A. Jazayeri-Tehrani, S. M. Rezayat, S. Mansouri et al., "Nano-curcumin improves glucose indices, lipids, inflammation, and Nesfatin in overweight and obese patients with non-alcoholic fatty liver disease (NAFLD): a double-blind randomized placebo-controlled clinical trial," *Nutrition & Metabolism*, vol. 16, no. 1, pp. 1–13, 2019.

[9] C. Wang, J. D. Jiang, W. Wu, and W. J. Kong, "The compound of mangiferin-berberine salt has potent activities in modulating lipid and glucose metabolisms in HepG2 cells," *BioMed Research International*, vol. 2016, no. 5, pp. 1–14, 2016.

[10] C. M. Byrd, D. W. Grosenbach, A. Berhanu et al., "Novel benzoxazole inhibitor of dengue virus replication that targets the NS3 helicase," *Antimicrobial Agents and Chemotherapy*, vol. 57, no. 4, pp. 1902–1912, 2013.

[11] M. P. Gaidhu and R. B. Ceddia, "Remodeling glucose and lipid metabolism through AMPK activation: relevance for treating obesity and type 2 diabetes," *Clinical Lipidology*, vol. 4, no. 4, pp. 465–477, 2009.

[12] B. B. Zhang, G. Zhou, and C. Li, "AMPK: an emerging drug target for diabetes and the metabolic syndrome," *Cell Metabolism*, vol. 9, no. 5, pp. 407–416, 2009.

[13] E. A. Day, R. J. Ford, and G. R. Steinberg, "AMPK as a therapeutic target for treating metabolic diseases," *Trends in Endocrinology & Metabolism*, vol. 28, no. 8, pp. 545–560, 2017.

[14] Y. Ogawa, K. Imajo, Y. Honda et al., "Palmitate-induced lipotoxicity is crucial for the pathogenesis of nonalcoholic fatty liver disease in cooperation with gut-derived endotoxin," *Scientific Reports*, vol. 8, no. 1, pp. 1–14, 2018.

[15] G. C. Farrell, F. Haczeyni, and S. Chitturi, "Pathogenesis of NASH: how metabolic complications of overnutrition favour lipotoxicity and pro-inflammatory fatty liver disease," *Obesity, Fatty Liver and Liver Cancer*, vol. 1061, pp. 19–44, 2018.

[16] Z. Wang, S. Zhang, Y. Xiao et al., "NLRP3 inflammasome and inflammatory diseases," *Oxidative Medicine and Cellular Longevity*, vol. 2020, 11 pages, 2020.

[17] A. di, S. Xiong, Z. Ye et al., "The TWIK2 potassium efflux channel in macrophages mediates NLRP3 inflammasome-induced inflammation," *Immunity*, vol. 49, no. 1, pp. 56–65.e4, 2018.

[18] J. Shi, Y. Zhao, K. Wang et al., "Cleavage of GSDMD by inflammatory caspases determines pyroptotic cell death," *Nature*, vol. 526, no. 7575, pp. 660–665, 2015.

[19] Y. Y. Yuan, S. L. Wang, and L. W. Yuan, "Inflammatory caspase-related pyroptosis: mechanism, regulation and therapeutic potential for inflammatory bowel disease," *Gastroenterology Report*, vol. 6, no. 3, pp. 167–176, 2018.

[20] B. Xu, M. Jiang, Y. Chu et al., "Gasdermin D plays a key role as a pyroptosis executor of non-alcoholic steatohepatitis in humans and mice," *Journal of Hepatology*, vol. 68, no. 4, pp. 773–782, 2018.

[21] J. Wu, S. Lin, B. Wan, B. Velani, and Y. Zhu, "Pyroptosis in liver disease: new insights into disease mechanisms," *Aging and Disease*, vol. 10, no. 5, pp. 1094–1108, 2019.

[22] A. S. Sasdelli, L. Brodosi, and G. Marchesini, "NAFLD-associated hepatocellular carcinoma: a threat to patients with metabolic disorders," *Current Hepatology Reports*, vol. 15, no. 2, pp. 1–10, 2016.

[23] S. Saha, P. Sadhukhan, and P. C. Sil, "Mangiferin: a xanthonoid with multipotent anti-inflammatory potential," *BioFactors*, vol. 42, no. 5, pp. 459–474, 2016.

[24] F. Gold-Smith, A. Fernandez, and K. Bishop, "Mangiferin and cancer: mechanisms of action," *Nutrients*, vol. 8, no. 7, p. 396, 2016.

[25] C. Yon, T. Teramoto, N. Mueller et al., "Modulation of the nucleoside triphosphatase/RNA helicase and 5′-RNA triphosphatase activities of dengue virus type 2 nonstructural protein 3 (NS3) by interaction with NS5, the RNA-dependent RNA polymerase," *The Journal of Biological Chemistry*, vol. 280, no. 29, pp. 27412–27419, 2005.

[26] L. Na, Q. Zhang, S. Jiang et al., "Mangiferin supplementation improves serum lipid profiles in overweight patients with hyperlipidemia: a double-blind randomized controlled trial," *Scientific Reports*, vol. 5, p. 10344, 2015.

[27] J. I. Beier and J. M. Banales, "Pyroptosis: an inflammatory link between NAFLD and NASH with potential therapeutic implications," *Journal of Hepatology*, vol. 68, no. 4, pp. 643–645, 2018.

[28] S. Joshi-Barve, S. S. Barve, K. Amancherla et al., "Palmitic acid induces production of proinflammatory cytokine interleukin-8 from hepatocytes," *Hepatology*, vol. 46, no. 3, pp. 823–830, 2007.

[29] G. Musso, M. Cassader, and R. Gambino, "Non-alcoholic steatohepatitis: emerging molecular targets and therapeutic strategies," *Nature Reviews. Drug Discovery*, vol. 15, no. 4, pp. 249–274, 2016.

[30] M. Pinky Gaidhu and R. B. Ceddia, "Remodeling glucose and lipid metabolism through AMPK activation: relevance for treating obesity and type 2 diabetes," *Clinical Lipidology*, vol. 4, no. 4, pp. 465–477, 2009.

[31] H.-W. Chao, S. W. Chao, H. Lin, H. C. Ku, and C. F. Cheng, "Homeostasis of glucose and lipid in non-alcoholic fatty liver disease," *International Journal of Molecular Sciences*, vol. 20, no. 2, p. 298, 2019.

[32] P. Apontes, Z. Liu, K. Su et al., "Mangiferin stimulates carbohydrate oxidation and protects against high fat diet induced metabolic disorders," *Diabetes*, 2014.

[33] Y. Shao, G. Yuan, J. Zhang, and X. Guo, "Liraglutide reduces lipogenetic signals in visceral adipose of db/db mice with AMPK activation and Akt suppression," *Drug Design Development & Therapy*, vol. 2015, no. 9, pp. 1177–1184, 2015.

[34] A. M. Fritzen, A. M. Lundsgaard, A. B. Jordy et al., "New Nordic diet-induced weight loss is accompanied by changes in metabolism and AMPK signaling in adipose tissue," *Journal of Clinical Endocrinology & Metabolism*, vol. 100, no. 9, pp. 3509–3519, 2015.

[35] D. De Nardo and E. Latz, "NLRP3 inflammasomes link inflammation and metabolic disease," *Trends in Immunology*, vol. 32, no. 8, pp. 373–379, 2011.

[36] C. Lebeaupin, E. Proics, C. H. D. de Bieville et al., "ER stress induces NLRP3 inflammasome activation and hepatocyte death," *Cell Death & Disease*, vol. 6, no. 9, article ???, 2015.

[37] A. Wree, M. D. McGeough, C. A. Peña et al., "NLRP3 inflammasome activation is required for fibrosis development in NAFLD," *Journal of Molecular Medicine (Berlin, Germany)*, vol. 92, no. 10, pp. 1069–1082, 2014.

[38] F. Angelico, M. Del Ben, R. Conti et al., "Insulin resistance, the metabolic syndrome and non alcoholic fatty liver disease (NAFLD)," *Nutrition Metabolism & Cardiovascular Diseases*, vol. 13, no. 5, p. 327, 2003.

[39] N. Ikarashi, T. Toda, T. Okaniwa, K. Ito, W. Ochiai, and K. Sugiyama, "Anti-obesity and anti-diabetic effects of acacia polyphenol in obese diabetic KKAy mice fed high-fat diet," *Evidence-Based Complementary and Alternative Medicine*, vol. 2011, no. 5, 10 pages, 2011.

Hindawi
Journal of Immunology Research
Volume 2021, Article ID 4973589, 13 pages
https://doi.org/10.1155/2021/4973589

*Research Article*

# Dysbiosis of Gut Microbiota Promotes Hepatocellular Carcinoma Progression by Regulating the Immune Response

**Nan Zhang,[1] Yusong Gou,[2] Shan Liang,[2] Ning Chen,[1] Yali Liu,[2] Qiushui He ,[1,3] and Jing Zhang [2]**

[1]*Department of Medical Microbiology, Capital Medical University, No. 10, Youwai Xitoutiao Street, Fengtai District, Beijing 100069, China*
[2]*The Third Unit, Department of Hepatology, Beijing Youan Hospital, Capital Medical University, No. 8 Youwai Xitoutiao Street, Fengtai District, Beijing 100069, China*
[3]*Department of Medical Microbiology, University of Turku, Kiinamyllynkatu 10, Turku 20520, Finland*

Correspondence should be addressed to Qiushui He; qiushui.he@utu.fi and Jing Zhang; zjyouan@ccmu.edu.cn

Received 10 July 2021; Revised 3 September 2021; Accepted 24 September 2021; Published 20 October 2021

Academic Editor: Lifei Wang



*Background and Aim*. Dysbiosis of gut microbiota is important in the development of hepatocellular carcinoma (HCC). However, little is known about whether and how dysbiosis impacts HCC progression. This cross-sectional study is aimed at evaluating microbiome dysbiosis, gut damage, and microbial translocation in different stages of HCC. *Method*. This study included 74 Chinese male patients with HCC. They were divided into early ($n = 19$), intermediate ($n = 37$), and terminal ($n = 18$) groups, referred to as Barcelona Clinic Liver Cancer stage 0+A, B, and C+D, respectively. Paired fecal and plasma samples were collected. Microbial composition and profiles were analyzed by 16S rRNA gene sequencing. The levels of gut damage marker (regenerating islet-derived protein 3$\alpha$ (REG3$\alpha$)) and microbial translocation markers (soluble CD14 (sCD14), lipopolysaccharide-binding protein (LBP), peptidoglycan recognition proteins (PGRPs)) were determined in plasma samples of patients by ELISA. Twenty plasma cytokine and chemokines were determined by Luminex. *Results*. In early, intermediate, and terminal groups, the abundance of the *Bifidobacteriaceae* family decreased significantly (3.52%, 1.55%, and 0.56%, respectively, $P = 0.003$), while the abundance of the *Enterococcaceae* family increased significantly (1.6%, 2.9%, and 13.4%, respectively, $P = 0.022$). Levels of REG3$\alpha$ and sCD14 were markedly elevated only in the terminal group compared with the early ($P = 0.025$ and $P = 0.048$) and intermediate groups ($P = 0.023$ and $P = 0.046$). The level of LBP significantly increased in the intermediate ($P = 0.035$) and terminal ($P = 0.025$) groups compared with the early group. The PGRP levels were elevated only in the terminal group compared with the early group ($P = 0.018$). The ratio of *Enterococcaceae* to *Bifidobacteriaceae* was significantly associated with the levels of REG3$\alpha$, LBP, sCD14, and PGRPs. With HCC progression, increased levels of inflammatory cytokines accompanied by a T cell-immunosuppressive response and microbial translocation were observed. *Conclusion*. Gut microbiota compositional and functional shift, together with elevated gut damage and microbial translocation, may promote HCC development by stimulating inflammatory response and suppressing T cell response.

## 1. Introduction

Hepatocellular carcinoma (HCC) is the third leading cause of cancer mortality worldwide [1]. However, the underlying mechanism is poorly understood. Recently, increasing evidence has indicated the relationship between dysbiosis of gut microbiome and HCC development [2–4]. However, there has been only one report in which the abundance of proinflammatory bacteria *Enterobacteriaceae* tended to increase parallelly with the progression of HCC [5]. The findings demonstrated that microbiota dysbiosis could regulate the innate immune system and advance liver disease [6–8].

Besides microbiome dysbiosis, gut permeability was also found to correlate with HCC. A recent study reported that gut permeability was significantly higher in patients with

HCC compared with healthy individuals [9]. The effect of microbial translocation on cirrhosis was well studied [10], but was not researched in HCC. Therefore, this cross-sectional study is aimed at evaluating microbiome dysbiosis, gut damage, and microbial translocation in 74 male patients in different stages of HCC. The levels of cytokines, which reflect inflammation and immune response, were also measured. It was speculated that dysbiosis together with increased microbial translocation might impact HCC progression by regulating systemic inflammation and immune response.

## 2. Materials and Methods

*2.1. Patient Selection.* Patients with HCC admitted to Beijing Youan Hospital from June 2018 to September 2019 were recruited in this study. The study was approved by the ethics committee of Beijing Youan Hospital, Capital Medical University (No. 2018-038). All patients provided written informed consents.

The diagnosis of HCC was made following the international guidelines [11]. The inclusion criteria were as follows: HCC; age ≥ 18 years; male sex; and hepatitis B virus (HBV) surface antigen-positive or anti-hepatitis C virus (anti-HCV) antibody positive. The exclusion criteria were as follows: patients suffering from other causes of liver diseases, such as nonalcoholic fatty liver disease, alcoholic liver disease, and cholestatic liver disease. Patients with irritable bowel syndrome or inflammatory bowel disease; other cancers besides HCC; and autoimmune disease or serious cardiac, kidney, and respiratory diseases were also excluded. No antibiotic, probiotic, and immunosuppressive drugs were taken within 2 weeks before sample collection.

HCC was staged according to the Barcelona Clinic Liver Cancer (BCLC) staging system [12]. Stage 0 referred to single nodule < 2 cm and Child-Pugh A. Stage A was defined as single or three nodules < 3 cm and Child-Pugh A or B. Stage B referred to patients with multinodules and Child-Pugh A or B. Stage C comprised patients with portal invasion or extrahepatic spread and Child-Pugh A or B. Stage D included patients with HCC and Child-Pugh C. In the present study, patients with HCC were divided into early, intermediate, and terminal groups, which referred to stage 0+A, B, and C+D, respectively.

*2.2. Fecal Sample Collection, DNA Extraction, and Polymerase Chain Reaction Sequencing.* Each fresh fecal sample was split into two tubes containing bacterial RNA LOCKER (Youkang, Nanjing, China) and stored at -80°C. Total bacterial DNA was isolated from stool samples using the QIAamp Fast DNA Stool Mini Kit (Qiagen, Hilden, Germany) following the manufacturer's instructions and diluted to 1 ng/$\mu$L using sterile water. The V4-V5 regions of the prokaryotic 16S rRNA gene were amplified using the universal primer pair 515F (5′-GTGYCAGCMGCCGCGGTA-3′) and 909R (5′-CCCCGYCAATTCMTTTRAGT-3′) with barcode and then sequenced and analyzed [13]. The reason to choose the V4-V5 regions was that we also wanted to detect low abundant bacteria in the samples [5, 14]. Paired stool samples from 20 patients were sequenced to validate the results. Sequencing libraries were generated using TruSeq DNA Polymerase Chain Reaction- (PCR-) Free Sample Preparation Kit (Illumina, USA), and index codes were added. The amplification products were sequenced on an Illumina HiSeq 2500 platform, and 250 bp paired-end reads were generated. Sequencing data were analyzed using Quantitative Insights into Microbial Ecology (QIIME) platform version 1.9 and R v3.3.1 [15]. The paired-end reads from the DNA fragments were merged using FLASH (v1.2.7) [16].

*2.3. Operational Taxonomy Unit Clustering and Taxonomy Annotation.* Sequences with more than 97% similarity were assigned to the same operational taxonomy units (OTUs). OTU classification was conducted by running a Basic Local Alignment Search Tool (BLAST) search against the Greengenes database using the representative sequence set as a query. A representative sequence for each OTU was screened for further annotation. The sequences were annotated using RDP classifier V.2.6 according to the developer's documents (http://rdp.cme.msu.edu/classifier/class_help.jsp#conf) [17].

*2.4. Bacterial Diversity Analysis.* Bacterial diversity was determined by sampling-based OTU analysis. It is presented by Observed species index, Chao1 index, Shannon index, and Simpson index, all of which were calculated using the R vegan program package [18].

*2.5. Structure of Microbial Communities and OTU Biomarker Identification.* Principal component analysis (PCA) was conducted by R package (http://www.R-project.org/). The weighted and unweighted UniFrac distances were calculated with the phyloseq package [19]. The linear discriminant analysis (LDA) effect size (LEfSe) model was used to identify differences in microbiota composition for phylotypes [20]. Based on the normalized relative abundance matrix, taxa with significantly different abundances were determined by LEfSe using Kruskal-Wallis rank sum test.

*2.6. Determination of Plasma Biomarkers of Gut Damage and Microbial Translocation.* The plasma marker of gut damage, regenerating islet-derived protein (REG3$\alpha$), was determined using the ELISA kit (R&D Systems, ON, Canada). Soluble CD14 (sCD14), lipopolysaccharide-binding protein (LBP), and peptidoglycan recognition proteins (PGRPs) were selected as microbial translocation markers. The ELISA kits were Human CD14 Quantikine ELISA kit (Bio-Techne Ltd., Abingdon, United Kingdom), Human LBP DuoSet ELISA kit (Bio-Techne Ltd.), and Human PGRPs ELISA kit (Thermo Fisher, Merelbeke, Belgium). All assays were performed in duplicate following the manufacturer's protocol.

*2.7. Determination of Plasma Cytokines and Chemokines.* An inflammation 20-Plex Human ProcartaPlex Panel (EPX200-12185-901, Affymetrix eBioscience, Vienna, Austria) was used to detect the expression of 20 cytokines and chemokines. They were granulocyte colony-stimulating factor (GM-CSF), intercellular cell adhesion molecule-1 (ICAM-

1), interferon-$\alpha$ (IFN-$\alpha$), IFN-$\gamma$, interleukin-1$\alpha$ (IL-1$\alpha$), IL-1$\beta$, IL-4, IL-6, IL-8, IL-10, IL-12p70, IL-13, IL-17A, interferon-induced protein-10 (IP-10), monocyte chemoattractant protein-1 (MCP-1), macrophage inflammatory protein 1$\alpha$ (MIP-1$\alpha$), MIP-1$\beta$, sE-selectin, sP-selectin, and tumor necrosis factor-$\alpha$ (TNF-$\alpha$).

*2.8. Statistical Analysis.* One-way analysis of variance was used to evaluate the differences among the three groups. Continuous variables were compared using the Wilcoxon rank sum test between the two groups. Fisher's exact test compared categorical variables. Correlations were performed using a nonparametric Spearman test. A two-sided $P$ value < 0.05 indicated a significant difference. The threshold logarithmic LDA score for discriminative features was 2. Statistical analyses were conducted using GraphPad Prism 6.0 (La Jolla, CA, USA). Multivariate analysis was performed using SPSS 24.0 (IBM SPSS). Correlations analysis was performed by R i386 software (v.4.0.5).

In addition, an index was introduced to measure the degree of dysbiosis. This index was calculated based on the ratio of the relative abundance of *Enterococcaceae* family to that of *Bifidobacteriaceae* family. The ratio was calculated as follows:

$$\text{Ratio} = \frac{\log_{10}(100 \times Enterococcaceae + 1)}{\log_{10}(100 \times Bifidobacteriaceae + 1)}. \quad (1)$$

## 3. Results

*3.1. Patient Characteristics.* Altogether, 74 male patients with HCC were included. The average age was 61.00 (53.00–65.00) years. Of them, the early group included 7 patients with stage 0 and 12 with stage A HCC; the intermediate group included 37 patients with stage B HCC; and the terminal group included 8 patients with stage C and 10 with stage D HCC. Among them, 37 patients had HBV and the others had HCV. The demographics and laboratory results are listed in Table 1 and Supplementary Table 1.

*3.2. Gut Microbial Diversity Decreased with HCC Progression.* The OTU number in early, intermediate, and terminal groups was 322 ± 68, 314 ± 76, and 303 ± 66, respectively. Observed species and Chao1 indexes decreased significantly from early to intermediate and terminal groups (Observed species, $P = 0.023$ and 0.038; Chao1, $P = 0.013$ and 0.042; Figures 1(a) and 1(b)), while evenness reduced (Shannon, $P = 0.027$ and 0.039; Simpson, $P = 0.017$ and 0.028; Figures 1(c) and 1(d)). The results suggested that the alterations of OTUs were evenly contributed with HCC progression.

*3.3. Gut Microbial Profiles and Compositions Shifted with HCC Progression.* The PCA of the $\beta$-diversity index allowed a separation between any two groups, suggesting that the bacterial profiles of each group were distinguished (Figure 1(e)). The different taxa among the three groups identified by LDA analysis are summarized in Figure 1(f). And the ratio of *Enterococcaceae* to *Bifidobacteriaceae* family significantly increased from the early group to the terminal group (1.5 vs. 9.6, $P = 0.034$; Figure 1(g)). The abundance of *Actinobacteria* phylum (4.46% vs. 0.88%, $P = 0.020$; Figure 2(a)), *Bifidobacteriaceae* family (3.52% vs. 0.56%, $P = 0.003$; Figure 2(b)), and *Bifidobacterium* genus (3.51% vs. 0.56%, $P = 0.003$; Figure 2(c)) significantly decreased in the terminal group compared with the early group. Meanwhile, the abundance of *Enterococcaceae* (1.6% vs. 13.4%, $P = 0.022$), *Enterococcus* genus (1.6% vs. 13.4%, $P = 0.022$), and *Enterobacteriaceae* family (7.7% vs. 10.3%, $P = 0.046$) markedly increased with disease progression. *Lachnospiraceae*, *Peptostreptococcaceae*, unidentified *Clostridiales*, *Coriobacteriaceae*, and *Christensenellaceae* families were enriched in the early group; however, they significantly decreased or were even undetectable in the terminal group (all $P$ values < 0.05). Correspondingly, at the genus level, five genera belonging to the *Lachnospiraceae* family (*Blautia*, *Fusicatenibacter*, *Agathobacter*, *Anaerostipes*, and *Dorea*), one genus belonging to the *Clostridiales* family (unidentified *Clostridiales)*, and two genera belonging to the *Peptostreptococcaceae* family (*Romboutsia* and *Intestinibacter*) were also enriched in the early group and decreased or were even undetectable in the terminal group. All the alterations of the short-chain fatty acid- (SCFA-) producing bacteria mentioned earlier contributed to the decrease in richness along with HCC progression.

*3.4. Gut Damage Increased in Patients in the Terminal Group.* REG3$\alpha$ is a well-known marker of gut damage [21]. The plasma levels of REG3$\alpha$ significantly increased in patients in the terminal group (17,830 ± 3257 pg/mL) than in the early (11,591 ± 2388 pg/mL, $P = 0.025$) and intermediate groups (10,881 ± 2298 pg/mL, $P = 0.023$; Figure 3(a)).

*3.5. Plasma Levels of Microbial Translocation Markers Elevated in Patients in the Terminal Group.* Plasma sCD14 elevated in the terminal group (1504 ± 174 ng/mL) compared with the early (1148 ± 100 ng/mL, $P = 0.048$) and intermediate groups (1115 ± 53 ng/mL, $P = 0.046$; Figure 3(b)). The LBP level elevated in the intermediate (3984 ± 412 ng/mL) and terminal groups (4037 ± 911 ng/mL) compared with the early group (2818 ± 488 ng/mL, $P = 0.035$ and 0.025; Figure 3(c)). The PGRP level significantly increased in the terminal group (20.01 ± 2.17 ng/mL) compared with the early group (13.41 ± 1.62 ng/mL, $P = 0.018$; Figure 3(d)).

*3.6. Cytokine and Chemokine Levels.* The T cell immune response-related cytokines and chemokines, including IFN-$\gamma$, IL-4, IL-12p70, IL-13, and IL-17A, showed a decreased tendency from the early to the intermediate and terminal groups, but with no significant differences. The MCP-1 level decreased significantly in the terminal group (74.69 ng/mL) compared with the early (108.26 ng/mL, $P = 0.005$) and intermediate groups (90.70 ng/mL, $P = 0.015$; Figure 4(a)). The levels of chemokines, including GM-CSF, sE-selectin, and sP-selectin, tended to decrease in the terminal group without significant differences. The levels of other proinflammatory cytokines, including IL-1$\alpha$, IL-6, IL-10, IP-10,

Table 1: Clinical characteristics of patients with hepatocellular carcinoma (HCC).

| Clinical and pathological indexes | Early group ($n = 19$) | Intermediate group ($n = 37$) | Terminal group ($n = 18$) | p1# | p2# | p3# |
|---|---|---|---|---|---|---|
| Age (years) | 61.00 (53.00-65.00) | 59.00 (53.00-63.00) | 59.00 (47.75-65.75) | 1 | 1 | 1 |
| ALT (U/L) | 30.10 (22.40-39.30) | 30.20 (18.85-45.35) | 42.15 (27.90-57.28) | 1 | 0.462 | 0.148 |
| AST (U/L) | 31.30 (25.50-45.00) | 36.50 (26.65-55.95) | 65.45 (52.43-122.50) | 1 | **<0.001** | **<0.001** |
| TBIL ($\mu$mol/L) | 18.50 (15.40-30.10) | 25.90 (14.35-42.90) | 57.00 (34.55-155.50) | 1 | **0.001** | **0.005** |
| DBIL ($\mu$mol/L) | 9.50 (5.90-14.00) | 10.80 (7.70-16.55) | 35.45 (19.78-144.20) | 0.905 | **<0.001** | **0.001** |
| GGT (U/L) | 38.85 (19.00-68.50) | 57.30 (38.40-123.80) | 164.90 (92.53-240.30) | 0.684 | **<0.001** | **0.003** |
| ALP (U/L) | 79.75 (60.90-99.53) | 97.30 (77.40-115.70) | 158.55 (120.80-271.50) | 0.276 | **<0.001** | **<0.001** |
| ALB (g/L) | 34.40 (30.50-40.30) | 34.40 (31.60-38.00) | 32.05 (27.18-35.10) | 1 | 0.202 | 0.152 |
| CRE ($\mu$mol/L) | 67.60 (52.40-77.60) | 61.40 (52.35-66.90) | 66.90 (53.93-85.65) | 0.669 | 1 | 0.223 |
| CHE (U/L) | 3866.50 (2975.00-5406.00) | 3651.00 (3001.00-4964.00) | 1764.50 (1289.00-2892.00) | 1 | **<0.001** | **<0.001** |
| TBA ($\mu$mol/L) | 34.00 (14.23-42.25) | 19.30 (6.90-57.10) | 53.00 (27.00-133.70) | 1 | 0.097 | **0.006** |
| WBC (10*E*4/L) | 3.68 (1.91-4.47) | 4.20 (2.69-5.57) | 5.06 (3.37-6.39) | 0.25 | **0.041** | 0.25 |
| HGB (g/L) | 129.00 (109.00-138.00) | 123.00 (105.00-149.00) | 105.00 (96.25-132.50) | 0.473 | 0.26 | 0.398 |
| PLT (10*E*9/L) | 87.00 (57.50-97.50) | 82.00 (53.5-119.50) | 93.50 (47.00-148.50) | 1 | 1 | 1 |
| INR | 1.21 (1.07-1.39) | 1.19 (1.09-1.36) | 1.20 (1.11-1.32) | 1 | 1 | 1 |
| MELD score | 60.47 (56.36-62.13) | 60.12 (56.90-63.55) | 64.71 (62.23-67.03) | 1 | 0.307 | 0.408 |
| Child-Pugh | | | | | | |
| A | 13 (0.684) | 21 (0.568) | 1 (0.056) | 0.397 | **<0.001** | **<0.001** |
| B | 6 (0.316) | 16 (0.432) | 7 (0.389) | 0.397 | 0.737 | 0.759 |
| C | 0 (0.000) | 0 (0.000) | 10 (0.556) | — | **<0.001** | **<0.001** |

One-way analysis of variance was used to evaluate the difference among the three groups. Continuous variables were compared using Wilcoxon rank sum test between the two groups. Fisher's exact test compared categorical variables. ALT: alanine aminotransferase; AST: aspartate aminotransferase; TBIL: total bilirubin; DBIL: direct bilirubin; GGT: gamma glutamyl transpeptidase; ALP: alkaline phosphatase; ALB: albumin; CRE: creatinine; CHE: cholinesterase; TBA: total serum bile acid; WBC: white blood count; HGB: hematoglobin; PLT: platelets; INR: prothrombin time international standardized ratio; MELD: model for end-stage liver disease. Values indicate median and 25%-75% percentile. #p1 referred to early vs. intermediate, p2 referred to early vs. terminal, and p3 referred to intermediate vs. terminal.

MIP-1$\alpha$, and MIP-1$\beta$, increased in the terminal group, but showed no significant difference. The IL-8 level significantly increased in the terminal group (16.31 ng/mL) compared with the early (7.42 ng/mL, $P = 0.04$) and intermediate groups (6.80 ng/mL, $P = 0.004$; Figure 4(b)). These results suggested that HCC progression was characterized by an elevated inflammatory response and suppressed T cell immune responses. The plasma levels of 20 cytokines and chemokines are summarized in Supplementary Table 2.

*3.7. Relationship between HCC Progression, Gut Damage, Microbial Translocation, and Inflammatory Cytokines in Patients with HCC.* The IL-6 and IL-8 levels positively correlated with markers of microbial translocation, but did not correlate with REG3$\alpha$ or bacterial changes. The IL-6 level positively correlated with the sCD14 level ($r = 0.299$, $P = 0.015$) and the LBP level ($r = 0.261$, $P = 0.034$; Figures 5(a) and 5(b)). They were markers of Gram-negative bacterial translocation. The IL-8 level correlated with the sCD14 ($r = 0.347$, $P = 0.004$) and PGRP ($r = 0.411$, $P = 0.001$; Figures 5(c) and 5(d)) levels, which was a marker of Gram-positive bacterial translocation. The MCP-1 level inversely correlated with the LBP ($r = -0.296$, $P = 0.016$) and PGRP levels ($r = -0.245$, $P = 0.047$; Figures 5(e) and 5(f)). No correlation was found between plasma TNF-$\alpha$ level and any of the aforementioned indexes.

*3.8. The Ratio of Enterococcaceae to Bifidobacteriaceae Correlated with the Levels of REG3α and Markers of Bacterial Translocation.* Both $\alpha$-diversity and $\beta$-diversity could distinguish terminal HCC groups from the other two groups, so did gut damage and microbial translocation markers. Hence, whether gut-associated microbiota changes correlated with the loss of gut barrier integrity and circulating microbial translocation during HCC progression was evaluated. The LDA level revealed a decreased abundance of *Bifidobacteriaceae* family and increased abundance of *Enterococcaceae* family along with HCC progression. The ratio of *Enterococcaceae* to *Bifidobacteriaceae* was associated with the expression of gut damage marker REG3$\alpha$ ($r = 0.366$, $P = 0.003$) and bacterial translocation markers, sCD14 ($r = 0.322$, $P = 0.008$), LBP ($r = 0.386$, $P = 0.001$), and PGRP ($r = 0.405$, $P = 0.001$; Table 2). However, the ratio did not correlate with levels of IL-6 and IL-8.

## 4. Discussion

The findings of this study first showed that alterations in gut microbiota, elevated gut damage, and bacterial translocation were associated with HCC progression. Gut dysbiosis of HCC was characterized by increased abundance of *Enterococcaceae* and *Enterobacteriaceae* and decreased abundance of *Bifidobacteriaceae* and SCFA-producing bacteria.

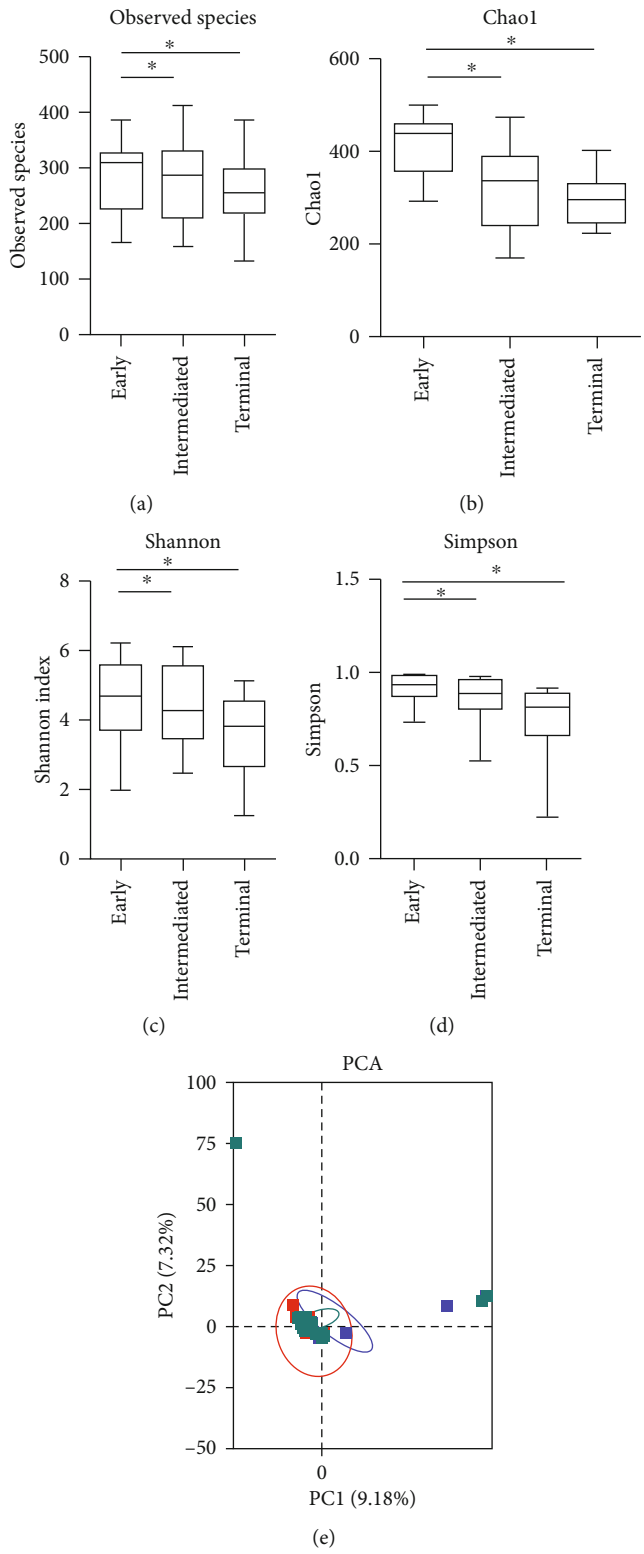


Figure 1: Continued.

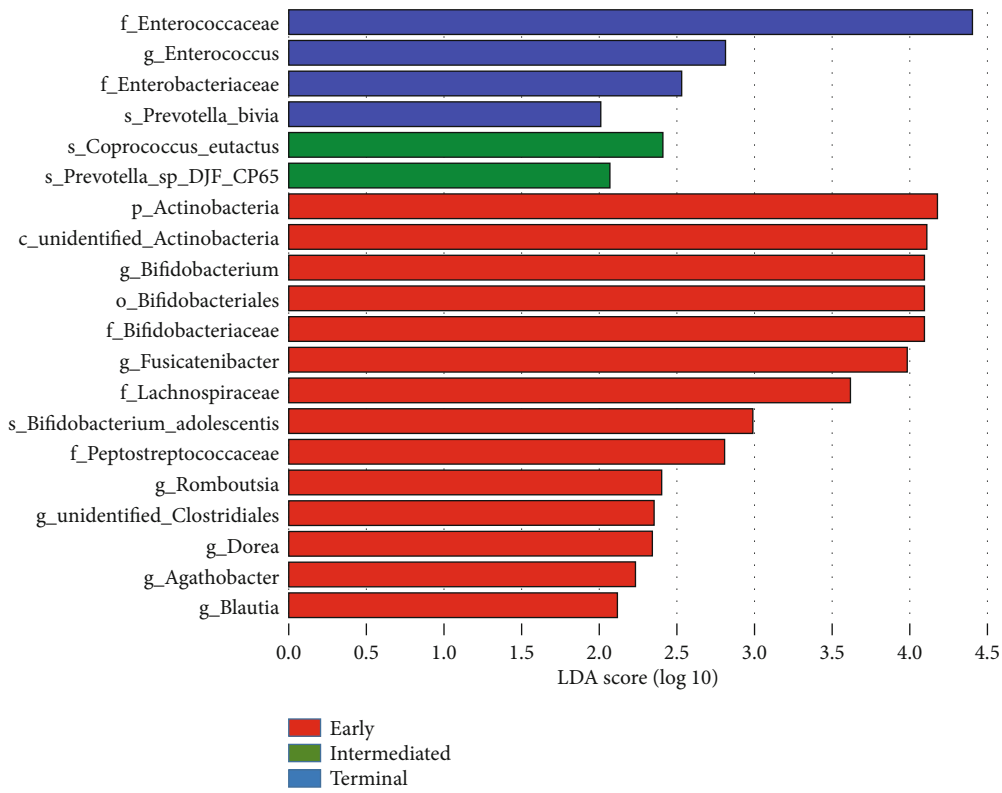


(f)

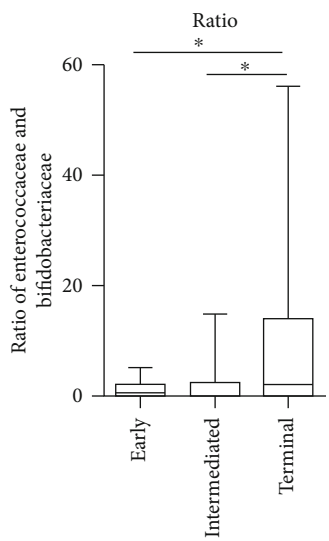


(g)

Figure 1: Gut microbiota richness, profiles, and compositions shifted in patients with hepatocellular carcinoma (HCC) progression. Microbial $\alpha$-diversity showed decreased (a) Observed species and (b) Chao1 index in patients with HCC progression, indicating reduced richness. (c) Shannon index and (d) Simpson index decreased significantly with HCC progression. This diminished number of bacteria was accompanied by decreased evenness. The box plots show the smallest and largest values, 25% and 75% quartiles, the median, and outliers. Significant difference ($P < 0.05$) was indicated by an asterisk. (e) Comparison of principal component analysis (PCA) using weighted UniFrac distance showed that the overall fecal microbiota composition ($\beta$-diversity) distinguished bacterial profiles among early, intermediate, and terminal groups of patients with HCC. Each dot represented one sample, and the distance between the samples represented the difference in community composition of the samples. (f) Histogram of the linear discriminant analysis (LDA) scores for differentially abundant taxa among patients with HCC in the early, intermediate, and terminal groups. Red indicates early group HCC, green indicates intermediated group HCC, and blue indicates terminal group HCC. (g) Change in the ratio of *Enterococcaceae* to *Bifidobacteriaceae* with HCC progression.

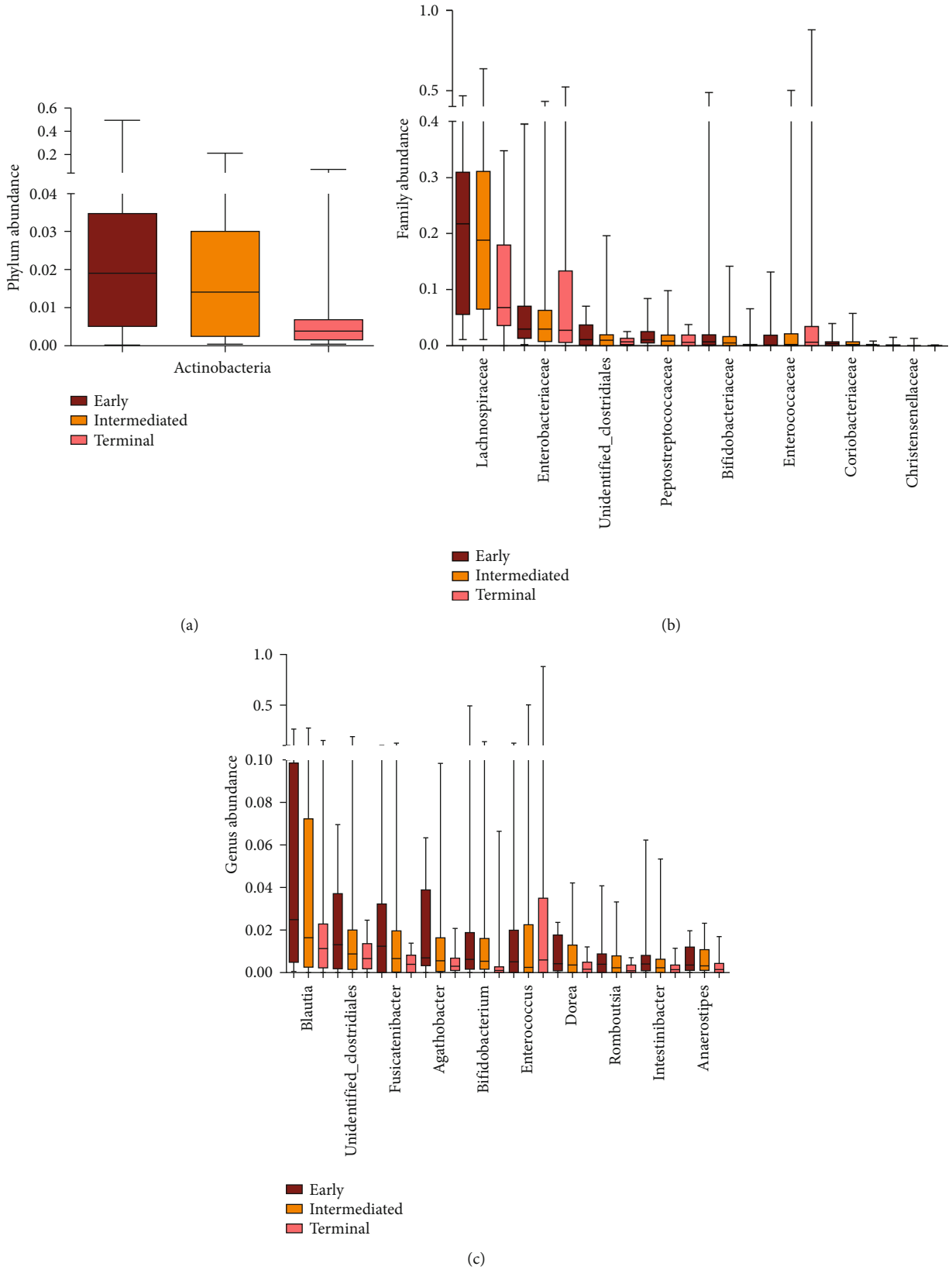


Figure 2: Difference in the abundance of gut microbiota in patients with different groups at the (a) phylum level, (b) family level, and (c) genus level. The difference in the abundance of presented taxon was significant (all $P$ values were less than 0.05). The box presented the 95% confidence intervals; the line inside denoted the median, and the symbol "+" denoted the mean value. Red indicates early group HCC, orange indicates intermediated group HCC, and pink indicates terminal group HCC.

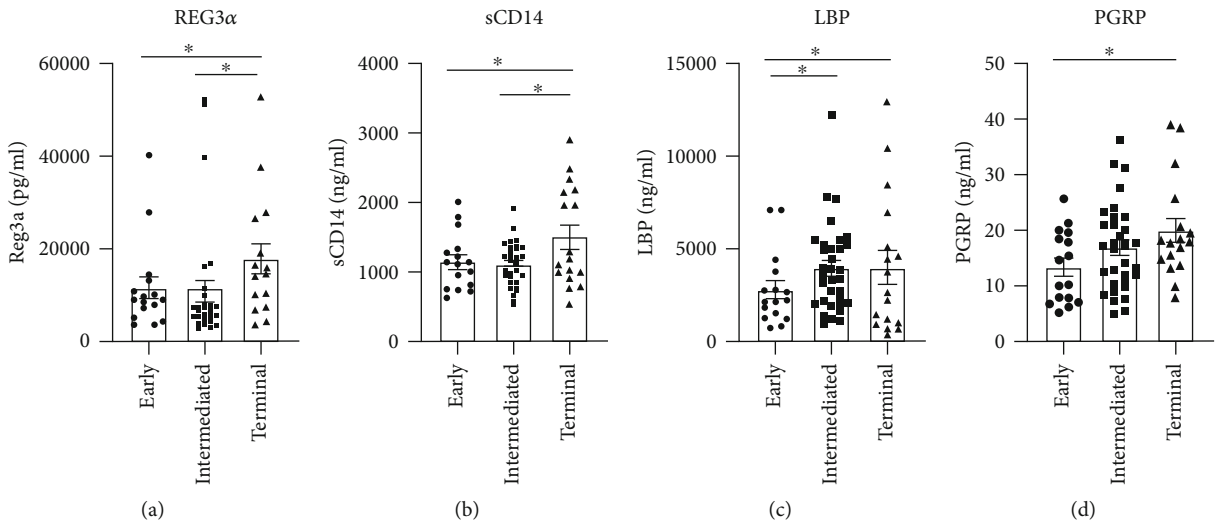


Figure 3: Assessment of gut barrier integrity marker and plasma level of microbial translocation markers in patients with HCC progression. (a) The level of gut damage marker of regenerating islet-derived protein 3$\alpha$ (REG3$\alpha$) significantly increased in patients in the terminal group compared with the early and intermediate groups. The levels of Gram-negative bacterial translocation markers, (b) soluble CD14 (sCD14) and (c) lipopolysaccharide-binding protein (LBP), also elevated in patients with HCC in the terminal group. (d) The levels of Gram-positive translocation marker, peptidoglycan recognition proteins (PGRPs), showed that an increased tendency with HCC progression even significantly elevated in patients with HCC in the terminal group compared with the early group. Each dot represented one sample. Significant difference ($P < 0.05$) was indicated by an asterisk.

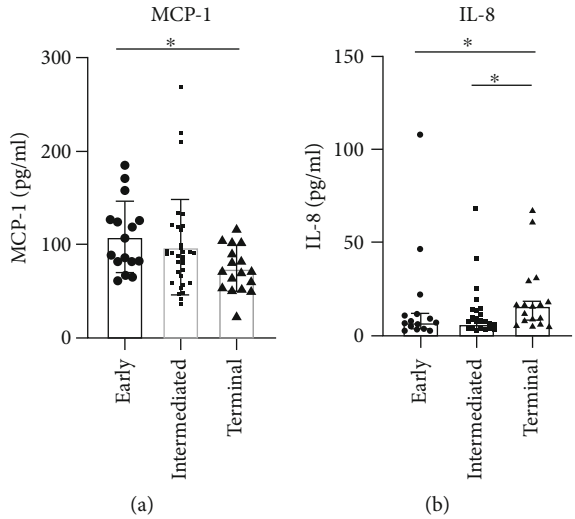


Figure 4: Evaluation of plasma level of inflammatory markers in patients with HCC progression. (a) The plasma level of monocyte chemoattractant protein-1 (MCP-1) showed a decreased tendency with HCC progression, which significantly reduced in the terminal group compared with the early group. (b) The plasma level of IL-8 significantly increased in patients with HCC in the terminal group compared with other groups. Each dot represented one sample. Significant difference ($P < 0.05$) was indicated by an asterisk.

Elevation of inflammatory response and suppression of T cell immunity induced by microbial products might be one of the mechanisms of HCC progression.

The data in the present study showed that gut microbial richness decreased significantly in the terminal group compared with the early group. The decrease in richness was mainly due to the reduction in the abundance of SCFA-producing bacteria. The result was consistent with that of a previous study. The study showed that $\alpha$-diversity significantly reduced in patients with BCLC stage C and D HCC compared with patients in stage A HCC [5]. Another similar study showed that the abundance of SCFA-producing family members declined significantly in patients with HCC compared with patients with hepatitis B [4]. SCFA-producing bacteria are known to participate in the process of fermenting diet fibers to SCFAs [22]. SCFAs are a major energy source of the intestinal enterocytes and are essential for maintaining the tight junction and intestinal barrier integrity [23]. However, in this study, the abundance of SCFA-producing bacteria did not correlate with the expression of

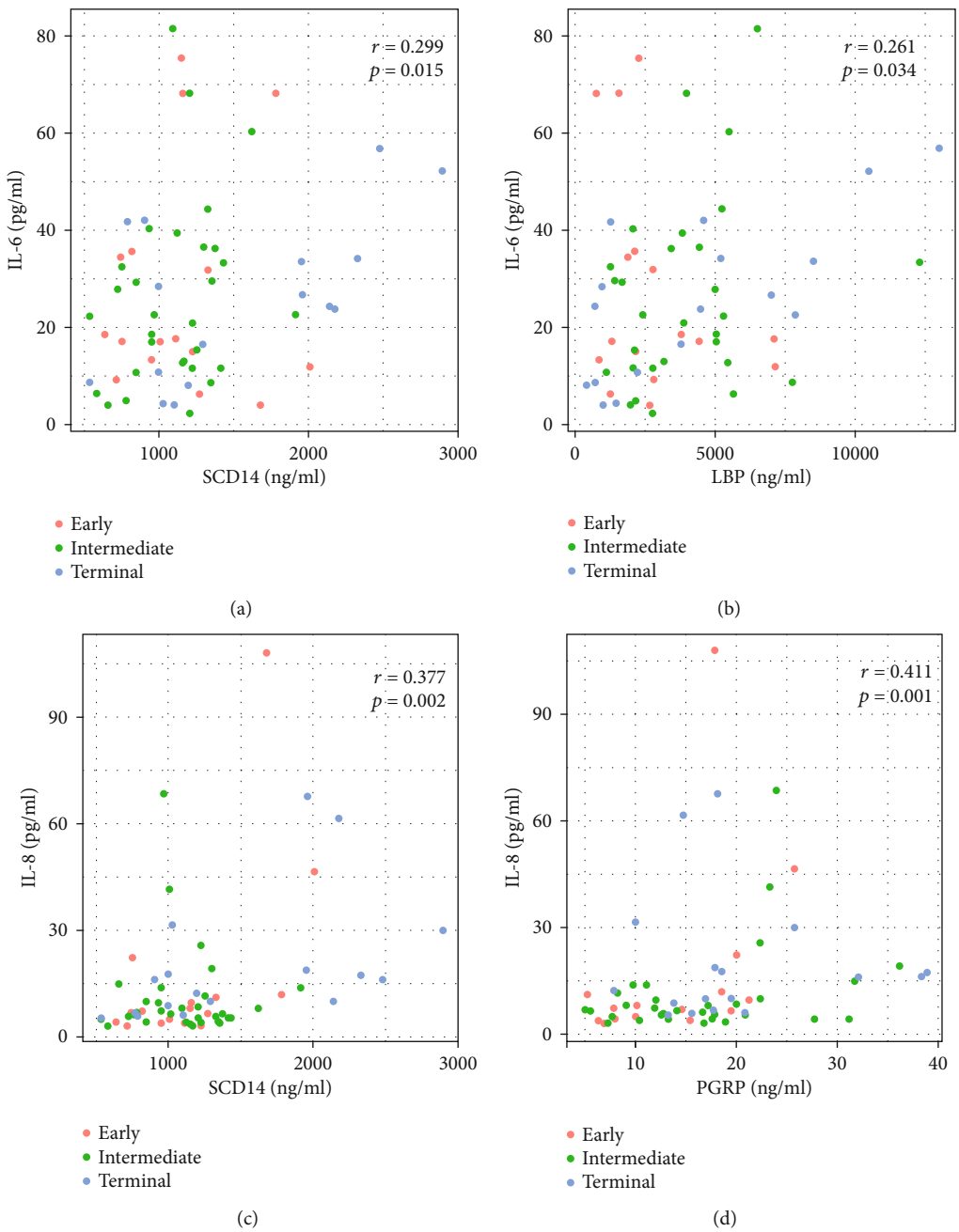


Figure 5: Continued.

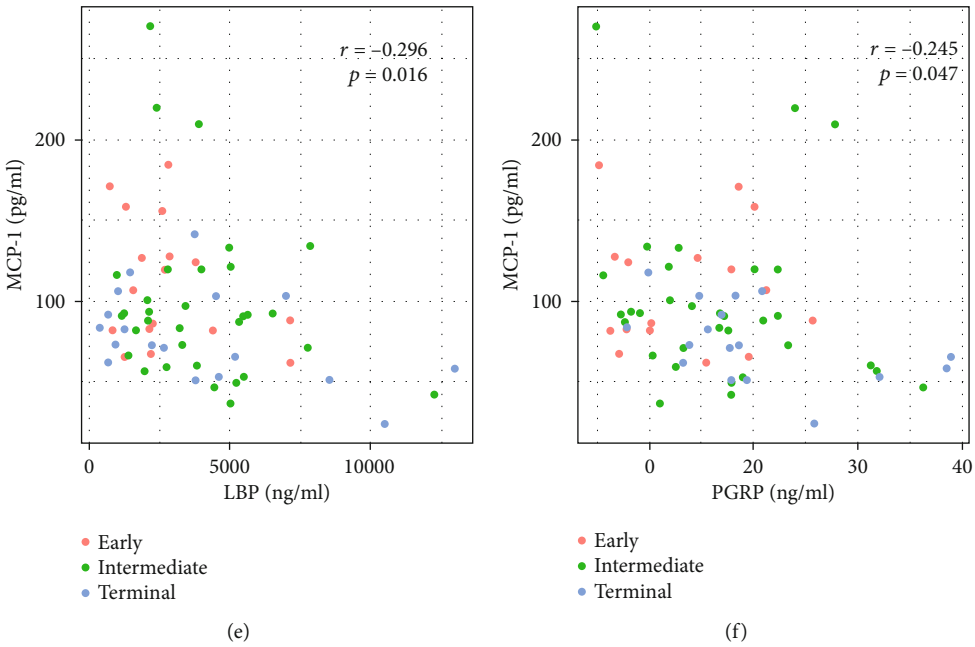


Figure 5: Plasma levels of IL-6, IL-8, and MCP-1 were associated with the markers of microbial translocation. Plasma levels of IL-6 correlated with those of (a) sCD14 and (b) LBP. IL-8 levels correlated with (c) sCD14 and (d) marker of Gram-positive bacterial translocation peptidoglycan recognition proteins (PGRPs). Level of MCP-1 inversely correlated with that of (e) LBP and (f) PGRP. Each dot represented one sample. Red indicates early group HCC, green indicates intermediated group HCC, and blue indicates terminal group HCC.

Table 2: Correlation between the ratio of *Enterococcaceae* and *Bifidobacteriaceae* or different cytokines and plasma levels of REG3$\alpha$ or markers of microbial translocation in HCC patients.

| | Ratio of *Enterococcaceae* and *Bifidobacteriaceae* | IL-6 | IL-8 | MCP-1 |
|---|---|---|---|---|
| REG3$\alpha$ | **$r = 0.366$**<br>**$P = 0.003$** | $r = 0.035$<br>$P = 0.783$ | $r = 0.081$<br>$P = 0.520$ | $r = -0.201$<br>$P = 0.106$ |
| sCD14 | **$r = 0.322$**<br>**$P = 0.008$** | **$r = 0.299$**<br>**$P = 0.015$** | **$r = 0.347$**<br>**$P = 0.004$** | $r = -0.183$<br>$P = 0.142$ |
| LBP | **$r = 0.386$**<br>**$P = 0.001$** | **$r = 0.261$**<br>**$P = 0.034$** | $r = 0.102$<br>$P = 0.414$ | **$r = -0.296$**<br>**$P = 0.016$** |
| PGRP | **$r = 0.405$**<br>**$P = 0.001$** | $r = 0.198$<br>$P = 0.111$ | **$r = 0.411$**<br>**$P = 0.001$** | **$r = -0.245$**<br>**$P = 0.047$** |

MCP-1: monocyte chemoattractant protein-1; REG3$\alpha$: regenerating islet-derived protein 3$\alpha$; sCD14: soluble CD14; LBP: lipopolysaccharide-binding protein; PGRP: peptidoglycan recognition protein.

the serum markers of gut damage and microbial translocation. It was speculated that multiple mechanisms might be involved in SCFA production and did not necessarily depend only on the change in the abundance of SCFA-producing bacteria.

Besides the changes in gut microbiota mentioned earlier, another predominant change was that the abundance of *Bifidobacteriaceae* decreased along with HCC progression accompanied by an increase in the abundance of *Enterococcaceae*. *Bifidobacteria* can reinforce gut barrier function, reduce mucosa inflammation, and protect the liver from injury [24]. Administration of *Bifidobacteria* could mitigate diethylnitrosamine- (DEN-) induced hepatocarcinogenesis in mouse models [25]. *Enterococcus* is regarded as pathogenic bacteria. The overgrowth of *Enterococcus* leads to the release of large amounts of polysaccharide A and LPS, which, in turn, increases gut permeability and facilitates microbial translocation. In this study, the ratio of *Enterococcaceae* to *Bifidobacteriaceae* correlated significantly with the expression of the serum markers of gut damage, microbial translocation, and HCC progression. Therefore, the ratio was considered an ideal quantitative marker of gut dysbiosis in patients with HCC. The ratio of abundance of *Firmicutes* to *Bacteroidetes* [26] or ratio of abundance of genus *Bifidobacterium* to the family *Enterobacteriaceae* was associated with the progression of chronic liver diseases [27]. However, both the ratios were similar among the three groups in this study. More studies should be performed in the future to confirm these results.

The changes in gut damage and microbial translocation biomarkers were subsequently detected due to the close relationship between gut dysbiosis and microbial translocation. REG3$\alpha$ is a C-type lectin antimicrobial peptide secreted into the gut lumen by Paneth cells [28]. REG3$\alpha$ invades into the bloodstream when gut barrier integrity is damaged [29]. Hence, the circulating level of REG3$\alpha$ is well accepted as a marker of gut damage. Previous studies reported that increasing REG3$\alpha$ level was always observed in patients with enteropathies, such as Crohn's and celiac diseases, ulcerative colitis, and graft-versus-host disease [29–31]. The results of this study suggested that gut damage worsened gradually along with HCC progression and facilitated the transfer of

more microbial products into the bloodstream [32, 33]. This study was the first to show the relationship between gut damage and HCC progression.

This study also found that bacterial translocation increased with HCC progression. LBP is a well-known marker of bacterial translocation [34]. sCD14 is a marker of Gram-negative bacterial translocation, which is secreted by activated myeloid cells after LPS stimulation [35]. PGRP is a peptidoglycan recognition protein and a marker of Gram-positive bacterial translocation [10]. The present study results showed an elevation in the levels of the aforementioned markers with HCC progression. Moreover, increased LBP and sCD14 levels correlated with IL-6 levels, while increased sCD14 and PGRP levels correlated with IL-8 levels. In theory, elevated sCD14 and LBP levels indicated increased circulation of LPS. LPS resulted in the release of proinflammatory cytokines, such as IL-6 and IL-8, by T cells. Chronic inflammation contributed to liver damage and HCC progression [36, 37]. Therefore, it is reasonable that bacterial translocation correlated with HCC progression. However, no relationship was found between gut permeability and microbial translocation. This might be due to bacterial translocation via different mechanisms other than gut integrity. On the contrary, the damage of gut barrier alone might also not be sufficient to cause bacterial translocation, unless additional mechanisms in the complex interactions between host and microbes in the gut failed. A similar result was also observed in patients with alcohol use disorder. In this study, no correlation with intestinal permeability marker was observed, although the levels of all the three markers elevated significantly [10].

Another finding of this study was the elevation of inflammatory response profile during HCC progression, represented by IL-6 and IL-8. IL-8 is a key factor in neutrophil recruitment and activation, which also promoted angiogenesis and metastasis [38, 39]. One previous study found that high serum IL-8 was one of the meaningful predictive cytokines in patients with HBV- and HCV-related HCC [40]. Moreover, as a T cell-attracting chemokine, MCP-1 level decreased significantly in the terminal group, indicating a reduction in T cell immune response. The levels of other cytokines, such as IFN-$\gamma$, the signature cytokine of the Th1 cell; IL-4 and IL-13, the signature cytokines of the Th2 cell; and IL-17, the signature cytokine of the Th17 cell, reduced simultaneously but without significant differences. These results reflected comprehensive immunity suppression in terminal HCC. The results were in accordance with an *ex vivo* study. The study showed that bacterial extracts from patients with HCC microbiota elicited a T cell-immunosuppressive phenotype [41]. It is well known that SCFAs could promote and regulate the differentiation and apoptosis of Treg cells [42]. According to the results of a previous study and this study, a distinctive microbiome, characterized by decreased abundance of SCFA-producing bacteria, could modulate the peripheral immune response and result in HCC progression.

One limitation of this study was that no causation relationship could be deduced. Whether the alterations of gut microbial profiles, gut permeability, or bacterial translocation was the reason or the result of HCC progression needs further validation in animal models. The other limitation of this study was the lack of geographical representation of the study cohort. In a big hospital in Beijing, most patients came from North China. The third limitation was the lack of age-matched healthy controls. However, this study was designed to evaluate and compare microbiome dysbiosis in different stages of HCC and their relationship with gut damage and microbial translocation. In consideration of the effect of sex on gut microbiota, only male patients were included. The cause of HCC was only HBV and HCV, so the results need further validation in terms of other causes. Finally, the T cell function should be detected directly to confirm the results in this study.

## 5. Conclusions

This study indicated that the dysbiosis of gut microbiota, together with increased gut permeability and microbial translocation, was associated with elevated circulating inflammatory response and reduction in T cell response during HCC progression. The findings obtained in this study also suggested that gut microbiota might be a potential target for HCC treatment and intervention, especially in terminal HCC.

## Abbreviations

HBV: Hepatitis B virus
HCC: Hepatocellular carcinoma
HCV: Hepatitis C virus
LBP: Lipopolysaccharide-binding protein
LPS: Lipopolysaccharide
MT: Microbial translocation
OTUs: Operational taxonomy units
PGRPs: Peptidoglycan recognition proteins
REG3$\alpha$: Regenerating islet-derived protein 3$\alpha$
sCD14: Soluble CD14
SCFAs: Short-chain fatty acids.

## Data Availability

The data of clinical characteristics, relative abundance of gut microbiota, and plasma levels of REG3$\alpha$, sCD14, LBP, PGRPs, cytokines, and chemokines of individuals used to support the findings of this study are included within the Supplementary Tables.

## Additional Points

*Lay Summary/Key Points*. This study revealed that gut microbiota compositional and functional shifts correlated with hepatocellular carcinoma (HCC) progression, especially in the terminal stage. The mechanism might include elevated gut permeability and microbial translocation relevant to dysbiosis. The accompanying systemic inflammatory increase and immune suppression appeared to promote HCC progression. An increased ratio of *Enterococcaceae* to *Bifidobacteriaceae* could serve as a biomarker of dysbiosis in HCC progression.

## Disclosure

The funding bodies had no role in the study design, data collection, data analysis or interpretation, or writing of the report.

## Conflicts of Interest

All authors report no conflicts of interest relevant to this study.

## Authors' Contributions

Q.H., N.Z., and J.Z. conceptualized and designed the study. Y.G., N.Z., H.Y., S.L., N.C., Y.L., and J.Z. performed sample collection and data acquisition. N.Z., Y.G., J.Z., and Q.H. analyzed and interpreted the data. N.Z., Y.G., Q.H., and J.Z. prepared the original draft. Q.H. and J.Z. wrote and reviewed the manuscript. All authors read and agreed to the published version of the manuscript. Nan Zhang and Yusong Gou contributed equally to this study.

## Acknowledgments

The authors thank all patients who agreed to participate in this study. This study was partly supported by the open funding of the Key Laboratory of Translational Research on Hepatitis B and Hepatocellular Carcinoma of Beijing Youan Hospital (BJYAHKF2018002); the fund of Clinical Research of Beijing Youan Hospital, CMU (YNKTTS20180108); and the fund of National Microbial Resource Center (No. NMRC-2021-2) and National Pathogen Resource Center (NPRC-32).

## Supplementary Materials

*Supplementary 1*. Supplementary Table 1: detailed information of study subjects.

*Supplementary 2*. Supplementary Table 2: concentrations of 20 plasma cytokines and chemokines in the early, intermediated, and terminal groups of HCC patients.

## References

[1] C. Mattiuzzi and G. Lippi, "Cancer statistics: a comparison between World Health Organization (WHO) and Global Burden of Disease (GBD)," *European Journal of Public Health*, vol. 30, no. 5, pp. 1026-1027, 2020.

[2] Z. Ren, A. Li, J. Jiang et al., "Gut microbiome analysis as a tool towards targeted non-invasive biomarkers for early hepatocellular carcinoma," *Gut*, vol. 68, no. 6, pp. 1014–1023, 2019.

[3] T. Inoue, J. Nakayama, K. Moriya et al., "Gut dysbiosis associated with hepatitis C virus infection," *Clinical Infectious Diseases*, vol. 67, no. 6, pp. 869–877, 2018.

[4] Q. Liu, F. Li, Y. Zhuang et al., "Alteration in gut microbiota associated with hepatitis B and non-hepatitis virus related hepatocellular carcinoma," *Gut Pathogens*, vol. 11, no. 1, p. 1, 2019.

[5] J. Ni, R. Huang, H. Zhou et al., "Analysis of the relationship between the degree of dysbiosis in gut microbiota and prognosis at different stages of primary hepatocellular carcinoma," *Frontiers in Microbiology*, vol. 10, p. 1458, 2019.

[6] B. Chassaing, L. Etienne-Mesmin, and A. T. Gewirtz, "Microbiota-liver axis in hepatic disease," *Hepatology*, vol. 59, no. 1, pp. 328–339, 2014.

[7] F. Shen, R. D. Zheng, X. Q. Sun, W. J. Ding, X. Y. Wang, and J. G. Fan, "Gut microbiota dysbiosis in patients with non-alcoholic fatty liver disease," *Hepatobiliary & Pancreatic Diseases International*, vol. 16, no. 4, pp. 375–381, 2017.

[8] J. S. Bajaj, D. M. Heuman, P. B. Hylemon et al., "Altered profile of human gut microbiome is associated with cirrhosis and its complications," *Journal of Hepatology*, vol. 60, no. 5, pp. 940–947, 2014.

[9] X. Wang, M. M. Li, Y. Niu et al., "Serum zonulin in HBV-associated chronic hepatitis, liver cirrhosis, and hepatocellular carcinoma," *Disease Markers*, vol. 2019, Article ID 5945721, 6 pages, 2019.

[10] L. Maccioni, B. Gao, S. Leclercq et al., "Intestinal permeability, microbial translocation, changes in duodenal and fecal microbiota, and their associations with alcoholic liver disease progression in humans," *Gut Microbes*, vol. 12, no. 1, p. 1782157, 2020.

[11] M. Omata, A. L. Cheng, N. Kokudo et al., "Asia-Pacific clinical practice guidelines on the management of hepatocellular carcinoma: a 2017 update," *Hepatology International*, vol. 11, no. 4, pp. 317–370, 2017.

[12] A. Forner, M. E. Reig, C. Rodriguez de Lope, and J. Bruix, "Current strategy for staging and treatment: the BCLC update and future prospects," *Seminars in Liver Disease*, vol. 30, no. 1, pp. 061–074, 2010.

[13] J. Ni, X. Li, Z. He, and M. Xu, "A novel method to determine the minimum number of sequences required for reliable microbial community analysis," *Journal of Microbiological Methods*, vol. 139, pp. 196–201, 2017.

[14] R. Huang, T. Li, J. Ni et al., "Different sex-based responses of gut microbiota during the development of hepatocellular carcinoma in liver-specific Tsc1-knockout mice," *Frontiers in Microbiology*, vol. 9, p. 1008, 2018.

[15] M. von Bergen, N. Jehmlich, M. Taubert et al., "Insights from quantitative metaproteomics and protein-stable isotope probing into microbial ecology," *The ISME Journal*, vol. 7, no. 10, pp. 1877–1885, 2013.

[16] T. Magoc and S. L. Salzberg, "FLASH: fast length adjustment of short reads to improve genome assemblies," *Bioinformatics*, vol. 27, no. 21, pp. 2957–2963, 2011.

[17] Q. Wang, G. M. Garrity, J. M. Tiedje, and J. R. Cole, "Naive Bayesian classifier for rapid assignment of rRNA sequences into the new bacterial taxonomy," *Applied and Environmental Microbiology*, vol. 73, no. 16, pp. 5261–5267, 2007.

[18] N. Christian, B. K. Whitaker, and K. Clay, "Microbiomes: unifying animal and plant systems through the lens of community ecology theory," *Frontiers in Microbiology*, vol. 6, 2015.

[19] P. J. McMurdie and S. Holmes, "phyloseq: an R package for reproducible interactive analysis and graphics of microbiome census data," *PLoS One*, vol. 8, no. 4, article e61217, 2013.

[20] N. Segata, J. Izard, L. Waldron et al., "Metagenomic biomarker discovery and explanation," *Genome Biology*, vol. 12, no. 6, p. R60, 2011.

[21] S. Isnard, R. Ramendra, F. P. Dupuy et al., "Plasma levels of C-type lectin REG3$\alpha$ and gut damage in people with human immunodeficiency virus," *The Journal of Infectious Diseases*, vol. 221, no. 1, pp. 110–121, 2020.

[22] J. M. Wong, R. de Souza, C. W. Kendall, A. Emam, and D. J. Jenkins, "Colonic health: fermentation and short chain fatty acids," *Journal of Clinical Gastroenterology*, vol. 40, no. 3, pp. 235–243, 2006.

[23] H. B. Wang, P. Y. Wang, X. Wang, Y. L. Wan, and Y. C. Liu, "Butyrate enhances intestinal epithelial barrier function via up-regulation of tight junction protein Claudin-1 transcription," *Digestive Diseases and Sciences*, vol. 57, no. 12, pp. 3126–3135, 2012.

[24] M. Xu, B. Wang, Y. Fu et al., "Changes of fecal Bifidobacterium species in adult patients with hepatitis B virus-induced chronic liver disease," *Microbial Ecology*, vol. 63, no. 2, pp. 304–313, 2012.

[25] H. L. Zhang, L. X. Yu, W. Yang et al., "Profound impact of gut homeostasis on chemically-induced pro-tumorigenic inflammation and hepatocarcinogenesis in rats," *Journal of Hepatology*, vol. 57, no. 4, pp. 803–812, 2012.

[26] V. W. Wong, C. H. Tse, T. T. Lam et al., "Molecular characterization of the fecal microbiota in patients with nonalcoholic steatohepatitis–a longitudinal study," *PLoS One*, vol. 8, no. 4, article e62885, 2013.

[27] H. Lu, Z. Wu, W. Xu, J. Yang, Y. Chen, and L. Li, "Intestinal microbiota was assessed in cirrhotic patients with hepatitis B virus infection. Intestinal microbiota of HBV cirrhotic patients," *Microbial Ecology*, vol. 61, no. 3, pp. 693–703, 2011.

[28] C. L. Bevins and N. H. Salzman, "Paneth cells, antimicrobial peptides and maintenance of intestinal homeostasis," *Nature Reviews. Microbiology*, vol. 9, no. 5, pp. 356–368, 2011.

[29] I. Marafini, A. di Sabatino, F. Zorzi et al., "Serum regenerating islet-derived 3-alpha is a biomarker of mucosal enteropathies," *Alimentary Pharmacology & Therapeutics*, vol. 40, no. 8, pp. 974–981, 2014.

[30] J. L. Ferrara, A. C. Harris, J. K. Greenson et al., "Regenerating islet-derived 3-alpha is a biomarker of gastrointestinal graft-versus-host disease," *Blood*, vol. 118, no. 25, pp. 6702–6708, 2011.

[31] D. Zhao, Y. H. Kim, S. Jeong et al., "Survival signal REG3$\alpha$ prevents crypt apoptosis to control acute gastrointestinal graft-versus-host disease," *The Journal of Clinical Investigation*, vol. 128, no. 11, pp. 4970–4979, 2018.

[32] R. Ramendra, S. Isnard, V. Mehraj et al., "Circulating LPS and (1→3)-$\beta$-D-glucan: a folie à deux contributing to HIV-associated immune activation," *Frontiers in Immunology*, vol. 10, p. 465, 2019.

[33] J. D. Estes, L. D. Harris, N. R. Klatt et al., "Damaged intestinal epithelial integrity linked to microbial translocation in pathogenic simian immunodeficiency virus infections," *PLoS Pathogens*, vol. 6, no. 8, article e1001052, 2010.

[34] J. R. Stehle Jr., X. Leng, D. W. Kitzman, B. J. Nicklas, S. B. Kritchevsky, and K. P. High, "Lipopolysaccharide-binding protein, a surrogate marker of microbial translocation, is associated with physical function in healthy older adults," *The Journals of Gerontology. Series A, Biological Sciences and Medical Sciences*, vol. 67, no. 11, pp. 1212–1218, 2012.

[35] J. M. Brenchley, D. A. Price, T. W. Schacker et al., "Microbial translocation is a cause of systemic immune activation in chronic HIV infection," *Nature Medicine*, vol. 12, no. 12, pp. 1365–1371, 2006.

[36] S. M. Riordan and R. Williams, "The intestinal flora and bacterial infection in cirrhosis," *Journal of Hepatology*, vol. 45, no. 5, pp. 744–757, 2006.

[37] C. Pande, A. Kumar, and S. K. Sarin, "Small-intestinal bacterial overgrowth in cirrhosis is related to the severity of liver disease," *Alimentary Pharmacology & Therapeutics*, vol. 29, no. 12, pp. 1273–1281, 2009.

[38] B. Zhu, N. Lin, M. Zhang et al., "Activated hepatic stellate cells promote angiogenesis via interleukin-8 in hepatocellular carcinoma," *Journal of Translational Medicine*, vol. 13, no. 1, p. 365, 2015.

[39] X. T. Fu, Z. Dai, K. Song et al., "Macrophage-secreted IL-8 induces epithelial-mesenchymal transition in hepatocellular carcinoma cells by activating the JAK2/STAT3/Snail pathway," *International Journal of Oncology*, vol. 46, no. 2, pp. 587–596, 2015.

[40] J. Estevez, V. L. Chen, O. Podlaha et al., "Differential serum cytokine profiles in patients with chronic hepatitis B, C, and hepatocellular carcinoma," *Scientific Reports*, vol. 7, no. 1, p. 11867, 2017.

[41] J. Behary, N. Amorim, X. T. Jiang et al., "Gut microbiota impact on the peripheral immune response in non-alcoholic fatty liver disease related hepatocellular carcinoma," *Nature Communications*, vol. 12, no. 1, p. 187, 2021.

[42] Y. Furusawa, Y. Obata, S. Fukuda et al., "Commensal microbe-derived butyrate induces the differentiation of colonic regulatory T cells," *Nature*, vol. 504, no. 7480, pp. 446–450, 2013.

Hindawi
Journal of Immunology Research
Volume 2021, Article ID 1007126, 9 pages
https://doi.org/10.1155/2021/1007126

*Review Article*

# The Emerging Roles of Tripartite Motif Proteins (TRIMs) in Acute Lung Injury

**Yingjie Huang**,[1] **Yue Xiao**,[2] **Xuekang Zhang**,[1] **Xuan Huang**,[3] **and Yong Li**[1]

[1]*Department of Anesthesiology, The First Affiliated Hospital of Nanchang University, Nanchang, China*
[2]*The First Clinical Medical College, Nanchang University, Nanchang 330006, China*
[3]*The National Engineering Research Center for Bioengineering Drugs and the Technologies, Institute of Translational Medicine, Nanchang University, Nanchang, China*

Correspondence should be addressed to Xuekang Zhang; kang7139@163.com, Xuan Huang; huangxuan@ncu.edu.cn, and Yong Li; liyong@ncu.edu.cn

Received 12 July 2021; Accepted 9 October 2021; Published 19 October 2021

Academic Editor: Elizabeth Soares Fernandes



Acute lung injury (ALI) is an inflammatory disorder of the lung that causes high mortality and lacks any pharmacological intervention. Ubiquitination plays a critical role in the pathogenesis of ALI as it regulates the alveolocapillary barrier and the inflammatory response. Tripartite motif (TRIM) proteins are one of the subfamilies of the RING-type E3 ubiquitin ligases, which contains more than 80 distinct members in humans involved in a broad range of biological processes including antivirus innate immunity, development, and tumorigenesis. Recently, some studies have shown that several members of TRIM family proteins play important regulatory roles in inflammation and ALI. Herein, we integrate emerging evidence regarding the roles of TRIMs in ALI. Articles were selected from the searches of PubMed database that had the terms "acute lung injury," "ubiquitin ligases," "tripartite motif protein," "inflammation," and "ubiquitination" using both MeSH terms and keywords. Better understanding of these mechanisms may ultimately lead to novel therapeutic approaches by targeting TRIMs for ALI treatment.

## 1. Introduction

Acute lung injury (ALI) is an acute hypoxic respiratory insufficiency caused by various direct (pulmonary) or indirect (extrapulmonary) injuries including sepsis syndrome, ischemia-reperfusion, pneumonia, and mechanical ventilation, which leads to the destruction of the barrier of alveolar epithelial cells and capillary endothelial cells, resulting in overinfiltration of inflammatory cells and diffuse pulmonary interstitial and alveolar edema [1]. In 1994, the diagnostic criteria of ALI were put forward by the American–European Consensus Conference: an acute onset; oxygenation index $(PaO_2/FiO_2) >$ 200 mm Hg and < 300 mm Hg (1 mmHg = 0.133 kPa); patchy shadows in both lungs on the chest X-ray; pulmonary artery wedge pressure ≤ 18 mmHg or no clinical evidence of left atrial hypertension; etc. [2]. Due to the lack of drug intervention, ALI remains a significant cause of morbidity and mortality in the critically ill patient population [2]. More severe situations with $PaO_2/FiO_2 \leq 200$ mm Hg, ALI turns to the worse stage acute respiratory distress syndrome (ARDS) [3].

Pathological hallmarks of ALI are injury to the vascular endothelium/alveolar epithelium, activation of innate immune response, and enhanced coagulation [4]. Exposure to several risk factors (i.e., pneumonia, sepsis, and shock) firstly leads to endothelial and/or epithelial monolayers damage, increasing permeability and impairing their barrier function [4]. A large amount of protein-rich fluid and inflammatory cells leaks into the alveoli and lung interstitium, resulting in pulmonary edema, neutrophil infiltration, cytokine and reactive oxygen species-mediated inflammation coagulation disorders, and pulmonary fibrosis [5]. Notedly, mast cells (MCs) and polymorphonuclear neutrophils (PMNs) are the main inflammatory cells, which play a critical role in the pathogenesis of ALI [6, 7]. MC activation induces tryptase release to trigger ALI [8], which is supported by the finding that MCs "stabilizers" can reduce ALI severity [9].

At present, there is still no effective pharmaceutical intervention for ALI; mechanical ventilation is the main approach to prevent respiratory failure and, combined with intensive care support, could improve health condition [10]. However, mechanical ventilation can exacerbate preexisting lung injury or even induce de novo injury in healthy lungs, which is called ventilator-induced lung injury (VILI) [11, 12]. In recent years, researchers have paid close attention to the identification of new routes at cellular level which could provide a better understanding of the physiopathology of ALI, but the precise cellular and molecular underlying mechanisms are still to be fully elucidated. Chen et al. recently summarized and introduced the role of lncRNAs in ALI in detail [13]. However, emerging evidence points out to the ubiquitination which functions as an important regulator in the pathobiology of ALI since it regulates the proteins evolved in the modulation of the alveolocapillary barrier and inflammatory response, opening a highly promising research field for the treatment of lung diseases [14].

## 2. Ubiquitination in ALI

Ubiquitination is the major protein posttranslational modification in cells by which ubiquitin (Ub) covalently attached the target protein for degradation through the 26S proteasome or lysosome or nonproteolytic modifications [15]. It plays crucial roles in diverse biological processes such as DNA repair, cell proliferation, signal transduction, apoptosis, and inflammation, whose dysregulation leads to many diseases [16]. However, bacterial infection or inflammatory stimulation often disrupts the process of protein ubiquitination. We and some other investigators have shown that expressions of some E3 Ub ligases were altered by infection or inflammation thus affecting the levels and functions of their target proteins. Thus, uncovering new E3 Ub ligase-related molecular mechanisms and signaling pathways will provide a unique opportunity for the potential design of new strategies to alleviate ALI.

*2.1. The Ubiquitin System.* As a multicomponent regulatory system, the Ub system is composed of three types of Ub enzymes, which is a highly controlled mechanism of protein degradation and turnover in cells, starting with approximately 8 kDa monomeric Ub [17]. Ub is activated by a Ub-activating enzyme (E1) in an adenosine-triphosphate- (ATP-) dependent manner and then conjugated by a ubiquitin conjugating enzyme (E2), finally resulting in transfer of Ub to an internal lysine of the substrate protein by an E3 ligase [18]. To date, there are only two E1 enzymes (UBA1 and UBA6) [19], around 40 E2 enzymes [20], but more than 600 E3 ligases [21] existed in the human genome. Although the addition of Ub moieties to specific residues on a substrate protein is partly because of E2/E3 enzymes pairings, E3 ligases were considered the predominant source of substrate specificity [22].

*2.2. E3 Ligases.* As a direct mediator of substrate tagging and ubiquitin chain elongation, E3 ligase is considered an essential component in the ubiquitin system that determines substrate specificity. In human genome, more than 600 putative E3 ligases have been identified [21]. There are three major kinds of E3 ligases divided by the molecular structure and functional mechanism, including HECT (homologous to the E6-associated protein carboxyl-terminus) domain family, RING (really interesting new gene) finger family, and the RBR (RING in-between-RING) E3 ubiquitin ligases [23]. HECT E3 ligase contains an N-terminal lobe which is responsible for E2 binding and substrate recognition, and a C-terminal HECT domain containing a catalytic cysteine that receives and passes an ubiquitin molecule from the E2 enzyme before conjugating ubiquitin to a substrate protein [24]. RING finger E3 ligases constitute the largest family of E3 ligases which are characterized based on the presence of a RING domain [25]. Interestingly, the canonical RING domain is a type of zinc finger with a RING fold structure while another type is the U-box domain which possesses the same RING fold but without zinc [26]. Unlike HECT E3 ligase, RING finger E3 ligase mediates the direct transfer of ubiquitin to a substrate protein by binding to a ubiquitin-charging E2 enzyme as a scaffold [27]. Notably, RING E3 ligases function either as monomers (e.g., c-CBL, E4B), homodimers (e.g., cIAP, CHIP), heterodimers (e.g., Mdm2-MdmX), or large multisubunit complexes, such as the Cullin-RING ligases (CRLs), which make up a distinct subtype characterized by their common Cullin scaffold protein [23]. RBR E3 ligases contain two RING domains (RING1 and RING2) with an in-between-RING (IBR) domain and share the common features of both HECT and RING finger E3 ligases which function as a hybrid of these two types of E3 ligases [28]. Specifically, the RING1 domain binds to ubiquitin-loaded E2 and transfers ubiquitin onto the RING2 domain at a catalytic cysteine residue before conjugation to the substrate protein [29].

*2.3. Role of E3 Ligases in ALI.* Although ubiquitination has been reported to play a pivotal role in multiple biological functions, its function in ALI remains poorly understood. Recently, the key regulative role of ubiquitination in ALI has been mentioned increasingly [14]. Of them, most studies have been focused on the E3 ubiquitin ligases and the conventional K48-ubiquitination which leads to the substrate proteins degradation via the 26S proteasome [30]. Accumulating evidence has demonstrated that E3 ligase plays a critical role in the pathobiology of ALI since it modulates critical proteins involved in the alveolocapillary barrier and the inflammatory response [14].

Tight junctions form a highly selective diffusion barrier between endothelial cells and epithelial cells by preventing most dissolved molecules and ions from passing freely through the paracellular pathway [31]. The function impairment of tight junction is a sign of ALI [32]. E3 ligase Itch, a member of the HECT Ub ligases, could directly interact with and degrade the tight junction-specific protein occludin [33] via ubiquitination. E-cadherin, a well-studied member of the classical cadherin family, is a central component in the cell-cell adhesion junction and plays a critical role in maintaining cell polarity and the integrity of epithelial cells [34]. Dysfunction of E-cadherin contributes to the pathogenesis of ALI [35]. A RING finger E3 ligase Hakai induces

E2-dependent ubiquitination and endocytosis of E-cadherin complex in epithelial cells [36]. Recently, Dong et al. found that the HECT E3 ligase Smurf2 induced $\mu$-opioid receptor 1 (MOR1) degradation in the ubiquitin-proteasome system in lung epithelial cells, and MOR1 has a potential effect in lung repair and remodeling after ALI [37].

E3 ligase Cblb inhibits the MyD88-dependent Toll-like receptor 4 (TLR4) signaling and attenuates acute lung inflammation induced by polymicrobial sepsis [38]. The ST2L receptor for interleukin 33 (IL-33) mediates pulmonary inflammation during ALI, which is bound and ubiquitinated by FBXL19, a member of the Skp1-Cullin-F-box family of E3 ubiquitin ligases [39]. In addition, E3 ligase FBXO3 targets the TRAF inhibitor FBXL2 for its destabilization and potently stimulates cytokine release, leading to changes in lung permeability, alveolar edema, and ALI [40]. FBXO17 has been described as an E3 ligase that recognizes and mediates the ubiquitination and degradation of GSK3$\beta$ to reduce inflammatory responses in lung epithelial cells after LPS injury [41]. Most recently, Lear et al. reported that E3 ligase KIAA0317 targets SOCS2 for ubiquitination and degradation by the proteasome and exacerbates pulmonary inflammation [42]. These studies have proved that ubiquitin-proteasome system especially E3 ligases is closely related to the pathogenesis of lung injury.

## 3. TRIMs in ALI

TRIM proteins are regarded as a subfamily of the RING finger E3 ligase, which contain more than 80 distinct members in humans [43]. TRIMs are composed by conserved three zinc-binding domains, an N-terminal RING domain, one or two B-boxes, and a central coiled-coiled domain (CDD) [44]. We recently found that TRIM65 selectively targeted vascular cell adhesion molecule 1 (VCAM-1) and promoted its ubiquitination and degradation, by which it critically controlled the duration and magnitude of pulmonary inflammation in ALI [45]. Particularly, Whitson and his colleagues reported that TRIM72 (also known as MG53) could function as a novel therapeutic protein to treat ALI [46]. Here, we discuss our current understanding of TRIMs as E3 ligases that executes its effector functions in ALI (Table 1).

*3.1. TRIM8.* TRIM8, as a member of TRIM family, has a common structural feature of a typical RBCC motif as well as a monopartite nuclear localization signal (NLS), which allows shuttling and functioning into the nucleus [47]. It has been reported that TRIM8 can regulate NF-$\kappa$B signaling both in the nucleus and cytoplasm: TRIM8 inhibited PIAS3-mediated negative regulation of p65 to enhance NF-$\kappa$B activity in the nucleus [48] and can also positively regulate NF-$\kappa$B pathway through k63-linked polyubiquitination of cytoplasmic protein TAK1 [49]. TRIM8 is ubiquitously expressed in human and mouse tissues, which has higher expression levels in the central nervous system, kidney, and lens, and lower expression level in digestive tract [44]. TRIM8 plays a key role in the immune response and participates in various fundamental biological processes such as cell survival, apoptosis, autophagy, differentiation, inflammation, and carcinogenesis [50].

Recently, studies have revealed that TRIM8 is involved in the regulation of sepsis and ALI. TRIM8 was significantly upregulated in LPS (lipopolysaccharide) sepsis-induced acute hepatic injury (AHI), which was a direct target of miR-373-3p [51]. Moreover, inhibition of TRIM8 by downregulation of long noncoding RNA (lncRNA) LINC00472, which served as a sponge for miR-373-3p and negatively regulated its expression, could reduce sepsis-induced expression of main proinflammatory cytokines such as IL-6, IL-10, and TNF-$\alpha$ [51]. Xiaoli et al. found that TRIM8 was increased in a time-dependent manner during LPS-induced ALI, promoting inflammatory response and ROS generation via the inactivation of p-AMPK$\alpha$. In addition, suppression of TRIM8 markedly downregulated mRNA levels of interleukin-1$\beta$ (IL-1$\beta$), IL-6, and tumor necrosis factor-$\alpha$ (TNF-$\alpha$) in lung epithelial cells mainly through blocking the NF-$\kappa$B signaling pathway and alleviated oxidative stress by regulating Nrf2 signaling and heme oxygenase-1 (HO-1) expression [52]. Although TRIM8 has been revealed to play an important role in acute lung injury, precise regulatory mechanisms such as whether it depends on the activity of E3 ubiquitin ligase and its specific target proteins need to be further clarified.

*3.2. TRIM14.* TRIM14 was originally known as KIAA0129 [53], and its overexpression was first found in human immunodeficiency virus- (HIV-) infected human and simian non-Hodgkin's lymphoma infected with simian immunodeficiency virus (SIV) [54, 55]. TRIM14 is a noncanonical member of the TRIM family, since it lacks the N-terminal RING domain of the typical RBCC motif which can exert an E3 ubiquitin ligase [56]. Studies have shown that TRIM14 can perform various functions via partners with which directly interact with its PRYSPRY domain [57]. Interestingly, TRIM14 was reported to be an important mediator of antiviral immunity both in DNA virus and double-stranded RNA virus infection [58, 59]. Furthermore, several groups found that TRIM14 may be involved in tumorigenesis [60–64].

Recently, we found that TRIM14 was overexpressed in human vascular endothelial cells (ECs) and markedly induced by inflammatory stimuli such as LPS [65]. TRIM14 was a new positive regulator of endothelial activation via activating the NF-$\kappa$B signaling pathway, which can directly bind to the promoter of *TRIM14* gene and control its transcription [65]. Zhou et al. revealed that TRIM14 underwent Lys-63-linked autopolyubiquitination at Lys-365 and served as a platform and recruited NEMO to the mitochondrial antiviral signal (MAVS) complex, leading to the activation of interferon regulatory factor 3 (IRF3) and NF-$\kappa$B signaling in human lung epithelial cells, which boost antiviral innate immune response [66]. TRIM14 also can recruit USP14 to cleave the K63-linked ubiquitin chain at lysine 332/338/341 of p100/p52, hinder the recognition of receptor p62, and inhibit the autophagy degradation of p100/p52, thus promoting the atypical activation of NF-$\kappa$B *in vivo* and *in vitro* [67]. Considering endothelial inflammation and dysfunction play a prominent role in development of ALI and NF-$\kappa$B is a central transcriptional factor in ALI, it is

Table 1: Role of TRIMs in acute lung inflammation.

| TRIMs | Models | Cell types | Mechanisms | Ref No. |
|---|---|---|---|---|
| TRIM8 | LPS-induced AHI | Human liver cells | LINC00472/miR-373-3p/TRIM8 axis | [51] |
| | LPS-induced ALI | Lung epithelial cells | p-AMPK$\alpha$/NF-$\kappa$B/Nrf2/ROS/HO-1 axis | [52] |
| TRIM14 | LPS-induced ALI | Human vascular endothelial cells | NEMO/TAK1/NF-$\kappa$b/TRIM14 pathway | [63] |
| TRIM21 | LPS-induced ALI | Lung microvascular endothelial cells | NF-$\kappa$B signaling | [79] |
| TRIM65 | ALI | Human vascular endothelial cells | VACM-1 ubiquitination and degradation | [45] |
| TRIM72 | Ischaemia-reperfusion and overventilation-induced ALI | Lung epithelial cells | Cell membrane repair | [97] |
| | Influenza virus -induced ALI | Macrophage<br>Lung tissue | NF-$\kappa$B signaling<br>Inhibition of pyroptosis | [98, 106] |
| | Hemorrhagic shock/contusive ALI | Human bronchial epithelial cells | Cell membrane repair | [46] |

suggested that TRIM14 may be involved in the pathological process of ALI, which needs further study.

*3.3. TRIM21.* TRIM21, also known as Ro52, has a typical RBCC motif and E3 ligase activity [68]. It is broadly expressed in most human tissues and cells and predominantly expressed in hematopoietic cells and endothelial and epithelial cells [69]. TRIM21 was identified as a major autoantigen in autoimmune diseases including Sjögren's syndrome, systemic lupus erythematosus (SLE), and rheumatoid arthritis [70–72]. Later studies revealed that TRIM21 is a highly conserved IgG receptor with high cytoplasmic affinity and specificity [73, 74], which can be induced by interferon to exert antiviral effect [75]. TRIM21 serves as a multifaceted regulator in viral immunity and can not only promote the production of type I interferon [76] and triggers an innate immune response via RIG-1 and cGAS sensing [77] but also negatively regulate innate immunity by targeting and degrading the viral DNA sensor DEAD (Asp-Glu-Ala-Asp) box polypeptide 41 (DDX41) [78]. The biological function and application of TRIM21 in antiviral immunity are described in detail in other reviews [79].

Using TRIM21-deficient mice, Yoshimi and colleagues found that TRIM21 is a negative regulator of NF-$\kappa$B-dependent proinflammatory cytokine production induction in fibroblasts after TLR ligands (poly(I:C), CpG, and LPS) stimulation [80]. In addition, TRIM21 deletion can lead enhanced production of proinflammatory cytokines and systemic autoimmunity though the IL-23-Th17 pathway [81]. Recently, Li et al. reported that TRIM21 exhibited an anti-inflammatory property against LPS-induced lung endothelial dysfunction and monocytes adhesion to endothelial cells [82]. TRIM21 can be monoubiquitylated and lysosomal degraded in response to LPS and may contribute to the pathogenesis of ALI [52]. TRIM21 can be used as a therapeutic target for endothelial dysfunction induced by sepsis, such as acute lung injury [83]. However, whether ubiquitination of TRIM21 is dependent on its phosphorylation and the specific phosphorylation or ubiquitination sites needs to be further clarified.

*3.4. TRIM65.* Human TRIM65 is a 517-amino acid protein, containing a N-terminal RING domain, a B-box, a coiled-coil domain, and a SPRY domain, is first known as a gene associated with white matter lesions [84, 85]. Using a systematic discovery-type proteomic analysis, Li et al. found that TRIM65 can negatively regulate miRNA-mediated mRNA translation inhibition through ubiquitination and subsequent degradation of trinucleotide repeat containing six (TNRC6) [86, 87]. Like other TRIMs, TRIM65 also participates in the antiviral innate immune response by ubiquitination of MDA5 [88, 89]. Over the years, several reports suggest that TRIM65 acts as a ubiquitin E3 ligase, targeting p53, ANXA2, Axin1, and ARHGAP35 to regulate carcinogenesis [90–93]. Most recently, Liu et al. published a review to introduce TRIM65 in white matter lesions, innate immunity and tumor [94].

We recently found that TRIM65 may control the magnitude and duration of LPS-induced lung inflammation and injury [45]. TRIM65-deficient (TRIM65$^{-/-}$) mice are more sensitive to LPS-induced death due to sustained and severe pulmonary inflammation. Further studies showed that monocytes/macrophages were higher in the BAL from TRIM65$^{-/-}$ mice, by which TRIM65 selectively targets vascular cell adhesion molecule 1 (VCAM-1) and directly induces its ubiquitination degradation in endothelial cells. It is worth noting that TRIM65 does not affect the MAPK and NF-$\kappa$B signaling pathways in ALI, although some studies have revealed that TRIM65 can activate the Erk1/2 pathway [95, 96], which suggests that TRIM65 has diverse functions in different cells and under distinct pathological conditions. Furthermore, TRIM65 is enriched in endothelial cells and declined at the early stage during endothelial activation; the mechanisms that precisely regulate TRIM65 levels in endothelial inflammation remain unknown. Further studies are necessary to understand the regulatory mechanisms that control TRIM65 expression.

*3.5. TRIM72.* TRIM72 (also known as MG53) is composed of a typical TRIM family protein RBCC structure and a PRY-SPRY subdomain which is mainly expressed in cardiac and skeletal muscle, as well as in renal and alveolar epithelial cells, monocyte, and macrophages with detectable amount level [97–100]. Cai et al. first revealed that TRIM72 acted as a key component of the sarcolemma cell plasma membrane repair machinery [101]. Upon the membrane injurious stimuli, TRIM72 oligomerized by oxidizing the thiol group of cysteine at position 242 and a leucine zipper

motif to induce the intracellular vesicles coated with TRIM72 to nucleate at the injured site, resulting in resealing the damaged membrane [102, 103]. At the membrane, TRIM72 protein binds to phosphatidyl serine to mediate the recruitment of vesicles at the injured site [104]. Interestingly, TRIM72 can be secreted and circulate throughout the entire body to reach all tissues and organs, allowing the recombinant TRIM72 protein to have therapeutic benefit in treatment of injuries to multiple tissues, such as the heart, kidney, lung, brain, liver, skin, skeletal muscle, and cornea [105].

Ablation of the TRIM72 gene leads to increased susceptibility to ischemia-reperfusion and overventilation-induced ALI in mice [97]. Recently, Sermersheim and his colleagues found that knockdown of TRIM72 in macrophages results in activation of NF-$\kappa$B signaling and increased inflammatory factor interleukin-1$\beta$ upon influenza virus infection, and knockout of TRIM72 promotes $CD45^+$ cells infiltration and IFN$\beta$ elevation in the lung [98]. Kenney et al. found that exogenous injection of recombinant human TRIM72 protein could protect ALI caused by lethal influenza virus infection [106]. Recombinant TRIM72 protein significantly decreased the level of inflammatory cytokines of IFN$\beta$, IL-6, and IL-1$\beta$ and infiltrating $CD11b^+$ lymphocytes in lung tissues [106]. It is reported that intravenous (IV) delivery or inhalation of recombinant human TRIM72 protein reduces symptoms in rodent models of ALI and emphysema [97]. The extracellular recombinant protein protects cultured lung epithelial cells against anoxia/reoxygenation-induced injuries [97]. Most recently, Whitson et al. had evaluated the therapeutic benefits of recombinant human TRIM72 protein in porcine models of ALI and found that recombinant TRIM72 protein can mitigate lung injury in the porcine model of combined hemorrhagic shock/contusive lung injury and reduce warm ischemia-induced injury to the isolated porcine lung through ex vivo lung perfusion administration [46]. These findings revealed that TRIM72 plays a critical role in ALI, and exogenous-recombinant TRIM72 protein may be a shelf stable therapeutic agent with the potential to restore lung function and lessen the impact of ALI.

## 4. Conclusions

TRIMs are a wide and well-conserved family of proteins defined as a subfamily of the RING-type E3 Ub ligases, which have been implicated in a broad range of biological processes including antiviral immunity, cell differentiation, development, and carcinogenesis. Accumulating evidence has shown that several TRIM members have unique and vital roles in ALI using distinct mechanisms (Table 1). Particularly, the regulation of ALI by targeting cell membrane repair has been a focus of intense research in the last few years. Interestingly, systemically administered recombinant human TRIM72 proteins could recognize injury to both epithelial and endothelial layers in the lung, which can effectively preserve lung structure and function in ALI. TRIM72 will be one of the most promising therapeutic agents with the potential to restore lung function and lessen the impact of ALI. Further work is needed to understand full contribution of TRIMs including discovered and undiscovered members to ALI. Identification of TRIM proteins with the potential to serve as therapeutic targets of ALI may help to novel drug development of ALI treatment.

## Data Availability

No data were used to support this study.

## Conflicts of Interest

The authors declare that they have no conflicts of interest.

## Acknowledgments

This work was supported by the grants from the National Natural Science Foundation of China (31760329, 31960147, 32170793, and 82160133) and Research and Training Fund for Young Talents in the First Affiliated Hospital of Nanchang University (YFYPY202003).

## References

[1] G. D. Rubenfeld, E. Caldwell, E. Peabody et al., "Incidence and outcomes of acute lung injury," *The New England Journal of Medicine*, vol. 353, no. 16, pp. 1685–1693, 2005.

[2] G. R. Bernard, A. Artigas, K. L. Brigham et al., "The American-European Consensus Conference on ARDS. Definitions, mechanisms, relevant outcomes, and clinical trial coordination," *American Journal of Respiratory and Critical Care Medicine*, vol. 149, no. 3, pp. 818–824, 1994.

[3] L. B. Ware and M. A. Matthay, "The acute respiratory distress syndrome," *The New England Journal of Medicine*, vol. 342, no. 18, pp. 1334–1349, 2000.

[4] V. Fanelli and V. M. Ranieri, "Mechanisms and clinical consequences of acute lung injury," *Annals of the American Thoracic Society*, vol. 12, Supplement 1, pp. S3–S8, 2015.

[5] E. R. Johnson and M. A. Matthay, "Acute lung injury: epidemiology, pathogenesis, and treatment," *Journal of Aerosol Medicine and Pulmonary Drug Delivery*, vol. 23, no. 4, pp. 243–252, 2010.

[6] H. Virk, G. Arthur, and P. Bradding, "Mast cells and their activation in lung disease," *Translational Research*, vol. 174, pp. 60–76, 2016.

[7] T. R. Martin, "Neutrophils and lung injury: getting it right," *The Journal of Clinical Investigation*, vol. 110, no. 11, pp. 1603–1605, 2002.

[8] X. Gan, D. Liu, P. Huang, W. Gao, X. Chen, and Z. Hei, "Mast-cell-releasing tryptase triggers acute lung injury induced by small intestinal ischemia-reperfusion by activating PAR-2 in rats," *Inflammation*, vol. 35, no. 3, pp. 1144–1153, 2012.

[9] C. Chen, Z. Zhang, F. Tan et al., "Stabilizing mast cells improves acute lung injury after orthotopic liver transplantation via promotion of apoptosis in polymorphonuclear neutrophils," *American Journal of Physiology. Lung Cellular and Molecular Physiology*, vol. 320, no. 2, pp. L266–L275, 2021.

[10] M. A. Matthay, D. McAuley, and L. B. Ware, "Clinical trials in acute respiratory distress syndrome: challenges and opportunities," *The Lancet*, vol. 5, no. 6, pp. 524–534, 2017.

[11] D. Dreyfuss and G. Saumon, "Ventilator-induced lung injury: lessons from experimental studies," *American Journal of*

*Respiratory and Critical Care Medicine*, vol. 157, no. 1, pp. 294–323, 1998.

[12] E. K. Wolthuis, A. P. J. Vlaar, G. Choi, J. J. T. H. Roelofs, N. P. Juffermans, and M. J. Schultz, "Mechanical ventilation using non-injurious ventilation settings causes lung injury in the absence of pre-existing lung injury in healthy mice," *Critical Care*, vol. 13, no. 1, p. R1, 2009.

[13] C. Chen, Y. He, Y. Feng, W. Hong, G. Luo, and Z. Ye, "Long non-coding RNA review and implications in acute lung inflammation," *Life Sciences*, vol. 269, p. 119044, 2021.

[14] N. D. Magnani, L. A. Dada, and J. I. Sznajder, "Ubiquitin-proteasome signaling in lung injury," *Translational Research*, vol. 198, pp. 29–39, 2018.

[15] K. N. Swatek and D. Komander, "Ubiquitin modifications," *Cell Research*, vol. 26, no. 4, pp. 399–422, 2016.

[16] R. B. Damgaard, "The ubiquitin system: from cell signalling to disease biology and new therapeutic opportunities," *Cell Death and Differentiation*, vol. 28, no. 2, pp. 423–426, 2021.

[17] J. Callis, "The ubiquitination machinery of the ubiquitin system," *The Arabidopsis Book*, vol. 12, article e0174, 2014.

[18] C. C. Goetzke, F. Ebstein, and T. Kallinich, "Role of proteasomes in inflammation," *Journal of Clinical Medicine*, vol. 10, no. 8, p. 1783, 2021.

[19] J. Jin, X. Li, S. P. Gygi, and J. W. Harper, "Dual E1 activation systems for ubiquitin differentially regulate E2 enzyme charging," *Nature*, vol. 447, no. 7148, pp. 1135–1138, 2007.

[20] M. D. Stewart, T. Ritterhoff, R. E. Klevit, and P. S. Brzovic, "E2 enzymes: more than just middle men," *Cell Research*, vol. 26, no. 4, pp. 423–440, 2016.

[21] W. Li, M. H. Bengtson, A. Ulbrich et al., "Genome-wide and functional annotation of human E3 ubiquitin ligases identifies MULAN, a mitochondrial E3 that regulates the organelle's dynamics and signaling," *PLoS One*, vol. 3, no. 1, article e1487, 2008.

[22] A. Hershko and A. Ciechanover, "The ubiquitin system," *Annual Review of Biochemistry*, vol. 67, no. 1, pp. 425–479, 1998.

[23] N. Zheng and N. Shabek, "Ubiquitin ligases: structure, function, and regulation," *Annual Review of Biochemistry*, vol. 86, no. 1, pp. 129–157, 2017.

[24] J. M. Huibregtse, M. Scheffner, S. Beaudenon, and P. M. Howley, "A family of proteins structurally and functionally related to the E6-AP ubiquitin-protein ligase," *Proceedings of the National Academy of Sciences of the United States of America*, vol. 92, no. 11, p. 5249, 1995.

[25] K. L. Lorick, J. P. Jensen, S. Fang, A. M. Ong, S. Hatakeyama, and A. M. Weissman, "RING fingers mediate ubiquitin-conjugating enzyme (E2)-dependent ubiquitination," *Proceedings of the National Academy of Sciences of the United States of America*, vol. 96, no. 20, pp. 11364–11369, 1999.

[26] C. W. Vander Kooi, M. D. Ohi, J. A. Rosenberg et al., "The Prp19 U-box crystal structure suggests a common dimeric architecture for a class of oligomeric E3 ubiquitin ligases," *Biochemistry*, vol. 45, no. 1, pp. 121–130, 2006.

[27] F. E. Morreale and H. Walden, "Types of ubiquitin ligases," *Cell*, vol. 165, no. 1, pp. 248–248.e1, 2016.

[28] C. E. Berndsen and C. Wolberger, "New insights into ubiquitin E3 ligase mechanism," *Nature Structural & Molecular Biology*, vol. 21, no. 4, pp. 301–307, 2014.

[29] D. M. Wenzel, A. Lissounov, P. S. Brzovic, and R. E. Klevit, "UBCH7 reactivity profile reveals parkin and HHARI to be RING/HECT hybrids," *Nature*, vol. 474, no. 7349, pp. 105–108, 2011.

[30] I. Vadász, C. H. Weiss, and J. I. Sznajder, "Ubiquitination and proteolysis in acute lung injury," *Chest*, vol. 141, no. 3, pp. 763–771, 2012.

[31] C. Zihni, C. Mills, K. Matter, and M. S. Balda, "Tight junctions: from simple barriers to multifunctional molecular gates," *Nature Reviews Molecular Cell Biology*, vol. 17, no. 9, pp. 564–580, 2016.

[32] Y. Liu, S. Mu, X. Li, Y. Liang, L. Wang, and X. Ma, "Unfractionated heparin alleviates sepsis-induced acute lung injury by protecting tight junctions," *The Journal of Surgical Research*, vol. 238, pp. 175–185, 2019.

[33] A. Traweger, D. Fang, Y. C. Liu et al., "The Tight junction-specific protein occludin is a functional target of the E3 ubiquitin-protein ligase Itch," *The Journal of Biological Chemistry*, vol. 277, no. 12, pp. 10201–10208, 2002.

[34] M. C. Nawijn, T. L. Hackett, D. S. Postma, A. J. M. van Oosterhout, and I. H. Heijink, "E-cadherin: gatekeeper of airway mucosa and allergic sensitization," *Trends in Immunology*, vol. 32, no. 6, pp. 248–255, 2011.

[35] G. W. Tu, M. J. Ju, Y. J. Zheng et al., "CXCL16/CXCR6 is involved in LPS-induced acute lung injury via P38 signalling," *Journal of Cellular and Molecular Medicine*, vol. 23, no. 8, pp. 5380–5389, 2019.

[36] Y. Fujita, G. Krause, M. Scheffner et al., "Hakai, a c-Cbl-like protein, ubiquitinates and induces endocytosis of the E-cadherin complex," *Nature Cell Biology*, vol. 4, no. 3, pp. 222–231, 2002.

[37] S. Dong, J. Liu, L. Li et al., "The HECT ubiquitin E3 ligase Smurf2 degrades $\mu$-opioid receptor 1 in the ubiquitin-proteasome system in lung epithelial cells," *American Journal of Physiology Cell Physiology*, vol. 316, no. 5, pp. C632–C640, 2019.

[38] K. Bachmaier, S. Toya, X. Gao et al., "E3 ubiquitin ligase Cblb regulates the acute inflammatory response underlying lung injury," *Nature Medicine*, vol. 13, no. 8, pp. 920–926, 2007.

[39] J. Zhao, J. Wei, R. K. Mialki et al., "F-box protein FBXL19-mediated ubiquitination and degradation of the receptor for IL-33 limits pulmonary inflammation," *Nature Immunology*, vol. 13, no. 7, pp. 651–658, 2012.

[40] B. B. Chen, T. A. Coon, J. R. Glasser et al., "A combinatorial F box protein directed pathway controls TRAF adaptor stability to regulate inflammation," *Nature Immunology*, vol. 14, no. 5, pp. 470–479, 2013.

[41] T. Suber, J. Wei, A. M. Jacko et al., "$SCF^{FBXO17}$ E3 ligase modulates inflammation by regulating proteasomal degradation of glycogen synthase kinase-3$\beta$ in lung epithelia," *The Journal of Biological Chemistry*, vol. 292, no. 18, pp. 7452–7461, 2017.

[42] T. B. Lear, A. C. McKelvey, J. W. Evankovich et al., "KIAA0317 regulates pulmonary inflammation through SOCS2 degradation," *JCI insight*, vol. 4, no. 19, 2019.

[43] S. Hatakeyama, "TRIM family proteins: roles in autophagy, immunity, and carcinogenesis," *Trends in Biochemical Sciences*, vol. 42, no. 4, pp. 297–311, 2017.

[44] A. Reymond, G. Meroni, A. Fantozzi et al., "The tripartite motif family identifies cell compartments," *The EMBO Journal*, vol. 20, no. 9, pp. 2140–2151, 2001.

[45] Y. Li, X. Huang, F. Guo et al., "TRIM65 E3 ligase targets VCAM-1 degradation to limit LPS-induced lung inflammation," *Journal of Molecular Cell Biology*, vol. 12, no. 3, pp. 190–201, 2020.

[46] B. A. Whitson, K. Mulier, H. Li et al., "MG53 as a novel therapeutic protein to treat acute lung injury," *Military Medicine*, vol. 186, Supplement_1, pp. 339–345, 2021.

[47] U. Bhaduri and G. Merla, "Rise of TRIM8: a molecule of duality," *Molecular Therapy Nucleic Acids*, vol. 22, pp. 434–444, 2020.

[48] D. Tomar, L. Sripada, P. Prajapati, R. Singh, A. K. Singh, and R. Singh, "Nucleo-cytoplasmic trafficking of TRIM8, a novel oncogene, is involved in positive regulation of TNF induced NF-$\kappa$B pathway," *PLoS One*, vol. 7, no. 11, article e48662, 2012.

[49] Q. Li, J. Yan, A. P. Mao et al., "Tripartite motif 8 (TRIM8) modulates TNF$\alpha$- and IL-1 -triggered NF-$\kappa$B activation by targeting TAK1 for K63-linked polyubiquitination," *Proceedings of the National Academy of Sciences of the United States of America*, vol. 108, no. 48, pp. 19341–19346, 2011.

[50] F. Marzano, L. Guerrini, G. Pesole, E. Sbisa, and A. Tullo, "Emerging roles of TRIM8 in health and disease," *Cell*, vol. 10, 2021.

[51] L. Li, Y. He, X. J. He, M. R. Bi, Y. H. Qi, and W. W. Zhu, "Down-regulation of long noncoding RNA LINC00472 alleviates sepsis-induced acute hepatic injury by regulating miR-373-3p/TRIM8 axis," *Experimental and Molecular Pathology*, vol. 117, p. 104562, 2020.

[52] L. Xiaoli, Z. Wujun, and L. Jing, "Blocking of tripartite motif 8 protects against lipopolysaccharide (LPS)-induced acute lung injury by regulating AMPK$\alpha$ activity," *Biochemical and Biophysical Research Communications*, vol. 508, no. 3, pp. 701–708, 2019.

[53] T. Nagase, N. Seki, A. Tanaka, K. Ishikawa, and N. Nomura, "Prediction of the coding sequences of unidentified human genes. IV. The coding sequences of 40 new genes (KIAA0121-KIAA0160) deduced by analysis of cDNA clones from human cell line KG-1," *DNA Research*, vol. 167-174, pp. 199–210, 1995.

[54] V. Tarantul, A. Nikolaev, H. Hannig et al., "Detection of abundantly transcribed genes and gene translocation in human immunodeficiency virus-associated non–Hodgkin's lymphoma," *Neoplasia (New York, N.Y.)*, vol. 3, no. 2, pp. 132–142, 2001.

[55] V. Z. Tarantul, A. I. Nikolaev, A. Martynenko, H. Hannig, G. Hunsmann, and W. Bodemer, "Differential gene expression in B-cell non-Hodgkin's lymphoma of SIV-infected monkey," *AIDS Research and Human Retroviruses*, vol. 16, no. 2, pp. 173–179, 2000.

[56] R. Rajsbaum, A. García-Sastre, and G. A. Versteeg, "TRIMmunity: the roles of the TRIM E3-ubiquitin ligase family in innate antiviral immunity," *Journal of Molecular Biology*, vol. 426, no. 6, pp. 1265–1284, 2014.

[57] Y. Yu, L. Liang, Y. Jin, and Y. Yin, "The TRIM14 PRYSPRY domain mediates protein interaction via its basic interface," *FEBS Letters*, vol. 593, no. 10, pp. 1122–1129, 2019.

[58] M. Chen, Q. Meng, Y. Qin et al., "TRIM14 inhibits cGAS degradation mediated by selective autophagy receptor p62 to promote innate immune responses," *Molecular Cell*, vol. 64, no. 1, pp. 105–119, 2016.

[59] P. Tan, L. He, J. Cui et al., "Assembly of the WHIP-TRIM14-PPP6C mitochondrial complex promotes RIG-I-mediated antiviral signaling," *Molecular Cell*, vol. 68, no. 2, article e295, pp. 293–307.e5, 2017.

[60] G. Xu, Y. Guo, D. Xu et al., "TRIM14 regulates cell proliferation and invasion in osteosarcoma via promotion of the AKT signaling pathway," *Scientific Reports*, vol. 7, no. 1, p. 42411, 2017.

[61] J. Hai, C. Q. Zhu, T. Wang, S. L. Organ, F. A. Shepherd, and M. S. Tsao, "TRIM14 is a putative tumor suppressor and regulator of innate immune response in non-small cell lung cancer," *Scientific Reports*, vol. 7, no. 1, p. 39692, 2017.

[62] Z. Tan, L. Song, W. Wu et al., "TRIM14 promotes chemoresistance in gliomas by activating Wnt/$\beta$-catenin signaling via stabilizing Dvl2," *Oncogene*, vol. 37, no. 40, pp. 5403–5415, 2018.

[63] S. Feng, X. Cai, Y. Li, X. Jian, L. Zhang, and B. Li, "Tripartite motif-containing 14 (TRIM14) promotes epithelial-mesenchymal transition via ZEB2 in glioblastoma cells," *Journal of Experimental & Clinical Cancer Research*, vol. 38, no. 1, p. 57, 2019.

[64] J. Chen, L. Huang, J. Quan, and D. Xiang, "TRIM14 regulates melanoma malignancy via PTEN/PI3K/AKT and STAT3 pathways," *Aging*, vol. 13, no. 9, pp. 13225–13238, 2021.

[65] X. Huang, Y. Li, X. Li, D. Fan, H. B. Xin, and M. Fu, "TRIM14 promotes endothelial activation via activating NF-$\kappa$B signaling pathway," *Journal of Molecular Cell Biology*, vol. 12, no. 3, pp. 176–189, 2020.

[66] Z. Zhou, X. Jia, Q. Xue et al., "TRIM14 is a mitochondrial adaptor that facilitates retinoic acid-inducible gene-I-like receptor-mediated innate immune response," *Proceedings of the National Academy of Sciences of the United States of America*, vol. 111, no. 2, pp. E245–E254, 2014.

[67] M. Chen, Z. Zhao, Q. Meng et al., "TRIM14 promotes noncanonical NF-$\kappa$B activation by modulating p100/p52 stability via selective autophagy," *Advanced Science*, vol. 7, no. 1, p. 1901261, 2020.

[68] K. Wada and T. Kamitani, "Autoantigen Ro52 is an E3 ubiquitin ligase," *Biochemical and Biophysical Research Communications*, vol. 339, no. 1, pp. 415–421, 2006.

[69] D. A. Rhodes, G. Ihrke, A. T. Reinicke et al., "The 52 000 MW Ro/SS-A autoantigen in Sjogren's syndrome/systemic lupus erythematosus (Ro52) is an interferon-gamma inducible tripartite motif protein associated with membrane proximal structures," *Immunology*, vol. 106, no. 2, pp. 246–256, 2002.

[70] E. Ben-Chetrit, R. I. Fox, and E. M. Tan, "Dissociation of immune responses to the ss-a (ro) 52-kd and 60-kd polypeptides in systemic lupus erythematosus and sjögren's syndrome," *Arthritis and Rheumatism*, vol. 33, no. 3, pp. 349–355, 1990.

[71] E. Ben-Chetrit, E. K. Chan, K. F. Sullivan, and E. M. Tan, "A 52-kD protein is a novel component of the ss-a/ro antigenic particle," *The Journal of Experimental Medicine*, vol. 167, no. 5, pp. 1560–1571, 1988.

[72] S. Salomonsson, S. E. Sonesson, L. Ottosson et al., "Ro/SSA autoantibodies directly bind cardiomyocytes, disturb calcium homeostasis, and mediate congenital heart block," *The Journal of Experimental Medicine*, vol. 201, no. 1, pp. 11–17, 2005.

[73] A. H. Keeble, Z. Khan, A. Forster, and L. C. James, "TRIM21 is an IgG receptor that is structurally, thermodynamically, and kinetically conserved," *Proceedings of the National Academy of Sciences of the United States of America*, vol. 105, no. 16, pp. 6045–6050, 2008.

[74] D. L. Mallery, W. A. McEwan, S. R. Bidgood, G. J. Towers, C. M. Johnson, and L. C. James, "Antibodies mediate intracellular immunity through tripartite motif-containing 21 (TRIM21)," *Proceedings of the National Academy of Sciences*

*of the United States of America*, vol. 107, no. 46, pp. 19985–19990, 2010.

[75] M. Sjöstrand, A. Ambrosi, S. Brauner et al., "Expression of the immune regulator tripartite-motif 21 is controlled by IFN regulatory factors," *Journal of Immunology*, vol. 191, no. 7, pp. 3753–3763, 2013.

[76] H. Liu, M. Li, Y. Song, and W. Xu, "TRIM21 restricts Coxsackievirus B3 replication, cardiac and pancreatic injury via interacting with MAVS and positively regulating IRF3-mediated type-I interferon production," *Frontiers in Immunology*, vol. 9, p. 2479, 2018.

[77] R. E. Watkinson, W. A. McEwan, J. C. H. Tam, M. Vaysburd, and L. C. James, "TRIM21 promotes cGAS and RIG-I sensing of viral genomes during infection by antibody-opsonized virus," *PLoS Pathogens*, vol. 11, no. 10, article e1005253, 2015.

[78] Z. Zhang, M. Bao, N. Lu, L. Weng, B. Yuan, and Y. J. Liu, "The E3 ubiquitin ligase TRIM21 negatively regulates the innate immune response to intracellular double-stranded DNA," *Nature Immunology*, vol. 14, no. 2, pp. 172–178, 2013.

[79] S. Foss, M. Bottermann, A. Jonsson, I. Sandlie, L. C. James, and J. T. Andersen, "TRIM21-from intracellular immunity to therapy," *Frontiers in Immunology*, vol. 10, p. 2049, 2019.

[80] R. Yoshimi, T. H. Chang, H. Wang, T. Atsumi, H. C. Morse III, and K. Ozato, "Gene disruption study reveals a nonredundant role for TRIM21/Ro52 in NF-kappaB-dependent cytokine expression in fibroblasts," *Journal of Immunology*, vol. 182, no. 12, pp. 7527–7538, 2009.

[81] A. Espinosa, V. Dardalhon, S. Brauner et al., "Loss of the lupus autoantigen Ro52/Trim21 induces tissue inflammation and systemic autoimmunity by disregulating the IL-23-Th17 pathway," *The Journal of Experimental Medicine*, vol. 206, no. 8, pp. 1661–1671, 2009.

[82] L. Li, J. Wei, R. K. Mallampalli, Y. Zhao, and J. Zhao, "TRIM21 mitigates human lung microvascular endothelial cells' inflammatory responses to LPS," *American Journal of Respiratory Cell and Molecular Biology*, vol. 61, no. 6, pp. 776–785, 2019.

[83] V. Natarajan, "Mind the gap between the endothelium and E3 ubiquitin ligase: TRIM21 is a viable therapeutic target in sepsis-induced endothelial dysfunction," *American Journal of Respiratory Cell and Molecular Biology*, vol. 61, no. 6, pp. 676-677, 2019.

[84] H. Schmidt, P. Freudenberger, S. Seiler, and R. Schmidt, "Genetics of subcortical vascular dementia," *Experimental Gerontology*, vol. 47, no. 11, pp. 873–877, 2012.

[85] P. Freudenberger, R. Schmidt, and H. Schmidt, "Genetics of age-related white matter lesions from linkage to genome wide association studies," *Journal of the Neurological Sciences*, vol. 322, no. 1-2, pp. 82–86, 2012.

[86] S. Li, L. Wang, B. Fu, and M. E. Dorf, "Trim65: a cofactor for regulation of the microRNA pathway," *RNA Biology*, vol. 11, no. 9, pp. 1113–1121, 2014.

[87] S. Li, L. Wang, B. Fu, M. A. Berman, A. Diallo, and M. E. Dorf, "TRIM65 regulates microRNA activity by ubiquitination of TNRC6," *Proceedings of the National Academy of Sciences of the United States of America*, vol. 111, no. 19, pp. 6970–6975, 2014.

[88] X. Lang, T. Tang, T. Jin, C. Ding, R. Zhou, and W. Jiang, "TRIM65-catalized ubiquitination is essential for MDA5-mediated antiviral innate immunity," *The Journal of Experimental Medicine*, vol. 214, no. 2, pp. 459–473, 2017.

[89] J. Meng, Z. Yao, Y. He et al., "ARRDC4 regulates enterovirus 71-induced innate immune response by promoting K63 polyubiquitination of MDA5 through TRIM65," *Cell Death & Disease*, vol. 8, no. 6, article e2866, 2017.

[90] Y. Li, C. Ma, T. Zhou, Y. Liu, L. Sun, and Z. Yu, "TRIM65 negatively regulates p53 through ubiquitination," *Biochemical and Biophysical Research Communications*, vol. 473, no. 1, pp. 278–282, 2016.

[91] W. S. Wei, X. Chen, L. Y. Guo et al., "TRIM65 supports bladder urothelial carcinoma cell aggressiveness by promoting ANXA2 ubiquitination and degradation," *Cancer Letters*, vol. 435, pp. 10–22, 2018.

[92] Y. F. Yang, M. F. Zhang, Q. H. Tian, and C. Z. Zhang, "TRIM65 triggers $\beta$-catenin signaling via ubiquitylation of Axin1 to promote hepatocellular carcinoma," *Journal of Cell Science*, vol. 130, no. 18, pp. 3108–3115, 2017.

[93] D. Chen, Y. Li, X. Zhang et al., "Ubiquitin ligase TRIM65 promotes colorectal cancer metastasis by targeting ARHGAP35 for protein degradation," *Oncogene*, vol. 38, no. 37, pp. 6429–6444, 2019.

[94] B. Liu, Y. Tang, P. Yang, C. Wu, and Y. Huang, "TRIM65 in white matter lesions, innate immunity and tumor," *Current Molecular Pharmacology*, vol. 14, 2021.

[95] J. Wang, X. Liang, T. Yu et al., "TRIM65 is a potential oncogenic protein via ERK1/2 on Jurkat and Raji cells: a therapeutic target in human lymphoma malignancies," *Cell Biology International*, vol. 42, no. 11, pp. 1503–1510, 2018.

[96] Y. T. Wu, S. Y. Ma, W. Q. Sun et al., "TRIM65 promotes invasion of endometrial stromal cells by activating ERK1/2/C-myc signaling via ubiquitination of DUSP6," *The Journal of Clinical Endocrinology and Metabolism*, vol. 106, no. 2, pp. 526–538, 2021.

[97] Y. Jia, K. Chen, P. Lin et al., "Treatment of acute lung injury by targeting MG53-mediated cell membrane repair," *Nature Communications*, vol. 5, no. 1, 2014.

[98] M. Sermersheim, A. D. Kenney, P. H. Lin et al., "MG53 suppresses interferon-$\beta$ and inflammation via regulation of ryanodine receptor-mediated intracellular calcium signaling," *Nature Communications*, vol. 11, no. 1, p. 3624, 2020.

[99] P. Duann, H. Li, P. Lin et al., "MG53-mediated cell membrane repair protects against acute kidney injury," *Science Translational Medicine*, vol. 7, no. 279, p. 279ra236, 2015.

[100] C. S. Lee, J. S. Yi, S. Y. Jung et al., "TRIM72 negatively regulates myogenesis via targeting insulin receptor substrate-1," *Cell Death and Differentiation*, vol. 17, no. 8, pp. 1254–1265, 2010.

[101] C. Cai, H. Masumiya, N. Weisleder et al., "MG53 nucleates assembly of cell membrane repair machinery," *Nature Cell Biology*, vol. 11, no. 1, pp. 56–64, 2009.

[102] M. Hwang, J. K. Ko, N. Weisleder, H. Takeshima, and J. Ma, "Redox-dependent oligomerization through a leucine zipper motif is essential for MG53-mediated cell membrane repair," *American Journal of Physiology Cell Physiology*, vol. 301, no. 1, pp. C106–C114, 2011.

[103] M. K. Ahn, K. J. Lee, C. Cai et al., "Mitsugumin 53 regulates extracellular $Ca^{2+}$ entry and intracellular $Ca^{2+}$ release via Orai1 and RyR1 in skeletal muscle," *Scientific Reports*, vol. 6, no. 1, p. 36909, 2016.

[104] T. Tan, Y. G. Ko, and J. Ma, "Dual function of MG53 in membrane repair and insulin signaling," *BMB Reports*, vol. 49, no. 8, pp. 414–423, 2016.

[105] Z. Li, L. Wang, H. Yue et al., "MG53, a tissue repair protein with broad applications in regenerative medicine," *Cell*, vol. 10, no. 1, p. 122, 2021.

[106] A. D. Kenney, Z. Li, Z. Bian et al., "Recombinant MG53 protein protects mice from lethal influenza virus infection," *American Journal of Respiratory and Critical Care Medicine*, vol. 203, no. 2, pp. 254–257, 2021.

Hindawi
Journal of Immunology Research
Volume 2021, Article ID 3598135, 9 pages
https://doi.org/10.1155/2021/3598135

*Research Article*

# Elevated Serum Chloride Levels Contribute to a Poor Prognosis in Patients with IgA Nephropathy

**Yaling Zhai,[1,2] Xingchen Yao,[1,2] Yuanyuan Qi,[1,2] Jingge Gao,[1,2] Yazhuo Chen,[1,2] Xinnian Wang,[1,2] Feng Wu,[1,2] and Zhanzheng Zhao[1,2]**

[1]*Department of Nephrology, The First Affiliated Hospital of Zhengzhou University, Zhengzhou, China*
[2]*The Renal Research Institution of Zhengzhou University, Zhengzhou, China*

Correspondence should be addressed to Zhanzheng Zhao; zhanzhengzhao@zzu.edu.cn

Received 6 April 2021; Revised 18 July 2021; Accepted 27 August 2021; Published 8 October 2021

Academic Editor: Meng-Hao Huang



*Introduction*. The identification of reliable prognostic factors is a crucial requirement for patients with IgA nephropathy (IgAN). Here, we explored the relationship between serum chloride levels and prognosis in patients with IgAN. *Methods*. We recruited all patients with primary IgAN, as diagnosed by renal biopsy, between 1st January 2015 and 1st April 2019. Patients were divided two groups (high chloride group and low chloride group) based on the best cut-off values from survival receiver operating characteristic (ROC) curves. The baseline clinicopathological characteristics of two groups were then compared. Cox proportional hazard models were used to determine the prognostic value of serum chloride levels in patients with IgAN. Finally, we screened reliable prognostic indicators and built a clinical prediction model and validated the performance of the model. *Results*. Compared with patients in the high chloride group, patients in the low chloride group had significantly lower levels of 24-hour urinary total protein (24 h-UTP), serum creatinine (sCr), and higher levels of hemoglobin (Hb), albumin (all $p < 0.05$), and less proportion of Oxford classification grade E1 (endothelial cell proliferation) and T2 (renal tubule atrophy or renal interstitial fibrosis). Cox analysis revealed that serum chloride level ≥ 105.4 mmol/L was a significant and independent risk factor for prognosis in patients with IgAN ($p < 0.05$). Serum chloride, sCr, T, hypertension, and Hb were used to generate a predictive model for prognosis. The*c*-indices of our predictive model were 0.80, 0.86, and 0.78, for 1, 2, and 3 years, respectively; Brier scores were 0.06, 0.09, and 0.16, respectively. *Conclusions*. A serum chloride level ≥ 105.4 mmol/l was identified as a significant and independent risk factor for the prognosis of patients with IgAN. A predictive prognosis model was generated using serum chloride, sCr, T, hypertension, and Hb; this model exhibited a good predictive effect.

## 1. Introduction

Primary IgA nephropathy (IgAN) is the most common type of idiopathic glomerulonephritis in the world and the main cause of end-stage renal disease (ESRD) in patients with primary glomerular disease [1]. At present, the most accepted pathogenic mechanism underlying IgAN relates to the "multiple hits" theory [2], "Hit-1," production of galactose-deficient IgA1 (Gd-IgA1) in circulation, "Hit-2," production of antibodies against Gd-IgA1, "Hit-3," formation of Gd-IgA1 containing circulating immune complex (CIC), and "Hit-4," deposition of CIC in kidney that contributes to renal injury. The important role of immunological and inflammatory mechanisms in the occurrence and development of IgAN has gradually become widely recognized [2–4]. Moreover, researchers have gradually identified a number of predictors for the prognosis of patients with IgAN based on clinical, pathological, genetic, and noninvasive biological markers [5]. However, these parameters are associated with poor sensitivity, trauma, and high costs. Therefore, there is a clear need to identify a more convenient and accurate predictor of prognosis for patients with IgAN.

The progressive loss of the kidney function is inevitably associated with a number of electrolyte and acid-based alterations [6–9]. Most of these disorders are intricately linked to the morbidity and mortality of patients with kidney disease [10], particularly with regards to potassium imbalance, metabolic acidosis, and the dysregulation of bone mineral

metabolism. The chloride ion is the most abundant anion in the extracellular fluid and plays a crucial role in regulating a number of functions in the human body [11], including the maintenance of osmotic pressure, acid-based balance, muscular activity, and the movement of water between fluid compartments [11]. Over time, studies have increasingly begun to recognize the importance of chloride, especially with ongoing investigations relating to acid-base mechanisms [12] and chloride ion channels [13]. However, very few studies have investigated the relationship between serum chloride and the renal prognosis of IgAN. Based on previous studies, serum chloride disorders may exert an adverse effect on renal function; it is currently believed that hyperchloremia is more closely related to the severity of kidney injury than hypochloremia [14]. Higher levels of serum chloride can cause the release of thromboxane [15] and enhance the response of renal vasoconstrictors, such as angiotensin II [16]. In addition, high chloride levels can induce a glomerular feedback mechanism in dense plaques, thus causing the contraction of afferent arterioles and the glomerular mesentery; this process may also reduce glomerular filtration rate [17]. In addition, high chloride levels are often associated with metabolic acidosis [12]. Perchloric acidosis increases the production of endothelin-1 and aldosterone, thus leading to tubulointerstitial inflammation and injury, thereby accelerating the progression of chronic kidney disease (CKD) [10]. Therefore, we hypothesized that serum chloride levels will affect the clinical and pathological indicators and prognosis of IgAN. The main objective of this study was to explore the relationship between serum chloride and the clinical and pathological indicators of IgAN, as well as the prognosis of patients with this condition.

## 2. Materials and Methods

*2.1. Study Population.* We enrolled patients with a biopsy-based diagnosis of primary IgAN between 1st January 2015 and 1st April 2019 in the First Affiliated Hospital of Zhengzhou University. The inclusion criteria included the following items: (1) primary IgAN was diagnosed by renal biopsy, (2) the follow-up time was more than 6 months, and (3) no glucocorticoid or immunosuppressants were used before renal biopsy and (4) an initial estimated glomerular filtration rate (eGFR) $\geq 15\,\mathrm{mL/min/1.73\,m^2}$ at the time of renal biopsy. The following exclusion criteria were applied: (1) patients with secondary IgAN, including those with chronic hepatitis B, Henoch-Schonlein purpura, ankylosing spondylitis, systemic lupus erythematosus, and rheumatoid arthritis; (2) patients for whom the number of glomeruli in renal biopsy specimens was <10; (3) patients who did not have a complete set of clinicopathological data; (4) patients with an $\mathrm{eGFR} < 15\,\mathrm{mL \cdot min^{-1}}\ (1.73\,\mathrm{m^2})^{-1}$; (5) patients with acute kidney failure at the time of renal biopsy; and (6) patients who had used choride-containing fluids before renal biopsy.

*2.2. Acquisition of Clinical, Biochemical, and Histopathological Data.* Baseline clinicopathological data were recorded at the time of the renal biopsy. The Oxford classification was used to score each patient's condition; this involved two renal pathologists who were blinded to the clinical data. First, the data were independently diagnosed by a junior nephrology pathologist and then reviewed by a senior nephrology pathologist. If these physicians had different opinions, the diagnosis of a senior nephrologist was prevail [18]. The mesangial cell proliferation score (M) was defined as M0 if the score was ≤0.5 and M1 if the score was>0.5. Endothelial cell hyperplasia (E) and segmental sclerosis or adhesion (S) were defined as E0 and S0 if absent and E1 and S1 if present. Renal tubule atrophy or renal interstitial fibrosis (T) was defined as T0 if 0% -25% of the cortical area was associated with renal tubule atrophy or renal interstitial fibrosis, T1 for 26% -50%, and T2 for >50%. Crescentic lesions (C) were defined as C0 if there were no crescents, C1 for <25% globular crescents, or C2 for ≥25% globular crescents. The degree of vascular injury (A) was defined as A0 if there were no obvious abnormalities, A1 if there was vascular wall thickening, and A2 if there was vascular wall thickening and other lesions, such as fibrinoid necrosis and vitreous degeneration. Renal tubular necrosis was scored as 0 if absent and 1 if present. Immunofluorescence results relating to immunoglobulin G (IgG), immunoglobulin M (IgM), immunoglobulin A (IgA), and glomerular C3 were scored as follows: 0 represents -/+, 1 represents +, 2 represents ++, 3 represents +++, and 4 represents ++++.

Serum creatinine (sCr), serum urea nitrogen (BUN), uric acid (UA), 24-hour urinary total protein (24 h-UTP), serum complements 3(sC3) and 4 (sC4), and serum immunoglobulins were detected by a sarcosine oxidase enzymatic method, a urease method, a urase-peroxidase coupling method, a biuret method, and an immunoturbidimetry method, respectively, using a Roche Cobas 8000c702 Automatic Biochemical Analyzer. Albumin and electrolytes were detected by bromocresol green colorimetry and an indirect ion selective electrode method, respectively, using a Roche Cobas 8000c701 Automatic Biochemical Analyzer. Hemoglobin was detected by a sodium dodecyl sulfate method using a Beckman Coulter LH750 Blood Cell Analyzer.

In order to analyze prognosis, we used an established definition for the composite endpoint: a doubling in sCr level when compared to baseline data, ESRD, death, or a decline in eGFR that was >30% [19]. ESRD was defined as when the eGFR was $\leq 15\,\mathrm{mL/min}$ per $1.73\,\mathrm{m^2}$ or when the patient required renal replacement therapy(RRT) (including hemodialysis, peritoneal dialysis, or renal transplantation).

*2.3. Statistical Methods.* The SurvivalROC package in *R* software (version 3.6.3; http://www.R-project.org) was used to calculate the best cut-off point for serum chloride. Normally distributed quantitative variables were expressed as means ± standard deviations (SDs), and based on the homogeneity of variance, the *t*-test or corrected *t*-test was used for comparisons between groups. Nonnormally distributed features were expressed as medians and interquartile ranges, and the Wilcoxon rank sum test was used for comparisons between groups. Categorical variables were expressed by frequency and percentage, and the chi-square test was used for comparison between groups. Kaplan-Meier survival curves,

along with unadjusted and adjusted Cox proportional hazards models, were used to analyze the relationship between serum chloride level and the prognosis of patients with IgAN. Age, sex, hypertension, 24 h-UTP, sCr, and Oxford classification scores were adjusted in multivariable-adjusted Cox proportional hazards models [20–23]. Furthermore, we built a predictive model for prognosis. Initial clinicopathological variables associated with survival were evaluated using univariate Cox regression (Supplemental Material Table 1). Then, we used forward-backward selection with the Akaike information criterion (AIC) to identify the final predictive factors. On the basis of this analysis, we used serum chloride, hypertension, sCr, hemoglobin (Hb), and Oxford classification grade T, in our final predictive model. A nomogram was then created to present the model in a visual manner. The internal stability of the model was then tested using the bootstrap approach. The model performance was evaluated based on the predictive accuracy for individual outcomes (discriminating ability) and the accuracy of point estimates of the survival function (calibration). SPSS version 21 software (SPSS Inc., Chicago, IL, USA) and *R* software (version 3.6.3, http://www.R-project.org) were used for statistical analysis. $p < 0.05$ was considered to be statistically significant.

## 3. Results

*3.1. Demographic and Clinicopathological Characteristics.* Between 1st January 2015 and 1st April 2019, we identified 394 patients with primary IgAN whose follow-up time exceeded 6 months. The clinical and pathological characteristics at baseline are summarized in Table 1. In total, 212 (54%) patients were male, and the mean age at biopsy was $35 \pm 12$ years, 154 (39%) patients had hypertension, the mean serum chloride level was $104.10 \pm 3.47$ mmol/l, the sCr was 85.25 (68.00, 120.00) umol/L, and 24 h-UTP was 1.86 (0.95,4.04) g/d. In Oxford classification, 91 (23%) patients were in the M1 group, 117 (30%) patients were in the E1 group, and 253 (64%) patients were in the S1 group, patients count with T0, T1, and T2 that was 275 (70%), 52 (13%), 67 (17%), and C0, C1, and C2 were 246 (63%),135 (34%), and 12 (3%), respectively. Patients were followed for 14 (9, 24 months) months, and 46 patients reached the composite endpoint.

*3.2. Experimental Grouping Based on Serum Chloride Levels.* According to survivalROC, the areas under the receiver operating characteristic curves (AUCs) for 1 year, 2 years, and 3 years were 0.63, 0.70, and 0.61, respectively; the best cut-off points were 105.50 for 1 year and 105.40 mmol/l for 2 years and 3 years (shown in Figure 1). The patients were divided into two groups (a low chloride group and a high chloride group) according to the cut-off value of 105.40 mmol/L. There were no significant differences in subsequent analyses regardless of whether the grouping was based on a cut-off of 105.40 mmol/L or 105.50 mmol/L. There were 247 patients in the low chloride group and 159 patients in the high chloride group.

*3.3. Patients with Higher Serum Chloride Levels Had More a Severe Clinical and Pathological Presentation.* The clinical and pathological characteristics of the 394 patients in the low chloride group and the high chloride group are shown in Table 1. The 24 h-UTP and sCr in the low chloride group were significantly lower than in the high chloride group [24-UTP: 1.46 (0.84, 3.44) vs. 2.64 (1.28, 4.98) g, $p < 0.001$; sCr: 83.00 (67.00, 111.25) vs. 94.50 (70.00, 145.00) $\mu$mol/l, $p = 0.004$]. Serum albumin and Hb levels in the low chloride group were significantly higher than those in the high chloride group [serum albumin: 39.10 (34.30, 42.90) vs. 33.80 (24.95, 38.95) g/l, $p < 0.001$; Hb: $130.40 \pm 19.30$ vs. $125.20 \pm 19.10$, $p = 0.010$]. In addition, we found that serum urea nitrogen, sC3, serum sodium, serum calcium, serum magnesium, and serum immunoglobulin G also showed significant differences when compared between the two groups. No difference between the two groups existed in other indicators including hypertension, UA, urine red blood cell, sC4, phosphorus, potassium, serum immunoglobulin A, and serum immunoglobulin M.

Furthermore, we also identified significantly fewer patients with an Oxford classification grade of E1 and an Oxford classification grade of T2 in the low chloride group [E: 185 (77)/55 (23) vs. 92 (60)/62 (40), $p < 0.001$; T: 178 (74)/30 (13)/32 (13) vs. 97 (63)/22 (14)/35 (23), $p = 0.012$]. there was no significant difference in the rest indicators including Oxford classification grade of M, S, C, and IgG, IgM, IgA, glomerular C3, A, tubular necrosis, and glomerular sclerosis, as well as segmental sclerosis.

*3.4. Serum Chloride Level Was Able to Predict the Prognosis of Patients with IgAN.* In order to investigate the relationship between serum chloride level and the prognosis of patients with IgAN, we first plotted a Kaplan-Meier renal survival curve for patients with IgAN according to serum chloride levels; results indicated that patients in the low chloride group had a significantly better renal survival rate than those in the high chloride group ($p < 0.001$) (Figure 2). Then, we performed unadjusted Cox regression analyses with no other adjusted factor except for serum chloride. These analyses showed that a significantly higher number of patients in the high chloride group reached the composite end point (hazard ratio (HR), 3.22; 95% confidence interval (95% CI), 1.76-5.86, $p < 0.001$) (Table 2). Then, we applied three adjusted Cox proportional hazards models. Our reasons for choosing these indicators were as follows. Firstly, in clinical research, age and gender need to be adjusted initially in the Cox proportional hazards model, irrespective of whether there are significant differences or not [20–23]. Secondly, hypertension, 24 h-UTP, sCr, and Oxford classification scores have been proven to be vital risk factors for the prognosis of patients with IgAN [20–23]. When adjusted for sex, age, sCr, 24 h-UTP, hypertension, and Oxford classification scores, a serum chloride level ≥ 105.4 mmol/L still showed a significant association with a poor renal outcome in patients with IgAN (model 1: HR, 3.09; 95% CI, 1.69-5.64, $p < 0.001$; model 2: HR, 2.33; 95% CI, 1.20-4.55, $p = 0.01$; model 3: HR, 2.05; 95% CI, 1.03-4.07, $p = 0.04$). These results revealed that a serum chloride level ≥ 105.40 mmol/l was an independent risk factor for the prognosis of patients with IgAN (Table 2).

Table 1: Relationship between the serum chloride and demographic, clinical, and pathologic data.

| Characters | Total ($n = 394$) | Low group ($n = 247$) | High group ($n = 159$) | $p$ value |
|---|---|---|---|---|
| Demographic data | | | | |
| Age (years) | 35 ± 12 | 34 ± 12 | 36.±12 | 0.050 |
| Male ($n$%) | 212 (54) | 125 (52) | 87 (57) | 0.392 |
| Clinical data | | | | |
| Hypertension ($n$%) | 154 (39%) | 89 (36%) | 65 (41%) | 0.309 |
| BUN (mmol/l) | 5.80 (4.50, 7.70) | 5.62 (4.40, 7.15) | 6.20 (4.62, 8.31) | 0.043 |
| sCr (umol/l) | 85.25 (68.00, 120.00) | 83.00 (67.00, 111.25) | 94.50 (70.00, 145.00) | 0.004 |
| UA (umol/l) | 341.00 (283.00,422.00) | 329.00 (271.00, 415.00) | 369.00 (293.75, 427.25) | 0.093 |
| ALB (g/l) | 37.30 (29.20, 41.50) | 39.10 (34.30, 42.90) | 33.80 (24.95, 38.95) | <0.001 |
| 24 h-UTP (g/d) | 1.86 (0.95,4.04) | 1.46 (0.84,3.44) | 2.64 (1.28,4.98) | <0.001 |
| Urine RBC (/HP) | 42.00 (9.00,181.00) | 41.00 (10.00,161.00) | 49.00 (8.00,187.00) | 0.730 |
| Serum C3 (g/l) | 1.16 (0.93,1.41) | 1.20 (0.98,1.48) | 1.11 (0.90,1.26) | 0.004 |
| Serum C4 (g/l) | 0.26 (0.21,0.32) | 0.25 (0.21,0.31) | 0.28 (0.21,0.33) | 0.124 |
| Hb (g/l) | 128.40 ± 19.40 | 130.40 ± 19.30 | 125.20 ± 19.10 | 0.010 |
| K (mmol/l) | 4.42 ± 0.49 | 4.38 ± 0.45 | 4.47 ± 0.55 | 0.091 |
| Na (mmol/l) | 143.00 ± 3.00 | 142.00 ± 3.00 | 144.00 ± 3.00 | <0.001 |
| Ca (mmol/l) | 2.20 ± 0.17 | 2.24 ± 0.16 | 2.14 ± 0.18 | <0.001 |
| Mg(mmol/l) | 0.94 ± 0.11 | 0.95 ± 0.10 | 0.93 ± 0.11 | 0.016 |
| P (mmol/l) | 1.24 ± 0.24 | 1.24 ± 0.22 | 1.24 ± 0.26 | 0.812 |
| SIgA (g/l) | 2.89 (2.12,3.88) | 2.86 (2.17,3.95) | 2.89 (1.97,3.75) | 0.459 |
| SIgG (g/l) | 9.69 (6.57,11.80) | 10.20 (7.99,12.80) | 8.63 (5.32,10.97) | 0.009 |
| SIgM (g/l) | 1.01 (0.76,1.43) | 1.06 (0.83,1.40) | 0.91 (0.66,1.50) | 0.137 |
| Histopathological data | | | | |
| M [M0/M1, $n$ (%)] | 303 (77)/91 (23) | 192 (80)/48 (20) | 111 (72)/43 (28) | 0.069 |
| E [E0/E1, $n$ (%)] | 277 (70)/117 (30) | 185 (77)/55 (23) | 92 (60)/62 (40) | <0.001 |
| S [S0/S1, $n$ (%)] | 141 (36)/253 (64) | 87 (36)/153 (64) | 54 (35)/100 (65) | 0.811 |
| T [T0/T1/T2, $n$ (%)] | 275 (70)/52 (13)/67 (17) | 178 (74)/30 (13)/32 (13) | 97 (63)/22 (14)/35 (23) | 0.012 |
| C [C0/C1/C2, $n$ (%)] | 246 (63)/135 (34)/12 (3) | 155 (65)/78 (33)/6 (3) | 91 (59)/57 (37)/6 (4) | 0.227 |
| IgG [0/1/2, $n$ (%)] | 325 (83)/50 (13)/18 (5) | 195 (82)/33 (14)/11 (5) | 130 (84)/17 (11)/7 (5) | 0.491 |
| IgM (0/1/2/3, $n$ (%)] | 115 (29)/200 (51)/66 (17)/4 (1) | 70 (30)/123 (53)/38 (16)/3 (1) | 45 (30)/77 (51)/28 (18)/1 (0.7) | 0.835 |
| IgA [0/1/2/3/4, $n$ (%)] | 4 (1)/22 (6)/277 (71)/88 (22)/1 (0.3) | 2 (0.8)/10 (4)/168 (71)/57 (24)/1 (0.4) | 2 (1)/12 (8)/109 (71)/31 (20)/0 (0) | 0.133 |
| C3 [0/1/2/3, $n$ (%)] | 108 (28)/82 (21)/165 (42)/33 (9) | 62 (26)/55 (23)/100 (42)/19 (8) | 46 (31)/27 (18)/65 (42)/14 (9) | 0.909 |
| A [0/1/2, $n$ (%)] | 133 (34)/83 (21)/178 (45) | 90 (38)/46 (19)/104 (43) | 43 (28)/37 (24)/74 (48) | 0.131 |
| Tubular necrosis [0/1, $n$ (%)] | 37 (95)/19 (5) | 229 (95)/11 (5) | 146 (95)/8 (5) | 0.782 |
| GS% | 0.10 (0.00,0.27) | 0.10 (0.00,0.26) | 0.09 (0.00,0.34) | 0.707 |
| SS% | 0.04 (0.00,0.10) | 0.03 (0.00,0.10) | 0.04 (0.00,0.11) | 0.703 |

Low group: serum chloride < 105.4 mmol/L and high group: serum choride ≥ 105.4 mmol/L. BUN: blood urine nitrogen; sCr: serum creatinine; UA: urine acid; ALB: albumin; 24 h-UTP: 24hour-urine protein; urine RBC: urine red blood cell; serum C3: serum complement 3; serum C4: serum complement 4; Hb: hemoglobin; K: potassium; Na: sodium; Ca: calcium; Mg: magnesium; P: phosphorus; SIgA: serum immunoglobulin A; SIgG: serum immunoglobulin G; SIgM: serum immunoglobulin M. For Oxford classification, mesangial cell proliferation score (M): M0 for score ≤ 0.5, M1 for score > 0.5; endothelial cell hyperplasia (E): E0 for absent and E1 for present; segmental sclerosis or adhesion (S): S0 for absent and S1 for present; renal tubule atrophy or renal interstitial fibrosis (T): T0 for 25% renal tubule atrophy or renal interstitial fibrosis, T1 for 26% ~ 50% ,and T2 ≥ 50%; crescentic lesions (C): C0 is no crescent, C1 is <25% globular crescent and C2 is ≥25% globular crescent. For immunofluorescence, immunoglobulin G(IgG): 0 for -/+, 1 for +, and 2 for ++; IgM, immunoglobulin M(IgM): 0 for -/+, 1 for +, 2 for ++, and 3 for +++; immunoglobulin A(IgA): 0 for-/+, 1 for +, 2 for ++, 3 for +++, and 4 for ++++; complement 3(C3): 0 for-/+, 1 for +, 2 for ++, and 3 for+++; the degree of vascular injury (A): 0 for no obvious abnormality, 1 for simple vascular wall thickening and 2 for not only vascular wall thickening, but also other lesions, such as fibrinoid necrosis and vitreous degeneration; renal tubular necrosis: 0 for no necrosis and 1 for necrosis. GS: glomerular sclerosis; SS: segmental sclerosis.

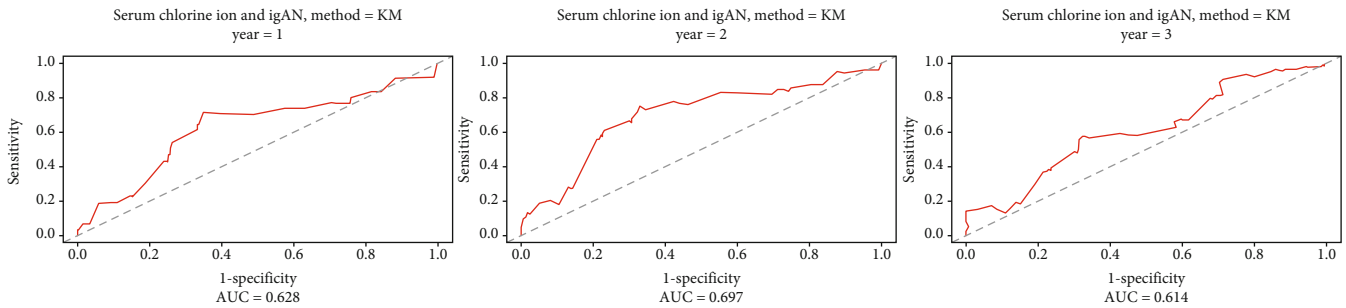


Figure 1: Survival receiver operating characteristic (ROC) curves for 1-, 3-, and 3-year survival. The areas under the receiver operating characteristics curves (AUCs) were 0.63, 0.70, and 0.61 for 1-, 2-, and 3-year follow-up, respectively. The cut-off values were 105.50 for 1-year follow-up and 105.40 for 2- and 3- ear follow-up.

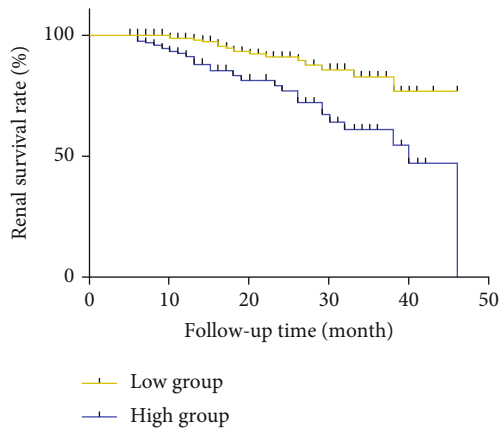


Figure 2: Kaplan-Meier renal survival curves for patients with IgA nephropathy (IgAN) according to serum chloride levels. Patients with IgAN were classified into two groups according to serum chloride levels: a low chloride group (<105.4 mmol/L, red line) and a high chloride group (≥105.4 mmol/L, blue line). Log-rank rest revealed that the cumulative renal survival rates in the high chloride group were significantly worse than those in the low chloride group ($p < 0.001$).

Table 2: Cox regression analysis of the effect of serum chloride ion on the prognosis of IgAN patients.

| Models | HR (95% CI) | $p$ value |
|---|---|---|
| Unadjusted | 3.22 (1.76-5.86) | <0.001 |
| Model1[a] | 3.09 (1.69-5.64) | <0.001 |
| Model2[b] | 2.33 (1.20-4.55) | 0.01 |
| Model3[c] | 2.05 (1.03-4.07) | 0.04 |

HR: hazard ratio; 95% CI: 95% confidence interval. Unadjusted model only included serum chloride which as qualitative data (<105.4 mmol/L and ≥105.4 mmol/L). Serum chloride < 105.4 mmol/L was reference. [a]Model 1 was adjusted for sex and age. Sex was analyzed as dichotomous data, and the male was used as reference. [b]Model 2 was adjusted for covariates in model 1 plus serum creatinine, 24-hour urine protein, and hypertension (yes or no), and no hypertension was used as reference. [c]Model 3 was adjusted for covariates in model 2 plus Oxford classification grade M (mesangial hypercellularity), E (the presence of endocapillary proliferation), S (segmental glomerulosclerosis/adhesion), T (severity of tubular atrophy/interstitial fibrosis), and C (presence of crescent) scores. The latter five variables were analyzed as categorical data. M0/E0/S0/T0/C0 was used as references.

*3.5. Generation of a Predictive Prognostic Model Based on Clinical and Pathological Parameters and Internal Validation.* According to univariate Cox regression analysis, we incorporated serum chloride level (<105.40 mmol/L or ≥105.40 mmol/L), hypertension (yes or no), sCr, UA, 24 h-UTP, serum phosphorus, Hb, and Oxford classification grade (T, M, S, and A) as our initial prognostic features (Supplemental Material Table 1). Then, these parameters were reduced to the five most useful potential predictors: serum chloride (<105.40 mmol/L or ≥105.40 mmol/L), sCr, Oxford classification grade T, hypertension, and Hb using forward-backward selection with the AIC. A nomogram based on the prognosis model was then constructed to estimate 1-, 2- and 3-year renal survival (shown in Figure 3). Then, bootstrap validation, with 200 re-tests, was employed for internal validation. The discriminative ability of the final model was then assessed using $C$ statistics. The $c$-index of this model was 0.80 (95% CI 0.65-0.94) for 1 year, 0.86 (95% CI 0.77-0.94) for 2 years, and 0.78 (95% CI 0.55-0.97) for 3 years. The calibration was evaluated using calibration plots and Brier scores. The Brier score for this model was 0.06 (95% CI 0.04-0.09) for 1 year, 0.09 (95% CI 0.05-0.13) for 2 years, and 0.16 (95% CI 0.06-0.32) for 3 years; calibration plots are shown in Figure 4.

## 4. Discussion

In the present study, we demonstrated that a serum chloride level ≥ 105.4 mmol/L at the time of renal biopsy was associated with more severe clinical and pathological manifestation and worse renal outcomes.

The early identification or prediction of a poor prognosis in patients with IgAN is often very difficult but remains a critical requirement. In recent years, an increasing number of prognostic indicators for IgAN have been investigated [24]. Of these, hypertension, massive proteinuria, renal impairment, albumin, and severe histological findings have been widely accepted [25]. However, these indicators are also associated with some disadvantages, such as limited sensitivity, trauma, or high costs. Over recent years, there has been significant interest in the investigation of biomarkers and genetic indicators [2]; however, these indicators can be relatively expensive and are therefore likely to create an economic burden for some patients. Therefore, there is a clear need to identify a convenient, cheap, specific, and highly sensitive indicator.

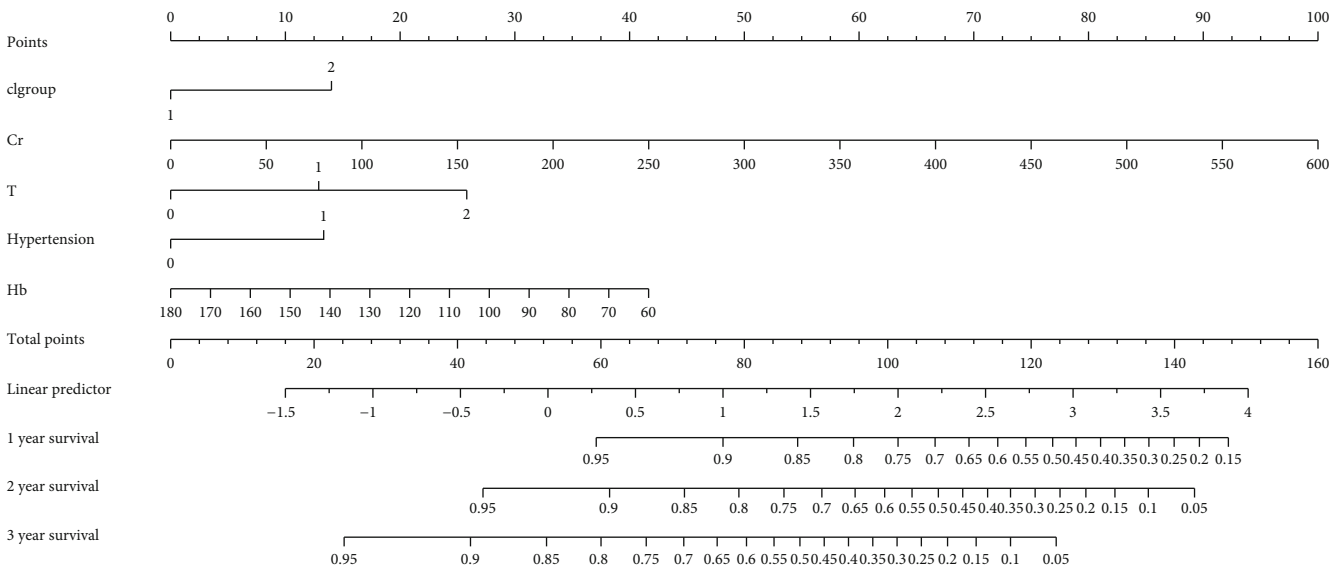


Figure 3: A nomogram predicting the probabilities of 1-, 2-, and 3-year renal survival. We built a nomogram based on the prognostic model (including sCr, hypertension, T, Hb, and serum chloride (<105.40 mmol/L or ≥105.40 mmol/L)). Higher total scores based on the sum of the assigned number of points for each factor in the nomogram were associated with a worse prognosis.

In a previous study, Mary et al. demonstrated that hypertonic NaCl in dogs led to transient renal vasodilation that was probably related to plasma hypertonicity followed by sustained renal vasoconstriction and reduced eGFR [15]. In another study, Tanake et al. used stroke-prone spontaneously hypertensive rats (SHRSP) to demonstrate that chloride ions amplified microangiopathy by exacerbating hypertension and potentially by increasing plasma renin activity (PRA), potentially by constricting the renal afferent arteriole [16]. In addition, chloride ions can induce a glomerular feedback mechanism in dense plaques that involves the contraction of afferent arterioles and the glomerular mesentery; this process can also reduce the glomerular filtration rate [26]. In addition, a high level of chloride may not only influenced IgAN by itself, and it may also be accompanied by metabolic acidosis, a process that is also known to cause damage to renal function [11]. Evidence to support a relationship between metabolic acidosis and the prognosis of patients with IgAN remains limited; although, metabolic acidosis has been associated with accelerated CKD progression and elevated all-cause mortality, thus providing new clues for the pathogenesis of IgAN [27].

In the present study, we used survivalROC software to divide our patients into two groups according to chloride levels. Although variable statistical methods are available for cut-off point selection [24], these tend not to relate to cut-off points for disease prognosis and early prediction, thus reducing clinical applicability and reducing statistical power [28]. Previous research has revealed that survivalROC software can facilitate the development of eligibility criteria for clinical trials [28]; this meant that our cut-off value was not only useful for experimental grouping but they were also useful for the early prediction of disease and prognosis.

When comparing the demographic, clinical, and pathological data between the two groups at baseline, we found that the clinical and pathological indicators of IgAN were more serious when the serum chloride level was ≥105.4 mmol/L.

According to univariate and multivariate Cox regression analyses, a serum chloride level ≥ 105.4 mmol/L was an independent and significant risk factor for IgAN. Although the range for serum chloride levels in the clinical laboratory dictates a higher limit of 106-107 mmol/L, we specifically considered the relationship between serum chloride level and the prognosis of patients with IgAN. Therefore, we believe that the higher limit of serum chloride level in such patients should be 105.4 mmol/L. This finding suggested that clinicians should pay close attention to changes in serum chloride level when treating patients with IgAN and to ensure that the level remains below 105.4 mmol/L.

In addition, we also established a clinical model for predicting prognosis that included sCr, serum chloride level (< 105.4 mmol/l or ≥105.4 mmol/l), hypertension, Oxford classification grade T, and Hb. Our predictive model for prognosis exhibited a good discriminative ability according to *c* -index. However, the calibration plots did not demonstrate very good agreement.

Next, we considered our findings in relation to a number of factors. Firstly, 0.9% NaCl solution is widely used in clinical work; this contains a concentration of chloride ions that is higher than the normal physiological range [29]. This could cause hyperchloremia and metabolic acidosis [30]. Considering the influence of serum chloride level on IgAN, it might be possible to replace NaCl solution with other solutions or restrict the use of NaCl solution; these possibilities should be investigated further. However, some articles in the existing literature may

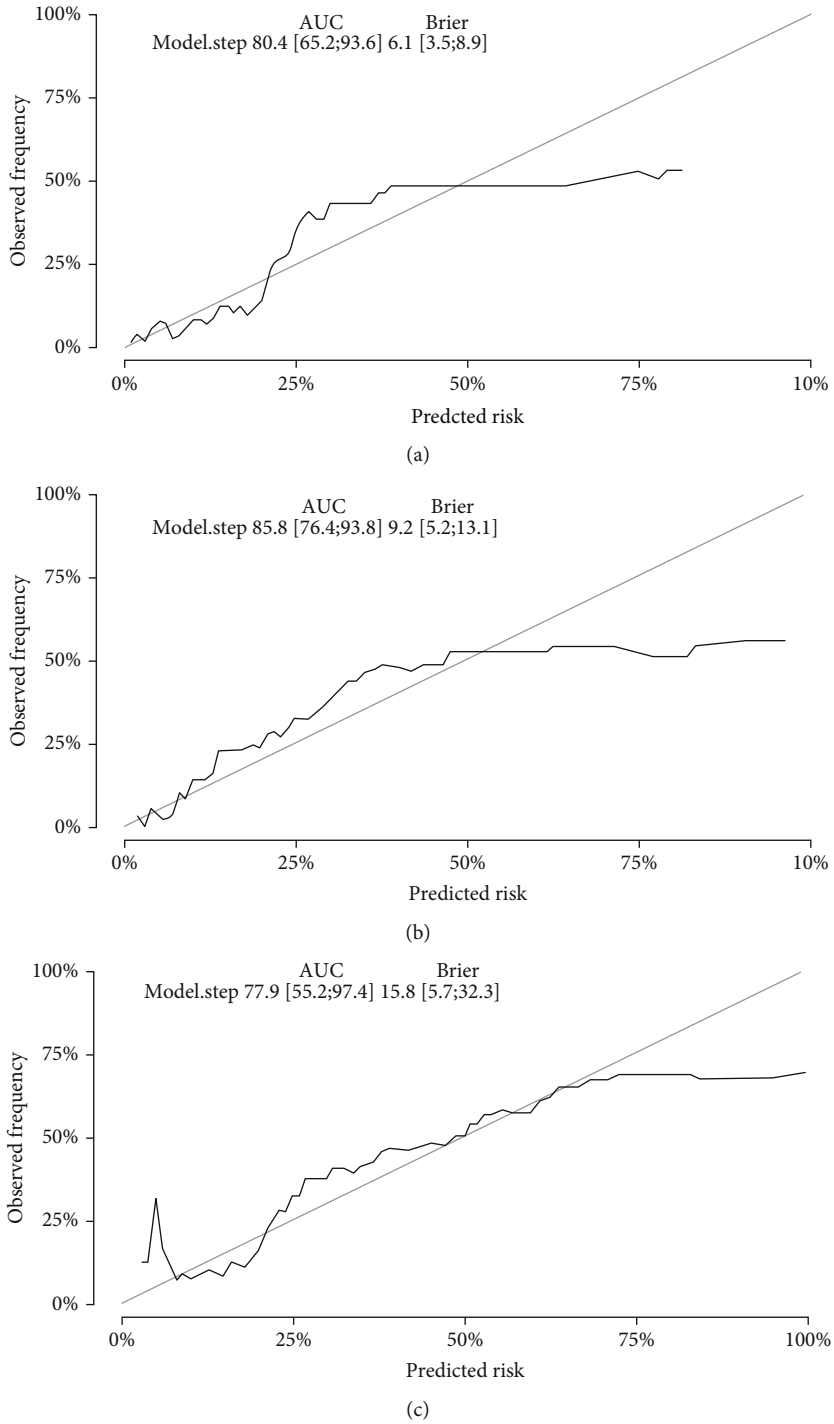


Figure 4: *c*-indices and calibration curves for the new model. 200 sample bootstrapped calibration plots for the prediction of 1–3-year renal survival are shown. The gray line represents the ideal fit while the black line represents practical fit. The *c*-indices for 1-3 years were 0.80 (95% CI: 0.65-0.94), 0.86 (95% CI: 0.77-0.94). and 0.78 (95% CI: 0.55-0.97), respectively. Brier scores were 0.06 (95% CI: 0.04-0.09), 0.09 (95% CI: 0.05-0.13). and 0.16 (95% CI: 0.06-0.32), respectively.

support our suggestions [17, 30]. For example, Malley et al. used a double-blinded method to compare the outcomes of renal transplantation patients involving lactated Ringer's solution and 0.9% NaCl solution [30]. Data showed that hyperchloremia and metabolic acidosis were more common in the group of patients receiving 0.9%NaCl. In another study, Yunos et al. proved that restricting the use of chlorine-rich fluids in a tertiary ICU reduced the incidence of acute kidney injury and renal replacement therapy requirements [30]. It is important to highlight that the blood samples acquired from patients in our study were collected on the morning of the day of renal biopsy before the use of any chlorine-containing fluids, thus indicating that our results were

not influenced by confounding factors. Secondly, 99.1% of chloride ions are reabsorbed by the kidney [26]. It may be possible to improve the prognosis of IgAN patients with high serum chloride levels by reducing the reabsorption of chloride ions in the kidney. Further research is now required to identify pathways that could inhibit the reabsorption of chloride ions. There are many mechanisms related to the reabsorption of chloride ions in the kidney [11, 31]. Of these, the most important process occurs in the latter half of the proximal tubule, where chloride ions are transported into cells via the $Cl^-$ -$HCO_3^-$ exchanger located on the top membrane of the epithelial cell; chloride ions that enter the cell are then transported to the intercellular fluid via the $K^+$-$Cl^-$ symporter on the basilar membrane and then absorbed into the blood. In addition, chloride ions can also be reabsorbed via a paracellular pathway [31]. Therefore, it may be possible to inhibit the reabsorption of chloride ions by inhibiting the transmembrane transport of chloride ions in the proximal renal tubules or the paracellular pathway, thereby reducing the serum levels of chloride and improving the prognosis of patients with IgAN. However, this possibility needs to be investigated further.

Our study has certain limitations that need to considered. First, this was a retrospective study carried out in a single-center. Second, we did not investigate the mechanisms underlying the elevation of serum chloride levels. In addition, our study has not been validated in other races.

## 5. Conclusions

In conclusion, serum chloride level $\geq 105.4$ mmol/L is an independent and significant risk factor for the prognosis of patients with IgAN. These findings indicate that we should pay more attention to serum chloride levels in patients with IgAN.

## Data Availability

Raw data used during the current study are available from the corresponding author on reasonable request for non-commercial use.

## Ethical Approval

The Medical Ethics Committee of The First Affiliated Hospital of Zhengzhou University approved the study protocol, and informed written consent was obtained from each participant. All methods reported here were carried out in accordance with the relevant guidelines and regulations of The First Affiliated Hospital of Zhengzhou University.

## Disclosure

Our manuscript has been presented as "pre-print" in "research square" according to the following link https://www.researchsquare.com/article/rs-124116/v1.

## Conflicts of Interest

The authors declare no competing interests.

## Authors' Contributions

Conceived and designed experiments were contributed by Yaling Zhai and Xingchen Yao. Data collection was contributed by Xingchen Yao, Jingge Gao, and Xinnian Wang. Xingchen Yao, Yazhuo Chen, Yuanyuan Qi, and Feng Wu analyzed the data. Zhanzheng Zhao contributed reagents/materials/analysis tools. Xingchen Yao wrote the paper. All authors read and approved the final manuscript. Yaling Zhai and Xingchen Yao are co-first authors.

## Acknowledgments

We would like to express our gratitude to all patients involved in this study and all colleagues in the nephrology lab and in the renal pathology department, who did a lot of work during the treatment follow-up of IgAN patients. The work was supported by the National Natural Science Foundation for Youths of China (Grant No. 81600555) and China Postdoctoral Science Foundation (Grant No. 2018M640684), National Natural Science Foundation of China (Grant No. 81873611), Science and Technology Innovation Team of Henan (Grant No. 17IRTSTHN020), and Foundation for Leading Personnel of Central Plains of China (Grant No. 194200510006).

## Supplementary Materials

Supplemental Table 1: univariate Cox regression for screening out variates into predictive prognosis mode. *(Supplementary Materials)*

## References

[1] R. J. Wyatt and B. A. Julian, "IgA nephropathy," *The New England Journal of Medicine*, vol. 368, no. 25, pp. 2402–2414, 2013.

[2] C. C. Szeto and P. K. Li, "MicroRNAs in IgA nephropathy," *Nature Reviews Nephrology*, vol. 10, no. 5, pp. 249–256, 2014.

[3] H. Li, M. H. Huang, J. D. Jiang, and Z. G. Peng, "Hepatitis C: from inflammatory pathogenesis to anti-inflammatory/hepatoprotective therapy," *World Journal of Gastroenterology*, vol. 24, no. 47, pp. 5297–5311, 2018.

[4] M. Huang, H. G. Kim, X. Zhong et al., "Sestrin 3 protects against diet-induced nonalcoholic steatohepatitis in mice through suppression of transforming growth factor $\beta$ signal transduction," *Hepatology*, vol. 71, no. 1, pp. 76–92, 2020.

[5] Y. Tomino, "Predictors of prognosis in IgA nephropathy," *The Kaohsiung Journal of Medical Sciences*, vol. 28, no. 10, pp. 517–520, 2012.

[6] G. Corona, C. Giuliani, J. G. Verbalis, G. Forti, M. Maggi, and A. Peri, "Hyponatremia improvement is associated with a reduced risk of mortality: evidence from a meta-analysis," *PLoS One*, vol. 10, no. 4, article e0124105, 2015.

[7] K. L. Raphael, G. Wei, B. C. Baird, T. Greene, and S. Beddhu, "Higher serum bicarbonate levels within the normal range are associated with better survival and renal outcomes in

African Americans," *Kidney International*, vol. 79, no. 3, pp. 356–362, 2011.

[8] C. P. Kovesdy, J. E. Anderson, and K. Kalantar-Zadeh, "Association of serum bicarbonate levels with mortality in patients with non-dialysis-dependent CKD," *Nephrology Dialysis Transplantation*, vol. 24, no. 4, pp. 1232–1237, 2008.

[9] J. Luo, S. M. Brunelli, D. E. Jensen, and A. Yang, "Association between serum potassium and outcomes in patients with reduced kidney function," *Clinical Journal of the American Society of Nephrology*, vol. 11, no. 1, pp. 90–100, 2016.

[10] T. Dhondup and Q. Qian, "Electrolyte and Acid-Base Disorders in Chronic Kidney Disease and End-Stage Kidney Failure," *Blood Purification*, vol. 43, no. 1-3, pp. 179–188, 2017.

[11] K. Berend, L. H. van Hulsteijn, and R. O. Gans, "Chloride: the queen of electrolytes?," *European Journal of Internal Medicine*, vol. 23, no. 3, pp. 203–211, 2012.

[12] G. T. Shires and J. Holman, "Dilution acidosis," *Annals of Internal Medicine*, vol. 28, no. 3, pp. 557–559, 1948.

[13] I. E. Veizis and C. U. Cotton, "Role of kidney chloride channels in health and disease," *Pediatric Nephrology*, vol. 22, no. 6, pp. 770–777, 2007.

[14] J. A. Neyra, F. Canepa-Escaro, X. Li et al., "Association of hyperchloremia with hospital mortality in critically Ill septic patients," *Critical Care Medicine*, vol. 43, no. 9, pp. 1938–1944, 2015.

[15] E. M. Bullivant, C. S. Wilcox, and W. J. Welch, "Intrarenal vasoconstriction during hyperchloremia: role of thromboxane," *American Journal of Physiology-Renal Physiology*, vol. 256, no. 1, pp. F152–F157, 1989.

[16] M. Tanaka, O. Schmidlin, J. L. Olson, S. L. Yi, and R. C. Morris, "Chloride-sensitive renal microangiopathy in the stroke-prone spontaneously hypertensive rat," *Kidney International*, vol. 59, no. 3, pp. 1066–1076, 2001.

[17] N. M. Yunos, R. Bellomo, N. Glassford, H. Sutcliffe, Q. Lam, and M. Bailey, "Chloride-liberal vs. chloride-restrictive intravenous fluid administration and acute kidney injury: an extended analysis," *Intensive Care Medicine*, vol. 41, no. 2, pp. 257–264, 2015.

[18] S. Liang, G. Y. Cai, Z. Y. Duan et al., "Urinary sediment miRNAs reflect tubulointerstitial damage and therapeutic response in IgA nephropathy," *BMC Nephrology*, vol. 18, no. 1, p. 63, 2017.

[19] "KDIGO glomerulonephritis (GN) guideline," 2012, http://kdigo.org/guidelines/gn/.

[20] W. Y. Guo, L. Zhu, S. J. Meng et al., "Mannose-binding lectin levels could predict prognosis in IgA nephropathy," *Journal of the American Society of Nephrology*, vol. 28, no. 11, pp. 3175–3181, 2017.

[21] X. Yang, J. Ou, H. Zhang et al., "Urinary matrix metalloproteinase 7 and prediction of IgA nephropathy progression," *American Journal of Kidney Diseases*, vol. 75, no. 3, pp. 384–393, 2020.

[22] B. Zhu, W. H. Liu, D. R. Yu et al., "The association of low hemoglobin levels with IgA nephropathy progression: a two-center cohort study of 1, 828 cases," *American Journal of Nephrology*, vol. 51, no. 8, pp. 624–634, 2020.

[23] S. J. Barbour, R. Coppo, H. Zhang et al., "Evaluating a New International Risk-Prediction Tool in IgA Nephropathy," *JAMA Internal Medicine*, vol. 179, no. 7, pp. 942–952, 2019.

[24] M. Mazumdar and J. R. Glassman, "Categorizing a prognostic variable: review of methods, code for easy implementation and applications to decision-making about cancer treatments," *Statistics in Medicine*, vol. 19, no. 1, pp. 113–132, 2000.

[25] Z. Ni, Y. Yuan, Q. Wang et al., "Time-averaged albumin predicts the long-term prognosis of IgA nephropathy patients who achieved remission," *Journal of Translational Medicine*, vol. 12, no. 1, p. 194, 2014.

[26] N. M. Yunos, R. Bellomo, D. Story, and J. Kellum, "Bench-to-bedside review: Chloride in critical illness," *Critical Care*, vol. 14, no. 4, p. 226, 2010.

[27] S. N. Shah, M. Abramowitz, T. H. Hostetter, and M. L. Melamed, "Serum bicarbonate levels and the progression of kidney disease: a cohort study," *American Journal of Kidney Diseases*, vol. 54, no. 2, pp. 270–277, 2009.

[28] P. J. Heagerty, T. Lumley, and M. S. Pepe, "Time-dependent ROC curves for censored survival data and a diagnostic marker," *Biometrics*, vol. 56, no. 2, pp. 337–344, 2000.

[29] A. Durward, S. Skellett, A. Mayer, D. Taylor, S. M. Tibby, and I. A. Murdoch, "The value of the chloride: sodium ratio in differentiating the aetiology of metabolic acidosis," *Intensive Care Medicine*, vol. 27, no. 5, pp. 828–835, 2001.

[30] C. M. N. O'Malley, R. J. Frumento, M. A. Hardy et al., "A randomized, double-blind comparison of lactated Ringer's solution and 0.9% NaCl during renal transplantation," *Anesthesia & Analgesia*, vol. 100, no. 5, pp. 1518–1524, 2005.

[31] G. Planelles, "Chloride transport in the renal proximal tubule," *Pflügers Archiv*, vol. 448, no. 6, pp. 561–570, 2004.

Hindawi
Journal of Immunology Research
Volume 2021, Article ID 7316456, 13 pages
https://doi.org/10.1155/2021/7316456

*Review Article*

# HIV-Related Immune Activation and Inflammation: Current Understanding and Strategies

**Tingxia Lv**,[1,2] **Wei Cao**,[1] **and Taisheng Li**[1,3,4]

[1]*Department of Infectious Diseases, Peking Union Medical College Hospital, Chinese Academy of Medical Sciences & Peking Union Medical College, Beijing 100730, China*
[2]*Department of Infectious Diseases, Beijing Friendship Hospital, Capital Medical University, Beijing, China*
[3]*Department of Basic Medical Sciences, School of Medicine, Tsinghua University, Beijing 100084, China*
[4]*Tsinghua-Peking Center for Life Sciences, Beijing 100084, China*

Correspondence should be addressed to Taisheng Li; litsh@263.net

Received 19 July 2021; Accepted 20 September 2021; Published 29 September 2021

Academic Editor: Xuan Huang



Although antiretroviral therapy effectively controls human immunodeficiency virus (HIV) replication, a residual chronic immune activation/inflammation persists throughout the disease. This aberrant immune activation and inflammation are considered an accelerator of non-AIDS-related events and one of the driving forces of $CD4^+$ T cell depletion. Unfortunately, HIV-associated immune activation is driven by various factors, while the mechanism of excessive inflammation has not been formally clarified. To date, several clinical interventions or treatment candidates undergoing clinical trials have been proposed to combat this systemic immune activation/inflammation. However, these strategies revealed limited results, or their nonspecific anti-inflammatory properties are similar to previous interventions. Here, we reviewed recent learnings of immune activation and persisting inflammation associated with HIV infection, as well as the current directions to overcome it. Of note, a more profound understanding of the specific mechanisms for aberrant inflammation is still imperative for identifying an effective clinical intervention strategy.

## 1. Introduction

With the development of well-tolerated and highly effective antiretroviral therapy (ART), HIV/AIDS has changed from a fatal disease into a chronic and controllable condition [1]. As a result, the life expectancy of HIV-infected patients with a high $CD4^+$ T cell count and an undetectable viral after ART is gradually approaching that of the uninfected population [2]. However, abnormal immune activation and inflammation are accompanied by the whole infection process, and antiviral therapy alone is challenging to solve these clinical problems. For example, people living with HIV (PLWH) after successful ART still showed a higher level of immune activation, characterized by elevated biomarkers such as IL-6, D-dimer, C-reactive protein (CRP), and sCD14 [3, 4]. Chronic immune system activation is a hallmark of HIV infection and better predicts disease outcome than plasma viral load [5]. However, clinical data suggested that only up to 30% of patients after ART present a modest rise of $CD4^+$ T cell levels, far from effective immune reconstitution. Moreover, levels of inflammation are associated with disease progression in PLWH [6–8], which predicts an accelerated and accentuated onset of serious non-AIDS events (SNAEs), such as neurocognitive disorders, coronary artery disease, chronic liver/kidney dysfunction, metabolic syndrome, osteoporosis, and non-HIV-associated cancers [8, 9]. As a result, patients remain susceptible to opportunistic infections and are more prone to disease progression and poor outcomes in this setting.

Admittedly, the persistence of the HIV-1 reservoir after ART is an important reason for HIV-related immune activation and inflammation [10, 11]. However, HIV-related immune activation and inflammation are a systematic and long-term process, and many other factors and mechanisms are also involved. Given its complexity and burden for patients, treatment for abnormal immune activation and inflammation has

gradually become indispensable, and clinical trials using anti-inflammatory properties are underway to eliminate this phenomenon. This review will systematically elucidate the current mechanisms and therapeutic strategies/drugs for HIV-related immune activation and inflammation.

## 2. Driving Factors for HIV-Related Immune Activation

After the antigenic stimulation of the HIV, T cell is activated and induces the innate and adaptive immune response. However, the immune activation continues even after the HIV-1 viral load decreased to an undetectable level. The underlying mechanisms of persistent immune activation are complex, and various factors have been proposed to date.

*2.1. The Persistence of HIV Viral Reservoirs.* Continuous production of viral particles by reservoir cells in ART patients remains an important source of immune activation [12]. Admittedly, viral load and inflammation were decreased and $CD4^+$ T cell elevated after ART [13]. However, after combined antiretroviral therapy (cART), a small amount of HIV in the reservoirs cannot be eliminated. Consequently, its expression products activate lymphocytes and macrophages to cause immune activation. For example, HIV envelope glycoprotein 120 (gp120) induces IL-1$\beta$ release from macrophages through binding to the chemokine receptor CCR5 and coupling to G(i)alpha protein [14]. HIV-1 structural proteins, p17, p24, and gp41, act as viral pathogen-associated molecular pattern (PAMP) signaling through TLR2 and its heterodimers leading to significantly increased immune activation via the NF$\kappa$B signaling pathway [15]. Likewise, HIV-1 ssRNA interacts with the pattern recognition receptors TLR-7 and TLR-9 in plasmacytoid dendritic cells and induces the production of IFN-$\alpha$ and may therefore contribute to chronic immune activation [16]. Thus, HIV-1 persistence in individuals is at an increased risk for developing non-AIDS-related comorbidities [17, 18]. It is reported that pretreatment $CD8^+$ T cell activation, nadir $CD4^+$ T count, and CD4 : CD8 ratio might predict reservoir size [19]. Studies also have shown that administration of integrase inhibitors could partially reduce the reservoirs, decrease the number of infected memory $CD4^+$ T cells, and significantly decrease immune activation levels such as $CD38^+CD8^+$ T cells [20–22]. Based on the current understanding of HIV, therapy targeting HIV repositories is undoubtedly one of the critical strategies.

*2.2. Intestinal Microbial Translocation.* The disturbance in gut microbiota has been widely reported in HIV-infected subjects compared with healthy controls [23, 24]. Generally, HIV destroys the $CCR5^+CD4^+$ T cells, which are abundantly present in the gut-associated lymphoid tissues, leading to the destruction of the intestinal mucosal barrier. Then, many intestinal microbial and their metabolites entered the blood circulation, inducing immune activation and hyperinflammatory response [25, 26]. Circulating lipopolysaccharide (LPS), an indicator of microbial translocation, was significantly increased in chronically HIV-infected individuals and simian immunodeficiency virus- (SIV-) infected rhesus macaques [5, 27]. The microbial translocation is also associated with the proportion of $CD8^+$ T cells overexpressing CD38, IFN concentration in the blood [26], and sustained failure during $CD4^+$ T cell reconstitution in treated patients [28]. On the other hand, the high inflammatory state of intestinal mucosa and apoptosis of intestinal epithelial cells further promoted intestinal microbial translocation [29]. Therefore, dysregulation of intestinal microbial and microbial translocation is significantly correlated with immune and inflammatory activation [30].

*2.3. Depletion of Regulatory T (Treg) Cells.* The distribution of Treg cells, the potent natural regulator, changed during chronic HIV infection and was accompanied by a shift of $CD4^+CD25^+$ Treg from the peripheral blood to peripheral lymph nodes and mucosal lymphoid tissues [31–33]. Treg cells can inhibit T cell activation and proliferation through contact-dependent mechanisms, but Treg cell itself is vulnerable to HIV infection, leading to a significant functional deficit [34, 35]. Treg cells were also reported to control immune activation during HIV-1 infection through impairing IL-2 production [36]. Even in HIV elite controllers, the decreased Treg cells are strongly associated with immune activation and can increase the incidence of atherosclerosis and other related inflammatory diseases [37, 38]. In other words, growing Treg cells may reduce HIV-associated immune activation, which is the basis of current clinical trials using statins to suppress immune activation [39].

*2.4. Coinfection with Other Viruses.* Compared to HIV-monoinfected individuals, patients with other virus infections have elevated soluble inflammatory biomarkers and surface markers of T cell activation [40–43]. HIV infection also leads to the lower immune function of the body and often causes the reactivation of some viruses that have been lurking in the body for a long time, such as cytomegalovirus (CMV) and human herpesvirus (HSV). Margolick et al. showed that in well-controlled HIV-infected patients, the body's specific T cell response to CMV would affect chronic immune activation [44]. Active HSV infection, regardless of symptoms, involves the recruitment of activated $CD4^+$ T cells to the genital area and can lead to breaks in the mucosal layer through which HIV can enter [45, 46]. HIV-1 infection also impairs HSV-specific $CD4^+$ and $CD8^+$ T cell response by reducing Th1 cytokines and CCR5 ligand secretion [47], while HSV-2 infection significantly increases the susceptibility of the host to acquire HIV and promotes the shedding of the latter during the coinfection [48]. In addition, in patients coinfected with HIV and HCV, the inflammatory response, platelet activation, and oxidative stress are more intense, indicating its enhanced immune activation [49, 50].

## 3. Pathogenesis of HIV-Related Inflammation

*3.1. Toll-Like Receptors (TLRs) and Nuclear Factor-Kappa B (NF-κB) Activation.* Toll-like receptors (TLR1-10) are pattern recognition receptors (PRRs) expressed on the surface or inside various immune cells, which could recognize

multiple PAMPs such as LPS, peptidoglycan, virus, and nucleic acid [51]. HIV single-stranded RNA (ssRNA) and double-stranded RNA (dsRNA) are formed during their life cycle and can be recognized by intracellular TLRs. For example, TLR7 recognizes the HIV ssRNA, leading to the destruction of T cells and the release of inflammatory cytokines [52]. Inflammatory activation caused by TLR3 recognition of HIV dsRNA is linked with HIV-associated blood-brain barrier disorders and neurological dysfunction [53]. HIV infection can also lead to the expression changes of TLRs. For example, TLR3 and TLR4 are not expressed in T cells of healthy people, but their expression is significantly increased after HIV infection [54]. HIV-1 ssRNA stimulation of neutrophils leads to enhanced expression of TLR7/8, RIG-I, and MDA5, decreased expression of TLR2, induction of cytokines (TNF-$\alpha$ and IL-6), and production of ROS [55]. In addition, after HIV infection, the gp120 activates IKK$\beta$, which subsequently leads to endogenous I$\kappa$B$\alpha$ phosphorylation, nuclear translocation of NF-$\kappa$B, and then overexpression of IL-6 and IL-8 [56]. HIV-associated neurocognitive disorders (HAND), which exist in approximately 50% of infected individuals even after a highly active antiretroviral therapy, correlate with the activation of NF-$\kappa$B [57]. For example, in central nervous system lesions, HIV transactivator of transcription (Tat) protein induces the expression of proinflammatory genes in astrocytes, which ultimately activates NF-$\kappa$B and upregulates the expressions of MCP-1, IL-8, CXCL10, etc. [58]. Additionally, decrement in excitatory amino acid transporter 2 (EAAT-2) in astrocyte plasma membranes leads to elevated levels of extracellular glutamate, while this increased EAAT-2 inhibition via the NF-$\kappa$B signaling pathway during HAND [59].

*3.2. Interferon and Interferon-Stimulated Genes.* HIV triggers the induction of type I IFN (IFN-$\alpha/\beta$), providing a crucial mechanism of antiviral defense and inflammation response [60, 61]. Interferon regulatory factors also participate in the induction of type I interferon, and interferon-stimulated genes (ISG) produce many subsequent effects [62]. It was reported that IFN-$\alpha/\beta$ binding to cell surface receptors induces the expression of ISG-15 by activating the downstream JAK-STAT pathway [53, 63]. The expression of ISG-15 was positively correlated with plasma viral load and $CD4^+$ T cell count in HIV-1 chronically infected patients [64]. Moreover, ISG-15 increases the expression of IP-10, a critical inflammatory factor in HIV-induced immune dysfunction and disease progression, by activating NF-$\kappa$B, suggesting the crosstalk between the NF-$\kappa$B and interferon signaling [65]. In addition, the expression of IP-10 is also negatively regulated by miR-21, and the increased expression of ISG-15 can also reduce the inhibitory effect of miR-21 on IP-10 [66].

*3.3. Cysteinyl Aspartate-Specific Protease- (Caspase-) Induced Cell Apoptosis and Pyroptosis.* Caspase family participates in apoptosis/pyroptosis under various stimulation, such as cytokines and DNA damage, of which caspase-3/8/9 is the main effector of cell apoptosis and caspase-1 mediated the pyroptosis [67]. HIV-infected cells exhibited increased programmed cell death, such as apoptosis, pyroptosis, and ferroptosis than uninfected cells [68]. The decrease of $CD4^+$ T cells can be simultaneously mediated by apoptosis and pyroptosis, while the immune activation is more closely related to pyroptosis during HIV infection [69, 70]. It is reported that the main pattern of $CD4^+$ T cell death caused by HIV is caspase-1-mediated pyroptosis (about 95%), while the proportion of cell apoptosis is less than 5% [70]. In HIV-infected patients without ART, caspase-1/3 expression in $CD4^+$ T cells and caspase-3 expression in $CD8^+$ T cells were significantly increased [71]. Meanwhile, there was a positive correlation between HLA-$DR^+CD38^+CD8^+$ T cells and $CD4^+$ T cells with high expression of caspase-1 [71]. In addition, caspase-1-mediated cell apoptosis plays a vital role in the occurrence and development of immune reconstitution inflammatory syndrome (IRIS), as evidenced by the increased serum cytokine levels and caspase-1/5 in HIV-associated tuberculosis infection patients with IRIS [72]. Besides cell death, caspases are also centrally involved in inflammation responses, among which the secretion of IL-1$\beta$ and IL-18 plays a key role [73]. After HIV infection, bystander $CD4^+$ T cells produce HIV-1 DNA, which is recognized by the host DNA receptor interferon-$\gamma$-inducible protein 16 (IFI16) and then binds to apoptosis-associated speckle-like protein (ASC) and procaspase-1 to form a functional inflammasome [74]. Then, the inflammasome mediated the cleavage and mature of pre-IL-1$\beta$ and pre-IL-18. Meanwhile, the activated caspase-1 also leads to increased cell permeability, edema/rupture, and the release of other damage-related molecular patterns (DAMP) such as HMG-B1, IL-33, and inflammatory cytokines [67, 70, 71]. It is worth mentioning that the transmission of HIV between cells promotes pyroptosis, while free virus particles could not induce pyroptosis of $CD4^+$ T cells [75].

## 4. Strategies to Reduce HIV-1 Related Immune Activation and Inflammation

Currently, the strategies aimed at coping with HIV-1-related immune activation and inflammation are still challenging due to the complexity of immune activation, the differences of the PLWH population, and uneven inclusion criteria. However, some drugs are emerging in the experimental stage though there is still a long way to go before eradicating immune activation.

### *4.1. Immunosuppressive Drugs*

*4.1.1. Prednisolone.* In 2012, Kasang et al. reported that prednisolone has beneficial effects on immunological correlates of HIV disease progression in untreated HIV-infected patients ($CD38^+CD8^+$%, $CD38^+CD4^+$%, sCD14, and LPS-binding protein (LBP)), but no additional beneficial effects in patients treated with ART [76]. Consistent with this viewpoint, Wallis et al. reported that no effect on markers of cell activation or apoptosis after eight weeks of prednisone (40 mg/d) treatment as an adjunct to ART in 24 HIV-infected subjects with >200 $CD4^+$ T cells/$\mu$L [77]. Similarly, a randomized clinical trial of prednisolone (5 mg/day, two

years) applied in ART naïve patients showed a significant decrease in immune activation (sCD14, suPAR, and CD38/HLA-DR/CD8$^+$) and an increase in CD4$^+$ T counts, while no significant effect on the primary endpoint of HIV disease progression to AIDS although viral load increased quickly than placebo [78]. Therefore, these facts might illuminate that prednisolone is more possibly associated with a stabilization of CD4$^+$ T cell count [79, 80], which predicted the promising application of prednisolone in abnormal immune activation after clearance of HIV.

*4.1.2. Chloroquine/Hydroxychloroquine (CQ/HCQ).* Agents with immunosuppressive properties were first tried in PLWH in 1998, which could both break the vicious cycle that leads to the slow attrition of the lymphocyte pools [81]. Both CQ and HCQ have been widely used in treating autoimmune conditions, such as lupus and arthritis, and they could also suppress the HIV-1 replication in patients [82]. In 2010, Murray et al. reported the combination usage of CQ with ART in PLWH and indicated a reduced activation and proliferation of memory CD8$^+$ T cells (proportions of HLA-DR, CD38, and Ki67 expression), as well as plasma LPS levels [83]. Piconi and colleagues also reported that HCQ (400 mg daily) reduced the level of activated CD4$^+$(-CD4$^+$/Ki67$^+$), CD14$^+$(CD14$^+$/CD69$^+$) T cells, and IL-6/TNF-$\alpha$, but increased the proportion of Tregs [84]. However, a placebo-controlled trial in the United Kingdom in 2012 showed that among HIV-infected patients not taking ART, 48 weeks of HCQ monotherapy (400 mg/d) did not reduce CD8$^+$ T cell activation and IL-6/D-dimer level but did result in a more significant decline in CD4$^+$ T cell count and increased viral replication [85]. Furthermore, Routy et al. conducted an open-labeled single-arm study and found no substantial changes in the levels of immune activation or inflammation markers (HLA-DR, CD38, and IL-6) after 24 weeks of ART+CQ (250 mg/d) [86]. Therefore, the role of CQ/HCQ in HIV-induced immune activation/inflammation is limited, especially in the presence of HIV. Of note, the conflicting results among different studies might be partially derived from the insufficient dosage of CQ/HCQ.

*4.1.3. Cyclosporin A (CsA).* Clinical trials suggested that CsA treatment was associated with modest but transient increases in the CD4$^+$ T count and delayed progression to AIDS [87–89]. Cyclosporin treatment also significantly decreased the production of various cytokines (IL-2, TNF-$\alpha$, and IFN-$\gamma$) in vitro [90]. Rizzardi et al. enrolled nine patients with primary HIV infection to receive CsA (0.3-0.6 mg/kg) in conjunction with ART for eight weeks, after which CsA was discontinued and ART continued for another 58 weeks. Results showed that patients with CsA treatment experienced a significant rise in CD4$^+$ T count compared to the HAART-only control. Additionally, the proportion of IFN-$\gamma$-secreting CD4+CCR7-T cells was significantly higher in the CsA group during treatment [91]. However, it is essential to underscore that CsA must be used with ART; otherwise, patients' conditions might deteriorate quickly [89, 92, 93].

*4.1.4. Rapamycin (RAPA).* As known to date, RAPA is a macrocyclic lactone antibiotic with immunosuppressive properties and is currently used for prophylaxis of rejection in patients following organ transplantation. RAPA exerts its immunosuppressive function by inhibiting the mammalian target of rapamycin (mTOR) and further prevents cytokine-mediated T cell proliferation [94, 95]. In addition, RAPA can repress HIV-1 replication and reduce the release of IL-8 and MIP-1$\alpha$ in PBMC induced by $\alpha$CD3/$\alpha$CD28 [90, 96]. Coadministration of RAPA with CsA achieved a more obvious suppressive effect for HIV-1 reactivation in vitro and inhibited the production of cytokines such as IL-2, MCP-1, MIP-1$\alpha$, IL-1$\beta$, IFN-$\gamma$, TNF-$\alpha$, and IL-6 [90]. The first clinical trial of RAPA was conducted in six HIV-infected individuals (CD4$^+$ T cell count > 100/$\mu$L and VL < 50 copies/mL) who received liver transplantation, and results showed that patients who switched to RAPA monotherapy present improved control of HIV but no benefit in maintaining a higher CD4$^+$ T cell count compared to those treated with calcineurin inhibitors [97].

*4.1.5. Tripterygium wilfordii Hook F (TwHF).* As a traditional Chinese medication, TwHF has been widely used to treat different autoimmune diseases, including rheumatoid arthritis and active Crohn's disease [98, 99]. Among the significant bioactive component extracted from TwHF, triptolide has been demonstrated to reduce LPS-induced inflammation [100–103]. Li et al. creatively combined TwHF (10 mg, three times/d) with ART in 18 immune nonresponder HIV patients. After one year of treatment by TwHF extract, CD4$^+$ T cell count markedly increased, and the percentage of CD38$^+$HLA-DR$^+$ expressed on CD8$^+$ T and CD4$^+$ T cells decreased significantly during the 12-month treatment period [104]. Given these promising results, randomized placebo-controlled studies that enrolled more patients are warranted to evaluate the effects of TwHF extract on HIV patients.

*4.2. Stains.* Statins, including atorvastatin, fluvastatin, lovastatin, pitavastatin, pravastatin, rosuvastatin, and simvastatin, were generally used to decrease cholesterol. In recent years, statins have been tried for controlling HIV-associated inflammation but yielded mixed results. Ganesan et al. conducted a study in which 24 HIV-1-infected and ART naïve adults were enrolled to receive either atorvastatin 80 mg daily or placebo for eight weeks (phase A), followed by a washout phase of 4-6 weeks and a subsequent switch to complete additional 8 weeks (phase B) in the opposite assignment. The results showed that atorvastatin reduced the proportions of circulating CD4$^+$HLA-DR$^+$ (-2.5%), CD8$^+$HLA-DR$^+$ (-5%), CD8$^+$HLA-DR$^+$CD38$^+$ T cells (-3%) [105]. In contrast, in another study by Eckard et al., no statistically significant difference was observed in the percentage of hsCRP, IL-6, sTNFR-I/II, IP10, and D-dimer between rosuvastatin (10 mg daily for 24 weeks) and placebo at initial analysis [106]. However, the secondary analysis demonstrated that rosuvastatin reduced sCD14, Lp-PLA2, and IP-10 levels over 48 weeks, with a greater decrease in the proportion of activated (CD38$^+$HLA-DR$^+$) T cells

between the arms (−38.1% *vs.* −17.8%, or CD4+ cells and −44.8% *vs.* −27.4% for CD8+ cells) [107]. It is worth noting that the safety and drug-drug interactions regarding stains should be carefully considered. For example, atorvastatin appears to be relatively safe for long-term use at submaximal doses if monitored, while pravastatin, rosuvastatin, and pitavastatin appear to have the most benign safety profiles among statins when coadministered with ART and may not require dose adjustment [108].

### 4.3. Treatment on Microbial Translocation

*4.3.1. Probiotics/Prebiotics.* Given the crucial role of decreasing bacterial translocation and proinflammatory cytokine production in the maintenance of gut homeostasis, new therapies aimed at restoring the integrity of the epithelial and gut-associated lymphoid tissue (GALT) through oral prebiotics, probiotics, or synbiotics are promising for alleviating HIV-related disease progression. Disturbance in gut microbiota has been widely reported in HIV-infected subjects, and specific intestinal microbiota might benefit HIV-infected patients during ART by improving the microbiota composition and reducing mucosal and systemic inflammation [109, 110]. Probiotics/prebiotics was partially reported to improve gastrointestinal immunity in SIV-infected macaques [111] and decrease microbial translocation and immune activation in ART-treated HIV-infected individuals [109, 112, 113]. However, the results were not always encouraging. Hummelen et al.'s study enrolled 32 women infected with HIV and given probiotic supplementation for 25 weeks; the results showed that changes in IFN-$\gamma$, IL-10, IgG, and IgE did not differ from the placebo group, which is consistent with Villar-García et al.'s study [110, 114]. Additionally, based on the potential benefits of intestinal microorganisms, food additives such as vitamin [115], recombinant lactoferrin [116], and Mediterranean diet are also being explored in HIV patients [117]. In summary, the evidence for the efficacy of probiotics, prebiotics, and synbiotics in control inflammation as presented in current studies is insufficient, and further comprehensive studies are needed to reveal their exact effect.

*4.4. Hypoglycemic Agents.* Some hypoglycemic agents have been found to benefit microbiota composition, promote gut barrier integrity, and reduce inflammation in human and animal models of diabetes. For example, treatment with metformin in PLWH alleviated lipodystrophy syndrome, hyperlipidemia, and insulin sensitivity. Moreover, metformin prevented the progression of coronary artery calcification and calcified plaque volume in PLWH with metabolic syndrome [118]. In 6 nondiabetic PLWH, metformin decreased $CD4^+$ T cell expression of the marker of cell exhaustion programmed cell death-1 (PD-1) but not T cell activation markers CD38 and HLA-DR [119]. $CD4^+$ T cell counts, $CD4^+/CD8^+$ T cell ratios, and plasma markers of inflammation/gut damage underwent minor variations in the blood in response to metformin [120]. Furthermore, treatment of nondiabetic individuals with metformin controls inflammation by improving glucose metabolism and by regulating intracellular immunometabolic checkpoints [121]. Another hypoglycemic agent, sitagliptin, was previously reported to reduce inflammation and chronic immune cell activation in cART-treated HIV-infected adults with impaired glucose tolerance. After eight weeks of sitagliptin administration, plasma hsCRP and CXCL10 concentrations and adipose tissue MCP-1 abundance were significantly declined than placebo, while the $CD4^+/CD8^+$ helper/suppressor ratio, D-dimer, and IL-6 concentrations were not significantly different [122]. Based on these preliminary but various results, large-scale and long-term studies are needed to determine whether hypoglycemic agents reduce cardiovascular risk and events in HIV-infected adults.

### 4.5. Other Drugs

*4.5.1. Antiplatelet Agents.* Increased platelet activity has been reported in ART-treated HIV infection, and in vitro studies showed that HIV-1 plasma could activate healthy platelets, which in turn activated monocytes, implicating a direct role for activated platelets in immune activation [123]. In addition, a higher thrombogenicity and inflammation/immune activation contribute to the increased cardiovascular disease risk in PLWH [124]. Therefore, antiplatelet agents were tried in ART-experienced patients. For example, one week of low-dose aspirin treatment for ART-treated HIV-1-infected subjects exhibited a decreased activation marker of T cell (CD38 and HLA-DR) and monocyte (sCD14), as well as enhanced leukocyte responses to Toll-like receptor stimulation [123]. Unfortunately, the latest result published in 2019 showed that aspirin administration 81 mg daily in addition to ART did not benefit from decreasing inflammation, while another platelet inhibitor, clopidogrel, exhibited anti-inflammatory activity in PLWH [124]. Despite the mixed results to date, traditional interventions using antiplatelet agents to reduce CVD risk in HIV have been one choice, considering the overwhelming evidence that increased platelet activation is associated with an increased risk of cardiovascular events in PLWH.

*4.5.2. Cyclooxygenase Type 2 (COX-2) Inhibitor.* Cyclooxygenase is a critical-step enzyme in the inflammatory process, which results in the direct production of inflammatory mediators. Celecoxib, a COX-2 inhibitor, has been used for 12 weeks in PLWH without ART by Kvale's group in Norway and showed reduced $CD38^+CD8^+$ T%, $PD\text{-}1^+CD8^+$ T%, IgA levels, and enhanced Treg number [125]. In 2017, this group published another study based on a novel COX-2 inhibitor etoricoxib, which also obtains a sound effect for reducing activation of CD8 T cells and improving Gag-specific T cell responses in ART naïve patients. However, in this study, etoricoxib does not modulate soluble markers of inflammation (sCD25, IP10, CD163, CD14, IL-6, and CRP), and in a surprise twist, no significant immunological effects were observed in ART-treated patients [126].

*4.5.3. Medical Cannabis.* Previous human studies suggested that cannabis, to some extent, reduced the related symptoms (anorexia, cachexia, and neuropathic pain) and morbidity/mortality in PLWH [127, 128]. As for immune activation

Table 1: Current Interventions for HIV-related Immune Activation and Inflammation.

| Drug | Main inclusion criteria/groups | Case/control | Dose | Country | Efficiency/mechanism | Reference |
|---|---|---|---|---|---|---|
| Immunosuppressive drug | | | | | | |
| Prednisolone | CD4 > 300 cells/$\mu$L, absence of AIDS-defining symptoms, ART-naïve patients | Prednisolone ($n = 163$) /placebo ($n = 163$) | 5 mg, po, qd, 2 years | Tanzania & Germany | sCD14 ↓, CD38/HLA-DR/CD8$^+$ ↓, CD4 count ↑, HIV viral load ↑ | [78] |
| Prednisolone | 5 groups: (1) HIV-1 subjects untreated; (2) HIV-1 subjects treated with prednisolone; (3) HIV-1 with ART; (4) HIV-1 with ART+ prednisolone; (5) elite controllers | Untreated ($n = 10$); prednisolone ($n = 27$); ART ($n = 30$); prednisolone+ART ($n = 31$ ); elite controllers ($n = 3$) | 5 mg/day | Germany | CD38$^+$CD8$^+$% ↓, CD38$^+$CD4$^+$% (-), sCD14 ↓, LPS-binding protein (LBP) ↓, ART group vs. ART+prednisolone group: CD38$^+$CD8$^+$% (-), D38$^+$CD4$^+$% (-), sCD14 (-), LBP (-) | [76] |
| HCQ | ART-treated HIV patients, CD4 < 200 cells/L during the last 12 months of therapy, VL < 37 HIV RNA copies/mL | Prior/posttreatment ($n = 20$) | 400 mg/day, 6 w | Italy | Ki67CD4% ↓, CD69CD14% ↓; IL-6/TNF$\alpha$ ↓, Tregs↑, IFN-$\alpha$ secreting plasmacytoid DC ↓; LPS/TLR-mediated immune activation ↓; HLADRII, CD69, and CD38/ CD45RO CD8 T% ↓ | [84] |
| HCQ | 18 to 65 years, naive to ART or no therapy in the previous 12 months; CD4$^+$T ≥ 400 cells/$\mu$L, VL ≥ 1000 copies/mL | HCQ ($n = 42$)/placebo ($n = 41$) | 400 mg, 48 w | UK | CD8$^+$ T cell activation (-), CD4$^+$ T cell activation (-), D-dimer (-), IL-6 (-), Ki67$^+$CD4, Ki67$^+$CD8, CD4 cell count ↓ | [85] |
| CQ | Off-ART (arms A and B): HIV-1-infected; on-ART (arms C and D) participants: ART ≥ 24 months, VL < 400 copies/mL, CD4 cell count < 350 cells/$\mu$L | Arm A ($n = 16$); arm B ($n = 17$) Arm C ($n = 18$); arm D ($n = 19$) | Arms A and C: CQ (250 mg,12 w)/ placebo (12 w); arms B and D: placebo (12 w)→CQ (250 mg, 12 w) | US | On-ART cohort: HLA-DR$^+$CD8$^+$ ↓, CD38$^+$CD8$^+$ ↓, IP10 ↓ | NCT00819390 |
| Cyclosporine | Primary HIV infection (HIV-1 antibody negative, HIV-1 RNA positive in plasma, and ≥3 bands in western blot) | CsA+ART ($n = 9$), ART ($n = 29$) | 0.3-0.6 mg/kg po, q12 h, 8 w | Switzerland, Italy | CsA+HAART constantly maintained higher levels of CD4+ T cells; week 48: HIV-1-specific IFN-$\gamma$-secreting CD4 T% is higher than ART alone cohort | [91] |
| TwHF | cART ≥ 2 years, plasma HIV-1 VL < 40 copies/mL and suboptimal CD4 cell recovery | INRs ($n = 9$)/inadequate responders ($n = 9$) | 10 mg, po, tid, 12 months | China | Both groups: CD4 T cell count ↑, CD38$^+$HLA-DR$^+$CD8 T cell% ↓, CD38$^+$HLA-DR$^+$CD4 T cell% ↓ | [104] |
| Stains | | | | | | |
| Atorvastatin | No ART, CD4$^+$T > 350/$\mu$L, HIV-1 RNA > 1000 copies/mL, LDL < 130 mg/dL | Atorvastatin ($n = 34$) /control ($n = 24$) | 80 mg, qd, 8 w | US | CD4$^+$HLA-DR$^+$% ↓; CD8$^+$HLA-DR$^+$% ↓; CD8$^+$HLA-DR$^+$CD38$^+$ T cells% ↓, CD4T (-), CD4$^+$HLA-DR$^+$CD38$^+$ T cells% (-), CD4$^+$CD38$^+$% (-), CD8$^+$CD38$^+$% (-) TC ↓, LDL ↓ | [105] |
| Rosuvastatin | ART duration ≥ 6 months, HIV-1 RNA < 1000 copies/mL, LDL cholesterol ≤ 130 mg/dL; hsCRP ≥ 2 mg/L and/or expression of CD38 and HLA-DR antigens ≥19% of CD8$^+$ T cells at screening | Statin ($n = 72$)/placebo ($n = 75$) | 10 mg, po, qd | US | hsCRP, IL-6, sTNFR-I/II, IP10 and D-dimer (-) Lp-PLA2 level ↓; DL cholesterol level ↓ | |

Table 1: Continued.

| Drug | Main inclusion criteria/groups | Case/control | Dose | Country | Efficiency/mechanism | Reference |
|---|---|---|---|---|---|---|
| Treatment on microbial translocation | | | | | | |
| Probiotic | Women, 18–45 years, not-normal vaginal microbiota, no ART (CD4 count > 200 cells/$\mu$L) | Probiotics ($n = 32$)/placebo ($n = 33$) | Lactobacillus rhamnosus GR-1 and Lactobacillus reuteri RC-14 ($2 \times 10^9$ colony forming units), bid, 25 w | London, Netherlands | Insignificant changes in the immune parameters IFN-$\gamma$, IL-10, IgG, and IgE | [110] |
| Synbiotic dietary supplement | Adult females, currently taking ART, CD4 count > 200 cells/$\mu$L | Synbiotic ($n = 14$)/fiber group ($n = 13$) | SynBiotic 2000®, fibers, qd, 4 w | USA | $DR^+$38-PD1-CD4% ↓, $CD38^+CD8^+$ T cells ↓, CD38, HLA-DR, PD-1% on CD4 or CD8(-), monocyte activation (-); CRP (-) | [112] |
| Probiotics | 18-80 years, without history of drug failure | Probiotics ($n = 20$)/healthy donors ($n = 11$) | 1 g(a), 48 w | Italy | $CD4^+CD38^+HLA\text{-}DR^+$ T cell ↓, $CD8^+CD38^+HLA\text{-}DR^+$ T cells ↓, IL6 ↓, CRP ↓, sCD14 (-), D-dimer (-) | [109] |
| Recombinant lactoferrin | ≥ 40 years, ART > 1 year, HIV RNA level < 200 copies/mL | A rhlactoferrin then placebo sequence (A-P, $n = 28$), placebo then rhlactoferrin (P-A, $n = 26$) | A-P: M1-3 rhlactoferrin,1500 mg bid, M5-8 placebo<br>P-A: M1-3 placebo, M5-8 rhlactoferrin,1500 mg bid | US | sCD163 ↓, IL-6 (-), D-dimer (-), sCD14 (-), $CD8^+PD1^+$% (-), $CD8^+KI67^+$% (-), $D8^+CD38^+HLADR^+$% (-), $CD4^+PD1^+$% (-), $CD4^+KI67^+$% (-), $CD4^+CD38^+HLADR^+$% (-) | [116] |
| Synbiotics | 18-65 years, ART-naïve (stage A or B), CD4 T > 350 cells/$\mu$L | Probiotic ($n = 5$), synbiotic ($n = 5$), prebiotic ($n = 5$), placebo ($n = 5$) | Lactobacillus rhamnosus HN001 +Bifidobacterium lactis Bi-07 at $10^9$ cfu/mL as probiotics, 10 g of agave inulin as prebiotic, and the combination of both as symbiotic | Mexico | IL-6 ↓, TNF-$\alpha$ (-), IL-1$\beta$ (-), IL-10 (-) | [113] |
| Hypoglycemic agents | | | | | | |
| Metformin | Age > 45 years, stable > 1 year on ART, HIV RNA < 50 copies/mL | Metformin ($n = 6$)/control ($n = 6$) | Metformin 500 mg, 24 w | Hawaii | $PD1^+$ ↓, $PD1^+TIGIT^+$ ↓, $PD1^+TIGIT^+TIM3^+CD4$ T ↓ | [119] |
| Sitagliptin | cART for the prior 6 months, $CD4^+$ T cell count ≥ 300 cells/$\mu$L, HIV RNA < 100 copies/mL | Sitagliptin 100 mg/d ($n = 18$)/placebo ($n = 20$) | 100 mg, qd, 8 w | US | hsCRP ↓, CXCL10 ↓, $CD4^+/CD8^+$ ratio (-), D-dimer (-), IL-6 (-) | [122] |
| Other drugs | | | | | | |
| Aspirin | ART for ≥48 w, HIV RNA below quantification limit for ≥48 w | HIV ($n = 15$)/control ($n = 14$) | Aspirin: 81 mg, clopidogrel: 75 mg 24 w | US | sCD14 ↑, sCD163 (-), D-dimer (-), sTNFR1 (-), sTNFR2 (-), sIL-6 (-), thrombogenicity (-), sCD14 (-) | [124] |
| Celecoxib | 18–65 years, asymptomatic, HIV-1-positive patients off ART (HIV RNA > 6000 copies/mL, $CD4^+$ T cell count > 300 cells/$\mu$L) | Celecoxib arm ($n = 17$ )/control arm ($n = 12$) | 400 mg, bid, 12 w | Norway | $CD38^+CD8^+$ T% ↓, IgA ↓, a combined score for inflammatory markers ↓, PD-$1^+CD8^+$ T% ↓, $CD3^+$ $CD4^+$ $CD25^+$ $CD127^{low/-}$ Treg ↑ | [125] |
| Cannabis | HIV-1-infected ART-treated participants | Control ($n = 128$)<br>Moderate ($n = 40$)<br>Heavy ($n = 14$) | Moderate (cannabis: 5.1-69.9 $\mu$g/L), heavy users (cannabis: ≥70 $\mu$g/L) | USA | $HLA\text{-}DR^+CD38^+CD4$% ↓, $HLA\text{-}DR^+CD38^+CD8$% ↓, $CD14^{++}CD16^-$% ↑, $CD11c^+CD123^-$ ↓ | [129] |
| Pyridostigmine | No ART, D4 T cell counts ≥ 300/$\mu$L | Pyridostigmine ($n = 9$ )/placebo ($n = 10$) | 30 mg tid, 1 w | Mexico | CD69CD4 ↓, Treg ↑, T cell proliferation ↓, IFN-$\gamma$ ↓, TNF ↓, IL4/5/10 ↑ | [131] |
| Lisinopril | HIV VL < 40-75 copies/mL, $CD4^+T$ < 350 cells/$\mu$L in INRs and ≥350 cells/$\mu$L in IRs | Lisinopril ($n = 16$)/placebo ($n = 15$) | Lisinopril 20 mg, 24 w | US | $CD38^+HLA\text{-}DR^+$ $CD4^+$ (-), $CD38^+HLA\text{-}DR^+$ $CD8^+$ (-) | |

VL: viral load; INRs: immunologic nonresponders; IRs: immunologic responders; LDL: low-density lipoprotein.

and inflammation in HIV patients, Manuzak et al. clarified that heavy cannabis users had decreased frequencies of HLA-DR$^+$CD38$^+$CD4$^+$ and CD8$^+$ T cell, increased frequencies of classical monocyte subsets (CD14$^{++}$CD16$^-$), and reduced frequencies of IL-23 and TNF-$\alpha$ producing antigen-presenting cells [129]. Moreover, recent cannabis use was associated with lower levels of inflammatory biomarkers, in both cerebrospinal fluid (CSF) and blood, suggesting its specific antineuroinflammatory effects [130]. Although there are promising benefits of cannabis for HIV/AIDS sufferers, the potential psychoactive side effects (impaired memory, euphoria, anxiety, and paranoia) and minor nonpsychoactive effects (sleepiness, tiredness, dry mouth, and red eyes) continue to be a barrier to its medical use. Also, the similar drug heroin was being tried in PLWH for treating immune activation and cardiovascular risk in HIV (NCT03976258), but no study results were posted to date.

Besides, following treatment of pyridostigmine, an ACh-esterase inhibitor, in 9 treatment-naïve HIV-1 patients with CD4$^+$ T cell count over 300 cells/$\mu$L, the fraction of CD69$^+$CD4$^+$ T cells, IFN-$\gamma$, and TNF-$\alpha$ was significantly decreased, and Treg was dampened, while IL-4/6/10 were increased compared with placebo [131]. Dipyridamole was demonstrated to inhibit the replication of HIV-1 [132]; however, in virally suppressed persons with HIV on ART, it did not decrease the soluble markers of inflammation levels but modestly reduced the levels of CD8$^+$ T cell activation [133]. Administration of mesalazine to subjects with poor CD4$^+$ T cell gain on virologically suppressive cART did not affect markers of peripheral inflammation [134]. Moreover, leflunomide was proven to reduce the proliferation of activated T cells in vitro [135], but when applied in a small RCT in cART-naive patients, it showed no significant changes in activated CD4$^+$ and CD8$^+$ T cells [136]. Finally, the potential benefits for immune activation/inflammation among HIV-1-infected subjects of other drugs, such as isotretinoin (NCT01969058) and methotrexate (NCT01949116), require additional investigation [137].

## 5. Conclusion and Perspective

In conclusion, though many pathogeneses of HIV-related immune activation and inflammation, such as HIV-1 reservoir, coinfections, and various inflammatory signaling, have been clarified, the current understanding for this complex disease does not meet the need to develop specific therapeutic approaches. Moreover, non-AIDS-related events also accelerated the disease progression. Currently, though numerous approaches and strategies have been proposed for curing HIV (Table 1), no scalable solution has yet been reached. Therefore, on the one hand, a further understanding of the specific pathogenesis or their interaction causing aberrant HIV-associated immune activation/inflammation and effective intervention strategies is still imperative. On the other hand, drug intervention at the very early stage before the HIV reservoir is composed might be a promising strategy.

## Data Availability

The data used to support the review are included within the article.

## Conflicts of Interest

The authors declare that there is no conflict of interest regarding the publication of this paper.

## Acknowledgments

This work was supported by the National Key Technologies R&D Program for the 13th Five-year Plan (2017ZX10202101) and Chinese Academy of Medical Sciences (CAMS) Innovation Fund for Medical Sciences (CAMS-12M) (2017-12M-1-014).

## References

[1] S. G. Deeks, S. R. Lewin, and D. V. Havlir, "The end of AIDS: HIV infection as a chronic disease," *The Lancet*, vol. 382, no. 9903, pp. 1525–1533, 2013.

[2] A. J. Rodger, R. Lodwick, M. Schechter et al., "Mortality in well controlled HIV in the continuous antiretroviral therapy arms of the SMART and ESPRIT trials compared with the general population," *AIDS*, vol. 27, no. 6, pp. 973–979, 2013.

[3] K. A. So-Armah, J. P. Tate, C. H. Chang et al., "Do biomarkers of inflammation, monocyte activation, and altered coagulation explain excess mortality between HIV infected and uninfected people?," *Journal of Acquired Immune Deficiency Syndromes*, vol. 72, no. 2, pp. 206–213, 2016.

[4] A. Kamat, V. Misra, E. Cassol et al., "A plasma biomarker signature of immune activation in HIV patients on antiretroviral therapy," *PLoS One*, vol. 7, no. 2, article e30881, 2012.

[5] J. M. Brenchley, D. A. Price, T. W. Schacker et al., "Microbial translocation is a cause of systemic immune activation in chronic HIV infection," *Nature Medicine*, vol. 12, no. 12, pp. 1365–1371, 2006.

[6] A. Ganesan, P. K. Chattopadhyay, T. M. Brodie et al., "Immunologic and virologic events in early HIV infection predict subsequent rate of progression," *The Journal of Infectious Diseases*, vol. 201, no. 2, pp. 272–284, 2010.

[7] A. J. Rodger, Z. Fox, J. D. Lundgren et al., "Activation and coagulation biomarkers are independent predictors of the development of opportunistic disease in patients with HIV infection," *The Journal of Infectious Diseases*, vol. 200, no. 6, pp. 973–983, 2009.

[8] P. W. Hunt, J. Brenchley, E. Sinclair et al., "Relationship between T cell activation and CD4+T cell count in HIV-seropositive individuals with undetectable plasma HIV RNA levels in the absence of therapy," *The Journal of Infectious Diseases*, vol. 197, no. 1, pp. 126–133, 2008.

[9] C. T. Longenecker, C. Sullivan, and J. V. Baker, "Immune activation and cardiovascular disease in chronic HIV infection," *Current Opinion in HIV and AIDS*, vol. 11, no. 2, pp. 216–225, 2016.

[10] Z. Kruize and N. A. Kootstra, "The role of macrophages in HIV-1 persistence and pathogenesis," *Frontiers in Microbiology*, vol. 10, p. 2828, 2019.

[11] M. Massanella, R. Fromentin, and N. Chomont, "Residual inflammation and viral reservoirs," *Current Opinion in HIV and AIDS*, vol. 11, no. 2, pp. 234–241, 2016.

[12] P. Corbeau and J. Reynes, "Immune reconstitution under antiretroviral therapy: the new challenge in HIV-1 infection," *Blood*, vol. 117, no. 21, pp. 5582–5590, 2011.

[13] C. Bourgeois, J. Gorwood, A. Olivo et al., "Contribution of adipose tissue to the chronic immune activation and inflammation associated with HIV infection and its treatment," *Frontiers in Immunology*, vol. 12, article 670566, 2021.

[14] R. Cheung, V. Ravyn, L. Wang, A. Ptasznik, and R. G. Collman, "Signaling mechanism of HIV-1 gp120 and virion-induced IL-1$\beta$ release in primary human macrophages," *Journal of Immunology*, vol. 180, no. 10, pp. 6675–6684, 2008.

[15] B. M. Henrick, X. D. Yao, K. L. Rosenthal, and the INFANT study team, "HIV-1 structural proteins serve as PAMPs for TLR2 heterodimers significantly increasing infection and innate immune activation," *Frontiers in Immunology*, vol. 6, p. 426, 2015.

[16] M. Younas, C. Psomas, J. Reynes, and P. Corbeau, "Immune activation in the course of HIV-1 infection: causes, phenotypes and persistence under therapy," *HIV Medicine*, vol. 17, no. 2, pp. 89–105, 2016.

[17] M. G. Katusiime, G. U. Van Zyl, M. F. Cotton, and M. F. Kearney, "HIV-1 persistence in children during suppressive ART," *Viruses*, vol. 13, no. 6, p. 1134, 2021.

[18] T. Lyu, Y. Yue, E. Hsieh et al., "HIV-1 CRF01_AE subtype and HIV-1 DNA level among patients with chronic HIV-1 infection: a correlation study," *BMC Infectious Diseases*, vol. 20, no. 1, p. 66, 2020.

[19] S. D. Ismail, C. Riou, S. B. Joseph et al., "Immunological correlates of the HIV-1 replication-competent reservoir size," *Clinical Infectious Diseases*, 2021.

[20] K. Wu, S. Zhang, X. Zhang et al., "IL-21 expands HIV-1-specific $CD8^+$ T memory stem cells to suppress HIV-1 replication in vitro," *Journal of Immunology Research*, vol. 2019, Article ID 1801560, 13 pages, 2019.

[21] A. Vallejo, C. Gutierrez, B. Hernandez-Novoa et al., "The effect of intensification with raltegravir on the HIV-1 reservoir of latently infected memory CD4 T cells in suppressed patients," *AIDS*, vol. 26, no. 15, pp. 1885–1894, 2012.

[22] J. M. Llibre, M. J. Buzon, M. Massanella et al., "Treatment intensification with raltegravir in subjects with sustained HIV-1 viraemia suppression: a randomized 48-week study," *Antiviral Therapy*, vol. 17, no. 2, pp. 355–364, 2011.

[23] P. Nowak, M. Troseid, E. Avershina et al., "Gut microbiota diversity predicts immune status in HIV-1 infection," *AIDS*, vol. 29, no. 18, pp. 2409–2418, 2015.

[24] B. W. Wolf, K. B. Wheeler, D. G. Ataya, and K. A. Garleb, "Safety and tolerance of *Lactobacillus reuteri* supplementation to a population infected with the human immunodeficiency virus," *Food and Chemical Toxicology*, vol. 36, no. 12, pp. 1085–1094, 1998.

[25] A. S. Zevin, L. McKinnon, A. Burgener, and N. R. Klatt, "Microbial translocation and microbiome dysbiosis in HIV-associated immune activation," *Current Opinion in HIV and AIDS*, vol. 11, no. 2, pp. 182–190, 2016.

[26] J. M. Brenchley, T. W. Schacker, L. E. Ruff et al., "CD4+ T cell depletion during all stages of HIV disease occurs predominantly in the gastrointestinal tract," *The Journal of Experimental Medicine*, vol. 200, no. 6, pp. 749–759, 2004.

[27] L. Huang, J. Deng, R. Lang, G. Liao, and W. Jiang, "Enriched LPS staining within the germinal center of a lymph node from an HIV-infected long-term nonprogressor but not from progressors," *Journal of Immunology Research*, vol. 2020, Article ID 7471380, 5 pages, 2020.

[28] G. Marchetti, G. M. Bellistrì, E. Borghi et al., "Microbial translocation is associated with sustained failure in CD4+ T-cell reconstitution in HIV-infected patients on long-term highly active antiretroviral therapy," *AIDS*, vol. 22, no. 15, pp. 2035–2038, 2008.

[29] G. Marchetti, C. Tincati, and G. Silvestri, "Microbial translocation in the pathogenesis of HIV infection and AIDS," *Clinical Microbiology Reviews*, vol. 26, no. 1, pp. 2–18, 2013.

[30] D. M. Dinh, G. E. Volpe, C. Duffalo et al., "Intestinal microbiota, microbial translocation, and systemic inflammation in chronic HIV infection," *The Journal of Infectious Diseases*, vol. 211, no. 1, pp. 19–27, 2015.

[31] J. Nilsson, A. Boasso, P. A. Velilla et al., "HIV-1-driven regulatory T-cell accumulation in lymphoid tissues is associated with disease progression in HIV/AIDS," *Blood*, vol. 108, no. 12, pp. 3808–3817, 2006.

[32] H. J. Epple, C. Loddenkemper, D. Kunkel et al., "Mucosal but not peripheral FOXP3+ regulatory T cells are highly increased in untreated HIV infection and normalize after suppressive HAART," *Blood*, vol. 108, no. 9, pp. 3072–3078, 2006.

[33] J. Andersson, A. Boasso, J. Nilsson et al., "Cutting edge: the prevalence of regulatory T cells in lymphoid tissue is correlated with viral load in HIV-infected patients," *Journal of Immunology*, vol. 174, no. 6, pp. 3143–3147, 2005.

[34] M. E. Moreno-Fernandez, W. Zapata, J. T. Blackard, G. Franchini, and C. A. Chougnet, "Human regulatory T cells are targets for human immunodeficiency virus (HIV) infection, and their susceptibility differs depending on the HIV type 1 strain," *Journal of Virology*, vol. 83, no. 24, pp. 12925–12933, 2009.

[35] T. Bopp, C. Becker, M. Klein et al., "Cyclic adenosine monophosphate is a key component of regulatory T cell-mediated suppression," *The Journal of Experimental Medicine*, vol. 204, no. 6, pp. 1303–1310, 2007.

[36] V. Terzieva, D. Popova, M. Kicheva et al., "Correlation between the degree of immune activation, production of IL-2 and FOXP3 expression in CD4+CD25+ T regulatory cells in HIV-1 infected persons under HAART," *International Immunopharmacology*, vol. 9, no. 7-8, pp. 831–836, 2009.

[37] P. W. Hunt, A. L. Landay, E. Sinclair et al., "A low T regulatory cell response may contribute to both viral control and generalized immune activation in HIV controllers," *PLoS One*, vol. 6, no. 1, article e15924, 2011.

[38] J. M. Shaw, P. W. Hunt, J. W. Critchfield et al., "Short communication: HIV+ viremic slow progressors maintain low regulatory T cell numbers in rectal mucosa but exhibit high T cell activation," *AIDS Research and Human Retroviruses*, vol. 29, no. 1, pp. 172–177, 2013.

[39] A. L. Rodriguez-Perea, C. J. Montoya, S. Olek, C. A. Chougnet, and P. A. Velilla, "Statins increase the frequency of circulating $CD4^+FOXP3^+$ regulatory T cells in healthy individuals," *Journal of Immunology Research*, vol. 2015, Article ID 762506, 8 pages, 2015.

[40] M. L. Freeman, J. C. Mudd, C. L. Shive et al., "CD8 T-cell expansion and inflammation linked to CMV coinfection in

ART-treated HIV infection," *Clinical Infectious Diseases*, vol. 62, no. 3, pp. 392–396, 2016.

[41] A. Boulougoura and I. Sereti, "HIV infection and immune activation," *Current Opinion in HIV and AIDS*, vol. 11, no. 2, pp. 191–200, 2016.

[42] Z. A. Sullivan, E. B. Wong, T. Ndung'u, V. O. Kasprowicz, and W. R. Bishai, "Latent and active tuberculosis infection increase immune activation in individuals co-infected with HIV," *eBioMedicine*, vol. 2, no. 4, pp. 334–340, 2015.

[43] P. W. Hunt, J. N. Martin, E. Sinclair et al., "Valganciclovir reduces T cell activation in HIV-infected individuals with incomplete $CD4^+$ T cell recovery on antiretroviral therapy," *The Journal of Infectious Diseases*, vol. 203, no. 10, pp. 1474–1483, 2011.

[44] J. B. Margolick, J. H. Bream, T. L. Nilles et al., "Relationship between T-cell responses to CMV, markers of inflammation, and frailty in HIV-uninfected and HIV-infected men in the multicenter AIDS cohort study," *The Journal of Infectious Diseases*, vol. 218, no. 2, pp. 249–258, 2018.

[45] K. J. Looker, J. A. R. Elmes, S. L. Gottlieb et al., "Effect of HSV-2 infection on subsequent HIV acquisition: an updated systematic review and meta-analysis," *The Lancet Infectious Diseases*, vol. 17, no. 12, pp. 1303–1316, 2017.

[46] P. van de Perre, M. Segondy, V. Foulongne et al., "Herpes simplex virus and HIV-1: deciphering viral synergy," *The Lancet Infectious Diseases*, vol. 8, no. 8, pp. 490–497, 2008.

[47] P. A. Rubbo, E. Tuaillon, N. Nagot et al., "HIV-1 infection impairs HSV-specific $CD4^+$ and $CD8^+$ T-cell response by reducing Th1 cytokines and CCR5 ligand secretion," *Journal of Acquired Immune Deficiency Syndromes*, vol. 58, no. 1, pp. 9–17, 2011.

[48] A. R. Retamal-Diaz, A. M. Kalergis, S. M. Bueno, and P. A. Gonzalez, "A herpes simplex virus type 2 deleted for glycoprotein D enables dendritic cells to activate $CD4^+$ and $CD8^+$ T cells," *Frontiers in Immunology*, vol. 8, p. 904, 2017.

[49] J. A. Moreno, L. M. Beltran, A. Rubio-Navarro, J. Puig, J. M. Amaro-Villalobos, and J. Egido, "Influence of immune activation and inflammatory response on cardiovascular risk associated with the human immunodeficiency virus," *Vascular Health and Risk Management*, vol. 11, pp. 35–48, 2015.

[50] M. Huang, J. D. Jiang, and Z. Peng, "Recent advances in the anti-HCV mechanisms of interferon," *Acta Pharmaceutica Sinica B*, vol. 4, no. 4, pp. 241–247, 2014.

[51] H. Li, M. H. Huang, J. D. Jiang, and Z. G. Peng, "Hepatitis C: from inflammatory pathogenesis to anti-inflammatory/hepatoprotective therapy," *World Journal of Gastroenterology*, vol. 24, no. 47, pp. 5297–5311, 2018.

[52] J. J. Chang, A. Lacas, R. J. Lindsay et al., "Differential regulation of toll-like receptor pathways in acute and chronic HIV-1 infection," *AIDS*, vol. 26, no. 5, pp. 533–541, 2012.

[53] K. Shuai and B. Liu, "Regulation of JAK-STAT signalling in the immune system," *Nature Reviews Immunology*, vol. 3, no. 11, pp. 900–911, 2003.

[54] C. M. Sanders, J. M. Cruse, and R. E. Lewis, "Toll-like receptors, cytokines and HIV-1," *Experimental and Molecular Pathology*, vol. 84, no. 1, pp. 31–36, 2008.

[55] D. M. Giraldo, J. C. Hernandez, and S. Urcuqui-Inchima, "HIV-1-derived single-stranded RNA acts as activator of human neutrophils," *Immunologic Research*, vol. 64, no. 5-6, pp. 1185–1194, 2016.

[56] A. Shah, A. S. Verma, K. H. Patel et al., "HIV-1 gp120 induces expression of IL-6 through a nuclear factor-kappa B-dependent mechanism: suppression by gp120 specific small interfering RNA," *PLoS One*, vol. 6, no. 6, article e21261, 2011.

[57] A. R. Nookala and A. Kumar, "Molecular mechanisms involved in HIV-1 Tat-mediated induction of IL-6 and IL-8 in astrocytes," *Journal of Neuroinflammation*, vol. 11, no. 1, p. 214, 2014.

[58] G. S. Youn, D. J. Kwon, S. M. Ju et al., "Celastrol ameliorates HIV-1 Tat-induced inflammatory responses via NF-kappaB and AP-1 inhibition and heme oxygenase-1 induction in astrocytes," *Toxicology and Applied Pharmacology*, vol. 280, no. 1, pp. 42–52, 2014.

[59] X. Ye, Y. Zhang, Q. Xu et al., "HIV-1 Tat inhibits EAAT-2 through AEG-1 upregulation in models of HIV-associated neurocognitive disorder," *Oncotarget*, vol. 8, no. 24, pp. 39922–39934, 2017.

[60] B. He, J. T. Tran, and D. J. Sanchez, "Manipulation of type I interferon signaling by HIV and AIDS-associated viruses," *Journal of Immunology Research*, vol. 2019, Article ID 8685312, 10 pages, 2019.

[61] F. Wan and M. J. Lenardo, "The nuclear signaling of NF-$\kappa$B: current knowledge, new insights, and future perspectives," *Cell Research*, vol. 20, no. 1, pp. 24–33, 2010.

[62] P. M. Pitha, "Innate antiviral response: role in HIV-1 infection," *Viruses*, vol. 3, no. 7, pp. 1179–1203, 2011.

[63] A. Okumura, G. Lu, I. Pitha-Rowe, and P. M. Pitha, "Innate antiviral response targets HIV-1 release by the induction of ubiquitin-like protein ISG15," *Proceedings of the National Academy of Sciences of the United States of America*, vol. 103, no. 5, pp. 1440–1445, 2006.

[64] C. Scagnolari, K. Monteleone, C. Selvaggi et al., "ISG15 expression correlates with HIV-1 viral load and with factors regulating T cell response," *Immunobiology*, vol. 221, no. 2, pp. 282–290, 2016.

[65] S. Darb-Esfahani, B. V. Sinn, M. Rudl et al., "Interferon-stimulated gene, 15 kDa (ISG15) in ovarian high-grade serous carcinoma," *International Journal of Gynecological Pathology*, vol. 33, no. 1, pp. 16–22, 2014.

[66] X. Wu, L. L. Zhang, L. B. Yin et al., "Deregulated microRNA-21 expression in monocytes from HIV-infected patients contributes to elevated IP-10 secretion in HIV infection," *Frontiers in Immunology*, vol. 8, p. 1122, 2017.

[67] E. A. Miao, J. V. Rajan, and A. Aderem, "Caspase-1-induced pyroptotic cell death," *Immunological Reviews*, vol. 243, no. 1, pp. 206–214, 2011.

[68] Z. Q. Yao, D. Cao, S. Khanal et al., "A matter of life or death: productively infected and bystander CD4 T cells in early HIV infection," *Frontiers in Immunology*, vol. 11, article 626431, 2020.

[69] W. H. V. Carvalho-Silva, J. L. Andrade-Santos, F. O. Souto, A. V. C. Coelho, S. Crovella, and R. L. Guimaraes, "Immunological recovery failure in cART-treated HIV-positive patients is associated with reduced thymic output and RTE CD4+ T cell death by pyroptosis," *Journal of Leukocyte Biology*, vol. 107, no. 1, pp. 85–94, 2020.

[70] G. Doitsh, N. L. Galloway, X. Geng et al., "Cell death by pyroptosis drives CD4 T-cell depletion in HIV-1 infection," *Nature*, vol. 505, no. 7484, pp. 509–514, 2014.

[71] R. Cai, L. Liu, B. Luo et al., "Caspase-1 activity in CD4 T cells is downregulated following antiretroviral therapy for HIV-1

infection," *AIDS Research and Human Retroviruses*, vol. 33, no. 2, pp. 164–171, 2017.

[72] R. P. J. Lai, G. Meintjes, K. A. Wilkinson et al., "HIV-tuberculosis-associated immune reconstitution inflammatory syndrome is characterized by toll-like receptor and inflammasome signalling," *Nature Communications*, vol. 6, no. 1, p. 8451, 2015.

[73] N. Van Opdenbosch and M. Lamkanfi, "Caspases in cell death, inflammation, and disease," *Immunity*, vol. 50, no. 6, pp. 1352–1364, 2019.

[74] T. P. Hurst, A. Aswad, T. Karamitros, A. Katzourakis, A. L. Smith, and G. Magiorkinis, "Interferon-inducible protein 16 (IFI16) has a broad-spectrum binding ability against ssDNA targets: an evolutionary hypothesis for antiretroviral checkpoint," *Frontiers in Microbiology*, vol. 10, p. 1426, 2019.

[75] N. L. Galloway, G. Doitsh, K. M. Monroe et al., "Cell-to-cell transmission of HIV-1 is required to trigger pyroptotic death of lymphoid-tissue-derived CD4 T cells," *Cell Reports*, vol. 12, no. 10, pp. 1555–1563, 2015.

[76] C. Kasang, A. Ulmer, N. Donhauser et al., "HIV patients treated with low-dose prednisolone exhibit lower immune activation than untreated patients," *BMC Infectious Diseases*, vol. 12, no. 1, p. 14, 2012.

[77] R. S. Wallis, R. Kalayjian, J. M. Jacobson et al., "A study of the immunology, virology, and safety of prednisone in HIV-1-infected subjects with CD4 cell counts of 200 to 700 mm −3," *Journal of Acquired Immune Deficiency Syndromes*, vol. 32, no. 3, pp. 281–286, 2003.

[78] C. Kasang, S. Kalluvya, C. Majinge et al., "Effects of prednisolone on disease progression in antiretroviral-untreated HIV infection: a 2-year randomized, double-blind placebo-controlled clinical trial," *PLoS One*, vol. 11, no. 1, article e0146678, 2016.

[79] A. Ulmer, M. Muller, B. Bertisch-Mollenhoff, and B. Frietsch, "Low dose prednisolone reduces CD4+ T cell loss in therapy-naive HIV-patients without antiretroviral therapy," *European Journal of Medical Research*, vol. 10, no. 3, pp. 105–109, 2005.

[80] J. M. Andrieu, W. Lu, and R. Levy, "Sustained increases in CD4 cell counts in asymptomatic human," *The Journal of Infectious Diseases*, vol. 171, no. 3, pp. 523–530, 1995.

[81] C. Argyropoulos and A. Mouzaki, "Immunosuppressive drugs in HIV disease," *Current Topics in Medicinal Chemistry*, vol. 6, no. 16, pp. 1769–1789, 2006.

[82] K. Sperber, T. H. Kalb, V. J. Stecher, R. Banerjee, and L. Mayer, "Inhibition of human immunodeficiency virus type 1 replication by hydroxychloroquine in T cells and monocytes," *AIDS Research and Human Retroviruses*, vol. 9, no. 1, pp. 91–98, 1993.

[83] S. M. Murray, C. M. Down, D. R. Boulware et al., "Reduction of immune activation with chloroquine therapy during chronic HIV infection," *Journal of Virology*, vol. 84, no. 22, pp. 12082–12086, 2010.

[84] S. Piconi, S. Parisotto, G. Rizzardini et al., "Hydroxychloroquine drastically reduces immune activation in HIV-infected, antiretroviral therapy-treated immunologic nonresponders," *Blood*, vol. 118, no. 12, pp. 3263–3272, 2011.

[85] N. I. Paton, R. L. Goodall, D. T. Dunn et al., "Effects of hydroxychloroquine on immune activation and disease progression among HIV-infected patients not receiving antiretroviral Therapy," *JAMA*, vol. 308, no. 4, pp. 353–361, 2012.

[86] J. P. Routy, J. B. Angel, M. Patel et al., "Assessment of chloroquine as a modulator of immune activation to improve CD4 recovery in immune nonresponding HIV-infected patients receiving antiretroviral therapy," *HIV Medicine*, vol. 16, no. 1, pp. 48–56, 2015.

[87] R. Levy, J. P. Jais, J. M. Tourani, P. Even, and J. M. Andrieu, "Long-term follow-up of HIV positive asymptomatic patients having received cyclosporin A," *Advances in Experimental Medicine and Biology*, vol. 374, pp. 229–234, 1995.

[88] T. Diaz, S. Y. Chu, J. W. Buehler et al., "Socioeconomic differences among people with AIDS: results from a multistate surveillance project," *American Journal of Preventive Medicine*, vol. 10, no. 4, pp. 217–222, 1994.

[89] J. M. Andrieu, P. Even, A. Venet et al., "Effects of cyclosporin on T-cell subsets in human immunodeficiency virus disease," *Clinical Immunology and Immunopathology*, vol. 47, no. 2, pp. 181–198, 1988.

[90] A. R. Martin, R. A. Pollack, A. Capoferri, R. F. Ambinder, C. M. Durand, and R. F. Siliciano, "Rapamycin-mediated mTOR inhibition uncouples HIV-1 latency reversal from cytokine-associated toxicity," *The Journal of Clinical Investigation*, vol. 127, no. 2, pp. 651–656, 2017.

[91] G. P. Rizzardi, A. Harari, B. Capiluppi et al., "Treatment of primary HIV-1 infection with cyclosporin A coupled with highly active antiretroviral therapy," *The Journal of Clinical Investigation*, vol. 109, no. 5, pp. 681–688, 2002.

[92] L. H. Calabrese, M. M. Lederman, J. Spritzler et al., "Placebo-controlled trial of cyclosporin-A in HIV-1 disease: implications for solid organ transplantation," *Journal of Acquired Immune Deficiency Syndromes*, vol. 29, no. 4, pp. 356–362, 2002.

[93] A. Phillips, M. A. Wainberg, R. Coates et al., "Cyclosporine-induced deterioration in patients with AIDS," *CMAJ*, vol. 140, no. 12, pp. 1456–1460, 1989.

[94] A. Heredia, A. Amoroso, C. Davis et al., "Rapamycin causes down-regulation of CCR5 and accumulation of anti-HIV $\beta$-chemokines: an approach to suppress R5 strains of HIV-1," *Proceedings of the National Academy of Sciences of the United States of America*, vol. 100, no. 18, pp. 10411–10416, 2003.

[95] J. Gonzalez, T. Harris, G. Childs, and M. B. Prystowsky, "Rapamycin blocks IL-2-driven T cell cycle progression while preserving T cell survival," *Blood Cells, Molecules & Diseases*, vol. 27, no. 3, pp. 572–585, 2001.

[96] J. Roy, J. S. Paquette, J. F. Fortin, and M. J. Tremblay, "The immunosuppressant rapamycin represses human immunodeficiency virus type 1 replication," *Antimicrobial Agents and Chemotherapy*, vol. 46, no. 11, pp. 3447–3455, 2002.

[97] F. di Benedetto, S. di Sandro, N. de Ruvo et al., "First report on a series of HIV patients undergoing rapamycin monotherapy after liver transplantation," *Transplantation*, vol. 89, no. 6, pp. 733–738, 2010.

[98] R. Goldbach-Mansky, M. Wilson, R. Fleischmann et al., "Comparison of *Tripterygium wilfordii* Hook F versus sulfasalazine in the treatment of rheumatoid arthritis," *Annals of Internal Medicine*, vol. 151, no. 4, p. 229, 2009.

[99] J. Ren, Q. Tao, X. Wang, Z. Wang, and J. Li, "Efficacy of T2 in active Crohn's disease: a prospective study report," *Digestive Diseases and Sciences*, vol. 52, no. 8, pp. 1790–1797, 2007.

[100] Y. Lu, X. Bao, T. Sun, J. Xu, W. Zheng, and P. Shen, "Triptolide attenuate the oxidative stress induced by LPS/D-GalN in

mice," *Journal of Cellular Biochemistry*, vol. 113, no. 3, pp. 1022–1033, 2012.

[101] V. Premkumar, M. Dey, R. Dorn, and I. Raskin, "MyD88-dependent and independent pathways of toll-like receptors are engaged in biological activity of triptolide in ligand-stimulated macrophages," *BMC Chemical Biology*, vol. 10, no. 1, p. 3, 2010.

[102] R. Matta, X. Wang, H. Ge, W. Ray, L. D. Nelin, and Y. Liu, "Triptolide induces anti-inflammatory cellular responses," *American Journal of Translational Research*, vol. 1, no. 3, pp. 267–282, 2009.

[103] J. Ma, M. Dey, H. Yang et al., "Anti-inflammatory and immunosuppressive compounds from _Tripterygium wilfordii_," *Phytochemistry*, vol. 68, no. 8, pp. 1172–1178, 2007.

[104] T. Li, J. Xie, Y. Li et al., "*Tripterygium wilfordii* Hook F extract in cART-treated HIV patients with poor immune response: a pilot study to assess its immunomodulatory effects and safety," *HIV Clinical Trials*, vol. 16, no. 2, pp. 49–56, 2015.

[105] A. Ganesan, N. Crum-Cianflone, J. Higgins et al., "High dose atorvastatin decreases cellular markers of immune activation without affecting HIV-1 RNA levels: results of a double-blind randomized placebo controlled clinical trial," *The Journal of Infectious Diseases*, vol. 203, no. 6, pp. 756–764, 2011.

[106] A. R. Eckard, Y. Jiang, S. M. Debanne, N. T. Funderburg, and G. A. McComsey, "Effect of 24 weeks of statin therapy on systemic and vascular inflammation in HIV-infected subjects receiving antiretroviral therapy," *The Journal of Infectious Diseases*, vol. 209, no. 8, pp. 1156–1164, 2014.

[107] N. T. Funderburg, Y. Jiang, S. M. Debanne et al., "Rosuvastatin reduces vascular inflammation and T-cell and monocyte activation in HIV-infected subjects on antiretroviral therapy," *Journal of Acquired Immune Deficiency Syndromes*, vol. 68, no. 4, pp. 396–404, 2015.

[108] M. J. Feinstein, C. J. Achenbach, N. J. Stone, and D. M. Lloyd-Jones, "A systematic review of the usefulness of statin therapy in HIV-infected patients," *The American Journal of Cardiology*, vol. 115, no. 12, pp. 1760–1766, 2015.

[109] G. d'Ettorre, G. Ceccarelli, N. Giustini et al., "Probiotics reduce inflammation in antiretroviral treated, HIV-infected individuals: results of the "Probio-HIV" clinical trial," *PLoS One*, vol. 10, no. 9, article e0137200, 2015.

[110] R. Hummelen, J. Changalucha, N. L. Butamanya et al., "Effect of 25 weeks probiotic supplementation on immune function of HIV patients," *Gut Microbes*, vol. 2, no. 2, pp. 80–85, 2011.

[111] N. R. Klatt, L. A. Canary, X. Sun et al., "Probiotic/prebiotic supplementation of antiretrovirals improves gastrointestinal immunity in SIV-infected macaques," *The Journal of Clinical Investigation*, vol. 123, no. 2, pp. 903–907, 2013.

[112] M. Schunter, H. Chu, T. L. Hayes et al., "Randomized pilot trial of a synbiotic dietary supplement in chronic HIV-1 infection," *BMC Complementary and Alternative Medicine*, vol. 12, no. 1, p. 84, 2012.

[113] L. A. González-Hernández, L. F. Jave-Suarez, M. Fafutis-Morris et al., "Synbiotic therapy decreases microbial translocation and inflammation and improves immunological status in HIV-infected patients: a double-blind randomized controlled pilot trial," *Nutrition Journal*, vol. 11, no. 1, p. 90, 2012.

[114] J. Villar-García, J. J. Hernández, R. Güerri-Fernández et al., "Effect of probiotics (Saccharomyces boulardii) on microbial translocation and inflammation in HIV-treated Patients," *Journal of Acquired Immune Deficiency Syndromes*, vol. 68, no. 3, pp. 256–263, 2015.

[115] B. Lebouché, M. A. Jenabian, J. Singer et al., "The role of extended-release niacin on immune activation and neurocognition in HIV-infected patients treated with antiretroviral therapy - CTN PT006: study protocol for a randomized controlled trial," *Trials*, vol. 15, no. 1, p. 390, 2014.

[116] O. Sortino, K. H. Hullsiek, E. Richards et al., "The effects of recombinant human lactoferrin on immune activation and the intestinal microbiome among persons living with human immunodeficiency virus and receiving antiretroviral therapy," *The Journal of Infectious Diseases*, vol. 219, no. 12, pp. 1963–1968, 2019.

[117] C. Stradling, G. N. Thomas, K. Hemming, S. Taylor, and S. Taheri, "Randomized parallel-group pilot trial (Best foods for your heart) comparing the effects of a Mediterranean Portfolio diet with a low saturated fat diet on HIV dyslipidemia," *Clinical Nutrition*, vol. 40, no. 3, pp. 860–869, 2021.

[118] K. Fitch, S. Abbara, H. Lee et al., "Effects of lifestyle modification and metformin on atherosclerotic indices among HIV-infected patients with the metabolic syndrome," *AIDS*, vol. 26, no. 5, pp. 587–597, 2012.

[119] C. M. Shikuma, G. M. Chew, L. Kohorn et al., "Short communication: metformin reduces CD4 T cell exhaustion in HIV-infected adults on suppressive antiretroviral therapy," *AIDS Research and Human Retroviruses*, vol. 36, no. 4, pp. 303–305, 2020.

[120] D. Planas, A. Pagliuzza, R. Ponte et al., "LILAC pilot study: effects of metformin on mTOR activation and HIV reservoir persistence during antiretroviral therapy," *eBioMedicine*, vol. 65, article 103270, 2021.

[121] J. P. Routy, S. Isnard, V. Mehraj et al., "Effect of metformin on the size of the HIV reservoir in non-diabetic ART-treated individuals: single-arm non-randomised Lilac pilot study protocol," *BMJ Open*, vol. 9, no. 4, article e028444, 2019.

[122] C. Best, H. Struthers, E. Laciny, M. Royal, D. N. Reeds, and K. E. Yarasheski, "Sitagliptin reduces inflammation and chronic immune cell activation in HIV+ adults with impaired glucose tolerance," *The Journal of Clinical Endocrinology and Metabolism*, vol. 100, no. 7, pp. 2621–2629, 2015.

[123] M. O'Brien, E. Montenont, L. Hu et al., "Aspirin attenuates platelet activation and immune activation in HIV-1-infected subjects on antiretroviral therapy," *Journal of Acquired Immune Deficiency Syndromes*, vol. 63, no. 3, pp. 280–288, 2013.

[124] M. P. O'Brien, M. U. Zafar, J. C. Rodriguez et al., "Targeting thrombogenicity and inflammation in chronic HIV infection," *Science Advances*, vol. 5, no. 6, 2019.

[125] F. O. Pettersen, E. A. Torheim, A. E. Dahm et al., "An exploratory trial of cyclooxygenase type 2 inhibitor in HIV-1 infection: downregulated immune activation and improved T cell-dependent vaccine responses," *Journal of Virology*, vol. 85, no. 13, pp. 6557–6566, 2011.

[126] C. Prebensen, M. Trøseid, T. Ueland et al., "Immune activation and HIV-specific T cell responses are modulated by a cyclooxygenase-2 inhibitor in untreated HIV-infected individuals: an exploratory clinical trial," *PLoS One*, vol. 12, no. 5, article e0176527, 2017.

[127] E. E. Lutge, A. Gray, N. Siegfried, and Cochrane HIV/AIDS Group, "The medical use of cannabis for reducing morbidity and mortality in patients with HIV/AIDS," *Cochrane Database of Systematic Reviews*, no. 4, article CD005175, 2013.

[128] F. Grotenhermen and K. Muller-Vahl, "The therapeutic potential of cannabis and cannabinoids," *Deutsches Ärzteblatt International*, vol. 109, no. 29-30, pp. 495–501, 2012.

[129] J. A. Manuzak, T. M. Gott, J. S. Kirkwood et al., "Heavy Cannabis use associated with reduction in activated and inflammatory immune cell frequencies in antiretroviral therapy-treated human immunodeficiency virus-infected individuals," *Clinical Infectious Diseases*, vol. 66, no. 12, pp. 1872–1882, 2018.

[130] R. J. Ellis, S. N. Peterson, Y. Li et al., "Recent cannabis use in HIV is associated with reduced inflammatory markers in CSF and blood," *Neurol Neuroimmunol Neuroinflamm*, vol. 7, no. 5, 2020.

[131] S. I. Valdes-Ferrer, J. C. Crispin, P. F. Belaunzaran, C. G. Cantu-Brito, J. Sierra-Madero, and J. Alcocer-Varela, "Acetylcholine-esterase inhibitor pyridostigmine decreases T cell overactivation in patients infected by HIV," *AIDS Research and Human Retroviruses*, vol. 25, no. 8, pp. 749–755, 2009.

[132] K. A. Metcalf Pate and J. L. Mankowski, "HIV and SIV associated thrombocytopenia: an expanding role for platelets in the pathogenesis of HIV," *Drug Discovery Today: Disease Mechanisms*, vol. 8, no. 1-2, pp. e25–e32, 2011.

[133] B. J. C. Macatangay, E. K. Jackson, K. Z. Abebe et al., "A randomized, placebo-controlled, pilot clinical trial of dipyridamole to decrease human immunodeficiency virus-associated chronic inflammation," *The Journal of Infectious Diseases*, vol. 221, no. 10, pp. 1598–1606, 2020.

[134] M. Somsouk, R. M. Dunham, M. Cohen et al., "The immunologic effects of mesalamine in treated HIV-infected individuals with incomplete CD4+ T cell recovery: a randomized crossover trial," *PLoS One*, vol. 9, no. 12, article e116306, 2014.

[135] H. M. Cherwinski, R. G. Cohn, P. Cheung et al., "The immunosuppressant leflunomide inhibits lymphocyte proliferation by inhibiting pyrimidine biosynthesis," *The Journal of Pharmacology and Experimental Therapeutics*, vol. 275, no. 2, pp. 1043–1049, 1995.

[136] S. W. Read, M. DeGrezia, E. J. Ciccone et al., "The effect of leflunomide on cycling and activation of T-cells in HIV-1-infected participants," *PLoS One*, vol. 5, no. 8, article e11937, 2010.

[137] P. Y. Hsue, H. J. Ribaudo, S. G. Deeks et al., "Safety and impact of low-dose methotrexate on endothelial function and inflammation in individuals with treated human immunodeficiency virus: AIDS Clinical Trials Group study A5314," *Clinical Infectious Diseases*, vol. 68, no. 11, pp. 1877–1886, 2019.

Hindawi
Journal of Immunology Research
Volume 2021, Article ID 1125199, 10 pages
https://doi.org/10.1155/2021/1125199

*Research Article*

# Remote Inflammatory Preconditioning Alleviates Lipopolysaccharide-Induced Acute Lung Injury via Inhibition of Intrinsic Apoptosis in Rats

**Yong Liu, Jiahang Xu, Liang Zhao, Jing Cheng, and Baojun Chen**

*Department of Thoracic Surgery, The Central Hospital of Wuhan, Tongji Medical College, Huazhong University of Science and Technology, Wuhan 430011, China*

Correspondence should be addressed to Yong Liu; liuyong7575@163.com and Baojun Chen; baojunchen1962@126.com

Received 5 July 2021; Revised 7 August 2021; Accepted 26 August 2021; Published 21 September 2021

Academic Editor: Yisong Qian



*Background*. Acute lung injury (ALI) always leads to severe inflammation. As inflammation and oxidative stress are the common pathological basis of endotoxin-induced inflammatory injury and ischemic reperfusion injury (IRI), we speculate that remote ischemic preconditioning (RIPC) can be protective for ALI when used as remote inflammatory preconditioning (RInPC). *Method*. A total of 21 Sprague-Dawley rats were used for the animal experiments. Eighteen rats were equally and randomly divided into the control (NS injection), LPS (LPS injection), and RInPC groups. The RInPC was performed prior to the LPS injection via tourniquet blockage of blood flow to the right hind limb and adopted three cycles of 5 min tying followed by 5 min untying. Animals were sacrificed 24 hours later. There were 2 rats in the LPS group and 1 in the RInPC group who died before the end of the experiment. Supplementary experiments in the LPS and RInPC groups were conducted to ensure that 6 animals in each group reached the end of the experiment. *Results*. In the present study, we demonstrated that the RInPC significantly attenuated the LPS-induced ALI in rats. Apoptotic cells were reduced significantly by the RInPC, with the simultaneous improvement of apoptosis-related proteins. Reduction of MPO and MDA and increasing of SOD activity were found significantly improved by the RInPC. Increasing of TNF-$\alpha$, IL-1$\beta$, and IL-6 induced by the LPS was inhibited, while IL-10 was significantly increased by RInPC, compared to the LPS group. *Conclusion*. RInPC could inhibit inflammation and attenuate oxidative stress, thereby reducing intrinsic apoptosis and providing lung protection in the LPS-induced ALI in rats.

## 1. Introduction

Acute lung injury (ALI) is a life-threatening parenchymal lung disease caused by various pathogenic factors. The ALI is characterized by hypoxemia, lung gas and blood barrier damage, bilateral pulmonary inflammatory infiltration, and noncardiogenic interstitial edema. It often progresses to acute respiratory distress syndrome (ARDS) and requires mechanical ventilation. Uncontrolled inflammation is the main cause of death, with a mortality rate of over 30% [1]. At present, the treatment for ALI/ARDS is mainly supportive, and novel therapeutic strategies are urgently needed.

Sepsis is the most common cause of ALI. Lipopolysaccharide (LPS), the endotoxin derived from the outer membrane of Gram-negative bacteria, which is believed to be one of the most frequent triggers of sepsis, is a powerful causative agent of systemic inflammation. The LPS can directly damage the alveolar-capillary barrier, lung epithelial cells, and pulmonary vascular endothelial cells [2]. Alveolar macrophages (AM) activated by LPS can release cytokines such as TNF-$\alpha$ and IL-1$\beta$ to initiate the inflammatory cascade, producing a large number of inflammatory mediators and factors, and reactive oxygen species (ROS). The ROS can destroy the gas and blood barrier by damaging pulmonary vascular endothelial cells and alveolar epithelial cells, increasing their permeability, and causing pulmonary edema; it can also upregulate the expression of inflammatory factors and induce inflammation [3]. It has been elucidated that several different forms of programmed cell death (PCD), including autophagy, apoptosis, and pyroptosis, have

been correlated with the LPS-induced ALI in rat models [4–6].

Pyroptosis is triggered in response to infection. The LPS has been reported to directly stimulate the activation of caspase-11, which cleaves gasdermin D (GSDMD) resulting in membrane rupture and cell lysis in rodents [7]. The innate immune response can be activated by LPS through the activation of TLR4 receptors [8], leading to the transcription of MyD88-dependent genes, which encode proinflammatory cytokines including inactive proforms of IL-1$\beta$ and inflammasome components [9]. Multiple studies elucidated the role of the Fas/FasL system in the extrinsic epithelial apoptosis in LPS-induced ALI [6]. DNA damage, hypoxia, and metabolic stress can induce intrinsic apoptosis, which begins with mitochondrial outer membrane permeabilization (MOMP) and leads to the release of mitochondrial proteins into the cytosol [10]. The ROS may stimulate the cell death pathways and trigger inflammation, resulting in inflammasome activation, pyroptosis [11], and intrinsic apoptosis.

Ischemia-reperfusion injury (IRI) refers to the irreversible tissue damage caused by insufficient oxygen supply following tissue ischemia and subsequent restoration of blood supply. Oxidative stress, inflammation, and calcium ion overload were involved with the ischemia-reperfusion injury [12]. Ischemic preconditioning (IPC) is currently known as an effective protection strategy against the IRI. Remote IPC (RIPC) can be used to offer a protective effect to the target organ by transient ischemic interventions in organs or tissues far away from the target. In previous studies, the protective effect of the RIPC against myocardial IRI and cerebral IRI has been demonstrated in rat models [13, 14]. Its protective mechanism was related to the reduction of oxidative stress and the alleviation of intrinsic apoptosis.

Based on the results from this study, we speculate that the RIPC can also be used as a novel protective strategy in LPS-induced ALI via alleviating intrinsic apoptosis. To facilitate the distinction, RInPC, a short-term ischemic intervention in organs or tissues far away from the target organ before inflammation occurs, is termed to stand for remote inflammatory preconditioning, which is distinguished from RIPC. The LPS-induced ALI rat models were used with the RInPC during the preinflammatory stage to verify this hypothesis and explore its intrinsic apoptosis-related mechanisms.

## 2. Materials and Methods

*2.1. Ethics Statement.* All animals were taken care of and treated in agreement with the Animal Research: Reporting of In Vivo Experiments (ARRIVE) guidelines for this study. Further, all animal procedures were performed following the guidelines of Institutional Animal Care. The ethics approval has been obtained from the Ethics Committee of the Central Hospital of Wuhan affiliated to Tongji Medical College, Huazhong University of Science and Technology, before the onset of the study.

*2.2. Animals.* A total of 21 Sprague-Dawley rats weighing 250 to 270 g were obtained from the Beijing Vital River Laboratory Animal Technology Co., Ltd. (Certificate Number: SCXK-2003-001; Beijing, China). The animal experiment occurred at the animal experimental center of the Biofavor Biotech Company in Wuhan, Hubei, China. Animals were maintained in an air-conditioned atmosphere at 25°C with a 12-hour light-dark cycle exposure and were provided with free access to pelleted food and ad libitum water. After a one-week acclimation, the animals were randomly assigned into three groups, six rats per group. The first group was maintained as the control. The second group (LPS group) had the LPS intravenous injection. The third group (RInPC group) was treated the same as the LPS group with additional 30 minutes of remote stimuli before the LPS injection. There were 2 rats in the LPS group and 1 rat in the RInPC group that died before the end of the experiment. Supplementary experiments for the LPS and RInPC groups were conducted to include 6 animals that reached the end of the experiment in each group.

*2.3. Drugs.* The LPS (O127: B8; Sigma, St. Louis, MO, USA) used in this study was derived from Escherichia coli (O127) endotoxin, and it was dissolved in sterile saline.

*2.4. Experimental Protocol.* The animal model of LPS-induced ALI was developed with some modifications as described by Hagiwara et al. [15]. Briefly, the rat model was created by injection of LPS (5 mg/kg) via the tail vein. The same volume of normal saline (NS) was administered to the animals in the control group through the same route. All animals were injected intravenously under ether inhalation anesthesia.

The RInPC was performed for 30 minutes ahead of the LPS injection via tourniquet blockage of blood flow to the right hind limb and adopted three cycles of 5 min tying followed by 5 min of untying. Circulatory arrest in the limbs was identified by observing the empurpled limb skin and confirmed using a vascular Doppler. This method has been developed and standardized in a previous study [16].

Twenty-four hours after the injection, the animals were sacrificed following heart blood sampling under overanesthesia. The serum was separated by centrifugation of the blood sample at 3000 g for 15 minutes. Lung samples were collected with inflation after the chest was opened. The left lungs were used to measure the wet/dry ratio. The right upper lungs were stored in 4% paraformaldehyde for histological studies. And the right lower lungs were stored at −80°C for biochemical assay and protein analysis by western blotting.

*2.5. Histology and Morphology.* Complete random cross-sections of the rat lungs were fixed in 4% neutral phosphate-buffered formaldehyde, embedded in paraffin, sectioned (5 $\mu$m), and stained with hematoxylin and eosin (H&E). The sections were viewed by an experienced morphologist who knew nothing about the sample identity. Ten randomly chosen microscopic fields (×200) were viewed for each lung sample, and all 6 samples were viewed for each animal group. Histological evidence suggesting ALI was also evaluated by a blinded investigator according to Hofbauer

and colleagues' method [17]. In which, alveolar membrane thickness and cellularity were evaluated by estimating the fraction of the microscopic field occupied by the parenchymal tissue as opposed to the empty alveolar spaces. The average values of ALI were represented by a histological index of quantitative assessment (IQA) using the following criteria. Samples were graded from normal to severe, which was expressed by 0 (<15% of the space occupied by tissue and >85% by alveolar space), 1+ (15%-25% occupied by tissue and 75%-85% by alveolar space), 2+ (25%-50% occupied by tissue and 50%-75% by alveolar space), 3+ (50%-75% occupied by tissue and 25%-50% by alveolar space), and 4+ (75%-100% occupied by tissue and 0%–25% by alveolar space).

*2.6. Lung Wet-to-Dry Weight Ratio Measurement.* To assess tissue edema, the weight of rat lungs (six lungs per group) was measured, followed by a drying step of the lungs in an oven at 80°C for 48 h until the weight of the samples became constant. Then, the lung wet-to-dry weight ratio was calculated.

*2.7. Assay of Serum Lactate Acid.* Serum lactate measurement was performed in all groups using a lactate assay kit (Nanjing Jiancheng Bioengineering Institute, Nanjing, Jiangsu, China), according to the manufacturer's instructions.

*2.8. Enzyme-Linked Immunosorbent Assay (ELISA).* The levels of TNF-$\alpha$, IL-1$\beta$, IL-6, and IL-10 in serum were detected using the specific mouse or human ELISA kits (Elabscience Biotechnology Co. Ltd., Wuhan, Hubei, China). The optical density was measured at 450/540 nm wavelength using an automated ELISA reader (Flexstation3, Molecular Devices, LLC, Sunnyvale, CA, USA). All standards and samples were run in triplicate.

*2.9. Assays of Malondialdehyde (MDA), Myeloperoxidase (MPO), and Superoxide Dismutase (SOD).* These three oxidative stress indicators were detected in serum, as previously reported by using commercial assay kits (Nanjing Jiancheng Bioengineering Institute), according to the manufacturer's instructions [18]. The unit of measurement for MDA was nmol per milligram of protein. MPO and SOD activities were expressed as units per milligram of protein.

*2.10. Terminal Deoxynucleotidyl Transferase-Mediated dUTP Nick End Labeling (TUNEL) Assay.* The TUNEL technique was carried out using the "In Situ Cell Death Detection Kit." Briefly, the lung sections on the microscopic slides were dewaxed and incubated with proteinase K. Then, the slides were stained using a TUNEL kit (Biovision Inc., Mountain View, CA, USA), according to the manufacturer's instructions. Subsequently, the slides were examined under a fluorescence microscope (Olympus BX53, Olympus, Japan). Images were captured to determine the percentage of positive cells and intensity of staining and then used to calculate the percentage of positive nuclei in three representative areas from three samples per group as the apoptotic index for statistical analysis.

*2.11. Western Blotting Analysis.* The right lower lung specimens (approximately 100 mg each) were dissected out and stored at -80°C. The protein expressions of Bcl-2, Bax, Cyt-c, AIF, caspase-3, cleaved caspase-3, caspase-9, and cleaved caspase-9 in the lung were detected by western blotting analysis, which was described in the literature [19]. Briefly, the protein concentration was determined by the Bicinchoninic Acid (BCA) method. The protein sample was boiled and denatured; then, SDS-PAGE gel electrophoresis was performed. The protein was transferred onto the nitrocellulose membrane. Next, the proteins were blocked with 5% skim milk at 37°C for 1 h. The membranes were incubated overnight at 4°C with diluted primary antibody and GADPH primary antibody (1 : 1000). The next day, the membrane was washed three times with TBST and incubated with a secondary antibody diluted with the blocking solution at 37°C for 2 hours. The enhanced chemiluminescence (ECL) was developed, and the protein bands were photographed after washing. The integral optical density (IOD) of each target band was determined using Bandscan 5.0 software (*Bio Marin Pharmaceutical*, San Rafael, CA, USA). The expressions of the target proteins were normalized by the ratio of integrated optical density (IOD) of proteins to the IOD of GADPH. The expressions of Cyt-c and AIF in the mitochondria were normalized by the ratio of the IOD of proteins to the IOD of COX4.

*2.12. Statistical Analysis.* The significant differences were calculated using one-way ANOVA among multiple groups with the Prism 8.0 software (GraphPad Software, Inc., San Diego, CA, USA). Results were expressed as means ± standard deviation (SD). Values are shown using a column diagram. $P < 0.05$ was considered significant.

## 3. Results

*3.1. RInPC Attenuated the LPS-Induced ALI in Rats.* The survival percentages of the three groups of models were 100% (6/6), 75.0% (6/8), and 85.7% (6/7), respectively (Figure 1(a)). Histological evaluations of lung tissue changes by H&E staining were compared among the three groups. Similar to the description by Du et al. [20], the morphology in the control group was normal with no fluid in the alveolar space. No evidence of inflammatory cell infiltration or hemorrhage on the alveolar wall was found. Diffuse edema in alveolar spaces, inflammatory cell infiltration, and thickened interlobular septa were found in both the LPS and RInPC groups. A significantly higher ALI score represented by IQA was observed in the LPS group compared to the others. The IQA score of the RInPC group was significantly lower than that of the LPS group (control vs. RInPC vs. LPS: $0.71 \pm 0.24$ vs. $1.96 \pm 0.10$ vs. $3.00 \pm 0.16$, $P < 0.001$) (Figures 1(b) and 1(e)).

The wet/dry lung weight ratio was significantly increased in the LPS group ($8.66 \pm 2.34$ vs. $6.02 \pm 0.60$, $P < 0.05$) compared to the control group. The wet/dry ratio in the RInPC group was between the control and LPS groups, without any significant differences (Figure 1(c)).

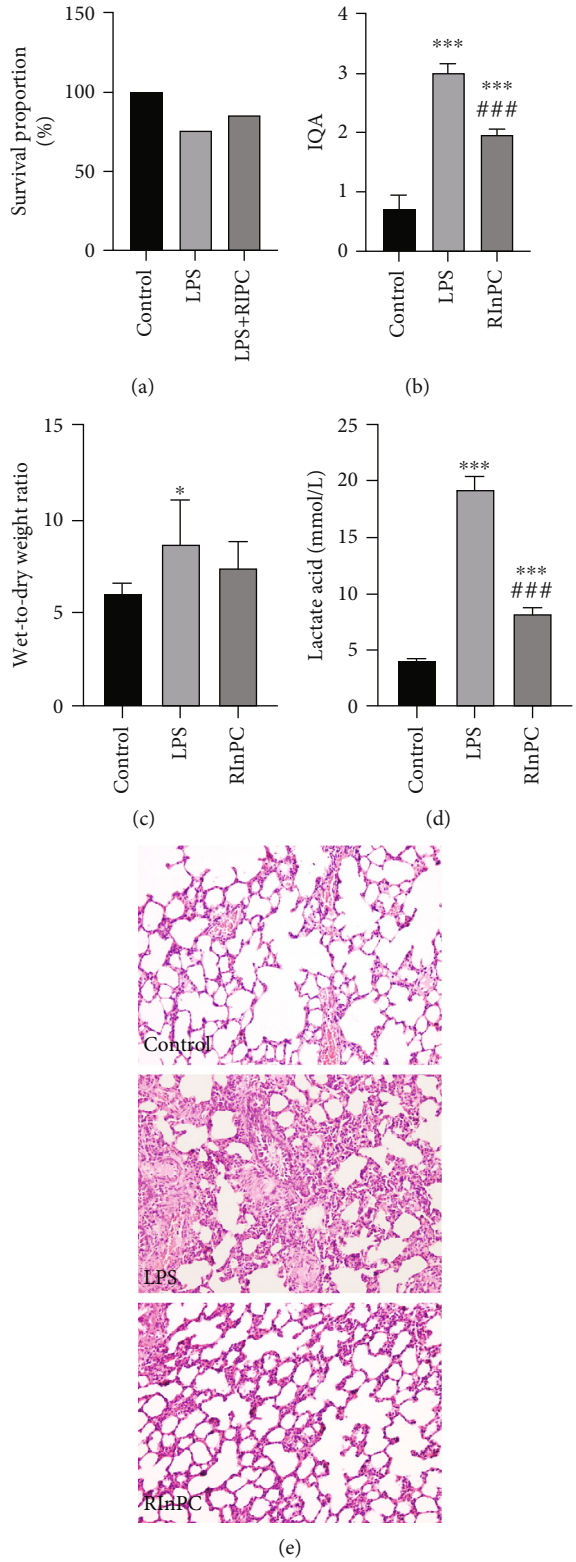


Figure 1: RInPC attenuated LPS-induced ALI in rats. (a) Comparison of survival proportion among three groups. (b) Comparison of ALI represented by IQA between each group. (c) Comparison of wet/dry ratio between each group. (d) Comparison of lactic acid in the serum of each group. (e) Histological changes of lung tissue in each group (H&E; 200x). Control: control group; LPS: LPS injury group; RInPC: LPS +RInPC group. In comparison, the LPS injury group showed diffuse edema in alveolar spaces and interstitium of the lung, hemorrhage, severe inflammatory cell infiltration and serous exudation in the alveolar space, and thickened interlobular septa. These changes were significantly mitigated in the RInPC group. $^{*}P < 0.05$; $^{**}P < 0.01$; $^{***}P < 0.001$ vs. control group; $^{\#}P < 0.05$; $^{\#\#}P < 0.01$; $^{\#\#\#}P < 0.001$ vs. LPS group ($n = 6$); IQA: index of quantitative assessment.

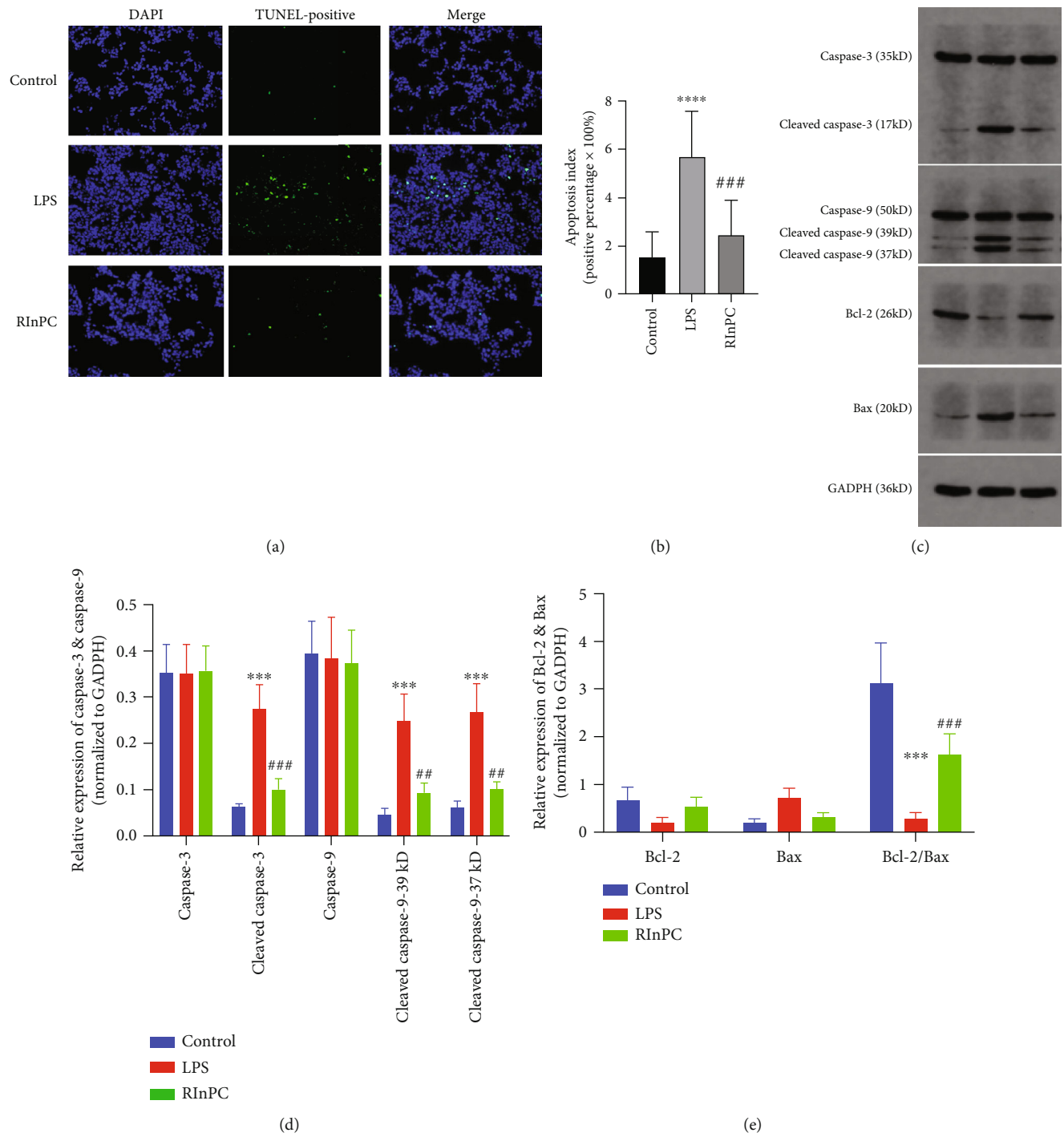


Figure 2: Continued.

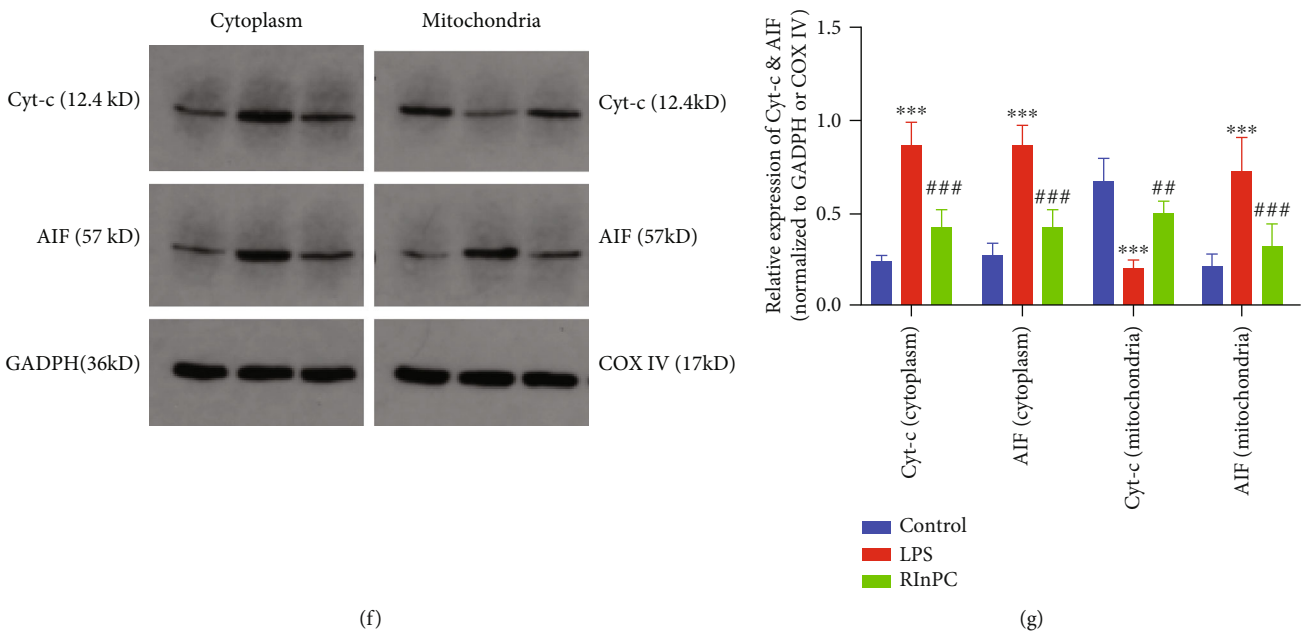


Figure 2: RInPC prevented apoptosis via an intrinsic pathway in LPS-induced ALI in rats. (a) Fluorescent images of the TUNEL results under a fluorescence microscope in ALI rats induced by LPS (original magnification: 400x). (b) Comparison of apoptosis index between each group. (c) WB bands of caspase-3, cleaved caspase-3, caspase-9, cleaved caspase-9, Bcl-2, and Bax. (d) Comparison of caspase-3, cleaved caspase-3, caspase-9, and cleaved caspase-9 between each group. (e) Comparison of Bcl-2, Bax, and Bcl-2/Bax ratio between each group. (f) WB bands of Cyt-c and AIF expressed in the cytoplasm and mitochondria. (g) Comparison of Cyt-c and AIF in the cytoplasm and mitochondria between each group. $^{***}P < 0.001$; $^{****}P < 0.0001$ vs. control; $^{\#\#}P < 0.01$; $^{\#\#\#}P < 0.001$ vs. LPS ($n = 3$). DAPI: 4′,6-diamidino-2-phenylindole; WB: western blot; Cyt-c: cytochrome c; AIF: apoptosis-inducing factor; GAPDH: glyceraldehyde 3-phosphate dehydrogenase; COX4: cytochrome c oxidase subunit 4.

The value of lactate acid in both the LPS group and the RInPC group was significantly increased compared to the control, while the value in the RInPC group was significantly lower than that in the LPS group. The values of the three groups were $3.98 \pm 0.33$, $19.33 \pm 1.03$, and $8.22 \pm 0.51$, respectively ($P < 0.001$) (Figure 1(d)).

*3.2. RInPC Prevented Apoptosis via an Intrinsic Pathway in LPS-Induced ALI in Rats.* To determine the protective effects of the RInPC against LPS-induced apoptosis, TUNEL was performed. In vivo, LPS-challenged animals exhibited a significant increase in green fluorescence apoptotic cells, which was significantly reduced by the RInPC (Figures 2(a) and 2(b)).

Although the values of both caspase-3 and caspase-9 were not changed in the lung specimen, cleaved caspase-3 and cleaved caspase-9 were upregulated significantly ($P < 0.001$ compared with the control group). The RInPC inhibited the LPS-induced upregulation of cleaved caspase-3 and cleaved caspase-9 ($P < 0.01$ compared with the LPS group) (Figures 2(c) and 2(d)).

The intrinsic pathway of apoptosis, which means mitochondrial-dependent apoptosis, is mediated through the release of cytochrome c (Cyt-c) and apoptosis-inducing factor (AIF), leading to ultimately caspase activation. In the present study, significantly increased Cyt-c in the cytoplasm and decreased Cyt-c in the mitochondria were observed ($P < 0.001$ compared with the control group), which was alleviated by the RInPC ($P < 0.001$ compared with the LPS group). Simultaneously, increased AIF both in cytoplasm and mitochondria were observed ($P < 0.001$ compared with the control group), which was also alleviated by the process of RInPC ($P < 0.001$ compared with the LPS group) (Figures 2(f) and 2(g)).

Additionally, the present study investigated the changes in the expression levels of the Bcl-2 family proteins (Bcl-2 and Bax) in lung tissue. The LPS injection resulted in the downregulation of the antiapoptotic protein Bcl-2 and upregulation of the proapoptotic protein Bax. Although no significant differences of Bcl-2 and Bax were observed among the three groups, a significantly decreased Bcl-2/Bax ratio was observed ($P < 0.001$ compared with the control group), and the RInPC prevented this decreased ratio ($P < 0.001$ compared with the LPS group). These results indicated that intravenous administration of LPS induced lung cell apoptosis, which was significantly alleviated by the treatment with the RInPC (Figures 2(c) and 2(e)).

*3.3. RInPC Palliated the Oxidative Stress in Lung Induced by LPS Injection.* To determine the antioxidative effects of the RInPC against LPS-induced ALI in rats, the MDA, MPO, and SOD levels in serum were measured. The LPS injection induced a 2.30-fold elevation of MDA level, a 2.13-fold elevation of MPO activity, and a 71.0% reduction of SOD activity, respectively, compared with the control group. In contrast, these oxidative markers were significantly

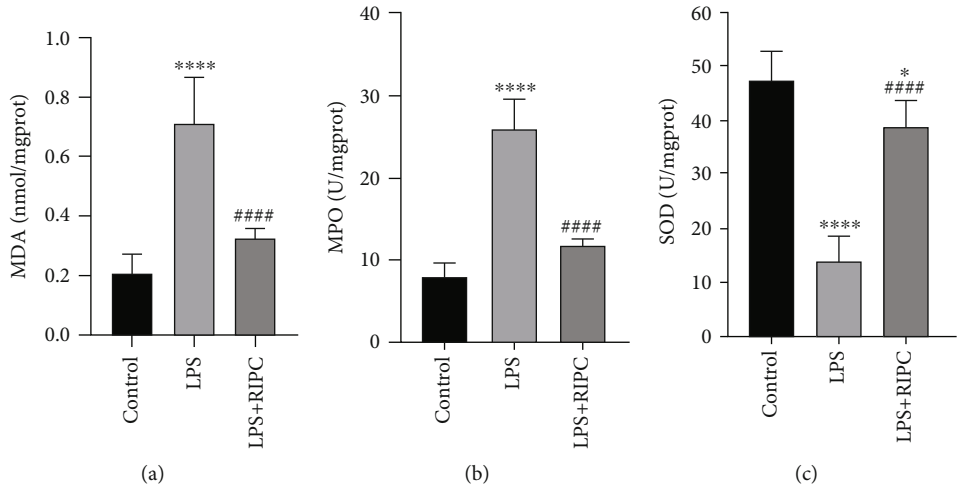


Figure 3: The RInPC palliated the oxidative stress in the lung induced by the LPS. (a) Comparison of MDA between each group. (b) Comparison of MPO between each group. (c) Comparison of SOD between each group. $^{*}P < 0.05$; $^{****}P < 0.0001$ vs. control group; $^{\#\#\#\#}P < 0.0001$ vs. LPS group ($n = 6$). MPO: myeloperoxidase; MDA: malondialdehyde; SOD: superoxide dismutase.

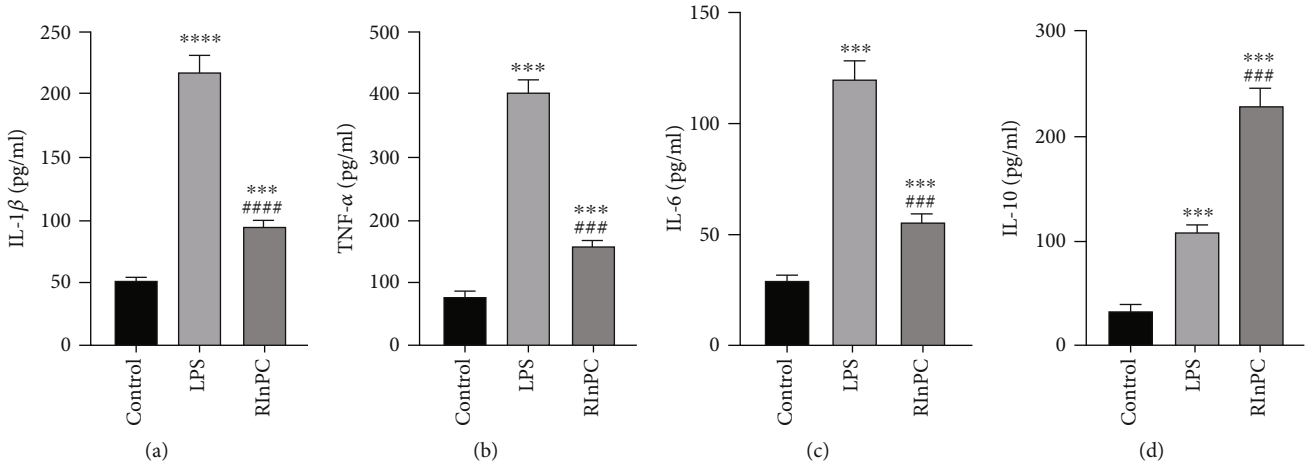


Figure 4: The RInPC reduced proinflammatory cytokine secretion induced by the LPS. (a) Comparison of TNF-$\alpha$ between each group. (b) Comparison of IL-1$\beta$ between each group. (c) Comparison of IL-6 between each group. (d) Comparison of IL-10 between each group. $^{***}P < 0.001$; $^{****}P < 0.0001$ vs. control group; $^{\#\#\#}P < 0.001$; $^{\#\#\#\#}P < 0.0001$ vs. LPS group ($n = 6$). TNF-$\alpha$: tumor necrosis factor-alpha; IL-1$\beta$: interleukin-1$\beta$; IL-6: interleukin-6; IL-10: interleukin-10.

improved by the RInPC in the LPS-injected rats. The MDA and MPO were reduced to levels close to the control group, and SOD was elevated to a level which was almost 84.5% of the control group (Figures 3(a)–3(c)).

*3.4. The RInPC Reduced Proinflammatory Cytokine Secretion Induced by LPS.* To investigate the anti-inflammatory effects of the RInPC in the lung of LPS-intoxicated rats, TNF-$\alpha$, IL-1$\beta$, IL-6, and IL-10 levels were measured. The LPS injection induced a 4.22-, 3.28-, 3.11-, and 2.20-fold elevation of TNF-$\alpha$, IL-1$\beta$, IL-6, and IL-10 levels, respectively, compared with the control group. Conversely, proinflammatory cytokines were significantly improved by the RInPC of LPS-injected rats. The TNF-$\alpha$, IL-1$\beta$, and IL-6 levels were improved to a level which was less than half of the level in the LPS group, with a significant increase of anti-inflammatory cytokine, IL-10, to a level which was more than 2-fold of the level in the LPS group (Figures 4(a)–4(d)).

## 4. Discussion

In this study, we demonstrated that the RInPC significantly attenuated the LPS-induced ALI in rats, possibly via an inhibition of intrinsic apoptosis, associated with reductions in both oxidative stress and proinflammatory cytokines. Although investigations on the inhibition of pyroptosis [7] and extrinsic apoptosis [6] in the LPS-induced ALI have been reported previously, we have not found a similar research result about intrinsic apoptosis and LPS-induced ALI.

Gram-negative bacteria have been associated with approximately 50% of infectious ALI, usually from

pneumonia or sepsis [21]. The LPS, as a common endotoxin, is critical for organ dysfunction and mortality associated with severe Gram-negative infections [22, 23]. It has been well established that intravenous administration of LPS can induce a model of ALI [24–26].

The RIPC was originally one of the strategies to alleviate organ IRI. It has been reported to exert a protective effect against ischemia/reperfusion injury in rat hearts, brains, and other organs, which may be associated with inhibiting the opening of mPTP [27, 28]. It has also been demonstrated to regulate the human myocardial apoptosis and inflammation, which is associated with the caspase cascade [29]. The protective mechanism has been known to be related to inhibiting inflammation, reducing oxidative stress, and reducing intrinsic apoptosis. Although different mechanisms about cell death are involved between IRI and ALI, the RInPC, which we abbreviated to stand for remote inflammatory preconditioning, was suspected to be protective in this rats' ALI model induced by LPS based on the effect related to inhibition of intrinsic apoptosis.

The animal model was established through intravenous injection of LPS (5 mg/kg) in the present study, based on a previous report [30, 31]. It was observed with significant lung injury and dysfunction following LPS administration, evidenced by the deterioration of histopathology, increased wet/dry weight ratio of the lung, and elevated lactate acid in serum, which is consistent with the other studies [26, 31–33]. The ALI in rats was attenuated by the performance of RInPC, which was reflected by improved histopathological changes and decreased wet/dry ratio and lactate acid in serum compared to the LPS group. Although the value of $PaO_2/FiO_2$ was not clarified, lactate acid has been certified to be an indicator of anoxemia of the organ, especially in lung injury. The lactate level has long been used as a marker of resuscitation, for risk stratification, and as a mortality prediction tool in sepsis with the commonly held belief that elevated lactate levels in sepsis occur as a consequence of anaerobic metabolism from tissue malperfusion [34]. Cytopathic hypoxia and direct mitochondrial impairment have been proposed as a cause of hyperlactemia, although the exact mechanism remains incompletely understood [35].

Through TUNEL detection, it was confirmed that the apoptosis of lung cells existed in the ALI model, and the RInPC significantly reduced the occurrence of apoptosis. Intrinsic apoptosis, mitochondrial-dependent apoptosis, was activated through the mitochondrial release of Cyt-c, AIF, and Smac [36]. When Cyt-c entered the cytoplasm, the apoptosome assembly was released from the apoptotic protease-activating factor 1, ATP, and procaspase-9, leading to cellular apoptosis via the activation of caspase-3 and caspase-7 [37]. To further elucidate the present hypothesis of intrinsic apoptosis, the Cyt-c and AIF levels in the cytoplasm and mitochondria were measured. The RInPC was demonstrated to improve the mitochondrial release of the Cyt-c into the cytoplasm and thus the expression of AIF.

The apoptosis-related proteins play pivotal roles in apoptosis. The caspase-3 and caspase-9 are activated and regulated by the apoptotic pathway mediated by the Bcl-2/Bax ratio [38, 39]. The present results demonstrated that the RInPC significantly downregulated the expression of caspase-9 and caspase-3, the proapoptosis protein, and the executive protein of apoptosis in vivo. In addition, the antiapoptosis protein Bcl-2 and the proapoptosis protein Bax, both involved in the regulation of the opening of mitochondrial permeability transition pore (mPTP), were also analyzed. The values indicated that the RInPC could attenuate the opening of mPTP through regulation of the Bcl-2/Bax ratio to inhibit the release of Cyt-c and AIF.

To explore the ability of the RInPC in regulating oxidative stress, we tested the contents of MDA and MPO and the activity of SOD. The MDA indirectly reflects the severity of the cells being attacked by free radicals. The MPO activity is an indicator of neutrophil infiltration in the lung. The SOD is an important oxygen-free radical scavenger [40]. It was shown that the LPS injection caused an increase in MDA production, MPO secretion, and SOD consumption in rats, suggesting an induced imbalance of oxidative stress. It was also demonstrated that the RInPC was found to be a good alleviator for the imbalance of oxidative stress induced by the LPS.

In this rat model of LPS-induced ALI, it was observed that the secretion of proinflammatory cytokines, including TNF-$\alpha$, IL-$\beta$, and IL-6, as well as the anti-inflammatory cytokine IL-10, was all increased significantly after the administration of the LPS, consistent with previous studies [15, 41]. Monocytes and macrophages secrete cytokines such as TNF-$\alpha$, IL-$\beta$, and IL-6 during the early stage of the inflammatory response when activated by the LPS, which play an important role in the occurrence and development of ALI/ARDS [32, 42, 43]. TNF-$\alpha$ is a primary mediator of inflammation [32, 43]. The IL-1$\beta$ also appears in the early stage of ALI and cooperates with the TNF-$\alpha$ to promote an inflammatory response. Levels of the IL-6 positively correlate with mortality in experimental models of sepsis. Measuring the IL-6 levels in at-risk patients can accurately predict individuals who are at significant risk of death as a result of sepsis [44]. The IL-10 inhibits the expression of proinflammatory cytokines, chemokines, and chemokine receptors as well as allergen tolerance in allergen-specific immunotherapy [42]. The RInPC significantly suppressed the secretion of TNF-$\alpha$, IL-$\beta$, and IL-6, promoting the secretion of IL-10, which suggested that the RInPC could reduce the inflammatory response in this ALI model.

Pyroptosis exerts a cell type-dependent role in inflammation and immunity. The caspase-11-dependent noncanonical pyroptosis was activated by cytosolic LPS from invading Gram-negative bacteria in macrophages, monocytes, or other cells in rodent animals [7]. As intrinsic apoptosis is always induced by DNA damage, hypoxia, and metabolic stress; we speculated that the intrinsic apoptosis may have been secondary to noncanonical pyroptosis in the LPS-induced ALI models, and further research is needed.

Some limitations in this study exist because of the experimental design. First of all, the protective effect of the RInPC on ALI was discussed only in rodent in vivo models. To determine whether there is a similar effect on other animals or humans, more elucidations are warranted. The second is that the in vitro experiments have not been applied to

explore whether cells treated with hypoxia and reoxygenation can better resist the endotoxin damage. Another one is that the wet/dry ratio was showed to have a significant difference between the control group and the LPS group, but that of the RInPC group was without any significant differences compared to the other two groups. Measurement of the protein level in BALF may be a better choice in future experiments. The last one is that the study showing some protective effects of RInPC on the LPS-induced ALI correlated with the intrinsic apoptosis is still observational. The mechanism mediating this protection has not been fully investigated.

## 5. Conclusion

In the present study, the RInPC inhibited the inflammatory response and attenuated the oxidative stress, thereby reducing intrinsic apoptosis and ultimately providing lung protection in the LPS-induced ALI model in rats. If a similar effect could be found in other animal models or human beings, we may get a new strategy to fight against ALI and ARDS.

## Data Availability

The datasets used and/or analyzed during the current study are available from the corresponding authors on reasonable request.

## Ethical Approval

This study was performed in agreement with the ARRIVE guidelines. The ethics approval has been obtained from the Ethics Committee of the Central Hospital of Wuhan affiliated to Tongji Medical College, Huazhong University of Science and Technology. Great efforts were made to minimize the suffering of animals.

## Consent

No consent was necessary.

## Conflicts of Interest

All authors declare that they have no conflict of interest.

## Authors' Contributions

Yong Liu and Baojun Chen contributed to the study conception and design. Material preparation, animal operation, data collection, and analysis were performed by Yong Liu, Jiahang Xu, Liang Zhao, and Jing Cheng. The first draft of the manuscript was written by Yong Liu, and the final version of the manuscript was revised by Baojun Chen and Yong Liu. All authors have read and approved the final version of the manuscript.

## Acknowledgments

This study was supported by the Natural Science Foundation of Hubei Province (ZRMS2019000195), China.

## References

[1] M. Xiang and J. Fan, "Pattern recognition receptor-dependent mechanisms of acute lung injury," *Molecular Medicine*, vol. 16, no. 1-2, pp. 69–82, 2010.

[2] F. Anjum, K. Joshi, N. Grinkina, S. Gowda, M. Cutaia, and R. Wadgaonkar, "Role of sphingomyelin synthesis in pulmonary endothelial cell cytoskeletal activation and endotoxin-induced lung injury," *American Journal of Respiratory Cell and Molecular Biology*, vol. 47, no. 1, pp. 94–103, 2012.

[3] X. F. Qi, Y. C. Teng, Y. S. Yoon, D. H. Kim, D. Q. Cai, and K. J. Lee, "Reactive oxygen species are involved in the IFN-gamma-stimulated production of Th2 chemokines in HaCaT keratinocytes," *Journal of Cellular Physiology*, vol. 226, no. 1, pp. 58–65, 2011.

[4] C. Fu, X. Dai, Y. Yang, M. Lin, Y. Cai, and S. Cai, "Dexmedetomidine attenuates lipopolysaccharide-induced acute lung injury by inhibiting oxidative stress, mitochondrial dysfunction and apoptosis in rats," *Molecular Medicine Reports*, vol. 15, no. 1, pp. 131–138, 2017.

[5] M. Ju, B. Liu, H. He et al., "MicroRNA-27a alleviates LPS-induced acute lung injury in mice via inhibiting inflammation and apoptosis through modulating TLR4/MyD88/NF-κB pathway," *Cell Cycle*, vol. 17, no. 16, pp. 2001–2018, 2018.

[6] P. S. Tang, M. Mura, R. Seth, and M. Liu, "Acute lung injury and cell death: how many ways can cells die?," *American Journal of Physiology. Lung Cellular and Molecular Physiology*, vol. 294, no. 4, pp. L632–L641, 2008.

[7] N. Kayagaki, S. Warming, M. Lamkanfi et al., "Non-canonical inflammasome activation targets caspase-11," *Nature*, vol. 479, no. 7371, pp. 117–121, 2011.

[8] B. Beutler and E. T. Rietschel, "Innate immune sensing and its roots: the story of endotoxin," *Nature Reviews. Immunology*, vol. 3, no. 2, pp. 169–176, 2003.

[9] A. Pfalzgraff and G. Weindl, "Intracellular lipopolysaccharide sensing as a potential therapeutic target for sepsis," *Trends in Pharmacological Sciences*, vol. 40, no. 3, pp. 187–197, 2019.

[10] D. Tang, R. Kang, T. V. Berghe, P. Vandenabeele, and G. Kroemer, "The molecular machinery of regulated cell death," *Cell Research*, vol. 29, no. 5, pp. 347–364, 2019.

[11] R. Zhou, A. S. Yazdi, P. Menu, and J. Tschopp, "A role for mitochondria in NLRP3 inflammasome activation," *Nature*, vol. 469, no. 7329, pp. 221–225, 2011.

[12] Q. Zhao, J. Wu, Q. Hua et al., "Resolvin D1 mitigates energy metabolism disorder after ischemia-reperfusion of the rat lung," *Journal of Translational Medicine*, vol. 14, no. 1, p. 81, 2016.

[13] S. B. Zhu, Y. Liu, Y. Zhu et al., "Remote preconditioning, perconditioning, and postconditioning: a comparative study of their cardio-protective properties in rat models," *Clinics (São Paulo, Brazil)*, vol. 68, no. 2, pp. 263–268, 2013.

[14] X. Zhou, Y. Liu, Y. Huang, S. Zhu, J. Zhu, and R. Wang, "Hypertonic saline infusion suppresses apoptosis of hippocampal cells in a rat model of cardiopulmonary resuscitation," *Scientific Reports*, vol. 7, no. 1, p. 5783, 2017.

[15] S. Hagiwara, H. Iwasaka, S. Matumoto, S. Hidaka, and T. Noguchi, "Effects of an angiotensin-converting enzyme inhibitor on the inflammatory response in in vivo and in vitro models," *Critical Care Medicine*, vol. 37, no. 2, pp. 626–633, 2009.

[16] R. K. Kharbanda, U. M. Mortensen, P. A. White et al., "Transient limb ischemia induces remote ischemic preconditioning in vivo," *Circulation*, vol. 106, no. 23, pp. 2881–2883, 2002.

[17] B. Hofbauer, A. Saluja, M. Bhatia et al., "Effect of recombinant platelet-activating factor acetylhydrolase on two models of experimental acute pancreatitis," *Gastroenterology*, vol. 115, no. 5, pp. 1238–1247, 1998.

[18] J. Yao, D. Pan, Y. Zhao et al., "Wogonin prevents lipopolysaccharide-induced acute lung injury and inflammation in mice via peroxisome proliferator-activated receptor gamma-mediated attenuation of the nuclear factor-kappaB pathway," *Immunology*, vol. 143, no. 2, pp. 241–257, 2014.

[19] Y. She, L. Shao, Y. Zhang, Y. Hao, Y. Cai, Z. Cheng et al., "Neuroprotective effect of glycosides in Buyang Huanwu Decoction on pyroptosis following cerebral ischemia-reperfusion injury in rats," *Journal of Ethnopharmacology*, vol. 242, p. 112051, 2019.

[20] Q. du, C. Wang, N. Zhang et al., "In vivo study of the effects of exogenous hydrogen sulfide on lung mitochondria in acute lung injury in rats," *BMC Anesthesiology*, vol. 14, no. 1, p. 117, 2014.

[21] K. Xie, Y. Yu, Y. Huang et al., "Molecular hydrogen ameliorates lipopolysaccharide-induced acute lung injury in mice through reducing inflammation and apoptosis," *Shock*, vol. 37, no. 5, pp. 548–555, 2012.

[22] O. Kumpf, E. J. Giamarellos-Bourboulis, A. Koch et al., "Influence of genetic variations in TLR4 and TIRAP/Mal on the course of sepsis and pneumonia and cytokine release: an observational study in three cohorts," *Critical Care*, vol. 14, no. 3, p. R103, 2010.

[23] J. M. Cavaillon, "Exotoxins and endotoxins: inducers of inflammatory cytokines," *Toxicon*, vol. 149, pp. 45–53, 2018.

[24] H. Koga, S. Hagiwara, C. Shingu, S. Matsumoto, I. Yokoi, and T. Noguchi, "Human atrial natriuretic peptide ameliorates LPS-induced acute lung injury in rats," *Lung*, vol. 188, no. 3, pp. 241–246, 2010.

[25] G. Matute-Bello, C. W. Frevert, and T. R. Martin, "Animal models of acute lung injury," *American Journal of Physiology. Lung Cellular and Molecular Physiology*, vol. 295, no. 3, pp. L379–L399, 2008.

[26] X. Li, C. Shan, Z. Wu, H. Yu, A. Yang, and B. Tan, "Emodin alleviated pulmonary inflammation in rats with LPS-induced acute lung injury through inhibiting the mTOR/HIF-1$\alpha$/VEGF signaling pathway," *Inflammation Research*, vol. 69, no. 4, pp. 365–373, 2020.

[27] M. A. Moskowitz and C. Waeber, "Remote ischemic preconditioning: making the brain more tolerant, safely and inexpensively," *Circulation*, vol. 123, no. 7, pp. 709–711, 2011.

[28] V. Sharma, R. Marsh, B. Cunniffe, M. Cardinale, D. M. Yellon, and S. M. Davidson, "From protecting the heart to improving athletic performance - the benefits of local and remote ischaemic preconditioning," *Cardiovascular Drugs and Therapy*, vol. 29, no. 6, pp. 573–588, 2015.

[29] M. Albrecht, K. Zitta, B. Bein et al., "Remote ischemic preconditioning regulates HIF-1$\alpha$ levels, apoptosis and inflammation in heart tissue of cardiosurgical patients: a pilot experimental study," *Basic Research in Cardiology*, vol. 108, no. 1, p. 314, 2013.

[30] J. S. Choi, H. S. Lee, K. H. Seo et al., "The effect of post-treatment N-acetylcysteine in LPS-induced acute lung injury of rats," *Tuberculosis and Respiratory Diseases*, vol. 73, no. 1, pp. 22–31, 2012.

[31] W. Shen, J. Gan, S. Xu, G. Jiang, and H. Wu, "Penehyclidine hydrochloride attenuates LPS-induced acute lung injury involvement of NF-$\kappa$B pathway," *Pharmacological Research*, vol. 60, no. 4, pp. 296–302, 2009.

[32] Y. Butt, A. Kurdowska, and T. C. Allen, "Acute lung injury: a clinical and molecular review," *Archives of Pathology & Laboratory Medicine*, vol. 140, no. 4, pp. 345–350, 2016.

[33] K. T. Hughes and M. B. Beasley, "Pulmonary manifestations of acute lung injury: more than just diffuse alveolar damage," *Archives of Pathology & Laboratory Medicine*, vol. 141, no. 7, pp. 916–922, 2017.

[34] G. Wardi, J. Brice, M. Correia, D. Liu, M. Self, and C. Tainter, "Demystifying lactate in the emergency department," *Annals of Emergency Medicine*, vol. 75, no. 2, pp. 287–298, 2020.

[35] C. Adrie, M. Bachelet, M. Vayssier-Taussat et al., "Mitochondrial membrane potential and apoptosis peripheral blood monocytes in severe human sepsis," *American Journal of Respiratory and Critical Care Medicine*, vol. 164, no. 3, pp. 389–395, 2001.

[36] E. W. Childs, B. Tharakan, F. A. Hunter, J. H. Tinsley, and X. Cao, "Apoptotic signaling induces hyperpermeability following hemorrhagic shock," *American Journal of Physiology. Heart and Circulatory Physiology*, vol. 292, no. 6, pp. H3179–H3189, 2007.

[37] S. A. Lakhani, A. Masud, K. Kuida et al., "Caspases 3 and 7: key mediators of mitochondrial events of apoptosis," *Science*, vol. 311, no. 5762, pp. 847–851, 2006.

[38] J. W. Dong, H. F. Zhu, W. Z. Zhu, H. L. Ding, T. M. Ma, and Z. N. Zhou, "Intermittent hypoxia attenuates ischemia/reperfusion induced apoptosis in cardiac myocytes via regulating Bcl-2/Bax expression," *Cell Research*, vol. 13, no. 5, pp. 385–391, 2003.

[39] S. Orrenius, "Mitochondrial regulation of apoptotic cell death," *Toxicology Letters*, vol. 149, no. 1-3, pp. 19–23, 2004.

[40] D. Impellizzeri, E. Esposito, E. Mazzon et al., "Effect of apocynin, a NADPH oxidase inhibitor, on acute lung inflammation," *Biochemical Pharmacology*, vol. 81, no. 5, pp. 636–648, 2011.

[41] L. Shen, H. Mo, L. Cai et al., "Losartan prevents sepsis-induced acute lung injury and decreases activation of nuclear factor kappaB and mitogen-activated protein kinases," *Shock*, vol. 31, no. 5, pp. 500–506, 2009.

[42] M. Bhatia and S. Moochhala, "Role of inflammatory mediators in the pathophysiology of acute respiratory distress syndrome," *The Journal of Pathology*, vol. 202, no. 2, pp. 145–156, 2004.

[43] S. Soni, M. R. Wilson, K. P. O'Dea et al., "Alveolar macrophage-derived microvesicles mediate acute lung injury," *Thorax*, vol. 71, no. 11, pp. 1020–1029, 2016.

[44] D. G. Remick, G. R. Bolgos, J. Siddiqui, J. Shin, and J. A. Nemzek, "Six at six: interleukin-6 measured 6 h after the initiation of sepsis predicts mortality over 3 days," *Shock*, vol. 17, no. 6, pp. 463–467, 2002.

Hindawi
Journal of Immunology Research
Volume 2021, Article ID 9321196, 16 pages
https://doi.org/10.1155/2021/9321196

*Research Article*

# Administration of a Probiotic Mixture Ameliorates Cisplatin-Induced Mucositis and Pica by Regulating 5-HT in Rats

**Yuanhang Wu,[1] Jianlin Wu,[2] Zhikun Lin,[3] Qian Wang,[4] Ying Li,[1] Aman Wang,[1] Xiu Shan,[1] and Jiwei Liu[1]**

[1]*Department of Medical Oncology, The First Affiliated Hospital, Dalian Medical University, Dalian, China*
[2]*Affiliated Zhongshan Hospital of Dalian University, Dalian, China*
[3]*Department of Hepatobiliary Surgery, The First Affiliated Hospital of Dalian Medical University, Dalian, China*
[4]*Liaoning CapitalBio Technology Co., Ltd., Dalian, China*

Correspondence should be addressed to Jiwei Liu; liujiwei@dmu.edu.cn

Received 22 July 2021; Revised 18 August 2021; Accepted 21 August 2021; Published 16 September 2021

Academic Editor: Tingtao Chen



Probiotic-based therapies have been shown to be beneficial for chemotherapy-induced mucositis. Previous research has demonstrated that a probiotic mixture (*Bifidobacterium brevis*, *Lactobacillus acidophilus*, *Lactobacillus casei*, and *Streptococcus thermophilus*) can ameliorate chemotherapy-induced mucositis and dysbiosis in rats, but the underlying mechanism has not been completely elucidated. We aimed to determine the inhibitory effects of the probiotic mixture on cisplatin-induced mucositis and pica and the underlying mechanism, focusing on the levels of 5-hydroxytryptamine (5-HT, serotonin) regulated by the gut microbiota. A rat model of mucositis and pica was established by daily intraperitoneal injection of cisplatin (6 mg/kg) for 3 days. In the probiotic+cisplatin group, predaily intragastric injection of the probiotic mixture ($1 \times 10^9$ CFU/kg BW) was administrated for 1 week before cisplatin injection. This was then followed by further daily probiotic injections for 6 days. Histopathology, pro-/anti-inflammatory cytokines, oxidative status, and 5-HT levels were assessed on days 3 and 6. The structure of the gut microbiota was analyzed by 16S rRNA gene sequencing and quantitative PCR. Additionally, 5-HT levels in enterochromaffin (EC) cells (RIN-14B cell line) treated with cisplatin and/or various probiotic bacteria were also determined. The probiotic mixture significantly attenuated kaolin consumption, inflammation, oxidative stress, and the increase in 5-HT concentrations in rats with cisplatin-induced intestinal mucositis and pica. Cisplatin markedly increased the relative abundances of *Enterobacteriaceae_other*, *Blautia*, *Clostridiaceae_other*, and members of *Clostridium* clusters IV and XIVa. These levels were significantly restored by the probiotic mixture. Importantly, most of the genera increased by cisplatin were significantly positively correlated with colonic 5-HT. Furthermore, in vitro, the probiotic mixture had direct inhibitory effects on the 5-HT secretion by EC cells. The probiotic mixture protects against cisplatin-induced intestine injury, exhibiting both anti-inflammatory and antiemetic properties. These results were closely related to the reestablishment of intestinal microbiota ecology and normalization of the dysbiosis-driven 5-HT overproduction.

## 1. Introduction

Cisplatin is a chemotherapy agent used for the first-line treatment of the majority of cancer patients [1]. Although clinical trials have shown effectiveness, unfavorable cytotoxic side effects are a huge hurdle that impedes the clinical application of otherwise beneficial cisplatin-based treatments [2–4]. Intestinal mucositis, a serious chemotherapy-induced side effect, is characterized by local accumulation of inflammatory cells [5], cell loss in the epithelial barrier [6], increased oxidative stress [7], and reduced gastrointestinal digestive enzyme activities [8]. Clinical manifestations include nausea, vomiting, ulceration, bloating, anorexia, constipation, severe diarrhea, and subsequent weight loss [9–11], causing potentially life-threatening complications. Improved management of cisplatin-induced mucositis and nausea/vomiting may help avoid reductions in and discontinuation of chemotherapy among patients.

Advances during the past three decades have elucidated some of the mechanisms by which chemotherapeutic agents induce side effects. Among these mechanisms, the effect of the neurotransmitter 5-hydroxytryptamine (5-HT, serotonin) plays an important part in chemotherapy-induced mucositis [9]. Cisplatin treatment may cause free radical generation, leading to localized exocytotic release of 5-HT from the enterochromaffin (EC) cells [10]. Thereafter, 5-HT interacts with 5-HT3 receptors on vagal afferent terminals in the wall of the bowel and transmits the stimulus to the brain, resulting in emesis [10]. 5-HT also regulates interstitial cells of Cajal (ICCs) in the gastrointestinal (GI) tract [12] and aquaporin 3 (AQP3) expression in the colon [13], which is closely related to constipation and diarrhea. In addition, increased intestinal 5-HT level coincides with deregulation of the mucosal immune system, which in turn exacerbates damage [14]. Currently, most drugs used as prophylaxis for chemotherapy-induced side effects belong to the classes of 5-HT3 receptor antagonists [15]. As a result, the quality of life for cancer patients has improved to a certain degree. However, these antagonists can also cause central nervous system (CNS) side effects, such as headaches, dizziness, and abnormal vision [16]. Therefore, adjuvant therapy targeting the biosynthesis of 5-HT by EC cells is a promising way to ameliorate chemotherapy-induced mucositis.

More than 90% of the total 5-HT in the human body is synthesized, stored, and released by EC cells in the intestinal mucosa [17]. 5-HT biosynthesis by EC cells was recently found to be modulated by human gut bacteria, such as *Clostridium* spp. [18]. This suggests a critical interaction between the gut microbiota and chemotherapy-induced GI complications. Disturbance of the commensal microbial structure, so-called dysbiosis, will inevitably influence EC cells and eventually affect the 5-HT-mediated stimulation of the GI tract and brain [19]. In recent years, several studies have explored gut dysbiosis in patients taking cisplatin-based chemotherapy [8, 20–22]. However, few studies have systematically evaluated the possible correlation between gut dysbiosis and 5-HT-mediated GI mucositis. In addition, whether reduction of chemotherapy-induced dysbiosis by probiotics can ameliorate the 5-HT overproduction by EC cells remains unclear.

Although rats do not vomit [23], they exhibit pica behavior (eating of nonnutritive substances such as kaolin) in response to a variety of emetogenic stimuli, which can be used as a proxy variable for nausea and vomiting in rat models [24, 25]. In this study, we administered a probiotic mixture (*Bifidobacterium brevis* DM8310, *Lactobacillus acidophilus* DM8302, *Lactobacillus casei* DM8121, and *Streptococcus thermophilus* DM8309) to rats with cisplatin-induced mucosal damage and pica. We aimed to investigate its effects on inflammation, oxidative stress, gut microbiota modification, and the levels of serum and colonic 5-HT in the rats. Our results showed that the probiotic mixture ameliorated cisplatin-induced mucositis and pica in rats and normalized the dysbiosis-driven 5-HT overproduction. These effects may be closely related to the effects of the probiotic mixture on gut dysbiosis in the cisplatin-treated rats.

## 2. Materials and Methods

*2.1. Bacterial Strains and Drugs.* A probiotic mixture, including the following strains: *Bifidobacterium brevis* DM8310, *Lactobacillus acidophilus* DM8302, *Lactobacillus casei* DM8121, and *Streptococcus thermophilus* DM8309, was provided by Dalian Medical University and prepared as described in a previous study [26]. Briefly, the strains were cultured separately on solid media under anaerobic condition, at 37°C for 24 h. After that, single colonies were picked and inoculated into MRS liquid medium and cultured for 24 hours. The bacteria were then mixed by centrifugation at $5{,}000 \times g$, 4°C for 2 min, and resuspended in 2 mL PBS before administration to rats. Cisplatin was obtained from Qilu Pharmaceutical Co., Ltd. (China) and dissolved in saline. Kaolin, acquired from China Pharmaceutical Chemical Reagents Co., Ltd. (China), was prepared and processed as previously described [21].

*2.2. Animal Study.* Sprague-Dawley (SD) male rats aged 8 weeks old and weighing 180~200 g each were supplied by the Specific Pathogen Free animal centre of Dalian Medical University and were kept on a 12 h light/dark cycle with access to food and water ad libitum in a temperature-controlled room (25°C). The kaolin pellets were introduced into the rats 6 days prior to cisplatin injection. Most of the rats stopped taking Kaolin on the third day, and those that were still interested in kaolin were excluded. The remaining rats were randomly divided into 3 experimental groups ($n = 10$ each), and toxicity was induced by daily intraperitoneal injection of cisplatin to rats with the dosage of 6 mg/kg for 3 days. The rats in the control group (Con) were subjected to saline (0.9% NaCl) injection every day and saline daily by gavage. The cisplatin group (Cis-p) received saline daily by gavage. The probiotic+cisplatin group (PM) was given cisplatin injection daily for 3 days and administration of probiotic mixture ($1 \times 10^9$ CFU/kg-BW) daily for 6 days. Probiotic mixture was administered one week before cisplatin injection. The general conditions of rats were examined every day, including activities, fur, appetite, breath, and stool. The body weight and consumption of kaolin were recorded every 24 h until the rats were sacrificed after anesthesia with sodium pentobarbital on the assigned day of each experiment. The small intestine (corresponding to the jejunum and ileum, resp.) and colon were removed. All animal work was performed according to the laboratory's animal ethics guidelines, and protocols were approved by the Dalian Medical University Institutional Animal Care and Use Committee (SYXK [Liao] 2017-0003).

*2.3. Intestinal Histology and Immunofluorescence Staining.* The colon of the rat was cut into distal, medial, and proximal sections, and 1 cm of different sections was fixed in 4% paraformaldehyde overnight at 4°C and then embedded in paraffin, and 4 $\mu$m thick sections were prepared. For histological analysis, sections were stained with hematoxylin/eosin (HE) and analyzed. The severity of colon damage was semi-quantitatively scored according to a histological scoring scale previously described [27]. For double-label immunofluorescence immunohistochemistry, slides were blocked with

10% NDS containing 0.3% Triton X-100 at 4°C for 2 h and incubated with rabbit anti-mouse CgA (1 : 500, Abcam) in combination with a rat anti-mouse 5-HT (1 : 50; Abcam) antibody at 20°C. After washing, the sections were incubated with a mixture of Alexa Fluor 488-conjugated donkey anti-rabbit IgG and Alexa Fluor 594-conjugated donkey anti-rat IgG (Invitrogen, Rockford, IL, USA; 1 : 1,000) secondary antibodies at 20°C for 3 h while protected from light. The sections were then mounted on glass slides and finally embedded with Fluoromount/Plus (K048, Diagonostic Biosystems, Pleasanton, CA, USA) after drying at room temperature for 30 min.

*2.4. ELISA.* The levels of lipopolysaccharides (LPS, USCN, USA), malondialdehyde (MDA, Nanjing Jiancheng Bioengineering Institute, China), serotonin, and cytokines (USCN, USA) including TNF-$\alpha$, IL-6, and IL-10 in sera and/or supernatant of tissue homogenates were detected by ELISA according to the manufacturer's instructions. Readings from tissue samples were normalized to total protein content as detected by the BCA assay (Thermo Pierce). Data that compiled across multiple experiments are expressed as concentrations normalized to controls within each experiment.

*2.5. The Quantitative Real-Time PCR (qPCR) Detection.* The extraction of total RNA and the synthesization of the complementary DNA (cDNA) were performed as previously described [28]. For detection of rat genes, amplification was performed in triplicates in 384 well plates (QuantStudio 6 Flex Real-Time PCR System) using ChamQ Universal SYBR qPCR Master Mix (Vazyme). The expression levels were calculated using the comparative $2^{-\triangle\triangle ct}$ method. For detection of fecal bacterial groups of rats, amplification and detection were performed as previously described [26]. Bacterial quantity was expressed as log10 bacteria/g of fecal content. qPCR primers are listed in Table 1.

*2.6. 16S rRNA Gene Sequencing and Analysis.* The fecal metagenomic DNA of rats was extracted using the QIAamp DNA Stool Mini Kit (Qiagen, Hilden, Germany). The primer pair 520F/802R was used to amplify the V3-V4 hypervariable region of the bacterial 16S rDNA from bacteria in rat feces of six groups ($n = 4$-5 each). HiSeq sequencing and data analysis were subsequently performed using a method described previously [29]. Operational taxonomic units (OTUs) present in 50% or more of the fecal samples were identified as core OTUs. Principal component analysis (PCA) was then conducted according to the distance matrices to analyze the diversity between groups.

*2.7. RIN-14B In Vitro Culture Experiments.* RIN-14B cells were purchased from ATCC (ATCC No. CCL 89) and seeded into 24-well plates at a density of $2 \times 10^5$ cells/0.5 mL RPMI1640 medium (Invitrogen-Japan) with 10% FCS (Thermo Fischer Scientific), 1% penicillin and streptomycin (Thermo Fisher Scientific) at 37°C, and 5% $CO_2$. 1 mL of the bacteria culture broths (OD600 = 1.5) was centrifuged at 2500 rpm for 5 minutes, and supernatants were filtered through 0.2 $\mu$m pore syringe filters. Cultured RIN-14B cells were incubated with different bacterial filtrates for 1 h at 37°C. For cisplatin treatment, cells were incubated with cisplatin (1 $\mu$g/mL), passed through 0.2 $\mu$m pore syringe filters, while for the cisplatin combined with PM treatment, cells were incubated with cisplatin (1 $\mu$g/mL) and 1 mL probiotic mixture. After incubation, the supernatant was collected, which was then centrifuged $6000 \times g$ for 5 min and frozen for downstream 5-HT analysis.

*2.8. Statistical Analysis.* All quantitative data were expressed as the mean ± standard error of the mean (SEM). Statistical analyses were performed using two-tailed, unpaired Student's $t$-test for comparisons of two groups when data obey normal distribution and even variance and using one-way ANOVA followed by the Kruskal-Wallis rank sum test for multigroup comparisons. Pearson's correlation test was used to analyze the correlation between the differential microbes and colon 5-HT level. Significance was set at $^{*}p < 0.05$, $^{**}p < 0.01$, $^{***}p < 0.001$, and $^{****}p < 0.0001$.

## 3. Results

*3.1. Probiotic Mixture Ameliorates Cisplatin-Induced Pica and Mucositis in Rats.* We established a rat model of pica and intestinal mucositis by intraperitoneally injecting cisplatin. The experiment design is shown in Figure 1(a). During the 6 d experiment, one rat died after cisplatin treatment in the Cis-p group on day 5 (Figure 1(b)). No other rats died. The body weight and kaolin consumption level (indicating the degree of pica) were measured. The body weight of rats in the Cis-p group decreased ($p < 0.0001$ vs. the Con group, Figure 1(c)). The probiotic mixture ameliorated the decreased body weight to a certain extent ($p = 0.0002$ vs. the Cis-p group, Figure 1(c)). Before the first injection of cisplatin, the rats in the different experimental groups consumed a similar amount of kaolin ($p > 0.05$ between each pair of groups). After injection of cisplatin, the kaolin consumption was significantly increased in the cisplatin-only rats compared to the control rats. Kaolin consumption in the PM group decreased to a certain extent, indicating that the probiotic mixture can ameliorate cisplatin-induced pica in rats (Figure 1(d)).

*3.2. Probiotic Mixture Improves the Intestinal Barrier Function in Cisplatin-Induced Mucositis.* Morphologic observation of the colon tissue of rats after cisplatin treatment revealed severe mucosal lesions with villous atrophy, irregular arrangement and architecture of the epithelial cell, and crypt disruption in the colon mucosa compared to the control rats. Compared to the cisplatin-only rats, the probiotic mixture protected the colon mucosa from cisplatin-induced injury by improving these factors (Figure 2(a)). The histological score of the colon in rats treated with cisplatin was higher compared with control and the probiotic mixture administrated rats (day 3: Con vs. Cis-p, $p < 0.0001$; Cis-p vs. PM, $p < 0.0001$; day 6: Con vs. Cis-p, $p < 0.0001$; Cis-p vs PM, $p = 0.0082$; Figure 2(b)). A significantly elevated serum lipopolysaccharide (LPS) level, which indicates gut permeability, was found in the cisplatin-only rats ($p = 0.0003$), and the probiotic mixture significantly

Table 1: List of PCR primers used for qPCR detection of gene expression and bacterial groups.

| Gene/bacterial group | Sequences (5′-3′) of primers | Size (bp) | Reference |
|---|---|---|---|
| MUC-2 | Forward: GGCTATGGCAGACTTTGT<br>Reverse: GCATTTGCGAGTTATCAG | 262 bp | This study |
| TPH1 | Forward: ACCATCTTCCGAGAGCTGAA<br>Reverse: GATGGAAAACCCTGTGCGTT | 162 bp | [71] |
| TPH2 | Forward: ATCCCAAGTTTGCTCAGTTTT<br>Reverse: GATGGACGAAAGTAACCCTG | 167 bp | [71] |
| SERT | Forward: AACTGGCAGAAACTCTTGGA<br>Reverse: GAAGATGACGAAGCCAGAGA | 195 bp | [71] |
| $\beta$-Actin | Forward: TGGCACCACACTTTCTACAAT<br>Reverse: GGTACGACCAGAGGCATACA | 189 bp | This study |
| *Clostridium cluster XIVa* | Forward: AAATGGACGGTACCTGACTAA<br>Reverse: CTTTGAGTTTCATTCTTGCGAA | 441 bp | [72] |
| *Clostridium cluster IV* | Forward: TTACTGGGTGTAAAGGG<br>Reverse: CTTCCTCCGTTTTGTCAA | 580 bp | [73] |

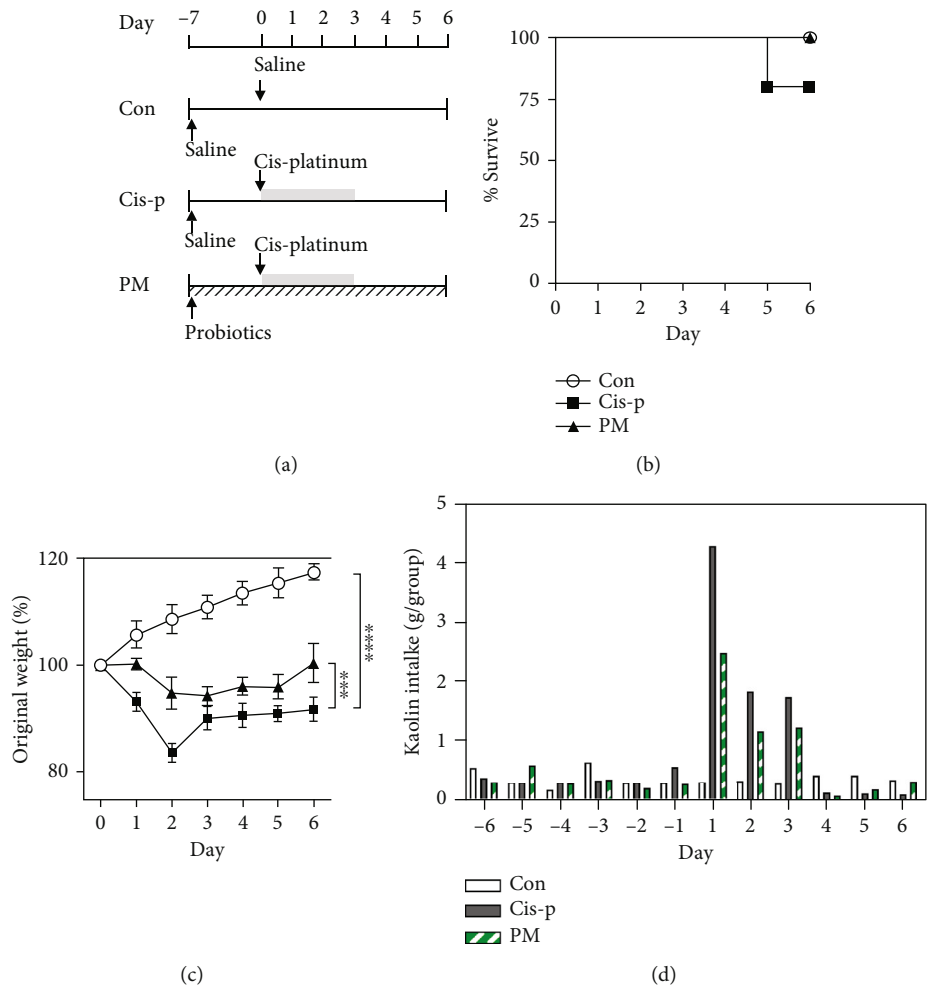


Figure 1: Effects of probiotic mixture on cisplatin-induced mucositis and pica in rats ($n = 5$): (a) experimental setup, (b) survival rate, (c) body weight, and (d) kaolin consumption. Con: normal control group; Cis-p: cisplatin-treated model group; PM: probiotic mixture- and cisplatin-treated group.

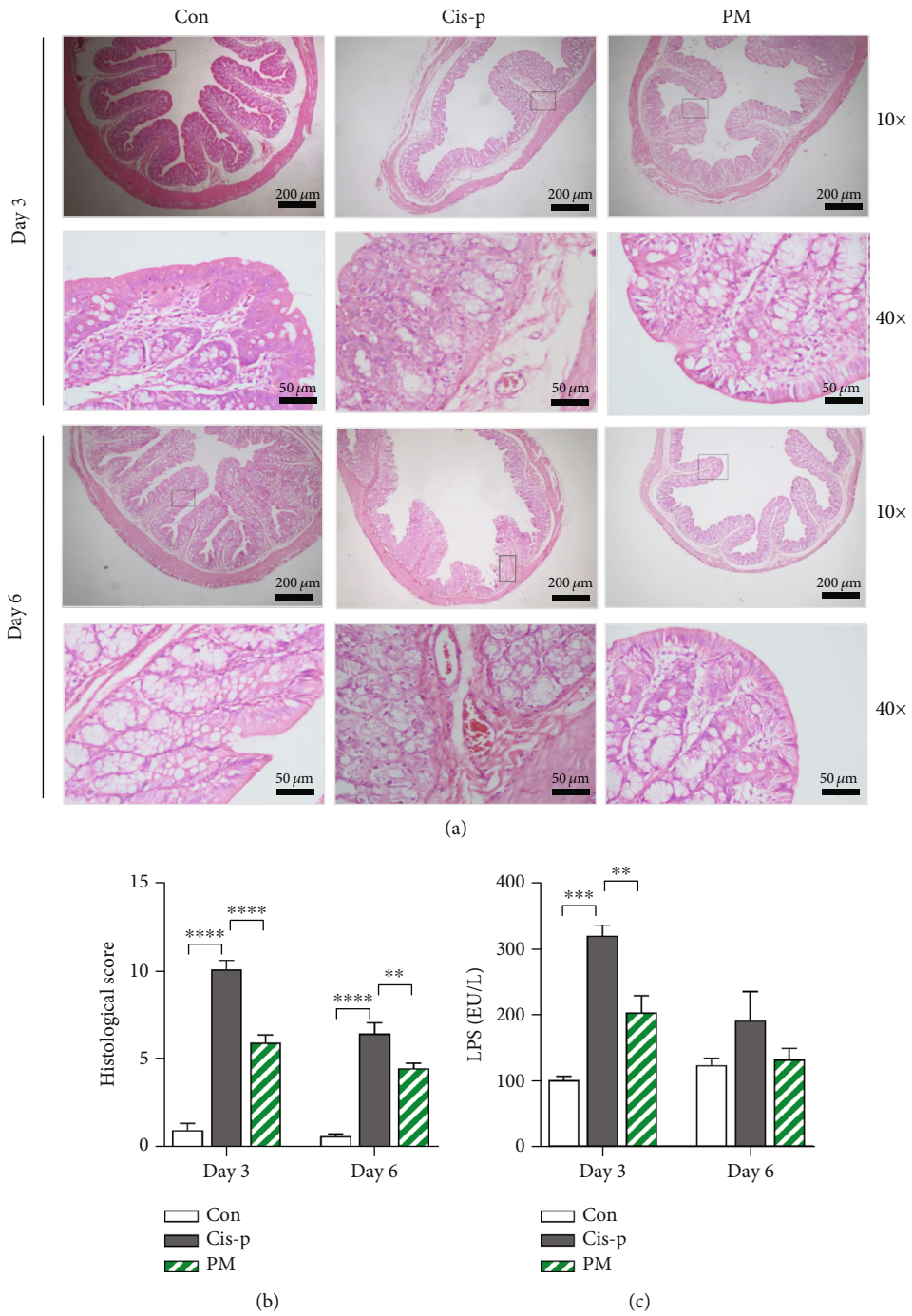


Figure 2: Continued.

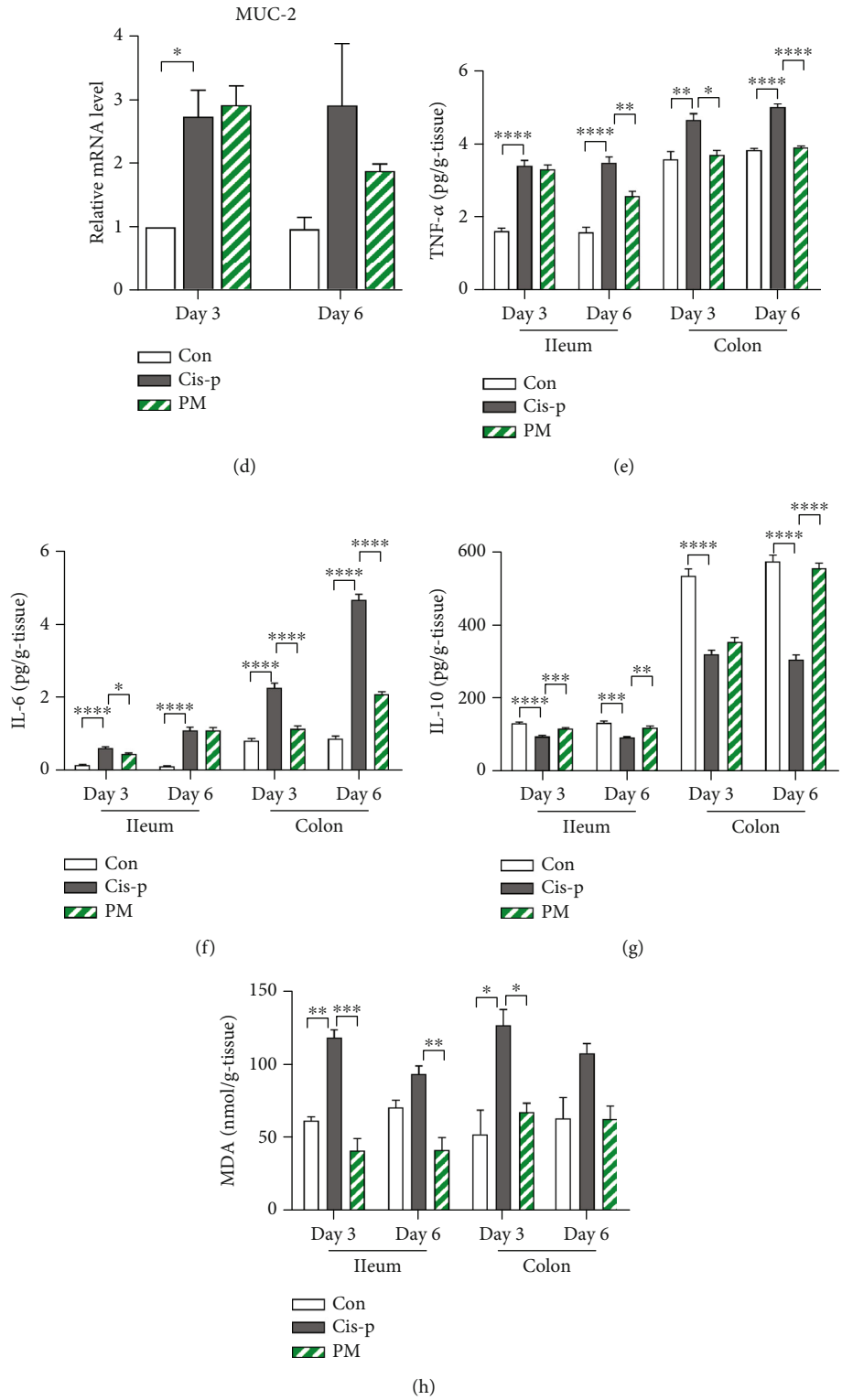


Figure 2: Effects of probiotic mixture on the intestinal barrier function in cisplatin-induced mucositis. (a) H&E staining of rat colon sections. (b) Histopathological analysis of H&E-stained sections. (c) Serum LPS were detected by ELISA. (d) Relative mRNA expression of mucin-2 (MUC-2) in colon tissues of rats, detected by quantitative PCR. Levels of tumor necrosis factor- (TNF-) $\alpha$ (e), interleukin- (IL-) 6 (f), IL-10 (g), and malondialdehyde (MDA) (h) in the ileum and colon. Data are expressed as mean ± SEM ($n = 3$-5): $^{*}p < 0.05$, $^{**}p < 0.01$, $^{***}p < 0.001$, and $^{****}p < 0.0001$.

inhibited this increase ($p = 0.0088$; Figure 2(c)). Mucin-2 (MUC-2) is the key constituent of the mucosal barrier that protects the mucosal epithelial layer. The mRNA expression levels of MUC-2 in the colon were significantly increased in the Cis-p group on day 3 ($p = 0.0142$; Figure 2(d)) and non-significantly decreased in the PM group on day 6. Additionally, compared to the Cis-p group, the probiotic mixture led to further beneficial effects on both days 3 and 6, such as reducing the elevated intestinal level of inflammatory tumor necrosis factor- (TNF-) $\alpha$ (ileum: $p = 0.0025$ [day 6]; colon: $p = 0.0107$ [day3]; $p < 0.0001$ [day 6]; Figure 2(e)) and interleukin- (IL-) 6 (ileum: $p = 0.0136$ [day 3]; colon: $p < 0.0001$ [day3]; $p < 0.0001$ [day 6]; Figure 2(f)) and promoting the secretion of IL-10 (ileum: $p = 0.0008$ [day 3]; $p = 0.006$ [day 6]; colon: $p < 0.0001$ [day 6]; Figure 2(g)). These results suggested that the probiotic mixture has an anti-inflammatory effect on cisplatin-induced intestinal mucositis in rats. Malondialdehyde (MDA), a product of lipid peroxidation, is an oxidative stress biomarker. Cisplatin increased the MDA level in intestinal tissues on both days 3 and 6, while the probiotic mixture significantly decreased the MDA concentration (ileum: $p = 0.0008$ [day 3]; $p = 0.006$ [day 6]; colon: $p = 0.0001$ [day 3]; Figure 2(h)). Together, these data indicated that the probiotic mixture had significant effects on the intestinal barrier functions, including the mechanical, immune, and chemical barrier functions.

*3.3. Probiotic Mixture Reduces Serum and Colonic 5-HT Overproduction.* As cisplatin-induced emesis is associated with an increase in 5-HT concentration, produced by EC cells, we conducted immunofluorescent staining of rat colon tissues in the three groups and also determined the colonic and serum levels of 5-HT. Double staining of chromogranin A (GI endocrine cell marker) and 5-HT showed that cisplatin-induced increases in 5-HT were localized to the colonic EC cells (Figure 3(a)). The levels of 5-HT in the colon and serum of the cisplatin-only rats were significantly increased in comparison to the control group (colon: $p = 0.0171$ [day 3]; $p = 0.0327$ [day 6]; serum: $p = 0.0056$ [day 3]; $p = 0.0277$ [day 6]; Figures 3(b) and 3(c)), and the probiotic mixture reduced the cisplatin-induced increases in colonic and serum levels of 5-HT, with significant differences on both days 3 and 6 (colon: $p = 0.018$ [day 3]; $p = 0.0148$ [day 6]; serum: P =0.0012 [day 3]; $P = 0.0238$ [day 6]; Figures 3(b) and 3(c)).

To investigate whether the inhibitory effects of the probiotic mixture on 5-HT levels in rats are due to the regulation of 5-HT synthesis or transport, we assessed the mRNA expression of tryptophan hydroxylases (TPH1 and TPH2) and the serotonin reuptake transporter (SERT) by quantitative real-time PCR. After cisplatin administration, TPH2 expression increased significantly in the colon of rats compared to the control group on day 3 ($p = 0.008$, Figure 3(e)). The probiotic mixture greatly downregulated TPH1 ($p = 0.042$) and TPH2 ($p = 0.013$) in the colon of rats compared to the levels in the cisplatin-only rats (Figures 3(d) and 3(e)). The expression level of SERT in the colon of rats showed no significant differences (Figure 3(f)).

*3.4. Regulation of Cisplatin-Induced Gut Dysbiosis in Rats by Probiotic Mixture Is Associated with Changes in the 5-HT Level.* To reveal the effects of the probiotic mixture on the gut microbiota during cisplatin-induced mucositis, sequencing targeting the V3–V4 region of the 16S rDNA was performed. Principal component analysis (PCA) revealed that the microbiota in the three groups were distinct from each other on day 3, especially regarding principal component 1 (PC1; 51.2%) (Figure 4(a)), indicating that cisplatin causes variation in the gut flora.

To further compare the gut microbiota composition among the three groups, histograms of the relative abundances were constructed, as shown in Figure 4(b) for phyla and Figure 4(c) for genera. The two most abundant bacterial phyla in rat were *Firmicutes* and *Bacteroidetes*. In the cisplatin-only rats, the relative abundance of *Firmicutes* increased (Figure S1A), while the relative abundance of *Bacteroidetes* decreased (Figure S1B), and the ratio of *Firmicutes* to *Bacteroidetes* (*F*/*B*) increased (Figure S1C), compared to the other two groups on day 3. Significant differences at the genus level were also observed (Figure 4(d)). Notably, the cisplatin-only rats had greater relative abundances of *Enterobacteriaceae_other* and *Blautia* on day 3 and *Blautia* and *Clostridiaceae_other* on day 6 but lower abundances of *Lactobacillus* (day 3) and *Roseburia* (day 6) than in the control group, suggesting that cisplatin closely affects the microbiota composition. Interestingly, in the PM group, *Proteus*, *Fusobacterium*, and *Flexispira* were clearly increased on day 3 compared to those in the cisplatin-only group. The relative abundances of *Lactobacillus*, *Enterobacteriaceae_other*, *Blautia*, *Roseburia*, and *Clostridiaceae_other* decreased.

*3.5. Probiotic Mixture Reduces Specific Bacteria That Promote Colonic 5-HT Biosynthesis In Vivo and Inhibit 5-HT Secretion by EC (RIN-14B) Cells In Vitro.* According to our finding that 5-HT levels were decreased in the colons of probiotic+cisplatin rats compared to the cisplatin-only rats, we therefore hypothesized that specific microbes are associated with affecting the host 5-HT pathways. Using Pearson's correlation analysis, bacteria that were significantly related to the colonic 5-HT variation were identified and plotted. We found that the genera *Ruminococcaceae_other*, *Blautia*, *Ruminococcus*, and *Dorea* were all significantly positively correlated with colonic 5-HT (Figure 5(a)). Relative quantification of selected 5-HT-associated bacterial groups was performed by quantitative real-time PCR. The results further revealed that the members of *Clostridium* clusters IV and XIVa (butyrate producers) were significantly increased in the cisplatin-only rats compared to the control rats. The PM group showed decreased abundances of *Clostridium* cluster IV and XIVa compared to the cisplatin-only group, especially on day 6 ($p = 0.015$, Figure 5(b); $p = 0.03$, Figure 5(c)).

To determine whether the protective effects of the probiotic mixture were directly associated with the inhibition of 5-HT secretion by EC cells, we further subjected RIN-14B cells to no treatment (control), one of the four bacteria in the probiotic mixture or the mixture itself, cisplatin only, or cisplatin plus the probiotic mixture. We found that all four bacteria and the mixture itself significantly decreased

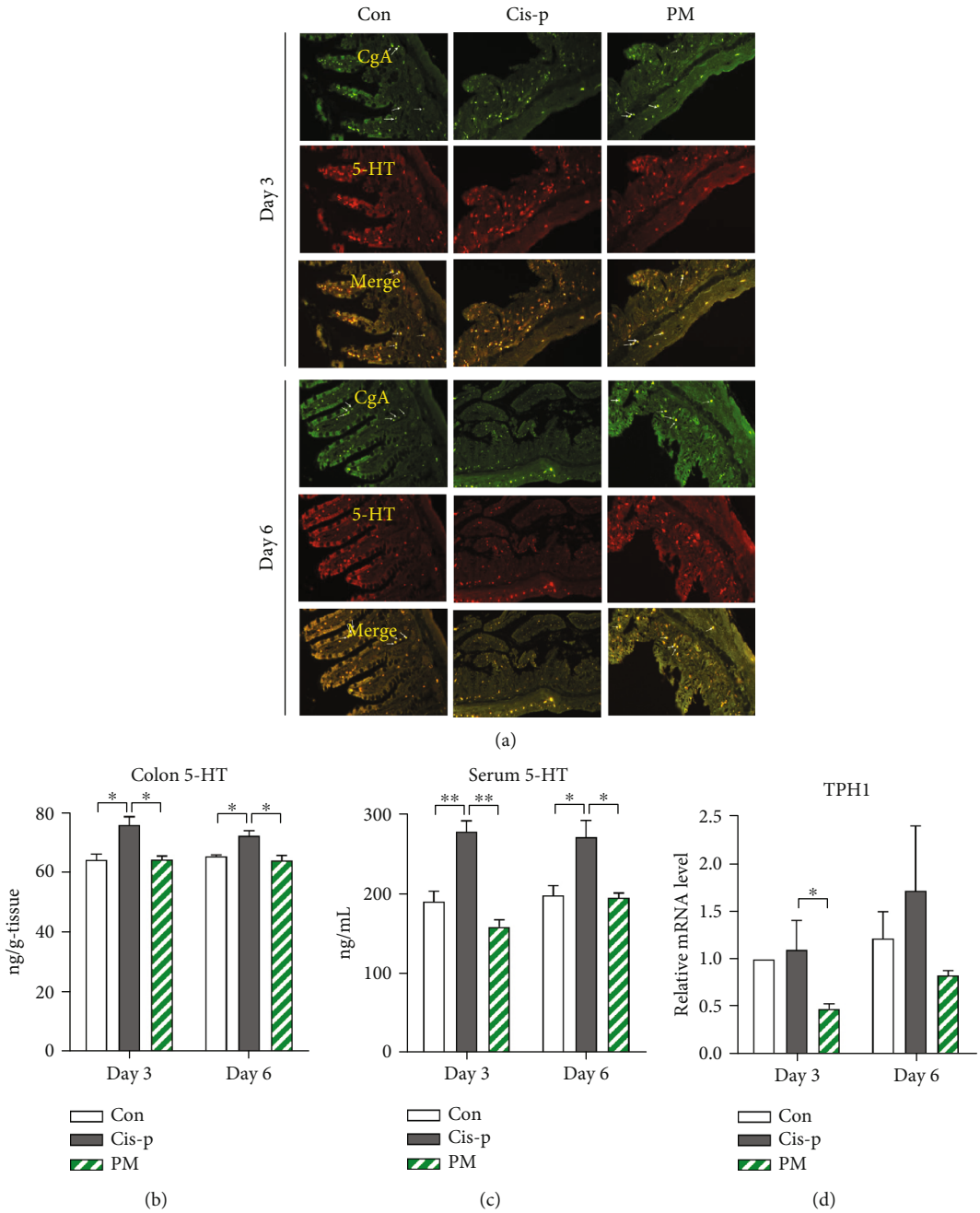


Figure 3: Continued.

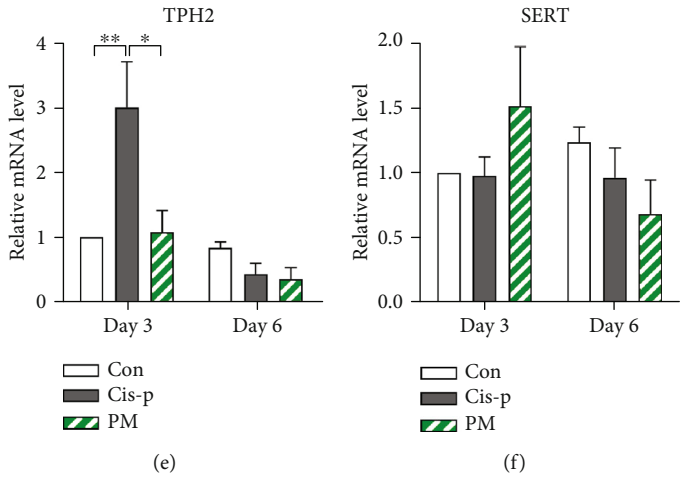


Figure 3: Effects of probiotic mixture on cisplatin-induced colonic 5-HT biosynthesis in rats. (a) Representative images of colons with chromogranin A (gastrointestinal endocrine cell marker, green) and 5-HT (red) staining. Levels of colonic (b) and serum (c) 5-HT. Colonic expression of TPH1 (d), TPH2 (e), and SERT (f) relative to $\beta$-actin. Data are normalized to expression levels in the control rats on day 3. Data are expressed as mean ± SEM ($n = 4$-5): $^{*}p < 0.05$ and $^{**}p < 0.01$.

5-HT secretion compared to the control cells (*S. thermophilus*, $p = 0.003$; *L. casei*, $p = 0.002$; *L. acidophilus*, $p = 0.013$; *B. brevis*, $p = 0.005$; PM, $p = 0.009$; Figure 5(d)). Furthermore, the probiotic mixture significantly reduced cisplatin-induced 5-HT overproduction (Cis-p vs. control, $p = 0.002$; PM vs. Cis-p, $p = 0.018$; Figure 5(d)). This suggested that the probiotic mixture not only reduced 5-HT-associated bacteria but also had direct inhibitory effects on 5-HT biosynthesis in EC cells.

## 4. Discussion

In this study, the inhibitory effects of a probiotic mixture on cisplatin-induced mucositis and pica in rats were investigated. We found that the underlying mechanisms involved gut microbiota-induced alteration of gut-derived 5-HT biosynthesis.

Chemotherapy-induced mucositis and nausea/vomiting are common and major debilitating side effects of chemotherapy, which severely affects quality of life among cancer patients, even reducing their compliance with chemotherapy [30]. Cisplatin, a cytotoxic agent, is widely prescribed in chemotherapy regimens for various human cancers due to its affinity for DNA [31]. Cisplatin causes both acute and delayed GI tract disorders (<24 and >24 hours after administration, respectively) [32]. Our results are consistent with those of prior studies in which cisplatin caused significant mucositis and pica in rats [8, 33–35]. Another study revealed that treatment with the probiotic mixture used in our study (*Bifidobacterium brevis* DM8310, *Lactobacillus acidophilus* DM8302, *Lactobacillus casei* DM8121, and *Streptococcus thermophilus* DM8309) alleviates 5-fluorouracil-induced mucositis in rats [26]. Our study demonstrated that this probiotic mixture also attenuated cisplatin-induced mucositis and pica in rats, which involved reducing inflammation and oxidative stress. A clinical study found that treatment with *B. breve* ameliorated intestinal mucositis in pediatric cancer patients taking chemotherapy [36]. *L. acidophilus* and *L. casei* both significantly improved the inflammatory and functional aspects of 5-fluorouracil-induced intestinal mucositis in mice [37, 38]. Furthermore, oral ingestion of *S. thermophilus* alleviated the symptoms of methotrexate-induced mucositis [39]. Thus, the probiotic mixture used in this study potentially improves GI function.

Intestinal barrier integrity is critical for intestinal function. Emerging data suggest that chemotherapy exerts detrimental effects on intestinal permeability, contributing to inflammation [40]. We detected histological abnormalities in the colon of mice treated with cisplatin, which were reversed by the probiotic mixture (Figure 2). In addition, compared to the cisplatin-only group, as indicated by the decreased endotoxin LPS in the serum. Although MUC-2 has been shown to have protective capacities, we found that it was upregulated during cisplatin-induced mucositis, especially on day 3, and it reverted to a normal level by day 6 in the probiotic+cisplatin group. MUC-2 upregulation may be a counterreaction by the intestine to protect against mucositis [41], which was also observed in methotrexate-induced damage [42, 43]. The mechanism may involve short-chain fatty acids (SCFAs) regulating prostaglandin production, thus stimulating MUC-2 expression in intestinal epithelial cells [44]. Our results also indicated that cisplatin-induced inflammation was attenuated by the probiotic mixture. The probiotic mixture inhibited cisplatin-induced generation of TNF-$\alpha$ and IL-6 and promoted the secretion of IL-10. In the cisplatin-only rats, the increase in inflammatory cytokines may be attributable to the degradation of the epithelial barrier; furthermore, this may trigger dysbiosis and elicit secondary inflammation, ultimately resulting in intestinal mucositis [45]. Oxidative stress is also a critical component of cisplatin-induced intestinal injury [46]. There is evidence that some lactic acid bacteria (*Bifidobacterium*, *Lactobacillus*, *Lactococcus*, and *Streptococcus thermophilus*) exerted antioxidant activity [47]. Our results also revealed that the

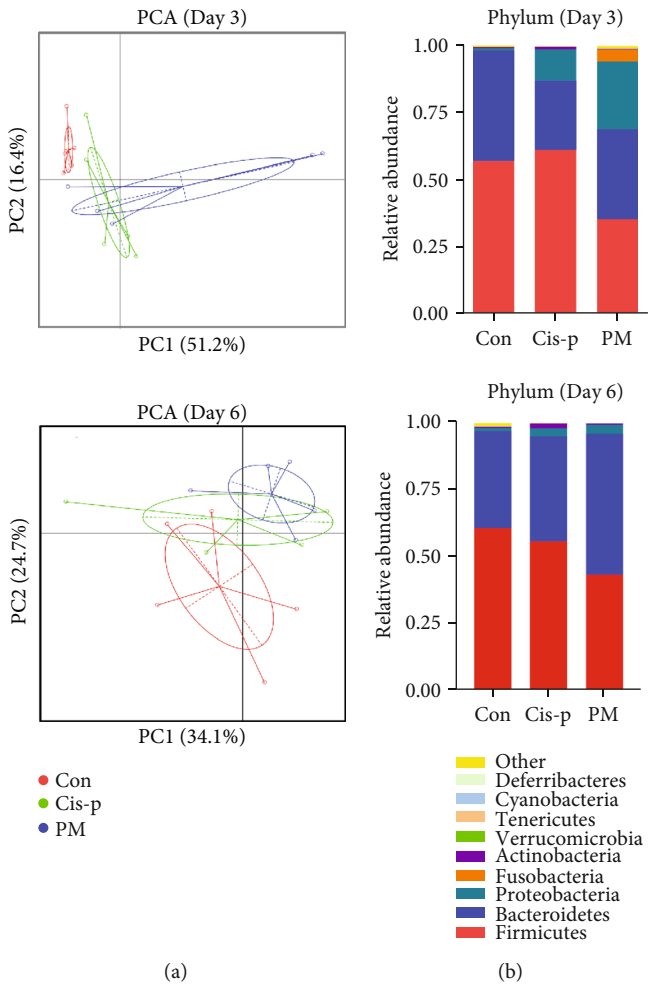


Figure 4: Continued.

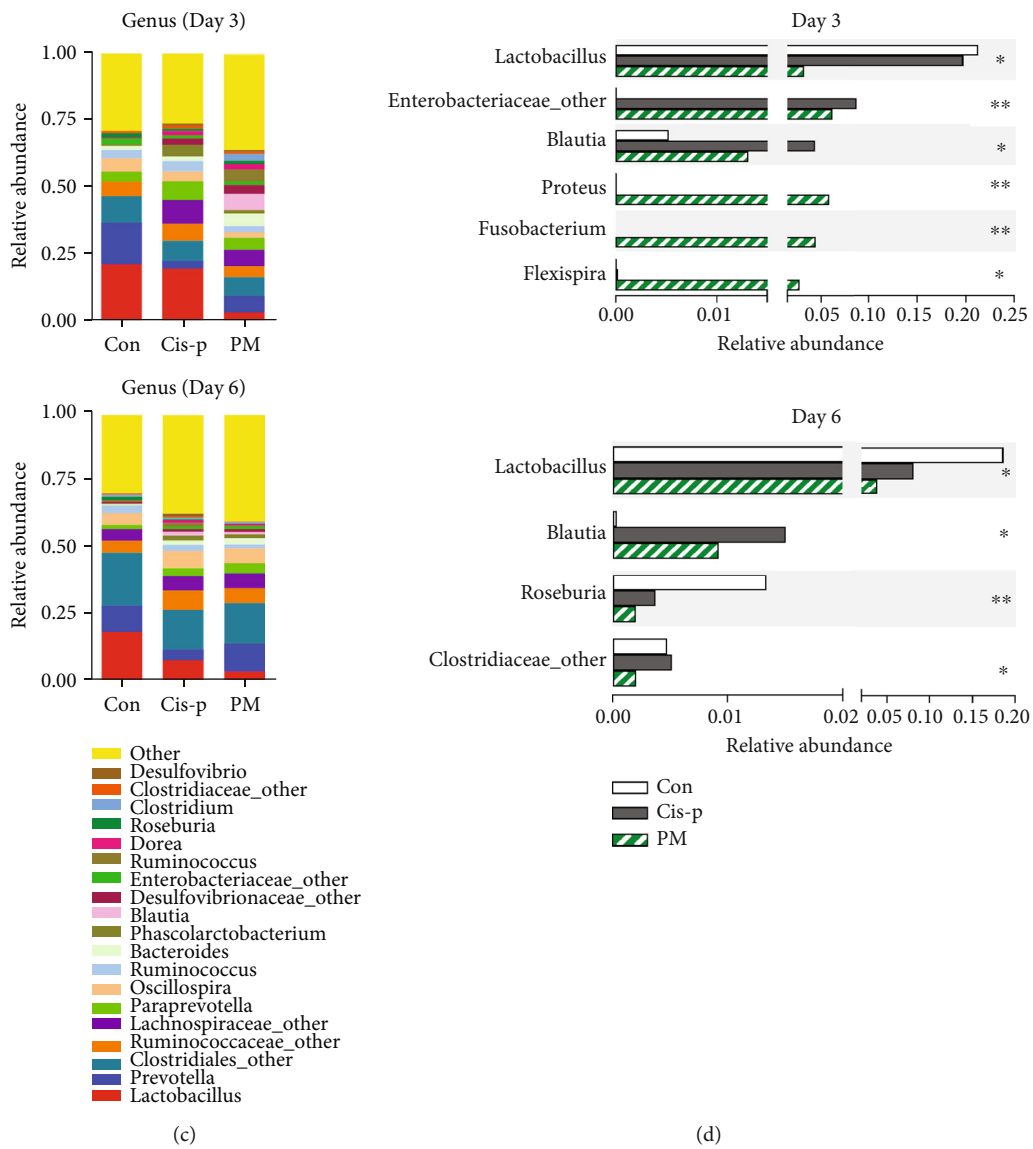


Figure 4: Probiotic mixture modulated intestinal bacterial composition in cisplatin-treated rats ($n = 4$-5). (a) Principal component analysis (PCA) among different samples. (b) Mean abundances in the gut microbiota at the phylum level. (c) Bar charts of the gut microbiota at the genus level. (d) Species differences among the three groups at the genus level. $^{*}p < 0.05$ and $^{**}p < 0.01$.

probiotic mixture (*Bifidobacterium*, *Lactobacillus*, and *Streptococcus thermophilus*) reduced oxidative stress by decreasing MDA concentrations in both colon and ileum tissues. Thus, all the data suggested that the probiotic mixture has potentially anti-inflammatory and antioxidant activities.

It has been suggested that acute GI tract disorders involve 5-HT secretion from EC cells, which are a subset of enteroendocrine cells that reside within the intestinal mucosa [48]. A rate-limiting enzyme in 5-HT biosynthesis is TPH, which is present in two isoforms (TPH1 and TPH2). TPH1 is primarily expressed in the EC cells of the gut, whereas TPH2 is expressed in serotonergic neurons [49]. TPH expression can be considered an indirect biomarker of 5-HT synthesis. 5-HT is inactivated by SERT-mediated uptake into mucosal epithelial cells or enteric neurons [50]. Therefore, TPH and SERT are important for determining the 5-HT concentration and dynamics. A preliminary study revealed that cisplatin significantly increased TPH1 mRNA expression, but not TPH2 and SERT mRNA expression, in ileal tissue [51]. Another study demonstrated that cisplatin increased TPH1 and TPH2 mRNA expression in the ileum and medulla oblongata, respectively, indicating that cisplatin accelerates 5-HT synthesis through upregulating TPH, but has no effect on SERT [34]. We found that cisplatin significantly increased TPH1 and TPH2 levels in the colon but did not affect the SERT level. Thus, the increase in colonic TPH activity after cisplatin administration may be due to an increase in the number of EC cells and enteric neurons that express TPH1 and TPH2 mRNA. Furthermore, the probiotic mixture significantly inhibited the increase in 5-HT levels in the colon and serum, probably because it inhibited 5-HT synthesis in the colon (Figure 3).

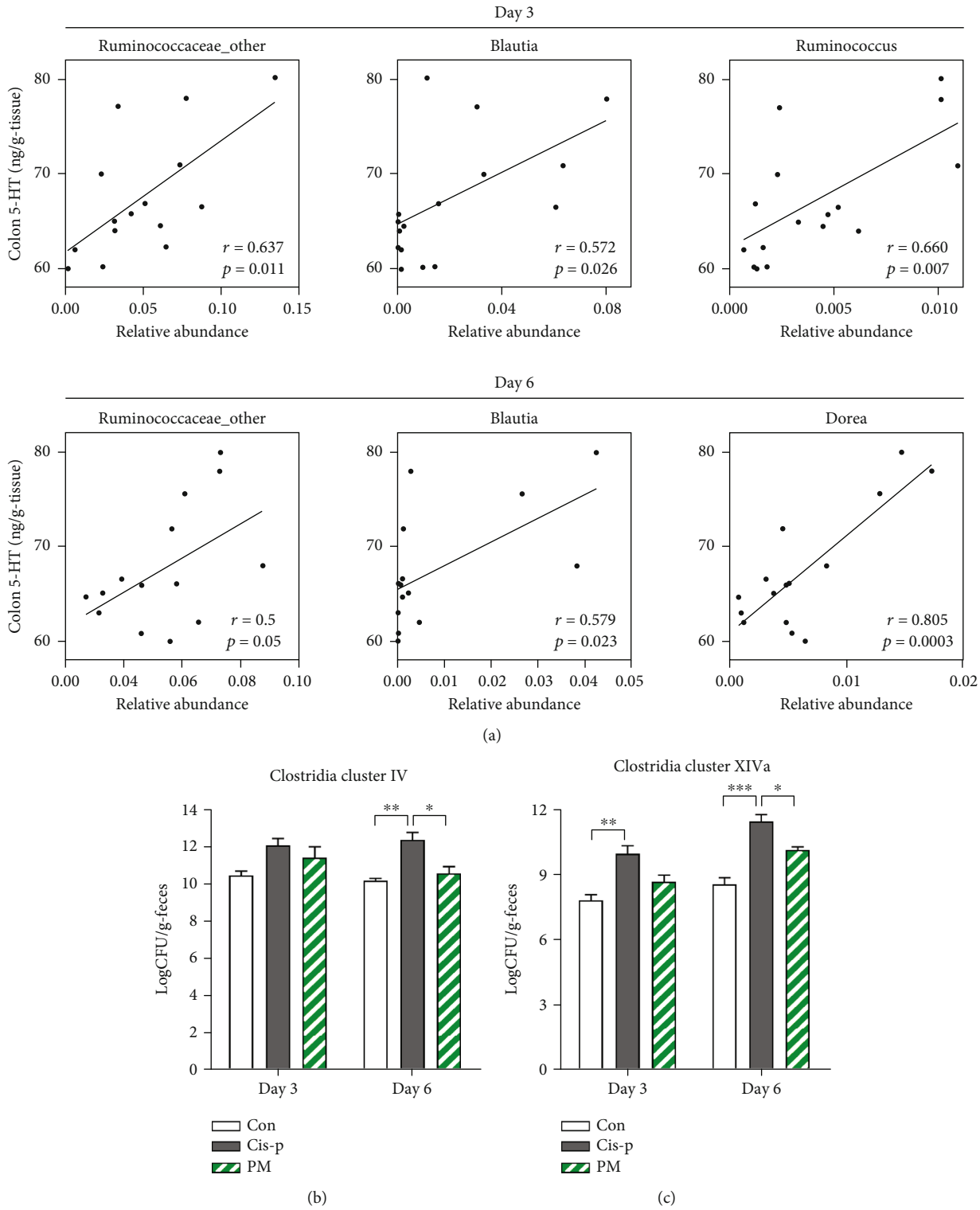


Figure 5: Continued.

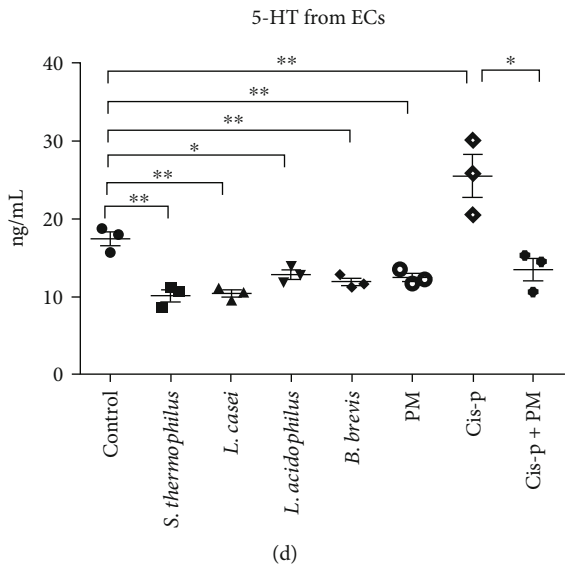


Figure 5: Probiotic mixture reduced 5-HT-associated bacteria and inhibited 5-HT secretion by RIN-14B cells. (a) Correlations between the abundances of differential species and colonic 5-HT level. Abundances of Clostridium cluster IV (b) and XIVa (c) in the feces of rats in different groups detected by quantitative PCR. Data are presented as the mean logarithm of bacterial colony-forming units (CFU) per gram of feces. (d) Levels of 5-HT released from RIN-14B cells after exposure to various bacteria or cisplatin. Data are expressed as mean ± SEM ($n = 3$–5): $^{*}p < 0.05$, $^{**}p < 0.01$, and $^{***}p < 0.001$.

The gut microbiota plays an important role in promoting levels of colonic and serum 5-HT. Yano et al. [18] found that germ-free mice exhibited significantly decreased levels of colonic and serum 5-HT compared to specific pathogen-free (SPF) controls, and the study suggested that the microbiota regulated 5-HT metabolism primarily by affecting host colonic EC cells. Gut dysbiosis is known to be involved in the pathogenesis of chemotherapy-induced mucositis, and restoring gut microbiota homeostasis may accelerate intestinal healing [40, 52, 53]. The probiotic mixture reversed cisplatin-induced gut dysbiosis—as indicated by the increased *F*/*B* ratio [54, 55]. We found that cisplatin treatment caused a significant increase in several gut bacterial taxa such as *Enterobacteriaceae_other*, *Blautia*, and *Clostridiaceae_other*, which were significantly restored by the probiotic mixture. Similar trends were observed in the abundances of *Ruminococcaceae_other*, *Ruminococcus*, and *Dorea*, although the differences were not significant. Notably, *Ruminococcaceae_other*, *Blautia*, *Ruminococcus*, and *Dorea* were all significantly positively correlated with colonic 5-HT (Figure 5). The abundances of *Enterobacteriaceae* and *Blautia* have been reported to be increased in chemotherapy-induced dysbiosis [56–58]. Consistent with our results, *Ruminococcaceae* and *Ruminococcus* have been reported to be positively correlated with 5-HT [59, 60]. However, we also found that *Proteus*, *Fusobacterium*, and *Flexispira*, as putative gastrointestinal pathogens [61–63], were clearly increased in the PM group on day 3 compared with the other two groups (Figure 4(d)). We considered that the sample size in the Illumina Hiseq sequencing was not enough; further studies based on a larger number of samples should be conducted to confirm the results. Importantly, the gut microbiota compositions of the three groups are different on days 3 and 6, which due to the gut epithelium have remarkable self-renewal capacity, and the intestinal microbiota also has the recovery ability to repair damaged mucosal barrier [64, 65]. Furthermore, the probiotic mixture accelerated recovery of cisplatin-induced intestinal damage.

It is worth noting that SCFAs are well-known metabolites produced by the microbiota. They have been suggested to influence 5-HT secretion. The SCFAs' butyrate and acetate, which are produced in abundance by distal gut microbes in vivo, significantly affect enteric 5-HT production by promoting TPH1 transcription [66]. *Clostridia* are anaerobic *Firmicutes* that produce a large array of metabolites. Moreover, *Clostridium* clusters IV and XIVa (also known as the *Clostridium leptum* and *Clostridium coccoides* groups, respectively) contain butyrate-producing species [67]. We therefore explored the link between *Clostridium* clusters IV and XIVa and cisplatin-induced intestinal injury. Riezzo et al. reported that a clinically relevant combination of irinotecan and 5-FU decreased *Clostridium* cluster IV and increased *Clostridium* cluster XIVa [68]. However, other studies showed that both an irinotecan regimen and 5-FU decreased the abundances of *Clostridium* cluster XIVa [26, 56]. Due to different drugs and different sampling times, our results demonstrated that cisplatin significantly increased members of *Clostridium* clusters IV and XIVa, which produce butyrate and thereby promote 5-HT secretion by EC cells. Therefore, we speculated that the probiotic mixture ameliorated cisplatin-induced mucositis and pica in rats partly by normalizing the dysbiosis-driven 5-HT overproduction. Additionally, probiotic bacterial species and probiotic supplements have a tendency to directly reduce colonic 5-HT [69, 70]. We confirmed that the probiotic mixture also had direct inhibitory effects against 5-HT biosynthesis in EC cells in vitro. To sum up, the probiotic mixture supplementation in cisplatin-treated rats reestablished the intestinal ecosystem, particularly

the populations of probiotic bacteria, which in turn attenuated the increased 5-HT.

## 5. Conclusion

In this study, the protective effects of a probiotic mixture against cisplatin-induced mucositis and pica and the potential underlying mechanisms were evaluated. The probiotic mixture significantly ameliorated kaolin consumption, inflammation, oxidative stress, and the increased 5-HT concentrations caused by cisplatin. Furthermore, the probiotic mixture mitigated the gut dysbiosis and attenuated the altered metabolic profiles induced by cisplatin. The mechanism underlying the attenuation of cisplatin-induced intestinal injury may involve the probiotic mixture modulating the dysbiosis-driven 5-HT overproduction. The findings of this study indicate that the probiotic mixture may be useful for treating intestinal injury induced by cisplatin-based chemotherapy. However, more optimized study design and a larger sample size would benefit future studies. Further studies are required to fully understand the in-deep mechanisms of how the probiotic mixture supplementation ameliorates the cisplatin-induced mucositis and pica.

## Data Availability

The raw data used to support the findings of this study will be made available by the authors, without undue reservation, to any qualified researcher.

## Ethical Approval

All experimental protocols were approved by the Animal Ethical Committee of Dalian Medical University.

## Conflicts of Interest

The authors have declared that no conflict of interest exists.

## Authors' Contributions

YW performed the data analyses and wrote the manuscript. JW contributed to the conception of the study and obtained the funding. ZL and YL performed the experiments. QW and AW contributed significantly to analysis and manuscript preparation. XS helped perform the analysis with constructive discussions. JL contributed to the conception of the study and revised the manuscript. All authors read and approved the final manuscript.

## Acknowledgments

This study was supported by the National Natural Science Foundation of China (82071911).

## Supplementary Materials

Figure S1: composition analysis of gut microbiota at the phylum level ($n = 4$-5). (A) Proportion of *Firmicutes*; (B) proportion of *Bacteroidetes*; (C) the ratio of *Firmicutes* to *Bacteroidetes*. $^{*}p < 0.05$. *(Supplementary Materials)*

## References

[1] N. Devarajan, R. Manjunathan, and S. K. Ganesan, "Tumor hypoxia: the major culprit behind cisplatin resistance in cancer patients," *Critical Reviews in Oncology/Hematology*, vol. 162, p. 103327, 2021.

[2] G. Babolmorad, A. Latif, I. K. Domingo et al., "Toll-like receptor 4 is activated by platinum and contributes to cisplatin-induced ototoxicity," *EMBO Reports*, vol. 22, no. 5, article e51280, 2021.

[3] C. Rui, S. N. Shi, W. Ren et al., "The multitargeted kinase inhibitor KW-2449 ameliorates cisplatin-induced nephrotoxicity by targeting RIPK1-mediated necroptosis," *Biochemical Pharmacology*, vol. 188, p. 114542, 2021.

[4] S. Gong, Y. Feng, Y. Zeng et al., "Gut microbiota accelerates cisplatin-induced acute liver injury associated with robust inflammation and oxidative stress in mice," *Journal of Translational Medicine*, vol. 19, no. 1, p. 147, 2021.

[5] F. A. L. Barroso, L. C. L. de Jesus, C. P. de Castro et al., "Intake of Lactobacillus delbrueckii (pExu:hsp65) prevents the inflammation and the disorganization of the intestinal mucosa in a mouse model of mucositis," *Microorganisms*, vol. 9, no. 1, p. 107, 2021.

[6] Y. Zhang, B. Zhang, L. Dong, and P. Chang, "Potential of omega-3 polyunsaturated fatty acids in managing chemotherapy- or radiotherapy-related intestinal microbial dysbiosis," *Advances in Nutrition*, vol. 10, no. 1, pp. 133–147, 2019.

[7] L. S. Fideles, J. A. L. de Miranda, C. D. S. Martins et al., "Role of rutin in 5-fluorouracil-induced intestinal mucositis: prevention of histological damage and reduction of inflammation and oxidative stress," *Molecules*, vol. 25, no. 12, p. 2786, 2020.

[8] C. H. Wu, J. L. Ko, J. M. Liao et al., "D-Methionine alleviates cisplatin-induced mucositis by restoring the gut microbiota structure and improving intestinal inflammation," *Therapeutic Advances in Medical Oncology*, vol. 11, p. 175883591882102, 2019.

[9] P. J. Hesketh, "Chemotherapy-induced nausea and vomiting," *The New England Journal of Medicine*, vol. 358, no. 23, pp. 2482–2494, 2008.

[10] R. M. Navari and M. Aapro, "Antiemetic prophylaxis for chemotherapy-induced nausea and vomiting," *The New England Journal of Medicine*, vol. 374, no. 14, pp. 1356–1367, 2016.

[11] V. L. Batista, T. F. da Silva, L. C. L. de Jesus et al., "Probiotics, prebiotics, synbiotics, and paraprobiotics as a therapeutic alternative for intestinal mucositis," *Frontiers in Microbiology*, vol. 11, p. 544490, 2020.

[12] M. M. Wouters, S. J. Gibbons, J. L. Roeder et al., "Exogenous serotonin regulates proliferation of interstitial cells of Cajal in mouse jejunum through 5-$HT_{2B}$ receptors," *Gastroenterology*, vol. 133, no. 3, pp. 897–906, 2007.

[13] R. Kon, N. Ikarashi, A. Hayakawa et al., "Morphine-induced constipation develops with increased aquaporin-3 expression in the colon via increased serotonin secretion," *Toxicological Sciences*, vol. 145, no. 2, pp. 337–347, 2015.

[14] Y. Dong, Y. Han, Z. Wang et al., "Role of serotonin on the intestinal mucosal immune response to stress-induced diarrhea in weaning mice," *BMC Gastroenterology*, vol. 17, no. 1, p. 82, 2017.

[15] A. Eliasen, K. Dalhoff, R. Mathiasen et al., "Pharmacogenetics of antiemetics for chemotherapy-induced nausea and vomiting: a

systematic review and meta-analysis," *Critical Reviews in Oncology/Hematology*, vol. 149, p. 102939, 2020.

[16] R. Juza, P. Vlcek, E. Mezeiova, K. Musilek, O. Soukup, and J. Korabecny, "Recent advances with 5-HT3 modulators for neuropsychiatric and gastrointestinal disorders," *Medicinal Research Reviews*, vol. 40, no. 5, pp. 1593–1678, 2020.

[17] J. D. Matute, J. Duan, and R. S. Blumberg, "Microbial RNAs pressure piezo1 to respond," *Cell*, vol. 182, no. 3, pp. 542–544, 2020.

[18] J. M. Yano, K. Yu, G. P. Donaldson et al., "Indigenous bacteria from the gut microbiota regulate host serotonin biosynthesis," *Cell*, vol. 161, no. 2, pp. 264–276, 2015.

[19] H. Szőke, Z. Kovács, I. Bókkon et al., "Gut dysbiosis and serotonin: intestinal 5-HT as a ubiquitous membrane permeability regulator in host tissues, organs, and the brain," *Reviews in the Neurosciences*, vol. 31, no. 4, pp. 415–425, 2020.

[20] A. Perales-Puchalt, J. Perez-Sanz, K. K. Payne et al., "Frontline science: microbiota reconstitution restores intestinal integrity after cisplatin therapy," *Journal of Leukocyte Biology*, vol. 103, no. 5, pp. 799–805, 2018.

[21] X. Feng, Q. Cheng, Q. Meng, Y. Yang, and K. Nie, "Effects of ondansetron and [6]-gingerol on pica and gut microbiota in rats treated with cisplatin," *Drug Design Development and Therapy*, vol. 13, pp. 2633–2641, 2019.

[22] Y. T. Zou, J. Zhou, C. Y. Wu et al., "Protective effects of *Poria cocos* and its components against cisplatin-induced intestinal injury," *Journal of Ethnopharmacology*, vol. 269, p. 113722, 2021.

[23] C. C. Horn, B. A. Kimball, H. Wang et al., "Why can't rodents vomit? A comparative behavioral, anatomical, and physiological study," *PLoS One*, vol. 8, no. 4, article e60537, 2013.

[24] N. Takeda, S. Hasegawa, M. Morita, and T. Matsunaga, "Pica in rats is analogous to emesis: an animal model in emesis research," *Pharmacology Biochemistry and Behavior*, vol. 45, no. 4, pp. 817–821, 1993.

[25] Y. L. Liu, N. Malik, G. J. Sanger, M. I. Friedman, and P. L. Andrews, "Pica–a model of nausea? Species differences in response to cisplatin," *Physiology & Behavior*, vol. 85, no. 3, pp. 271–277, 2005.

[26] Y. Tang, Y. Wu, Z. Huang et al., "Administration of probiotic mixture DM1 ameliorated 5-fluorouracil-induced intestinal mucositis and dysbiosis in rats," *Nutrition*, vol. 33, pp. 96–104, 2017.

[27] M. Li, P. Liang, Z. Li et al., "Fecal microbiota transplantation and bacterial consortium transplantation have comparable effects on the re-establishment of mucosal barrier function in mice with intestinal dysbiosis," *Frontiers in Microbiology*, vol. 6, p. 692, 2015.

[28] Y. Y. Li, H. Liu, H. Qi et al., "Probiotic fermentation of *Ganoderma lucidum* fruiting body extracts promoted its immunostimulatory activity in mice with dexamethasone-induced immunosuppression," *Biomedicine & Pharmacotherapy*, vol. 141, p. 111909, 2021.

[29] M. Li, B. Wang, X. Sun et al., "Upregulation of intestinal barrier function in mice with DSS-induced colitis by a defined bacterial consortium is associated with expansion of IL-17A producing gamma delta T cells," *Frontiers in Immunology*, vol. 8, p. 824, 2017.

[30] L. Lohr, "Chemotherapy-induced nausea and vomiting," *Cancer Journal*, vol. 14, no. 2, pp. 85–93, 2008.

[31] M. R. Trendowski, O. El Charif, P. C. Dinh Jr., L. B. Travis, and M. E. Dolan, "Genetic and modifiable risk factors contributing to cisplatin-induced toxicities," *Clinical Cancer Research*, vol. 25, no. 4, pp. 1147–1155, 2019.

[32] H. Takeda, C. Sadakane, T. Hattori et al., "Rikkunshito, an herbal medicine, suppresses cisplatin-induced anorexia in rats via 5-HT2 receptor antagonism," *Gastroenterology*, vol. 134, no. 7, pp. 2004–2013, 2008.

[33] H. Yamamoto, K. Ishihara, Y. Takeda, W. Koizumi, and T. Ichikawa, "Changes in the mucus barrier during cisplatin-induced intestinal mucositis in rats," *BioMed Research International*, vol. 2013, Article ID 276186, 8 pages, 2013.

[34] Q. Cheng, X. Feng, Q. Meng et al., "[6]-Gingerol ameliorates cisplatin-induced pica by regulating the TPH/MAO-A/SERT/5-HT/5-HT3 receptor system in rats," *Drug Design Development and Therapy.*, vol. 14, pp. 4085–4099, 2020.

[35] Y. Q. Li, Y. H. Yang, G. L. Zhang et al., "RNA-Seq reveals inflammatory mechanisms of Xiao-Ban-Xia-Tang decoction to ameliorate cisplatin-induced emesis in a rat pica model," *Biomedicine & Pharmacotherapy*, vol. 131, p. 110699, 2020.

[36] Y. Yamashiro and S. Nagata, "Beneficial microbes for premature infants, and children with malignancy undergoing chemotherapy," *Beneficial Microbes*, vol. 1, no. 4, pp. 357–365, 2010.

[37] P. F. Justino, L. F. Melo, A. F. Nogueira et al., "Regulatory role of Lactobacillus acidophilus on inflammation and gastric dysmotility in intestinal mucositis induced by 5-fluorouracil in mice," *Cancer Chemotherapy and Pharmacology*, vol. 75, no. 3, pp. 559–567, 2015.

[38] C. Y. Yeung, J. S. Chiang Chiau, M. L. Cheng et al., "Modulations of probiotics on gut microbiota in a 5-fluorouracil-induced mouse model of mucositis," *Journal of Gastroenterology and Hepatology*, vol. 35, no. 5, pp. 806–814, 2020.

[39] K. L. Tooley, G. S. Howarth, K. A. Lymn, A. Lawrence, and R. N. Butler, "Oral ingestion of streptococcus thermophilus diminishes severity of small intestinal mucositis in methotrexate treated rats," *Cancer Biology & Therapy*, vol. 5, no. 6, pp. 593–600, 2006.

[40] S. Zhong, Z. Zhou, Y. Liang et al., "Targeting strategies for chemotherapy-induced peripheral neuropathy: does gut microbiota play a role?," *Critical Reviews in Microbiology*, vol. 45, no. 4, pp. 369–393, 2019.

[41] B. A. de Koning, M. van der Sluis, D. J. Lindenbergh-Kortleve et al., "Methotrexate-induced mucositis in mucin 2-deficient mice," *Journal of Cellular Physiology*, vol. 210, no. 1, pp. 144–152, 2007.

[42] M. Verburg, I. B. Renes, H. P. Meijer et al., "Selective sparing of goblet cells and Paneth cells in the intestine of methotrexate-treated rats," *The American Journal of Physiology-Gastrointestinal and Liver Physiology*, vol. 279, no. 5, pp. G1037–G1047, 2000.

[43] M. Verburg, I. B. Renes, D. J. Van Nispen et al., "Specific responses in rat small intestinal epithelial mRNA expression and protein levels during chemotherapeutic damage and regeneration," *Journal of Histochemistry & Cytochemistry*, vol. 50, no. 11, pp. 1525–1536, 2002.

[44] L. E. Willemsen, M. A. Koetsier, S. J. van Deventer, and E. A. van Tol, "Short chain fatty acids stimulate epithelial mucin 2 expression through differential effects on prostaglandin E(1) and E(2) production by intestinal myofibroblasts," *Gut*, vol. 52, no. 10, pp. 1442–1447, 2003.

[45] S. Kato, N. Hamouda, Y. Kano et al., "Probiotic Bifidobacterium bifidum G9-1 attenuates 5-fluorouracil-induced intestinal

mucositis in mice via suppression of dysbiosis-related secondary inflammatory responses," *Clinical and Experimental Pharmacology & Physiology*, vol. 44, no. 10, pp. 1017–1025, 2017.

[46] J. N. Hu, J. Y. Yang, S. Jiang et al., "*Panax quinquefolium* saponins protect against cisplatin evoked intestinal injury via ROS-mediated multiple mechanisms," *Phytomedicine*, vol. 82, p. 153446, 2021.

[47] A. Amaretti, M. di Nunzio, A. Pompei, S. Raimondi, M. Rossi, and A. Bordoni, "Antioxidant properties of potentially probiotic bacteria: in vitro and in vivo activities," *Applied Microbiology and Biotechnology*, vol. 97, no. 2, pp. 809–817, 2013.

[48] G. M. Mawe and J. M. Hoffman, "Serotonin signalling in the gut–functions, dysfunctions and therapeutic targets," *Nature Reviews Gastroenterology & Hepatology*, vol. 10, no. 8, pp. 473–486, 2013.

[49] S. Matthes and M. Bader, "Peripheral serotonin synthesis as a new drug target," *Trends in Pharmacological Sciences*, vol. 39, no. 6, pp. 560–572, 2018.

[50] M. D. Gershon and J. Tack, "The serotonin signaling system: from basic understanding to drug development for functional GI disorders," *Gastroenterology*, vol. 132, no. 1, pp. 397–414, 2007.

[51] C. Ju, N. Hamaue, T. Machida et al., "Anti-inflammatory drugs ameliorate opposite enzymatic changes in ileal 5-hydroxytryptamine metabolism in the delayed phase after cisplatin administration to rats," *The European Journal of Pharmacology*, vol. 589, no. 1-3, pp. 281–287, 2008.

[52] H. Wang, M. S. Geier, and G. S. Howarth, "Prebiotics: a potential treatment strategy for the chemotherapy-damaged gut?," *Critical Reviews in Food Science and Nutrition*, vol. 56, no. 6, pp. 946–956, 2016.

[53] E. Montassier, T. Gastinne, P. Vangay et al., "Chemotherapy-driven dysbiosis in the intestinal microbiome," *Alimentary Pharmacology & Therapeutics*, vol. 42, no. 5, pp. 515–528, 2015.

[54] X. B. Lin, L. A. Dieleman, A. Ketabi et al., "Irinotecan (CPT-11) chemotherapy alters intestinal microbiota in tumour bearing rats," *PLoS One*, vol. 7, no. 7, article e39764, 2012.

[55] M. Fijlstra, M. Ferdous, A. M. Koning, E. H. Rings, H. J. Harmsen, and W. J. Tissing, "Substantial decreases in the number and diversity of microbiota during chemotherapy-induced gastrointestinal mucositis in a rat model," *Supportive Care in Cancer*, vol. 23, no. 6, pp. 1513–1522, 2015.

[56] J. Tong, X. Zhang, Y. Fan et al., "Changes of intestinal microbiota in ovarian cancer patients treated with surgery and chemotherapy," *Cancer Management and Research*, vol. Volume 12, pp. 8125–8135, 2020.

[57] Y. M. Kim, A. M. Snijders, C. J. Brislawn et al., "Light-stress influences the composition of the murine gut microbiome, memory function, and plasma metabolome," *Frontiers in Molecular Biosciences*, vol. 6, p. 108, 2019.

[58] A. T. Mudd, K. Berding, M. Wang, S. M. Donovan, and R. N. Dilger, "Serum cortisol mediates the relationship between fecal Ruminococcus and brain N-acetylaspartate in the young pig," *Gut Microbes*, vol. 8, no. 6, pp. 589–600, 2017.

[59] C. S. Reigstad, C. E. Salmonson, J. F. R. III et al., "Gut microbes promote colonic serotonin production through an effect of short-chain fatty acids on enterochromaffin cells," *The FASEB Journal*, vol. 29, no. 4, pp. 1395–1403, 2015.

[60] K. Atarashi, T. Tanoue, T. Shima et al., "Induction of colonic regulatory T cells by indigenous Clostridium species," *Science*, vol. 331, no. 6015, pp. 337–341, 2011.

[61] A. L. Hamilton, M. A. Kamm, S. C. Ng, and M. Morrison, "Proteus spp. as putative gastrointestinal pathogens," *Clinical Microbiology Reviews*, vol. 31, no. 3, article e00085, 2018.

[62] A. D. Kostic, D. Gevers, C. S. Pedamallu et al., "Genomic analysis identifies association of Fusobacterium with colorectal carcinoma," *Genome Research*, vol. 22, no. 2, pp. 292–298, 2012.

[63] M. Ying, Q. Yu, B. Zheng et al., "Cultured *Cordyceps sinensis* polysaccharides modulate intestinal mucosal immunity and gut microbiota in cyclophosphamide-treated mice," *Carbohydrate Polymers*, vol. 235, p. 115957, 2020.

[64] A. Gregorieff, Y. Liu, M. R. Inanlou, Y. Khomchuk, and J. L. Wrana, "Yap-dependent reprogramming of Lgr5(+) stem cells drives intestinal regeneration and cancer," *Nature*, vol. 526, no. 7575, pp. 715–718, 2015.

[65] Q. Hou, L. Ye, H. Liu et al., "*Lactobacillus* accelerates ISCs regeneration to protect the integrity of intestinal mucosa through activation of STAT3 signaling pathway induced by LPLs secretion of IL-22," *Cell Death & Differentiation*, vol. 25, no. 9, pp. 1657–1670, 2018.

[66] Y. Touchefeu, E. Montassier, K. Nieman et al., "Systematic review: the role of the gut microbiota in chemotherapy- or radiation-induced gastrointestinal mucositis - current evidence and potential clinical applications," *Alimentary Pharmacology & Therapeutics*, vol. 40, no. 5, pp. 409–421, 2014.

[67] H. Li, P. Wang, L. Huang, P. Li, and D. Zhang, "Effects of regulating gut microbiota on the serotonin metabolism in the chronic unpredictable mild stress rat model," *Journal of Neurogastroenterology and Motility*, vol. 31, no. 10, article e13677, 2019.

[68] G. Riezzo, G. Chimienti, A. Orlando, B. D'Attoma, C. Clemente, and F. Russo, "Effects of long-term administration of Lactobacillus reuteri DSM-17938 on circulating levels of 5-HT and BDNF in adults with functional constipation," *Beneficial Microbes*, vol. 10, no. 2, pp. 137–147, 2019.

[69] H. Yang, H. J. Kim, E. J. Hong, B. J. Pyun, B. S. Ko, and H. W. Lee, "Antidepressant effect of Tetragonia tetragonoides (Pall.) Kuntze extract on serotonin turnover," *Evidence-based Complementary and Alternative Medicine*, vol. 2019, Article ID 7312842, 7 pages, 2019.

[70] T. Matsuki, K. Watanabe, J. Fujimoto, T. Takada, and R. Tanaka, "Use of 16S rRNA gene-targeted group-specific primers for real-time PCR analysis of predominant bacteria in human feces," *Applied and Environmental Microbiology*, vol. 70, no. 12, pp. 7220–7228, 2004.

[71] M. I. Van Dyke and A. J. McCarthy, "Molecular biological detection and characterization of Clostridium populations in municipal landfill sites," *Applied and Environmental Microbiology*, vol. 68, no. 4, pp. 2049–2053, 2002.

[72] H. Yang, R. Cai, Z. Kong et al., "Teasaponin ameliorates murine colitis by regulating gut microbiota and suppressing the immune system response," *Frontiers of Medicine*, vol. 7, p. 584369, 2020.

[73] M. Mulder, D. Radjabzadeh, J. C. Kiefte-de Jong et al., "Long-term effects of antimicrobial drugs on the composition of the human gut microbiota," *Gut Microbes*, vol. 12, no. 1, article 1795492, 2020.

Hindawi
Journal of Immunology Research
Volume 2021, Article ID 7377685, 7 pages
https://doi.org/10.1155/2021/7377685

*Research Article*

# Correlation between Hyperalgesia and Upregulation of TNF-$\alpha$ and IL-1$\beta$ in Aqueous Humor and Blood in Second Eye Phacoemulsification: Clinical and Experimental Investigation

**Ruibo Yang**,[1] **Chang Liu**,[1] **Di Yu**,[1] **Lechong Ma**,[2] **Yan Zhang**,[1] **and Shaozhen Zhao**[1]

[1]*Tianjin Key Laboratory of Retinal Functions and Diseases, Tianjin Branch of National Clinical Research Center for Ocular Disease, Eye Institute and School of Optometry, Tianjin Medical University Eye Hospital, No. 251, FuKang Road, Nankai District, Tianjin 30384, China*
[2]*University of California Santa Cruz, 1156 High Street, Santa Cruz, CA 95064, USA*

Correspondence should be addressed to Yan Zhang; yanzhang9927@163.com and Shaozhen Zhao; zhaosz1997@sina.com

Received 16 June 2021; Revised 12 July 2021; Accepted 3 August 2021; Published 26 August 2021

Academic Editor: Lifei Wang



The aim of this study was to explore the correlation between intraoperative hyperalgesia of the second eye and the dynamic changes of tumor necrosis factor (TNF)-$\alpha$ and interleukin (IL)-1$\beta$ levels in aqueous humor (AH) of the second eye and whole blood after the first eye cataract surgery. A rabbit model of monocular phacoemulsification was established by administration of 0.3% levofloxacin. Whole blood and AH samples from non-surgical eyes in the experimental group (n =25) and second eye in the blank control group (n =15) were obtained and corneal sensitivity was examined after surgery (1, 3, 7, 14, and 21 days postoperatively). TNF-$\alpha$ and IL-1$\beta$ levels in AH and TNF-$\alpha$ mRNA and IL-1$\beta$ mRNA levels in whole blood were measured. In a clinical study, 30 patients who underwent bilateral phacoemulsification within 1 month were divided into six groups in accordance with the operation intervals (1, 3, 7, 10, 14, and 21days). TNF-$\alpha$ and IL-1$\beta$ levels in AH were measured at the beginning of surgery and intraoperative pain was assessed immediately after surgery. Corneal sensitivity ($F=244.910$, $P<0.05$), TNF-$\alpha$ and IL-1$\beta$ levels in AH ($F=184.200$, 82.900, $P<0.05$) of non-surgical eyes and in whole blood ($F=272.800$, 193.530, $P<0.05$) in the experimental group were significantly higher than the baseline levels after phacoemulsification. In the clinical study, NRS scores of second eye surgery were higher than those of the first eye($P=0.0025$) and 19 (63.3%) patients reported more pain during the second eye surgery. TNF-$\alpha$ and IL-1$\beta$ concentrations in AH of the second eye were significantly higher than those of the first eye ($F=123.60$, $P<0.05$; $F=59.60$, $P<0.05$). In conclusion, within 1 month after the first eye phacoemulsification, higher pain sensitivity (hyperalgesia) exists in the second eye, which may be related to dynamic changes in TNF-$\alpha$, IL-1$\beta$ levels in AH or whole blood.

## 1. Introduction

Phacoemulsification and intraocular lens implantation surgery under topical anesthesia is widely performed worldwide. Because of the inconsistent visual function of both eyes, many patients undergo second eye surgery a short time after the first eye surgery [1–3]. However, more eye pain and discomfort are commonly reported by patients with bilateral cataract during the second eye surgery, despite the same surgeon, anesthetic mode, procedure, and even operation circumstances, which is considered to be related to hyperalgesia [4–9]. Intraoperative hyperalgesia may reduce a patient's willingness to cooperate, increase surgical difficulty and risk, and reduce patient postoperative satisfaction. However, the mechanism by which the pain experience is stronger during the second eye phacoemulsification is not entirely understood.

In recent years, it has been verified that tumor necrosis factor (TNF)-$\alpha$ and interleukin (IL)-1$\beta$ not only induce

leukocyte activation, chemotaxis, and inflammatory responses, but also act as neuromodulators in the nervous system to enhance the sensitivity of sensory neurons, which will lead to neuropathic pain that includes hyperalgesia [10, 11].

In the current study, TNF-$\alpha$, IL-1$\beta$ levels in aqueous humor (AH) of non-surgical eyes and TNF-$\alpha$ and IL-1$\beta$ mRNA levels in blood were measured and compared with baseline levels in the phacoemulsification rabbit model. Subsequently, the TNF-$\alpha$, IL-1$\beta$ levels in AH were further verified between the first and second eye in clinical phacoemulsification as well as pain assessment between both eyes. The purpose of this study was to explore the correlation between intraoperative hyperalgesia of the second eye and dynamic changes of TNF-$\alpha$ and IL-1$\beta$ levels in AH of the second eye and in whole blood after the first eye cataract surgery. To our knowledge, studies on this subject remain insufficient. Therefore, the findings from the current study may broaden our understanding on the mechanism of hyperalgesia in the second eye surgery.

## 2. Materials and Methods

*2.1. Experimental Study.* Animal experiments were approved by the Ethics Committee for Animal Studies at Tianjin Medical Eye Hospital and were in accordance with the Guide for the Care and Use of Laboratory Animals of the National Institutes of Health.

*2.1.1. Animals and Grouping.* Forty New Zealand white rabbits (2 – 2.5 kg; Beijing Vital River Laboratory Animal Technology Co., Ltd. Beijing, China) were randomly divided into two experimental groups (group A, n = 25, monocular phacoemulsification) and blank control group (group B, n = 15). The rabbits were equally divided into five subgroups: postoperative 1, 3, 7, 14, and 21 day groups. Surgical eyes in group A and first eyes in group B were selected in accordance with a random number table. All animals were maintained under a 12-h light–dark cycle at 25 ± 1°C with 55% –75% humidity.

*2.1.2. Experimental Procedure.* Rabbits were administered 0.3% levofloxacin (Santen Pharmaceutical Co, Ltd, Tokyo, Japan) four times daily for 3 days prior to the surgery. AH samples were obtained through a lateral corneal incision at the beginning of surgery in surgical eyes of group A. Surgeries were performed by the same surgeon under topical anesthesia using 0.5% proparacaine combined with intramuscular anesthetization (Xylazin Hydrochloride Injection, 0.3 mL▪kg$^{-1}$, ShengDa Animal Medicine Company, DunHua, China). Topical Tobradex eye drops (0.3% tobramycin and 0.1% dexamethasone; Alcon Laboratories, Inc, Fort Worth, TX, USA) were administered four times a day postoperatively and tapered off for 1 month after surgery. Conjunctival congestion, corneal edema, and reaction in the anterior chamber were recorded preoperatively as well as postoperatively on days 1, 3, 7, 14, and 21. To measure baseline levels of TNF-$\alpha$ and IL-1$\beta$ in AH and whole blood, AH of surgical eyes in group A and first eyes in group B and blood in both groups were obtained preoperatively and corneal sensitivity of non-surgical eyes in group A and second eyes in group B was assessed preoperatively. Only the surgical eyes (25 eyes) in group A were subjected to unilateral phacoemulsification uneventfully. Corneal sensitivity and inflammation cytokines (TNF-$\alpha$ and IL-1$\beta$) in AH of non-surgical eyes in group A and the second eyes in group, and TNF-$\alpha$ and IL-1$\beta$ levels in whole blood of both groups were analyzed on days 1, 3, 7, 14, and 21 postoperatively. AH and blood samples from both groups were obtained and stored at −80°C. TNF-$\alpha$ and IL-1$\beta$ levels in AH were measured by ELISAs. TNF-$\alpha$ and IL-1$\beta$ mRNA levels in blood were measured by real-time quantitative PCR (qPCR).

*2.1.3. Measurement of Corneal Sensitivity.* Corneal sensitivity was measured using a Cochet–Bonnet esthesiometer (Luneau Ophthalmologie, Chartres, France) after the rabbits were in good mental state and placed in a quiet indoor environment. Blinking and escape behavior were considered a positive response. Measurement by the esthesiometer started with a length of 60 mm nylon filament that was gently applied perpendicularly to the central surface of the cornea. The length of filament was shortened in steps of 5 mm until a positive response of the rabbit was observed, which was considered a positive result of corneal sensitivity. Corneal sensitivity is presented as the length of the nylon filament (mm); as the length of the nylon filament increases, the corneal sensitivity increases. The same procedure was repeated three times with a 30-minute interval; then, an average value of corneal sensitivity was taken.

*2.1.4. Quantitative Real-Time Polymerase Chain Reaction.* Expression of TNF-$\alpha$ and IL-1$\beta$ mRNA in blood was measured by qPCR using the ABI 7900 System (CA, USA). The primer sequences were as follows. GAPDH: sense, 5′-GATGCTGGTGCCGAGTAC-3′ and antisense 5′-GCTG AGATGATGACCCTT-3′; TNF-$\alpha$: sense, 5′-ATGAGC ACTGAAAGCAT-3′ and antisense 5′-GAGGGCTGATT AGAGAG-3′; IL-1$\beta$: sense, 5′-GTCTTCCTAAAGCAAG CC-3′ and antisense 5′- GGGGTGTCACAATCTGTT-3′.

*2.1.5. Enzyme-Linked Immunosorbent Assays.* Total proteins were extracted from AH of rabbits. The concentrations of TNF-$\alpha$ and IL-1$\beta$ in AH were measured by Enzyme-linked immunosorbent assay (ELISA) kits (TNF-$\alpha$, Bio-Swamp Company, Wuhan, China; IL-1$\beta$, Bio-Swamp Company) in accordance with the manufacturer's procedures. Absorbance was read with a microplate reader (Tecan, Switzerland) at 450 nm at a reference wavelength of 570 nm. The procedure was the same for clinical samples.

*2.2. Clinical Study.* This prospective, single-blind, randomized study was conducted at Tianjin Medical University Eye Hospital between June 2018 and October 2019, which was approved by the institutional ethics committee of Tianjin Medical University Eye Hospital and followed the principles of the Declaration of Helsinki. Written informed consent was obtained from all patients. The study was registered at http://www.clinicaltrials.gov/ (registration number: ChiCTR1900023178).

*2.2.1. Inclusion and Exclusion Criteria.* Thirty age-related cataract patients with bilateral similar grades of lens opacity and willingness to undergo bilateral cataract surgery within 1 month were recruited. Patients with any of the following were excluded: history of previous ocular surgery and other ocular diseases, and systemic diseases such as diabetes mellitus, immune diseases, and other concomitant diseases. Patients who had systemic medication history, such as sedatives, analgesics, anti-inflammatory drugs or steroids, were also excluded.

*2.2.2. Surgical Procedures and Grouping.* The first eye was selected randomly. The timing of the second eye surgery was determined in accordance with the recovery of the first eye and the patients' willingness. The patients were divided into six groups in accordance with the interval between the two eye surgeries (1, 3, 7, 10, 14, and 21 days). Bilateral surgeries were performed by the same surgeon sequentially and uneventfully within 1 month with the same anesthetic mode (topical anesthesia, proparacaine 0.5%; Alcon, Inc, Fort Worth, TX, USA), procedures, phaco machine (Infiniti, Alcon Laboratories, Incorporated, Fort Worth, TX, USA), and operation circumstances. All surgeries were carried out between 9 and 12 am. Neither oral nor intravenous sedatives or analgesics were administered. AH samples were collected from separate single eye operations, which were obtained at the beginning of the phacoemulsification through an assisted corneal incision by inserting a 27 G needle into the anterior chamber. The samples were stored at −80°C until cytokine analysis.

*2.2.3. Assessment of Subjective Symptoms.* Intraoperative pain was assessed at the end of the surgery using a numerical rating scale (NRS) from 0 to 10 where 0, 1 – 3, 4 – 6, and 7 – 10 indicated no pain, mild pain, moderate pain, and severe pain, respectively. After second eye surgery patients were asked if they felt more pain during the first or second surgery, assumed answers were "I had more pain during the first surgery", "I had more pain during the second surgery", "I experienced the same pain during both surgeries", and "I forgot".

*2.2.4. Analysis of Cytokines in AH.* The procedure was the same as described for the experimental study.

*2.3. Statistical Analysis.* SPSS software version 20.0 (IBM-SPSS, Armonk, NY, USA) was used for all statistical analyses. The chi-squared test was used to determine subjective experience and NRS scores were subjected to the Wilcoxon matched-pairs signed-ranks test in the clinical study. Repeated measures analysis of variance (ANOVA) and a post-hoc LSD test were used to assess the differences in corneal sensitivity as well as TNF-$\alpha$ and IL-1$\beta$ in blood and AH. $P < 0.05$ was considered statistically significant.

## 3. Results

*3.1. Experimental Study*

*3.1.1. Corneal Sensitivity.* The corneal sensitivity of non-surgical eyes in group A was significantly higher than baseline at 1, 3, 7, and 14 days after surgery ($F = 244.910$, $P < 0.05$), particularly on day 7 after surgery (58.53 ± 0.38 mm), which decreased gradually and reached the baseline level at 21 days after surgery (49.60 ± 0.68 mm). There was no statistical difference between the various time points in group B ($F = 1.344$, $P > 0.05$). (Figure 1).

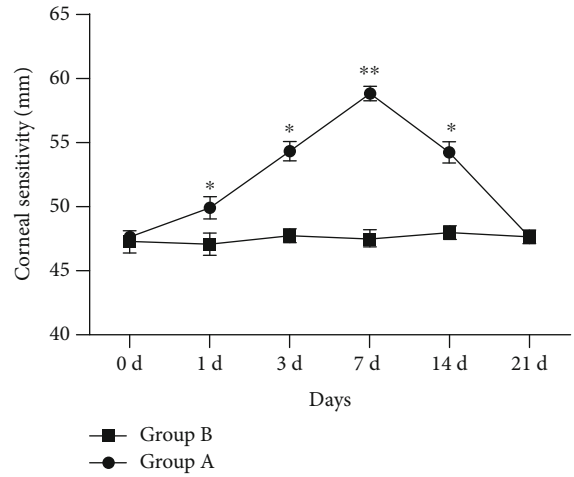


Figure 1: Corneal sensitivity of non-surgical eyes in group A and second-eye in group B. Group A: monocular phacoemulsification; Group B: blank control.

*3.1.2. Expressions of TNF-α and IL-1β mRNA in Blood.* The expression of TNF-$\alpha$ and IL-1$\beta$ mRNA in blood was significantly higher at 1, 3, 7, and 14 days after surgery compared with baseline levels in the experimental groups ($F = 272.800$, $P < 0.05$; $F = 193.530$, $P < 0.05$), which reached a peak on day 7 postoperatively (TNF-$\alpha$ mRNA: 14.95 ± 0.89; IL-1$\beta$ mRNA: 7.56 ± 0.46) and then decreased gradually. TNF-$\alpha$ and IL-1$\beta$ mRNAs returned to baseline levels on day 21 after surgery (TNF-$\alpha$ mRNA: 1.29 ± 0.27; IL-1$\beta$ mRNA: 1.03 ± 0.20). Statistical analysis demonstrated no significant differences in the second eye at various time points in the blank control group ($F = 1.612$, $P > 0.05$; $F = 0.626$, $P > 0.05$). (Figure 2).

*3.1.3. Concentrations of TNF-α and IL-1β in AH.* The concentrations of TNF-$\alpha$ and IL-1$\beta$ in AH of the non-surgical eye were significantly higher at 1, 3, 7, and 14 days after surgery than baseline levels in experimental groups ($F = 184.200$, $P < 0.05$; $F = 82.900$, $P < 0.05$), which reached a peak on day 7 postoperatively (TNF-$\alpha$: 162.34 ± 5.71 pg/ml; IL-1$\beta$: 16.68 ± 0.74 pg/ml) and then decreased gradually. TNF-$\alpha$ and IL-1$\beta$ concentrations returned to baseline levels on day 21 after surgery (TNF-$\alpha$: 58.37 ± 9.46 pg/ml; IL-1$\beta$: 9.64 ± 0.75 pg/ml). Statistical analysis demonstrated no significant differences in the second eye at the virous time points in the blank control group ($F = 1.140$, $P > 0.05$; $F = 0.820$, $P > 0.05$) (Figure 3).

*3.2. Clinical Study.* A total of 30 patients (60 eyes) were enrolled in the study. The average age was 72.2 ± 8.4 years. The average duration of first eye surgery was 11.5 ± 1.9 min

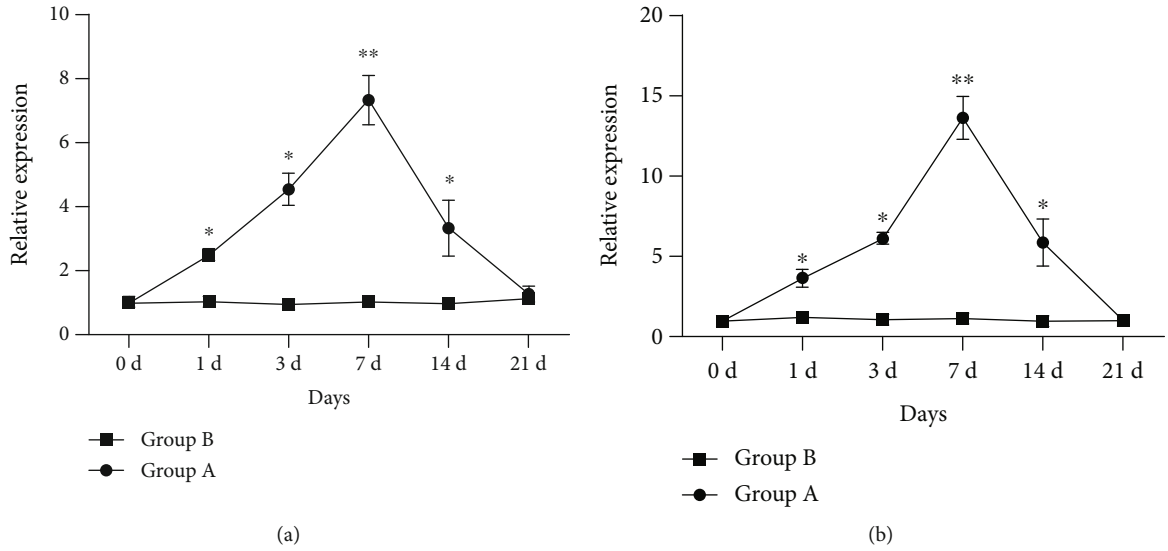


Figure 2: Expression of TNF-$\alpha$ mRNA and IL-1$\beta$ mRNAs in blood of experimental rabbits. Group A: monocular phacoemulsification; Group B: blank control.

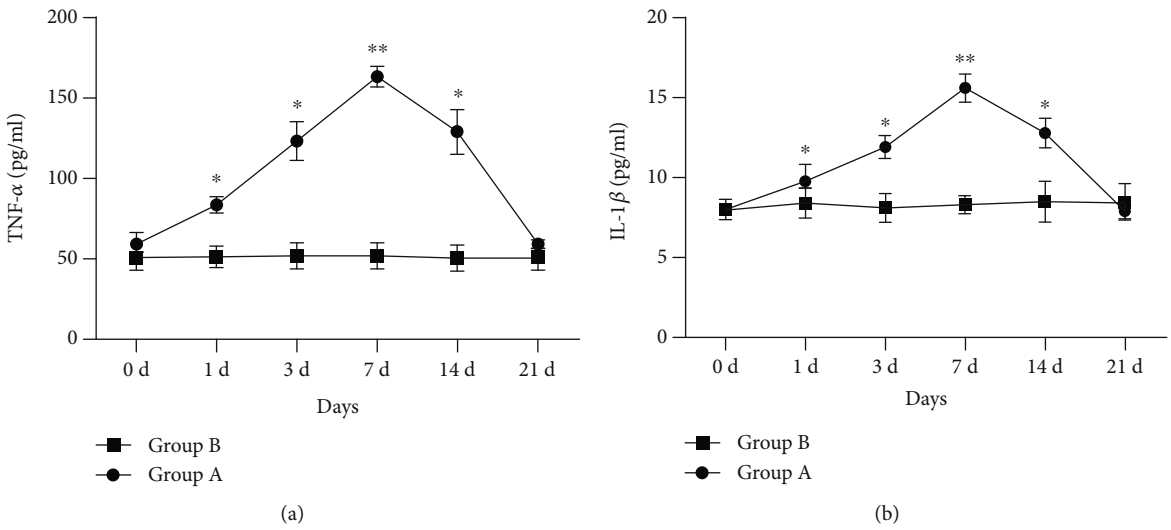


Figure 3: Concentrations of TNF-$\alpha$ and IL-1$\beta$ in AH of experimental rabbits. Group A: monocular phacoemulsification; Group B: blank control.

Table 1: Comparison of NRS scores during bilateral cataract surgery.

| | 1d | 3d | 7d | 10d | 14d | 21d | Total |
|---|---|---|---|---|---|---|---|
| 1st-eye surgery | 1.90 ± 0.74 | 2.10 ± 0.65 | 2.10 ± 0.74 | 1.90 ± 0.42 | 1.40 ± 0.55 | 2.10 ± 0.58 | 1.88 ± 0.12 |
| 2nd-eye surgery | 2.10 ± 0.65 | 2.30 ± 0.57 | 2.50 ± 0.50 | 2.30 ± 0.45 | 2.50 ± 0.50 | 2.50 ± 0.44 | 2.37 ± 0.10 |
| *P* value | 0.178 | 0.178 | 0.099 | 0.016* | 0.051 | 0.099 | 0.0025* |

Note: 1d, 3d, 7d, 10d, 14d, 21d represent the intervals between bilateral surgeries.

in the first eye, and 11.7 ± 1.8 min in second eye surgery. No significant difference was found between them (P >0.05).

*3.2.1. Evaluation of Eye Pain.* Using the NRS, eye pain was significantly higher in patients who underwent second eye surgery (t =4.568, p =0.0025), particularly when the interval between the two surgeries was 10 days (p =0.016) (Table 1). By comparing pain experiences between bilateral surgeries, 19 (63.3%) patients reported more pain during the second eye surgery, seven (23.3%) patients reported the same pain during the two surgeries, four (13.3%) patients reported more pain during the first eye surgery ($\chi^2 = 9.586$, P >0.05) (Figure 4).

*3.2.2. Concentrations of TNF-α and IL-1β in AH.* The concentrations of TNF-α and IL-1β were significantly higher in the second eye than the first eye in each group ($F = 123.60$, $P < 0.05$; $F = 59.60$, $P < 0.05$). Particularly at the 10-day interval, TNF-α and IL-1β levels ($6.88 \pm 0.71$ and $0.79 \pm 0.14$ pg/ml, respectively) were the highest in the second eye (Figure 5).

## 4. Discussion

Under topical anesthesia, it is common that patients complain more about pain and discomfort during the second eye cataract surgery [4–9, 12–14]. Intraoperative pain may increase surgical difficulty and risk, and cause patient postoperative dissatisfaction. However, the mechanism is not yet fully understood.

Previous studies have found that cataract patients are likely to have more pain during second eye surgery, which may be associated with decreased preoperative anxiety or the amnestic effects of intravenous sedation [5, 12]. Ursea et al. proposed the following three possible mechanisms. A psychological effect would be that patients are not as well prepared for the degree of wakefulness and magnitude of sensation that they will experience during the procedure in the second eye operation. A physiological response would be that sympathetic irritation sensitizes the second eye to painful stimuli after first eye surgery. A pharmacological explanation would be that the response to analgesic and sedative medications will decreased during the second operation because of previous exposure to those same medications during the first surgical procedure, which might result in drug tolerance [15]. Nevertheless, most previous studies have mainly focused on subjective psychological mechanisms and none of these hypotheses have been proven to date. Additionally, in some studies, local anesthetic decreases together with intravenous sedation and analgesics are applied commonly during the surgery [8, 12], and eye pain has been assessed using only self-report questionnaires [4, 5, 7, 12], which would result in bias in the pain experience of patients. We speculate that higher sensitivity to pain is not merely a psychological phenomenon and the involvement of physiopathological mechanism is possible.

Neuropathic pain is associated with chronic inflammation. The mechanism that underlies the role of TNF-α in the development of inflammatory hyperalgesia has been studied extensively, but mainly its role in the release of proinflammatory cytokines [16–19]. In general, TNF-α and IL-1β are weekly expressed in central and peripheral nervous systems, but cytokine expression upregulates after injury. TNF-α stimulates cascade release of other proinflammatory cytokines, such as IL-1β, interleukin-6 and interleukin-8, which triggers the release of the final inflammatory mediator prostaglandin E2 and sympathetic amines that directly sensitize nociceptors [20]. In models of neuropathic pain, these cytokines activate in the nervous tissue consistent with the emergence of painful behavior, namely allodynia and hyperalgesia. Verri Jr et al. [21] suggested that Granulocyte-colony stimulating factor-induced hyperalgesia might be mediated by the peripheral production of pronociceptive cytokines

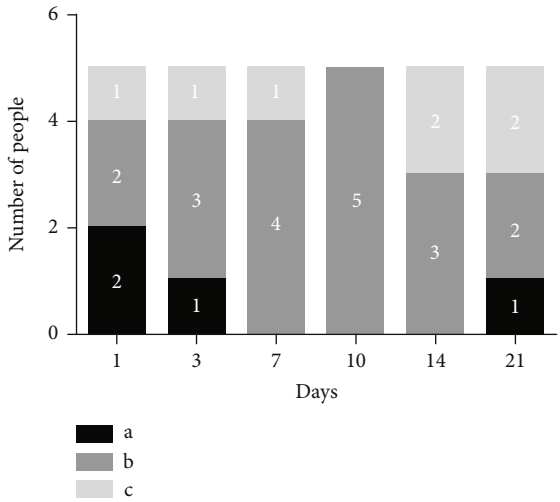


Figure 4: Comparison of pain experiences between bilateral surgeries. The days represent the various groups in accordance with the interval between bilateral surgeries. a: "I had more pain during the first surgery"; b: "I had more pain during the second surgery"; c: "I experienced the same pain during both surgeries". The bar graph shows the number of people who chose the option.

TNF-α and IL-1β. Cataract surgery is an invasive procedure that breaks the blood-aqueous humor barrier, which leads to an intraocular inflammatory response in the surgical eye. A previous study revealed that AH of the second eye has higher levels of TGF-β2 and MCP-1 during bilateral sequential cataract surgery [22–24, 25]. CCI is produced by loose ligation of the sciatic nerve in rats and the paw withdrawal threshold to mechanical stimulation is used to evaluate pain threshold changes. We indirectly evaluated changes in eye pain perception by measuring corneal sensitivity in rabbits by observing eye blinks and escape behaviors after mechanical stimulation. The results showed that the changes of corneal sensitivity in rabbits coincided with changes of TNF-α and IL-1β levels in AH and blood, which implies that intraoperative hyperalgesia is associated with the relative high levels of TNF-α and IL-1β in the second eye AH and whole blood after first eye cataract surgery. The high levels of TNF-α and IL-1β in AH and blood will probably lead to sensitization of the sensory branches of the trigeminal nerve, which will in turn lead to hyperalgesia of the eye. Therefore, we speculate that the increased sensitivity to pain in the second eye after the first cataract surgery is not just a simple psychological response, but a complex pathophysiological mechanism.

In this study, the increased sensitivity to pain in the second eye was manifested consistently in both experimental and clinical studies, which was particularly obvious during the early postoperative period (in 2 weeks after the first eye surgery). This finding suggests that the second eye cataract surgery should be scheduled more reasonably to avoid or reduce patient discomfort and complaints. In addition to visual function, patient comfort is a crucial part of the treatment experience. Nonsteroidal anti-inflammatory drugs or analgesics may be an appropriate choice for individuals

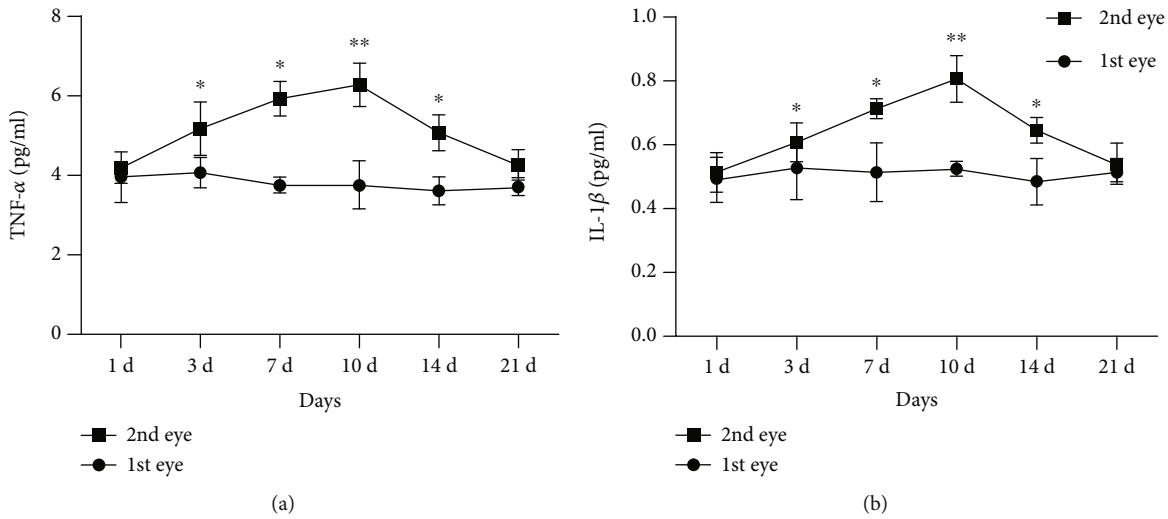


Figure 5: Concentrations of TNF-$\alpha$ and IL-1$\beta$ in AH of both eyes during bilateral cataract surgery.

who need a second eye operation within 1 month, especially within 7–10 days of the first eye surgery.

The current study had some unavoidable limitations that need to be considered. The expression of cytokines in whole blood samples of patients was not detected because such invasive practices would inflict additional pain on the patients. Because of the amount of AH samples, we could not evaluate more cytokines related to pain perception and inflammation.

## 5. Conclusions

In conclusion, within 1 month after the first eye phacoemulsification, higher pain sensitivity (hyperalgesia) exists in the second eye, which may be related to dynamic changes of TNF-$\alpha$, IL-1$\beta$ levels in AH and blood. The increased inflammatory cytokines levels in AH of the second eye or non-surgical eye and blood may be induced by the first eye surgical trauma. However, further studies should be conducted to verify the regulatory pathways responsible for the increased levels of TNF-$\alpha$ and IL-1$\beta$ in body fluids and the higher corneal sensitivity and intraoperative hyperalgesia of the second eye.

## Data Availability

The datasets used in this study are available from the corresponding author on resonable request.

## Conflicts of Interest

The authors declare that they have no conflicts of interest.

## Authors' Contributions

Ruibo Yang and Chang Liu contributed equally to this work. Ruibo Yang and Chang Liu are co-first authors.

## Acknowledgments

The research was funded by the Science & Technology Development Fund of Tianjin Education Commission for Higher Education (20140128), Tianjin Clinical Key Discipline (Specialty) Construction Project (TJLCZDXKM002), Tianjin Binhai New Area Key Science and Technology Project Supported by Key Health Commission (2019BWKZ008), General Project of Tianjin Natural Science Foundation (19JCYBJC25700).

## References

[1] P. N. Rosen, R. M. Kaplan, and K. David, "Measuring outcomes of cataract surgery using the quality of well-being scale and VF-14 visual function index," *Journal of Cataract and Refractive Surgery*, vol. 31, no. 2, pp. 369–378, 2005.

[2] J. Colin, S. El Kebir, E. Eydoux, T. Hoang-Xuan, P. Rozot, and M. Weiser, "Assessment of patient satisfaction with outcomes of and ophthalmic care for cataract surgery," *Journal of Cataract and Refractive Surgery*, vol. 36, no. 8, pp. 1373–1379, 2010.

[3] V. K. Gothwal, T. A. Wright, E. L. Lamoureux, J. Khadka, C. McAlinden, and K. Pesudovs, "Improvements in visual ability with first-eye, second-eye, and bilateral cataract surgery measured with the visual symptoms and quality of life questionnaire," *Journal of Cataract and Refractive Surgery*, vol. 37, no. 7, pp. 1208–1216, 2011.

[4] A. Bardocci, F. Ciucci, G. Lofoco, S. Perdicaro, and A. Lischetti, "Pain during second eye cataract surgery under topical anesthesia: an intraindividual study," *Graefe's Archive for Clinical and Experimental Ophthalmology*, vol. 249, no. 10, pp. 1511–1514, 2011.

[5] L. Jiang, K. Zhang, W. He, X. Zhu, P. Zhou, and Y. Lu, "Perceived pain during cataract surgery with topical anesthesia: a comparison between first-eye and second-eye surgery," *Journal of Ophthalmology*, vol. 2015, Article ID 383456, 6 pages, 2015.

[6] K. Kowalczuk, M. Cybulski, Ł. Cybulski, and E. Krajewska-Kułak, "Pain perception and acceptance of illness in patients

undergoing phacoemulsification cataract surgery under drip anesthesia," *Journal of Clinical Medicine*, vol. 8, no. 10, p. 1575, 2019.

[7] F. A. Adatia, M. Munro, I. Jivraj, A. Ajani, and R. Braga-Mele, "Documenting the subjective patient experience of first versus second cataract surgery," *Journal of Cataract and Refractive Surgery*, vol. 41, no. 1, pp. 116–121, 2015.

[8] N. S. Sharma, J. L. Ooi, E. C. Figueira et al., "Patient perceptions of second eye clear corneal cataract surgery using assisted topical anaesthesia," *Eye (London, England)*, vol. 22, no. 4, pp. 547–550, 2008.

[9] C. Shi, J. Yuan, and B. Zee, "Pain perception of the first eye versus the second eye during phacoemulsification under local anesthesia for patients going through cataract surgery: a systematic review and Meta-analysis," *Journal of Ophthalmology*, vol. 2019, Article ID 4106893, 8 pages, 2019.

[10] J. Li, G. H. Wei, H. Huang et al., "Nerve injury-related autoimmunity activation leads to chronic inflammation and chronic neuropathic pain," *Anesthesiology*, vol. 118, no. 2, pp. 416–429, 2013.

[11] K. Seno, S. Sase, A. Ozeki et al., "Advanced glycation end products regulate interleukin-1$\beta$ production in human placenta," *The Journal of Reproduction and Development*, vol. 63, no. 4, pp. 401–408, 2017.

[12] R. Ursea, M. T. Feng, M. Zhou, V. Lien, and R. Loeb, "Pain perception in sequential cataract surgery: comparison of first and second procedures," *Journal of Cataract and Refractive Surgery*, vol. 37, no. 6, pp. 1009–1014, 2011.

[13] S. Akkaya, Y. B. Özkurt, S. Aksoy, and H. K. Kökçen, "Differences in pain experience and cooperation between consecutive surgeries in patients undergoing phacoemulsification," *International Ophthalmology*, vol. 37, no. 3, pp. 545–552, 2017.

[14] A. Hari-Kovacs, P. Lovas, A. Facsko, and I. D. Crate, "Is second eye phacoemulsification really more painful?," *Wiener Klinische Wochenschrift*, vol. 124, no. 15-16, pp. 516–519, 2012.

[15] A. Bardocci, "Second-eye pain in cataract surgery," *Journal of Cataract and Refractive Surgery*, vol. 38, no. 9, p. 1705, 2012.

[16] P. Sacerdote, S. Franchi, S. Moretti et al., "Cytokine modulation is necessary for efficacious treatment of experimental neuropathic pain," *Journal of Neuroimmune Pharmacology*, vol. 8, no. 1, pp. 202–211, 2013.

[17] S. F. de Magalhães, L. P. Manzo, F. M. de Faria et al., "Inflammatory pain in peripheral tissue depends on the activation of the TNF-$\alpha$ type 1 receptor in the primary afferent neuron," *The European Journal of Neuroscience*, vol. 53, no. 2, pp. 376–389, 2021.

[18] N. T. Fiore and P. J. Austin, "Are the emergence of affective disturbances in neuropathic pain states contingent on supraspinal neuroinflammation?," *Brain, Behavior, and Immunity*, vol. 56, pp. 397–411, 2016.

[19] K. Okamoto, D. P. Martin, J. D. Schmelzer, Y. Mitsui, and P. A. Low, "Pro- and anti-inflammatory cytokine gene expression in rat sciatic nerve chronic constriction injury model of neuropathic pain," *Experimental Neurology*, vol. 169, no. 2, pp. 386–391, 2001.

[20] L. Wang, Z. Zhang, D. D. Koch, Y. Jia, W. Cao, and S. Zhang, "Anterior chamber interleukin 1$\beta$, interleukin 6 and prostaglandin E2in patients undergoing femtosecond laser-assisted cataract surgery," *The British Journal of Ophthalmology*, vol. 100, no. 4, pp. 579–582, 2016.

[21] T. T. Carvalho, S. M. Borghi, F. A. Pinho-Ribeiro et al., "Granulocyte-colony stimulating factor (G-CSF)-induced mechanical hyperalgesia in mice: role for peripheral TNF$\alpha$, IL-1$\beta$ and IL-10," *European Journal of Pharmacology*, vol. 749, pp. 62–72, 2015.

[22] X. J. Zhu, D. Wolff, K. K. Zhang et al., "Molecular inflammation in the contralateral eye after cataract surgery in the first eye," *Investigative Ophthalmology & Visual Science*, vol. 56, no. 9, pp. 5566–5573, 2015.

[23] Y. Chen, Y. Zhang, K. Sun, and H. Yan, "Higher TGF-$\beta$2 level in the aqueous humor of the second eye versus the first eye in the course of sequential cataract surgery," *Ocular Immunology and Inflammation*, vol. 28, no. 3, pp. 439–445, 2020.

[24] Y. Zhang, Y. Du, Y. Jiang, X. Zhu, and Y. Lu, "Effects of Pranoprofen on aqueous humor monocyte Chemoattractant Protein-1 level and pain relief during second-eye cataract surgery," *Frontiers in Pharmacology*, vol. 9, p. 783, 2018.

[25] L. W. Chu, K. I. Cheng, J. Y. Chen et al., "Loganin prevents chronic constriction injury-provoked neuropathic pain by reducing TNF-$\alpha$/IL-1$\beta$-mediated NF-$\kappa$B activation and Schwann cell demyelination," *Phytomedicine*, vol. 67, p. 153166, 2020.

Hindawi
Journal of Immunology Research
Volume 2021, Article ID 5123823, 14 pages
https://doi.org/10.1155/2021/5123823

*Research Article*

# Diabetic Bone Marrow Cell Injection Accelerated Acute Pancreatitis Progression

**Xiao-Min Luo,[1] Cen Yan,[1] Yue-Jie Zhang,[1] Ling-Jia Meng,[1] Guo-Tao Lu,[2] Ji-Ming Yin,[3] and Ying-Mei Feng[1]**

[1]*Department of Science and Technology, Beijing Youan Hospital, Capital Medical University, Beijing 100069, China*
[2]*Pancreatic Center, Department of Gastroenterology, Affiliated Hospital of Yangzhou University, Yangzhou University, Yangzhou 225099, China*
[3]*Beijing Hepatology Institute, Beijing 100069, China*

Correspondence should be addressed to Ying-Mei Feng; yingmeif13@sina.com

Received 10 June 2021; Accepted 6 August 2021; Published 25 August 2021

Academic Editor: Lifei Wang



Acute pancreatitis (AP) is one of the leading causes of hospital admission, 20% of which could progress to the severe type with extensive acinar cell necrosis. Clinical studies have reported that diabetes is an independent risk factor of the incidence of AP and is associated with higher severity than nondiabetic subjects. However, how diabetes participates in AP progression is not well defined. To investigate this question, wild-type (wt) and diabetic db/db mice at the age of 16 weeks were used in the study. AP was induced in wt recipients by 10 injections of 50 $\mu$g/kg caerulein with a 1 h interval. One hour after the last caerulein injection, bone marrow cells (BMC) isolated from wt and db/db mice were injected intraperitoneally into the recipients ($1 \times 10^7$ cells/recipient). The recipients with no BMC injection served as controls. Thirteen hours after BMC injection, serum lipase activity was 1.8- and 1.3-folds higher in mice that received db/db BMC, compared with those with no injection and wt BMC injection, respectively ($p \leq 0.02$ for both). By H&E staining, the overall severity score was 14.7 for no cell injection and 16.6 for wt BMC injection and increased to 22.6 for db/db BMC injection ($p \leq 0.002$ for both). In particular, mice with db/db BMC injection developed more acinar cell necrosis and vacuolization than the other groups ($p \leq 0.03$ for both). When sections were stained with an antibody against myeloperoxidase (MPO), the density of MPO+ cells in pancreatitis was 1.9- and 1.6-folds higher than wt BMC and no BMC injection groups, separately ($p \leq 0.02$ for both). Quantified by ELISA, db/db BMC produced more IL-6, GM-CSF, and IL-10 compared with wt BMC ($p \leq 0.04$ for all). In conclusion, BMC of db/db mice produced more inflammatory cytokines. In response to acinar cell injury, diabetic BMC aggravated the inflammation cascade and acinar cell injury, leading to the progression of acute pancreatitis.

## 1. Introduction

Diabetes is a common disease worldwide. According to the recent report, the number of diabetic patients was estimated at 415 million in 2015 and might be projected to be 642 million by 2040 [1]. Type 2 diabetes mellitus (T2DM) accounted for more than 90% among diabetic patients, which is featured as insulin resistance in peripheral organs and insufficient insulin production by dysfunctional pancreatic $\beta$ cells [1]. In a meta-analysis involving 698,782 T2DM patients, the hazard ratio was 2.00 (95% CI, 1.83-2.19) for coronary heart disease, 2.27 (95% CI, 1.95-2.65) for ischemic stroke, and 1.73 (95% CI, 1.51-1.98) for other vascular diseases, respectively, compared with nondiabetic subjects [2].

Apart from vascular complications described above, acute pancreatitis (AP) occurs more frequently in diabetic patients than nondiabetic ones [3, 4]. In a prospective study ($n = 547{,}554$), the adjusted hazard ratio of having acute pancreatitis was 1.53 (95% CI, 1.49-1.58) for diabetic patients after 8 years of follow-up. Moreover, the presence of diabetes was associated with a 1.46-fold increased risk of severe AP compared with nondiabetic ones [3]. Likewise, a meta-analysis of 354,880 patients revealed that the risk of having AP was 1.55 (95% CI, 1.27-1.90) for diabetic patients

compared with nondiabetic subjects. Furthermore, the risk of getting intensive care admission and organ failure was 1.80- and 1.59-folds greater in diabetic patients than nondiabetic individuals [4]. In line with clinical findings, when challenged with caerulein injection, diabetic db/db mice developed more severe AP than wt controls [5]. Nevertheless, how diabetes potentiates AP progression is not fully known.

As a sort of aseptic inflammation, AP is manifested as inflammatory cell infiltration and acinar cell necrobiosis. In the early stage of AP, acinar cells produce tumor necrosis factor- (TNF-) $\alpha$, IL-10, and monocyte chemoattractant protein-1 (MCP-1) which promote neutrophil and subsequent monocyte infiltration into the panaceas. These inflammatory cells enhance inflammatory cytokine production such as IL-6 and TNF-$\alpha$ and produce enzymes, both of which orchestrate acinar cell autoaggression and destruction [6, 7]. In type 2 diabetic patients, the ratio of neutrophils versus lymphocytes was higher than that of nondiabetic participants and subjects with impaired glucose tolerance [8]. Given that circulating white blood cells originated from bone marrow cells (BMC), we hypothesized that BMC from diabetic mice could contribute to AP progression than nondiabetic BMC. To investigate this question, wt mice received caerulein injections to induce AP. One hour after the last caerulein injection, BMC of C57BL/6 and age-matched diabetic db/db mice were isolated and injected intraperitoneally into the recipients to assess disease severity.

## 2. Method

*2.1. Animals.* Male C57BL/6 and db/db mice with a C57BL/6 background at the age of 8 weeks were purchased from Beijing Vital River Laboratory Animal Technology Co., Ltd. and GemPharmatech Co., Ltd., respectively. They were housed under specific pathogen-free (SPF) conditions in an air-conditioned animal facility at 24°C on a twelve-hour light/dark cycle. Animals had free access to water and standard laboratory chow ad libitum. The study protocol was approved by the experimental animal ethics committee of Capital Medical University.

As reported, db/db mice developed diabetes at the age of 14-16 weeks [9, 10]. Therefore, lipid and glucose levels, COFO data, and BMC isolation were performed in db/db mice and wt controls at the age of 16 weeks.

*2.2. Mouse Model of AP.* The murine model of AP could be induced by a series of intraperitoneal injections of caerulein [5, 11, 12]. After being fasted overnight, C57BL/6 mice at the age of 8 weeks received intraperitoneal injection of 50 $\mu$g/kg caerulein. A total of 10 injections with a one-hour interval were performed to establish AP. To obtain consistent induction of AP, a fresh solution of caerulein at the final concentration was prepared prior to each experiment (Cae, AnaSpec, Inc., San Jose, CA, USA).

*2.3. BMC Isolation and Cell Injection Experiment.* BMC were isolated from C57BL/6 and db/db mice at the age of 16 weeks. Briefly, tibias and femurs were dissected free. After making a small cut on one edge of the bone, the bone cavity was flushed with 5 mL sterile PBS. After, BMC were spun down by centrifugation at 700 g for 5 min. One hour after the $10^{th}$ caerulein injection of caerulein, BMC were administered intraperitoneally to the recipients with induced AP ($1 \times 10^7$ cells/recipient). The recipients were randomly assigned to 3 groups: no BMC injection ($n = 6$), C57BL/6 BMC injection ($n = 15$), and db/db BMC injection ($n = 15$). In parallel, the mice injected with saline alone served as pancreatitis-free controls.

Blood samples were obtained from the tail vein of the mice at 0, 12, and 24 hours before and after the first caerulein injection. The animals were anesthetized by intraperitoneal injection of sodium pentobarbital (50 mg/kg) and sacrificed 24 hours after the first caerulein injection. The pancreatic tissues were dissected, fixed in 4% paraformaldehyde in PBS, and embedded in paraffin for histological analysis.

*2.4. ELISA.* Plasma levels of total cholesterol and triglyceride were determined according to the protocols (Nanjing Jiancheng Corp., Nanjing, China). Fasting blood glucose levels were measured based on the manufacturer's instruction (Roche). Plasma insulin levels were measured by ELISA (Cat. No. CEA448Mu, Cloud-Clone Corp., Wuhan, China). Plasma lipase and amylase activities were measured by commercial kits and quantified by a Tecan Safire microplate reader (mouse amylase assay kit: ab102523, Abcam, Cambridge, MA; lipase kits: Nanjing Jiancheng Corp., Nanjing, China).

*2.5. Cytokine Measurement.* Proteins were extracted from BMC of wt and db/db mice using the RIPA buffer (MILLIPLEX® MAP, USA). Protein concentration was quantified by the BCA method (Thermo Scientific, USA). After calculation, 25 $\mu$g proteins of each sample were loaded to a 96-well plate and mixed with mouse high-sensitivity T cell antibody-immobilized premixed magnetic beads. A panel of cytokines was determined by MILLIPLEX® MAP following the manual instruction. The cytokines included granulocyte-macrophage colony-stimulating factor (GM-CSF), interferon-gamma (IFN-$\gamma$), interleukin-1alpha (IL-1$\alpha$), interleukin-1beta (IL-1$\beta$), interleukin-2 (IL-2), interleukin-4 (IL-4), interleukin-5 (IL-5), interleukin-6 (IL-6), interleukin-7 (IL-7), interleukin-10 (IL-10), interleukin-12 (IL-12) (p70), interleukin-13 (IL-13), interleukin-17A (IL-17A), keratinocyte chemokine (KC), lipopolysaccharide-induced CXC chemokine (LIX), MCP-1, macrophage inflammatory protein-2 (MIP-2), and TNF-$\alpha$.

*2.6. Histology.* The paraffin-embedded pancreatic tissue was cut into sections with a 4 $\mu$m thickness. After hematoxylin and eosin staining, the severity in the aspects of inflammation, acinar cell necrosis and vacuolization, and edema of the pancreas was scored to compute the total severity. Pathological changes were assessed by two investigators blinded to the experiments. At least six visual fields of each mouse were studied.

*2.7. Immunohistochemistry.* Paraffin-embedded sections were deparaffinized and incubated with a 0.3% $H_2O_2$ solution to remove endogenous peroxidase activity. Antigen retrieval was performed with a citrate buffer (pH 6.8). Goat serum

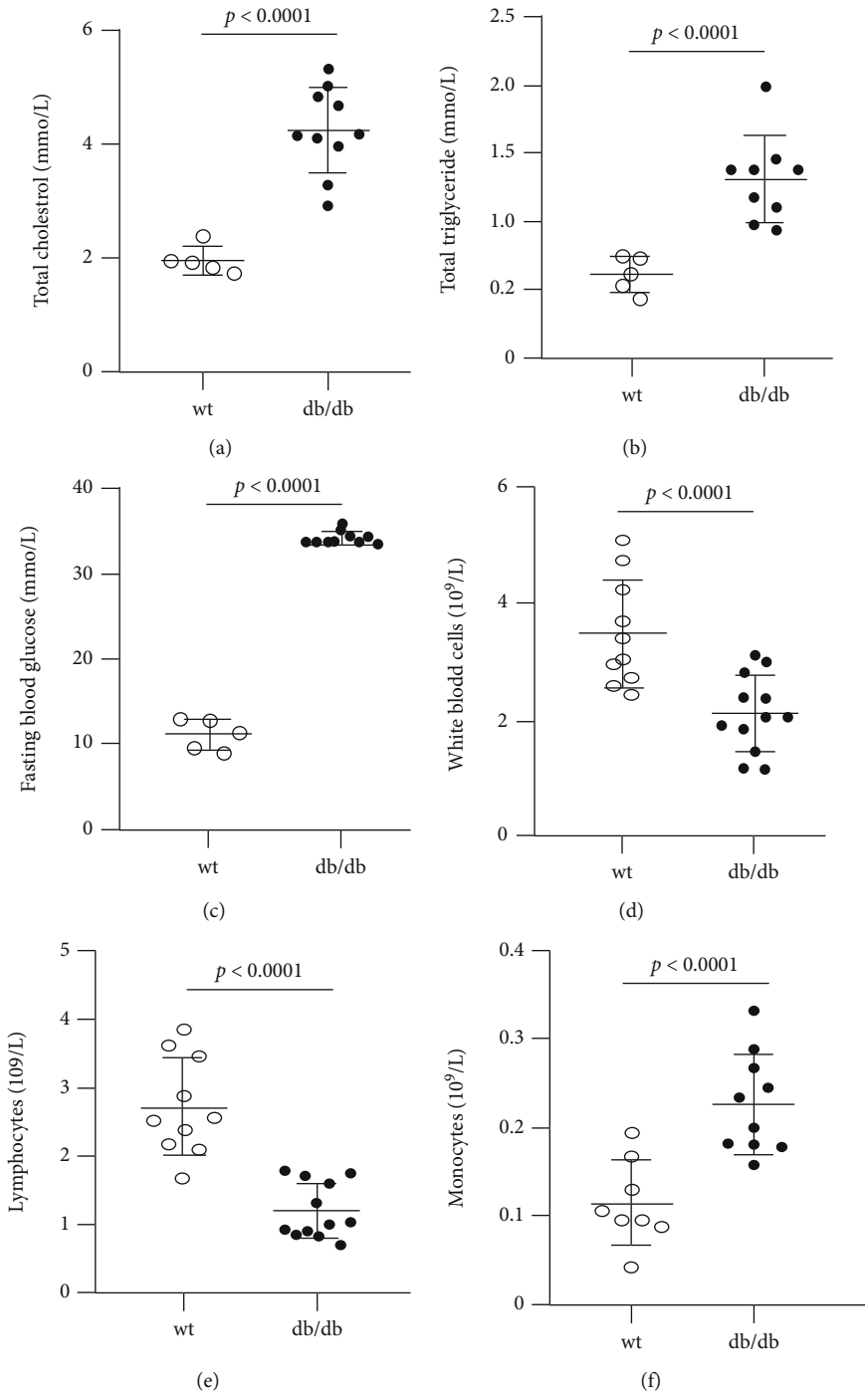


Figure 1: Continued.

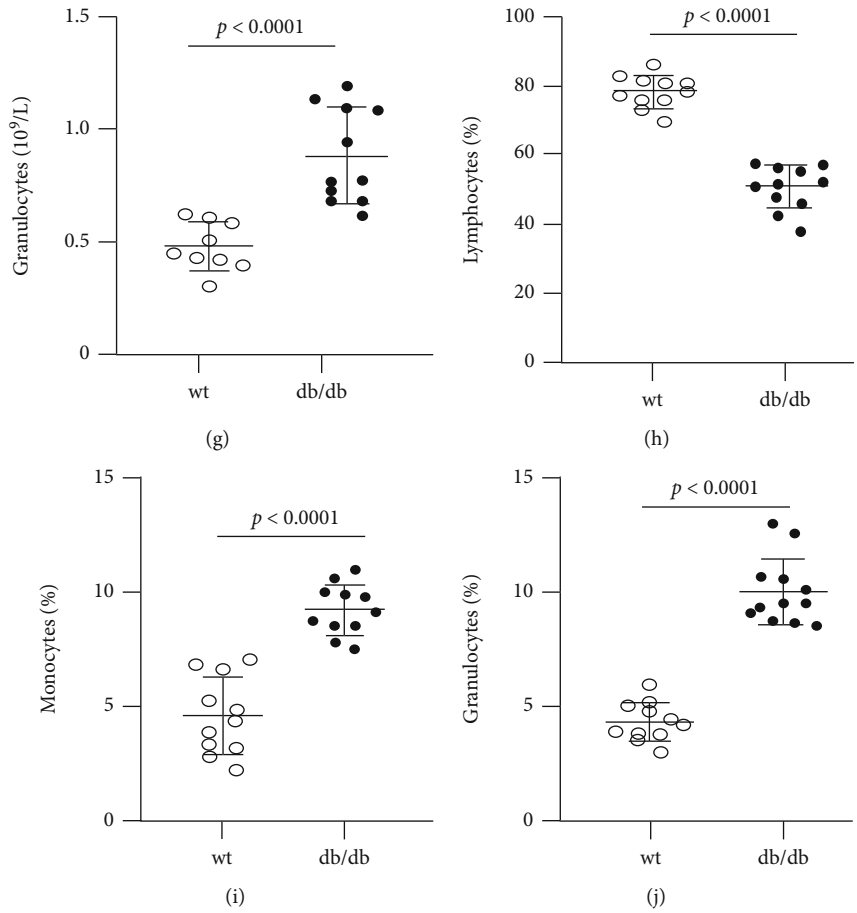


Figure 1: Phenotypic characteristics of wt and db/db mice at the age of 16 weeks. (a) Fasting plasma cholesterol, $n = 5\text{-}10$. (b) Fasting plasma triglyceride, $n = 5\text{-}10$. (c) Fasting blood glucose, $n = 10\text{-}12$. (d–g) White blood cell count and differential white blood cell count. (h–j) Proportion of lymphocytes, monocytes, and granulocytes among white blood cells, $n = 10\text{-}12$. wt: wild type.

Table 1: General characteristics of wild-type and db/db mice at the age of 16 weeks.

| | Wild-type mice | db/db mice | $p$ value |
|---|---|---|---|
| Number | 5-11 | 10-12 | |
| Total cholesterol (mmol/L) | 1.95 ± 0.24 | 4.24 ± 0.74 | 0.0001 |
| Total triglyceride (mmol/L) | 0.61 ± 0.13 | 1.55 ± 0.82 | 0.026 |
| Plasma glucose (mmol/L) | 11.02 ± 1.79 | 34.11 ± 0.82 | 0.0001 |
| White blood cells ($\times 10^9$/L) | 3.48 ± 0.92 | 2.09 ± 0.65 | 0.0005 |
| Lymphocytes ($\times 10^9$/L) | 2.72 ± 0.71 | 1.20 ± 0.40 | 0.0001 |
| Monocytes ($\times 10^9$/L) | 0.11 ± 0.04 | 0.22 ± 0.05 | 0.0003 |
| Granulocytes ($\times 10^9$/L) | 0.47 ± 0.10 | 0.88 ± 0.21 | 0.0001 |
| Lymphocytes (%) | 78.14 ± 4.68 | 50.69 ± 6.20 | 0.0001 |
| Monocytes (%) | 4.57 ± 1.71 | 9.26 ± 1.12 | 0.0001 |
| Granulocytes (%) | 17.27 ± 3.38 | 40.21 ± 5.88 | 0.0001 |
| Red blood cells ($\times 10^{12}$/L) | 2.92 ± 0.28 | 3.84 ± 0.23 | 0.0001 |
| Hemoglobin (gram) | 43.03 ± 4.55 | 57.90 ± 22.03 | 0.04 |
| Platelets ($\times 10^9$/L) | 785.80 ± 123.59 | 530.96 ± 129.93 | 0.0001 |
| Mean platelet volume (fL) | 12.67 ± 0.50 | 11.7 ± 1.69 | 0.07 |

Data were expressed as mean ± SD.

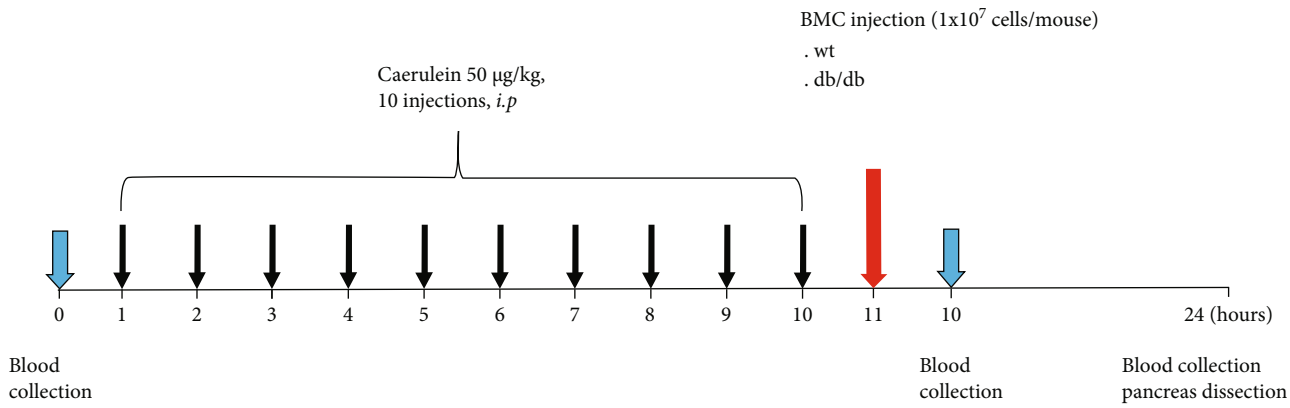


(a)

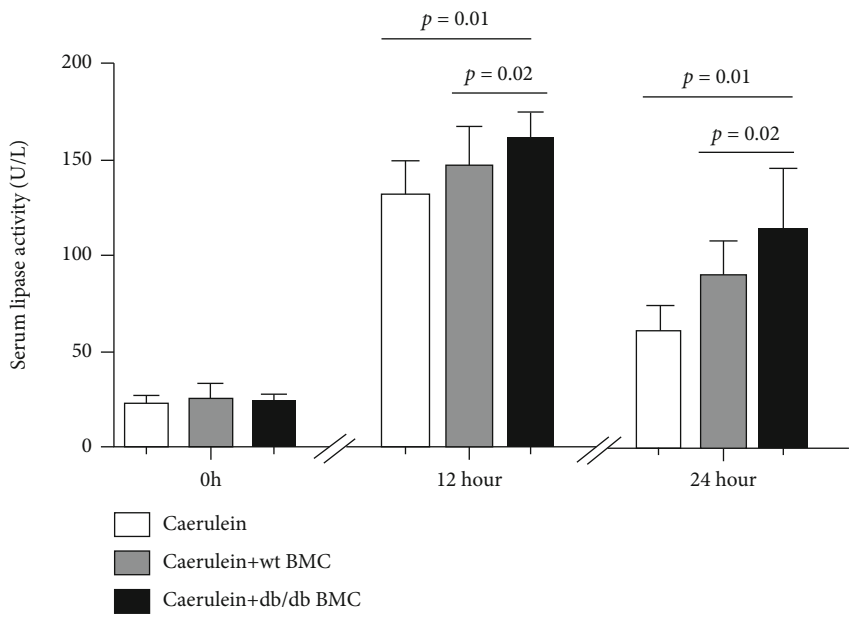


(b)

Figure 2: Continued.

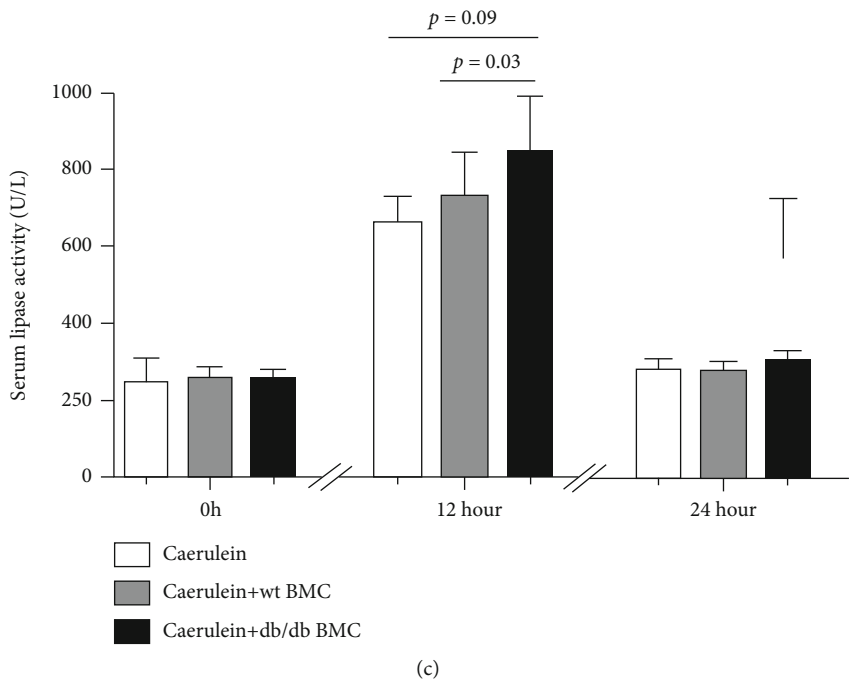


Figure 2: Biochemical analysis of AP in mice that received bone marrow cell (BMC) injection. (a) The scheme of the study design. (b, c) Serum lipase activity and serum amylase activity in mice with induced AP following BMC injection. AP was induced in wt recipients by ten caerulein injections. One hour after the last injection, BMC of wt or db/db donors were isolated and injected into mice with induced AP. AP: acute pancreatitis; wt: wild type; BMC: bone marrow cells.

was used to block nonspecific antigens. Then, paraffin sections were probed with a rabbit anti-mouse myeloperoxidase (MPO) polyclonal antibody (dilution: 1/1000; GB11224, Servicebio, Wuhan, China) or with an anti-insulin mouse monoclonal antibody (dilution: 1/500; GB13121, Servicebio, Wuhan, China). The next day, sections were incubated with a goat anti-rabbit secondary antibody or goat anti-mouse secondary antibody for 1 hour at room temperature. A diaminobenzene horseradish peroxidase color development kit was used for the color reaction. Finally, the sections were counterstained with hematoxylin and dehydrated. Sections stained only with the secondary antibody with the omission of the primary antibody served as negative controls. The staining-positive cells in the pancreas were counted using the ImageJ software. At least six visual fields of each mouse were studied. Data were expressed as MPO+ cells per microscopy field and the percentage of insulin+ cells in islets [13].

*2.8. Statistical Analysis.* Data were presented as mean ± SD. An unpaired, 2-tailed Student's test was applied to compare the means. One-way analysis of variance (ANOVA) with Dunnett's multiple comparison test was applied when there were more than two experimental groups. Significance was a two-tailed $p$ value of 0.05 or less.

## 3. Results

*3.1. Diabetic db/db Mice Were Featured as Myeloid Cell Expansion.* At the age of 16 weeks, plasma levels of cholesterol and triglyceride were 2.2- and 2.5-folds higher in db/db mice than wt controls (Figures 1(a) and 1(b)). Hyperglycemia started to appear in obese db/db mice at the age of 8 weeks and to progress following the age. By the age of 14-16 weeks, $\beta$ cell content was decreased in islets with a reduced $\beta$ cell mass and impaired insulin secretion, indicating $\beta$ cell dysfunction [9, 10]. Similar to these reports, fasting blood glucose levels were 11.02 mmol/L at wt mice but increased to 34.11 mmol/L at db/db mice (Figure 1(c)).

Compared with wt mice at 16 weeks old, the number of white blood cells and lymphocytes in the peripheral blood was 40% and 56% lower in db/db mice (white blood cells: $3.48 \pm 0.92 \times 10^9$/L vs. $2.10 \pm 0.66 \times 10^9$/L, $p = 0.01$, and $n = 11$-13; lymphocytes: $2.58 \pm 0.76 \times 10^9$/L vs. $1.32 \pm 0.53 \times 10^9$/L, $p = 0.0002$, and $n = 11$-13) (Figures 1(d) and 1(e)). The number of monocytes was comparable between two groups (monocytes: $0.16 \pm 0.08 \times 10^9$/L vs. $0.19 \pm 0.08 \times 10^9$/L, $p = 0.33$, and $n = 11$-13) (Figure 1(f)). However, granulocyte and monocyte counts were 1.8- and 2.0-folds higher in db/db mice, respectively, compared with wt controls (granulocytes: $0.48 \pm 0.11 \times 10^9$/L vs. $0.88 \pm 0.21 \times 10^9$/L, $p < 0.0001$, and $n = 11$-13; monocytes: $0.11 \pm 0.05 \times 10^9$/L vs. $0.23 \pm 0.06 \times 10^9$/L, $p = 0.0004$, and $n = 11$-13) (Figure 1(g)). Accordingly, the proportion of lymphocytes was 35% lower, but the percentage of monocytes and granulocytes was 2.0- and 2.3-folds higher in db/db mice, respectively, when compared with wt controls (lymphocytes: 78.1 ± 4.7% vs. 50.7 ± 6.2%, $p < 0.0001$; monocytes: 4.6 ± 1.7% vs. 9.3 ± 1.1%, $p < 0.0001$; and granulocytes: 17.3 ± 3.4% vs. 40.2 ± 5.9%, $p < 0.0001$) (Figures 1(h)–1(j)).

General characterization of age-matched male wt and db/db mice is summarized in Table 1.

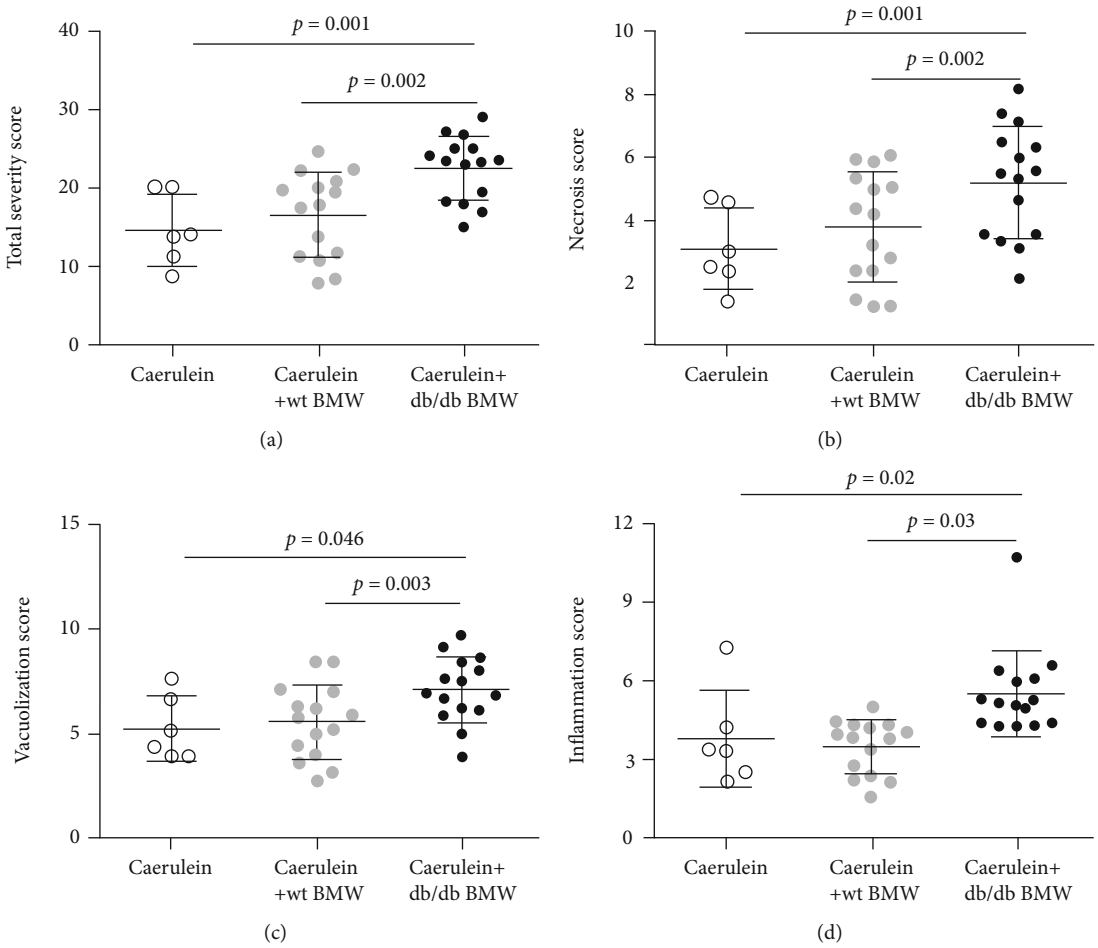


Figure 3: Continued.

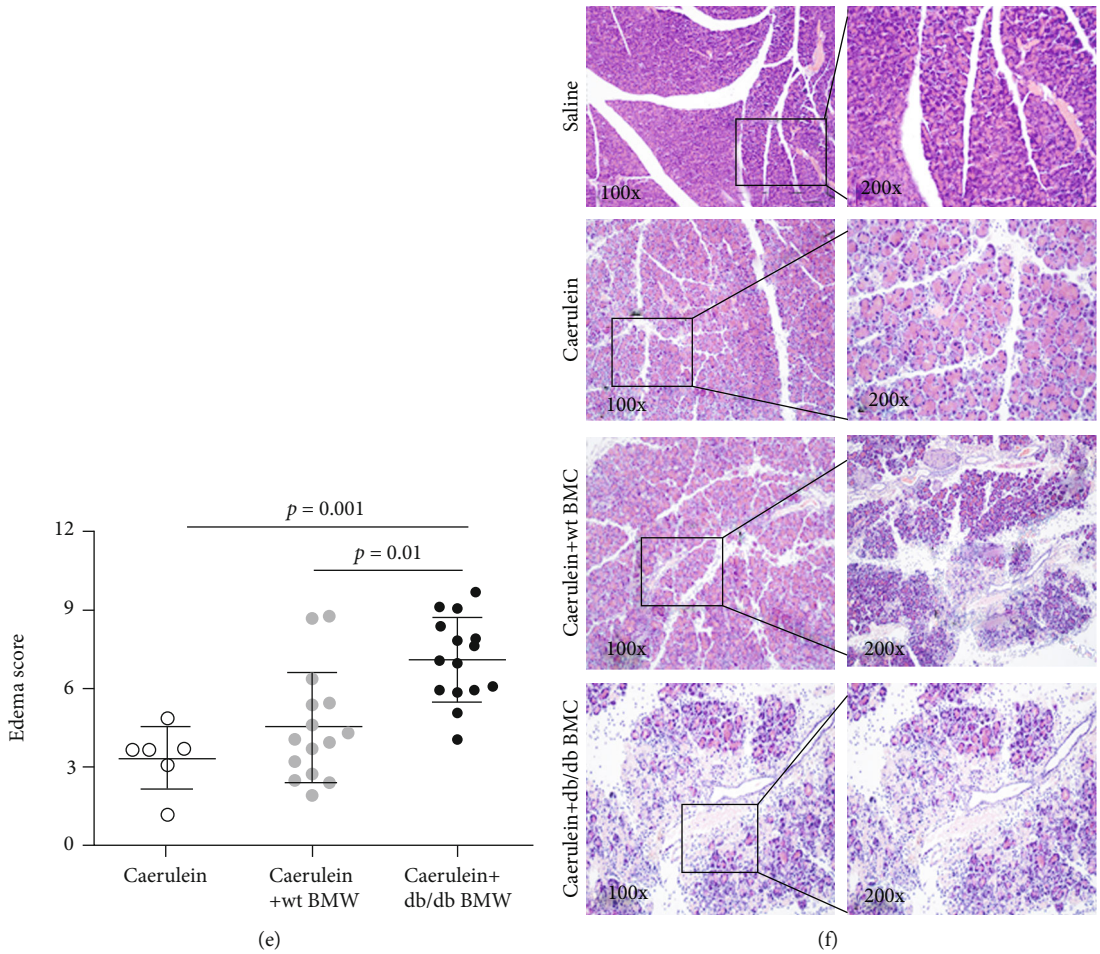


Figure 3: The effect of bone marrow cell injection on AP progression. The severity was assessed on H&E-stained sections in the aspects of acinar cell necrosis and vacuolization, inflammatory cell infiltration, and edema of the pancreas. The degree of severity was scored from 1 to 10. Total severity score (a) was the sum of necrosis (b), vacuolization (c), inflammation (d), and edema (e). $n = 6$-15. AP: acute pancreatitis.

*3.2. The Effect of BMC Injection on Serum Amyloid and Lipase Activity in Mice with Induced Acute Pancreatitis.* Previously, Gao et al. reported that db/db mice developed severe acinar damage than wt controls after caerulein injection [5]. To testify whether BMC contributed to acute pancreatitis progression, BMC were isolated from wt and db/db donors and injected peritoneally into the caerulein-injected mice. The recipients without BMC injection served as controls. The scheme of the experimental design is illustrated in Figure 2(a).

Quantified by ELISA, serum lipase activity was comparable prior to injection among three groups (no injection: 23.5 ± 3.8 U/L, $n = 3$; wt BMC: 25.4 ± 8.0 U/L, $n = 15$; and db/db BMC: 24.4 ± 4.5 U/L, $n = 15$; $p \geq 0.57$) (Figure 2(b)). Following the first injection, serum lipase levels were dramatically increased. One hour after BMC injection, serum lipase levels were increased to 132.5 U/L for the no injection group, 145.1 U/L for the wt BMC group, and 161.1 U/L for the db/db BMC group (132.5 ± 17.1 U/L vs. 145.1 ± 21.0 U/L vs. 161.1 ± 14.8 U/L, $n = 6$-15). Similar findings were observed at 13 hours after BMC injection (serum lipase levels: 62.0 ± 13.3 U/L vs. 89.6 ± 18.6 U/L vs. 113.6 ± 32.6 U/L) (Figure 2(b)).

Similar kinetics of serum amylase was detected. Compared with no BMC injection, serum amylase activity was 1.3- and 1.1-folds higher after 1 and 13 hours of db/db BMC injection (1 h: 663.3 ± 67.3 U/L vs. 845.8 ± 147.0 U/L, $n = 6$-15, and $p = 0.009$; 13 h: 279.7 ± 26.8 U/L vs. 302.7 ± 22.2 U/L, $n = 6$-15, and $p = 0.03$). By contrast, serum amylase activity was not altered between the wt BMC injection and no injection groups in the entire experiment (1 h after BMC injection: 663.3 ± 67.3 U/L vs. 735.3 ± 111.0 U/L, $n = 6$-15, and $p = 0.16$; 13 h after BMC injection: 279.7 ± 26.8 U/L vs. 282.5 ± 17.7 U/L, $n = 6$-15, and $p = 0.78$) (Figure 2(c)).

*3.3. The Effect of BMC Injection on Histological Changes in Mice with Induced Acute Pancreatitis.* As previously described [5, 14, 15], the pancreatitis damage was assessed in the aspects of inflammation as evidenced by infiltrated inflammatory cells, acinar cell vacuolization and necrosis, and edema in the pancreas. The overall total severity score was 14.7 for no injection, 16.6 for wt BMC injection, and 22.6 for db/db BMC injection ($p = 0.001$ for db/db BMC injection vs. no injection; $p = 0.002$ for db/db BMC vs. wt BMC) (Figure 3(a)). Compared with the normal pancreas,

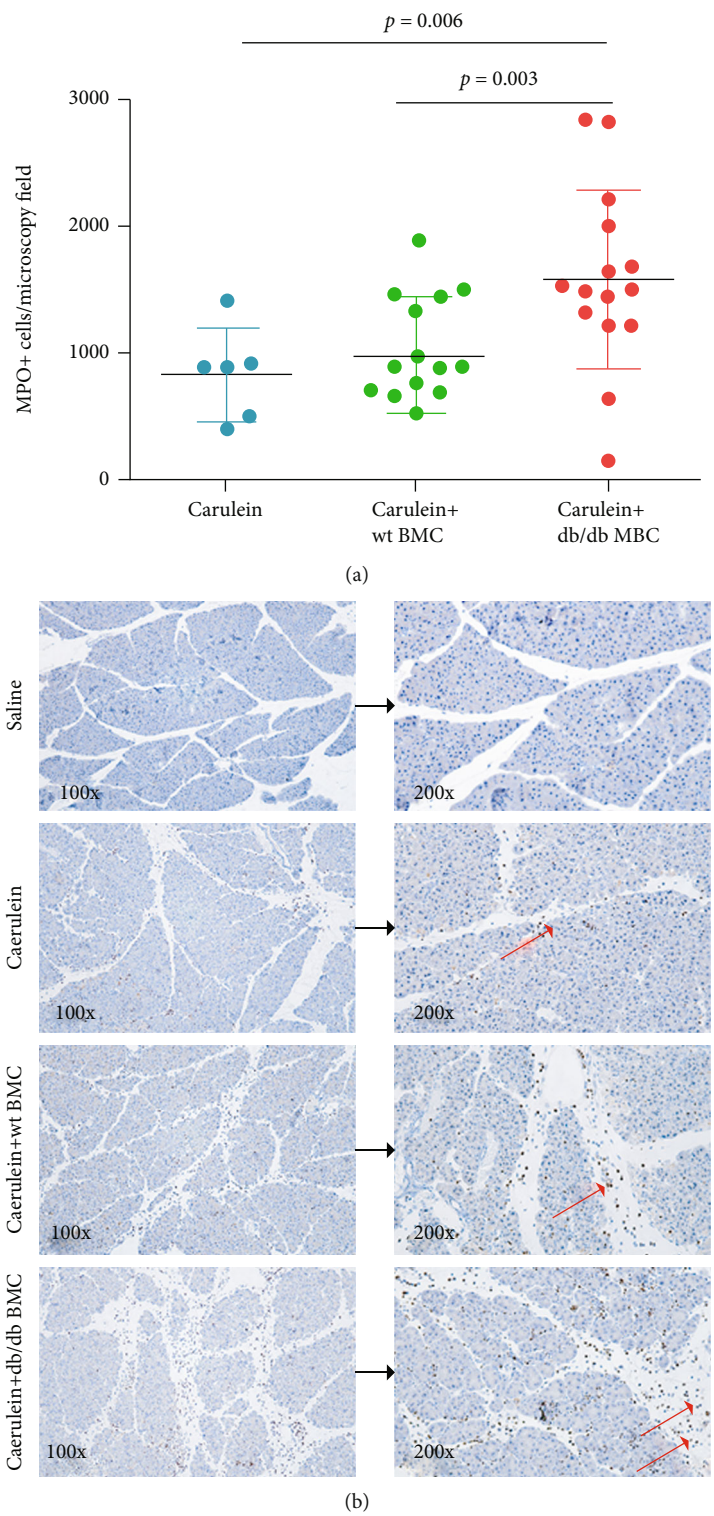


Figure 4: The effect of bone marrow cell injection on the inflammation of AP. Paraffin sections were stained with an antibody against MPO. (a) The number of MPO+ cells per microscopy field was numerated by ImageJ. (b) Representative pictures of MPO-stained sections in wt mice that received saline injection and caerulein injection without or with bone marrow cell injection. AP: acute pancreatitis; MPO: myeloperoxidase; wt: wild type.

the extent of pancreas injury induced by caerulein injection alone or with wt BMC injection was similar, both of which were presented by a low degree of edema and a small amount of infiltrated inflammatory cells and necrotic acinar cells. Compared with other groups, db/db BMC injection induced pronounced acinar cell necrosis and vacuolization, indicating the severe damage in situ (necrosis score: 3.1 ± 1.3 vs. 3.8 ± 1.8 vs. 5.2 ± 1.8, $n = 6$-15; vacuolization score: 3.8 ± 1.8 vs.

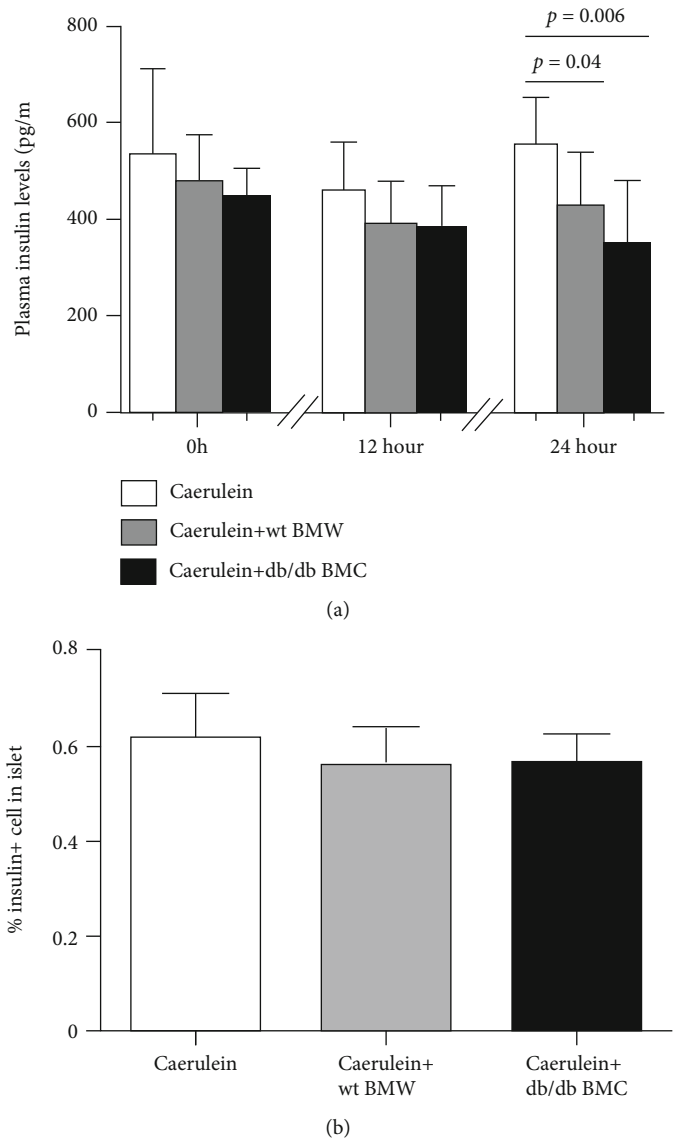


Figure 5: Continued.

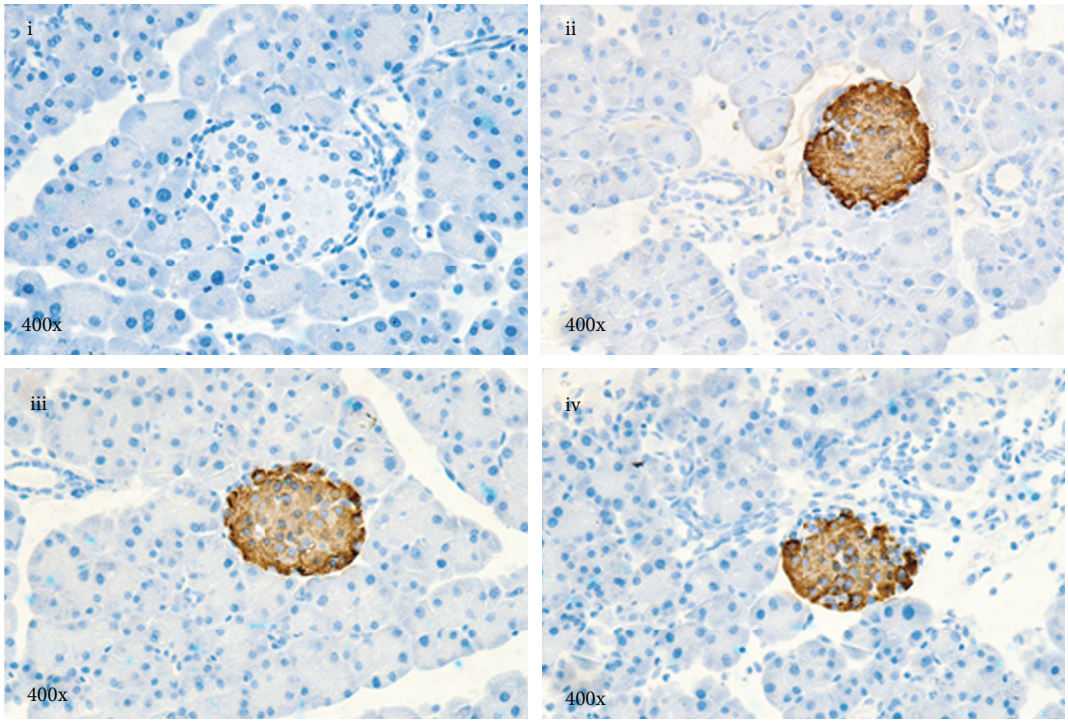


i. Negative control
ii. Caerulein
iii. Caerulein+wt BMW
iv. Caerulein+db/db BMC

(c)

Figure 5: The impact of cell injection on pancreatic $\beta$ cells. (a) Plasma insulin levels at baseline, 12 hours, and 24 hours after the first caerulein injection. $n = 6$-9. (b, c) Pancreas sections were stained with an antibody against insulin, and insulin+ cells in islets were analyzed. $n = 5$ for each group.

$3.5 \pm 1.0$ vs. $5.5 \pm 1.6$; $n = 6$-15) (Figures 3(b) and 3(c)). Accordingly, more severe inflammation and edema were observed in mice that received db/db BMC injection in comparison to the other groups (edema score: $3.3 \pm 1.2$ vs. $4.5 \pm 2.1$ vs. $7.1 \pm 1.6$; inflammation score: $5.3 \pm 1.6$ vs. $5.5 \pm 1.8$ vs. $7.1 \pm 1.6$; $n = 6$-15) (Figures 3(d) and 3(e)). The representative H&E sections are shown in Figure 3(f).

*3.4. The Effect of BMC Injection on Neutrophil Infiltration in Mice with Induced Acute Pancreatitis.* Conventionally, circulating neutrophils are the first cells homing to the injured site to participate in inflammation. To study the inflammatory status, the sections were stained with an antibody against MPO, the general marker of neutrophils. Similar to the severity score, the number of MPO+ cells per microscopy field was comparable between the no injection and wt BMC injection groups ($834.3 \pm 360.0$ cells/field vs. $984.9 \pm 448.8$ cells/field, $p = 0.47$). Nevertheless, the number of MPO+ cells was 1.9- and 1.6-folds higher in mice that received db/db BMC injection compared with wt BMC injection and no BMC injection, respectively ($p \leq 0.02$ for both) (Figure 4(a)). Moreover, MPO+ cells were 1.6-folds greater in mice injected with db/db BMC than those with wt BMC, indicating increased BMC homing to the injured pancreas ($1576.0 \pm 703.8$ cells/field vs. $984.9 \pm 448.8$ cells/field, $p = 0.01$). Representative MPO-stained sections of each group are shown in Figure 4(b).

By ELISA, plasma insulin levels were reduced in the recipients that received wt BMC and db/db BMC at sacrifice compared with those without cell injection (Figure 5(a)). Nonetheless, when pancreas sections were stained with an antibody against insulin, the percentage of $\beta$ cells in islets was comparable among the three groups ($p = 0.48$) (Figure 5(b)). Representative morphology of insulin-stained islets is shown in Figure 5(c).

Taken together, BMC of diabetic db/db mice triggered more inflammation and acinar cell damage in mice with AP. These data suggest that diabetic BMC were different from wt BMC with inherited inflammatory nature.

*3.5. Inflammatory Profile of Diabetic db/db BMC.* Finally, proteins were extracted from freshly isolated BMC to measure proinflammatory and anti-inflammatory cytokine and chemokine production. Quantified by the Bio-Plex Pro signaling assay, the intracellular levels of GM-CSF, IL-6, and IL-10 were all higher in db/db BMC compared with wt BMC (Figures 6(a)–6(c)). The cytokine and chemokine profiles of wt and db/db BMC are listed in Table 2.

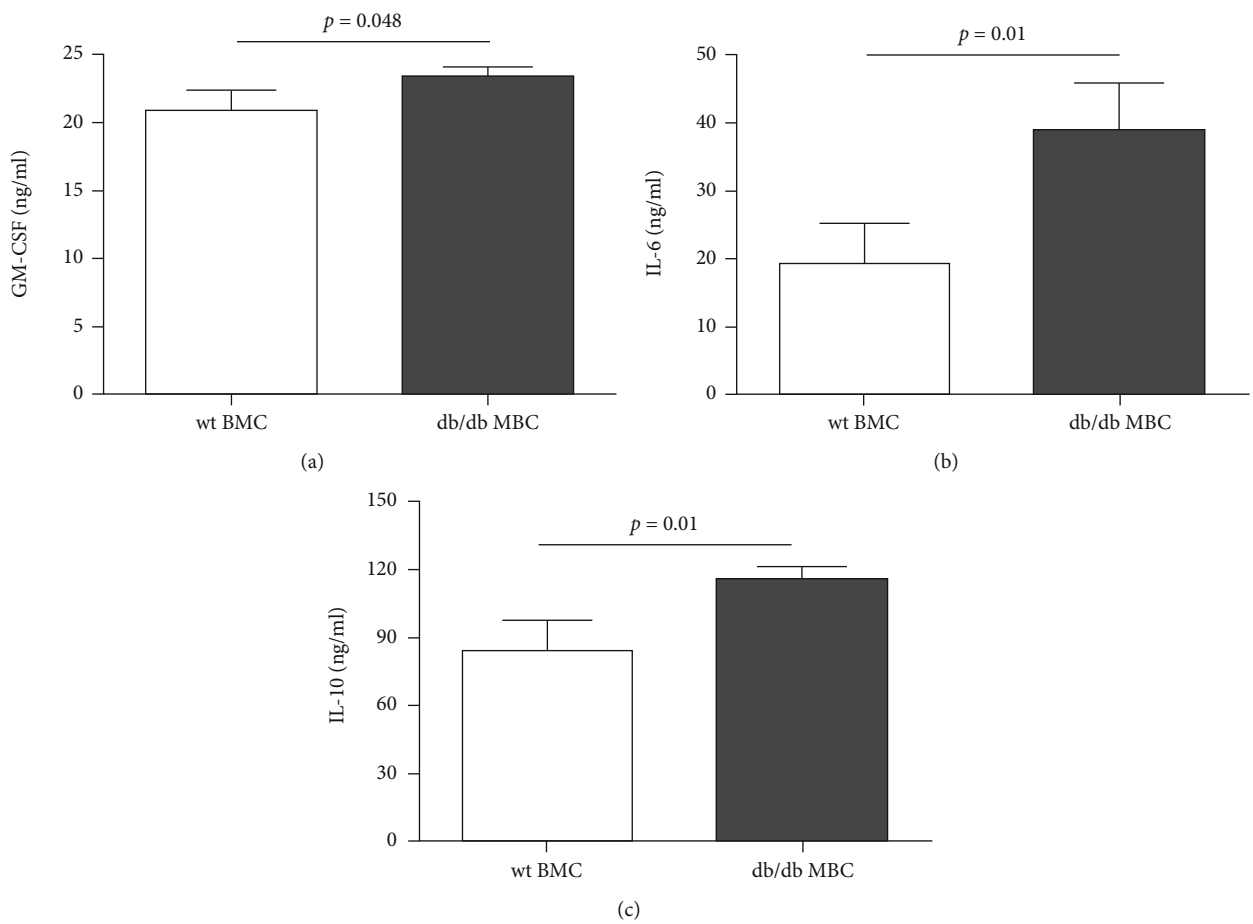


Figure 6: Cytokine production of GM-CSF (a), IL-6 (b), and IL-10 (c) in bone marrow cells isolated from wt and db/db mice at the age of 16 weeks. $n = 3$-4. wt: wild type; BMC: bone marrow cells.

## 4. Discussion

The main findings of the study include the following: (1) at the age of 16 weeks, diabetic db/db mice developed hyperglycemia and an increased amount of granulocytes and monocytes in the peripheral blood; (2) BMC of db/db mice produced more GM-CSF, IL-6, and IL-10 than that of wt controls; and (3) compared with no cell injection, injection of BMC isolated from db/db mice accelerated inflammation and acinar cell damage in mice with AP whereas injection of wt BMC did not aggravate disease progression.

AP is the leading cause of hospital admission in the United States and other countries, resulting in organ failure and mortality [16–18]. Gallstones, alcohol abuse, smoking, and hypertriglyceridemia are the well-known risk factors of AP [16–18]. From the pathological view, AP comprises two waves of inflammation. The first wave initiates from injured acinar cells that secrete inflammatory cytokines to recruit circulating granulocytes and monocytes homing to the lesion site. The second wave comes from infiltrating granulocytes and monocytes that elevate proinflammatory cytokine and chemokine production. Except for inflammatory cytokine secretion and oxidative stress induction, neutrophils release their DNA, histone proteins, high mobility group box 1, and granule components into the pancreas to form neutrophil extracellular traps (NETs), which facilitate inflammation by duct occlusion and trypsin activation [14, 19]. In parallel, NF-$\kappa$B and STAT3 pathways become activated in monocytes. Ultimately, the inflammatory cascades propagate, leading to systemic inflammation [19].

Recently, a growing body of evidence has indicated that diabetes not only exposes higher risk but also promotes more severe AP than nondiabetic ones [4]. From the mechanism insight, hereby, we demonstrated that BMC of db/db mice had distinct inflammatory cytokine profiles from BMC isolated from wt controls (Figure 5). This partially explains why diabetic BMC injection contributed substantially to the inflammation and acinar cell damage in acute pancreatitis. Among the cytokines that were differentially expressed in wt and diabetic BMC, IL-6 was the major one involved in AP. Via the IL-6 receptor expressed on acinar cells, IL-6/IL-6R activates signal transducers and activators of transcription 3 (STAT3) for acinar cell destruction [20]. The result of a meta-analysis comprising mild AP ($n = 896$), severe AP ($n = 700$), and healthy controls confirmed the positive correlation of plasma IL-6 levels and disease severity [21].

In the study, IL-10 production was increased in diabetic BMC when compared with wt BMC (Figure 5(b)). In line with our findings, Chen et al. reported that serum levels of IL-10 could discriminate the severe type from mild ones in

Table 2: Summary of cytokines produced by bone marrow cells from wild-type and db/db mice at the age of 16 weeks.

| Cytokines | Wild-type mice | db/db mice | $p$ value |
|---|---|---|---|
| Number | 4 | 4 | |
| GM-CSF (pg/mL) | 20.8 ± 1.5 | 24.1 ± 0.6 | 0.048 |
| IFN-$\gamma$ (pg/mL) | 5.98 ± 4.25 | 8.32 ± 1.09 | 0.13 |
| IL-1$\alpha$ (pg/mL) | 27.7 ± 3.1 | 30.9 ± 1.4 | 0.59 |
| IL-1$\beta$ (pg/mL) | 45.0 ± 20.5 | 54.9 ± 8.7 | 0.44 |
| IL-2 (pg/mL)* | 4.18 ± 1.67 | 3.61 ± 0.70 | 0.60 |
| IL-4 (pg/mL) | 4.19 ± 0.99 | 4.46 ± 0.80 | 0.80 |
| IL-5 (pg/mL) | 4.69 ± 0.54 | 4.84 ± 0.90 | 0.90 |
| IL-6 (pg/mL) | 19.3 ± 5.9 | 37.4 ± 7.0 | 0.01 |
| IL-7 (pg/mL) | 8.72 ± 2.37 | 12.25 ± 1.91 | 0.063 |
| IL-10 (pg/mL) | 84.2 ± 13.1 | 108.5 ± 11.6 | 0.03 |
| IL-12 (p70) (pg/mL) | 38.3 ± 3.3 | 42.6 ± 5.6 | 0.12 |
| KC (pg/mL) | 605.7 ± 918.5 | 112.0 ± 30.9 | 0.27 |
| MCP-1 (pg/mL) | 95.6 ± 60.4 | 71.6 ± 18.8 | 0.41 |
| TNF-$\alpha$ (pg/mL) | 7.22 ± 3.82 | 6.63 ± 0.61 | 0.75 |

GM-CSF: granulocyte-macrophage colony-stimulating factor; IFN-$\gamma$: interferon-gamma; IL-1$\alpha$: interleukin-1alpha; IL-1$\beta$: interleukin-1beta; IL-2: interleukin-2; IL-4: interleukin-4; IL-5: interleukin-5; IL-6: interleukin-6; IL-7: interleukin-7; IL-10: interleukin-10; IL-12 (p70): interleukin-12; IL-13: interleukin-13; IL-17A: interleukin-17A; KC: keratinocyte chemokine; LIX: lipopolysaccharide-induced CXC chemokine; MCP-1: monocyte chemotactic protein-1; MIP-2: macrophage inflammatory protein-2; TNF-$\alpha$: tumor necrosis factor-alpha. In the assay, the values of IL-13, IL-17 (IL-17A), LIX, and MIP-2 were under the detection limit in both groups. Data were expressed as mean ± SD.

AP [22]. IL-10 is produced by activated T cells such as Treg, Th17, and Th1 cells and macrophages stimulated by bacterial lipopolysaccharides and catecholamines or clearance of apoptotic cells [23]. Through binding to IL-10R1, Janus kinases Jak1 and Tyk2 are activated, resulting in STAT3 phosphorylation and nuclear translocation for target gene transcription. The anti-inflammatory property of IL-10 comes from the inhibition of inflammatory cytokine release and antigen presentation in monocytes and macrophages [23]. Intriguingly, IL-10 derived from plasma cells triggers myeloid lineage differentiation when cocultured in vitro [24]. Thus, how IL-10 participates in inflammation of AP needs future investigation.

Serum lipase and amylase are conventional markers to diagnose AP. Quantified by ELISA, the elevated lipase activity sustained much longer than amylase following the induction of AP by caerulein injection (Figure 2). The inconsistency between serum amylase activity and histological changes in the pancreas was noticed, which could be due to the different half-life and metabolism of these enzymes [25].

The limitations of the study are as follows. First, BMC injection was performed to evaluate the impact of diabetes on AP induced by caerulein injection. In this simplified model, we could not assess the global impact of diabetes such as hyperglycemia on disease progression. Second, we did not evaluate the migratory capacity of injected BMC in vivo. In the study, the recipient mice with induced AP received db/db BMC, wt BMC, or no BMC injection. By MPO staining, the number of MPO+ cells was more pronounced in the recipients that received db/db BMC than wt BMC, implying the increased BMC homing to the lesion site. Whether and how IMP stimulated BMC migration need future investigation. And third, we did not dissect the effect of lymphocytes and macrophages on the progression of AP. By staining with the anti-CD3 or anti-CD20 antibody, T- and B-lymphocytes were detected more in the interstitium than in the acini of patients with AP [26]. By contrast, as immune mediators, certain subtypes of lymphocytes could have a detrimental effect on secondary infection in AP [27]. Similarly, M1 and M2 macrophages have distinct properties in disease progression. M1 macrophages are proinflammatory and secrete inflammatory cytokines and chemokines in AP whereas M2 macrophages could facilitate stellate cells for fibrotic formation in chronic pancreatitis [28]. It would be of great interest to explore how these cells orchestrate the inflammatory progression of pancreatitis.

Taken together, following diabetes progression, the number of myeloid cells increases whereas lymphocytes decrease. BMC of diabetic db/db mice had different features from that of wt ones in that they produce more proinflammatory cytokines such as IL-6. In response to acinar cell injury, diabetic BMC aggravated the inflammation cascade and acinar cell injury, leading to AP progression.

## Data Availability

The data in the study are available from the corresponding author upon request.

## Conflicts of Interest

The authors declare that they have no conflicts of interest.

## Authors' Contributions

Xiao-Min Luo, Cen Yan, and Yue-Jie Zhang performed the animal experiments. Xiao-Min Luo analyzed the histological and immunohistochemistry data. Ling-Jia Meng and Guo-Tao Lu performed the histological experiments. Ji-Ming Yin performed the ELISA experiments. Ying-Mei Feng initiated the project, designed the experiment, analyzed the data, and prepared the draft.

## Acknowledgments

We thank Yang Zhang for his advice in the study. This work was supported by the National Natural Science Foundation of China (grant numbers 81670765 and 82070841) to Ying-Mei Feng.

## References

[1] S. Chatterjee, K. Khunti, and M. J. Davies, "Type 2 diabetes," *Lancet*, vol. 389, no. 10085, pp. 2239–2251, 2017.

[2] Emerging Risk Factors Collaboration, N. Sarwar, P. Gao et al., "Diabetes mellitus, fasting blood glucose concentration, and

risk of vascular disease: a collaborative meta-analysis of 102 prospective studies," *The Lancet*, vol. 375, no. 9733, pp. 2215–2222, 2010.

[3] H. N. Shen, Y. H. Chang, H. F. Chen, C. L. Lu, and C. Y. Li, "Increased risk of severe acute pancreatitis in patients with diabetes," *Diabetic Medicine*, vol. 29, no. 11, pp. 1419–1424, 2012.

[4] A. Mikó, N. Farkas, A. Garami et al., "Preexisting diabetes elevates risk of local and systemic complications in acute pancreatitis: systematic review and meta-analysis," *Pancreas*, vol. 47, no. 8, pp. 917–923, 2018.

[5] L. Gao, G. T. Lu, Y. Y. Lu et al., "Diabetes aggravates acute pancreatitis possibly via activation of NLRP3 inflammasome in db/db mice," *American Journal of Translational Research*, vol. 10, no. 7, pp. 2015–2025, 2018.

[6] G. A. Minkov, K. S. Halacheva, Y. P. Yovtchev, and M. V. Gulubova, "Pathophysiological mechanisms of acute pancreatitis define inflammatory markers of clinical prognosis," *Pancreas*, vol. 44, no. 5, pp. 713–717, 2015.

[7] A. Habtezion, "Inflammation in acute and chronic pancreatitis," *Current Opinion in Gastroenterology*, vol. 31, no. 5, pp. 395–399, 2015.

[8] M. Lou, P. Luo, R. Tang et al., "Relationship between neutrophil-lymphocyte ratio and insulin resistance in newly diagnosed type 2 diabetes mellitus patients," *BMC Endocrine Disorders*, vol. 15, no. 1, 2015.

[9] H. L. Kammoun, T. L. Allen, D. C. Henstridge et al., "Evidence against a role for NLRP3-driven islet inflammation in db/db mice," *Molecular Metabolism*, vol. 10, pp. 66–73, 2018.

[10] T. Kimura, A. Obata, M. Shimoda et al., "Protective effects of the SGLT2 inhibitor luseogliflozin on pancreatic $\beta$-cells indb/dbmice: the earlier and longer, the better," *Diabetes, Obesity & Metabolism*, vol. 20, no. 10, pp. 2442–2457, 2018.

[11] D. Qian, G. Song, Z. Ma et al., "MicroRNA-9 modified bone marrow-derived mesenchymal stem cells (BMSCs) repair severe acute pancreatitis (SAP) via inducing angiogenesis in rats," *Stem Cell Research & Therapy*, vol. 9, no. 1, p. 282, 2018.

[12] J. H. Tan, R. C. Cao, L. Zhou et al., "ATF6 aggravates acinar cell apoptosis and injury by regulating p53/AIFM2 transcription in severe acute pancreatitis," *Theranostics*, vol. 10, no. 18, pp. 8298–8314, 2020.

[13] X. Wang, L. Liang, and L. Du, "The effects of intrauterine undernutrition on pancreas ghrelin and insulin expression in neonate rats," *The Journal of Endocrinology*, vol. 194, no. 1, pp. 121–129, 2007.

[14] N. J. H. Warren and A. Eastman, "Reply to Koh: signaling dynamics of DNA damage response invoked by combination therapy are dose-dependent," *Journal of Biological Chemistry*, vol. 294, no. 6, p. 2192, 2019.

[15] Y. Zhang, W. He, C. He et al., "Large triglyceride-rich lipoproteins in hypertriglyceridemia are associated with the severity of acute pancreatitis in experimental mice," *Cell Death & Disease*, vol. 10, no. 10, p. 728, 2019.

[16] Y. W. Chien, T. Y. Chien, R. E. Bagdon, Y. C. Huang, and R. H. Bierman, "Transdermal dual-controlled delivery of contraceptive drugs: formulation development, in vitro and in vivo evaluations, and clinical performance," *Pharmaceutical Research*, vol. 6, no. 12, pp. 1000–1010, 1989.

[17] L. Boxhoorn, R. P. Voermans, S. A. Bouwense et al., "Acute pancreatitis," *Lancet*, vol. 396, no. 10252, pp. 726–734, 2020.

[18] M. A. Mederos, H. A. Reber, and M. D. Girgis, "Acute pancreatitis: a review," *JAMA*, vol. 325, no. 4, pp. 382–390, 2021.

[19] P. J. Lee and G. I. Papachristou, "New insights into acute pancreatitis," *Nature Reviews. Gastroenterology & Hepatology*, vol. 16, no. 8, pp. 479–496, 2019.

[20] Q. Wang, L. Bai, S. Luo et al., "TMEM16A $Ca^{2+}$-activated $Cl^{-}$ channel inhibition ameliorates acute pancreatitis via the $IP_3R/Ca^{2+}/NF\kappa B/IL\text{-}6$ signaling pathway," *Journal of Advanced Research*, vol. 23, pp. 25–35, 2020.

[21] N. Li, B. M. Wang, S. Cai, and P. L. Liu, "The role of serum high mobility group box 1 and interleukin-6 levels in acute pancreatitis: a meta-analysis," *Journal of Cellular Biochemistry*, vol. 119, no. 1, pp. 616–624, 2018.

[22] Y.-J. Chen, T.-L. Lin, Z. Cai, C.-H. Yan, S.-R. Gou, and Y.-D. Yao-Dong Zhuang, "Assessment of acute pancreatitis severity via determination of serum levels of has-miR-126-5p and IL-6," *Experimental and Therapeutic Medicine*, vol. 21, no. 1, pp. 1–1, 2020.

[23] R. Sabat, G. Grütz, K. Warszawska et al., "Biology of interleukin-10," *Cytokine & Growth Factor Reviews*, vol. 21, no. 5, pp. 331–344, 2010.

[24] L. Meng, L. N. Almeida, A. K. Clauder et al., "Bone marrow plasma cells modulate local myeloid-lineage differentiation via IL-10," *Front Immunol*, vol. 10, p. 1183, 2019.

[25] O. Z. Ismail and V. Bhayana, "Lipase or amylase for the diagnosis of acute pancreatitis?," *Clinical Biochemistry*, vol. 50, no. 18, pp. 1275–1280, 2017.

[26] E. I. Căluianu, D. O. Alexandru, E. A. Târtea et al., "Assessment of T- and B-lymphocytes and VEGF-A in acute pancreatitis," *Romanian Journal of Morphology and Embryology*, vol. 58, no. 2, pp. 481–486, 2017.

[27] L. Ding, Y. Yang, H. Li, H. Wang, and P. Gao, "Circulating lymphocyte subsets induce secondary infection in acute pancreatitis," *Frontiers in Cellular and Infection Microbiology*, vol. 10, p. 128, 2020.

[28] F. Hu, N. Lou, J. Jiao, F. Guo, H. Xiang, and D. Shang, "Macrophages in pancreatitis: mechanisms and therapeutic potential," *Biomedicine & Pharmacotherapy*, vol. 131, p. 110693, 2020.

Hindawi
Journal of Immunology Research
Volume 2021, Article ID 5317662, 10 pages
https://doi.org/10.1155/2021/5317662

*Research Article*

# The Ablation of Envelope Protein Glycosylation Enhances the Neurovirulence of ZIKV and Cell Apoptosis in Newborn Mice

**Yanqing Guo**,[1,2,3] **Linlin Bao**,[1,2,3] **Yanfeng Xu**,[1,2,3] **Fengdi Li**,[1,2,3] **Qi Lv**,[1,2,3] **Feiyue Fan**,[1,2,3] **and Chuan Qin**[1,2,3]

[1]*Comparative Medicine Center, Peking Union Medical College (PUMC) and, Institute of Laboratory Animal Sciences, Chinese Academy of Medical Sciences (CAMS), Beijing 100021, China*
[2]*Key Laboratory of Human Disease Comparative Medicine, Ministry of Health, Beijing 100021, China*
[3]*Beijing Key Laboratory for Animal Models of Emerging and Reemerging Infectious, Pan Jia Yuan Nan Li No. 5, Chao Yang District, Beijing 100021, China*

Correspondence should be addressed to Chuan Qin; qinchuan@pumc.edu.cn

Received 4 June 2021; Accepted 4 July 2021; Published 16 July 2021

Academic Editor: Meng-Hao Huang



Zika virus (ZIKV) has attracted the wide global attention due to its causal link to microcephaly. In this study, two amino acid (aa) mutation (E143K and R3394K) were identified at the fourth generation (named ZKC2P4) during the serial passage of ZIKV-Asian lineage ZKC2/2016 strain in the newborn mouse brain, while another seven aa deletions in envelope (E) protein were detected in ZKC2P6. ZKC2P6 is a novel nonglycosylated E protein Asian ZIKV we first identified and provides the first direct supporting evidence that glycosylation motif could be lost during the passage in neonatal mice. To study the impact of E protein glycosylation ablation, we compared the pathogenicity of ZKC2P6 with that of ZKC2P4. The results showed that the loss of E protein glycosylation accelerated the disease progression, as evidenced by an earlier weight loss and death, a thinner cerebral cortex, and more serious tissue lesions and inflammation/necrosis. Furthermore, ZKC2P6 exhibited a greater ability to replicate and caused severer cell apoptosis than that of ZKC2P4. Therefore, the ablation of E glycosylation generally enhances the neurovirulence of ZIKV and cell apoptosis in newborn mice.

## 1. Introduction

Zika virus (ZIKV), a member of the mosquito-borne Flaviviridae family, was originally isolated from a rhesus monkey from the Zika forest in 1947 [1]. Phylogenetic analyses have revealed two main ZIKV lineages, African and Asian, and the contemporary epidemics have been traced to the Asian lineage [2]. Currently, ZIKV has been causally linked to microcephaly during pregnancy and thus evolved into a new public health threat [3]. The genome of ZIKV is a positive-sense RNA that contains one open reading frame encoding a polyprotein, which can be cleaved into three structural proteins, including capsid (C), precursor membrane (PrM), and envelope (E), and seven nonstructural (NS) proteins [4, 5]. The E protein is involved in many crucial steps of the viral lifecycle, including the interactions with cellular surface attachment factors and receptors, the fusion of viral and cellular membranes, virus assembly, and liberation. To date, three types of mouse models, including the embryonic microcephaly model [6], the neonatal mouse model [7], and the adult mouse model lacking the IFN receptor (Ifnar$^{-/-}$ model) [8], were used to study the virulence of ZIKV. Although these three models have some degree of immune deficiency, the developmental state of the first two models is closer to that of human microcephalic fetus. The glycan on N154 of E protein projects from the viral surface and may be directly involved in cell receptor binding [9]. Glycosylation site deficiency can be achieved in two ways: the substitution of a single key aa (an aa in the

glycosylation motif NDT) or the deletion of a few aa spanning the N154 site. For example, the loss of the N154 glycosylation site via a deletion has been observed in the African ZIKV [4, 10] while the glycosylation site motif was lost because of a 1-aa substitution in dengue virus (DV) and ZIKV [4]. The loss of the N154 glycosylation site has been observed in some flaviviruses, and this phenomenon may be related to passaging in the mouse brain, but no direct evidence exists to support this hypothesis [4, 10].

In the present study, we obtained a novel nonglycosylated E protein Asian ZIKV, named ZKC2P6, via spontaneous amino acid deletion during neonatal Balb/c mice brain passage. The ablation of envelope protein glycosylation of ZKC2P6 enhanced its replication ability and induced severer histological lesions, inflammation/necrosis, and more cellular apoptosis in newborn mice. This finding also provides the first direct supporting evidence that glycosylation motif could be lost during brain passage in neonatal mice.

## 2. Materials and Methods

*2.1. Cells and Viruses.* Human neuroblastoma cell line SH-SY5Y (ATCC CRL-2266) was maintained in MEM containing 15% fetal bovine serum (FBS) (Gibco, USA) at 37°C with 5% $CO_2$. The Vero African green monkey kidney epithelial cell line (ATCC CCL81) was cultured in DMEM supplemented with 10% FBS. The ZIKV strain ZKC2/2016 (KX253996) was isolated from an imported case [11]. ZKC2P4 and ZKC2P6 were derived from ZKC2/2016 after four and six passages in suckling mice, respectively. The supernatant of the solution containing homogenized mouse brains at 5 days postinfection (DPI) was harvested, titrated using a real-time reverse transcription (RT)-PCR assay, and then stored at -80°C. ZIKV strains were purified three times using a plaque assay on Vero cells as described below. Studies with ZIKV were conducted under BSL2 and animal BAL3 conditions in the Institute of Laboratory Animal Sciences (ILAS) with Institutional Biosafety Committee approval.

*2.2. Plaque Assay.* ZIKV samples were serially diluted tenfold for 6 times in DMEM, and 1 ml virus in each dilution was added to Vero cell monolayers in 6-well plates and was then incubated at 37°C with 5% $CO_2$. After a 1 h incubation, the supernatants were discarded and washed with phosphate buffered saline (PBS). Then, 2 ml of DMEM containing 1% low-melting-point agarose (Sigma) was added to each well, the plates were incubated at 37°C with 5% $CO_2$ for 4 days, and the monoclonal virus was selected and amplified in 12-well plates.

*2.3. Reverse Transcription PCR (RT-PCR).* The virus RNA was extracted from preserved supernatant using an RNeasy Mini Kit (QIAGEN, Germany); then, the viral genome was amplified using the PrimeScript One-Step RT-PCR Kit (TaKaRa, China). Primers in this study were designed using the Oligo software (Supplemental Table 1). ZIKV RNA copies were determined using a specific probe (5′-FAM-CGGCATACAGCATCAGGTGCATAGGAG-MGB-3′) and primer set (ZIKA 835: TTGGTCATGATACTGCTGATTGC; ZIKA 911c: CCTTCCACAAAGTCCCTATTGC) [12]. Following the manufacturer's protocol, 25 $\mu$l reactions of the QuantiTect Probe RT-PCR Kit with 5 $\mu$l of RNA template were used to perform qRT-PCR assays using an ABI Step One Plus System. ZIKV RNA (535-1211), which was transcribed using the MEGAshortscript T7 Transcription Kit in vitro and the MEGAclear Transcription Clean-Up Kit (Invitrogen, USA), was used as the RNA standard to determine the number of viral copies in the samples.

*2.4. Genetic, Phylogenetic, and Structural Analyses.* ZIKV genomes were amplified via RT-PCR assays using the corresponding primers (Supplemental Table 1), assembled using the SeqMan software in the DnaStar package, and then aligned using the MEGA 5.05 software. Phylogenetic trees were generated using the maximum-likelihood method with default settings implemented by the MEGA 5.05 software. The structure of the E protein was predicted using the Swiss-Model online tool (https://swissmodel.expasy.org/), while the structure of glycan was built using ChemBioDraw Ultra. The structure around N154 in the E protein was interpreted using the PyMol software. The superposition of the predicted structure was conducted using the Chimera software.

*2.5. Virus Replication Kinetics.* The cell culture supernatants were discarded, and virus-medium (containing $1.5 \times 10^7$ viral copies) and 0.5 mL of fresh medium (MEM containing 4% FBS) were added when the SH-SY5Y cells reached 90% confluence in 12-well plates. The infected cells were cultured for indicated time points (0 h, 6 h, 12 h, 24 h, 48 h, and 72 h), and the corresponding supernatants were collected. Virus loads in supernatants were determined using quantitative RT-PCR.

*2.6. Animal Experiments.* One-day-old Balb/c mice were intracranially inoculated using 25 $\mu$l of ZKC2P4 or ZKC2P6 virus stocks (containing $1.5 \times 10^7$ viral copies) or uninfected supernatant of the solution containing the ground brains from age-matched mice. The animals were observed and weighed at 0, 1, 3, 5, and 7 DPI. The brains and spinal cords were collected at 3 and 5 DPI for histopathological analysis and the determination of viral copies. Mouse brains were collected at 5 DPI for western blot. The protocols were approved by the Animal Use and Care Committee of the Institute of Laboratory Animal Science, Peking Union Medical College (Permit Number: ILAS-BLL17007). The animal experiments were conducted following the guidelines for animal welfare of the World Organization for Animal Health.

*2.7. Histopathology and Immunofluorescence.* Tissues for paraffin embedding were processed routinely, and the 4 $\mu$m thickness sections were stained with Nissl staining. The Nissl-stained slides were viewed by light microscopy or Nano Zoomer S60. For immunofluorescence detection, the sections were incubated in 0.5% Triton X-100 in PBS for cell membrane penetration, in 0.01 M sodium citrate for antigens reparation, and blocked at RT for 1 h in 10% BSA (Sigma). The sections were then incubated in the primary antibody at 4°C overnight, washed with PBS, and incubated in the secondary antibody at RT for 1 h. After washing with PBS, the slides were finally stained with DAPI (Abcam, UK) for

5 min and then were viewed with a Leica Microsystems or Nano Zoomer S60 instrument. The antibodies used for immunofluorescence were as follows: Z6 provided by George Fu Gao (1 : 250) (Ma et al., 2016), anti-cleaved caspase-3 rabbit mAb (9664 s, 1 : 500; CST), anti-GFAP rabbit mAb (80788, 1 : 500; CST), anti-Sox2 rabbit mAb (23064, 1 : 500; CST), anti-NeuN rabbit mAb (24307, 1 : 500; CST), fluorescein-conjugated Affinipure goat anti-human IgG (H +L) (ZF0308, 1 : 500; ZSGB-BIO, China), and Alexa Fluor 594-conjugated anti-rabbit IgG (H+L) (8889 s, 1 : 1000; CST).

*2.8. Western Blot.* The western blot was performed as previously reported [13]. Briefly, the harvested brains were washed with cold PBS and fully lysed with RIPA buffer. The lysed brains were placed on the ice for 30 min and then were centrifuged for 30 min at 13,000 rpm at 4°C to remove tissue debris. The protein concentration was determined using the BCA method. Proteins were analyzed under denaturing conditions in 12% SDS-PAGE and transferred onto a nitrocellulose filter membrane. The membranes were blocked with 5% skim milk in TBST (TBS with 0.1% Tween 20) buffer for 1 h and then incubated overnight at 4°C with antibodies against PARP (9542 s, 1 : 1000; CST) and $\beta$-actin (4970 s, 1 : 1000; CST). After washing with TBST, the membranes were further incubated with the second antibody conjugated to HRP (7074 s, 1 : 5000; CST) for 1 h at room temperature and then were washed with TBST. The blots were exposed using ECL western blotting detection reagent and scanned using the Bio-Rad Quantity one Program.

*2.9. Statistical Analysis.* All the data were analyzed using GraphPad Prism 5.0 or SPSS 16.0 software. Survival curves were analyzed using the log-rank (Mantel-Cox) test. The weight changes were analyzed using a repeated measures ANOVA. Other results were analyzed using Student's unpaired $t$-test or a one-way ANOVA with Tukey's multiple comparison test. The data are presented as the means ± SD. The $p < 0.05$ was considered statistically significant.

## 3. Results

*3.1. Discovery of the Envelope Protein Glycosylation Ablation Zika Virus.* Similar to other flaviviruses, ZIKV can be passaged in the brain of newborn mice. In this study, we conducted the serial passage of ZKC2/2016, which was isolated from an imported case in China [11], in one-day-old neonatal mice, and then experimentally isolated a ZIKV strain with substantial neurovirulence. E143K and R3394K were found by sequencing and alignment in the fourth generation, and seven aa (from 445 to 451) were further deleted in the fifth to the eighth generations (Figure 1(a)). The fourth and sixth generations were purified three times using the plaque assay method and were named strains ZKC2P4 (MG674718) and ZKC2P6 (MG674719), respectively. As of May 2021, 66 other strains with a loss of N-linked glycosylation from aa deletion have been identified in 945 complete ZIKV sequences in GenBank. In our study, 12 representative strains were shown (Figure 1(a)) and phylogenetic analysis revealed that the ZKC2P6 strain is a novel nonglycosylated E protein strain occurring via aa deletion in the Asian lineage (Figure 1(b)). Additionally, ZKC2P6 provides the first direct supporting evidence that glycosylation motif could be lost during the passage in neonatal mice, which is consistent with the clinical findings of another two similar but not identical amino acid deletions [14, 15].

*3.2. Structure Prediction of the E Protein.* The deletion of a few aa spanning the N154 site of the ZKC2P6 strain may impact the E protein structure. To further determine its effect, the structure of the E protein of ZIKV (PDB codes: 5IZ7.2.H and 5IZ7.2.1) was used as a template for the E proteins of ZKC2P4 and ZKC2P6, respectively. The superposition of the ZKC2P4 and ZKC2P6 E proteins and the region spanning the N154 site (red in Figure 1(a)) showed that the loss of N-linked glycosylation in the E protein of the ZKC2P6 strain sharply impacts the local alpha-helix (Figures 1(c) and 1(d)). The E protein is responsible for virus entry by interacting with cell surface receptors and represents an important determinant of viral pathogenesis [16]. Therefore, the change in the ZKC2P6 E protein structure may impact viral pathogenesis.

*3.3. Envelope Protein Glycosylation Ablation Enhances the Neurovirulence of ZIKV in Neonatal Mice.* To determine the effect of E protein glycosylation ablation for the neurovirulence of ZIKV in neonatal mice, we compared the in vivo data of ZKC2P6 with those of ZKC2P4 in one-day-old Balb/c mice that underwent intracerebral injection inoculation. Notably, ZKC2P6-infected mice presented an earlier weight loss (Figure 2(a)), emergence of symptoms, including stomach emptying, motor weakness, and hind limb paralysis (data not shown), and death (Figure 2(b)) than did ZKC2P4. There was no obvious difference in body length and posture at 3 DPI, while significant differences were found at 5 DPI (Figure 2(c)). An inspection of the Balb/c mice at 3 and 5 DPI showed that the ZKC2P6 infection led to obviously microcephalic brains (Figures 2(d) and 2(e)). In addition, we noticed a thinner cortex in the ZKC2P6-infected brains (Figure 2(f)). The microcephaly phenotype caused by ZKC2P6 is similar to that observed in the study by Li et al. [6]. Histological lesions and inflammation/necrosis in the cerebral cortex, hippocampus, cervical spinal cord, cerebellum, and brain stem were observed at earlier time points and more severe after ZKC2P6 infection (Figure 2(g) and Table 1). More death of neurons and glial cells was also observed in the cerebral cortex, hippocampus, and cervical spinal cord in the ZKC2P6 group (Figure 2(g)). Meanwhile, edemas were found in the brains and cervical spinal cords of the ZKC2P6-infected group, while no lesions in the kidney were found in any of the three groups (Table 1). Therefore, envelope protein glycosylation ablation in ZKC2P6 is more virulent to newborn mice than ZKC2P4.

*3.4. Envelope Protein Glycosylation Ablation Significantly Enhances ZIKV Replication.* To study the effect of E glycosylation ablation for ZIKV replication, the ZIKV particles in the cerebral cortex and hippocampus of neonatal mice at 5 DPI were determined and the result showed that the virus

| | | Pr 143–148 | | | | | | E 441–453 | | | | | | | | | | | | | NS5 3394–3397 | | | |
|---|---|---|---|---|---|---|---|---|---|---|---|---|---|---|---|---|---|---|---|---|---|---|---|---|
| Asian | KX253996.1 ZKC2/2016 | E | A | I | S | F | P | M | I | V | N | D | T | G | H | E | T | D | E | N | R | I | I | G |
| | MG674718.1 ZKC2P4 | K | A | I | S | F | P | M | I | V | N | D | T | G | H | E | T | D | E | N | K | I | I | G |
| | MG674718.1 ZKC2P6 | K | A | I | S | F | P | M | I | V | N | - | - | - | - | - | - | - | E | N | K | I | I | G |
| | KY553111.1 AFMC-U | E | A | I | S | F | P | M | I | - | - | - | - | G | H | E | T | D | E | N | R | I | I | G |
| | MT439647.1 | ? | ? | ? | ? | ? | ? | M | I | - | - | - | - | G | H | E | T | D | E | N | R | I | I | G |
| African | HQ234498 MR766 | K | A | I | S | F | A | M | I | V | N | D | T | G | Y | E | T | D | E | N | R | I | I | G |
| | KF268949 ARB15076 | K | A | I | S | F | A | M | I | V | N | D | - | - | - | - | - | - | E | N | R | L | I | G |
| | KF383117 ArD128000 | K | A | I | S | F | A | M | - | - | - | - | - | G | H | E | T | D | E | N | R | I | I | G |
| | KF383115 ArB1362 | K | A | I | S | F | A | M | I | V | N | D | - | - | - | - | - | - | - | N | R | I | I | G |
| | KU963574 IbH-30656 | K | A | I | S | F | V | M | I | V | N | D | - | - | - | - | - | - | E | N | R | I | I | G |
| | LC629066.1 Deltal163 | K | A | I | S | F | A | M | T | - | - | - | - | G | Y | E | T | D | E | N | R | I | I | G |
| | LC629066.1 Deltal156 | K | A | I | S | F | A | M | T | V | N | - | - | - | - | - | - | D | E | N | R | I | I | G |
| | MH061909 MR766-P5 | K | A | I | S | F | A | M | I | - | - | - | - | G | Y | E | T | D | E | N | R | I | I | G |
| | NC012532.1 | K | A | I | S | F | A | M | I | - | - | - | - | G | Y | E | T | D | E | N | R | I | I | G |

(a)

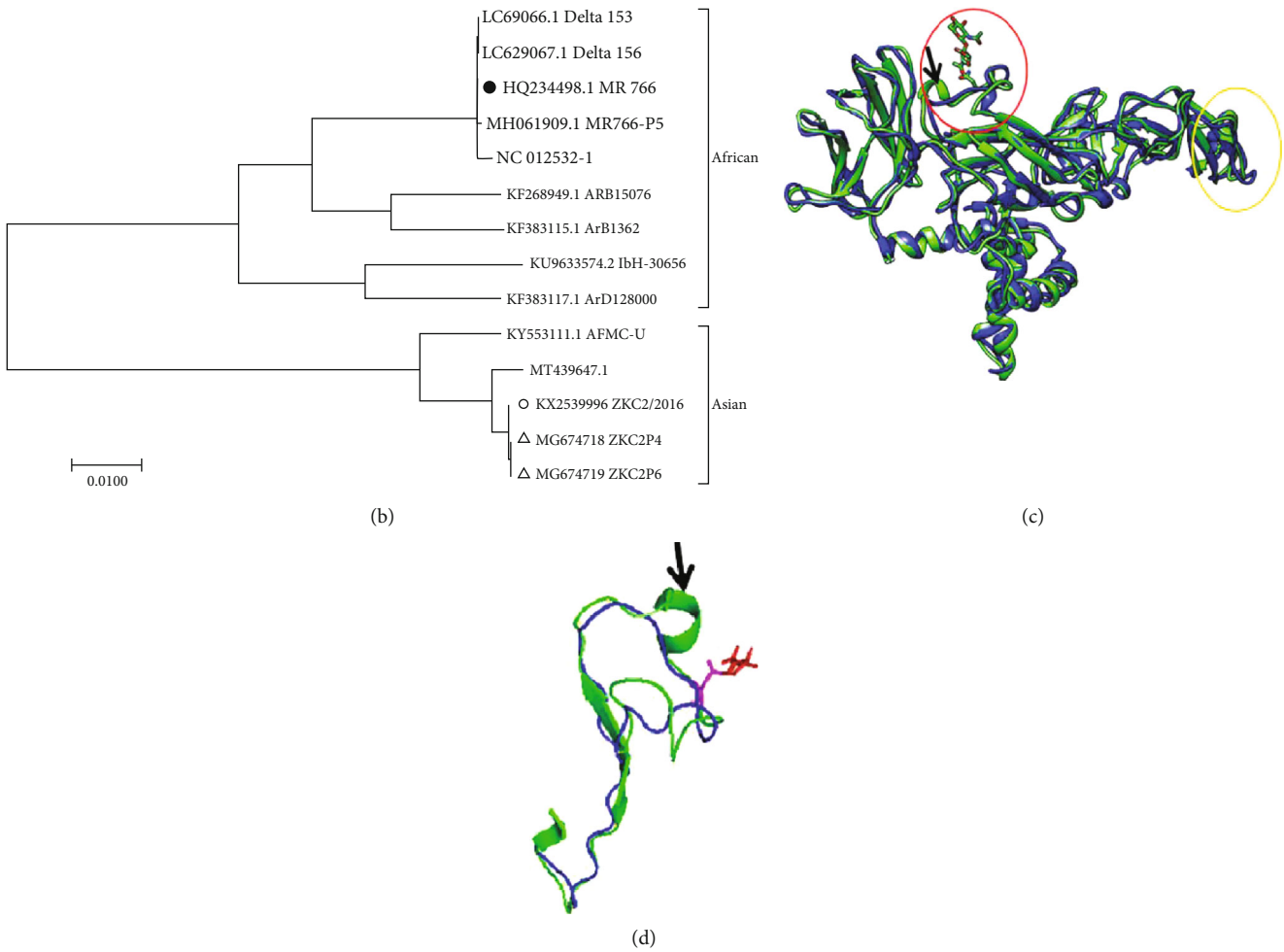


Figure 1: Mutation, phylogenetic, and structural analyses of the ZKC2P4 and ZKC2P6 strains. (a) The aa mutation (highlighted yellow) of the ZKC2P4 and ZKC2P6 strain are aligned to the corresponding aa of other ZIKV strains. "-" indicates an aa deficiency. Red indicates the N154 glycosylation site. (b) Phylogenetic tree constructed based on the nucleic acids of the complete open reading frame by the maximum-likelihood algorithm in the MEGA v5.05 software. "●" indicates the African lineage reference strain; "○" indicates the Asian lineage reference strain; "△" indicates the strains used in this study. (c) Superposition of the artist-rendered models of E proteins in the ZKC2P4 (green) and ZKC2P6 (blue). Red circle indicates the loop region surrounding the glycosylation site, and yellow circle indicates the glycan loop. (d) Superposition of the loop region surrounding the glycosylation site (140 to 177 in ZKC2P4 and 140 to 170 in ZKC2P6) of the E protein. The stick structure represents the glycan of the ZKC2P4 strain, and the alpha-helix is indicated by the black arrow.

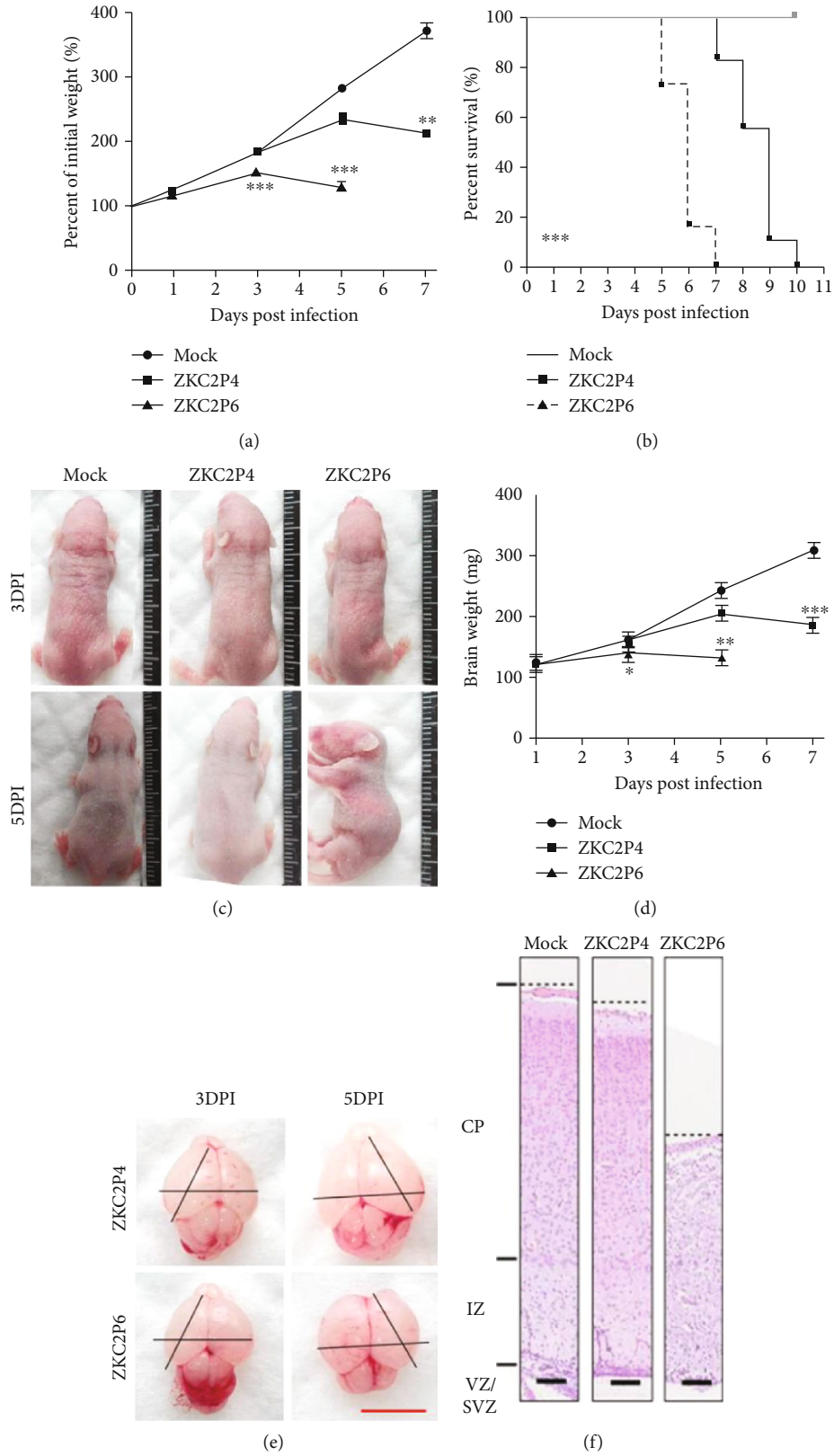


Figure 2: Continued.

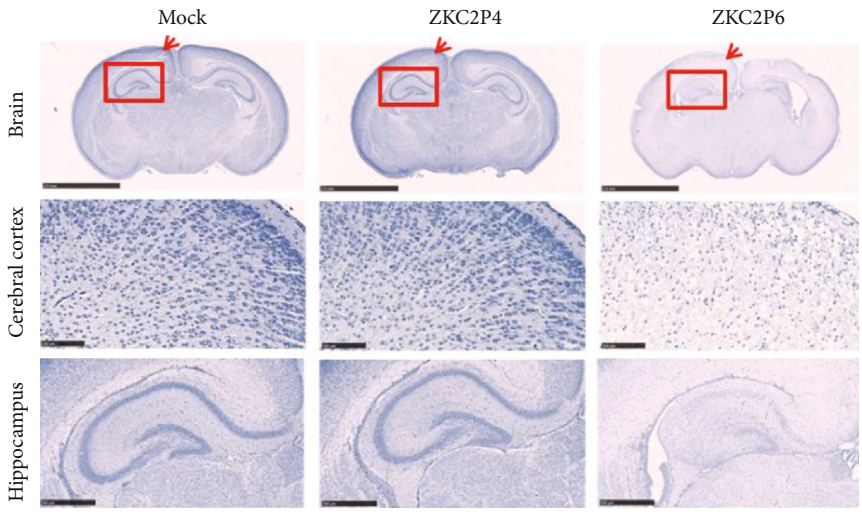


(g)

Figure 2: Envelope protein glycosylation ablation enhances the neurovirulence of ZIKV in neonatal mice. (a) The changes of body weight. $N = 18$, $^{***}p < 0.001$. (b) Survival rate in neonatal mice after $1.5 \times 10^7$ viral copies of ZKC2P4/ZKC2P6 infection or the uninfected supernatant injection. $N = 18$, $^{***}p < 0.001$. (c) Body length and posture of neonatal mice at 3 and 5 DPI. $N = 6$. (d) Brain weight of neonatal mice. $N = 6$, $^{*}p < 0.05$, $^{**}p < 0.01$, and $^{***}p < 0.001$. (e) Microcephalic brains from mice in the ZKC2P4 and ZKC2P6 groups. Black bars represent the brain width or cerebral cortex length, scale bar: 0.5 cm. (f) Brain cortices and (g) histopathological analysis of the cerebral cortex, hippocampus, and cervical spinal cord in each group at 5 DPI. Nissl staining, scale bar: 100 $\mu$m.

Table 1: Lesions of cervical spinal cord, kidney, and parts of brain on 3 and 5 DPI.

| DPI | Group | Cerebral cortex | Hippocampus | Cerebellum | Brain stem | Cervical spinal cord | Kidney |
|---|---|---|---|---|---|---|---|
| | Mock | - | - | - | - | - | - |
| 3 | ZKC2P4 | + | + | + | - | ± | - |
| | ZKC2P6 | ++ | ++ | + | + | ± | - |
| | Mock | - | - | - | - | - | - |
| 5 | ZKC2P4 | ++ | + | + | ± | ± | - |
| | ZKC2P6 | +++ | +++ | ++ | + | + | - |

Note: -, no lesions and inflammation/necrosis; ±, minor lesions, occasional neurons/glial cell inflammation and necrosis; +, mild lesions, a few neurons/glial inflammation and necrosis; ++, moderate lesions, more neurons/glial cell inflammation and necrosis; +++, severe lesions, large number of neurons/glial inflammation and necrosis.

loads were significantly higher in the ZKC2P6 group than that of the ZKC2P4 (Figure 3(a)). The quantification of ZIKV loads in the brain further verified the enhanced replication capability of ZKC2P6 (Figure 3(b)). Similar results were also observed in the cerebral cortex of neonatal mice at 3 DPI and hippocampus of neonatal mice (data not shown). Meanwhile, detailed location analysis in normal neural cells of neonatal mice suggested that ZKC2P6 did not infect the NeuN+ neurons, GFAP+ glial cells, and Sox2 + neural stem cells, as no colocalization of the virus was detected in the corresponding cells (Figure 3(c)). Furthermore, the enhanced ZIKV replication after E glycosylation ablation was further verified in human neuroblastoma cell line SH-SY5Y at 24, 48, and 72 h postinfection (Figure 3(d)). Therefore, E glycosylation ablation significantly enhances ZIKV replication in our study.

*3.5. Envelope Protein Glycosylation Ablation Significantly Enhances the Apoptosis of Nerve Cells in the Brain.* ZIKV infection can lead to caspase-3 (Cas3) activation in both neural precursor cells and embryonic mouse brain [17]. To determine whether ZKC2P6 accelerates the apoptosis of nerve cells in the brain, immunofluorescence for cleaved caspase-3 and western blotting for the cleaved PARP, one of the main cleavage targets of Cas3, were detected. We found that ZKC2P6 induced more apoptosis (cells positive for the cleaved Cas3) in the cerebral cortex and hippocampus of neonatal mice at 5 days postinfection of ZKC2P6 compared with the ZKC2P4 and mock groups (Figure 4(a)). Furthermore, the protein level of cleaved PARP (Figures 4(b) and 4(c)) in the ZKC2P6 group was higher than that of ZKC2P4 and mock groups. These results hinted that E glycosylation ablation significantly enhances the apoptosis of nerve cells in the brain.

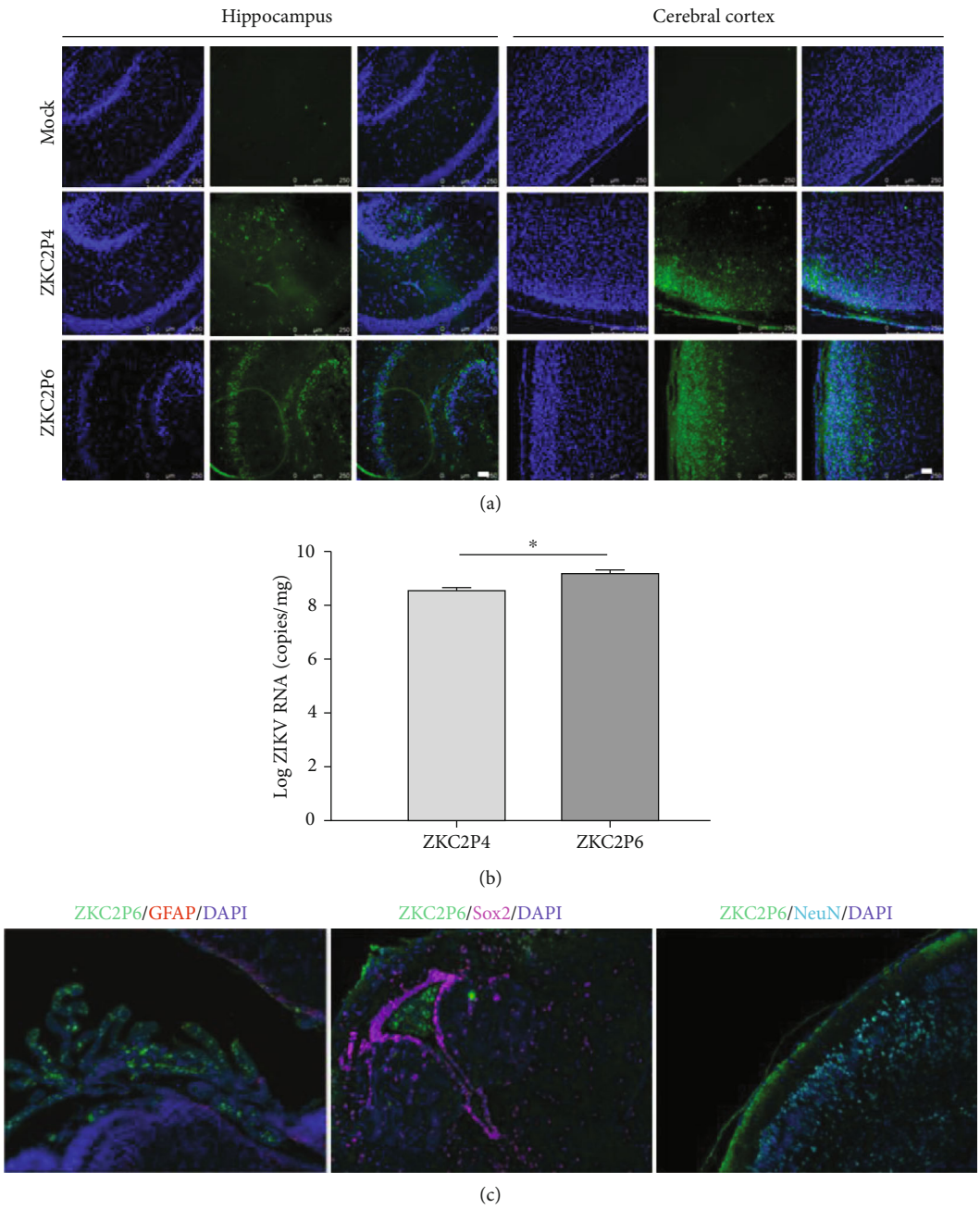


Figure 3: Continued.

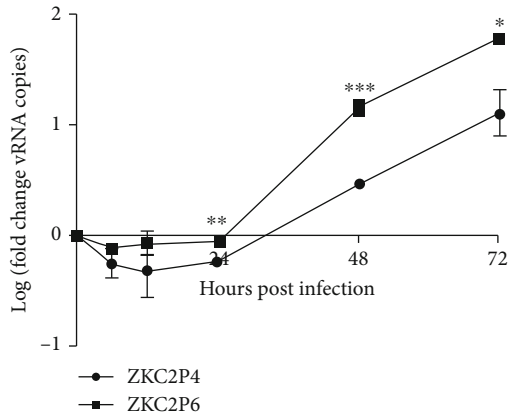


(d)

Figure 3: Envelope protein glycosylation ablation of ZIKV enhances viral replication in the brains of neonatal mice. (a) ZIKV viral particles (green) in the cerebral cortex and hippocampus at 5 DPI. Scale bar: 50 $\mu$m. (b) Qualification of ZIKV in the brains of one-day-old Balb/C mice at 5 DPI after $1.5 \times 10^7$ viral copies of ZKC2P4/ZKC2P6 infection. $N = 6$, $^{*}p < 0.05$. (c) Colocalization of ZKC2P6 with NeuN+ neurons, GFAP+ glial cells, and Sox2+ neural stem cells using immunofluorescence. (d) Growth curves of ZKC2P4 and ZKC2P6 in SH-SY5Y cells after $1.5 \times 10^7$ viral copy infection. $N = 3$, $^{**}p < 0.01$.

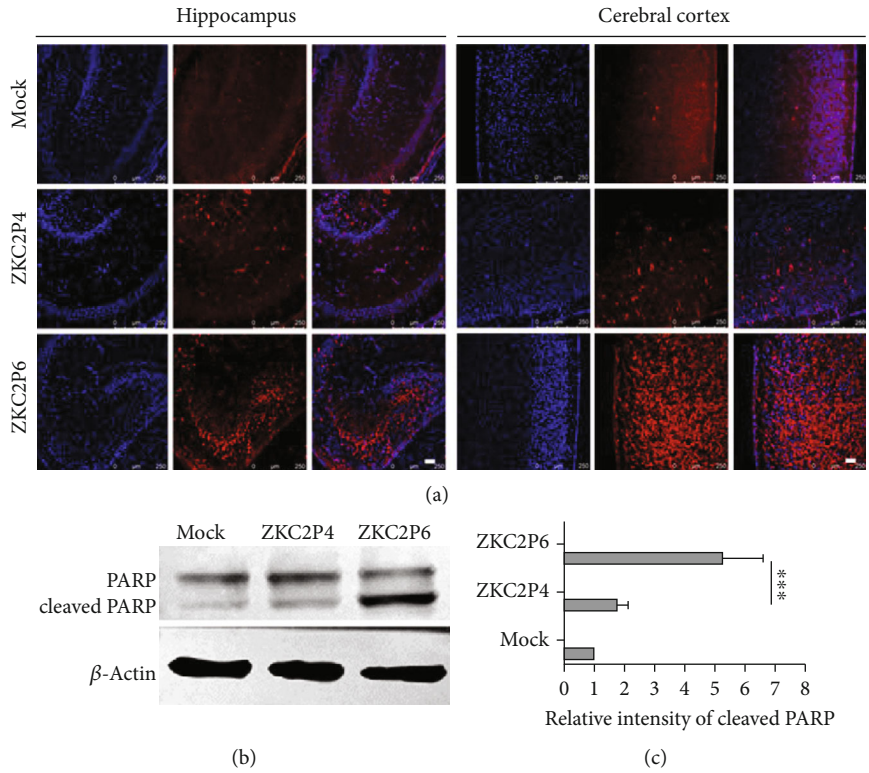


Figure 4: Envelope protein glycosylation ablation of ZIKV enhances the apoptosis of nerve cells. (a) Apoptosis of nerve cells in the cerebral cortex and hippocampus at 5 DPI. Red indicates the cleaved caspase-3 after immunofluorescence assay. Scale bar: 50 $\mu$m. (b, c) The expression of cleaved PARP in the brains at 5 DPI. $N = 6$, $^{***}p < 0.001$.

## 4. Discussion

Over the past decades, the loss of the glycosylation site has been observed in many flaviviruses, such as WNV [18], DV [19], KJV [20], and ZIKV [4]. Here, we purified two ZIKV strains (ZKC2P4 and ZKC2P6) with spontaneous aa substitution in PrM and NS protein region during the serial passage of ZKC2/2016 in the mouse brain and further observed 7 aa deletions spanning the glycosylation motif in ZKC2P6 stain. To our knowledge, the ZKC2P6 strain is the first Asian strain with a glycosylation motif deficiency spontaneously produced via aa deletion during brain passage in

newborn mice (Figure 1(b)). Envelope protein glycosylation mediated Zika virus pathogenesis [21]. In the present study, the ablation of E glycosylation in ZKC2P6 enhanced its capability of viral replication and neurovirulence, leading to histological lesions, inflammation/necrosis, cellular apoptosis, and death in the mouse brain.

Except for ~10 amino acids (aa) surrounding the N-linked glycosylation site (N154), the ZIKV structure is similar to other flavivirus structures [9, 22]. In this study, 7 aa spanning the N154 site are deleted in ZKC2P6, while similar but not the same strains with aa deletion spanning the N154 site (MT439647, KY553111, KF268949, KF383117, KF383115, KU963574, LC629066, LC629067, MH061909, and NC012532) were previously recorded in the complete ZIKV sequences from GenBank (Figure 1(a)). Our results during newborn mouse brain passage further provided the direct evidence to support this hypothesis that glycosylation motif may be lost during ZIKV passage histories [4]. Six to nine aa near the glycosylation site in E protein of ZIKV, which is longer than that in several (but not all) other flaviviruses, leads to the projection of the glycan on N154 from the viral surface [9]. The deletion of this seven aa in our study was predicted to influence the structure of the glycan loop (Figures 1(c) and 1(d)) and may influence the spatial structure of the E protein dimer for the existence of the glycan loop [9].

The E protein is responsible for virus entry and impacts viral fitness, infectivity, replication, and virulence in many flaviviruses [23]. In our study, envelope protein glycosylation ablation enhanced the ZIKV replication and neurovirulence in neonatal mice. Mossenta et al. proved that N-linked glycosylation at Asn-154 in ZIKV influences viral assembly and infectivity in vitro [24], while Fontes-Garfias and his colleagues demonstrated that E glycosylation was necessary for the ZIKV infection in Ifnar1-/- mice and mosquito hosts but did not significantly affect neurovirulence in newborn mice [25]. However, we observed that E protein glycosylation ablation enhanced the neurovirulence of ZIKV in newborn mice, which represents a discrepancy with the results by Fontes-Garfias et al. We speculated three possible reasons may explain this discrepancy. First, the CD-1 and Balb/C mice may have different sensitivities to ZIKV; second, the neurovirulence of ZKC2P6 in newborn mice may be related to aa near the N154 site besides glycan on N154, while the FSS13025 strain lost the glycosylation motif through a single aa substitution. Third, other 19 aa of FSS13025, including an important pathogenic site at position 139 [16], were different from the corresponding aa of ZKC2P6. Moreover, the hepacivirus genera HCV also belong to the family of the Flaviviridae, though not the flaviviruses [26]. Our results about the enhanced ZIKV replication, neurovirulence, tissue lesions, inflammation/necrosis, and apoptosis after E protein glycosylation ablation are in line with the fact that the deletion of N-glycosylation sites of HCV E1 envelope protein enhances specific cellular and humoral immune responses [27]. In the present study, we also verified that ZKC2P6 did not infect the GFAP+ glial cells, NeuN+ neurons, and Sox2 + neural stem cells (Figure 3(c)), which is consistent with the conclusion that ZIKV did not infect NeuN+ neurons and GFAP+ glial cells in normal adult human brain tissues [28]. However, ZIKV in Sox2+ and NeuN+ cells in the subventricular zone and dentate gyrus of the adult mouse brain were quantified in another study [29]. Meanwhile, consistent with the enhanced infectivity, envelope protein glycosylation ablation of ZKC2P6 predictively induced apoptosis of nerve cells in the brain in our study (Figure 4).

In conclusion, we identified a novel ZIKV strain, named ZKC2P6, that is the first Asian strain with a glycosylation motif deficiency caused by aa deletion during newborn mouse brain passage. Furthermore, we revealed that ZKC2P6 exhibited a greater ability to replicate and caused severer neurovirulence and cell apoptosis in newborn mice.

## Data Availability

The data supporting the conclusions of this article are included in the article.

## Conflicts of Interest

The authors have no conflicts of interest to declare.

## Authors' Contributions

Y.G. conducted all the experiments and drafted the manuscript. Q.L. performed the cell experiments. F.L. performed the animal experiments. Y.X. performed the histological assessments and immunofluorescence. Y.G., L.B., and F.F. designed the experiments and edited the manuscript. Q.C. provided overall supervision and financial support and prepared the final version of the manuscript. All the authors read and approved the final manuscript.

## Acknowledgments

This work was supported by the Chinese National Major S&T project (2017ZX10304402-001), the National Key Research and Development Project of China (2016YFD0500304), the CAMS Initiative for Innovative Medicine (2016-12M-1-014 and 2016-12M-006), the PUMC Youth Fund (2017310017 and 2017310050), and the Fundamental Research Funds for the Central Universities.

## Supplementary Materials

Supplemental information for this article includes one table. *(Supplementary Materials)*

## References

[1] G. W. Dick, S. F. Kitchen, and A. J. Haddow, "Zika virus. I. Isolations and serological specificity," *Transactions of the Royal Society of Tropical Medicine and Hygiene*, vol. 46, no. 5, pp. 509–520, 1952.

[2] S. J. Hung and S. W. Huang, "Contributions of genetic evolution to Zika virus emergence," *Frontiers in Microbiology*, vol. 12, p. 655065, 2021.

[3] L. G. Gallo, J. Martinez-Cajas, H. M. Peixoto et al., "Another piece of the Zika puzzle: assessing the associated factors to

microcephaly in a systematic review and meta-analysis," *BMC Public Health*, vol. 20, no. 1, p. 827, 2020.

[4] A. D. Haddow, A. J. Schuh, C. Y. Yasuda et al., "Genetic characterization of Zika virus strains: geographic expansion of the Asian lineage," *PLoS Neglected Tropical Diseases*, vol. 6, no. 2, p. e1477, 2012.

[5] G. Kuno and G. J. Chang, "Full-length sequencing and genomic characterization of Bagaza, Kedougou, and Zika viruses," *Archives of Virology*, vol. 152, no. 4, pp. 687–696, 2007.

[6] C. Li, D. Xu, Q. Ye et al., "Zika virus disrupts neural progenitor development and leads to microcephaly in mice," *Cell Stem Cell*, vol. 19, no. 1, pp. 120–126, 2016.

[7] W. C. Huang, R. Abraham, B. S. Shim, H. Choe, and D. T. Page, "Zika virus infection during the period of maximal brain growth causes microcephaly and corticospinal neuron apoptosis in wild type mice," *Scientific Reports*, vol. 6, no. 1, p. 34793, 2016.

[8] M. T. Aliota, E. A. Caine, E. C. Walker, K. E. Larkin, E. Camacho, and J. E. Osorio, "Characterization of lethal Zika virus infection in AG129 mice," *PLOS Neglected Tropical Diseases*, vol. 10, no. 4, 2016.

[9] D. Sirohi, Z. Chen, L. Sun et al., "The 3.8 A resolution cryo-EM structure of Zika virus," *Science*, vol. 352, no. 6284, pp. 467–470, 2016.

[10] O. Faye, C. C. M. Freire, A. Iamarino et al., "Molecular evolution of Zika virus during its emergence in the 20(th) century," *PLoS Neglected Tropical Diseases*, vol. 8, no. 1, p. e2636, 2014.

[11] L. Liu, S. Zhang, J. S. De Wu et al., "Identification and genetic characterization of Zika virus isolated from an imported case in China," *Infection, Genetics and Evolution*, vol. 48, pp. 40–46, 2017.

[12] R. S. Lanciotti, O. L. Kosoy, J. J. Laven et al., "Genetic and serologic properties of Zika virus associated with an epidemic, Yap State, Micronesia, 2007," *Emerging Infectious Diseases*, vol. 14, no. 8, pp. 1232–1239, 2008.

[13] M. H. Huang, H. Li, R. Xue et al., "Up-regulation of glycolipid transfer protein by bicyclol causes spontaneous restriction of hepatitis C virus replication," *Acta Pharmaceutica Sinica B*, vol. 9, no. 4, pp. 769–781, 2019.

[14] F. C. M. Iani, M. Giovanetti, V. Fonseca et al., "Epidemiology and evolution of Zika virus in Minas Gerais, Southeast Brazil," *Infection, Genetics and Evolution*, vol. 91, p. 104785, 2021.

[15] S. H. Gu, D. H. Song, D. Lee et al., "Whole-genome sequence analysis of Zika virus, amplified from urine of traveler from the Philippines," *Virus Genes*, vol. 53, no. 6, pp. 918–921, 2017.

[16] L. Yuan, X. Y. Huang, Z. Y. Liu et al., "A single mutation in the prM protein of Zika virus contributes to fetal microcephaly," *Science*, vol. 358, no. 6365, pp. 933–936, 2017.

[17] F. R. Cugola, I. R. Fernandes, F. B. Russo et al., "The Brazilian Zika virus strain causes birth defects in experimental models," *Nature*, vol. 534, no. 7606, pp. 267–271, 2016.

[18] T. J. Chambers, M. Halevy, A. Nestorowicz, C. M. Rice, and S. Lustig, "West Nile virus envelope proteins: nucleotide sequence analysis of strains differing in mouse neuroinvasiveness," *The Journal of General Virology*, vol. 79, no. 10, pp. 2375–2380, 1998.

[19] J. A. Mondotte, P. Y. Lozach, A. Amara, and A. V. Gamarnik, "Essential role of dengue virus envelope protein N glycosylation at asparagine-67 during viral propagation," *Journal of Virology*, vol. 81, no. 13, pp. 7136–7148, 2007.

[20] S. C. Adams, A. K. Broom, L. M. Sammels et al., "Glycosylation and antigenic variation among Kunjin virus isolates," *Virology*, vol. 206, no. 1, pp. 49–56, 1995.

[21] D. L. Carbaugh, R. S. Baric, and H. M. Lazear, "Envelope protein glycosylation mediates Zika virus pathogenesis," *Journal of Virology*, vol. 93, no. 12, 2019.

[22] V. A. Kostyuchenko, E. X. Y. Lim, S. Zhang et al., "Structure of the thermally stable Zika virus," *Nature*, vol. 533, no. 7603, pp. 425–428, 2016.

[23] D. L. Carbaugh and H. M. Lazear, "Flavivirus envelope protein glycosylation: impacts on viral infection and pathogenesis," *Journal of Virology*, vol. 94, no. 11, 2020.

[24] M. Mossenta, S. Marchese, M. Poggianella, J. L. Slon Campos, and O. R. Burrone, "Role of N-glycosylation on Zika virus E protein secretion, viral assembly and infectivity," *Biochemical and Biophysical Research Communications*, vol. 492, no. 4, pp. 579–586, 2017.

[25] C. R. Fontes-Garfias, C. Shan, H. Luo et al., "Functional analysis of glycosylation of Zika virus envelope protein," *Cell Reports*, vol. 21, no. 5, pp. 1180–1190, 2017.

[26] H. Li, M. H. Huang, J. D. Jiang, and Z. G. Peng, "Hepatitis C: from inflammatory pathogenesis to anti-inflammatory/hepatoprotective therapy," *World Journal of Gastroenterology*, vol. 24, no. 47, pp. 5297–5311, 2018.

[27] M. Liu, H. Chen, F. Luo et al., "Deletion of N-glycosylation sites of hepatitis C virus envelope protein E1 enhances specific cellular and humoral immune responses," *Vaccine*, vol. 25, no. 36, pp. 6572–6580, 2007.

[28] Z. Zhu, M. J. Gorman, L. D. McKenzie et al., "Zika virus has oncolytic activity against glioblastoma stem cells," *The Journal of Experimental Medicine*, vol. 214, no. 10, pp. 2843–2857, 2017.

[29] H. Li, L. Saucedo-Cuevas, J. A. Regla-Nava et al., "Zika virus infects neural progenitors in the adult mouse brain and alters proliferation," *Cell Stem Cell*, vol. 19, no. 5, pp. 593–598, 2016.

Hindawi
Journal of Immunology Research
Volume 2021, Article ID 9998517, 9 pages
https://doi.org/10.1155/2021/9998517

*Research Article*

# Alpinetin Attenuates Persistent Inflammation, Immune Suppression, and Catabolism Syndrome in a Septic Mouse Model

**Yukun Liu,[1] Kang Wang,[2] Qaunrui Feng,[3] Yongsheng Zhang,[3] Chuntao Wang,[3] Qinxin Liu,[3] Xinghua Liu,[3] Xiang Wang,[3] Wei Gao,[3] Xiangjun Bai,[3] Zhanfei Li,[3] and Yuchang Wang[3]**

[1]*Department of Plastic Surgery, Tongji Hospital of Tongji Medical College, Huazhong University of Science and Technology, Wuhan 430030, China*
[2]*Digestive Disease Center, Seventh Affiliated Hospital, Sun Yat-sen University, Shenzhen 518107, China*
[3]*Trauma Center/Department of Emergency and Traumatic Surgery, Tongji Hospital of Tongji Medical College, Huazhong University of Science and Technology, Wuhan 430030, China*

Correspondence should be addressed to Yuchang Wang; tjwangyuchang@tjh.tjmu.edu.cn

Received 24 March 2021; Revised 20 May 2021; Accepted 19 June 2021; Published 5 July 2021

Academic Editor: Meng-Hao Huang



Patients who survive the acute phase of sepsis can progress to persistent inflammation, immunosuppression, and catabolism syndrome (PICS), which usually results in extended recovery periods and multiple complications. Alpinetin is a flavonoid isolated from Alpinia katsumadai Hayata that has been demonstrated to have anti-inflammatory, antibacterial, and antioxidant activities. The aim of this study was to investigate whether the administration of alpinetin could attenuate PICS in a septic mouse model. Mice were randomly divided into four groups: the (1) sham-operated group, (2) sham+alpinetin (1 mg/kg intravenously infused for once per day after sham operation), (3) cecal ligation and puncture (CLP), and (4) CLP+alpinetin (50 mg/kg intravenously infused for once per day after CLP). Eight days after sham operation or CLP surgery, mice were euthanized for subsequent examination. Alpinetin significantly improved the survival of septic mice. Also, it attenuated the CLP-induced persistent inflammation, immunosuppression, and catabolism syndrome. The level of plasma proinflammatory cytokines and apoptosis of T lymphocytes were obviously decreased by alpinetin as well. Moreover, oxidative stress in the organs was compelling lower in the alpinetin-treated CLP mice. In this clinically relevant model of sepsis, alpinetin ameliorates CLP-induced organ dysfunction and improves the likelihood of survival, possibly through suppressing the inflammatory response, oxidative stress, and apoptosis. These findings suggested that alpinetin could be a potential novel therapeutic approach to prevent sepsis-induced PICS.

## 1. Introduction

The advancements of diagnosis and management have substantially improved the overall survival rate of sepsis in the past few decades. Unfortunately, long-term outcomes in sepsis survivors have not been improved over time, usually resulting in a state of chronic critical illness [1]. Some sepsis survivors present with typical syndromes that follow the SIRS-CARS reaction: persistent inflammation, immunosuppression, and catabolism syndrome (PICS), marked by recurrent nosocomial infections, inadequate nutrition, and the need for long-term skilled nursing. Physiologically, these states are generally characterized by sustained inflammation, suppressed host immunity, and the loss of lean muscle mass [2, 3]. Many patients are suffering from prolonged recovery times and often progress to chronic critical illness (CCI) with less than 50% of patients surviving 1 year after hospital discharge [4, 5]. Nevertheless, no specific and effective pharmacological intervention is currently available for PICS.

Although the PICS hypothesis has been validated early in 2012 [6], the precise mechanism remains as yet incomplete. Unbalance of persistent inflammation and progressive

immunosuppression were widely accepted to be the basic mechanisms of PICS. This persistent inflammation is characterized by increased concentration of plasma IL-6, neutrophilia, etc. The reason contributing to an immunosuppressive state is marked by T cell exhaustion and increased proportions of regulatory T cells (Tregs), lymphopenia, etc. [7]. Lymphopenia is considered a typical sign of immunosuppression in clinical practice [6]. Therefore, the development of new agents that have the ability of anti-inflammation in addition to modulating immunity may be useful for the treatment of PICS.

Alpinetin is a Chinese traditional medicine usually isolated from the plants of Alpinia katsumadai Hayata. This drug has been reported to have varieties of biological activities, including antibacterial, antioxidative, and anti-inflammatory [8, 9]. Numerous studies have suggested that alpinetin has a protective effect on ulcerative colitis and kidney injury in mice by regulating inflammation [8, 9]. However, whether alpinetin had protective effects against sepsis-induced PICS has not yet been fully explored. In the present study, we aimed to testify the protective effects of alpinetin on PICS.

## 2. Methods

*2.1. Animal.* Six-week-old male C57BL/6 mice were housed in standard environmental conditions with a 12 h/12 h light/-dark conditions and fed with standard commercial chow with free access to water. This study was approved by the local institutional review board, and the experiments were performed and were approved by the Animal Ethics Committee of Tongji Hospital, Tongji Medical College, Huazhong University of Science and Technology.

*2.2. PICS Model of Sepsis.* Sepsis-induced PICS models were established by CLP as previously described [3]. Briefly, seven- to eight-week-old male mice (22–26 g) were used in all experiments. Mice were anesthetized with pentobarbital sodium (40 mg/kg) injected intraperitoneally (i.p.). Sham-operated mice underwent the same protocol without the CLP procedure. Finally, mice were resuscitated with sterile saline (50 mL/kg) injected subcutaneously.

*2.3. Experimental Protocol.* C57BL/6 male mice were randomly divided into four groups: the (1) sham-operated group, (2) sham +alpinetin group, (3) CLP group, and (4) CLP+alpinetin (50 mg/kg) group. Eight days after sham operation or CLP surgery, mice were euthanized for subsequent examination. Alpinetin was purchased from the National Institute for the Control of Pharmaceutical and Biological Products (Beijing, China). The dose of alpinetin was selected according to previous reports [10].

*2.4. Flow Cytometry.* Single-cell suspensions of the spleen were prepared as previously described. Cell counts were determined using a Coulter Ac T 10 cell counter (Beckman Coulter, Brea, CA, USA). Cells were then resuspended in a flow cytometry buffer (1% bovine serum PBS), and nonspecific binding was blocked by a preincubation with 5% rat serum (Invitrogen, Life Technologies, Grand Island, NY, USA) and 1 $\mu$L/sample of Fc Block (BD Pharmingen, San Jose, CA, USA). The following cell types were identified using the following antibody combinations: neutrophils (Ly-6G and CD11b) and CD4 T cells, CD3 and CD4 T cells, and CD8 T cells (CD3 and CD8).

*2.5. ELISA.* TNF-$\alpha$ and IL-6 levels in serum were measured using ELISA kits (BioLegend, CA, USA) according to the manufacturer's instructions.

*2.6. Histological Examination.* Lung tissues were fixed overnight in 4% paraformaldehyde and embedded in paraffin. Then, sections were cut into 5 $\mu$m, and hematoxylin-eosin (H&E) staining was performed. Histopathological examinations were carried out using a microscope (RX51, Olympus Optical Co., Ltd., Tokyo, Japan). The histological examination was performed in a blinded fashion using a scoring system previously validated and described.

*2.7. Measurement of ROS and SOD Level.* Tissues of the lung and spleen were cut into cubes, and the dispersed cells filtered with a 300-mesh nylon net. After washing with cold PBS, the fluorescence intensity of ROS was measured with excitation wavelength at 500 nm and emission wavelength at 525 nm using reactive oxygen species assay kits (Nanjing Jiancheng Bioengineering Institute, China) following the manufacturer's protocols.

Tissues of the lung and spleen were homogenized using a tissue grinder and determined using BCA Protein Assay Kits. The activity of SOD was assessed using SOD assay kits (Nanjing Jiancheng Bioengineering Institute) according to the manufacturer's instructions.

*2.8. Statistical Analysis.* All statistical analyses were completed using GraphPad Prism 8.0 (USA). All data were presented as mean ± SD. Normally distributed data were determined by one-way analysis of variance (ANOVA), followed by the Tukey post hoc test. Nonnormally distributed data were analyzed with nonparametric Wilcoxon tests. Survival data were analyzed using the Kaplan-Meier method, and survival curves were compared using the log-rank test and Gehan-Breslow-Wilcoxon test in univariate analysis. Statistical significance was defined as $p$ value $< 0.05$.

## 3. Results

*3.1. Alpinetin Improved the Survival of CLP Septic Mice.* To evaluate the effect of alpinetin administration on the survival of CLP-operated mice, mice were divided into four groups as shown in Figure 1 and monitored for 8 days. The survival rate in the CLP group (survival: 6 of 30 mice, 20.0%) was significantly lower than that in the sham and sham+alpinetin groups (survival: 10 of 10 mice, 100% in sham and sham+alpinetin groups, $p < 0.001$). Interestingly, the administration of alpinetin significantly improved the survival rate to 53.3% in the CLP+alpinetin group (survival: 8 of 15 mice, $p < 0.05$).

*3.2. Alpinetin Alleviated Inflammation in CLP-Induced PICS in Mice.* To determine the effects of alpinetin on

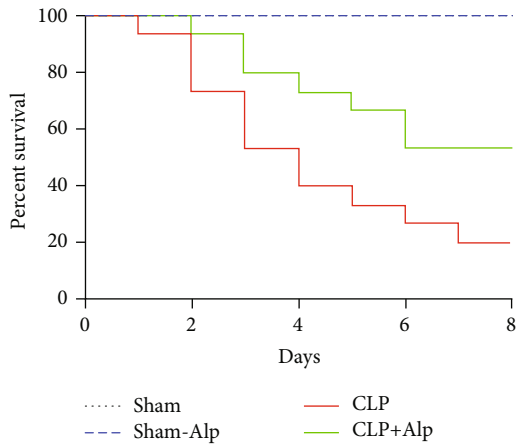


Figure 1: Effect of alpinetin on the survival of CLP septic mice. Mice were intravenously administered with alpinetin (50 mg/kg) in the sham+alpinetin and CLP+alpinetin groups, and the survival rates of the mice were monitored for 8 days. Survival data were analyzed using the Kaplan-Meier method, and survival curves were compared using the log-rank test and Gehan-Breslow-Wilcoxon test in univariate analysis. $^{***}p < 0.001$, CLP vs. sham; $^{\#}p < 0.05$, CLP-Alp vs. CLP.

inflammation, numbers of neutrophils in the spleen and blood were detected eight days after CLP. Weight of the spleen, splenocytes, and number of neutrophils in the spleen and blood increased in the CLP group, which were consistent with the characteristics of PICS. Alpinetin significantly decreased the weight of the spleen and the number of white blood cells compared with those in the CLP group (Figures 2(a) and 2(b)). Additionally, we observed that the number of neutrophils in the spleen and blood was significantly decreased in the CLP+alpinetin group (Figures 2(c) and 2(d)). Furthermore, there were notable increases in IL-6 and TNF-$\alpha$ levels in the serum of CLP which were reduced by alpinetin treatment (Figures 2(e) and 2(f)). These results suggested that alpinetin significantly attenuated inflammation in sepsis-induced PICS.

*3.3. Alpinetin Improved Immunosuppression in CLP-Induced PICS.* Lymphopenia (lymphocyte count < 800/mm$^3$) is considered to be an important clinical feature in PICS [6]. The loss of T cells is a key determinant of immune suppression. This is of particular importance as studies did reveal that persistent lymphopenia is related to increased mortality and secondary infections in severely ill intensive care patients [11]. In a murine PICS model, lymphopenia was depicted in a quantitative loss of CD4$^+$ and CD8$^+$ T cells [3]. In our study, we examined splenic T cell numbers eight days after CLP. We observed that the total CD4$^+$ and CD8$^+$ T cell numbers from septic mice are significantly decreased in the CLP group and significantly suppressed in the CLP+alpinetin group (Figures 3(a) and 3(b)), suggesting that alpinetin improved the immunosuppression in CLP-induced PICS.

*3.4. Alpinetin Improved Catabolism in CLP-Induced PICS.* Most septic patients display a rapid loss of lean muscle mass due to sustained catabolism. The decrease in muscle mass associated with sepsis is not due to a decline in protein synthesis, but rather attributed to an increase in protein breakdown [12]. Literature has implicated an ongoing inflammatory response as the driving force behind prolonged catabolism in sepsis [13]. In a murine PICS model, mice had a leg muscle mass loss of approximately 50% eight days after CLP [3]. To validate this, we evaluated the weight change and thigh muscle mass of mice. In our study, both weight and thigh muscle mass were significantly decreased in the CLP group, but largely increased in the CLP+alpinetin group (Figures 4(a) and 4(b)), suggesting that alpinetin may help to improve nutritional status in PICS.

*3.5. Alpinetin Treatment Inhibited Apoptosis of CD4$^+$ and CD8$^+$ T Cells.* Lymphocyte apoptosis has been reported to play an important role in the pathogenesis of sepsis and is thought to be the main reason that contributes to lymphopenia [14]. To further confirm the effects of alpinetin on T lymphocyte apoptosis, flow cytometry was used to detect the apoptosis of CD4$^+$ and CD8$^+$ T lymphocytes in vivo and apoptosis was labeled with caspase-3$^+$PI$^+$. The percentages of CD4$^+$ and CD8$^+$ T lymphocyte apoptosis were significantly increased in the CLP group, which was in accordance with the previous study. Interestingly, alpinetin administration significantly suppressed the apoptosis of CD4$^+$ and CD8$^+$ T lymphocytes (Figures 5(a) and 5(b)). In a word, our results demonstrated that alpinetin inhibited the activation of caspase-3-dependent apoptosis.

*3.6. Alpinetin Reduces Lung Injury and MPO Activity.* Sustained tissue damage and multiple organ failure are another characteristic of PICS. It is commonly accepted that the lung is the primary target of organ damage in sepsis. Thus, to further investigate the effect of alpinetin on lung inflammation, lung tissues were collected for cell H&E staining and MPO activity. Hemorrhage, alveolar septal thickening, and leukocyte infiltration were observed in PICS mice compared with the sham group. However, these histopathological changes and the lung injury score were significantly attenuated by alpinetin treatment (Figures 6(a) and 6(b)). Inflammatory cell infiltration plays a critical role in lung inflammation and is overwhelmingly the highest contributor to tissue damage. Additionally, myeloperoxidase (MPO) activity is considered to be a marker of inflammatory cell infiltration in lung tissues [15]. As shown in Figure 6(c), MPO activity significantly increased in lung tissues in PICS mice. However, MPO activity was dramatically reduced by the administration of alpinetin. These findings suggest that alpinetin has protective effects against inflammatory injury in PICS.

*3.7. Alpinetin Ameliorates Oxidative Stress in Septic Mice.* Sepsis is characterized by an excess of reactive oxygen species, inducing cellular damage and death, depletion of antioxidants, and accumulation of markers of oxidative stress [16]. Alleviating oxidative stress is considered one of the important mechanisms to treat lung injury [17, 18]. The level of oxidative stress was analyzed by determining ROS level and SOD activity in the lung and spleen. We observed an

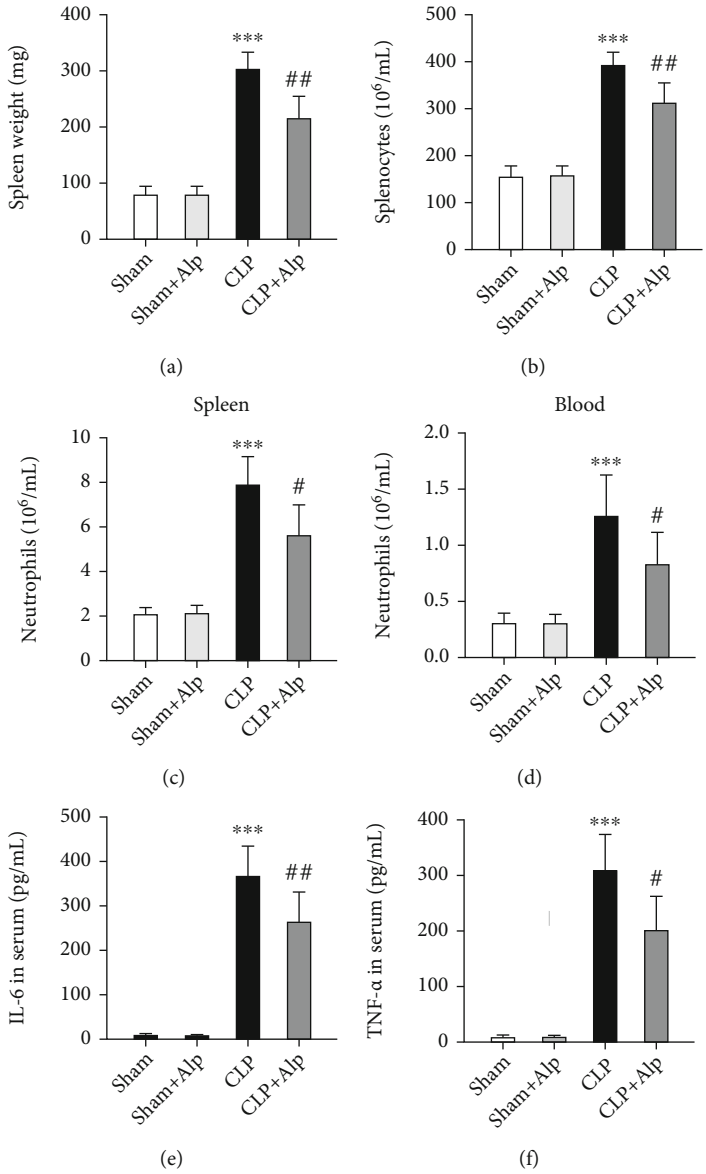


Figure 2: Effects of alpinetin on splenic myelopoiesis and leukocytosis eight days after the procedure. The spleen and blood were collected and analyzed eight days after the cecal ligation and puncture (CLP) operation. (a) Weight, (b) total number of WBCs, (c) neutrophils in the spleen, and (d) neutrophils in the blood. (e) IL-6 and (f) TNF-$\alpha$ in serum were quantified by using ELISA kits. Sham ($n = 10$), sham+Alp ($n = 10$), CLP ($n = 6$), and CLP+Alp ($n = 8$). Data are shown as mean ± SD. $^{***}p < 0.001$, CLP vs. sham; $^{\#}p < 0.05$, $^{\#\#}p < 0.01$, CLP-Alp vs. CLP.

increased ROS in the lung and spleen in the PICS group, and alpinetin reverts back the level of these organs (Figure 7(b)). Regarding antioxidant enzymes, the SOD activity showed significant decrease after sepsis in the meanwhile, and alpinetin was effective in increasing SOD activity level in the lung and spleen (Figure 7(b)).

## 4. Discussion

In this study, we used a rational and scientific method to demonstrate that the CLP procedure evoked PICS, characterized by elevated neutrophil number, increased plasma levels of IL-6 and TNF-$\alpha$, lymphopenia, and loss of weight, which were improved by alpinetin in a mouse model of sepsis-induced PICS. As a result, the intravenous administration of alpinetin improved the survival of the CLP septic mice. Furthermore, alpinetin significantly reduced the apoptosis of $CD4^+$ and $CD8^+$ T lymphocyte and lung injury and reduced lung and spleen superoxide production in PICS mice. Accordingly, these findings suggest that alpinetin attenuates CLP-induced PICS and may be useful as a therapeutic agent to relieve related organ injury.

Alpinetin, a novel plant flavonoid isolated from Alpinia katsumadai Hayata, has anti-inflammatory and antioxidative effects on variable disease processes, such as ulcerative colitis, acute kidney injury, and endometritis [8–10, 19]. In the mouse model of LPS-induced liver injury, alpinetin inhibited

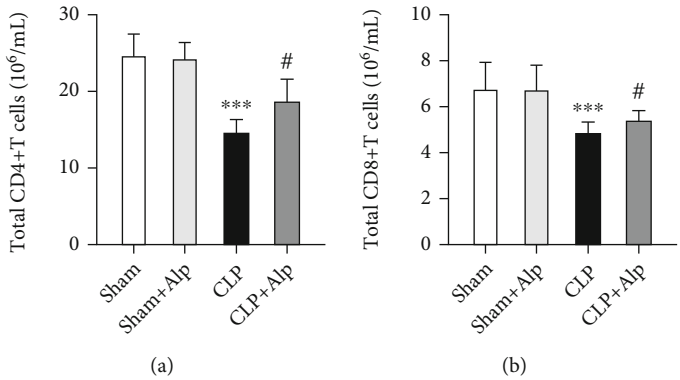


Figure 3: Effects of alpinetin on splenic T cells eight days after the procedure. After eight days, animals were sacrificed and the spleens were removed. Flow cytometry was then used to characterize the number of (a) total $CD4^+$ T cells and (b) total $CD8^+$ T cells in each group. Sham ($n = 10$), sham+Alp ($n = 10$), CLP ($n = 6$), and CLP+Alp ($n = 8$). Data are shown as mean ± SD. $^{***}p < 0.001$, CLP vs. sham; $^{\#}p < 0.05$, CLP-Alp vs. CLP.

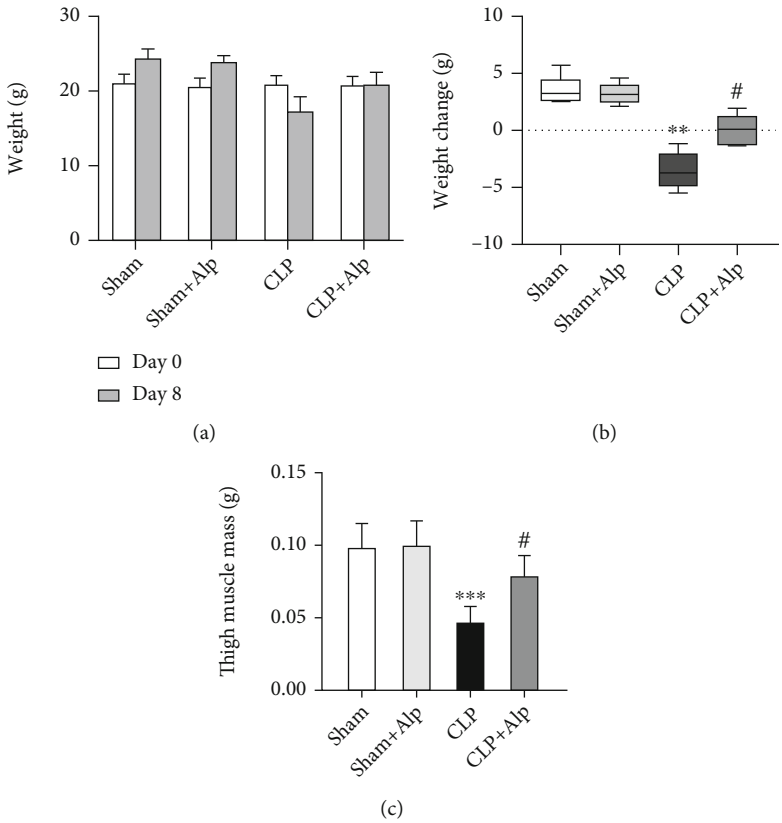


Figure 4: Effects of alpinetin on weight changes after the procedure. (a) Mice were weighed before the operation (day 0) and on the eighth day after the procedure (day 8). Groups were then compared in terms of (b) absolute change in weight and (c) thigh muscle weight. Sham ($n = 10$), sham+Alp ($n = 10$), CLP ($n = 6$), and CLP+Alp ($n = 8$). Data are shown as mean ± SD. $^{**}p < 0.01$, $^{***}p < 0.001$, CLP vs. sham; $^{\#}p < 0.05$, CLP-Alp vs. CLP.

liver injury through reducing inflammatory cell infiltration and proinflammatory cytokine release [9]. In an in vivo model of ulcerative colitis, dextran sulfate sodium-induced intestinal barrier dysfunction, inflammation, and oxidative stress were attenuated or prevented by alpinetin [8].

The CLP model has been widely used as the gold standard in sepsis models, as it closely mimics the clinical condition of human sepsis [20]. The previous study has implicated that mice which survived eight days after CLP displayed PICS characteristics including lymphocyte depletion, circulating myeloid cell increase, and weight loss [3]. In our present study, results showed that mice that survived eight days not only displayed PICS characteristic but also accompanied by lung injury.

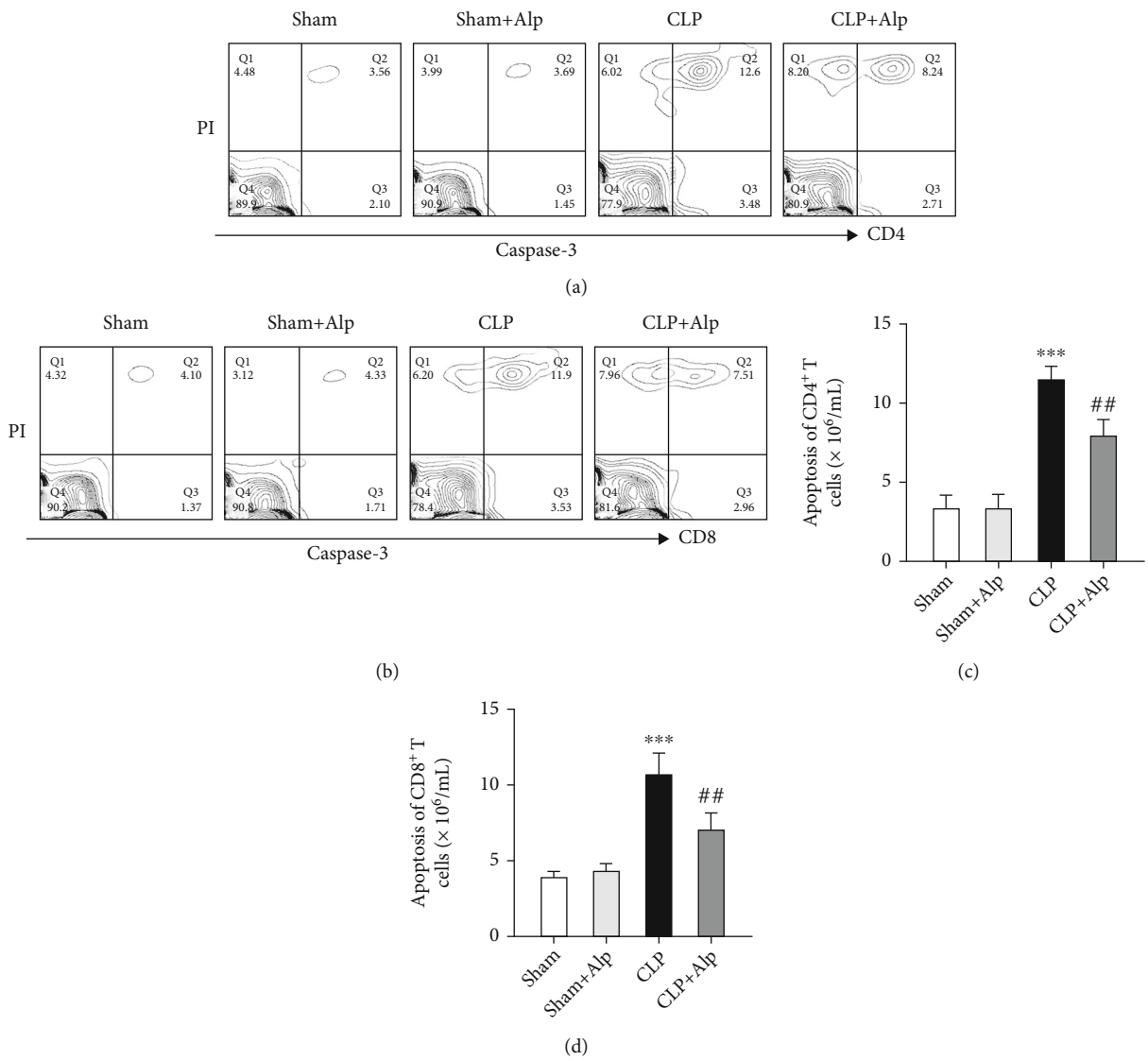


Figure 5: Effects of alpinetin on apoptosis of $CD4^+$ and $CD8^+$ T cells in the spleen. Flow cytometry was then used to evaluate the apoptosis by detecting caspase-3 activation and cell death (PI positive) of $CD4^+$ (a, c) and $CD8^+$ (b, d) T cells in the spleen on the eighth day. Sham ($n = 8$), sham+Alp ($n = 8$), CLP ($n = 6$), and CLP+Alp ($n = 8$). Data are shown as mean ± SD. $^{***}p < 0.001$, CLP vs. sham; $^{\#\#}p < 0.01$, CLP-Alp vs. CLP.

Recent studies demonstrated that the increasing apoptosis of immune cells plays a pivotal role in immunosuppression and consequent organ dysfunction, which were observed in sepsis [14, 21]. Animal studies showed that the blockade of cell apoptosis could improve the survival rate in a sepsis model [14]. Studies have revealed that alpinetin could attenuate chronic obstructive pulmonary disease (COPD) and colitis by inhibiting apoptosis [22, 23]. Su et al. have recently reported that alpinetin can reduce the activity of caspase-3 and caspase-9 in COPD rats, inhibit the occurrence of alveolar cell apoptosis, and reduce the release of inflammatory factors by reducing the activities of TGF-$\beta$1, TNF-$\alpha$, and $\alpha$-SMA [23]. In the present study, there was obvious downregulation of the expression of caspase-3 in T cells of PICS mice after alpinetin intervention. Alpinetin ameliorated lymphopenia and the apoptosis of $CD4^+$ T and $CD8^+$ T lymphocytes in the spleen of PICS mice. Results indicated that alpinetin could attenuate cell death and immunosuppression of T lymphocytes induced by sepsis. Additionally, apoptosis can be triggered by a variety of stimuli including inflammatory cytokines and ROS. ROS has been extensively implicated in T cell hyporesponsiveness, apoptosis, and activation [24, 25]. To validate this hypothesis, the levels of ROS and SOD were measured to assess the degree of oxidative stress in the spleen of PICS mice. In our study, PICS triggered ROS overproduction and SOD hypoactivity in the spleen, indicating that the elevated levels of oxidative stress exist and may facilitate T lymphocyte apoptosis in PICS mice. However, both apoptosis of T cells and oxidative stress in the spleen were suppressed by alpinetin. Therefore, alpinetin may exert its antiapoptotic effect by reducing the production of superoxide. Taken together, these results

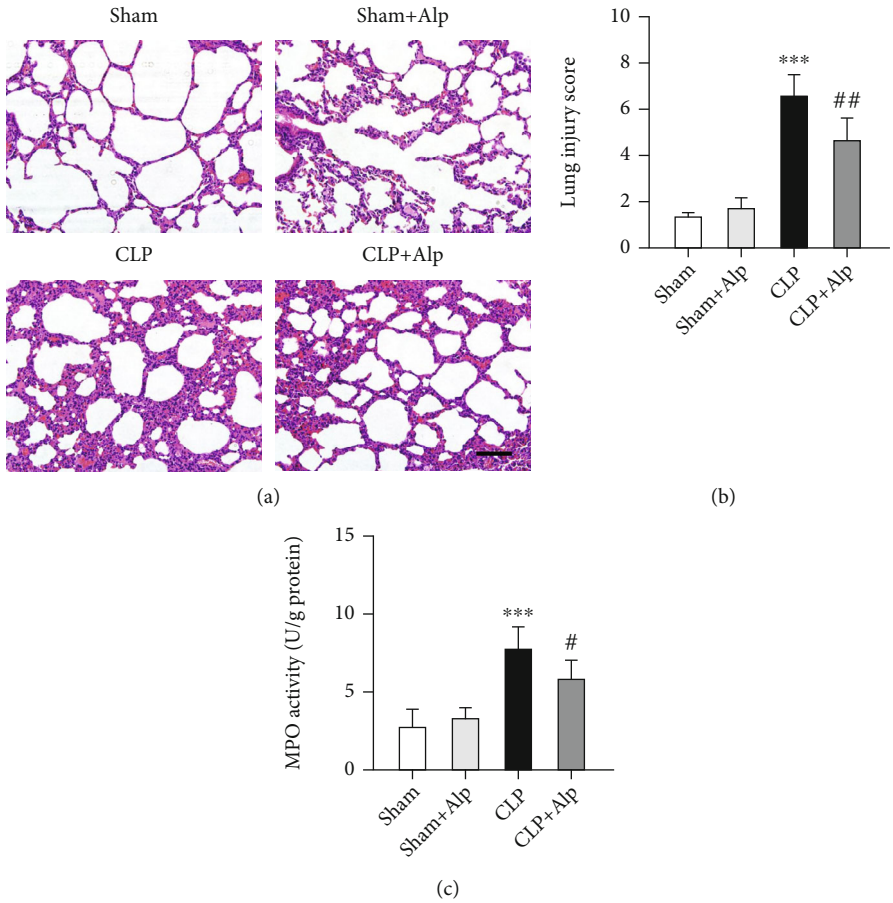


Figure 6: Effects of alpinetin on lung injury and MPO activity. (a) Representative images of H&E-stained lung tissues from different groups. (b) Lung injury score. (c) MPO activity was analyzed using MPO Assay Kits. The scale bar is 50 $\mu$m. Sham ($n = 8$), sham+Alp ($n = 8$), CLP ($n = 6$), and CLP+Alp ($n = 8$). Data are shown as mean ± SD. $^{***}p < 0.001$, CLP vs. sham; $^{\#\#}p < 0.01$, CLP-Alp vs. CLP.

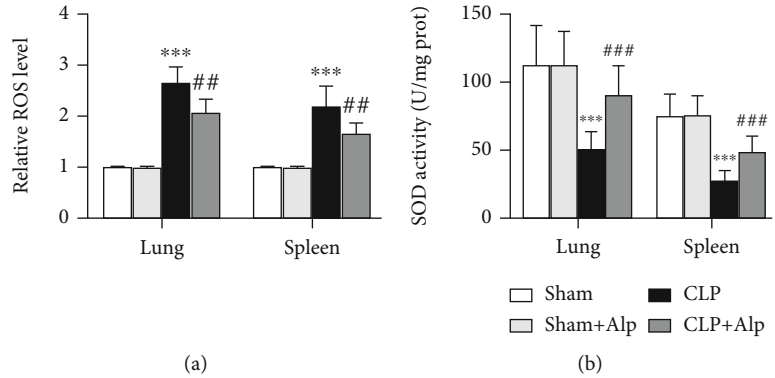


Figure 7: Effects of alpinetin on oxidative stress in CLP-induced PICS. After eight days, animals were sacrificed and the lung, liver, and kidney were removed. (a) The ROS levels in the mouse lung and spleen were assessed using commercial reactive oxygen species assay kits. (b) The SOD activity in mouse lung and spleen tissues was evaluated using commercial SOD assay kits. Sham ($n = 8$), sham+Alp ($n = 8$), CLP ($n = 6$), and CLP+Alp ($n = 6$). Data are shown as mean ± SD. $^{***}p < 0.001$, CLP vs. sham; $^{\#\#}p < 0.01$, $^{\#\#\#}p < 0.001$, CLP-Alp vs. CLP.

indicate that alpinetin attenuates CLP-induced PICS through its counterregulatory action to mediate the resolution of inflammation, oxidative stress, and apoptosis.

Death from sepsis is not thought to be related to infection itself but associated with organ failure that results from the systemic response to infection [26]. Lung injury is one of the most frequent organ dysfunctions in sepsis. We found that alpinetin administration exhibited the tendency to ameliorate lung injury as shown by decreased inflammatory cell infiltration and MPO. Evidence has indicated that oxidative

stress, which is induced by ROS accumulation and reduced activity of antioxidant enzymes, plays a crucial role in the progress of organ failure in sepsis [16, 18, 27–29]. In our study, along with the increase in ROS, the activity of SOD decreases in the lung of PICS mice. However, alpinetin exhibited antioxidative action in the lung of PICS as evidenced by upregulation of SOD, accompanied by the decrease in ROS. These findings indicated that alpinetin may attenuate inflammation and lung injury via inhibiting oxidative stress in the lung of PICS.

## 5. Conclusions

In conclusion, the present study described a novel function of alpinetin in alleviating CLP-induced PICS. Alpinetin attenuates PICS and related organ injury in the mouse model by anti-inflammation effect in addition to inhibiting apoptosis of T lymphocytes, which may be involved in oxidative stress. Further studies, in particular clinical trials, are necessary to verify the potential adjuvant effect of alpinetin in PICS.

## Data Availability

The data are presented within the paper. Additional raw data are available on request from the corresponding author.

## Ethical Approval

All animal procedures in this study complied with the guidelines provided by the Animal Ethics Committee of Tongji Hospital, Tongji Medical College, Huazhong University of Science and Technology.

## Conflicts of Interest

The authors declare no conflict of interest.

## Authors' Contributions

Yukun Liu, Yuchang Wang, and Zhanfei Li designed the project. Qaunrui Feng, Yongsheng Zhang, Chuntao Wang, Qinxin Liu, Xiang Wang, and Xinghua Liu performed the experiments. Wei Gao and Xiangjun Bai provided technical support. Yuchang Wang and Yukun Liu analyzed the data. Yukun Liu, Kang Wang, and Yuchang Wang wrote the manuscript.

## Acknowledgments

The authors would like to thank all staff from the Laboratory of Trauma Center, Tongji Hospital, for their technical assistance during the experimental study. This study was supported by grants from the National Natural Science Foundation of China (Grant Nos. 82002101, 82002096, 81571891, and 81772129).

## References

[1] M. Shankar-Hari and G. D. Rubenfeld, "Understanding long-term outcomes following sepsis: implications and challenges," *Current Infectious Disease Reports*, vol. 18, no. 11, p. 37, 2016.

[2] H. Horiguchi, T. J. Loftus, R. B. Hawkins et al., "Innate immunity in the persistent inflammation, immunosuppression, and catabolism syndrome and its implications for therapy," *Front Immunol.*, vol. 9, p. 595, 2018.

[3] A. M. Pugh, N. J. Auteri, H. S. Goetzman, C. C. Caldwell, and V. Nomellini, "A murine model of persistent inflammation, immune suppression, and catabolism syndrome," *International Journal of Molecular Sciences*, vol. 18, no. 8, p. 1741, 2017.

[4] R. B. Hawkins, S. L. Raymond, J. A. Stortz et al., "Chronic critical illness and the persistent inflammation, immunosuppression, and catabolism syndrome," *Frontiers in Immunology*, vol. 9, p. 1511, 2018.

[5] J. C. Mira, L. F. Gentile, B. J. Mathias et al., "Sepsis pathophysiology, chronic critical illness, and persistent inflammation-immunosuppression and catabolism syndrome," *Critical Care Medicine*, vol. 45, no. 2, pp. 253–262, 2017.

[6] L. F. Gentile, A. G. Cuenca, P. A. Efron et al., "Persistent inflammation and immunosuppression: a common syndrome and new horizon for surgical intensive care," *Journal of Trauma and Acute Care Surgery*, vol. 72, no. 6, pp. 1491–1501, 2012.

[7] C. B. Bergmann, N. Beckmann, C. E. Salyer, P. A. Crisologo, V. Nomellini, and C. C. Caldwell, "Lymphocyte immunosuppression and dysfunction contributing to persistent inflammation, immunosuppression and catabolism syndrome (PICS)," *Shock*, vol. 55, no. 6, pp. 723–741, 2020.

[8] Y. Tan and C. Zheng, "Effects of alpinetin on intestinal barrier function, inflammation and oxidative stress in dextran sulfate sodium-induced ulcerative colitis mice," *The American Journal of the Medical Sciences*, vol. 355, no. 4, pp. 377–386, 2018.

[9] T. G. Liu, K. H. Sha, L. G. Zhang, X. X. Liu, F. Yang, and J. Y. Cheng, "Protective effects of alpinetin on lipopolysaccharide/d-galactosamine-induced liver injury through inhibiting inflammatory and oxidative responses," *Microbial Pathogenesis*, vol. 126, pp. 239–244, 2019.

[10] Y. Huang, L. S. Zhou, L. Yan, J. Ren, D. X. Zhou, and S. S. Li, "Alpinetin inhibits lipopolysaccharide-induced acute kidney injury in mice," *International Immunopharmacology*, vol. 28, no. 2, pp. 1003–1008, 2015.

[11] C. Adrie, M. Lugosi, R. Sonneville et al., "Persistent lymphopenia is a risk factor for ICU-acquired infections and for death in ICU patients with sustained hypotension at admission," *Annals of Intensive Care*, vol. 7, no. 1, p. 30, 2017.

[12] M. Klaude, M. Mori, I. Tjader, T. Gustafsson, J. Wernerman, and O. Rooyackers, "Protein metabolism and gene expression in skeletal muscle of critically ill patients with sepsis," *Clinical Science (London, England)*, vol. 122, no. 3, pp. 133–142, 2012.

[13] M. Rosenthal, A. Gabrielli, and F. Moore, "The evolution of nutritional support in long term ICU patients: from multisystem organ failure to persistent inflammation immunosuppression catabolism syndrome," *Minerva Anestesiologica*, vol. 82, no. 1, pp. 84–96, 2016.

[14] Y. Y. Luan, Y. M. Yao, X. Z. Xiao, and Z. Y. Sheng, "Insights into the apoptotic death of immune cells in sepsis," *Journal of Interferon & Cytokine Research*, vol. 35, no. 1, pp. 17–22, 2015.

[15] Y. C. Wang, Q. X. Liu, Q. Zheng et al., "Dihydromyricetin alleviates sepsis-induced acute lung injury through inhibiting NLRP3 inflammasome-dependent pyroptosis in mice model," *Inflammation*, vol. 42, no. 4, pp. 1301–1310, 2019.

[16] K. Mantzarlis, V. Tsolaki, and E. Zakynthinos, "Role of oxidative stress and mitochondrial dysfunction in sepsis and potential therapies," *Oxidative Medicine and Cellular Longevity*, vol. 2017, Article ID 5985209, 10 pages, 2017.

[17] Y. L. Ni, H. T. Shen, C. H. Su et al., "Nerolidol suppresses the inflammatory response during lipopolysaccharide-induced acute lung injury via the modulation of antioxidant enzymes and the AMPK/Nrf-2/HO-1 pathway," *Oxidative Medicine and Cellular Longevity*, vol. 2019, Article ID 9605980, 10 pages, 2019.

[18] W. Xia, Z. Pan, H. Zhang, Q. Zhou, and Y. Liu, "Inhibition of ERR$\alpha$ aggravates sepsis-induced acute lung injury in rats via provoking inflammation and oxidative stress," *Oxidative Medicine and Cellular Longevity*, vol. 2020, Article ID 2048632, 9 pages, 2020.

[19] Y. Liang, T. Shen, Q. Ming et al., "Alpinetin ameliorates inflammatory response in LPS-induced endometritis in mice," *International Immunopharmacology*, vol. 62, pp. 309–312, 2018.

[20] L. Dejager, I. Pinheiro, E. Dejonckheere, and C. Libert, "Cecal ligation and puncture: the gold standard model for polymicrobial sepsis?," *Trends in Microbiology*, vol. 19, no. 4, pp. 198–208, 2011.

[21] M. Aziz, A. Jacob, and P. Wang, "Revisiting caspases in sepsis," *Cell Death & Disease*, vol. 5, no. 11, article e1526, 2014.

[22] Y. Miao, Q. Lv, S. Qiao et al., "Alpinetin improves intestinal barrier homeostasis via regulating AhR/suv39h1/TSC2/mTORC1/autophagy pathway," *Toxicology and Applied Pharmacology*, vol. 384, p. 114772, 2019.

[23] Y. Su, X. Tao, and J. Xu, "Protective effect of alpinetin on rats with chronic obstructive pulmonary disease," *Food Science & Nutrition*, vol. 8, no. 12, pp. 6603–6611, 2020.

[24] A. V. Belikov, B. Schraven, and L. Simeoni, "T cells and reactive oxygen species," *Journal of Biomedical Science*, vol. 22, no. 1, p. 85, 2015.

[25] A. Signorile, A. Ferretta, M. Ruggieri et al., "Mitochondria, oxidative stress, cAMP signalling and apoptosis: a crossroads in lymphocytes of multiple sclerosis, a possible role of nutraceutics," *Antioxidants*, vol. 10, no. 1, 2020.

[26] M. Singer, C. S. Deutschman, C. W. Seymour et al., "The Third International Consensus Definitions for Sepsis and Septic Shock (Sepsis-3)," *Journal of the American Medical Association*, vol. 315, no. 8, pp. 801–810, 2016.

[27] B. E. Minter, D. A. Lowes, N. R. Webster, and H. F. Galley, "Differential effects of mitoVitE, $\alpha$-tocopherol and trolox on oxidative stress, mitochondrial function and inflammatory signalling pathways in endothelial cells cultured under conditions mimicking sepsis," *Antioxidants*, vol. 9, no. 3, p. 195, 2020.

[28] J. Y. Kim, J. Leem, and H. L. Hong, "Protective effects of SPA0355, a thiourea analogue, against lipopolysaccharide-induced acute kidney injury in mice," *Antioxidants*, vol. 9, no. 7, p. 585, 2020.

[29] X. Zhong, J. He, X. Zhang et al., "UCP2 alleviates tubular epithelial cell apoptosis in lipopolysaccharide-induced acute kidney injury by decreasing ROS production," *Biomedicine & Pharmacotherapy*, vol. 115, p. 108914, 2019.

Hindawi
Journal of Immunology Research
Volume 2021, Article ID 9979843, 12 pages
https://doi.org/10.1155/2021/9979843

*Research Article*

# Acacetin Protects Myocardial Cells against Hypoxia-Reoxygenation Injury through Activation of Autophagy

**Chong Liu,[1,2] Minmin Zhang,[3] Shenyi Ye,[1,2] Chenliang Hong,[1,2] Jiaxi Chen,[1,2] Ruyue Lu,[1] Bingjie Hu,[1,2] Weijun Yang,[4] Bo Shen,[1,2] and Zhengyi Gu[4]**

[1]*Taizhou Hospital of Zhejiang Province Affiliated to Wenzhou Medical University, 317000 Taizhou, China*
[2]*Enze Hospital, Taizhou Enze Medical Center (Group), 317000 Taizhou, China*
[3]*YiLi Normal University, College of Chinese Language and Literature, YiLi, 835000 Xinjiang, China*
[4]*Xinjiang Institute of Materia Medica, Uygur, Xinjiang Province 830004, China*

Correspondence should be addressed to Weijun Yang; wilfred3106@163.com, Bo Shen; shenb@enzemed.com, and Zhengyi Gu; zhengyi087@126.com

Received 24 March 2021; Accepted 27 May 2021; Published 30 June 2021

Academic Editor: Tingtao Chen



Ischemic heart disease is a leading cause of mortality and morbidity worldwide. We previously demonstrated that acacetin protects against myocardial ischemia reperfusion injury in rats, although the underlying mechanism remains to be elucidated. In the present study, we investigated the effects of acacetin on autophagy during hypoxia/reoxygenation (H/R) injury by exposing H9c2 myocardial cells to H/R with or without acacetin pretreatment during hypoxia. Our results show that acacetin significantly increased cell viability in a dose-dependent manner, enhanced antioxidant capacity, and suppressed protein apoptosis of rat cardiomyocytes H9c2 cells following H/R injury. In addition, lentiviral infection of H9c2 cardiomyocytes revealed that acacetin pretreatment significantly enhanced the fluorescence intensity of autophagy proteins Beclin 1, LC3-II, and p62. These results indicate that acacetin protected H9c2 cardiomyocytes from H/R damage by enhancing autophagy. Moreover, we found that application of acacetin increased activation of the PI3K/Akt signaling pathway, whereas cotreatment with the PI3K inhibitor LY294002 reversed the inhibition of apoptosis and autophagy induced by acacetin. In conclusion, acacetin mitigated H/R injury by promoting autophagy through activating the PI3K/Akt/mTOR signaling pathway.

## 1. Introduction

Ischemic heart disease is a leading cause of mortality and morbidity worldwide [1]. Following an ischemic attack, reperfusion therapy is regarded as the most effective measure to save ischemic myocardium [2]. However, myocardial ischemic-reperfusion therapy may induce ultrastructural damage and functional impairment of cardiomyocytes, which aggravates ischemic myocardium injury [3–5]. Although reports describing therapeutic interventions and prognosis of myocardial injury have recently increased, available therapies still induce ultrastructural damage and functional impairments in cardiomyocytes [6]. Many researchers have discussed problems with optimizing myocardial injury therapy, but potential mechanisms and drug targets of myocardial injury remain to be elucidated. Thus, novel pharmacological or other effective targets are urgently needed to protect against myocardial hypoxia-reoxygenation (H/R) injury.

Acacetin, an effective constituent of the Chinese traditional herb *Ziziphora bungeana* (Juz.), was previously demonstrated to protect against myocardial ischemia reperfusion injury [7, 8]. However, the effective targets and mechanism of acacetin remain to be elucidated. Autophagy is a highly conserved catabolic process involving the degradation and recycling of macromolecules, which is important for both organelle formation and lysosome degradation [9]. Moreover, autophagy has a major role in the pathological process of myocardial infarction. As cardiac tissue is comprised of terminally differentiated cardiomyocytes, autophagy occurs at a basal level under normal conditions to maintain intracellular homeostasis by removing long-lived or excess protein aggregates and damaged organelles [9–12].

Hence, we hypothesized that acacetin may protect myocardial cells against H/R injury through autophagy and investigated its targets and potential mechanisms.

Recent studies show that the phosphoinositide 3 kinase (PI3K)/Akt/mechanistic target of rapamycin (mTOR) pathway plays crucial roles in regulating mitophagy and mitochondrial quality control [13–15]. Mitophagy may have restorative potential for myocardial H/R injury [13]. However, the ability of acacetin to induce autophagy effects and related signaling pathways is poorly understood. Thus, the purpose of this study was to determine whether the molecular mechanisms underlying the cardioprotective effects of acacetin are related to promotion of autophagy via activation of PI3K/Akt/mTOR signaling.

## 2. Materials and Methods

*2.1. Materials.* Acacetin (purity ≧ 98%) was purchased from the Xinjiang Urumqi Uygur Medicine Institute (Xinjiang, China).

*2.2. Cell Culture.* H9c2 cells exhibiting good growth were inoculated into 25 $cm^2$ flasks in low-glucose Dulbecco's Modified Eagle's Medium containing 10% fetal bovine serum and placed in an incubator at 37°C with 5% $CO_2$. When cell cultures reached 85%–90% confluence, they were washed twice with precooled phosphate-buffered saline (PBS), and then, the cells were digested from the culture flask with a 1 : 2 volume of 0.25% trypsin. Cells were passaged once every 2 to 3 days. Cells were inoculated into the corresponding culture plates during logarithmic growth phase [16].

*2.3. Detection of Acacetin Cytotoxicity.* Cells in logarithmic growth phase were prepared into cell suspensions that were subsequently inoculated into 96-well plates. To seed approximately $1 - 2 \times 10^4$ cells per well, approximately 100 $\mu$l of cell suspension was added into wells; one sample generated 4–6 replicates. Plates were then placed in a 37°C incubator to allow the cells to stably adhere. Subsequently, cells were incubated a gradient of acacetin concentrations (1.56, 3.13, 6.25, 12.50, 25.00, 50.00, 100.00, and 200.00 $\mu$g/ml) for 12, 24, and 36 h to observe cell growth. Cell Counting Kit 8 (CCK-8; Wuhan Boster Biotechnology, Wuhan, China) reagents were nontoxic to cells and reduced by the electron carrier to orange-deficient formazan by some dehydrogenases in the mitochondria of cells. Cell viability assay is according to a previously described protocol [16].

*2.4. Establishment of a Stimulated H/R Model in H9c2 Cardiomyocytes.* To mimic H/R-induced injury *in vitro*, ischemia followed by reperfusion was stimulated in H9c2 cells [17]. After transferring cells to a closed container with an oxygen-deficient zone (Mitsubishi Gas Chemical, Tokyo, Japan) for incubation in a 5% $CO_2$ incubator at 37°C to induce anoxia, cells were exposed to 4 h of simulated ischemia. Subsequently, the culture medium was replaced with normal medium, and cells were incubated in a 5% $CO_2$ incubator at 37°C for 4 h to simulate reperfusion [18].

*2.5. Detection of SOD, LDH, and MDA.* Cell samples were homogenized to extract enzymes for detection. Superoxide dismutase (SOD; Nanjing Institute of Bioengineering, Nanjing, China) and malondialdehyde (MDA; Nanjing Institute of Bioengineering), and lactate dehydrogenase (LDH, Nanjing Institute of Bioengineering) activities were detected by kits purchased from the Nanjing Institute of Bioengineering according to the manufacturer's directions.

*2.6. Western Blotting.* After 12 h treatment with varying concentrations of acacetin, simulation of ischemia for the final 4 h, cells were washed twice with cold PBS and immediately lysed in radioimmunoprecipitation assay lysis buffer (Wuhan Boster Biotechnology) supplemented with phenylmethylsulfonyl fluoride and protease and phosphatase inhibitor cocktail (Cat. No. P1260; Solarbio, Beijing, China). The resulting protein was boiled for 5 min in 1× loading buffer and electrophoresed according to a previously described method [19]. Following electrophoretic separation, protein samples were transferred to polyvinylidene fluoride membranes (Millipore, Burlington, MA, USA) and blocked with 3% bovine serum albumin for 2 h [20]. Subsequently, membranes were incubated with the following primary antibodies overnight at 4°C [14]: Bax [1 : 1000; Cat. No. 2772; Cell Signaling Technology (CST), Danvers, MA, USA], p-AKT (Ser473) (1 : 2000; Cat. No. 4060, CST), Bcl-2 (1 : 1000; Cat. No. abs131701; Absin, Shanghai, China), mTOR (1 : 1000; Cat. No. 2983, CST), PI3K (1 : 1000; Cat. No. 4257, CST), Beclin 1 (1 : 1000; Cat. No. abs117840, Absin), and LC3B (1 : 1000; Thermo Fisher, Waltham, MA, USA). After washing three times, membranes were incubated with goat anti-rabbit IgG-FITC (1 : 100; abs20004ss, Absin) and goat anti-rabbit IgG-HRP (1 : 5000; abs2004ss, Absin) for 2 h at room temperature (RT). Next, membranes were washed three times with Tris-buffered saline containing Tween [21] and subsequently developed using an enhanced chemiluminescence reagent. Protein expression levels were normalized to the level of $\beta$-actin in corresponding lanes using Image Lab™ Version 3.0 (Bio-Rad, Hercules, CA, USA) and ImageJ 1.41 (https://imagej.nih.gov/ij/) for densitometric analysis.

*2.7. Flow Cytometric Analysis of Apoptosis.* Annexin V, FITC, and PI are sensitive probes for identifying apoptotic cells. According to our previously described method [22], each group of cells was prepared for flow cytometry. Briefly, H9c2 cells were harvested by dissociation with trypsin-EDTA, washed twice with cold PBS, and then resuspended in 1× binding buffer [23]. Next, 100 $\mu$l of the solution ($1 \times 10^5$ cells) were transferred into a 5 ml culture tube. After adding 5 $\mu$l of Annexin V-FITC and 10 $\mu$l of PI, cells were gently vortexed and incubated for 15 min at RT (25°C) in the dark. Finally, 400 $\mu$l of 1× binding buffer was added to each tube, and cells were analyzed by flow cytometry within 1 h [24].

*2.8. Visualization of Autophagic Fluorescence Intensity by Microscopy.* Autophagic flux in primary mouse cardiomyocytes was monitored using stubRFP-sensGFP-LC3 lentivirus, a LC3 double-fluorescent lentivirus autophagy detection system optimized for monitoring of cell autophagy by flow

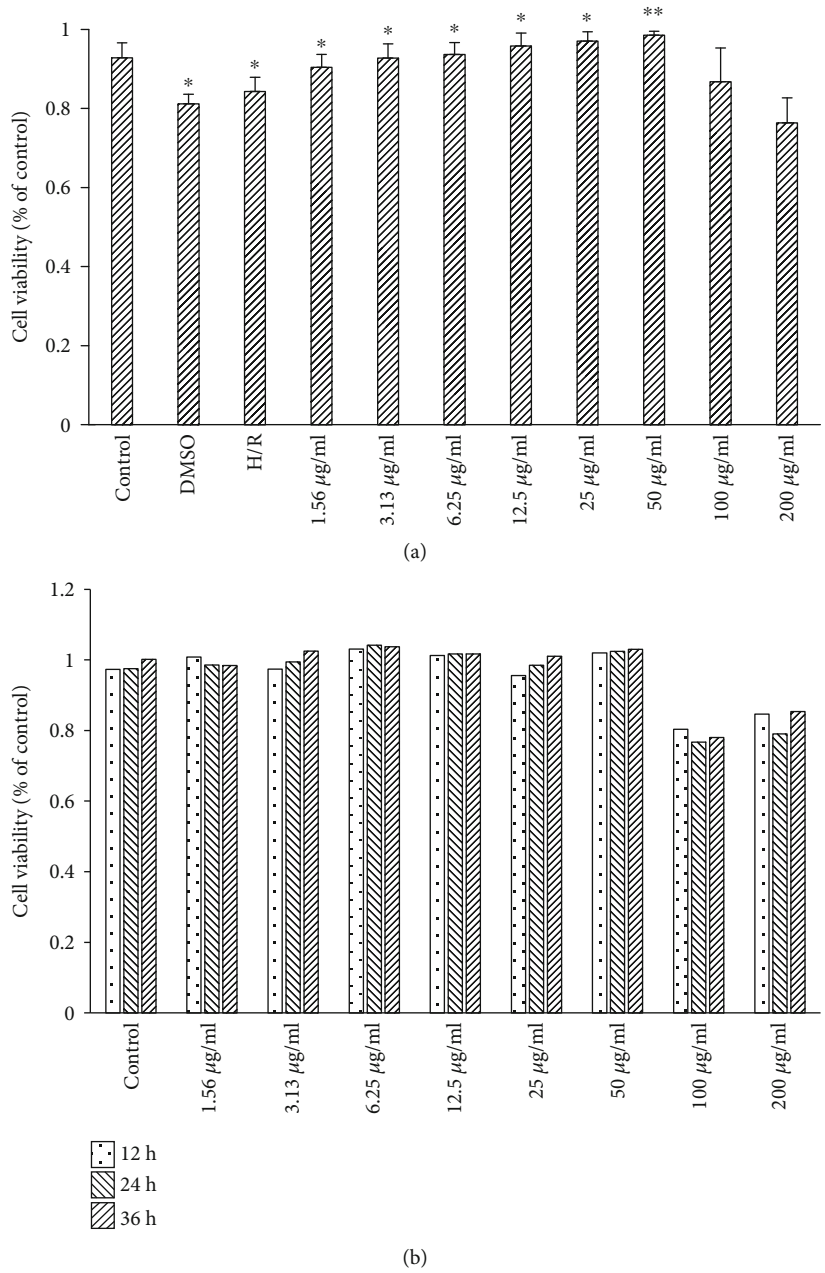


Figure 1: Effect of acacetin on viability of H9c2 cells. (a) Effect of acacetin on viability of H9c2 cells was detected by CCK-8 assay. (b) Effect of varying pretreatment time (12, 24, and 36 h) with acacetin on viability of H9c2 cells was detected by CCK-8 assay. Bars indicate mean ± standard deviation of three independent experiments. CCK-8: Cell Counting Kit 8.

cytometry. The fusion protein consists of a red fluorescent protein (Stub-RFP), green fluorescent protein (Sens-GFP), and autophagy-labeled protein LC3 [25]. Cardiomyocytes were transfected with stubRFP-sensGFP-LC3 lentivirus and seeded onto six-well plates. Twelve hours later, cardiomyocytes were exposed to different experimental conditions (control, H/R, or H/R + Acacetin). Cells were then analyzed with a U-LH100HG optical microscope (Olympus, Tokyo, Japan) [20].

*2.9. Statistical Analyses.* Statistical analysis was conducted with SPSS 22.0 software (IBM, Armonk, NY, USA. Data are expressed as mean ± standard deviation. $P < 0.05$ was considered to be statistically significant.

## 3. Results

*3.1. Cell Viability.* We first assayed the effect of acacetin on cell viability and found that viability gradually increased with increasing concentrations of acacetin in the range of 1.56–50 $\mu$g/ml. These results indicate that the activity elicited by acacetin occurred in a concentration-dependent manner. When the concentration of acacetin reached 100–200 $\mu$g/ml, cell viability was slightly decreased (Figure 1(a)). In addition,

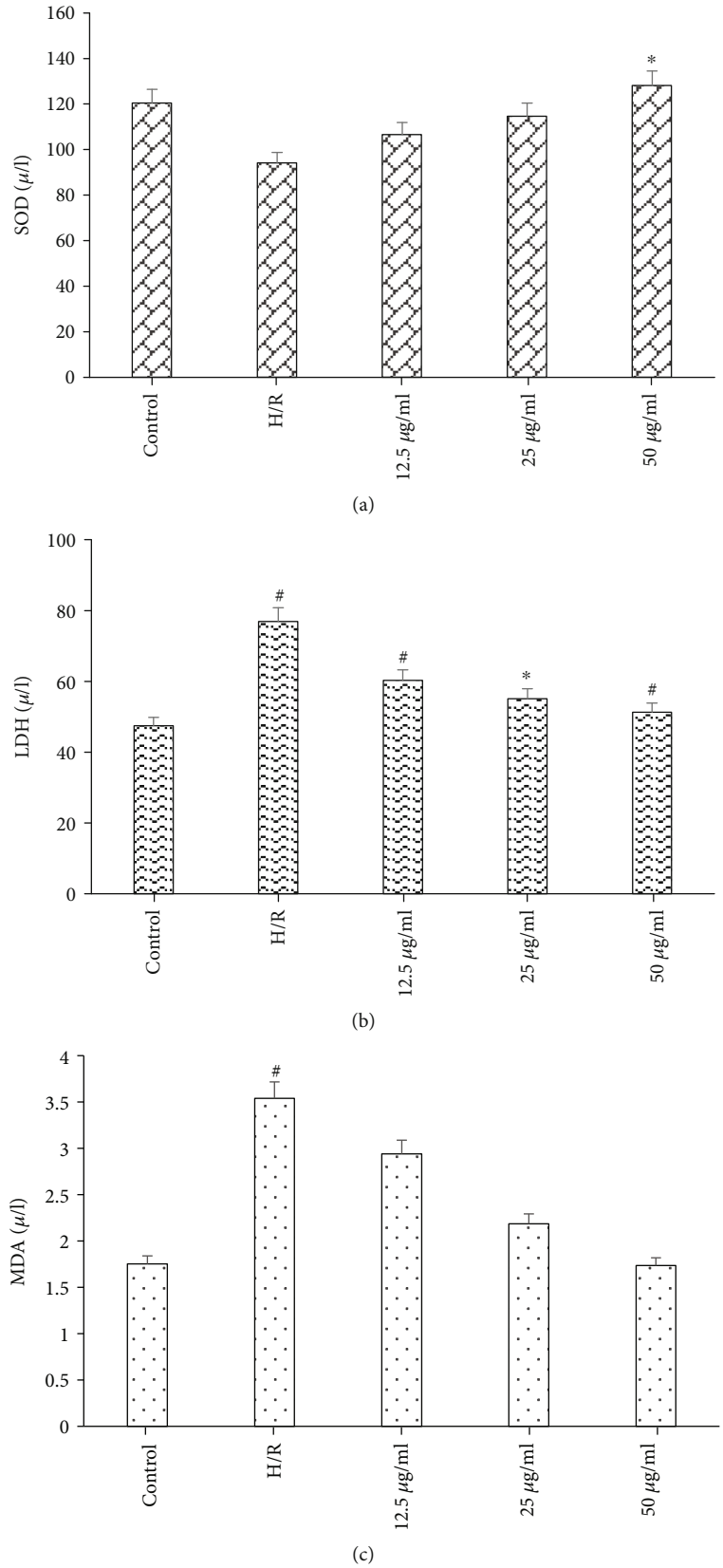


Figure 2: Release of SOD, LDH, and MDA at the end of H/R was determined. Results for control, H/R model, and H/R + acacetin (12.5, 25, and 50 $\mu$g/ml) groups are expressed as percentages of control and presented as mean ± standard deviation of five independent experiments. $^{\#}P < 0.05$ compared with control group; $^{\#}P < 0.05$ vs. $^{*}P < 0.01$ compared with H/R group. H/R: hypoxia/reoxygenation; LDH: lactate dehydrogenase; MDA: malondialdehyde; SOD: superoxide dismutase.

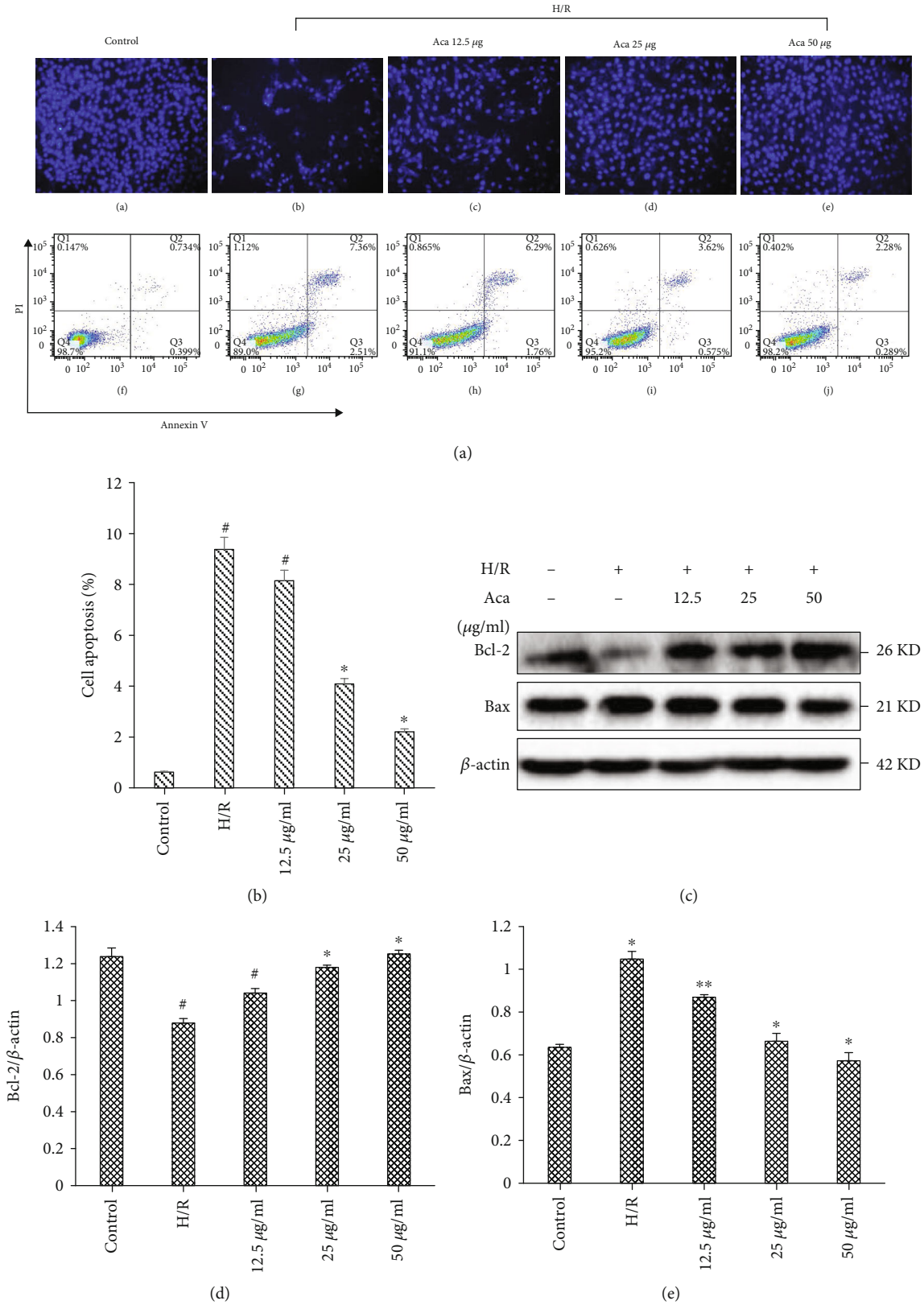


Figure 3: Acacetin suppresses apoptosis of H9c2 cells in H/R injury. H9c2 cells were divided into control, H/R model, and H/R + acacetin (12.5, 25, and 50 $\mu$g/ml) groups. (a) Cell apoptosis rates of each group were analyzed by flow cytometry, while cell survival rates were analyzed by DAPI staining. (b–d) Relative protein levels of cleaved Bax and Bcl-2 in each group were measured by Western blot. Bars indicate mean ± standard deviation of three independent experiments. $^{\#}P < 0.05$ compared with control group; $^{\#}P < 0.05$, $^{*}P < 0.01$ compared with H/R model group. DAPI: 4′,6-diamidino-2-phenylindole; H/R: hypoxia/reoxygenation.

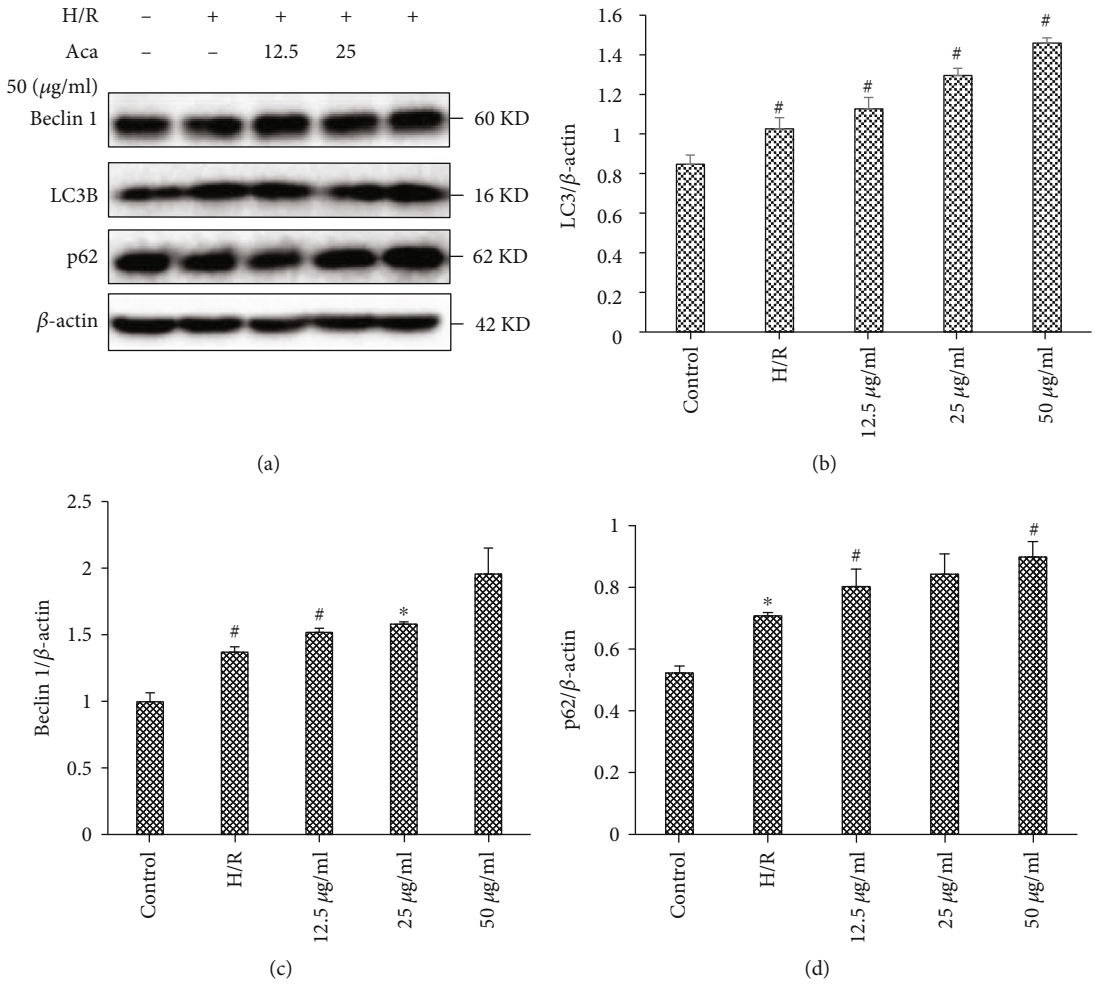


Figure 4: Continued.

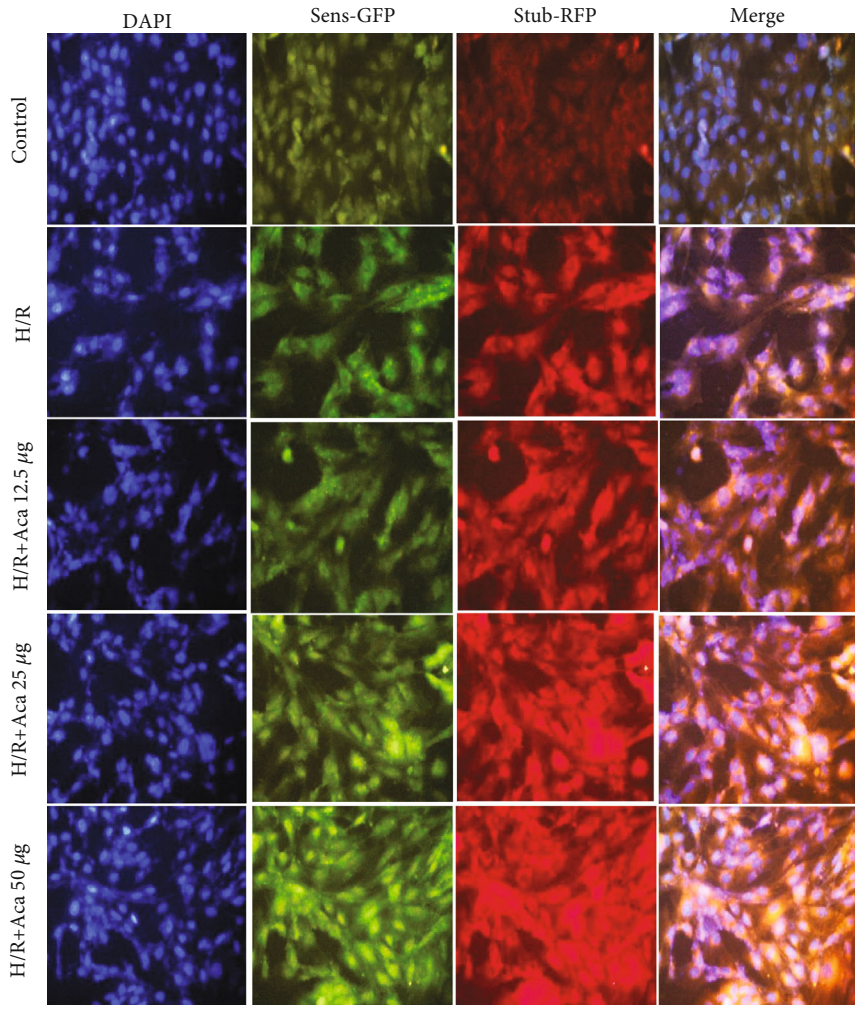


(e)

Figure 4: Acacetin promotes autophagy to suppress apoptosis of H9c2 cells following H/R injury. H9c2 cells were divided into control, H/R model, and H/R + acacetin (12.5, 25, and 50 $\mu$g/ml) groups. (a–d) Relative protein levels of beclin 1, p62, and LC3-II in each group were measured by Western blot. (e) Immunofluorescence of LC3 II in H9c2 cells as detected by fluorescence microscopy. Bars indicate mean ± standard deviation of three independent experiments. $^{\#}P < 0.05$ compared with control group; $^{\#}P < 0.05$, $^{*}P < 0.01$ compared with H/R model group. H/R: hypoxia/reoxygenation; LC3-II: microtubule-associated protein 1A/1B-light chain 3.

we further evaluated the effect of varying acacetin pretreatment time on the viability of cardiomyocytes. The rate of cell survival was the highest at 12 h, but decreased at 24 h and 36 h; thus, 12 h was selected as the pretreatment time for follow-up experiments (Figure 1(b)).

*3.2. Acacetin Enhanced the Antioxidant Capacity of Cardiomyocytes.* Antioxidant enzymes are important indicator of cardiac antioxidant capacity. Therefore, we investigated the effect of acacetin on protein levels of reactive antioxidant enzymes in cardiomyocytes. Protein levels of SOD, an important antioxidant enzyme [26], were significantly decreased by H/R but increased with acacetin pretreatment (Figure 2(a)). In addition, the activities of MDA and LDH were reduced in acacetin pretreatment groups, indicating that cell injury was inhibited by acacetin pretreatment (Figures 2(b) and 2(c)). This effect was most significant at concentration of 50 $\mu$g/ml acacetin, consistent with previous experimental results. These results indicate that following H/R, a large number of oxygen free radicals were released, biofilm lipidization was severe, and cell membrane permeability was increased [27], resulting in significant increases of LDH and MDA activities and a significant decrease of SOD activities compared with the control group.

*3.3. Acacetin Inhibited H/R-Induced Cell Apoptosis.* We further examined the effects of acacetin on cardiomyocytes following H/R injury by flow cytometry and 4′,6-diamidino-2-phenylindole (DAPI) staining. Both results showed that acacetin could inhibit cell apoptosis induced by H/R injury (Figures 3(a) and 3(b)). In addition, we evaluated Bcl-2 and Bax expression after H/R injury, and the protection elicited by acacetin. Our results show that compared with the H/R model group, Bax protein expression was significantly decreased, and Bcl-2 protein expression was significantly increased in cells pretreated with acacetin for 12 h

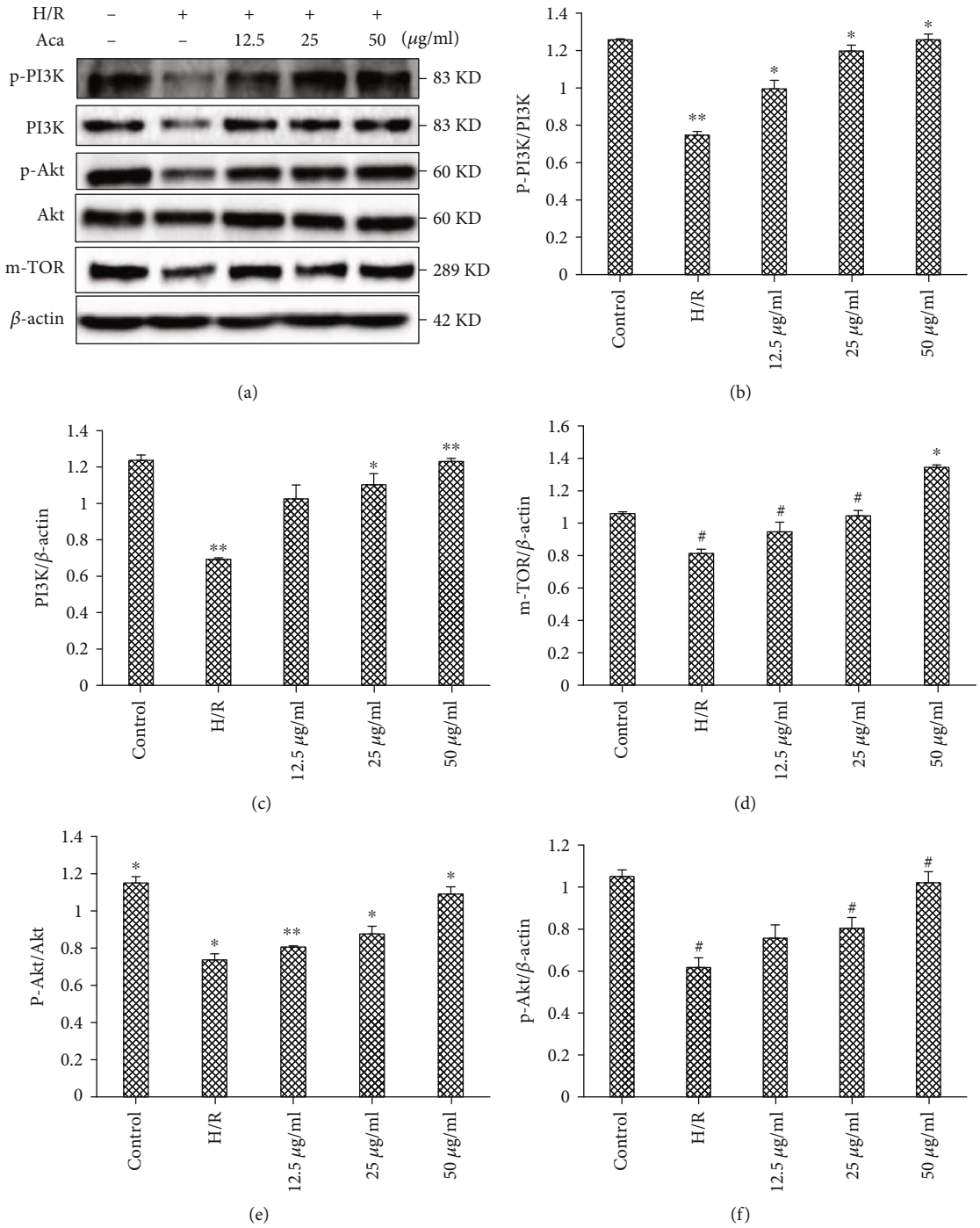


Figure 5: Acacetin mitigates H/R injury by regulating the PI3K/Akt/mTOR signaling pathway. H9c2 cells were divided into control, H/R, H/R + acacetin (12.5, 25, and 50 $\mu$g/ml), and H/R +50 $\mu$g/ml acacetin + LY294002 groups. (a–f) Relative protein levels of p-Akt, p-PI3K, and mTOR in each group were measured by Western blot. Bars indicate mean ± standard deviation of three independent experiments. $^{\#}P < 0.05$ compared with control group; $^{\#}P < 0.05$, $^{*}P < 0.01$ compared with H/R model group. H/R; hypoxia/reoxygenation; p-: phosphorylated; PI3K: phosphoinositide 3 kinase; mTOR: mechanistic target of rapamycin.

(Figures 3(c)–3(e)). These results suggest that the inhibitory effect of acacetin on cardiomyocyte apoptosis may be achieved by increasing Bcl-2 expression and inhibiting Bax activation.

*3.4. Acacetin Induced Autophagy to Protect Cardiomyocytes against H/R Injury.* Examination of autophagy-linked protein expression by Western blot showed that the accumulation of autophagy markers (including LC3-II, Beclin 1, and p62) elicited by acacetin occurred in a dose-dependent manner (Figure 4(a)). Our experimental results show that acacetin could protect H9c2 cells from H/R injury by promoting autophagy. Compared with the H/R group, acacetin pretreatment for 12 h enhanced the apoptosis-promoting effect of

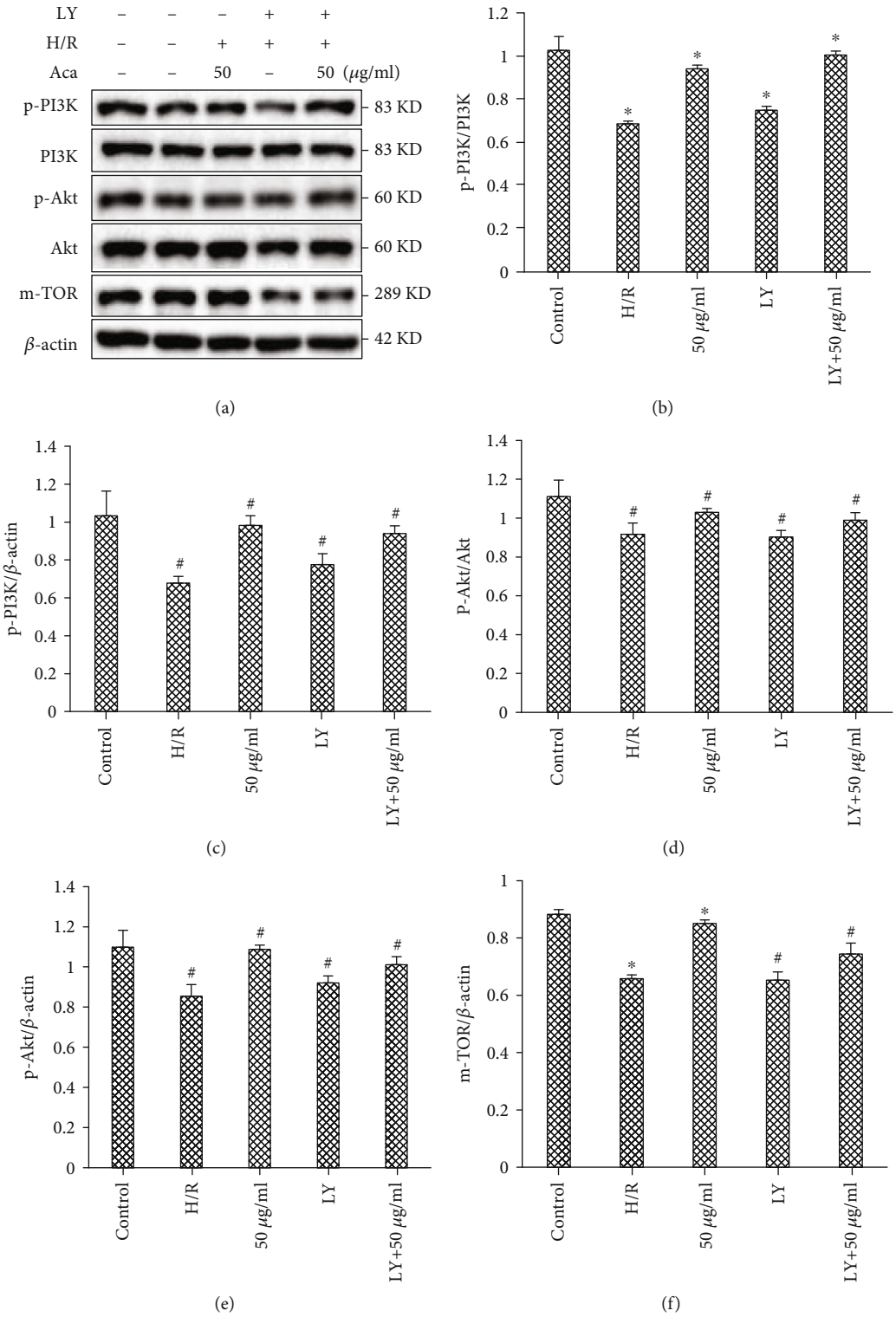


Figure 6: Continued.

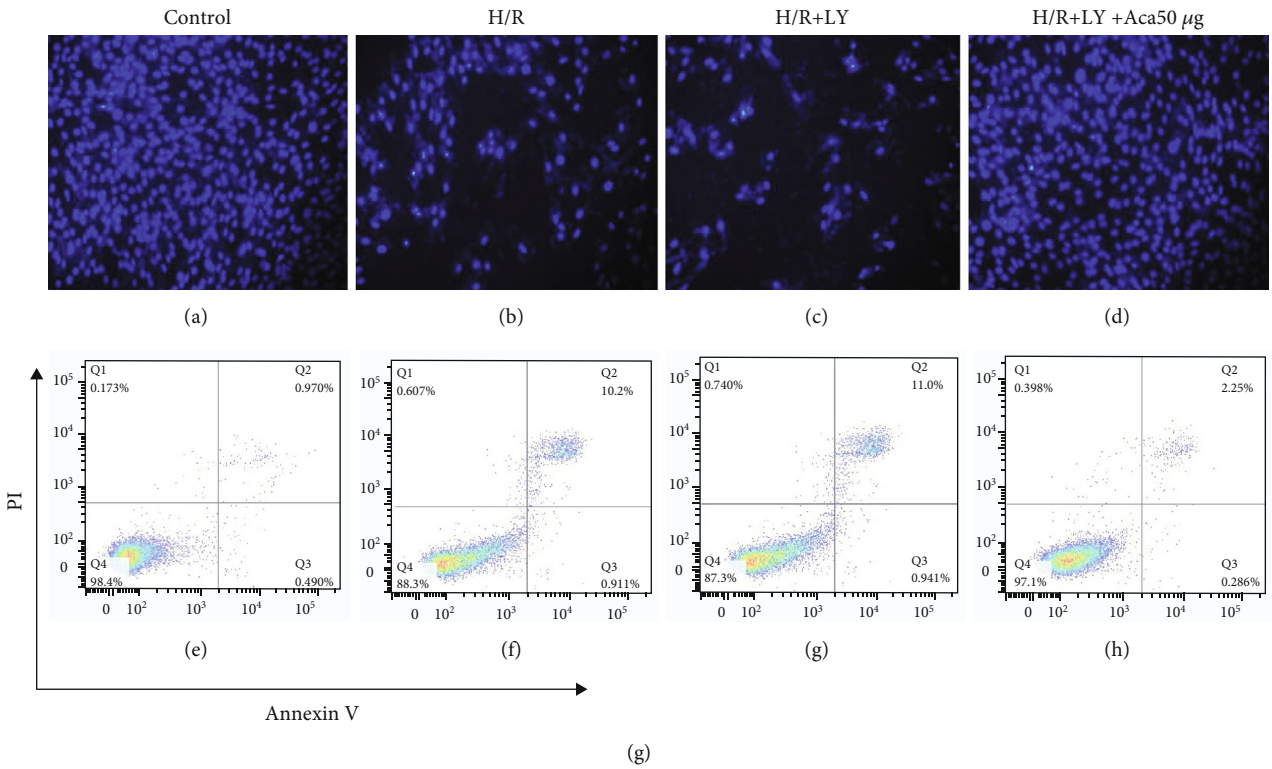


Figure 6: Acacetin induced autophagy in H9c2 cells by inhibiting the PI3K/Akt/mTOR pathway. H9c2 cells were divided into control, H/R model, H/R +50 μg/ml acacetin, H/R + LY294002, and H/R +50 μg/ml acacetin + LY294002 groups. (a–f) Relative protein levels of p-Akt, p-PI3K, and mTOR in each group as measured by Western blot. Bars indicate mean ± standard deviation of three independent experiments. $^{\#}P < 0.05$ compared with control group; $^{\#}P < 0.05$, $^{*}P < 0.01$ compared with H/R model group. (g) Cell apoptosis rates of each group were analyzed by flow cytometry. (f) Cell survival rates of each group were analyzed by DAPI staining. DAPI: 4′,6-diamidino-2-phenylindole; H/R: hypoxia/reoxygenation; PI3K: phosphoinositide 3 kinase; mTOR: mechanistic target of rapamycin.

H/R following blocking of autophagy flux, indicating that acacetin induced autophagy as a cytoprotective mechanism.

We further observed that acacetin promoted autophagy, as indicated by the aggregation of Stub-RFP and Sens-GFP on autophagosomes following lentiviral infection (Figure 4(e)). In this experiment, the intensity of red/green spots observed by fluorescence microscopy was used to judge the degree of autophagy of H9c2 cardiomyocytes in each experimental group after H/R. Compared with the H/R group, H9c2 cells treated with acacetin exhibited higher fluorescence intensity, confirming that acacetin induced autophagy in H9c2 cells. Compared with the H/R group, use of acacetin improved the autophagy activity of H9c2 cells.

*3.5. Acacetin Enhanced Autophagy via the PI3K/Akt Signaling Pathway.* The PI3K/Akt/mTOR signaling pathway is the most classical signaling pathway involved in the multiple prolongation mechanism of mTOR. We further verified the effect of acacetin on the expression of PI3K/Akt/mTOR signaling pathway-related proteins in H9c2 cells injured by H/R. Western blot results showed that compared with the control group, expression of PI3K, phosphorylated PI3K (p-PI3K), Akt, and phosphorylated Akt (p-Akt) proteins in the H/R model group were decreased. Indeed, compared with the H/R model group, PI3K, p-PI3K, Akt, and p-Akt gradually increased with increasing concentrations of acacetin (Figure 5). As shown in Figure 5, acacetin activated the PI3K/Akt/mTOR signaling pathway and participated in the protection of cardiomyocytes, thus inhibiting cell metabolism and promoting proliferation.

To verify the mechanism of acacetin, we determined whether the PI3K/Akt inhibitor LY294002 (LY, 20 mM) could abolish its activity. Cell viability of every group, as assessed by flow cytometry and DAPI assay, demonstrated that inhibition of PI3K/Akt abrogated the protection elicited by acacetin pretreatment (Figure 6). These results indicate that the efficacy of acacetin was abolished by LY294002.

## 4. Discussion

The objective of the current study was to determine whether the beneficial effect of acacetin on cardiomyocytes exposed to H/R injury involves autophagy as a protective mechanism. In this study, we showed that acacetin preconditioning suppressed myocardial cell apoptosis of rat cardiomyocytes following damage caused by H/R injury. Moreover, acacetin enhanced autophagy by regulating activity of the PI3K/Akt signaling pathway and enhancing the interaction of autophagosomes to maintain a higher level of autophagy, which offered a protective effect against H/R injury.

Acacetin is a natural product with antiproliferative and antioxidant activities. Acacetin has also been shown to exert

an antiproliferative effect by blocking cell cycle progression and inducing apoptosis. Moreover, acacetin has been shown to target mitochondria to induce apoptosis of chronic lymphocytic leukemia (CLL) B lymphocytes through increased reactive oxygen species formation, mitochondrial membrane potential collapse, mitochondrial permeability transition, release of cytochrome c, caspase 3 activation, and finally apoptosis, whereas normal healthy B lymphocytes were unaffected. In addition, oral administration of acacetin elicited potent *in vivo* anticancer activity in CLL xenograft mouse models [28]. Our present study found that acacetin preconditioning yielded beneficial effects and protected myocardial cells through activation of autophagy.

Under activating physiological conditions, autophagy can remove useless, superfluous, or damaged cells and organelles to maintain homeostasis of the body [29]. Previous studies revealed that moderate upregulation of autophagy could protect cardiomyocytes against H/R injury, whereas excessive autophagy could aggravate myocardial H/R injury [20, 30, 31]. LC3, p62, and Beclin 1 are central autophagy-related proteins involved in autophagy flux [12]. Our results clearly show that acacetin activated these autophagy-related proteins and increased cell viability, thereby maintaining the homeostasis of cells. During the early stage of autophagy, LC3-I was transformed into membrane LC3-II, leading Stub-RFP and Sens-GFP (red/green colocalized dots) to accumulate on autophagosomes. Our results showed that red/green fluorescence was the weakest in the control group. Compared with the H/R group, fluorescence intensity of the acacetin group was enhanced, indicating that acacetin could effectively activate autophagy in myocardial cells.

As an essential prosurvival pathway, PI3K/Akt signaling plays classical signal transduction roles in the development of cardioprotection against myocardial H/R injury. To further verify that acacetin induced autophagy in H9c2 cells by inhibiting the PI3K/Akt/mTOR pathway, we evaluated the contents of PI3K/Akt/mTOR proteins, which were significantly increased after adding inhibitors (Figure 6) [32, 33]. DAPI and flow cytometry results also indicated increase in cardiomyocyte apoptosis, suggesting that PI3K/AKT/mTOR pathway activation may promote the induction of autophagy in H9c2 cells. In addition, it was concluded that acacetin can inhibit expression of the proapoptotic factor Bax and enhance the expression of antiapoptotic factors Bcl-2 and mTOR, thus reducing apoptosis of H9c2 cardiomyocytes during H/R.

In summary, the results of this study suggest that acacetin inhibited apoptosis through the PI3K/Akt/mTOR signaling pathway to alleviate H/R injury in H9c2 cardiomyocytes by promoting autophagy. Thus, the clinical efficacy and safety of acacetin for reducing myocardial H/R injury warrant further study.

## Data Availability

The data used to support the findings of this study are available from the corresponding author upon request.

## Conflicts of Interest

The authors declare no competing interests.

## Authors' Contributions

W.C, J.Q.X., and B.S. contributed to the conception of this review. L.C. and M.M.Z. analyzed the literature and wrote the manuscript. C.L.H. and J.X.C. completed figure drawing. R.Y.L., B.J.H., and W.J.Y. revised the manuscript. Chong Liu and Minmin Zhang contributed equally to this work.

## Acknowledgments

This work was supported by the Science and Technology Project of Taizhou (20ywa10 and 1901ky28), the Science and Technology Project of Taizhou Enze Medical Center (Group) (20ezc41 and 19EZB13), the Natural Science Foundation of Zhejiang Province (LQ21H280006), and Medical Health Science and Technology Project of Zhejiang Provincial Health Commission (2021RC143).

## References

[1] G. W. Reed, J. E. Rossi, and C. P. Cannon, "Acute myocardial infarction," *The Lancet*, vol. 389, no. 10065, pp. 197–210, 2017.

[2] A. Lejay, F. Fang, R. John et al., "Ischemia reperfusion injury, ischemic conditioning and diabetes mellitus," *Journal of Molecular and Cellular Cardiology*, vol. 91, pp. 11–22, 2016.

[3] G. Aliev, M. E. Obrenovich, D. Seyidova, and J. C. de la Torre, "Exploring ischemia-induced vascular lesions and potential pharmacological intervention strategies," *Histology and Histopathology*, vol. 20, no. 1, pp. 261–273, 2005.

[4] S. K. Banerjee, A. K. Dinda, S. C. Manchanda, and S. K. Maulik, "Chronic garlic administration protects rat heart against oxidative stress induced by ischemic reperfusion injury," *BMC Pharmacology*, vol. 2, no. 1, p. 16, 2002.

[5] S. N. Goyal, S. Bharti, S. Arora, M. Golechha, and D. S. Arya, "Endothelin receptor antagonist BQ-123 ameliorates myocardial ischemic- reperfusion injury in rats: a hemodynamic, biochemical, histopathological and electron microscopic evidence," *Biomedicine & Pharmacotherapy*, vol. 64, no. 9, pp. 639–646, 2010.

[6] S. He, X. Wang, Y. Zhong et al., "Hesperetin post-treatment prevents rat cardiomyocytes from hypoxia/reoxygenation injury in vitro via activating PI3K/Akt signaling pathway," *Biomedicine & Pharmacotherapy*, vol. 91, pp. 1106–1112, 2017.

[7] W. J. Yang, C. Liu, Z. Y. Gu et al., "Protective effects of acacetin isolated from Ziziphora clinopodioides Lam. (Xintahua) on neonatal rat cardiomyocytes," *Chinese Medicine*, vol. 9, no. 1, p. 28, 2014.

[8] J. He, W. Yang, B. Cheng et al., "Integrated metabolomic and transcriptomic profiling reveals the tissue-specific flavonoid compositions and their biosynthesis pathways in Ziziphora bungeana," *Chinese Medicine*, vol. 15, no. 1, p. 73, 2020.

[9] L. Liu, Y. Wu, and X. Huang, "Orientin protects myocardial cells against hypoxia-reoxygenation injury through induction of autophagy," *European Journal of Pharmacology*, vol. 776, pp. 90–98, 2016.

[10] J. Bai, Y. K. Wu, K. M. Wu et al., "Triptolide induces autophagy of ovarian granulosa cells via PI3K/AKT/m TOR pathway," *Zhongguo Zhong Yao Za Zhi*, vol. 44, no. 16, pp. 3429–3434, 2019.

[11] Z. Long, B. Chen, Q. Liu et al., "The reverse-mode NCX1 activity inhibitor KB-R7943 promotes prostate cancer cell death by activating the JNK pathway and blocking autophagic flux," *Oncotarget*, vol. 7, no. 27, pp. 42059–42070, 2016.

[12] Y.-. M. Mei, L. Li, X.-. Q. Wang et al., "AGEs induces apoptosis and autophagy via reactive oxygen species in human periodontal ligament cells," *Journal of Cellular Biochemistry*, vol. 121, no. 8-9, pp. 3764–3779, 2020.

[13] C. Luo, Y. Zhang, H. Guo, X. Han, J. Ren, and J. Liu, "Ferulic acid attenuates hypoxia/reoxygenation injury by suppressing mitophagy through the PINK1/parkin signaling pathway in H9c2 cells," *Frontiers in Pharmacology*, vol. 11, p. 103, 2020.

[14] H. Mei, Y. Xiang, H. Mei et al., "Pterostilbene inhibits nutrient metabolism and induces apoptosis through AMPK activation in multiple myeloma cells," *International Journal of Molecular Medicine*, vol. 42, no. 5, pp. 2676–2688, 2018.

[15] L. Tang, Y. Mo, Y. Li et al., "Urolithin A alleviates myocardial ischemia/reperfusion injury via PI3K/Akt pathway," *Biochemical and Biophysical Research Communications*, vol. 486, no. 3, pp. 774–780, 2017.

[16] B. Yang, C. S. Pan, Q. Li et al., "Inhibitory effects of Chanling Gao on the proliferation and liver metastasis of transplanted colorectal cancer in nude mice," *PLoS One*, vol. 14, no. 2, article e0201504, 2019.

[17] B. Q. Guo, J. B. Xu, M. Xiao, M. Ding, and L. J. Duan, "Puerarin reduces ischemia/reperfusion-induced myocardial injury in diabetic rats via upregulation of vascular endothelial growth factor A/angiotensin-1 and suppression of apoptosis," *Molecular Medicine Reports*, vol. 17, no. 5, pp. 7421–7427, 2018.

[18] S. Hu, S. Cao, and J. Liu, "Role of angiopoietin-2 in the cardioprotective effect of fibroblast growth factor 21 on ischemia/reperfusion-induced injury in H9c2 cardiomyocytes," *Experimental and Therapeutic Medicine*, vol. 14, no. 1, pp. 771–779, 2017.

[19] R. Ma, Y. Zhang, W. Wang et al., "Inhibition of autophagy enhances the antitumour activity of tigecycline in multiple myeloma," *Journal of Cellular and Molecular Medicine*, vol. 22, no. 12, pp. 5955–5963, 2018.

[20] R. Zhao, E. Xie, X. Yang, and B. Gong, "Alliin alleviates myocardial ischemia-reperfusion injury by promoting autophagy," *Biochemical and Biophysical Research Communications*, vol. 512, no. 2, pp. 236–243, 2019.

[21] R. X. Tang, F. Y. Kong, B. F. Fan et al., "HBx activates Fas L and mediates Hep G2 cell apoptosis through MLK3-MKK7-JNKs signal module," *World Journal of Gastroenterology*, vol. 18, no. 13, pp. 1485–1495, 2012.

[22] K. M. Murphy, V. Ranganathan, M. L. Farnsworth, M. Kavallaris, and R. B. Lock, "Bcl-2 inhibits Bax translocation from cytosol to mitochondria during drug- induced apoptosis of human tumor cells," *Cell Death and Differentiation*, vol. 7, no. 1, pp. 102–111, 2000.

[23] T. Su, J. Li, M. Meng et al., "Bone marrow stromal cells induced activation of nuclear factor κB signaling protects non-Hodgkin's B lymphoma cells from apoptosis," *Tumour Biology*, vol. 37, no. 8, pp. 10745–10752, 2016.

[24] L. Li, J. Y. Yin, F. Z. He et al., "Long noncoding RNA SFTA1P promoted apoptosis and increased cisplatin chemosensitivity via regulating the hn RNP-U-GADD45A axis in lung squamous cell carcinoma," *Oncotarget*, vol. 8, no. 57, pp. 97476–97489, 2017.

[25] Z. R. Zhou, Z. Z. Yang, S. J. Wang et al., "The Chk 1 inhibitor MK-8776 increases the radiosensitivity of human triple-negative breast cancer by inhibiting autophagy," *Acta Pharmacologica Sinica*, vol. 38, no. 4, pp. 513–523, 2017.

[26] Y. Liu, M. Yang, L. Zheng et al., "Antioxidant responses of triangle sail mussel *Hyriopsis cumingii* exposed to toxic *Microcystis aeruginosa* and thermal stress," *The Science of the Total Environment*, vol. 743, article 140754, 2020.

[27] Y. Cai, Y. Lu, R. Chen, Q. Wei, and X. Lu, "Anti-hypoxia activity and related components of Rhodobryum giganteum par," *Phytomedicine*, vol. 18, no. 2-3, pp. 224–229, 2011.

[28] H. Liu, L. Yang, H. Wu et al., "Water-soluble acacetin prodrug confers significant cardioprotection against ischemia/reperfusion injury," *Scientific Reports*, vol. 6, no. 1, article 36435, 2016.

[29] Y. Yang and D. J. Klionsky, "Autophagy and disease: unanswered questions," *Cell Death and Differentiation*, vol. 27, no. 3, pp. 858–871, 2020.

[30] M. Ziegler, X. Wang, and K. Peter, "Platelets in cardiac ischaemia/reperfusion injury: a promising therapeutic target," *Cardiovascular Research*, vol. 115, no. 7, pp. 1178–1188, 2019.

[31] B. Trachtenberg and J. Hare, "Response by Trachtenberg and Hare to letter regarding the article, "inflammatory cardiomyopathic syndromes"," *Circulation Research*, vol. 122, no. 1, p. e2, 2018.

[32] B. J. Wang, W. L. Zheng, N. N. Feng et al., "The effects of autophagy and PI3K/AKT/m-TOR signaling pathway on the cell-cycle arrest of rats primary sertoli cells induced by zearalenone," *Toxins*, vol. 10, no. 10, p. 398, 2018.

[33] J. A. Cowgill, S. A. Francis, and D. B. Sawyer, "Anthracycline and peripartum cardiomyopathies," *Circulation Research*, vol. 124, no. 11, pp. 1633–1646, 2019.

Hindawi
Journal of Immunology Research
Volume 2021, Article ID 9975628, 14 pages
https://doi.org/10.1155/2021/9975628

*Research Article*

# Mechanism of Nucleic Acid Sensing in Retinal Pigment Epithelium (RPE): RIG-I Mediates Type I Interferon Response in Human RPE

**Joshua Schustak, Michael Twarog, Xiaoqiu Wu, Henry Y. Wu, Qian Huang, and Yi Bao**

*The Department of Ophthalmology, Novartis Institutes for BioMedical Research, 22 Windsor Street, Cambridge, MA, USA*

Correspondence should be addressed to Qian Huang; qian.huang@dragonflytx.com and Yi Bao; yi.bao@novartis.com

Received 30 March 2021; Revised 12 May 2021; Accepted 21 May 2021; Published 19 June 2021

Academic Editor: Yisong Qian



Age-related macular degeneration (AMD), a degenerative disease of the outer retina, is the leading cause of blindness among the elderly. A hallmark of geographic atrophy (GA), an advanced type of nonneovascular AMD (dry AMD), is photoreceptor and retinal pigment epithelium (RPE) cell death. Currently, there are no FDA-approved therapies for GA due to a lack of understanding of the disease-causing mechanisms. Increasing evidence suggests that chronic inflammation plays a predominant role in the pathogenesis of dry AMD. Dead or stressed cells release danger signals and inflammatory factors, which causes further damage to neighboring cells. It has been reported that type I interferon (IFN) response is activated in RPE cells in patients with AMD. However, how RPE cells sense stress to initiate IFN response and cause further damage to the retina are still unknown. Although it has been reported that RPE can respond to extracellularly added dsRNA, it is unknown whether and how RPE detects and senses internally generated or internalized nucleic acids. Here, we elucidated the molecular mechanism by which RPE cells sense intracellular nucleic acids. Our data demonstrate that RPE cells can respond to intracellular RNA and induce type I IFN responses via the RIG-I (DExD/H-box helicase 58, DDX58) RNA helicase. In contrast, we showed that RPE cells were unable to directly sense and respond to DNA through the cGAS-STING pathway. We demonstrated that this was due to the absence of the cyclic GMP-AMP synthase (cGAS) DNA sensor in these cells. The activation of IFN response via RIG-I induced expression of cell death effectors and caused barrier function loss in RPE cells. These data suggested that RPE-intrinsic pathways of nucleic acid sensing are biased toward RNA sensing.

## 1. Introduction

Age-related macular degeneration (AMD) is the most common cause of blindness among the elderly in the US and worldwide [1]. Although antiangiogenic drugs are currently in use for wet AMD, no Food and Drug Administration-(FDA-) approved treatments for intermediate AMD or geographic atrophy (GA) exist to date. A hallmark of AMD and GA is photoreceptor and retinal pigment epithelium (RPE) cell death. RPE, consisting of critical retinal cells and involved in AMD, is a unique epithelial tissue that interacts with photoreceptors on its apical side and with Bruch's membrane and the choriocapillaris on its basal side, making it essential for the maintenance of vision. Aging and other accumulated genetic and environmental risk factors might lead to RPE dysfunction, eventually resulting in RPE degeneration, and ultimately cell death, a major pathology of AMD. However, the cellular mechanisms causing degeneration of RPE are poorly understood.

Increasing evidence have indicated that chronic inflammatory events mediated by key pathways (e.g., complement, Toll-like receptor (TLR), NF-$\kappa$B, inflammasome, and interferon (IFN) response) play a central role in the pathogenesis and development of AMD [2, 3]. However, the molecular nature of these inflammatory mechanisms remains unclear. The immune status of the chorioretinal interface is known to be mainly regulated by RPE, with inflammation potentially having both physiological and pathological roles in RPE maintenance. Recent studies have suggested that type I IFN response is activated in RPE in patients with AMD. It was

shown that both the mRNA and protein levels of IFN-$\beta$ were increased in the RPE of patients with GA compared with age-matched controls [4]. In addition, it was reported that type I IFN pathway played an important role in animal models of retinal degeneration, most notably in A/J mice, as well as following the Alu-RNA subretinal delivery [4, 5]. However, the mechanisms by which RPE cells sense nucleic acids and induce downstream type I IFN response in the retina have not been fully addressed.

The type I family of IFNs is known to be responsible for inducing an antiviral response, playing a major role in restricting virus-infected cells. In addition to responding to foreign viral infections, they have also been implicated in sensing self-nucleic acids in the form of danger-associated molecular patterns (DAMPs). In particular, DAMPs have been shown to be released from dying or stressed cells and detected by pattern recognition receptors (PRRs) of the innate immune system. DAMPs induce inflammation and further damage to other cells. In mammalian cells, recognition of nucleic acids is known to involve multiple sensors. Specifically, members of the TLR family have been reported to sense RNA through TLR3, TLR7, and TLR8 and DNA via TLR9. In cytosol, RNA sensing is known to mainly occur through RIG-I-like receptors (RLRs), a group of RNA-specific PRRs. Intracellular DNA sensing, however, has been shown to mainly occur through the cGAS/STING axis, which detects cytosolic double-stranded DNA (dsDNA) [6, 7]. Once activated, these nucleic acid sensors trigger multiple signaling cascades and produce type I IFNs and proinflammatory cytokines via the activation of the interferon regulatory factor (IRF) and NF-$\kappa$B family of transcription factors [8, 9]. It was reported that treatment of poly(I:C) in culture medium could induce IRF3-mediated IFN-$\beta$ and NF-$\kappa$B-mediated cytokine release through TLR3 and further generate interferon stimulate genes (ISGs) in both ARPE-19 and primary human RPE cells [10, 11]. However, the mechanism by which this system of nucleic acid sensing works in RPE, as well as which sensors are responsible for internally generated or internalized nucleic acids and activating the type I IFN pathway in the retina, remains unknown.

In this study, we confirmed that RPE could both produce and respond to interferon-beta (IFN-$\beta$), leading to downstream signaling. Surprisingly, whereas RPE cells were demonstrated to directly respond to intracellular RNA, they did not respond directly to DNA due to lack of expression of the cyclic GMP-AMP synthase (cGAS) DNA sensor. We further identified the RNA sensor RIG-I (also known as DExD/H-box helicase 58, DDX58) as a key sensor for initiating the type I IFN response in RPE.

## 2. Materials and Methods

*2.1. Human samples.* Postmortem human eyes, including patients with geographic atrophy (GA) and non-AMD controls, were procured from the Lions Eye Institute for Transplant & Research (LEITR; Tampa FL) with consent of donors or donors' next of kin and in accordance with the law of US and Florida, the Declaration of Helsinki and FDA regulations, and Novartis guidelines of using human tissues in research. All study tissues were preserved within 6 hours postmortem or less. The donor information used for IHC and RNAscope is listed in Supplementary Table 1.

*2.2. Immunohistochemistry (IHC) and RNAscope.* For IHC, the eyes were fixed in Modified Davidson's Fixative (MDF, H0290-500ML, Sigma-Aldrich, St. Louis, MO) for 48 hours, followed with 70% alcohol for an additional 48 hours all at room temperature. The eyes were embedded in paraffin wax, serially sectioned at a thickness of 5 $\mu$m through the optic nerve, and processed for antibody staining using Leica Bond RX according to manufacturer's instructions. ×20 and ×40 images were taken by the Aperio AT2 scanner. The specificity of RIG-I (LsBIO LS-C344928, Lifespan Biosciences, Seattle, WA) antibody was validated using A549-Dual and A549-Dual KO-RIG-I cells (Supplementary Figure 1A-B) (InvivoGen, San Diego, CA). IgG antibody was used as a negative control (Supplementary Figure 1C).

For RNAscope, in situ hybridization on MDF-fixed paraffin-embedded retinal samples was performed using the RNAscope® 2.5 LS-Reagent Kit-RED (Advanced Cell Diagnostics, Hayward, CA) with RIG-I (NM_550268) specific probe according to the manufacturer's instructions. Probes for PPIB and DapB (Advanced Cell Diagnostics) were used as positive (data not shown) and negative controls (Supplementary Figure 1D), respectively.

*2.3. Image analysis for IHC and RNAscope.* IHC slides were scanned with Aperio at ×40 magnification, and scans were analyzed with the HALO image analysis platform (Indica labs, Albuquerque, New Mexico, USA). Analysis setting was Area quantification v1.0, and the area to be analyzed was assigned with circular annotation layers placed over the ONL and RPE layer in macula region.

RNAscope slides were scanned with Aperio at ×40 magnification, and scans were analyzed with the HALO image analysis platform (Indica Labs, Albuquerque, New Mexico, USA) using the Chromogenic RNA ISH Module. This allowed for thresholding and detection of positive probe staining on a single-cell basis to quantify average number of probe copies per cell. The area to be analyzed was assigned with circular annotation layers placed over all the layers in macula region.

*2.4. Cell cultures.* ARPE-19 was purchased from ATCC (Manassas, VA; CRL-2302). ARPE-19 was cultured in DMEM/F12 (Gibco Life Technologies, Carlsbad, CA) supplemented with 10% heat-inactivated fetal calf serum (FBS, Sigma-Aldrich) and 1% penicillin/streptomycin (Gibco BRL, Grand Island, NY) at 37°C and 5% $CO_2$. Cells were cultured at least 3 weeks postseeding to form mature monolayers unless otherwise specified. Cell morphology was monitored daily, and mycoplasma was measured by MycoAlert Mycoplasma Detection Kits (Lonza, Basel, Switzerland) every other month to avoid contaminations. iCell-RPE, an iPS-derived RPE cell line, was purchased from FUJIFILM Cellular Dynamics (Madison, WI). Cells were cultured in Lonza RtEGM medium (Lonza) at 37°C and 5% $CO_2$. iPS-RPE cells were cultured on tissue culture treated plates, or

on Falcon transmembrane inserts for polarization (Corning, Corning, NY; 353095). Cells were cultured at least 3 weeks postseeding to form mature monolayers. Maturation of cells was confirmed by pigmentations, immunofluorescence staining for ZO-1 (Thermo Fisher Scientific, Waltham, MA #33-9111) and BEST1 (Novus, #NB300-164), and transepithelial resistance (Supplementary Figure 2).

THP1-Dual, THP-1-Dual KO-cGAS, A549-Dual, and A549-Dual KO-RIG-I cells were purchased from InvivoGen, and cells were prepared and cultured following the manufacturer's protocols. KO cell lines were validated by western blotting.

*2.5. Generation of ARPE-19 RIG-I KO cell line.* ARPE-19 cells stably expressing the Cas9 gene (ARPE19-Cas9) were generated by lentiviral transduction of ARPE-19 cells. Virus was harvested from supernatants of HEK-293T cells (ATCC) cotransfected with the in-house lentiviral vector pNGx_LV_c010 [12] and Lentiviral Packaging Plasmid Mix (Cellecta, Mountain View, CA; #CPCP-K2A) using TransIT-293 Transfection Reagent (MirusBio, Madison, WI). ARPE19-Cas9 cells were selected with 125 $\mu$g/mL HygromycinB (Invitrogen, Carlsbad, CA), and Cas9 expression was verified by western blotting using Anti-FLAG primary antibody (Sigma-Aldrich #F1804, Supplementary Figure 3A-B). ARPE-19 RIG-I KO cells were generated by sgRNA expression in ARPE-19-Cas9 cells by lentiviral infection using the in-house lentiviral vector pNGx_LV_g003 [12]. The sgRNA sequence targeting DDX58/RIG-I is ACTCACCCTCCCTAAACCAG. Control sgRNA sequences were as follows: Ctrl1, GTAGCGAACGTGTC CGGCGT; Ctrl2, GACCGGAACGATCTCGCGTA; Ctrl3, GGCAGTCGTTCGGTTGATAT; and Ctrl4, GCTTGA GCACATACGCGAAT. Knockout was verified by western blot analysis (Supplementary Figure 3C).

*2.6. Reagents.* IFN-$\alpha$, IFN-$\beta$, IFN-$\gamma$, and IFN-$\lambda$1/2/3 were purchased from R&D Systems (Minneapolis, MN). Anti-IFN-$\beta$ antibody (InvivoGen) was used to neutralize IFN-$\beta$. dsDNA-EC, ISD (interferon stimulatory DNA), polydA:dT, poly(I:C)-LMW, and 3p-hpRNA were purchased from InvivoGen. Total nucleic acids (NA) were isolated from ARPE-19 using Nucleic Acid Isolation Kits (Thermo Fisher Scientific) according to the manufacturer's instructions. Transfection efficiency of each inducer (~80%) was confirmed using imaging of fluorescence labeled nucleic acids in ARPE-19 and iPS-RPE cells.

*2.7. Western blot analysis and enzyme-linked immunosorbent assay (ELISA).* Culture supernatants were harvested, and whole-cell lysates were extracted using RIPA cell lysis buffer (Cell Signaling Technology, Danvers, MA) for western blotting or cell lysis buffer (CST#9803) for ELISA, supplemented with protease and phosphatase inhibitors (Thermo Fisher Scientific) according to the manufacturer's protocol. All samples were stored at −80°C before use.

For western blotting, samples (30 $\mu$g of protein) were dissolved in sample buffer (Invitrogen) and boiled for 5 min at 100°C. The sample was then separated by Criterion™ TGX™ precast gel electrophoresis and electrotransferred onto nitrocellulose membranes (Bio-Rad, Hercules, CA). The MagicMark™ XP Western Protein Standard (Invitrogen) was used as a molecular weight indicator. The membrane was blocked for 1 h using 5% milk in Tris-buffered saline and Tween 20 (TBST). Following three washes with TBST, the membrane was incubated overnight with primary antibodies purchased from Cell Signaling Technology, including cGAS (CST#15102), IRF3 (CST#11904), RIG-I (CST#3743), Histone H3 (CST#4499), $\beta$-actin (CST#5125), and GAPDH (CST#8884), at 1 : 1000 dilution. After three washes with TBST, the membrane was incubated with a secondary antibody (anti-rabbit IgG-HRP-linked antibody, at 1 : 1000 dilution; Cell Signaling Technology) for 1 h. The immunoreactive proteins were detected using the SuperSignal™ West Femto Maximum sensitivity substrate (Thermo Fisher Scientific) and imaged on FluorChem M (ProteinSimple, San Jose, CA).

For ELISA, lysates or supernatants were measured in 384-well plates using antibody pairs for ISG15 (R&D #AF4845, #A-830), cGAS (Cayman #23853, CST#66546), IFN-$\alpha$1 (Abcam #ab215408), IFN-$\beta$ (R&D #DY814), IFN-$\gamma$ (R&D #DY285B), IFN-$\lambda$1/3 (R&D #DY1598B), or Human IL-6 DuoSet for IL-6 (R&D #DY206). For some experiments, assays were run using Meso Scale Discovery plates (Meso Scale Diagnostics, Rockville, MD), and IFN-$\beta$ secretion in supernatant was analyzed using the Human IFN-$\beta$ Tissue Culture Kit (MSD #K151ADB). Protein levels were measured according to manufacturer instructions.

*2.8. RNA interference.* RNA interference against key nodes of the type I IFN pathway was performed using Qiagen (Hilden, Germany) or Dharmacon (Lafayette, CO) small interfering RNAs (siRNAs). The AllStars and Negative Control siRNAs were purchased from Qiagen and used as negative controls. Transfection of siRNAs in ARPE-19 cells was carried out using Dharmafect 4 (Dharmacon) according to the instructions of the manufacturer. Cells were transfected with 1 pmol/96-well culture dish for IFN-$\beta$ release measurement by the IFN-$\beta$ Human Tissue Culture Kit (Mesoscale Discovery, Rockville, MD). At least three different siRNAs were used for targeting each key nodes of the pathway. The knockdown efficiency was validated using real-time reverse transcription- (RT-) PCR.

*2.9. Real-Time RT-PCR.* Messenger RNAs were isolated from ARPE-19 cells treated with indicated siRNAs using the TurboCapture 96 mRNA Kit (Qiagen), and RNA was reverse transcribed using the High-Capacity cDNA Reverse Transcription Kit (Applied Biosystems, Foster City, CA). Real-time PCR was performed using FAM-labeled TaqMan probes targeting genes of interest and a VIC-labeled TaqMan probe targeting $\beta$-actin as control (Applied Biosystems). Reactions were run with TaqMan Universal PCR Master Mix on the ViiA7 system (Applied Biosystems) according to the instructions of the manufacturer.

*2.10. RPE cell death.* RPE cell death was measured using CytoTox-Glo (Promega, Madison, WI) or propidium iodide (PI, Thermo Fisher Scientific) staining and real-time

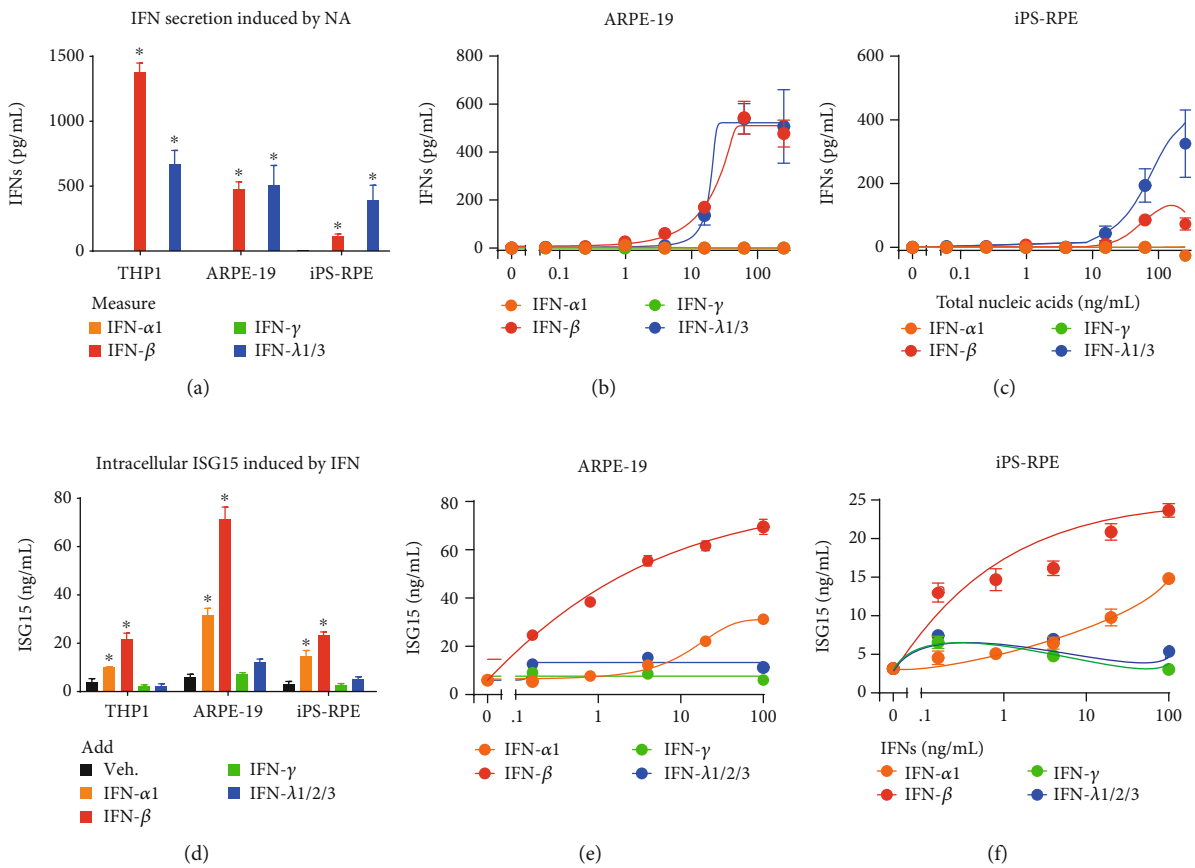


Figure 1: RPE cells respond to nucleic acids to secrete IFNs and also respond to secreted IFNs to generate ISGs. (a–c) Nucleic acid challenge-induced production of IFN-$\beta$ and IFN-$\lambda$ in RPE. Total nucleic acids (NA) were isolated from ARPE-19 cells and transfected into indicated cell types at 0.25 $\mu$g/mL. Secreted IFN proteins were measured using ELISA 24 h after stimulation; only IFN-$\beta$ and IFN-$\lambda$ were predominantly produced in RPE cells. Examples of dose-response curves in ARPE-19 (b) and iPS-RPE (c) cells. (d–f) RPE cells respond to IFN-$\alpha$ and IFN-$\beta$ to initiate downstream signaling and generate ISGs. Several key types of IFNs (100 ng/mL each) were added to RPE cells, with RPE cells primarily responding to IFN-$\alpha$ and IFN-$\beta$ by inducing intracellular ISG15 measured by ELISA 24 h after stimulation. Examples of dose-response curves in ARPE-19 (e) and iPS-RPE (f) cells. Each data point represents biological replicates ($n = 3$), and is indicated as mean ± SD. $^*p < 0.05$ compared with relative vehicle control groups.

monitoring using IncuCyte (Essen BioScience, Ann Arbor, MI). For CytoTox-Glo, cells were treated with indicated stimuli for 2, 6, 24, and 72 h, and then supernatants were collected and measured by CytoTox-Glo according to the instructions of the manufacturer. To monitor PI staining in real time, cells were treated with indicated stimuli and imaged in IncuCyte for bright field and red channel every 3 h according to the instructions of the manufacturer. Images were analyzed using the IncuCyte software.

*2.11. Transepithelial resistance (TER).* Barrier function of RPE cells was assessed by monitoring TER every 15 minutes by means of a cellZscope 2 (NanoAnalytics GmbH, Münster, Germany). The resistance values for individual monolayers at specific times ($\Omega$cm$^2$) were determined, subtracted for background resistance produced by the blank filter and culture medium (as 0%), and normalized to baseline resistance prior to stimulation (as 100%).

*2.12. Data Analysis.* Protein levels measured by ELISA were presented as absolute amount, and gene levels by qPCR were normalized by $\beta$-actin. Three independent experiments with triplicates within each experiment were performed, and values were presented as mean ± SD. Two groups were compared using Student's $t$-test. Multiple comparisons were made using analysis of variance followed by the post hoc *Newman–Keuls* test. Differences were considered significant at $p < 0.05$.

## 3. Results

*3.1. Retinal pigment epithelium cells both produced and responded to type I interferon.* Previous reports have shown that the type I IFN pathway is activated in patients with GA and enriched in RPE [4]. We thus decided to focus on the mechanisms through which such a response might be potentiated in RPE. We used ARPE-19, a spontaneously arising RPE cell line, and induced pluripotent stem- (iPS-) derived RPE cells from multiple donors in our in vitro assays. Although ARPE-19 is a widely used human-derived RPE-like cell line, it has been reported to lack some features of mature RPE, such as pigmentation and expression of

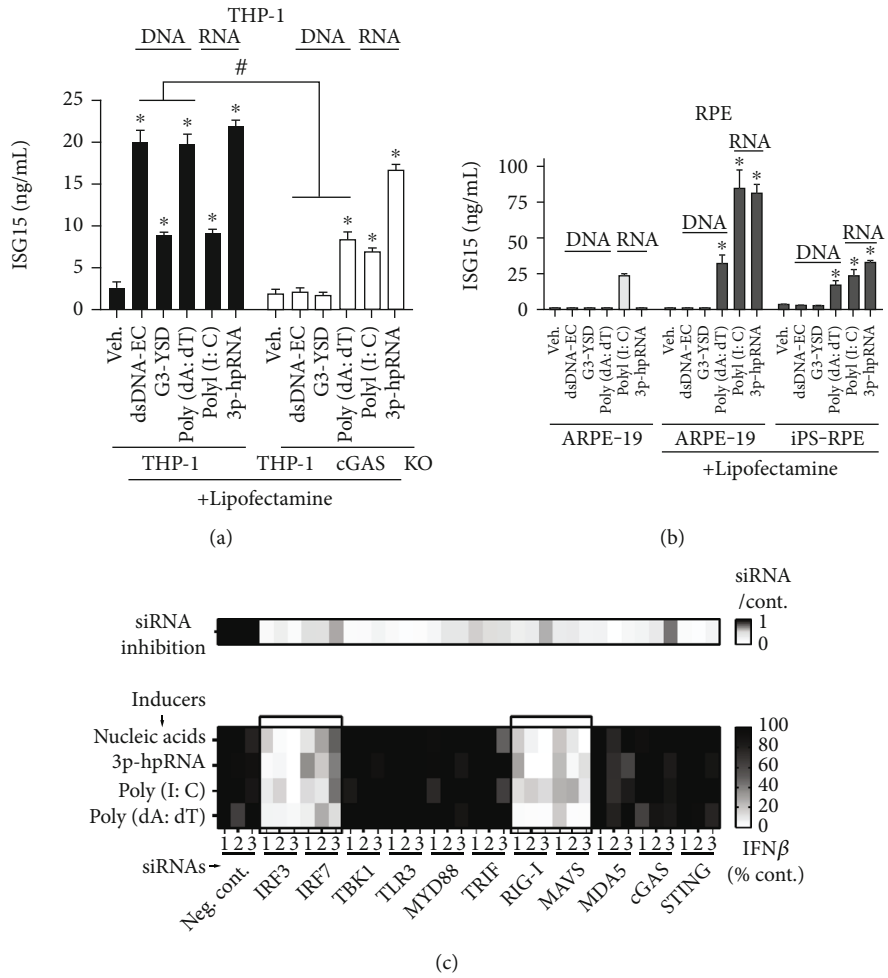


Figure 2: Identification of RIG-I as the key sensor in type I IFN response in RPE. (a, b) RNA but not DNA could be sensed by RPE to induce type I IFN response, suggesting the lack of DNA sensors in unstimulated RPE. THP-1 and THP-1 cGAS KO cells were used as controls (a). Cells were treated with indicated inducers at 0.25 $\mu$g/mL, with or without the Lipofectamine transfection reagent, and intracellular ISG15 was measured by ELISA 24 h after stimulation. Each bar represents biological replicates ($n = 3$) and is indicated as mean ± SD. Note that ARPE-19 without transfection did not respond to most tested inducers except for poly(I:C). $^{*}p < 0.05$ compared with corresponded vehicle-treated groups. $^{\#}p < 0.05$ compared with same induces in parental cells. (c) Type I IFN response was induced via the RIG-I–MAVS–IRF3 axis in ARPE-19 cells. ARPE-19 cells were cultured 10 d after reaching confluence for screening purposes. Different key nodes for the activation of the IFN pathway were knocked down using siRNAs (at least 3 different siRNAs for each gene). Cells were then treated with indicated nucleic acids, and the release of secreted IFN-$\beta$ was measured by ELISA 24 h after stimulation. Similar results were observed in 3 independent experiments with different inducers (indicated in different lines) or different siRNAs (shown as different column); a single representative experiment is shown as an example. A heatmap was used to better visualize the percentage (%) change in the results. The efficiency of the mRNA knockdown was validated by qPCR and shown at the top in the form of heatmap. About ~70% inhibition was observed in most tested siRNAs.

*RPE65*, while retaining some RPE features such as morphology, polarization, and phagocytosis [13]. Due to these limitations, we also utilized iPS-derived RPE cells to further support our interrogations. Prior to performing experiments, we confirmed the characteristics of mature RPE in iPS-RPE cells (Supplementary Figure 3), including barrier function, pigmentation, morphology, and expression of mature RPE markers (bestrophin 1 (*BEST1*), etc.).

There are 3 major types of IFN family members: type I (IFN-$\alpha$ and IFN-$\beta$), type II (IFN-$\gamma$), and type III (IFN-$\lambda$). To determine exactly which types of IFN are stimulated by exposure to nucleic acids in RPE, we measured the secretion of IFNs. We used a total cell nucleic acid (NA) fraction, including both DNA and RNA, to stimulate both ARPE-19 and iPS-RPE cells. We then detected the secretion of both IFN-$\beta$ and IFN-$\lambda$ in NA-transfected RPE cells (Figures 1(a)–1(c)) using ELISA, hence confirming that RPE could sense nucleic acids to generate IFNs. In addition, to determine whether IFNs participate in an autoregulatory feedback loop within RPE, we treated cells with recombinant IFNs and measured the induction of intracellular ISG15, one of the most strongly and rapidly induced interferon-stimulated genes (ISGs) [14–16], using ELISA. Upon treatment with different IFN types, our results indicated that RPE cells responded to type I IFN with downstream activation of ISG15 (Figures 1(d)–1(f)). Taken

together, these data showed that RPE cells have the necessary components to both produce IFN, namely IFN-$\beta$ and IFN-$\lambda$, and respond to IFN, primarily IFN-$\beta$, via the induction of downstream IFN signaling.

*3.2. Identification of RIG-I as a major sensor of intracellular RNA in retinal pigment epithelium.* Upon showing that RPE cells could both produce and respond to IFN, we next sought to determine the sensors responsible for recognition of nucleic acids, including both DNA and RNA. First, we used THP-1 cells to validate the quality of nucleic acid inducers (either DNA or RNA) used in RPE cells (Figure 2(a)). To this end, we challenged RPE cells with DNA or RNA, with or without transfection reagent, in order to capture both cell surface and internal NA sensors [4, 11, 17–19]. As shown in Figure 2(b), in the absence of transfection reagent, ARPE-19 cells did not respond to any inducers tested except for poly(I:C), which was consistent with previous reports that RPE responded to extracellular poly(I:C) through TLR3, a reported RNA sensor [10, 11, 19]. Next, we wanted to characterize the intracellular NA sensors in RPE cells. Specifically, we aimed to determine whether RPE cells could detect intracellular DNA, RNA, or both. To our surprise, we observed that in the presence of transfection reagent, both ARPE-19 and iPS-RPE cells responded to RNA but not DNA except for poly(dA:dT), a repetitive synthetic double-stranded DNA sequence (Figure 2(b)). This response was greater than that to nucleic acids applied without transfection reagent, which is consistent with a similar observation in endothelial cells [20]. Interestingly, as shown in Figure 2(a), poly(dA:dT)-induced IFN response was also demonstrated to only be partly reduced in THP-1-Dual KO-cGAS cells, suggesting that poly(dA:dT) might be recognized and initiate downstream signaling indirectly through a nonclassic DNA sensing system. This agreed with previous reports that poly(dA:dT) could indirectly activate IFN pathways through an RNA polymerase III-transcribed RNA intermediary [17, 21].

In order to pinpoint specific intracellular nucleic acid sensors in RPE, we performed an in vitro siRNA knockdown screen targeting key nodes of the IFN pathway in ARPE-19 cells. To this end, we tested different nucleic acids, including commercially available DNA/RNA mimics or isolated total nucleic acid content from cells as inducers, and evaluated the consequent secretion of IFN-$\beta$. We used a knockdown of the interferon regulatory factor 3 (IRF3) transcription factor, one of the master regulators of IFN [9, 22], as our positive control. We accordingly noted that IRF3 knockdown significantly inhibited the induction of the secretion of IFN-$\beta$ (Figure 2(c)). Interestingly, we found that the most pronounced reduction in the secretion of IFN-$\beta$ was observed in both RIG-I and MAVS knockdown groups (Figure 2(c)), regardless of whether RPE was stimulated with RNA or DNA or a RNA/DNA mixture. These results indicated that the RIG-I-mediated signaling pathway is responsible for sensing intracellular nucleic acids in RPE cells.

We performed further validation of the importance of RIG-I in the recognition of intracellular nucleic acids using a CRISPR/Cas9 KO in ARPE-19 cells. We generated an

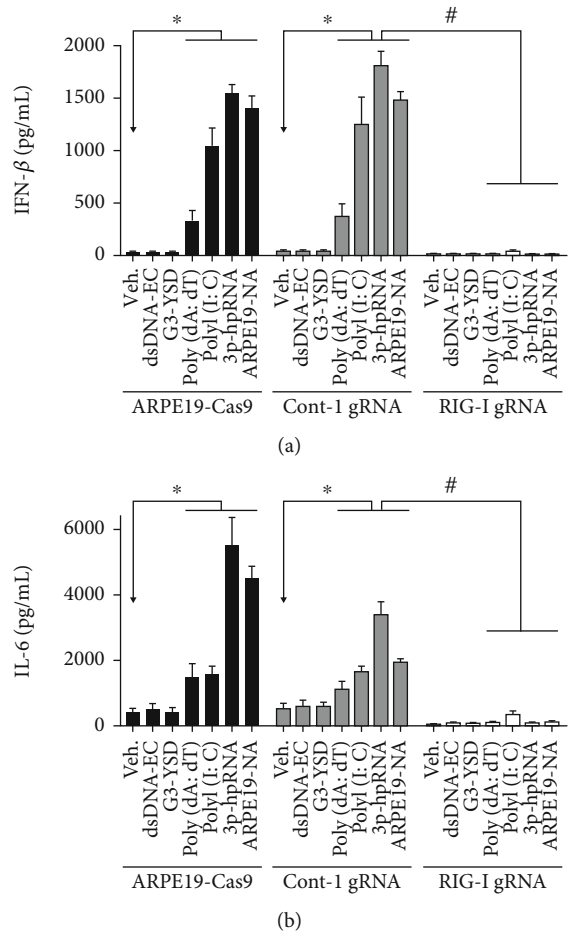


Figure 3: ARPE-19 cannot sense nucleic acids in RIG-I-deficient cells. The ARPE-19 RIG-I KO cell line was generated and validated using an ARPE-19-Cas9 line (see Supplementary Figure 3). Cells were stimulated with indicated inducers at 0.25 $\mu$g/mL, and the release of IFN-$\beta$ or IL-6 was measured by ELISA 24 h after stimulation. (a) The IFN response was abolished in RIG-I KO ARPE-19 cells. Similar to ARPE-19, Cas9-expressing ARPE-19 cells respond to RNA but not DNA. Interestingly, ARPE-19 RIG-I KO cells did not respond to any tested nucleic acids, further validating RIG-I as the major sensor in RPE cells. (b) The nucleic acid-induced release of IL-6 was also reduced in ARPE-19 RIG-I KO cells. Note that unlike other stimuli, the poly(I:C)-induced release of IL-6 was only partly reduced in RIG-I KO cells, suggesting the potential involvement of other sensors. $^{*}p < 0.05$ compared with corresponded vehicle-treated groups. $^{\#}p < 0.05$ compared with same inducers in control gRNA-transduced cells.

ARPE-19 cell line stably expressing Cas9 and control or RIG-I gRNA-transduced cells and validated them by western blotting (Supplementary Figure 3). Compared with parental cells, control gRNA-transduced cells were demonstrated to have a similar profile of nucleic acid sensing. However, the secretion of IFN-$\beta$ in RIG-I gRNA-transduced cells was shown to be completely abrogated (Figure 3(a)), confirming the role of RIG-I as a key sensor for type I IFN response in RPE cells in vitro.

In addition to IFN, RIG-I sensing of nucleic acids has also been shown to activate NF-$\kappa$B-mediated cytokine release,

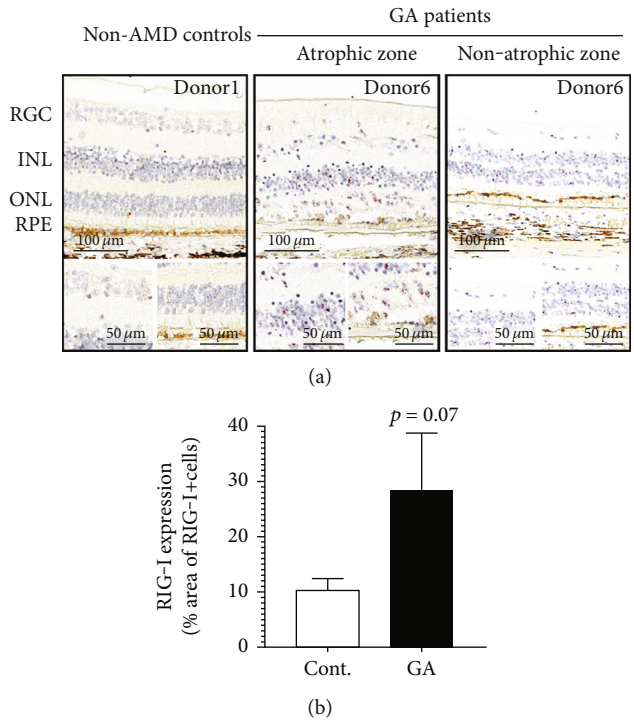


Figure 4: RIG-I mRNA is elevated in patients with GA. (a) The elevation in the levels of RIG-I mRNA in patients with GA relative to non-AMD controls was observed using RNAscope. Low levels of RIG-I signal (red dots) were detected in non-AMD control patients, whereas elevated signals were detected in RGC, ONL, INL, and RPE layers of patients with GA. Scale bars are indicated. $n = 3$/group, patient information is listed in Supplementary Table 1. DAPB was used as negative control (see Supplementary Figure 1D). In addition, the RIG-I signal in the macular region was analyzed by HALO, with the % area of RIG-I positive signals being shown in (b).

including interleukin 6 (IL-6). It was reported that RIG-I could directly regulate the expression of NF-κB [23] or indirectly regulate the activation of NF-κB through mitochondrial antiviral signaling protein (MAVS) and TANK-binding kinase 1 (TBK1) [24, 25]. Therefore, we used the secretion of IL-6 as a readout to evaluate the nucleic acid-induced RIG-I-mediated activation of NF-κB in RPE cells. We found that most of the secretion of IL-6 was abolished in RIG-I KO cells, indicating that the NF-κB-mediated cytokine release was RIG-I-dependent. Interestingly, in contrast to the IFN response, poly(I:C)-induced IL-6 release was shown to be only partially reduced in ARPE-19-RIG-I KO (Figure 3(b)), suggesting another RNA sensor, that is, TLR3, might be responsible for this poly(I:C)-induced cytokine release in RPE cells, in agreement with previous reports [11]. Furthermore, we noted that the poly(dA:dT)-induced response in ARPE-19 was abolished in RIG-I siRNA-treated or ARPE-19-RIG-KO cells, as shown in Figures 2(c) and 3(a), respectively, further confirming the RIG-I-dependent response of ARPE-19 cells to poly(dA:dT).

Our findings suggested that RIG-I is the key NA sensor in RPE cells. To determine whether these in vitro findings were relevant to AMD, we first sought to determine whether the expression of RIG-I was increased in samples from donors with AMD. We used RNAscope and immunohistochemistry (IHC) to analyze retinal sections from donors with AMD. We observed that the mRNA expression of RIG-I was low but detectable in control human donors, whereas it significantly upregulated in the retina of patients with GA, notably in retinal ganglion cells (RGCs), outer nuclear layer (ONL), inner nuclear layer (INL), and RPE layers (Figure 4). This was consistent with the role of RIG-I as a well-known mammalian ISG [26]. In order to further determine the expression of the RIG-I protein in human donors, we validated a RIG-I antibody for IHC using the A549 RIG-I KO cell line (Supplementary Figure 1A-B). We consistently observed that the levels of the RIG-I protein in RPE cells were increased in all 5 patients with GA compared with control donor samples (Supplementary Figure 5 and Figure 5), supporting the key role of RIG-I in mediating type I IFN response in RPE cells. Surprisingly, we found that in contrast to the transcript, the RIG-I protein was almost exclusively observed in RPE and choroid layers in both patients with GA and non-AMD controls (Figures 4(a) and 5(a)), suggesting that posttranscriptional mechanisms might be involved in regulating the expression of RIG-I in non-RPE cell types. Taken together, these results confirmed our in vitro findings that RPE could detect intracellular RNA via RIG-I.

*3.3. Expression of cGAS Was Not Detectable in Retinal Pigment Epithelium.* The cGAS DNA sensor has been reported to play a major role in sensing the Alu-RNA-induced IFN response and degeneration of RPE, in part through sensing mitochondrial DNA [4]. We were thus surprised that knockdown of cGAS was shown to have little

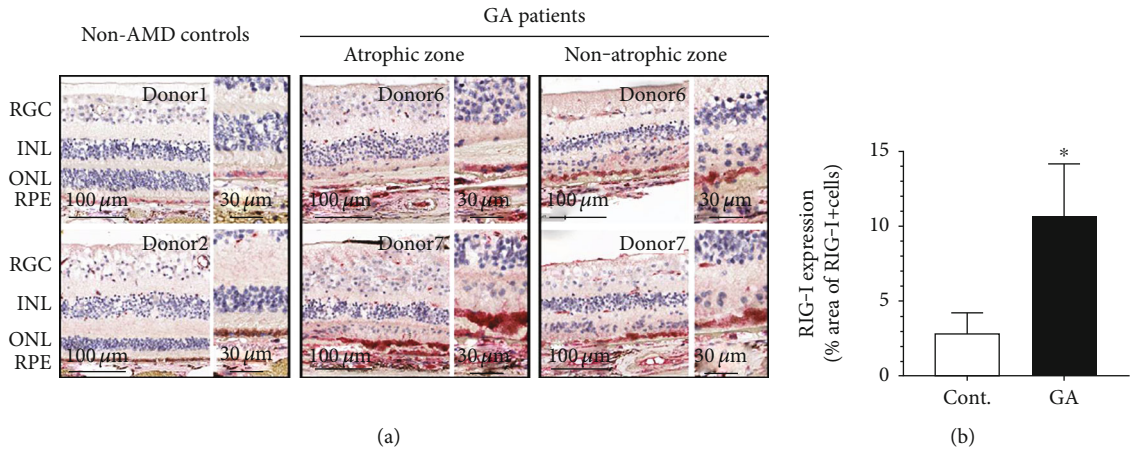


Figure 5: The RIG-I protein is expressed in human RPE, and elevated in patients with GA. (a) The expression of the RIG-I protein in non-AMD control and patients with GA was measured using IHC. Note that, unlike mRNA, RIG-I protein (red) was mainly enriched in RPE and choroid. The IgG control was used as negative control (see Supplementary Figure 1C). Examples of region selection for IHC and RNAscope from donor 6 (patient with GA) are shown in Supplementary Figure 4. In addition, the RIG-I signal in the macular region was analyzed by HALO, with the % area of RIG-I positive signals being shown in (b). Representative pictures of RIG-I IHC for each donor are shown in Supplementary Figure 5. Scale bars are indicated. $n = 5$/group, and patient information is listed in Supplementary Table 1. $^{*}p < 0.05$ compared with non-AMD control patients.

effect on the DNA-induced production of IFN within RPE (Figures 2(b) and 2(c)). Upon further investigation, cGAS transcripts were undetected in iPS-RPE, which are more similar to primary RPE cells, and detected only at very low levels in ARPE-19 cells (at least 1000-fold lower than housekeeping gene controls). Our findings were supported by recent analyses of single-cell transcripts from human donors [27] showing that cGAS was not detectable in RPE and only enriched in myeloid cells (Supplementary Figure 6). Next, we evaluated the level of the cGAS protein in RPE in vitro to confirm the lack of expression of this gene. We measured the level of the cGAS protein using a cGAS antibody validated in THP1-Dual KO-cGAS cells (Supplementary Figure 7A). Accordingly, we did not detect any cGAS protein in either ARPE-19 or iPS-RPE cells (Supplementary Figure 7A). We observed a similar pattern using ELISA, where cGAS was detected in THP-1 cells but undetectable in negative control THP1-Dual KO-cGAS cells and below the limit of detection in either ARPE-19 or iPS-RPE cells (Supplementary Figure 7B).

Previous reports suggested that cGAS was part of the induced ISG response machinery following activation of type I IFN response [28, 29]. However, when nucleic acids were used to stimulate cells in vitro, we were unable to detect the expression of cGAS in either ARPE-19 or iPS-RPE cells (Supplementary Figure 7A and 7B). This suggested that cGAS might not be expressed in RPE and was not induced in RPE following exposure to nucleic acids.

It has been reported that the cGAS protein might predominantly reside in the nucleus, interacting with, and potentially being sequestered by, genomic DNA [30]. To exclude this possibility within RPE, we applied high doses of salt to dissociate proteins and genomic DNA. We used histones as a control to show that chromatin-bound proteins were released after treatment with high-dose sodium chloride; however, cGAS was still undetectable (Supplementary Figure 7C). Collectively, these results confirmed that RPE have an undetectable expression of cGAS and consequently cannot directly respond to DNA stimulation through cGAS (Figures 2(b) and 2(c)).

*3.4. Activation of Interferon Induced Cell Death-Related Gene Expression and Altered the Barrier Function of Retinal Pigment Epithelium in Response to RNA.* In order to evaluate whether activation of the interferon pathway by nucleic acids can induce RPE cell degeneration, we measured iPS-RPE cell death using the following two methods: (1) enzyme release from dead cells by CytoTox-Glo and (2) real-time cell death monitoring by propidium iodide (PI) staining using IncuCyte. While cell death was observed in response to the positive control staurosporine, cell death was not observed in cells treated with nucleic acids (Figures 6(a) and 6(b)). The data suggest NA-mediated activation of the IFN pathway does not result in immediate RPE cell death.

We then examined the expression of cell death pathway genes, as it has been reported in other settings that type I IFN response can prime cells to become more sensitive toward cell death by upregulating the expression of key nodes in cell death pathways [31–35]. Indeed, as shown in Figures 6(c)–6(f), gene expression of key effectors of various types of cell death, including CASP7/8 (apoptosis), Gasdermin-D (GSDMD, pyroptosis), and MLKL (necroptosis), was induced upon RNA stimulation. This data supports the hypothesis that NA sensing in RPE cells may sensitize the cells to secondary insults by upregulating cell death effectors during degeneration during disease progression and eventually lead to RPE cell death.

Furthermore, to better understand the biological consequence of elevated type I IFN response on RPE cells, we set out to investigate the RPE barrier, as this is a key RPE cell

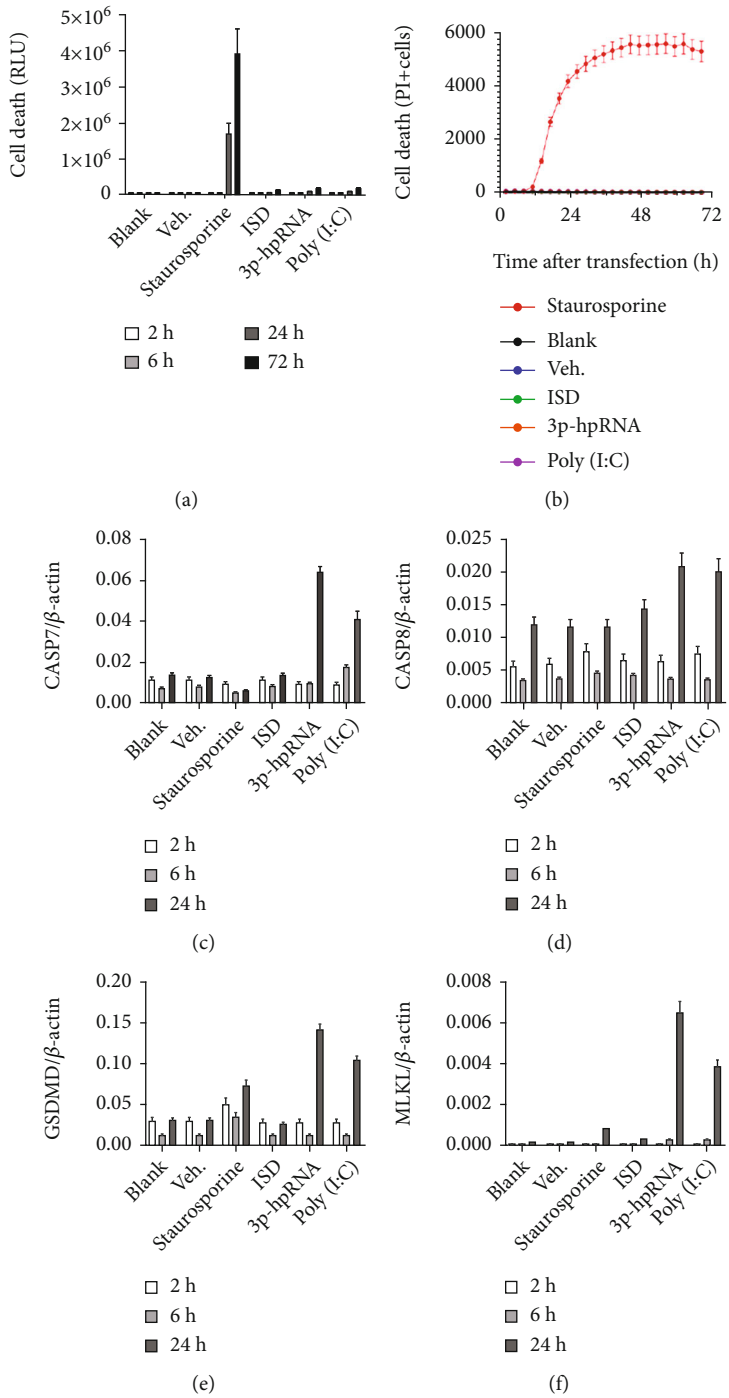


Figure 6: Nucleic acids do not induce RPE cell death but increase pro-cell death pathway genes. (a, b) Cell death in nucleic acid-transfected iPS-RPE cells (iCell) was measured by CytoTox-Glo (a) or propidium iodide (PI) staining (b). Staurosporine (10 $\mu$M) was used as positive control to induce apoptosis. None of the tested nucleic acids (1 $\mu$g/mL) induced RPE death. (c–f) Cell death pathway-relevant genes CASP7, CASP8, GSDMD, and MLKL were measured by qPCR in iCell at indicated times after transfection of nucleic acids (1 $\mu$g/mL). 3p-hpRNA and poly(I:C), but not ISD, induced upregulation of pro-death genes.

function [36, 37]. In order to evaluate the effects of IFNs on RPE barrier function, we measured the transepithelial resistance (TER) in polarized iPS-RPE cells cultured on a permeable transmembrane matrix. As shown in Figures 7(a) and 7(d), the barrier function was impaired in cells treated with IFN-$\beta$, and, as expected, an anti-IFN-$\beta$ antibody was able to prevent this IFN-$\beta$-induced leakage. Consistent with our findings, RNA but not DNA was shown to be capable of impairing TER (Figures 7(b) and 7(d)). We were able to further validate that the nucleic acid sensing-induced impaired barrier

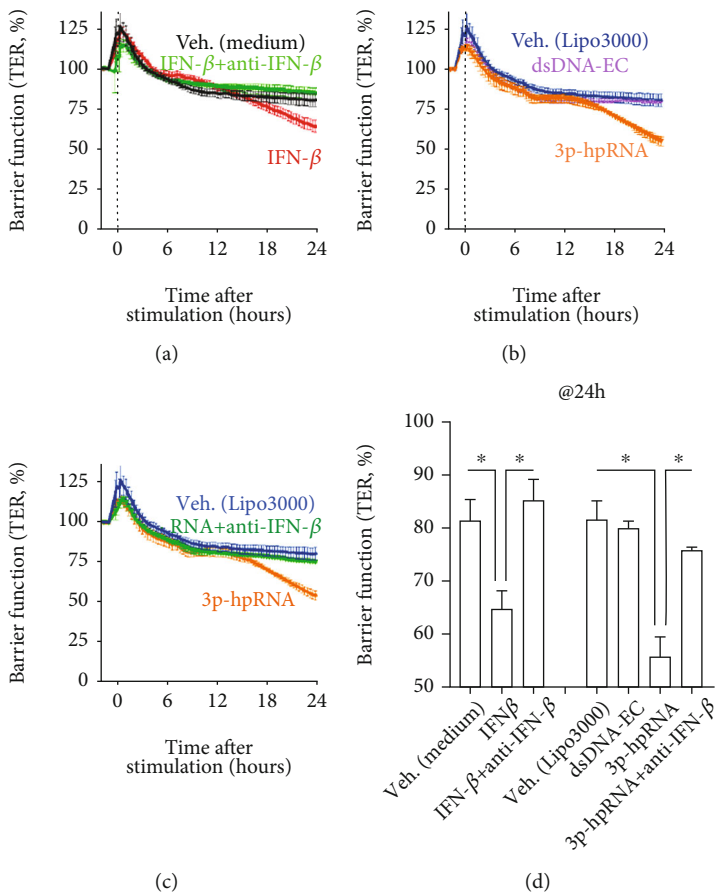


Figure 7: Type I IFN response alters RPE barrier function. iPS-RPE cells were cultured on transmembrane in 24-well plates, and TER was measured as an indicator of RPE barrier function. Note that treatment with IFN-$\beta$ at 100 ng/mL (a) or transfection with RNA but not DNA at 0.25 $\mu$g/mL (b) could reduce TER, whereas anti-IFN-$\beta$ could recover the IFN-$\beta$-induced (a) and RNA-induced loss of barrier function (c). Normalized TER after 24 h treatment is summarized in (d) as a bar graph indicating changes to the barrier function. Each data point represents biological replicates ($n = 3$). $^*p < 0.05$ compared with IFN-$\beta$- or 3p-hpRNA-induced group with TER loss.

function was dependent on secreted IFNs, as addition of an anti-IFN-$\beta$ antibody was sufficient to prevent the loss of TER in RPE (Figures 7(c) and 7(d)). These results further supported our findings that the IFN response in RPE cells is induced through RNA but not DNA sensors.

## 4. Discussion

Type I IFN signaling is known to play a critical role in host defense, especially in infectious diseases. Increasing evidence has suggested a role for the type I IFN response in chronic diseases with sterile inflammation, especially autoimmune diseases and aging-related diseases, such as systemic lupus erythematosus, multiple sclerosis, Sjogren's syndrome, atherosclerosis, and Alzheimer's disease [38–42]. Our data, in agreement with previous reports [4, 5], showed that this pathway is also involved in AMD, an age-related degenerative disease. In our study, RIG-I, one of the key node-sensing nucleic acids and an ISG in the IFN response, was significantly upregulated in patients with GA. In agreement with previous publications [4], our data revealed an increased type I IFN response in retina, exhibited by increased levels of IFN-$\beta$ in RPE of patients with GA.

There are many innate receptors responsible for sensing nucleic acids and activating the type I IFN pathway. In particular for RNA sensing, TLRs, especially TLR3, have been reported to recognize dsRNA to initiate an IFN response in RPE, with the TLR3 412Phe variant showing protective effects against GA [19, 43, 44]. Human RIG-I, encoded by DDX58, is a dsRNA helicase enzyme that has been demonstrated to play important roles in RNA sensing. In this study, we showed that there was no IFN response detected in cells responding to nucleic acids without transfection reagents except for poly(I:C) (Figure 2(b)), which is consistent with previous reports showing that TLR3 is responsible for extracellular poly(I:C)-induced cytokine release in RPE [10, 11]. Here, we hypothesized that both TLR3 and RIG-I might be important for initiating intracellular poly(I:C)-induced NF-$\kappa$B-dependent release of cytokines from RPE cells (Figure 3(b)). However, we found that knockdown of members of the TLR signaling pathway (e.g., TLR3, MYD88 innate immune signal transduction adaptor (MYD88), and Toll-like receptor adaptor molecule 1 (TICAM1, known as TRIF)) had no effect on IFN-$\beta$ production (Figure 2(c)), but knockdown or knockout of RIG-I abolishes IFN-$\beta$ and IL-6 production in RPE (Figures 2(c), 3(a), and 3(b)),

suggesting that RIG-I but not TLR3 is the key sensor for initiating a type I IFN response in responding to intracellular RNA in RPE.

While the production of type I IFN is known to be caused by viral and bacterial infections, it might also be the result of chronic sterile inflammation. Based on our results using bacterial dihydrodipicolinate reductase (dapB) as a negative control for RNAscope (Supplementary Figure 1D), we excluded the possibility of bacterial contamination in our human donor samples and considered that the elevation of type I IFN response observed in patients with GA was due to sterile inflammation. Endogenous nucleic acids, for example, might be abnormally released into the cytosol during cellular dysfunction and might then be recognized by corresponding sensors, resulting in the induction of different inflammatory mediators via specific signaling pathways [45, 46]. While both DNA and RNA might potentially activate IFN pathways, when studying this possibility in RPE cells, which are unique to the retina, we found that RNA, but not DNA, except for poly(dA:dT) as discussed above, induced an IFN response (Figure 2(b)). There might be several potential sources of RNA inducers in patients with AMD. For instance, mitochondrial dysfunction was highlighted as one of the main features observed in patients with AMD [47]. In addition to mtDNA release from dysregulated mitochondria triggering a type I IFN response via the cGAS-STING pathway [46], it was reported that mitochondrial double-stranded RNA (mtdsRNA) could trigger a type I IFN response through RIG-I and the melanoma differentiation-associated protein 5 (MDA5) RIG-I-like receptor [45]. Additionally, DICER dysregulation and Alu RNA accumulation were reported in patients with AMD, suggesting that this accumulation might cause mitochondrial dysfunction, mtDNA release, and subsequent initiation of the IFN response via the cGAS-STING pathway [4].

Our study, in contrast, showed that cGAS was not involved in nucleic acid sensing in RPE cells. Multiple methods were used, and we were unable to confirm any detectable expression of cGAS in either basal or induced RPE cells. Therefore, it is more likely that accumulated RNA directly activated type I IFN response in RPE cells via the RNA sensor RIG-I. This finding was in agreement with recently published results on human retina profiling using single-nucleus RNA-seq (NucSeq) [27]. This dataset was internalized and reanalyzed. Briefly, RIG-I (DDX58) is known to be widely expressed in most cells, including RPE, and even more highly enriched in astrocytes and Muller cells. However, interestingly, cGAS (MB21D1) is known to be only expressed in myeloid cells, but not RPE (Supplementary Figure 6), further supporting our findings on the lack of expression of cGAS in RPE (Supplementary Figure 7).

There might be several potential explanations for the discrepancies observed between reports on the activity of RIG-I and cGAS in the retina: (1) RPE cells might directly respond to Alu-RNA via RIG-I, potentially initiating a type I IFN response and then signaling to professional inflammatory cells, such as macrophages or microglia, to amplify this response in a cGAS-dependent manner; (2) macrophages/-microglia might initiate retinal damage via the cGAS/STING pathway and then activate/prime RPE cells to be more sensitive to RIG-I-recognized RNA inducers, thus helping amplify the signal to affect the whole retina. That is, other cell types, particularly macrophage/microglia, might be activated through cGAS/STING and subsequently lead to activation and damage of RPE cells. Therefore, it would be interesting to further explore the mechanisms by which other cell types in the retina communicate and are coactivated alongside the RPE.

The elevation of IFN signatures (i.e., ISGs), which is observed in patients with GA perhaps as a consequence of nucleic acid sensing, has been shown to be a sign of both activated IRF3-mediated type I IFN response and NF-$\kappa$B-mediated release of cytokines through nucleic acid sensors and the TBK1 essential mediator [8, 9, 23–25]. The induction of IFN pathway genes, including cell death effectors and other ISGs, could amplify the signal through a positive feedback loop. This might include key nodes of the IFN pathway, such as cGAS, RIG-I, interferon regulatory factor 7 (IRF7), and signal transducer and activator of transcription 1 (STAT1) [26, 48, 49], which could increase the sensitivity of the sensing of nucleic acids and thus keep activating NF-$\kappa$B and IRF3-mediated inflammation. Here, we showed that in addition to type I IFN response, the NF-$\kappa$B-mediated release of cytokines was also activated in RPE cells in response to nucleic acid sensing, specifically RNA (Figure 3(b)). Additionally, the RNA-induced release of cytokines was abolished in RIG-I KO cells, indicating that the secretion of cytokines in response to nucleic acid sensing was also RIG-I-dependent in RPE.

Interestingly, we observed the upregulation of RIG-I transcripts across the entire retina and RPE-choroid, and not confined to atrophic regions in patients with GA (Figure 4(a)). As RIG-I is one of the ISGs, this data suggested that IFN-mediated inflammation was amplified in the whole retina of patients with GA. It is possible that activation of type I IFN response in RPE cells may prime the cells and lead to further cell degeneration/death across the retina by upregulating ISGs, such as mixed lineage kinase domain-like pseudokinase (MLKL), caspase 8 (CASP8), and TNF superfamily member 10 (TNFSF10, known also as TRAIL) [31–35]. In our study, we found that 3p-hpRNA and poly(I:C) could induce CASP7/8, GSDMD, and MLKL gene expression (Figures 6(c)–6(f)), further supporting that although IFN activation did not directly induce RPE death, it induces key nodes of cell death pathways and may prime RPE cells toward death. This is consistent with the slow progressive nature of RPE degeneration in AMD and GA, where it may take years and often decades to develop atrophy and cause vision loss.

In the clinic, IFN-$\alpha$ is commonly used for the treatment of patients with hepatitis C, whereas IFN-$\beta$ is used as a first line immune-modulatory treatment for multiple sclerosis. While IFN-$\alpha$ and IFN-$\beta$ have been reported to exhibit similar systemic side effects, retinopathy is a frequently observed adverse effect of IFN-$\alpha$, with only a limited number of case reports on IFN-$\beta$-associated retinopathy being reported [50, 51]. Interestingly, the previously reported

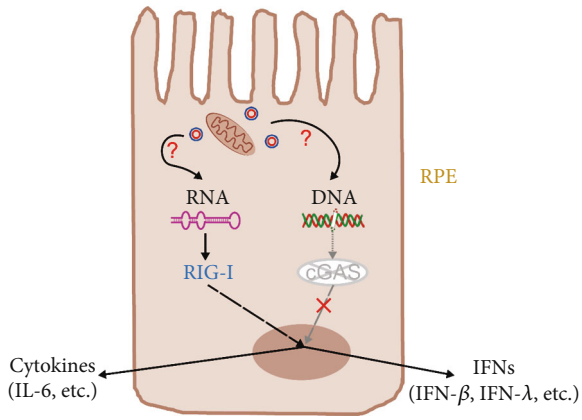


Figure 8: Schematic diagram for potential mechanism of intracellular nucleic acid sensing in RPE.

issue of ocular toxicity resulting from siRNA therapy [44] has been raised again for adeno-associated viral vector- (AAV-) based gene therapy [52]. A potential explanation, in addition to IFN-mediated effects on cell death, might be that IFN might impair RPE barrier function, as shown in our study (Figure 7).

In summary, we identified the RIG-I/DDX58 RNA sensor as the major sensor for intracellular nucleic acids in RPE cells. A schematic diagram to illustrate a potential mechanism is summarized in Figure 8. Our results illustrated the mechanism by which type I IFN response functions in RPE cells, and especially the means by which distinct cell types might contribute to common molecular mechanisms via different signaling pathways, thus giving new clues for the improved understanding of the mechanisms of action at the single-cell level through in vivo observations. The results of this study might help explain the mechanism through which nucleic acids can induce retinal degeneration and thereby identify a potential therapeutic target to reduce the IFN response and improve or delay retinal degeneration.

## Abbreviations

AMD: Age-related macular degeneration
RPE: Retinal pigment epithelium
IFN: Interferon
ISG: Interferon-stimulated gene
GA: Geographic atrophy
TLR: Toll-like receptor
DAMPs: Danger-associated molecular patterns
PRRs: Pattern recognition receptors
dsDNA: Double-stranded DNA
TER: Transepithelial resistance.

## Data Availability

The authors confirm that the data supporting the findings of this study are available within the article and/or its supplementary materials.

## Disclosure

Henry Y. Wu's current address is Q32 Bio, One Broadway, 11th Floor, Cambridge, MA, USA. Qian Huang's current address is Dragonfly Therapeutics, 35 Gatehouse Drive, Waltham, MA, USA.

## Conflicts of Interest

All authors of this manuscript, during the time of preparation, were employees of Novartis Pharma AG, Cambridge, USA.

## Authors' Contributions

Joshua Schustak and Michael Twarog contributed equally to this work.

## Acknowledgments

We thank Yubin Qiu for providing human samples, Angela Banks and Sandra Jose for bioinformatics support, and Dr. Robert Esterberg and Dr. Quintus G. Medley for their critical reading of the manuscript.

## Supplementary Materials

Table S1: patient information for this study. Figure S1: method optimization and validation for IHC and RNAscope. Figure S2: iPS-derived RPE cells show RPE phenotypes. Figure S3: the method of generation and validation of an ARPE-19-Cas9 cell line. Figure S4: examples of RIG-I mRNA (by RNAscope, (a)) and protein (by IHC, (b)) expression level from a GA patient (donor 6). Different areas were selected to show in higher magnifications. Figure S5: represented pictures of RIG-I IHC from 10 donors (5 non-AMD controls and 5 GA patients) show consistent upregulation of RIG-I proteins in GA patients to support Figure 5. Figure S6: RIG-I and cGAS expression patterns in human non-AMD control retina. Figure S7: no functional cGAS is detected in RPE. *(Supplementary Materials)*

## References

[1] W. L. Wong, X. Su, X. Li et al., "Global prevalence of age-related macular degeneration and disease burden projection for 2020 and 2040: a systematic review and meta-analysis," *The Lancet Global Health*, vol. 2, no. 2, pp. e106–e116, 2014.

[2] A. Kauppinen, J. J. Paterno, J. Blasiak, A. Salminen, and K. Kaarniranta, "Inflammation and its role in age-related macular degeneration," *Cellular and Molecular Life Sciences*, vol. 73, no. 9, pp. 1765–1786, 2016.

[3] J. E. Knickelbein, C. C. Chan, H. N. Sen, F. L. Ferris, and R. B. Nussenblatt, "Inflammatory mechanisms of age-related macular degeneration," *International Ophthalmology Clinics*, vol. 55, no. 3, pp. 63–78, 2015.

[4] N. Kerur, S. Fukuda, D. Banerjee et al., "cGAS drives noncanonical-inflammasome activation in age-related macular degeneration," *Nature medicine*, vol. 24, no. 1, pp. 50–61, 2018.

[5] D. Mustafi, T. Maeda, H. Kohno, J. H. Nadeau, and K. Palczewski, "Inflammatory priming predisposes mice to age-related retinal degeneration," *The Journal of Clinical Investigation*, vol. 122, no. 8, pp. 2989–3001, 2012.

[6] L. B. Ivashkiv and L. T. Donlin, "Regulation of type I interferon responses," *Nature Reviews. Immunology*, vol. 14, no. 1, pp. 36–49, 2014.

[7] M. Schlee and G. Hartmann, "Discriminating self from non-self in nucleic acid sensing," *Nature Reviews. Immunology*, vol. 16, no. 9, pp. 566–580, 2016.

[8] M. Iwanaszko and M. Kimmel, "NF-κB and IRF pathways: cross-regulation on target genes promoter level," *BMC Genomics*, vol. 16, no. 1, p. 307, 2015.

[9] K. Honda, A. Takaoka, and T. Taniguchi, "Type I interferon [corrected] gene induction by the interferon regulatory factor family of transcription factors," *Immunity*, vol. 25, no. 3, pp. 349–360, 2006.

[10] J. J. Hooks, C. N. Nagineni, L. C. Hooper, K. Hayashi, and B. Detrick, "IFN-beta provides immuno-protection in the retina by inhibiting ICAM-1 and CXCL9 in retinal pigment epithelial cells," *Journal of Immunology*, vol. 180, no. 6, pp. 3789–3796, 2008.

[11] M. Wornle, M. Merkle, A. Wolf et al., "Inhibition of TLR3-mediated proinflammatory effects by alkylphosphocholines in human retinal pigment epithelial cells," *Investigative Ophthalmology & Visual Science*, vol. 52, no. 9, pp. 6536–6544, 2011.

[12] R. DeJesus, F. Moretti, G. McAllister et al., "Functional CRISPR screening identifies the ufmylation pathway as a regulator of SQSTM1/p62," *Elife*, vol. 5, 2016.

[13] K. C. Dunn, A. E. Aotaki-Keen, F. R. Putkey, and L. M. Hjelmeland, "ARPE-19, a human retinal pigment epithelial cell line with differentiated properties," *Experimental Eye Research*, vol. 62, no. 2, pp. 155–170, 1996.

[14] Y. C. Perng and D. J. Lenschow, "ISG15 in antiviral immunity and beyond," *Nature Reviews. Microbiology*, vol. 16, no. 7, pp. 423–439, 2018.

[15] S. D. Der, A. Zhou, B. R. Williams, and R. H. Silverman, "Identification of genes differentially regulated by interferon alpha, beta, or gamma using oligonucleotide arrays," *Proceedings of the National Academy of Sciences of the United States of America*, vol. 95, no. 26, pp. 15623–15628, 1998.

[16] K. R. Loeb and A. L. Haas, "The interferon-inducible 15-kDa ubiquitin homolog conjugates to intracellular proteins," *The Journal of Biological Chemistry*, vol. 267, no. 11, pp. 7806–7813, 1992.

[17] A. Ablasser, F. Bauernfeind, G. Hartmann, E. Latz, K. A. Fitzgerald, and V. Hornung, "RIG-I-dependent sensing of poly(-dA:dT) through the induction of an RNA polymerase III-transcribed RNA intermediate," *Nature Immunology*, vol. 10, no. 10, pp. 1065–1072, 2009.

[18] N. Semenova, M. Bosnjak, B. Markelc, K. Znidar, M. Cemazar, and L. Heller, "Multiple cytosolic DNA sensors bind plasmid DNA after transfection," *Nucleic Acids Research*, vol. 47, no. 19, pp. 10235–10246, 2019.

[19] M. V. Kumar, C. N. Nagineni, M. S. Chin, J. J. Hooks, and B. Detrick, "Innate immunity in the retina: Toll-like receptor (TLR) signaling in human retinal pigment epithelial cells," *Journal of Neuroimmunology*, vol. 153, no. 1-2, pp. 7–15, 2004.

[20] D. Farkas, A. A. R. Thompson, A. R. Bhagwani et al., "Toll-like receptor 3 is a therapeutic target for pulmonary hypertension," *American Journal of Respiratory and Critical Care Medicine*, vol. 199, no. 2, pp. 199–210, 2019.

[21] Y. H. Chiu, J. B. Macmillan, and Z. J. Chen, "RNA polymerase III detects cytosolic DNA and induces type I interferons through the RIG-I pathway," *Cell*, vol. 138, no. 3, pp. 576–591, 2009.

[22] T. Tamura, H. Yanai, D. Savitsky, and T. Taniguchi, "The IRF family transcription factors in immunity and oncogenesis," *Annual Review of Immunology*, vol. 26, no. 1, pp. 535–584, 2008.

[23] H. X. Zhang, Z. X. Liu, Y. P. Sun et al., "Rig-I regulates NF-kappaB activity through binding to Nf-kappab1 3′-UTR mRNA," *Proceedings of the National Academy of Sciences of the United States of America*, vol. 110, no. 16, pp. 6459–6464, 2013.

[24] R. B. Seth, L. Sun, C. K. Ea, and Z. J. Chen, "Identification and characterization of MAVS, a mitochondrial antiviral signaling protein that activates NF-kappaB and IRF 3," *Cell*, vol. 122, no. 5, pp. 669–682, 2005.

[25] M. Bonnard, C. Mirtsos, S. Suzuki et al., "Deficiency of T2K leads to apoptotic liver degeneration and impaired NF-kappaB-dependent gene transcription," *The EMBO Journal*, vol. 19, no. 18, pp. 4976–4985, 2000.

[26] A. E. Shaw, J. Hughes, Q. Gu et al., "Fundamental properties of the mammalian innate immune system revealed by multispecies comparison of type I interferon responses," *PLoS biology*, vol. 15, no. 12, article e2004086, 2017.

[27] L. D. Orozco, H. H. Chen, C. Cox et al., "Integration of eQTL and a single-cell atlas in the human eye identifies causal genes for age-related macular degeneration," *Cell reports*, vol. 30, no. 4, pp. 1246–1259, 2020.

[28] F. Ma, B. Li, S. Y. Liu et al., "Positive feedback regulation of type I IFN production by the IFN-inducible DNA sensor cGAS," *Journal of Immunology*, vol. 194, no. 4, pp. 1545–1554, 2015.

[29] M. Xiong, S. Wang, Y. Y. Wang, and Y. Ran, "The regulation of cGAS," *Virologica Sinica*, vol. 33, no. 2, pp. 117–124, 2018.

[30] H. E. Volkman, S. Cambier, E. E. Gray, and D. B. Stetson, "Tight nuclear tethering of cGAS is essential for preventing autoreactivity," *Elife*, vol. 8, 2019.

[31] M. Chawla-Sarkar, D. J. Lindner, Y. F. Liu et al., "Apoptosis and interferons: role of interferon-stimulated genes as mediators of apoptosis," *Apoptosis*, vol. 8, no. 3, pp. 237–249, 2003.

[32] Y. Li, X. Guo, C. Hu et al., "Type I IFN operates pyroptosis and necroptosis during multidrug-resistant A. baumannii infection," *Cell Death and Differentiation*, vol. 25, no. 7, pp. 1304–1318, 2018.

[33] M. Stawowczyk, S. Van Scoy, K. P. Kumar, and N. C. Reich, "The interferon stimulated gene 54 promotes apoptosis," *The Journal of Biological Chemistry*, vol. 286, no. 9, pp. 7257–7266, 2011.

[34] R. J. Thapa, S. Nogusa, P. Chen et al., "Interferon-induced RIP1/RIP3-mediated necrosis requires PKR and is licensed by FADD and caspases," *Proceedings of the National Academy of Sciences of the United States of America*, vol. 110, no. 33, pp. E3109–E3118, 2013.

[35] J. Sarhan, B. C. Liu, H. I. Muendlein et al., "Constitutive interferon signaling maintains critical threshold of MLKL expression to license necroptosis," *Cell Death and Differentiation*, vol. 26, no. 2, pp. 332–347, 2019.

[36] O. Strauss, "The retinal pigment epithelium in visual function," *Physiological Reviews*, vol. 85, no. 3, pp. 845–881, 2005.

[37] Z. Ablonczy, M. Dahrouj, P. H. Tang et al., "Human retinal pigment epithelium cells as functional models for the RPE in vivo," *Investigative Ophthalmology & Visual Science*, vol. 52, no. 12, pp. 8614–8620, 2011.

[38] H. Li, J. A. Ice, C. J. Lessard, and K. L. Sivils, "Interferons in Sjogren's syndrome: genes, mechanisms, and effects," *Frontiers in Immunology*, vol. 4, p. 290, 2013.

[39] A. T. Reder and X. Feng, "Aberrant type I interferon regulation in autoimmunity: opposite directions in MS and SLE, shaped by evolution and body ecology," *Frontiers in Immunology*, vol. 4, p. 281, 2013.

[40] C. P. Mavragani, T. B. Niewold, A. Chatzigeorgiou et al., "Increased serum type I interferon activity in organ-specific autoimmune disorders: clinical, imaging, and serological associations," *Frontiers in Immunology*, vol. 4, p. 238, 2013.

[41] M. Du, X. Wang, X. Mao et al., "Absence of interferon regulatory factor 1 protects against atherosclerosis in apolipoprotein E-deficient mice," *Theranostics*, vol. 9, no. 16, pp. 4688–4703, 2019.

[42] J. M. Taylor, M. R. Minter, A. G. Newman, M. Zhang, P. A. Adlard, and P. J. Crack, "Type-1 interferon signaling mediates neuro-inflammatory events in models of Alzheimer's disease," *Neurobiology of Aging*, vol. 35, no. 5, pp. 1012–1023, 2014.

[43] A. K. Patel and A. S. Hackam, "Toll-like receptor 3 (TLR3) protects retinal pigmented epithelium (RPE) cells from oxidative stress through a STAT3-dependent mechanism," *Molecular Immunology*, vol. 54, no. 2, pp. 122–131, 2013.

[44] Z. Yang, C. Stratton, P. J. Francis et al., "Toll-like receptor 3 and geographic atrophy in age-related macular degeneration," *New England Journal of Medicine*, vol. 359, no. 14, pp. 1456–1463, 2008.

[45] A. Dhir, S. Dhir, L. S. Borowski et al., "Mitochondrial double-stranded RNA triggers antiviral signalling in humans," *Nature*, vol. 560, no. 7717, pp. 238–242, 2018.

[46] A. P. West, W. Khoury-Hanold, M. Staron et al., "Mitochondrial DNA stress primes the antiviral innate immune response," *Nature*, vol. 520, no. 7548, pp. 553–557, 2015.

[47] E. Bianchi, F. Scarinci, G. Ripandelli et al., "Retinal pigment epithelium, age-related macular degeneration and neurotrophic keratouveitis," *International Journal of Molecular Medicine*, vol. 31, no. 1, pp. 232–242, 2013.

[48] E. C. Baechler, F. M. Batliwalla, G. Karypis et al., "Interferon-inducible gene expression signature in peripheral blood cells of patients with severe lupus," *Proceedings of the National Academy of Sciences of the United States of America*, vol. 100, no. 5, pp. 2610–2615, 2003.

[49] L. Bennett, A. K. Palucka, E. Arce et al., "Interferon and granulopoiesis signatures in systemic lupus erythematosus blood," *The Journal of Experimental Medicine*, vol. 197, no. 6, pp. 711–723, 2003.

[50] L. Gaetani, P. S. Menduno, F. Cometa et al., "Retinopathy during interferon-beta treatment for multiple sclerosis: case report and review of the literature," *Journal of Neurology*, vol. 263, no. 3, pp. 422–427, 2016.

[51] E. Medhat, G. Esmat, E. Hamza et al., "Ophthalmological side effects of interferon therapy of chronic hepatitis C," *Hepatobiliary surgery and nutrition*, vol. 5, no. 3, pp. 209–216, 2016.

[52] W. Xiong, D. M. Wu, Y. Xue et al., "AAV cis-regulatory sequences are correlated with ocular toxicity," *Proceedings of the National Academy of Sciences of the United States of America*, vol. 116, no. 12, pp. 5785–5794, 2019.

Hindawi
Journal of Immunology Research
Volume 2021, Article ID 9117805, 15 pages
https://doi.org/10.1155/2021/9117805

*Research Article*

# Evaluation of the Effects of Different *Bacteroides vulgatus* Strains against DSS-Induced Colitis

**Sijia Li,[1,2] Chen Wang,[1,2] Chengcheng Zhang,[1,2] Yanhong Luo,[1,2] Qianqian Cheng,[1] Leilei Yu,[1,2] and Zhen Sun[1]**

[1]*School of Food Science and Technology, Jiangnan University, Wuxi, Jiangsu 214122, China*
[2]*State Key Laboratory of Food Science and Technology, Jiangnan University, Wuxi, Jiangsu 214122, China*

Correspondence should be addressed to Zhen Sun; zhsun@jiangnan.edu.cn

Received 17 April 2021; Revised 10 May 2021; Accepted 18 May 2021; Published 30 May 2021

Academic Editor: Tingtao Chen



Although the strain-dependent effects of *Bacteroides vulgatus* on alleviating intestinal inflammatory diseases have been demonstrated, the literature has rarely focused on the underlying causes of this effect. In this study, we selected four *B. vulgatus* strains (FTJS5K1, FTJS7K1, FSDTA11B14, and FSDLZ51K1) with different genomic characteristics and evaluated their protective roles against dextran sulfate sodium- (DSS-) induced colitis. Compared to the other three tested strains, *B. vulgatus* 7K1 more strongly ameliorated the DSS-induced weight loss, shortening of the colon length, increased disease activity index scores, colonic tissue injury, and immunomodulatory disorder. In contrast, *B. vulgatus* 51K1 significantly worsened the DSS-induced alterations in the tumor necrosis factor-alpha (TNF-$\alpha$) concentration and colonic histopathology. A comparative genomic analysis of *B. vulgatus* 7K1 and 51K1 showed that the beneficial effects of *B. vulgatus* 7K1 may be associated with some of its specific genes involved in the production of short-chain fatty acids or capsular polysaccharides and enhancement of its survivability in the gut. In conclusion, these findings indicate that the supplementation of *B. vulgatus* 7K1 is a potentially efficacious intervention for alleviating colitis and provides scientific support for the screening of probiotics with anticolitis effect.

## 1. Introduction

*Bacteroides*, one of the most abundant genera in the mammalian colon, has been a primary candidate for next-generation probiotics and has attracted considerable attention due to its role in the prevention of a series of metabolic disorders, including obesity [1, 2], diarrhea [3], viral encephalitis [4], and enteritis [5]. In particular, the protective effects of *Bacteroides* on inflammatory diseases in the gut are a hot topic. The results of human studies have indicated that the relative abundance of *Bacteroides* in patients with inflammatory bowel disease (IBD) is markedly lower than that in healthy participants [6, 7]. Furthermore, animal studies related to colitis have demonstrated that several strains of *Bacteroides*, including *Bacteroides fragilis* NCTC 9343, *Bacteroides thetaiotaomicron* DSM 2079, and *Bacteroides cellulosilyticus* DSM 14838, can expand the population of interleukin- (IL-) 10-producing $CD4^{+}CD45RB^{low}$ T cells [8], ameliorate the histopathological damage of the gut [9], and increase the levels of anti-inflammatory IL-10 and Treg cells [10]. These findings indicate that *Bacteroides* strains could be beneficial to the restoration of gut health in patients with intestinal inflammatory diseases. However, some studies have shown inconsistent results. One study found that the oral administration of enterotoxigenic *B. fragilis* 86-5443-2-2 isolated from piglets induced colitis in mice, which was manifested by the severe damage of colon tissue [11]. In addition, *Bacteroides eggerthii* 12986 has been reported to reduce survival, accelerate body weight loss, and increase intestinal bleeding in dextran sulfate sodium- (DSS-) treated mice, which then enhanced the severity of their colitis [12]. These reports suggest that the effects of *Bacteroides* on intestinal inflammatory diseases are species or even strain-specific.

The varying effects of different strains may be attributable to their physiological characteristics. The colonization ability of strains is a physiological characteristic related to the

protective functions of some strains against intestinal inflammatory disease. The type VI secretion system (T6SS) [13], antibacterial proteins [14], or capsular polysaccharides [15] of certain *Bacteroides* strains may increase their competitive fitness in the gut. Colitis-related studies have indicated that a high competitive colonization ability of *B. fragilis* could inhibit the intestinal adhesion of and further exposure to toxic pathogenic bacteria, and thus, prevent colitis [16]. The compounds produced by various strains also play a role in the development of intestinal inflammatory disease. For example, short-chain fatty acids (SCFAs), especially butyrate, may promote the intestinal epithelial barrier function [17], inhibit the central regulator of the inflammatory NF-$\kappa$B signaling pathway [18], and decrease oxidative stress [19], thereby preventing pathological damage of the colon associated with intestinal inflammatory disease. One study found that the administration of *B. fragilis* could improve the tight junction (TJ) integrity of the gut by increasing the number of SCFAs [20]. However, enterotoxins secreted by *B. fragilis* VPI 13784 have been reported to induce inflammation and significant colon tissue damage in lambs, rabbits, and rats after injection of the strain into their intestinal ligated loops [21]. The surface antigens of some strains can also affect intestinal inflammatory diseases. For example, polysaccharide A, a type of capsular polysaccharide present on *B. fragilis* NCTC 9343, has been reported to alleviate colitis [22] and colitis-associated colorectal cancer [23]. Another capsular zwitterionic polysaccharide TP2 from *B. fragilis* ZY-312 has been reported to protect rats from 2,4-dinitrobenzenesulfonic acid-triggered enteritis by reducing the degree of intestinal adhesion and the area of intestinal ulcers [5]. Moreover, the sphingolipids of *B. fragilis* NCTC9343 have been found to attenuate oxazolone-induced experimental colitis [24]. These results indicate that the effects of *Bacteroides* and even probiotics on alleviating intestinal inflammatory diseases are closely related to their physiological characteristics. Notably, the phenotype of bacteria is determined by their genome, and some studies have revealed that the functional differences between various probiotic strains on colitis remission are strongly associated with their genome [25, 26].

*Bacteroides vulgatus* is a representative species of the *Bacteroides* genus and is known to have a beneficial effect on the human colon health [27, 28]. Some studies have reported that *B. vulgatus* mpk can inhibit *Escherichia coli*-induced colitis [29] or *Yersinia enterocolitica*-induced inflammation [30], whereas other studies have demonstrated the proinflammatory effect of certain *B. vulgatus* strains. One study showed that *B. vulgatus* DESEP-B could induce colitis in HLA-B27 transgenic rats [31]. Another study found that *B. vulgatus* TUSVM 40G2-33 led to the enhancement of carrageenan-induced colitis in guinea pigs [32]. These results imply that the protective effect of *B. vulgatus* is strain-dependent. Furthermore, a previous study has revealed the considerable differences in inflammatory responses of guinea pigs administrated with seven different *B. vulgatus* strains in an experimental model for ulcerative colitis [33]. This demonstrated the variable ability of various *B. vulgatus* strains in the enhancement of colitis. However, most investigations of the effect of *B. vulgatus* on colitis have only focused on a single strain. Hence, it is important to investigate the complex relationship between *B. vulgatus* strains and colitis and the reasons for the varying effects of different strains. In this study, we selected four *B. vulgatus* strains with large differences in their genomes and assessed their roles in alleviating colitis. Due to its simplicity, reliability, and applicability, we used DSS to induce colitis in mice [34]. We then analyzed the genomic characteristics of the selected *B. vulgatus* strains to identify the functional genes that may play a role in alleviating the intestinal damage caused by the DSS.

## 2. Materials and Methods

*2.1. Bacterial Strains and Preparation.* We used *B. vulgatus* strains FTJS5K1 (5K1), FTJS7K1 (7K1), FSDTA11B14 (11B14), and FSDLZ51K1 (51K1) in this study, all of which had been isolated from the fecal samples of different volunteers. The 5K1 and 7K1 strains were deposited in the Culture Collection of Food Microorganisms (CCFM) of Jiangnan University (Wuxi, China). The four strains were grown anaerobically at 37°C for 18 h in a brain–heart infusion broth (Hopebio, China) supplemented with 5 $\mu$g/mL hemin (Sangon Biotech, China) and 0.5 $\mu$g/mL vitamin K1 (Sangon Biotech, China). A fresh culture of each strain was collected by centrifugation (5 min at 6000 g) and then washed twice with sterile phosphate-buffered saline (PBS). The final bacterial pellets were resuspended in sterile PBS at a concentration of $5 \times 10^9$ colony-forming units (CFUs)/mL.

*2.2. Animal Experimental Design.* Sixty specific pathogen-free C57BL/6J mice (male, 6 weeks old) purchased from the Shanghai Laboratory Animal Center were housed at five animals per cage at the Animal Experiment Center of Jiangnan University. The mice were provided with sufficient sterilized water and standard food ad libitum and were maintained under standard conditions (20–24°C, 50%–60% humidity, and a 12 h light/darkness cycle). All mice were given a 7-day period to acclimatize to their new environment. Then, they were randomly divided into six groups (10 mice in each group): control, DSS, DSS+5K1, DSS+7K1, DSS+51K1, and DSS+11B14. To induce acute colitis in the mice in the experimental groups, 3% DSS (36–50 kDa, MP Biomedicals, Carlsbad, CA, USA) was added to their sterile filtered drinking water for 7 days. During the trial, the mice in the control and DSS groups were orally gavaged with 0.2 mL of sterile PBS. The mice in the other groups were fed one of the four *B. vulgatus* strains at a dose of $1 \times 10^9$ CFUs/0.2 mL in sterile PBS by gavage. Three essential parameters of the disease activity index (DAI) were measured daily [35], including body weight, stool consistency, and fecal blood. Fecal occult blood was measured by using an Occult Blood Kit (Nanjing Jiancheng Co., Ltd., Nanjing, China). On day 7 after treatment, fresh stool samples were collected and instantly frozen at -80°C for further analysis. On day 8, euthanasia of mice was performed by carbon dioxide administration. The colons of all the mice were extracted, and their lengths were measured. The distal colon (5 mm) was then immersed in a 4% paraformaldehyde solution, and the remainder was stored at −80°C for subsequent testing. All the procedures related

Table 1: Primers sequences used for RT-qPCR.

| Gene | Forward | Reverse |
|---|---|---|
| Claudin-1 | 5′-GATGTGGATGGCTGTCATTG-3′ | 5′-CCTGGCCAAATTCATACCTG-3′ |
| Occludin | 5′-CACACTTGCTTGGGACAGAG-3′ | 5′-TAGCCATAGCCTCCATAGCC-3′ |
| ZO-1 | 5′-CTTCTCTTGCTGGCCCTAAAC-3′ | 5′-TGGCTTCACTTGAGGTTTCTG-3′ |
| Mucin 2 | 5′-TGCCCACCTCCTCAAAGAC-3′ | 5′-GTAGTTTCCGTTGGAACAGTGAA-3′ |
| $\beta$-Actin | 5′-GGCTGTATTCCCCTCCATCG-3′ | 5′-CCAGTTGGTAACAATGCCATGT-3′ |

to these animal experiments were approved by the Committee of Ethics in Jiangnan University, China (JN. NO. 20190930c0801120[249]).

*2.3. Genome Sequencing, Clusters of Orthologous Group (COG) Annotation, and Phylogenetic Tree Construction.* Genome sequencing of *B. vulgatus* strains was performed using the Illumina HiSeq System by Majorbio (China), as described in a previous study [36, 37]. GLIMMER software was used to predict the protein-coding sequences. To identify the relationships between different *B. vulgatus* strains, we used OrthoMCL1.4 to generate the orthologous genes of 14 strains. Among these 14 strains, the genome of ATCC 8482 (Genome accession number: NC_009614.1), mpK (Genome accession number: CP013020.1), PC510 (Genome accession number: NZ_ADKO00000000.1), AF34-15 (Genome accession number: NZ_QRPW00000000.1), AM44-21 (Genome accession number: NZ_QSEZ00000000.1), RH 1270 (Genome accession number: NZ_WCIG00000000.1), and RJ2H1 (Genome accession number: NZ_PHJG00000000.1) was downloaded from the National Center for Biotechnology Information (NCBI) database. The other 7 genome sequences of 5K1 (Genome accession number: JACBPX000000000), 7K1 (Genome accession number: JACBPY000000000), 11B14 (Genome accession number: JACBPW000000000), 51K1 (Genome accession number: JACBPV000000000), FBJS10K3 (Genome accession number: JACBPS000000000), FGSZY37K4 (Genome accession number: JACBPT000000000), and FJSWX62K35 (Genome accession number: JACBPU000000000) were from the current study. We then used PhyML3 software to construct a neighbor-joining phylogenetic tree based on the core gene alignment generated using MAFFT [38]. To distinguish the functional genes between the various strains, we annotated the gene functions against the Carbohydrate-Active enZyme (CAZy) database and the Clusters of Orthologous Groups (COG) protein database by BLASTp [39].

*2.4. Determination of Intestinal Permeability.* To assess the intestinal permeability of the mice, we used 4000-Da fluorescein isothiocyanate-dextran (DX-4000-FITC, Sigma-Aldrich, USA), as described in [40]. Briefly, the mice were orally administrated DX-4000-FITC at a dosage of 500 mg/kg of body weight after fasting for 6 h on day 7. After 1 h, their blood was collected to detect the concentration of DX-4000-FITC.

*2.5. Histological Evaluation.* The fixed colon tissues were embedded in paraffin, stained with hematoxylin and eosin, and finally scanned by a Digital Slide Scanner (Motic China Group Ltd.). The damage severity of colon section was evaluated and scored from 0 to 4 for ulceration of epithelium, crypt damage, depletion of goblet cells, edema, and inflammation by a pathologist in blinded fashion.

*2.6. Biochemical Analysis of the Colon.* Colon samples of a certain weight were homogenized in normal saline solution and then centrifuged at 12000 g (10 min at 4°C). The supernatant was used to determine the total protein concentration using a BCA protein assay kit (Beyotime Biotechnology, Shanghai, China). The contents of IL-6, IL-10, and TNF-$\alpha$ in the colon supernatant were determined using commercially available enzyme-linked immunosorbent assay kits (R&D Systems, Minneapolis, MN, USA).

*2.7. Gene Expression Analysis.* Total RNA isolation from the colon tissue was performed using a FastPure Cell/Tissue Total RNA Isolation Kit (Vazyme Biotech Co., Ltd., Nanjing, China), and then a RevertAid First Strand cDNA Synthesis Kit (Vazyme Biotech Co., Ltd., Nanjing, China) was used for cDNA synthesis. Real-time quantitative polymerase chain reaction (RT-qPCR) was performed using $\beta$-actin as an internal control to identify the expressions of mucin2 (MUC2), ZO-1, claudin-1, and occludin [41]. RT-qPCR was carried out on a CFX96 Real-Time System (Bio-Rad, Hercules, CA) using SYBR Green super mix (Bio-Rad, Hercules, CA) under the following program: 2 min at 95°C, 39 cycles of 30 s at 95°C, 30 s at 60°C, and 30 s at 72°C. The $2^{-\Delta\Delta Cq}$ method was used to analyze the results. Table 1 lists the sequences of primers used in this study.

*2.8. Fecal DNA Extraction, Sequencing, and Analysis.* The FastDNA Spin Kit for Feces (MP Biomedicals) was used to extract bacterial DNA from the stool samples of the mice. The gut microbiota genomes were sequenced according to the method described in a previous study [42]. Briefly, after amplification and purification, the DNA amplicons of the 16S rRNA sequences (V3-V4 region) in the bacterial DNA were sequenced by the MiSeq Illumina platform.

Principle coordinate analysis was performed to evaluate the beta diversity of the microbial communities. Microbial diversity was estimated by the Chao-1 index. LEfSe analysis was used to determine the intergroup differences in the fecal microbiota composition.

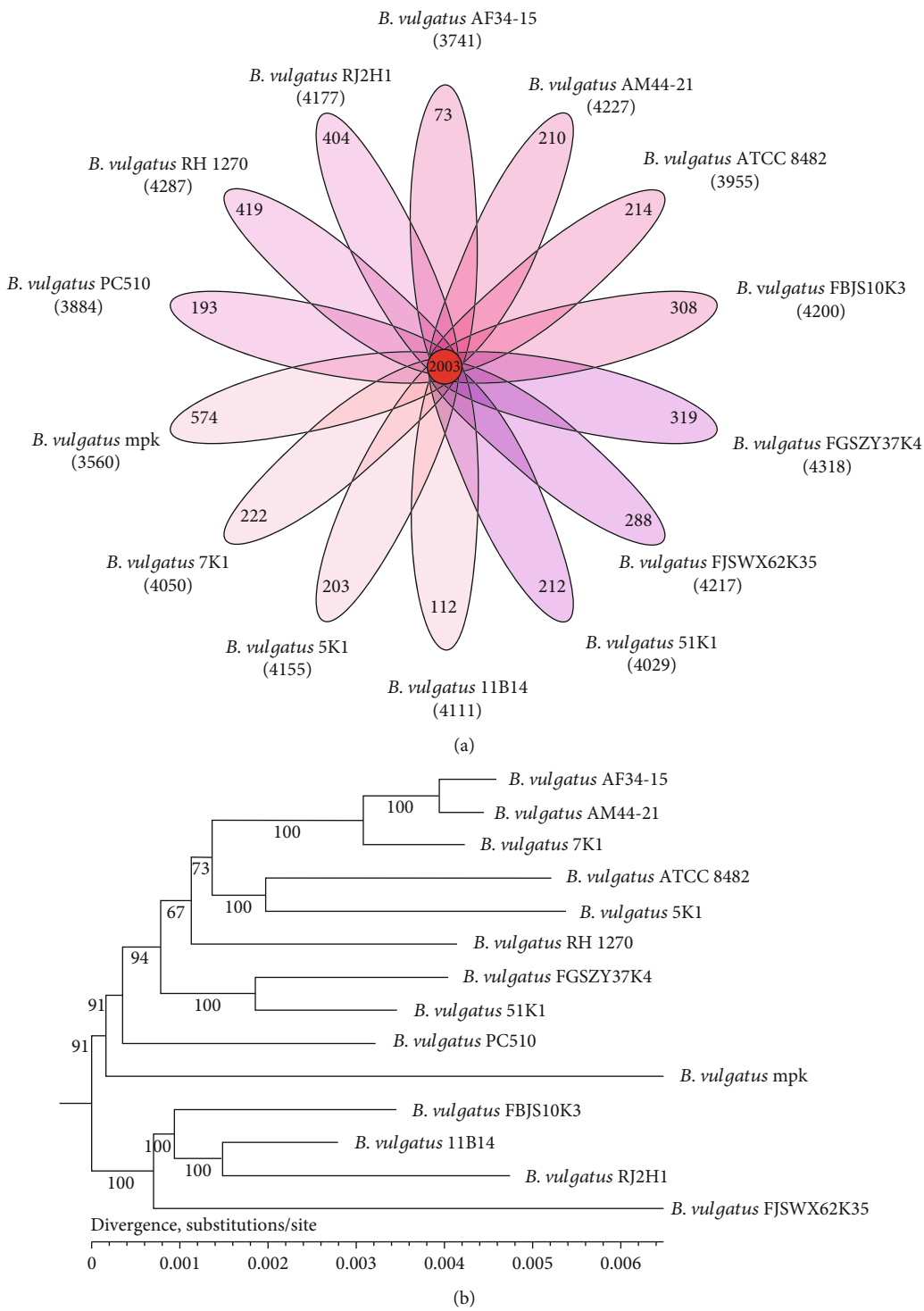


Figure 1: Core genes and phylogenetic analyses of 14 *Bacteroides vulgatus* strains. (a) Venn diagram of homologous clusters shared among the core genes. (b) Phylogenetic tree of 14 strains of *B. vulgatus*. Bootstrap confidence values were marked in the phylogenetic tree.

*2.9. Determination of Short-Chain Fatty Acids (SCFAs) in Feces.* To extract SCFAs (acetate, propionate, isobutyrate, butyrate, valerate, and isovalerate), the fecal samples were weighed, then soaked in saturated NaCl solution, acidified with sulfuric acid (10%), and treated with diethyl ether. Gas chromatography-mass spectrometry (GC-MS) was then performed to determine the SCFAs concentrations in the feces, as described in [43]. Briefly, helium was used as the carrier gas with a flow rate of 2 mL/min, and injection volume was 1 $\mu$L at an injection temperature of 240°C. The following GC-MS temperature program was used: initial temperature 100°C, increase to 140°C at 7.5°C/min, then rise to 200°C at

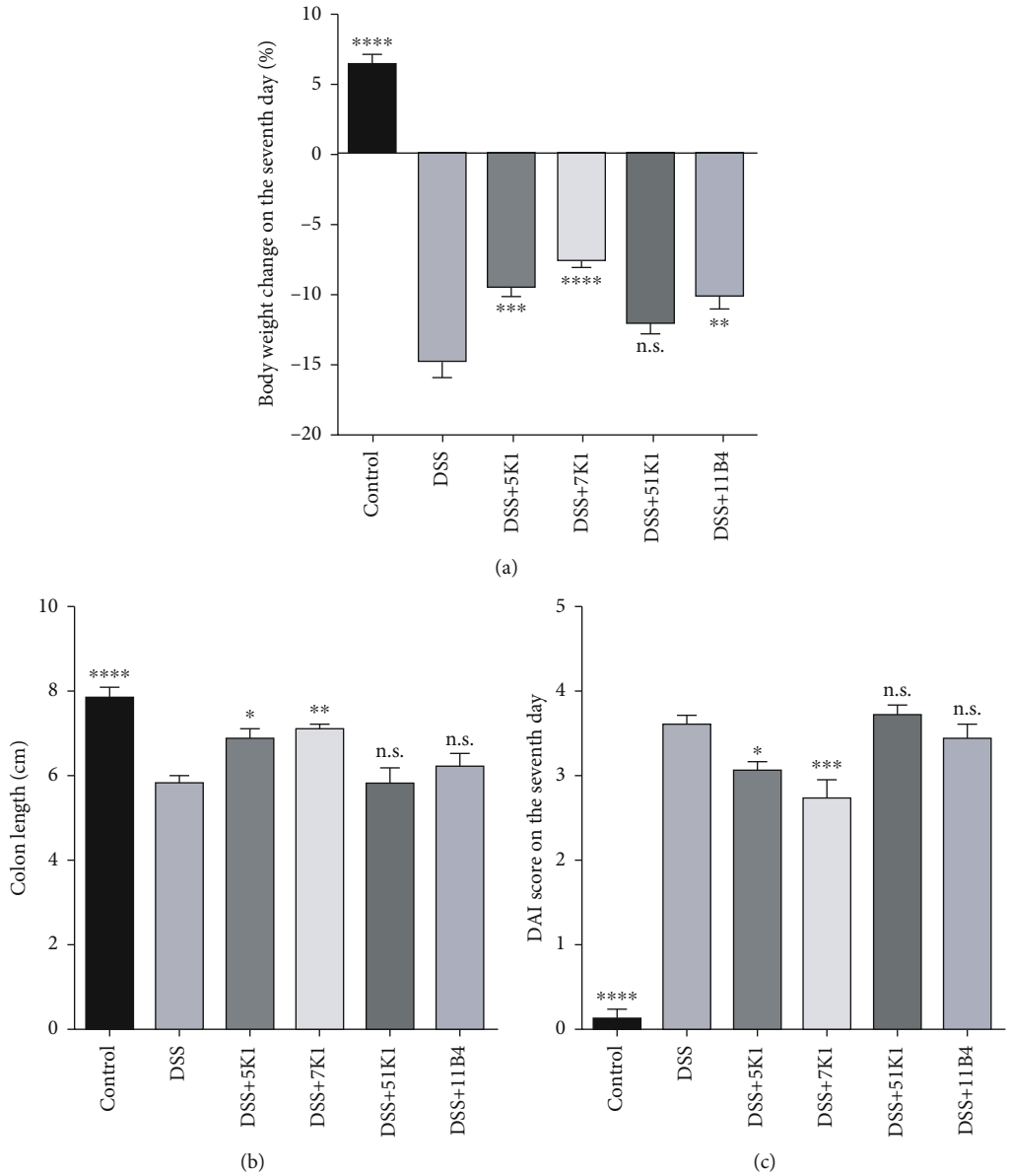


Figure 2: Effect of *Bacteroides vulgatus* on colitis symptoms. (a) Body weight. (b) Colon length. (c) Disease activity index (DAI). Six mice per group.

60°C/min with a hold time of 3 min and an ion source temperature of 220°C. The external standard method was used to calculate the SCFA concentrations.

*2.10. Statistical Analysis.* All statistical analyses were performed using GraphPad Prism software version 6.0. The experimental data are expressed as the mean ± the standard error of the mean. A one-way analysis of variance with Tukey's multiple comparison test was performed to determine the significance of the differences, and $p < 0.05$ was considered to be statistically significant. The symbol $*$ indicates that the difference between the DSS group and the treated groups is significant, with $*$, $**$, $***$, and $****$ indicating $p < 0.05$, $p < 0.01$, $p < 0.001$, and $p < 0.0001$, respectively. The symbol n.s. indicates that the difference between the DSS group and other groups has no significance.

## 3. Results

*3.1. Genetic Diversity and Evolution of B. vulgatus Strains.* The 14 *B. vulgatus* strains (7 strains from this study and 7 strains from the NCBI database) shared 2003 orthologous genes (Figure 1(a)). The neighbor-joining tree established on the basis of these 2003 core genes shows that the strains are distributed into several branches (Figure 1(b)). We selected four strains (5K1, 7K1, 51K1, and 11B14) located far from each other on the phylogenetic tree to evaluate their effects on alleviating DSS-induced colitis in mice.

*3.2. Effect of B. vulgatus on Colitis Symptoms.* DSS exposure was found to markedly deteriorate the intestinal physiology of the mice, accompanied with weight loss, shortening of the colon length, and increased DAI scores (Figure 2).

Notably, the administration of *B. vulgatus* strain 7K1, but not 5K1, 51K1, or 11B14, led to a significant recovery of these three physiological indicators.

*3.3. Effect of B. vulgatus on the Intestinal Permeability of DSS-Treated Mice.* To estimate the effect of *B. vulgatus* strains on the intestinal permeability of the mice, we determined the serum FITC levels. After the DSS challenge, the FITC levels in the mice serum were markedly increased compared with those in the control group (Figure 3). These levels were markedly reduced in the mice fed with *B. vulgatus* 5K1 or *B. vulgatus* 7K1. However, neither *B. vulgatus* 51K1 nor *B. vulgatus* 11B14 showed any intestinal protective effect.

*3.4. Effect of B. vulgatus on DSS-Induced Colonic Tissue Injury.* The colon tissues of the mice in the DSS group, as compared to the control group, exhibited severe inflammatory cell infiltration, submucosal edema, significant disappearance of goblet cells, and severe damage to the epithelial structure (Figure 4(a)). The histological scores are a quantifiable indication of colonic injury. Compared with the DSS-treated mice, the colon tissue damage, expressed as the integrity of the intestinal epithelium and the alleviation of submucosal edema, in the mice fed with *B. vulgatus* 7K1 was significantly reduced (Figure 4(b)), whereas it was obviously aggravated in the mice fed with *B. vulgatus* 5K1, 11B14, or 51K1.

*3.5. Effect of B. vulgatus on the Secretion of Inflammatory Factors in DSS-Treated Mice.* Treatment with DSS resulted in dramatic alterations in the colonic immunomodulatory indicators of the mice, including increases in the concentrations of the proinflammatory cytokines TNF-$\alpha$ and IL-6, and a decrease in the concentration of the anti-inflammatory cytokine IL-10 (Figure 5). Among the tested strains, *B. vulgatus* 7K1 was the most effective in restoring the expression of the three inflammatory cytokines by significantly inhibiting the increases in TNF-$\alpha$ and IL-6 concentrations and upregulating the IL-10 concentrations up to those found in the control group. However, apart from reducing the IL-6 concentrations (Figure 5(b)), *B. vulgatus* 5K1 induced no alterations in any of the other indicators. In addition, *B. vulgatus* 51K1 significantly increased the TNF-$\alpha$ concentrations (Figure 5(a)).

*3.6. Comparative Genomic Analysis of the Specific Genes in Different B. vulgatus Strains.* We performed COG annotation to predict the functional genes of *B. vulgatus* 7K1 and *B. vulgatus* 51K1, and we found that 30 COG families were present only in the *B. vulgatus* 7K1 genome (Table S1). Except for three genes assigned to the COG category "General function prediction only" and four assigned to the COG category "Function unknown," most of the genes were mainly related to metabolism, transport, replication, recombination, repair, and defense. In addition, according to the annotation results from the CAZy database, the abundance of genes from 14 glycoside hydrolase families (GH3, GH5, GH15, GH20, GH33, GH43_24, GH141, GH95, GH105, GH29, GH106, GH27, GH99, and GH109) and 3 glycosyl transferase families (GT28, GT6, and GT4) was relatively high in the *B. vulgatus* 7K1 genome (Table S2).

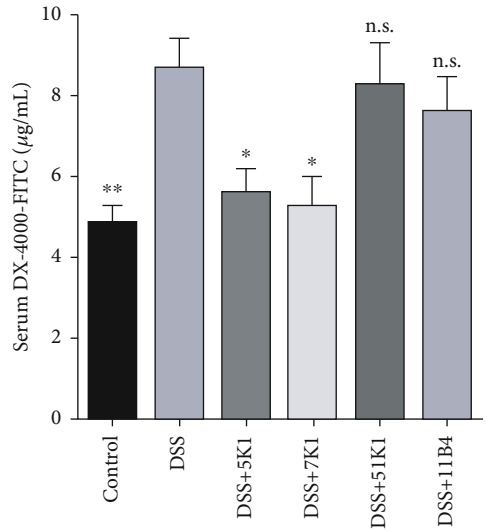


Figure 3: Effects of *Bacteroides vulgatus* on the intestinal permeability of mice. Four mice per group.

*3.7. Effect of B. vulgatus on SCFA Concentrations in Feces.* The concentrations of isobutyrate, valerate, and isovalerate in the fecal samples were not significantly different in the DSS group compared with the control group (Figure 6). Notably, after the oral administration of *B. vulgatus* 7K1, the concentrations of these SCFAs markedly increased. Furthermore, the concentrations of acetate, propionate, and butyrate were significantly decreased in the DSS group compared with the control group. Treatment with *B. vulgatus* 7K1 dramatically restored the acetate and butyrate concentrations close to their concentrations in the control group, but did not result in a significant change in the propionate concentrations.

*3.8. Effect of B. vulgatus on the mRNA Levels of Genes Related to the Intestinal Barrier in Colon Tissue.* To assess the intestinal mucosal barrier of the mice, we measured the relative expression levels of genes related to TJ proteins (ZO-1, occludin, and claudin-1) and MUC2. The results showed that the DSS treatment significantly decreased the expression of these four mucosal barrier indicators (Figure 7). Notably, oral gavage of *B. vulgatus* 7K1 played a protective role against DSS-induced alterations in ZO-1 and claudin-1 expression. Although the expression of occludin and MUC2 was upregulated by *B. vulgatus* 7K1, the results were not statistically significant.

*3.9. Effect of B. vulgatus on the Composition of the Bacterial Community.* Compared with the control group, DSS treatment was found to affect the composition of the gut microbiota (Figure 8(a)) and slightly decrease the microbial diversity (Figure 8(b)), although these results were not statistically significant. Cotreatments with DSS and *B. vulgatus* 7K1 induced similar results. At the genus level, *B. vulgatus* 7K1 treatment markedly increased the abundance of *Turicibacter* and *Romboutsia* in comparison with that in the DSS group (Figure 8(c)).

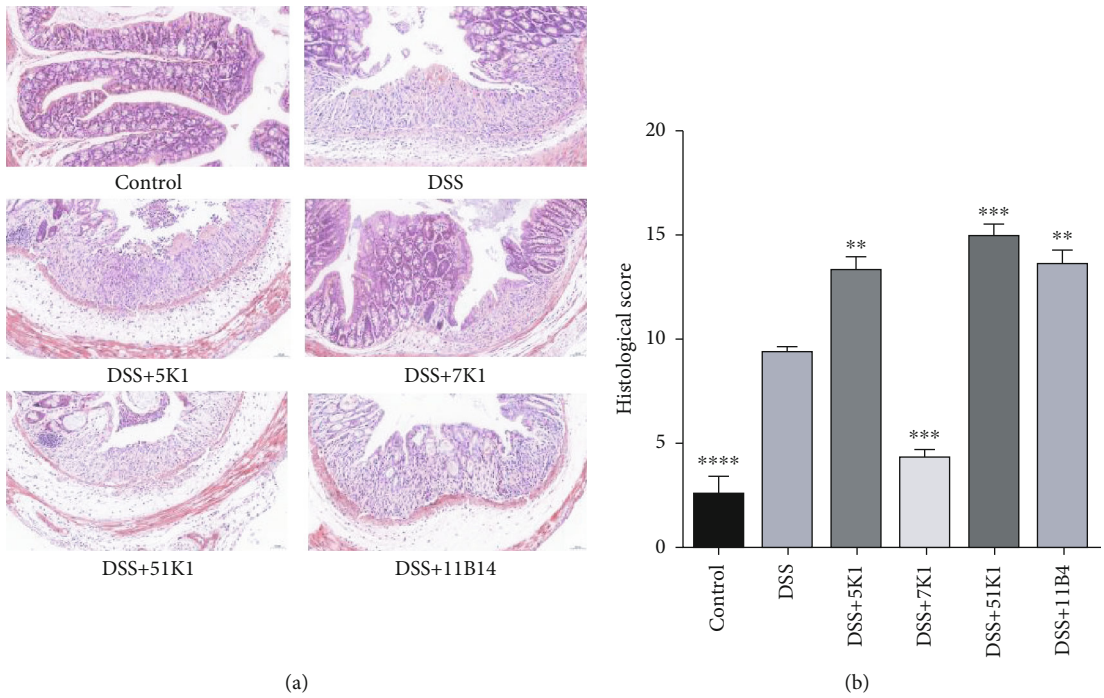


Figure 4: Effects of *Bacteroides vulgatus* on colonic tissue injury in mice. (a) Histological images. (b) Histological score. Four mice for the control group and three mice for each of the other groups.

## 4. Discussion

Numerous studies have shown that different strains of probiotics have different anticolitis effects [44–46]. *B. vulgatus*, a next-generation probiotic, has also been found to prevent colitis, depending on the strain [33]. Many factors influence the strain-specific effects of probiotics. The survivability of probiotics during transit through the gastrointestinal tract directly affects their abundance in the gut [47]. Several studies have shown that the protective effects of probiotic strains on the host health are dose-dependent [48–50]. Research has also revealed the enhanced ability of microencapsulated *Lactobacillus rhamnosus* GG to tolerate the stomach and small intestine environments, which can strengthen its efficacy in ameliorating the symptoms of colitis [51]. Hence, the ability of probiotics to resist the harsh environment of the gastrointestinal tract is a crucial factor that influences their colitis-ameliorating effects. Pathogenic bacteria such as *Citrobacter rodentium* and enterohemorrhagic *E. coli* can attach themselves to intestinal epithelial cells and then activate an immune response in the gut that can cause severe colitis [52, 53]. Hence, the ability of probiotics to inhibit pathogen colonization in the intestine is essential to their effectiveness against colitis. A study has revealed that the oral administration of *Lactobacillus acidophilus* can decrease the colonization and translocation of *C. rodentium* and then inhibit *C. rodentium*-induced colitis [54]. In addition, some probiotics can release antimicrobial factors such as hydrogen peroxide and bacteriocins, which can kill the pathogenic bacteria or inhibit their growth [55, 56]. Enhancement of the intestinal epithelial barrier function by some probiotics is also directly related to their alleviation effect on colitis [57, 58]. SCFAs, which are produced by certain probiotics, can promote mucin expression [59] or stimulate the expression of TJ proteins [60], which serve to maintain the intestinal integrity [61]. These findings suggest that the different anticolitis abilities of probiotic strains are attributable to their complex physiological characteristics.

Genomic diversity implies functional specificity. Several *Lactobacillus fermentum* strains with considerable genomic differences have been reported to exhibit different anti-inflammatory effects on colitis in mice [46]. Hence, we constructed an evolutionary tree and selected four *B. vulgatus* strains that have large genomic differences. We then assessed their efficacy in ameliorating DSS-induced colitis in mice. Our results showed that among the four *B. vulgatus* strains, only *B. vulgatus* 7K1 could significantly relieve five DSS-induced symptoms, including reduced body weight, a shortened colon, increased DAI scores, severe damage to the colon tissue, and increased intestinal permeability. An abnormal immune response is an important indicator of the pathogenesis of colitis. Proinflammatory cytokines TNF-$\alpha$ and IL-6 have been reported to result in mucosal inflammation and aggravate immune disorders [62, 63]. Reducing TNF-$\alpha$ and IL-6 in mice with colitis was considered to be a logical target for the treatment of colitis [64]. The experiment in IL-10-deficient mice has proved the vital role of IL-10 in preventing IBD [65]. As an anti-inflammatory cytokine, IL-10 has been reported to inhibit the expression of TNF-$\alpha$ in immune regulatory processes [66]. Moreover, the protective effects of *B. fragilis* NCTC 9343 against colitis induced by trinitrobenzene sulphonic acid (TNBS) or *Helicobacter hepaticus* largely attributed to its ability to increase the production of IL-10 [8, 22]. In our study, the oral administration of *B. vulgatus*

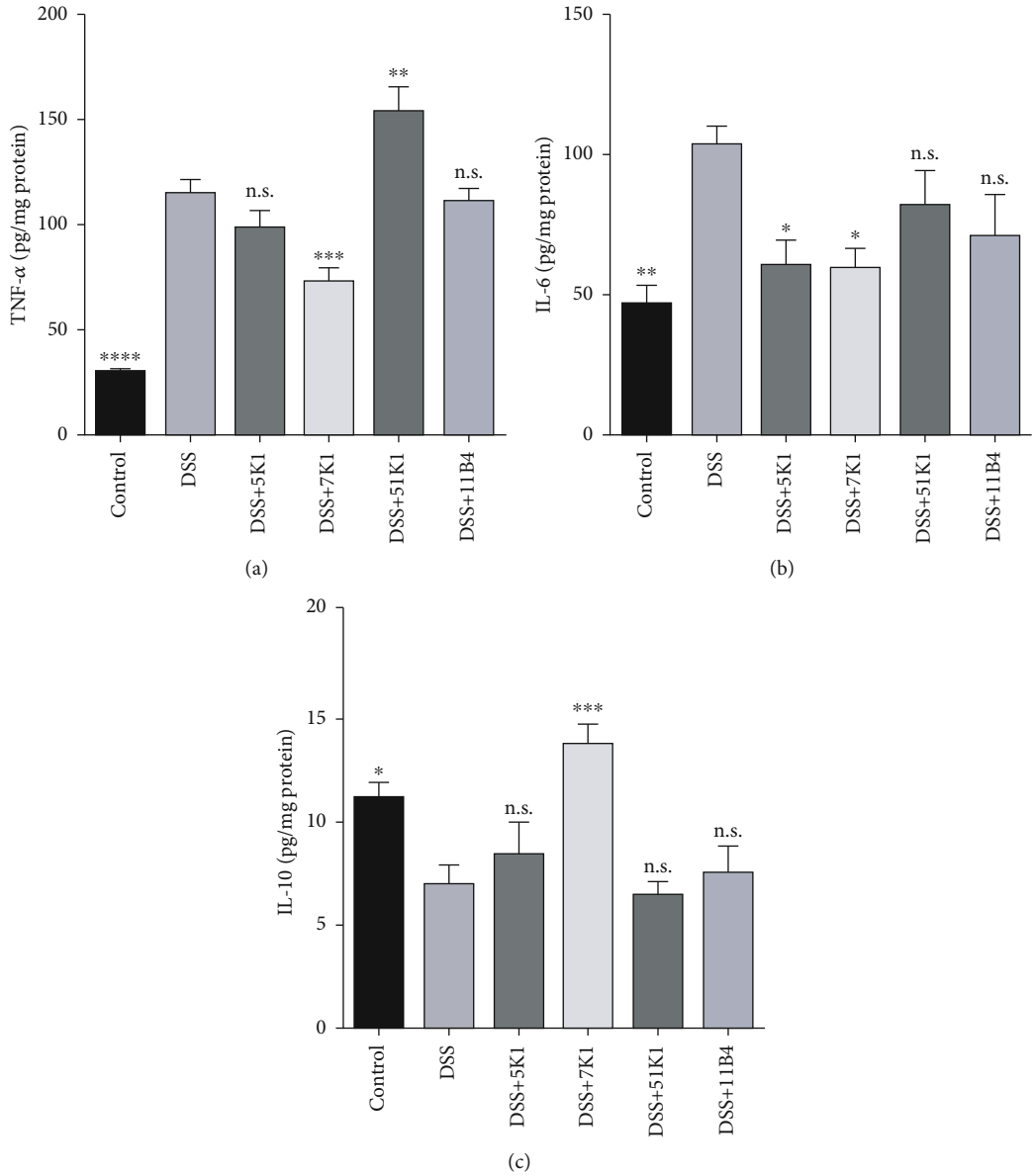


Figure 5: Effects of *Bacteroides vulgatus* on the concentrations of inflammatory cytokines. (a) TNF-$\alpha$. (b) IL-6. (c) IL-10. Six mice per group.

7K1, rather than *B. vulgatus* 5K1, not only significantly reduced the concentrations of TNF-$\alpha$ and IL-6 but also markedly increased the production of IL-10 in the colon tissue of mice. Hence, given these results, we found *B. vulgatus* 7K1 to be significantly more effective in relieving DSS-induced colitis in mice than the other *B. vulgatus* strains tested in this study. We note that *B. vulgatus* 51K1 was the only one of the four strains that failed to restore the weight loss, shortened colon, and increased DAI scores caused by DSS. Furthermore, *B. vulgatus* 51K1, but not the other three strains, significantly increased both the tissue damage and TNF-$\alpha$ concentration in the mouse colons, as compared to the DSS group. These results indicate that *B. vulgatus* 51K1 can dramatically aggravate colitis.

Subsequently, we performed a comparative genomic analysis to understand the differences in the anti-inflammatory effects of *B. vulgatus* 7K1 and *B. vulgatus* 51K1. Among the 30 strain-specific COGs for *B. vulgatus* 7K1, COG2977 is involved in secondary metabolite biosynthesis, transport, and catabolism and may be related to the production of SCFAs. Moreover, GH43_24, which is more abundant in the *B. vulgatus* 7K1 genome than in the *B. vulgatus* 51K1 genome, is mainly responsible for the hydrolysis of xylan. A previous study reported that feeding mice xylooligosaccharides can increase the production of fecal SCFAs [67]. In our experiments, *B. vulgatus* 7K1 significantly promoted the production of SCFAs, including acetate, butyrate, isobutyrate, valerate, and isovalerate (Figure 6).

The protective role of SCFAs, especially butyrate, acetate, and propionate, in intestinal inflammatory diseases has been widely demonstrated and is well recognized. Mechanistically, SCFAs may promote the integrity of the intestinal epithelial barrier by increasing the synthesis of mucins in the mucosal layer [68] and of TJ proteins in the epithelial monolayer

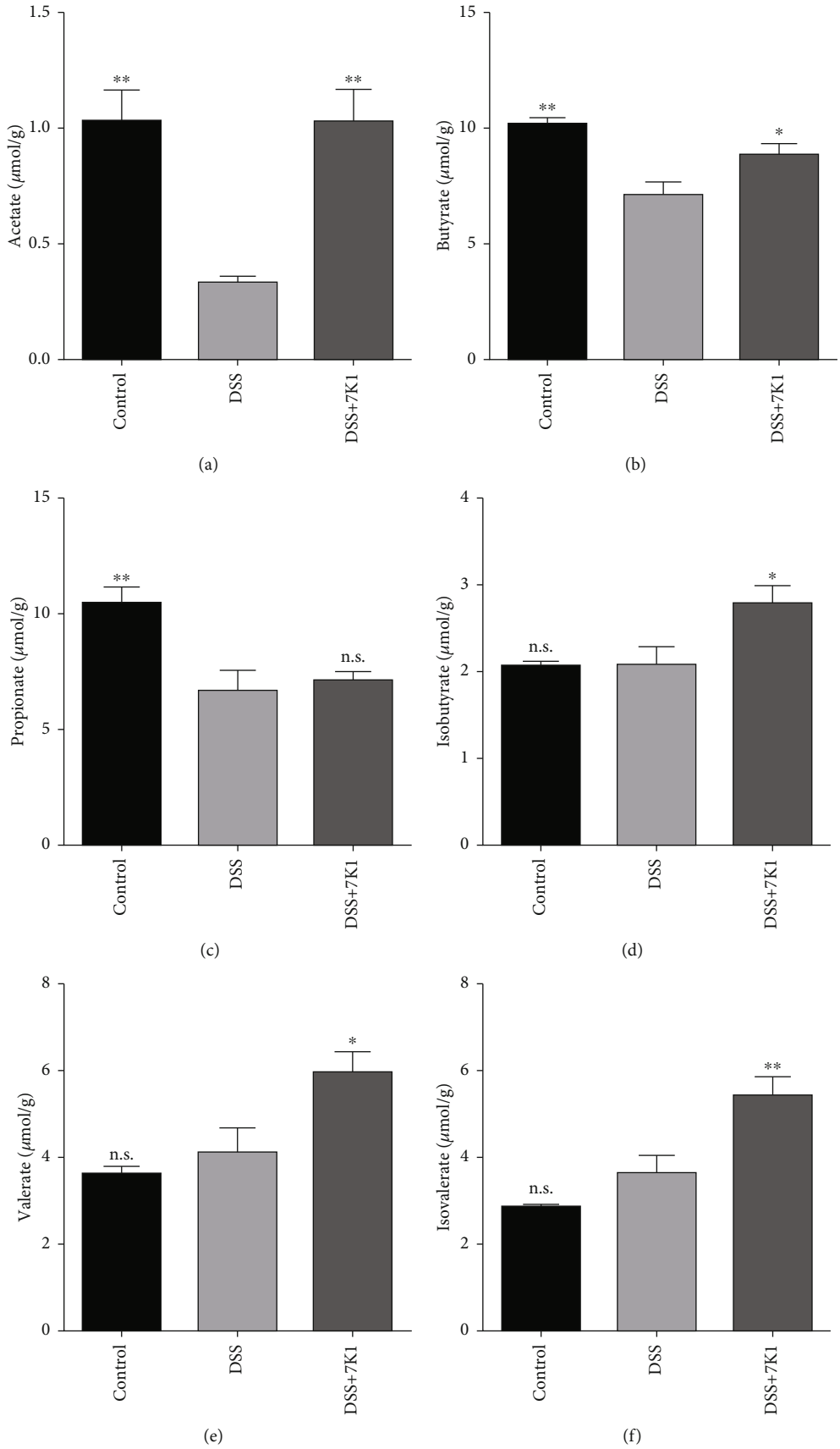


Figure 6: Effects of *Bacteroides vulgatus* on the concentrations of short-chain fatty acids in the fecal samples of mice. (a) Acetate. (b) Propionate. (c) Butyrate. (d) Isobutyrate. (e) Valerate. (f) Isovalerate. Five mice per group.

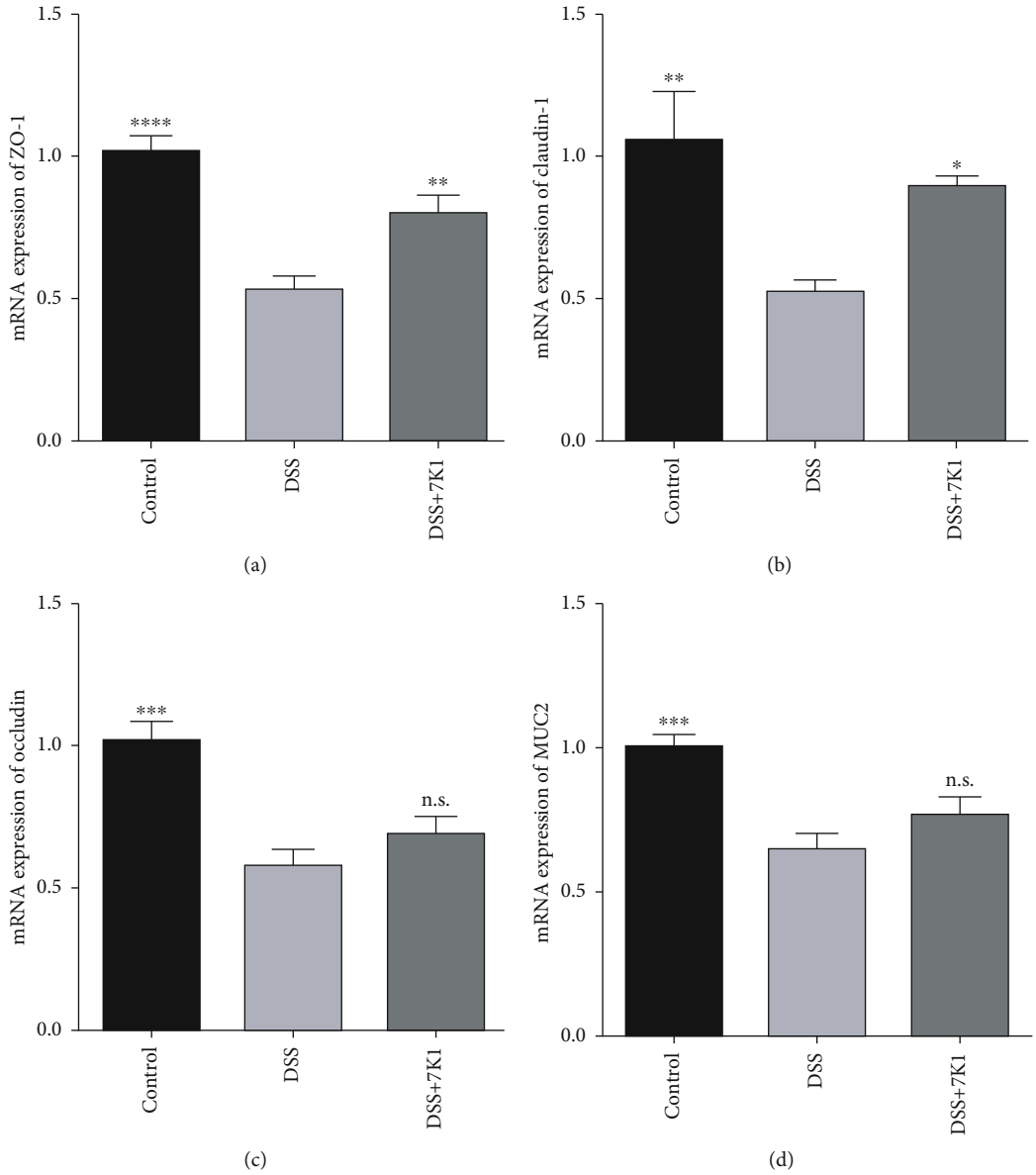


Figure 7: Effects of *Bacteroides vulgatus* on the intestinal barrier of mice. (a) ZO-1. (b) Claudin-1. (c) Occludin. (d) MUC2. Six mice per group.

[69, 70], and thus, contribute to the remission of colitis. In addition, SCFAs attenuate colitis in mice by restoring the balance of gut microbial dysbiosis [71, 72]. In this study, feeding *B. vulgatus* 7K1 to mice protected the TJs of their intestinal epithelial cells (Figure 7), but did not restore the balance of the gut microbial dysbiosis caused by DSS (Figure 8). Hence, enhancing the integrity of the epithelial monolayer by increasing the SCFAs may be a protective mechanism of *B. vulgatus* 7K1 against DSS-induced colitis.

COG4464, which is specific to *B. vulgatus* 7K1, is responsible for the biosynthesis of capsular polysaccharides. The anti-inflammatory effect of the capsular polysaccharide produced by certain *Bacteroides* strains has been reported in several studies [5, 10]. As the best-studied zwitterionic capsular polysaccharide, polysaccharide A has been confirmed to prevent colitis by inducing the expression of IL-10 in the colon [73]. Our results showed that *B. vulgatus* 7K1, but not *B. vulgatus* 51K1, markedly upregulated the IL-10 expression in the mouse colons (Figure 5). Thus, the gene belonging to COG4464 may partly account for the anti-inflammatory property of *B. vulgatus* 7K1.

The specific genes of *B. vulgatus* 7K1, denoted as COG0270, COG1343, and COG3392, are responsible for DNA replication, recombination, and repair and are integral to cell survival [74]. In addition, another specific gene, denoted as COG0610, belonging to *B. vulgatus* 7K1 is related to the type I site-specific restriction-modification system, which has been found to protect bacteria from bacteriophage infection [75]. Bacteriophages are members of the host gut

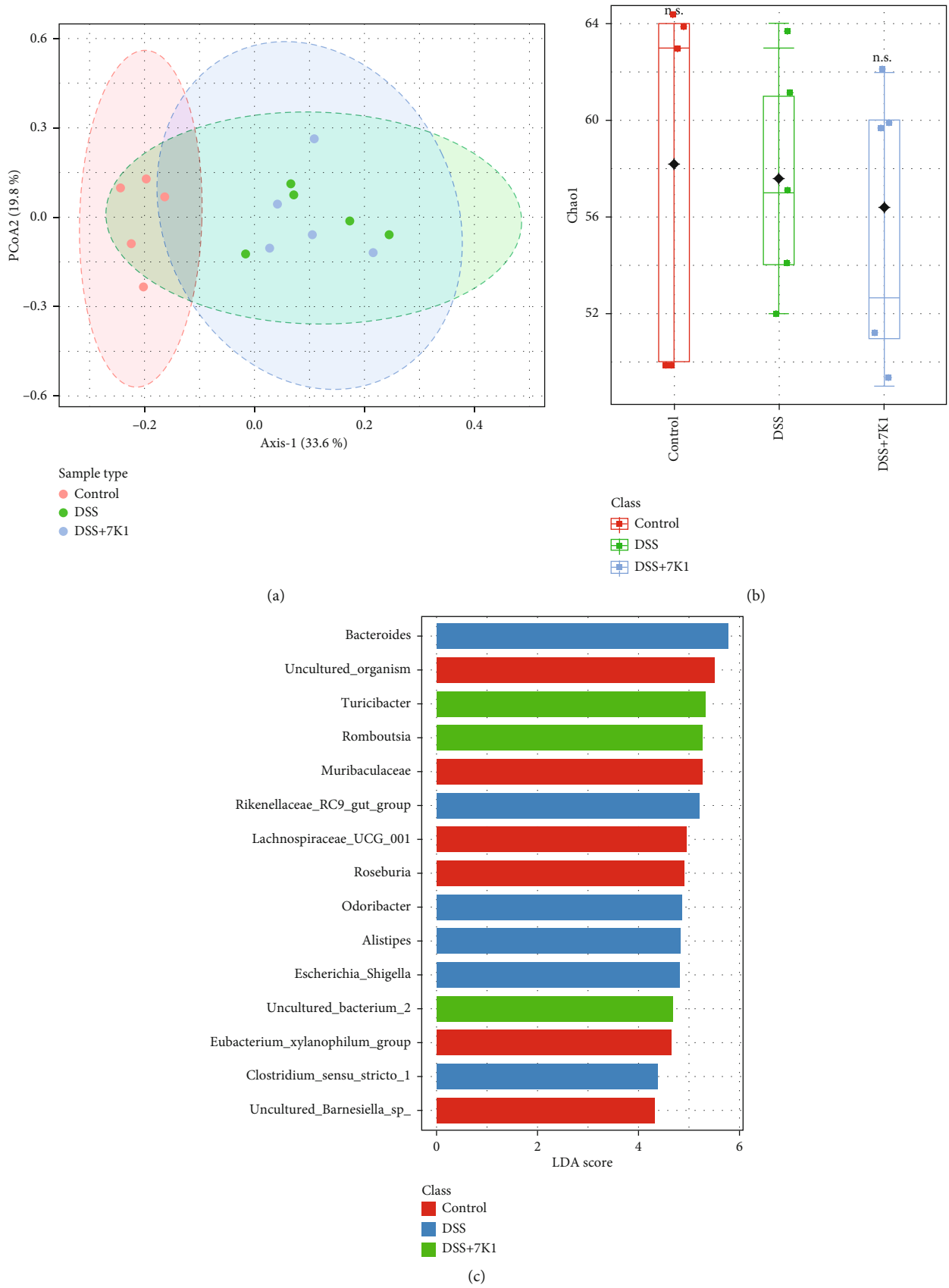


Figure 8: Effect of *Bacteroides vulgatus* on the intestinal microbiota of mice. (a) Principal component analysis of gut microbiota. (b) Alpha diversity indicated by Chao1 index. (c) LEfSe analysis of the different groups. Five mice per group.

microbiota. Environmental stimuli have been reported to induce the production of infectious bacteriophages that cause lysis in their bacterial host [76]. Hence, these genes may guarantee the survival of *B. vulgatus* 7K1 in the gut of DSS-treated mice and further ensure its protective role in the host health.

Compared with *B. vulgatus* 51K1, *B. vulgatus* 7K1 has more gene copy numbers for the families GH29, GH95, and GH141. The $\alpha$-L-fucosidases of these glycoside hydrolase families are involved in the synthesis of fucosyl-N-acetylglucosamine disaccharides [77]. It has been reported that some fucosyl-N-acetylglucosamine disaccharides inhibit the adhesion of certain enteropathogenic *E. coli* (EPEC) strains onto HT29 cells [78]. EPEC adherence onto intestinal epithelial monolayers can disrupt the barrier function [79]. Thus, the greater number of genes of these glycoside hydrolase families in *B. vulgatus* 7K1 may guarantee its protective effect on the intestinal barrier function.

## 5. Conclusion

The results of this study revealed that the protective roles of *B. vulgatus* strains selected from different clades of the phylogenetic tree against DSS-induced colitis are strain-specific. *B. vulgatus* 7K1 exhibited a significant protective effect against colitis, but *B. vulgatus* 51K1 markedly deteriorated the symptoms of colitis in mice. The results of further genomic comparisons showed that several specific genes present in the *B. vulgatus* 7K1 genome that are responsible for colonic SCFAs or capsular polysaccharide production and survival in the gut do not exist in the *B. vulgatus* 51K1 genome. This may explain the effective protection provided by *B. vulgatus* 7K1 against DSS-induced colitis, and the lack thereof by *B. vulgatus* 51K1.

## Data Availability

The data used to support the findings of this study are available from the corresponding author upon request.

## Conflicts of Interest

The authors declare no conflicts of interest.

## Acknowledgments

This work was supported by the National Natural Science Foundation of China [32001665], the Natural Science Foundation of Jiangsu Province [BK20180603], the National first-class discipline program of Food Science and Technology [JUFSTR20180102], and Collaborative Innovationcenter of Food Safety and Quality Control in Jiangsu Province.

## Supplementary Materials

Table S1: specific clusters of orthologous group (COG) categories in *Bacteroides vulgatus* 7K1. Table S2: details of the Carbohydrate-Active enZyme genes that are abundant in the genome of *Bacteroides vulgatus* 7K1. *(Supplementary Materials)*

## References

[1] R. Liu, J. Hong, X. Xu et al., "Gut microbiome and serum metabolome alterations in obesity and after weight- loss intervention," *Nature Medicine*, vol. 23, no. 7, pp. 859–868, 2017.

[2] J. Y. Yang, Y. S. Lee, Y. Kim et al., "Gut commensal *Bacteroides acidifaciens* prevents obesity and improves insulin sensitivity in mice," *Mucosal Immunology*, vol. 10, no. 1, pp. 104–116, 2017.

[3] W. Zhang, B. Zhu, J. Xu et al., "*Bacteroides fragilis* protects against antibiotic-associated diarrhea in rats by modulating intestinal defenses," *Frontiers in Immunology*, vol. 9, p. 1040, 2018.

[4] C. Ramakrishna, M. Kujawski, H. Chu, L. Li, S. K. Mazmanian, and E. M. Cantin, "*Bacteroides fragilis* polysaccharide A induces IL-10 secreting B and T cells that prevent viral encephalitis," *Nature Communications*, vol. 10, no. 1, article 2153, 2019.

[5] L. Zheng, M. Luo, G. Kuang et al., "Capsular polysaccharide from *Bacteroides fragilis* protects against ulcerative colitis in an undegraded form," *Frontiers in Pharmacology*, vol. 11, article 570476, 2020.

[6] K. Takahashi, A. Nishida, T. Fujimoto et al., "Reduced abundance of butyrate-producing bacteria species in the fecal microbial community in Crohn's disease," *Digestion*, vol. 93, no. 1, pp. 59–65, 2016.

[7] W. Zhong, X. Lu, H. Shi et al., "Distinct microbial populations exist in the mucosa-associated microbiota of diarrhea predominant irritable bowel syndrome and ulcerative colitis," *Journal of Clinical Gastroenterology*, vol. 53, no. 9, pp. 660–672, 2019.

[8] S. K. Mazmanian, J. L. Round, and D. L. Kasper, "A microbial symbiosis factor prevents intestinal inflammatory disease," *Nature*, vol. 453, no. 7195, pp. 620–625, 2008.

[9] M. Delday, I. Mulder, E. T. Logan, and G. Grant, "*Bacteroides thetaiotaomicron* ameliorates colon inflammation in preclinical models of Crohn's disease," *Inflammatory Bowel Diseases*, vol. 25, no. 1, pp. 85–96, 2019.

[10] C. P. Neff, M. E. Rhodes, K. L. Arnolds et al., "Diverse intestinal bacteria contain putative zwitterionic capsular polysaccharides with anti-inflammatory properties," *Cell Host & Microbe*, vol. 20, no. 4, pp. 535–547, 2016.

[11] E. C. Wick, S. Rabizadeh, E. Albesiano et al., "Stat3 activation in murine colitis induced by enterotoxigenic *Bacteroides fragilis*," *Inflammatory Bowel Diseases*, vol. 20, no. 5, pp. 821–834, 2014.

[12] R. Dziarski, S. Y. Park, D. R. Kashyap, S. E. Dowd, and D. Gupta, "Pglyrp-regulated gut microflora *Prevotella falsenii*, *Parabacteroides distasonis* and *Bacteroides eggerthii* enhance and *Alistipes finegoldii* attenuates colitis in mice," *PLoS One*, vol. 11, no. 1, article e0146162, 2016.

[13] M. Chatzidaki-Livanis, N. Geva-Zatorsky, and L. E. Comstock, "*Bacteroides fragilis* type VI secretion systems use novel effector and immunity proteins to antagonize human gut Bacteroidales species," *Proceedings of the National Academy of Sciences of the United States of America*, vol. 113, no. 13, pp. 3627–3632, 2016.

[14] M. Chatzidaki-Livanis, M. J. Coyne, K. G. Roelofs, R. R. Gentyala, J. M. Caldwell, and L. E. Comstock, "Gut symbiont *Bacteroides fragilis* secretes a eukaryotic-like ubiquitin protein that mediates intraspecies antagonism," *MBio*, vol. 8, no. 6, 2017.

[15] N. T. Porter, P. Canales, D. A. Peterson, and E. C. Martens, "A subset of polysaccharide capsules in the human symbiont *Bacteroides thetaiotaomicron* promote increased competitive fitness in the mouse gut," *Cell Host & Microbe*, vol. 22, no. 4, pp. 494–506.e8, 2017.

[16] A. L. Hecht, B. W. Casterline, Z. M. Earley, Y. A. Goo, D. R. Goodlett, and J. Bubeck Wardenburg, "Strain competition restricts colonization of an enteric pathogen and prevents colitis," *EMBO Reports*, vol. 17, no. 9, pp. 1281–1291, 2016.

[17] R. Corrêa-Oliveira, J. L. Fachi, A. Vieira, F. T. Sato, and M. A. R. Vinolo, "Regulation of immune cell function by short-chain fatty acids," *Clinical & Translational Immunology*, vol. 5, no. 4, p. e73, 2016.

[18] R. B. Canani, M. Di Costanzo, and L. Leone, "The epigenetic effects of butyrate: potential therapeutic implications for clinical practice," *Clinical Epigenetics*, vol. 4, no. 1, p. 4, 2012.

[19] J. Sauer, K. K. Richter, and B. L. Pool-Zobel, "Physiological concentrations of butyrate favorably modulate genes of oxidative and metabolic stress in primary human colon cells," *Journal of Nutritional Biochemistry*, vol. 18, no. 11, pp. 736–745, 2007.

[20] M. H. Sofi, Y. Wu, T. Ticer et al., "A single strain of *Bacteroides fragilis* protects gut integrity and reduces GVHD," *Jci Insight*, vol. 6, no. 3, article e136841, 2021.

[21] R. J. Obiso, D. M. Lyerly, R. L. van Tassell, and T. D. Wilkins, "Proteolytic activity of the *Bacteroides fragilis* enterotoxin causes fluid secretion and intestinal damage in vivo," *Infection and Immunity*, vol. 63, no. 10, pp. 3820–3826, 1995.

[22] J. L. Round and S. K. Mazmanian, "Inducible Foxp3$^+$ regulatory T-cell development by a commensal bacterium of the intestinal microbiota," *Proceedings of the National Academy of Sciences of the United States of America*, vol. 107, no. 27, pp. 12204–12209, 2010.

[23] Y. K. Lee, P. Mehrabian, S. Boyajian et al., "The protective role ofBacteroides fragilisin a murine model of colitis-associated colorectal Cancer," *mSphere*, vol. 3, no. 6, 2018.

[24] E. M. Brown, X. Ke, D. Hitchcock et al., "*Bacteroides*-derived sphingolipids are critical for maintaining intestinal homeostasis and symbiosis," *Cell Host & Microbe*, vol. 25, no. 5, pp. 668–680.e7, 2019.

[25] Q. Zhai, X. Shen, S. Cen et al., "Screening of *Lactobacillus salivarius* strains from the feces of Chinese populations and the evaluation of their effects against intestinal inflammation in mice," *Food & Function*, vol. 11, no. 1, pp. 221–235, 2020.

[26] Y. Liu, Y. Li, X. Yu et al., "Physiological characteristics of *Lactobacillus casei* strains and their alleviation effects against inflammatory bowel disease," *Journal of Microbiology and Biotechnology*, vol. 31, no. 1, pp. 92–103, 2021.

[27] J. Qin, R. Li, J. Raes et al., "A human gut microbial gene catalogue established by metagenomic sequencing," *Nature*, vol. 464, no. 7285, pp. 59–65, 2010.

[28] J. Tap, S. Mondot, F. Levenez et al., "Towards the human intestinal microbiota phylogenetic core," *Environmental Microbiology*, vol. 11, no. 10, pp. 2574–2584, 2009.

[29] M. Waidmann, O. Bechtold, J. S. Frick et al., "*Bacteroides vulgatus* protects against *Escherichia coli*-induced colitis in gnotobiotic interleukin-2-deficient mice," *Gastroenterology*, vol. 125, no. 1, pp. 162–177, 2003.

[30] J. S. Frick, K. Fink, F. Kahl et al., "Identification of commensal bacterial strains that modulate *Yersinia enterocolitica* and dextran sodium sulfate-induced inflammatory responses: implications for the development of probiotics," *Infection and Immunity*, vol. 75, no. 7, pp. 3490–3497, 2007.

[31] H. C. Rath, K. H. Wilson, and R. B. Sartor, "Differential induction of colitis and gastritis in HLA-B27 transgenic rats selectively colonized with *Bacteroides vulgatus* or *Escherichia coli*," *Infection and Immunity*, vol. 67, no. 6, pp. 2969–2974, 1999.

[32] A. B. Onderdonk, R. L. Cisneros, and R. T. Bronson, "Enhancement of experimental ulcerative colitis by immunization with *Bacteroides vulgatus*," *Infection and Immunity*, vol. 42, no. 2, pp. 783–788, 1983.

[33] A. B. Onderdonk, R. Bronson, and R. Cisneros, "Comparison of *Bacteroides vulgatus* strains in the enhancement of experimental ulcerative colitis," *Infection and Immunity*, vol. 55, no. 3, pp. 835-836, 1987.

[34] S. Wirtz, V. Popp, M. Kindermann et al., "Chemically induced mouse models of acute and chronic intestinal inflammation," *Nature Protocols*, vol. 12, no. 7, pp. 1295–1309, 2017.

[35] M. Murano, K. Maemura, I. Hirata et al., "Therapeutic effect of intracolonically administered nuclear factor kappa B (p65) antisense oligonucleotide on mouse dextran sulphate sodium (DSS)-induced colitis," *Clinical and Experimental Immunology*, vol. 120, no. 1, pp. 51–58, 2000.

[36] R. Q. Li, Y. R. Li, K. Kristiansen, and J. Wang, "SOAP: short oligonucleotide alignment program," *Bioinformatics*, vol. 24, no. 5, pp. 713-714, 2008.

[37] R. Q. Li, H. M. Zhu, J. Ruan et al., "De novo assembly of human genomes with massively parallel short read sequencing," *Genome Research*, vol. 20, no. 2, pp. 265–272, 2010.

[38] K. Katoh and D. M. Standley, "MAFFT multiple sequence alignment software version 7: improvements in performance and usability," *Molecular Biology and Evolution*, vol. 30, no. 4, pp. 772–780, 2013.

[39] J. S. Zheng, L. F. Ruan, M. Sun, and M. Gänzle, "A genomic view of *Lactobacilli* and *Pediococci* demonstrates that phylogeny matches ecology and physiology," *Applied & Environmental Microbiology*, vol. 81, no. 20, pp. 7233–7243, 2015.

[40] Q. X. Zhai, F. W. Tian, J. X. Zhao, H. Zhang, A. Narbad, and W. Chen, "Oral administration of probiotics inhibits absorption of the heavy metal cadmium by protecting the intestinal barrier," *Applied and Environmental Microbiology*, vol. 82, no. 14, pp. 4429–4440, 2016.

[41] Q. Xu, X. F. Li, E. Y. Wang et al., "A cellular model for screening of *Lactobacilli* that can enhance tight junctions," *RSC Advances*, vol. 6, no. 113, pp. 111812–111821, 2016.

[42] L. L. Wang, M. L. Pan, D. Y. Li et al., "Metagenomic insights into the effects of oligosaccharides on the microbial composition of cecal contents in constipated mice," *Journal of Functional Foods*, vol. 38, pp. 486–496, 2017.

[43] B. Y. Mao, D. Y. Li, C. Q. Ai, J. Zhao, H. Zhang, and W. Chen, "Lactulose differently modulates the composition of luminal and mucosal microbiota in C57BL/6J mice," *Journal of Agricultural and Food Chemistry*, vol. 64, no. 31, pp. 6240–6247, 2016.

[44] R. Zhai, X. Xue, L. Zhang, X. Yang, L. Zhao, and C. Zhang, "Strain-specific anti-inflammatory properties of two *Akkermansia muciniphila* strains on chronic colitis in mice," *Frontiers in Cellular and Infection Microbiology*, vol. 9, p. 239, 2019.

[45] D. Srutkova, M. Schwarzer, T. Hudcovic et al., "*Bifidobacterium longum* CCM 7952 promotes epithelial barrier function and prevents acute DSS-induced colitis in strictly strain-

specific manner," *PLoS One*, vol. 10, no. 7, article e0134050, 2015.

[46] Y. Zhao, C. Zhang, L. Yu et al., "Phylogenetic and comparative genomic analysis of *Lactobacillus fermentum* strains and the key genes related to their intestinal anti-inflammatory effects," *Engineering*, 2021.

[47] C. Dunne, L. O'Mahony, L. Murphy et al., "In vitro selection criteria for probiotic bacteria of human origin: correlation with in vivo findings," *American Journal of Clinical Nutrition*, vol. 73, no. 2, pp. 386S–392S, 2001.

[48] Y. Chen, Y. Jin, C. Stanton et al., "Dose-response efficacy and mechanisms of orally administered CLA-producing *Bifidobacterium breve* CCFM683 on DSS-induced colitis in mice," *Journal of Functional Foods*, vol. 75, no. 3, article 104245, 2020.

[49] M. Szulińska, I. Łoniewski, S. van Hemert, M. Sobieska, and P. Bogdański, "Dose-dependent effects of multispecies probiotic supplementation on the lipopolysaccharide (LPS) level and cardiometabolic profile in obese postmenopausal women: a 12-week randomized clinical trial," *Nutrients*, vol. 10, no. 6, p. 773, 2018.

[50] X. W. Gao, M. Mubasher, C. Y. Fang, C. Reifer, and L. E. Miller, "Dose-response efficacy of a proprietary probiotic formula of *Lactobacillus acidophilus* CL1285 and *Lactobacillus casei* LBC80R for antibiotic-associated diarrhea and clostridium difficile -associated diarrhea prophylaxis in adult patients," *American Journal of Gastroenterology*, vol. 105, no. 7, pp. 1636–1641, 2010.

[51] R. Li, Y. F. Zhang, D. B. Polk, P. M. Tomasula, F. Yan, and L. S. Liu, "Preserving viability of *Lactobacillus rhamnosus* GG *in vitro* and *in vivo* by a new encapsulation system," *Journal of Controlled Release*, vol. 230, pp. 79–87, 2016.

[52] D. J. Silberger, C. L. Zindl, and C. T. Weaver, "*Citrobacter rodentium*: a model enteropathogen for understanding the interplay of innate and adaptive components of type 3 immunity," *Mucosal Immunology*, vol. 10, no. 5, pp. 1108–1117, 2017.

[53] A. L. Glasser, J. Boudeau, N. Barnich, M. H. Perruchot, J. F. Colombel, and A. Darfeuille-Michaud, "Adherent invasive *Escherichia coli* strains from patients with Crohn's disease survive and replicate within macrophages without inducing host cell death," *Infection and Immunity*, vol. 69, no. 9, pp. 5529–5537, 2001.

[54] C. C. Chen, S. Louie, H. N. Shi, and W. A. Walker, "Preinoculation with the probiotic *Lactobacillus acidophilus* early in life effectively inhibits murine *Citrobacter rodentium* colitis," *Pediatric Research*, vol. 58, no. 6, pp. 1185–1191, 2005.

[55] R. N. Fedorak and K. L. Madsen, "Probiotics and the management of inflammatory bowel disease," *Inflammatory Bowel Diseases*, vol. 10, no. 3, pp. 286–299, 2004.

[56] C. Maciej, L. P. Hale, and L. Physiology, "Bacterial-mucosal interactions in inflammatory bowel disease—an alliance gone bad," *American Journal of Physiology-Gastrointestinal and Liver Physiology*, vol. 295, no. 6, pp. G1139–G1149, 2008.

[57] Y. Chen, Y. Jin, C. Stanton et al., "Alleviation effects of *Bifidobacterium breve* on DSS-induced colitis depends on intestinal tract barrier maintenance and gut microbiota modulation," *European Journal of Nutrition*, vol. 60, no. 1, pp. 369–387, 2021.

[58] G. Wang, Q. Xu, X. Jin et al., "Effects of *Lactobacilli* with different regulatory behaviours on tight junctions in mice with dextran sodium sulphate-induced colitis," *Journal of Functional Foods*, vol. 47, pp. 107–115, 2018.

[59] A. J. Leonel and J. I. Alvarez-Leite, "Butyrate: implications for intestinal function," *Current Opinion in Clinical Nutrition and Metabolic Care*, vol. 15, no. 5, pp. 474–479, 2012.

[60] H. Liu, J. Wang, T. He et al., "Butyrate: a double-edged sword for health?," *Advances in Nutrition*, vol. 9, no. 1, pp. 21–29, 2018.

[61] P. C. A. Moquet, L. Onrust, F. van Immerseel, R. Ducatelle, W. H. Hendriks, and R. P. Kwakkel, "Importance of release location on the mode of action of butyrate derivatives in the avian gastrointestinal tract," *World's Poultry Science Journal*, vol. 72, no. 1, pp. 61–80, 2016.

[62] T. Horiuchi, H. Mitoma, S.-I. Harashima, H. Tsukamoto, and T. Shimoda, "Transmembrane TNF-$\alpha$: structure, function and interaction with anti-TNF agents," *Rheumatology*, vol. 49, no. 7, pp. 1215–1228, 2010.

[63] I. A. Lee, E. A. Bae, J. H. Lee et al., "*Bifidobacterium longum* HY8004 attenuates TNBS-induced colitis by inhibiting lipid peroxidation in mice," *Inflammation Research*, vol. 59, no. 5, pp. 359–368, 2010.

[64] A. K. Pandurangan, S. Ismail, Z. Saadatdoust, and N. M. Esa, "Allicin alleviates dextran sodium sulfate- (DSS-) induced ulcerative colitis in BALB/c mice," *Oxidative Medicine & Cellular Longevity*, vol. 2015, article 605208, pp. 1–13, 2015.

[65] J. J. Hansen, L. Holt, and R. B. Sartor, "Gene expression patterns in experimental colitis in IL-10-deficient mice," *Inflammatory Bowel Diseases*, vol. 15, no. 6, pp. 890–899, 2009.

[66] S. K. Mittal and P. A. Roche, "Suppression of antigen presentation by IL-10," *Current Opinion in Immunology*, vol. 34, pp. 22–27, 2015.

[67] J. Yang, Q. Li, S. M. Henning et al., "Effects of prebiotic fiber xylooligosaccharide in adenine-induced nephropathy in mice," *Molecular Nutrition & Food Research*, vol. 62, no. 15, article e1800014, 2018.

[68] N. Burger-van Paassen, A. Vincent, P. J. Puiman et al., "The regulation of intestinal mucin MUC2 expression by short-chain fatty acids: implications for epithelial protection," *Biochemical Journal*, vol. 420, no. 2, pp. 211–219, 2009.

[69] H. B. Wang, P. Y. Wang, X. Wang, Y. L. Wan, and Y. C. Liu, "Butyrate enhances intestinal epithelial barrier function via up-regulation of tight junction protein claudin-1 transcription," *Digestive Diseases and Sciences*, vol. 57, no. 12, pp. 3126–3135, 2012.

[70] L. Peng, Z. R. Li, R. S. Green, I. R. Holzman, and J. Lin, "Butyrate enhances the intestinal barrier by facilitating tight junction assembly via activation of AMP-activated protein kinase in Caco-2 cell monolayers," *Journal of Nutrition*, vol. 139, no. 9, pp. 1619–1625, 2009.

[71] X. Dou, N. Gao, D. Yan, and A. Shan, "Sodium butyrate alleviates mouse colitis by regulating gut microbiota dysbiosis," *Animals*, vol. 10, no. 7, article 1154, 2020.

[72] Y.-M. Lu, J.-J. Xie, C.-G. Peng, B.-H. Wang, K.-C. Wang, and L.-J. Li, "Enhancing clinical efficacy through the gut microbiota: a new field of traditional Chinese medicine," *Engineering*, vol. 5, no. 1, pp. 40–49, 2019.

[73] H. Chu, A. Khosravi, I. P. Kusumawardhani et al., "Gene-microbiota interactions contribute to the pathogenesis of inflammatory bowel disease," *Science*, vol. 352, no. 6289, pp. 1116–1120, 2016.

[74] H. L. Klein and K. N. Kreuzer, "Replication, recombination, and repair: going for the gold," *Molecular Cell*, vol. 9, no. 3, pp. 471–480, 2002.

[75] J. Youell and K. Firman, "Mechanistic insight into type I restriction endonucleases," *Frontiers in Bioscience*, vol. 17, no. 7, pp. 2122–2139, 2012.

[76] J. M. Norman, S. A. Handley, M. T. Baldridge et al., "Disease-specific alterations in the enteric virome in inflammatory bowel disease," *Cell*, vol. 160, no. 3, pp. 447–460, 2015.

[77] P. Liu, H. Zhang, Y. Wang et al., "Screening and characterization of an $\alpha$-L-fucosidase from *Bacteroides fragilis* NCTC9343 for synthesis of fucosyl-N-acetylglucosamine disaccharides," *Applied Microbiology and Biotechnology*, vol. 104, no. 18, pp. 7827–7840, 2020.

[78] J. E. Becerra, J. M. Coll-Marqués, J. Rodríguez-Díaz, V. Monedero, and M. J. Yebra, "Preparative scale purification of fucosyl-N-acetylglucosamine disaccharides and their evaluation as potential prebiotics and antiadhesins," *Applied Microbiology and Biotechnology*, vol. 99, no. 17, pp. 7165–7176, 2015.

[79] J. Spitz, R. Yuhan, A. Koutsouris, C. Blatt, J. Alverdy, and G. Hecht, "Enteropathogenic *Escherichia coli* adherence to intestinal epithelial monolayers diminishes barrier function," *American Journal of Physiology-Gastrointestinal and Liver Physiology*, vol. 268, no. 2, pp. G374–G379, 1995.